The University of Nottingham

Elucidation of Potential NRP1 Interactors using BioID Technology

George Coney
MPharm

A Thesis Submitted to the University of Nottingham for the Degree of Doctor of Philosophy

April, 2025

I. Abstract

Background:

Neuropilin 1 (NRP1) is a transmembrane glycoprotein involved in diverse physiological processes, including angiogenesis, axonal guidance, immune regulation, cell adhesion, and recently, facilitation of SARS-CoV-2 entry and infectivity. Despite its functional importance, comprehensive analyses of the NRP1 interactome have been limited. Previous studies focused primarily on the N-terminal region, while the intracellular C-terminal portion, containing a PDZ domain, remains largely unexplored. Identifying NRP1 binding partners, particularly those interacting with its C-terminal region, is critical to fully understand its cellular roles.

Aims:

This study aimed to define the NRP1 interactome using BioID proximity labeling technology, both under basal conditions and following stimulation with its cognate ligand $VEGF_{165}$a. A particular focus was placed on characterizing interactions mediated by the intracellular C-terminal region. Selected candidate interactors were further validated using NanoLuciferase Bioluminescence Resonance Energy Transfer (NanoBRET) assays.

Results:

In HEK293T cells, BioID analysis identified 177 proteins enriched under basal conditions and 42 potential interactors upon $VEGF_{165}$a stimulation. Among a subset of proteins selected for further validation—Vesicle-associated membrane protein-associated protein A (VAPA), Occludin (OCLN), Zona occludens 1 (ZO1), Septin 9 (SEPT9), Hepatocyte growth factor-regulated tyrosine kinase substrate (HRS), and Integrin β1 (ITGB1)—positive interactions were particularly observed for OCLN and VAPA, associated with cell adhesion and vesicular trafficking, respectively. Further experiments using hTERT2-HUVEC cells, a more physiologically relevant endothelial model, revealed additional potential interactors, suggesting that NRP1 may exhibit context-dependent, cell-specific interactions.

Conclusions:

This study presents the most detailed analysis to date of the NRP1 interactome, highlighting the role of its C-terminal region in recruiting PDZ domain-containing proteins. BioID combined with NanoBRET validation demonstrates that NRP1 interactions are both ligand-dependent and cell-type-specific, particularly involving proteins implicated in adhesion and trafficking. These findings provide a foundation for understanding the molecular mechanisms underlying NRP1 function in diverse physiological and pathological contexts.

II. Acknowledgements

First and foremost, I would like to express my heartfelt gratitude to my incredible supervisors, Dr. Laura Kilpatrick, Dr. Daniel Booth, and Dr. Steve Hill, for their unwavering patience and guidance from the very beginning of the project through to its completion. From a challenging start — marked by multiple rounds of COVID infections — to the equally demanding write-up phase, with various personal hurdles in between, your support has been a constant. The lessons I've learned under your supervision will stay with me throughout my career and life.

Thank you again for fostering such a warm and welcoming research environment. I truly couldn't imagine undertaking my PhD in any other lab. It has been a privilege to work among such inspiring individuals.

I would also like to extend my sincere thanks to the members of my immediate lab groups. In the Booth Lab, the support from both past and present members has been integral to my development throughout the PhD. Particular thanks go to Eva, Grace, Pippa, Kathryn, Zarah, and Michaela — your friendship has meant the world to me. We are PhD trauma-bonded for life.

In COMPARE, I am grateful to Dr. Mark Soave for sticking with me during the early, cloning-heavy days of the project, and for his constant encouragement. A special thank you to Dr. Simon Platt for his continued advice throughout my PhD and for keeping the lab running smoothly — your efforts never go unnoticed. Thanks also to Marleen for her boundless passion for cell culture and for ensuring the tissue culture labs were always functioning flawlessly.

A heartfelt thank you to the Wellcome Trust for supporting this project, and to Prof. Jeanette Woolard for leading the Wellcome Trust programme at the University of Nottingham. I also wish to thank her ever-enthusiastic right-hand, Dr. Eddy Wragg. Though he joined later in my project, his input has had a positive and lasting impact. I'd also like to acknowledge Assistant Prof. Sam Cooper, whose evolving role within the programme has been matched by her consistent support throughout. Additional thanks go to Prof. Dave Bates, who served as the cohort lead during our first year exploring various facets of angiogenesis.

To my family and friends — thank you for always believing in me, especially during moments when I doubted myself. Finally, to my partner Noemi — thank you for never wavering in your belief in me. Your constant support, especially during the difficult write-up period, has been invaluable. I couldn't have done it without you.

III. Acronyms and Abbreviation

AF	Alexa Fluor
ANOVA	Analysis of variance
APEX	Ascorbate Peroxidase
AP-MS	Affinity purification - mass spectrometry
ATP	Adenosine triphosphate
BirA	Biotin ligase
BRET	Bioluminescence resonance energy transfer
BSA	Bovine serum albumin
CAV-ME	Caveolin-mediated endocytosis
CENPA	Centromere protein A
CME	Clathrin-mediated endocytosis
Co-IP	Co-immunoprecipitation
CUB	Complement, Uegf, BMP
DAPI	4',6-diamidino-2-phenylindole
DMEM	Dulbecco's modified eagle medium
DNA	Deoxyribonucleic acid
EC	Endothelial cell
ECD	Extracellular domain
ECM	Extracellular matrix
EGFR	Endothelial growth factor receptor
ER	Enrichment ratio
ESCRT	Endosomal sorting complex required for transport
FACS	Fluorescence-activated cell sorting
FCS	Foetal Calf Serum
FDR	False discovery rate
FITC	Fluorescein Isothiocyanate
FSC	Forward scatter
GFP	Green fluorescent protein
GO	Gene ontology
HBSS	Hank's balanced salt solution
HEK293T	Human embryonic kidney 293T
HRP	Horseradish peroxidase
HRS	Hepatocyte growth factor-regulated tyrosine kinase substrate
hTERT2	Human telomerase reverse transcriptase
HUVEC	Human umbilical vein endothelial cells
iBAQ	intensity based absolute quantification
IF	Immunofluorescence
ITGB1	Integrin B1
JAM	Junction adhesion molecule
KD	Kinase domain
KID	Kinase insert domain
LB	Luria Bertani
LC-MS	Liquid chromatography - mass spectrometry
LDS	Lithium dodecyl sulphate

LFQ	Label free quantification
MAM	Meprin/Antigen 5/Receptor Tyrosine Phosphatase μ
MAPK	Mitogen-activated protein kinase
MP	Macropinocytosis
MS	Mass Spectrometry
MVB	Multivesicular body
NanoLuc	Nano luciferase
NRP1	Neuropilin 1
nTMP	Normalised transcripts per million
OCLN	Occludin
PBS	Phosphate-buffered saline
PCR	Polymerase chain reaction
PDL	Poly-D-Lysine
PDZ	PSD95)/Discs large (Dlg)/Zonula occludens-1 (ZO-1)
PEI	Polyethylenimine
PEP	Posterior error probability
PFA	paraformaldehyde
PLA	Proximity ligation assay
PSM	Peptide spectrum match
RFP	Red fluorescent protein
riBAQ	relative intensity based absolute quantification
RNA	Ribonucleic acid
RT	Room temp
RTK	Receptor tyrosine kinase
SDS-PAGE	Sodium Dodecyl Sulfate-Polyacrylamide Gel Electrophoresis
SEM	Standard error of the mean
SEPT9	Septin 9
SNAP	Synaptosomal-associated protein
SNARE	Soluble N-ethylmaleimide-sensitive factor attachment protein receptor
SPR	Surface Plasmon Resonance
Squassh	Segmentation and quantification of subcellular shapes
SSC	Side scatter
TDC	Target decoy competition
TM	Transmembrane
VAMP	Vesicle-associated membrane protein
VAPA	Vesicle-associated membrane protein-associated protein A
VEGF	Vascular endothelial growth factor
VEGFR	Vascular endothelial growth factor receptor
WT	Wild type
ZO1	Zona occludens 1

IV. Figures and Tables List

Chapter 1: General Introduction

Page

Figure 1.1 – General morphology of vessel types in the cardiovascular system. 20
Figure 1.2 – Mechanisms of Vasculogenesis and angiogenesis. 24
Figure 1.3 – Mechanisms of transport across endothelial cells. 26
Figure 1.4 – Mechanisms of transcytosis across endothelial cells. 28
Figure 1.5 – Types of endothelial cell junctions. 31
Figure 1.6 – Composition of adherens junction. 33
Figure 1.7 – Composition of tight junction. 37
Figure 1.8 – Structure of the folded and unfolded focal adhesion complex. 41
Figure 1.9 – Schematic illustrating ligand-binding selectivity to VEGFR subtypes, NRP-1 and NRP-2. 43
Figure 1.10 – A schematic detailing the $VEGF_{165}$a structure and isoforms generated through alternative splicing. 49
Figure 1.11 – Structure and domains of Neuropilin-1. 52
Figure 1.12 – Internalisation and membrane recycling of VEGFR2 facilitated by NRP1 60
Figure 1.13 – Mechanism of viral entry of SARS-CoV-2 by binding of S1 protein to Neuropilin-1. 64
Figure 1.14 – Principles of using BioID technology to identify novel interactors with NRP1. 73
Figure 1.15 – Principles of NanoBRET. 74
Table 1.1 – Observed binding partners with Neuropilin-1 in the literature. 69

Chapter 2: General Materials and Methods

Figure 2.1 – Haemocytometer cell counting visualisation. 89
Table 2.1 – Sequence of oligos used in the PCR of mycBioID2, BioID2-HA and VEGFR3. 79
Table 2.2 – Details describing the volume of media, volume of PDL or gelatine, and number of cells (HEK293T or hTERT2-HUVEC) per well, relating to the culture vessel size. 89
Table 2.3 – Details regarding the amount of DNA, volume of polyethylenimine (PEI) and volume of NaCl used in PEI transfections per well. 91
Table 2.4 - Details regarding the amount of DNA, volume of FuGENE HD and volume of Opti-MEM used in FuGENE HD transfections per well. 92
Table 2.5 – Squassh analysis plug-in settings. 97
Table 2.6 – Composition of wash buffers used in the isolation of biotinylated proteins protocol. 100
Table 2.7 – Plasmids ordered from addgene containing potential NRP1 interacting partner identified during BioID screening. 106

Chapter 3: Molecular Cloning and BioID Evaluation

Figure 3.1 – Immunofluorescence images from unbound BioID1 BirA and BioID2 BirA transient transfections in HeLa Cells. 111
Figure 3.2 – Total cell fluorescence analysis of BioID1 compared with BioID2 112
Figure 3.3 – BioID2-CENPA cloning protocol and results. 113
Figure 3.4 – Immunofluorescence images from BioID1-CENPA and BioID2-CENPA transient transfections in HeLa Cells. 116

Figure 3.5 – Fluorescence intensity analysis of BioID1-CENPA compared with BioID2-CENPA. 118
Figure 3.6 – Schematic illustrating the BioID cloned plasmids of VEGFR2, VEGFR3, NRP1 and NRP1 and relative locations of the biotin ligase. 119
Figure 3.7 – mycBioID2-VEGFR3 cloning protocol and results. 120
Figure 3.8 – VEGFR3-BioID2-HA cloning protocol and results 122
Figure 3.9 – mycBioID2-VEGFR2 cloning protocol and results. 124
Figure 3.10 – VEGFR2-BioID2-HA cloning protocol and results. 126
Figure 3.11 – mycBioID2-NRP1 cloning protocol and results. 128
Figure 3.12 – NRP1-BioID2-HA cloning protocol and results. 130
Figure 3.13 – Immunofluorescence of HEK293T cell transfected with N-terminal BioID2 constructs 133
Figure 3.14 – Alternative images for mycBioID2-VEGFR2 and mycBioID2-VEGFR3 not representative of the cell population. 134
Figure 3.15 – Immunofluorescence of HEK293T cell transfected with C-terminal BioID2 constructs 135
Table 3.1 – Ligation reaction formula for insertion of CENPA into the mycBioID2 vector. 114
Table 3.2 – Results from the bacterial transformation of BioID2-CENPA ligation reactions in Chemically Competent DH5α E. Coli cells. 114
Table 3.3 – Ligation reaction formula for insertion of BioID2 into the VEGFR3 vector. 120
Table 3.4 – Results from the bacterial transformation of BioID2-VEGFR3 ligation reactions in Chemically Competent DH5α E. Coli cells. 121
Table 3.5 – Ligation reaction formula for insertion of BioID2-HA into the VEGFR3 vector. 122
Table 3.6 – Results from the bacterial transformation of VEGFR3-BioID2-HA ligation reactions in Chemically Competent DH5α E. Coli cells. 123
Table 3.7 – Ligation reaction formula for insertion of mycBioID2 into the VEGFR2 vector. 124
Table 3.8 – Results from the bacterial transformation of mycBioID2-VEGFR2 ligation reactions in Chemically Competent DH5α E. Coli cells. 125
Table 3.9 – Ligation reaction formula for insertion of BioID2-HA into the VEGFR2 vector. 126
Table 3.10 – Results from the bacterial transformation of VEGFR2-BioID2-HA ligation reactions in Chemically Competent DH5α E. Coli cells. 127
Table 3.11 – Ligation reaction formula for insertion of mycBioID2 into the NRP1 vector. 129
Table 3.12 – Results from the bacterial transformation of mycBioID-NRP1 ligation reactions in Chemically Competent DH5α E. Coli cells. 129
Table 3.13 – Ligation reaction formula for insertion of BioID2-HA into the NRP1 vector. 131
Table 3.14 – Results from the bacterial transformation of NRP1-BioID2-HA ligation reactions in Chemically Competent DH5α E. Coli cells. 131
Table 3.15 – Summary of the BioID plasmids synthesised in this project and their characteristics. 140

Chapter 4: NRP1 Interactome Analyses in HEK293T Cells

Figure 4.1 – A schematic depicting the BioID analysis protocol pipeline. 144
Figure 4.2 – Immunofluorescence of optimised transfection of NRP1-BioID2-HA in HEK293T cells. 146
Figure 4.3 – Initial streptavidin pulldown attempts with HEK293T cells transfected with mycBioID2-NRP1 analysed by western blot. 148
Figure 4.4 – Intermediate streptavidin pulldown attempts with HEK293T cells transfected with mycBioID2-NRP1 analysed by western blot. 149
Figure 4.5 – Optimised streptavidin pulldown with HEK293T cells transfected with mycBioID2-NRP1 analysed by western blot. 151

Figure 4.6 – A summary of the enriched proteins in the mycBioID2-NRP1 bioinformatic analysis in both $VEGF_{165}$a stimulated and basal conditions. 157
Figure 4.7 – Bioinformatic processing of MaxQuant output files analysis pipeline. 158
Figure 4.8 – Immunofluorescence of optimised transfection of NRP1-BioID2-HA in HEK293T cells. 159
Figure 4.9 – Depletion of biotin from standard Dulbecco's Modified Eagle Medium (DMEM) cultured with HEK293T cells transfected with NRP1-BioID2-HA. 161
Figure 4.10 – Optimised streptavidin pulldown with HEK293T cells transfected with NRP1-BioID2-HA analysed by western blot. 164
Figure 4.11 – A summary of the enriched proteins in the NRP1-BioID2-HA bioinformatic analyses in both $VEGF_{165}$a stimulated and basal conditions. 165
Figure 4.12 – Common proteins between 4 repeats of C-terminal NRP1-BioID2-HA stimulated with $VEGF_{165}$a. 166
Figure 4.13 – Molecular function gene ontology (GO) analysis of enriched proteins for NRP1-BioID2-HA treated with $VEGF_{165}$a. 169
Figure 4.14 – Biological processes gene ontology (GO) analysis of enriched proteins for NRP1-BioID2-HA treated with $VEGF_{165}$a. 171
Figure 4.15 – Cellular component gene ontology (GO) analysis of enriched proteins for NRP1-BioID2-HA treated with $VEGF_{165}$a. 172
Figure 4.16 – Common proteins between 4 repeats of C-terminal NRP1-BioID2-HA in basal conditions. 174
Figure 4.17 – Molecular function gene ontology (GO) analysis of enriched proteins for NRP1-BioID2-HA under basal conditions. 180
Figure 4.18 – Biological processes gene ontology (GO) analysis of enriched proteins for NRP1-BioID2-HA under basal conditions. 182
Figure 4.19 – Cellular component gene ontology (GO) analysis of enriched proteins for NRP1-BioID2-HA under basal conditions 185
Figure 4.20 – Immunofluorescence of transfection of NRP1-BioID2-HA in HEK293/HaloTag-VEGFR2 stable cell line. 188
Figure 4.21 – Immunofluorescence of transfection of SNAP-NRP1 in HEK293/HaloTag-VEGFR2 stable cell line. 189
Figure 4.22 – Immunofluorescence of transduction optimisation of pLV-NRP1-BioID2-HA in HEK293/HaloTag-VEGFR2 stable cell line. 191
Figure 4.23 – Immunofluorescence of blasticidin selected HEK293/HaloTag-VEGFR2/NRP1-BioID2-HA stable cell line. 192
Figure 4.24 – Fluorescence-activated cell sorting (FACS) of blasticidin selected HEK293/HaloTag-VEGFR2/NRP1-BioID2-HA stable cell line. 194
Figure 4.25 – Immunofluorescence of blasticidin selected HEK293/HaloTag-VEGFR2/NRP1-BioID2-HA stable cell line post-FACS. 196
Figure 4.26 – Optimised streptavidin pulldown with HEK293/HaloTag-VEGFR2/NRP1-BioID2-HA stable cell line. 198
Figure 4.27 - A summary of the enriched proteins in the NRP1-BioID2-HA bioinformatic analyses in conditions of NRP1 expression alone with $VEGF_{165}$a stimulated condtions vs basal conditions vs NRP1 coexpression with VEGFR2 and treated with $VEGF_{165}$a. 216
Table 4.1 – Example of generated UniProt reference database used in the bioinformatic analysis of the BioID samples sent for mass spectrometry. 152
Table 4.2 – Important parameters input into the MaxQuant software during bioinformatic processing of BioID samples. 153
Table 4.3 – Example of the types of output data in ‘proteinGroups’ generated by MaxQuant bioinformatic processing. 153

Table 4.4 – mycBioID2-NRP1 $VEGF_{165}$a stimulated enriched protein list using protein score analysis method. 154
Table 4.5 – mycBioID2-NRP1 $VEGF_{165}$a stimulated enriched protein list using iBAQ value analysis method. 155
Table 4.6 – mycBioID2-NRP1 $VEGF_{165}$a stimulated enriched protein list using riBAQ value analysis method. 156
Table 4.7 – mycBioID2-NRP1 under basal conditions enriched protein list using riBAQ value analysis method. 156
Table 4.8 – Enriched protein list in NRP1-BioID2-HA samples treated with $VEGF_{165}$a of proteins common between all 4 repeats. 167
Table 4.9 – Enriched protein list in NRP1-BioID2-HA samples treated with $VEGF_{165}$a of proteins common in 3 of the 4 repeats. 167
Table 4.10 – Enriched protein list in NRP1-BioID2-HA samples under basal conditions common between all 4 repeats. 174
Table 4.11 – Enriched protein list in NRP1-BioID2-HA samples under basal conditions common in 3 of the 4 repeats. 176
Table 4.12 – Enriched protein list in HEK293/HaloTag-VEGFR2/NRP1-BioID2-HA treated with $VEGF_{165}$a after 1 repeat. 199

Chapter 5: Validation of BioID Hits

Figure 5.1 – Principles of NanoBRET validation experiments. 220
Figure 5.2 – Immunofluorescence of HEK293T cells transfected with mEmerald-CENPA, with and without coexpression of NRP1-BioID2-HA 222
Figure 5.3 – Colocalisation of GFP-VAPA with NRP1-BioID2-HA in HEK293T Cells 224
Figure 5.4 – Colocalisation of mEmerald-OCLN with NRP1-BioID2-HA in HEK293T Cells. 226
Figure 5.5 – Colocalisation of GFP-ZO1 with NRP1-BioID2-HA in HEK293T Cells. 228
Figure 5.6 – Colocalisation of ITGB1-mEmerald with NRP1-BioID2-HA in HEK293T Cells. 230
Figure 5.7 – Colocalisation of mCherry-SEPT9 with NRP1-BioID2-HA in HEK293T Cells. 232
Figure 5.8 – Interaction Analysis using NanoBRET for GFP-VAPA and NRP1-NanoLuc. 235
Figure 5.9 – Interaction Analysis using NanoBRET for mEmerald-OCLN and NRP1-NanoLuc. 236
Figure 5.10 – Interaction Analysis using NanoBRET for mCherry-SEPT9 and NRP1-NanoLuc. 237
Figure 5.11 – Interaction Analysis using NanoBRET for HRS-RFP and NRP1-NanoLuc. 239
Figure 5.12– Interaction Analysis using NanoBRET for ITGB1-mEmerald and NRP1-NanoLuc 240
Figure 5.13 – Interaction Analysis using NanoBRET for GFP-ZO1 and NRP1-NanoLuc. 240
Table 5.1 – Plasmids sourced from Addgene for further investigation as potential NRP Interactors. 221
Table 5.2 – Common interactors between VAPA BioID experiments and the NRP1 BioID experiments in this project. 242
Table 5.3 – Common interactors between VAPB BioID experiments and the NRP1 BioID experiments in this project. 243
Table 5.4 – Related proteins to those identified interactors between VAPB BioID experiments and the NRP1 BioID experiments in this project. 243
Table 5.5 – Common interactors between OCLN BioID experiments and the NRP1 BioID experiments in this project. 245
Table 5.6 – Common interactors between ZO1 BioID experiments and the NRP1 BioID experiments in this project. 247
Table 5.7 – Summary of the investigations of the potential NRP1 interactors identified in the BioID experiments. 253

Chapter 6: NRP1 Interactome Analyses in hTERT2-HUVEC Cells

Figure 6.1 – Immunofluorescence of optimised transfection of electroporation of C1-mEmerald in hTERT2-HUVEC cells. 258
Figure 6.2 – Immunofluorescence of optimised transfection of electroporation of NRP1-BioID2-HA in hTERT2-HUVEC cells. 260
Figure 6.3 – Immunofluorescence of transduction optimisation of pLV-NRP1-BioID2-HA in hTERT2-HUVEC cells. 262
Figure 6.4 – Immunofluorescence of blasticidin selected hTERT2-HUVEC/NRP1-BioID2-HA stable cell line. 264
Figure 6.5 – Fluorescence-activated cell sorting (FACS) of blasticidin selected hTERT2-HUVEC/NRP1-BioID2-HA cell line. 266
Figure 6.6 – Immunofluorescence of FAC sorted hTERT2-HUVEC/NRP1-BioID2-HA stable cell line. 268
Figure 6.7 – Initial streptavidin pulldowns with hTERT2-HUVEC/NRP1-BioID2-HA stable cell line. 270
Figure 6.8 – Optimised streptavidin pulldown with hTERT2-HUVEC/NRP1-BioID2-HA stable cell line. 271
Figure 6.9 – A summary of the enriched proteins in the NRP1-BioID2-HA bioinformatic analyses in both $VEGF_{165}a$ stimulated and basal conditions in hTERT2/HUVEC cells. 272
Figure 6.10 – Cellular component gene ontology (GO) analysis of enriched proteins for hTERT2-HUVEC/NRP1-BioID2-HA cells treated with $VEGF_{165}a$. 276
Figure 6.11 – Molecular function gene ontology (GO) analysis of enriched proteins for hTERT2-HUVEC/NRP1-BioID2-HA under basal conditions. 280
Figure 6.12 – Biological processes gene ontology (GO) analysis of enriched proteins for hTERT2-HUVEC/NRP1-BioID2-HA under basal conditions. 281
Figure 6.13 – Cellular component gene ontology (GO) analysis of enriched proteins for hTERT2-HUVEC/NRP1-BioID2-HA under basal conditions. 282
Figure 6.14 – A comparison of NRP1 BioID enriched proteins in HEK293T and hTERT2-HUVEC cells when stimulated with $VEGF_{165}a$. 289
Figure 6.15 – A comparison of NRP1 BioID enriched proteins in HEK293T basal conditions and hTERT2-HUVEC cells when stimulated with $VEGF_{165}a$. 290
Figure 6.16 – A comparison of NRP1 BioID enriched proteins in HEK293T and hTERT2-HUVEC cells in basal conditions. 295
Figure 6.17 – A comparison of NRP1 BioID enriched proteins in HEK293T stimulated with $VEGF_{165}a$ and hTERT2-HUVEC cells in basal conditions. 296
Table 6.1 – Enriched protein list in hTERT2-HUVEC/NRP1-BioID2-HA treated with $VEGF_{165}a$ after 1 repeat. 273
Table 6.2 – Enriched protein list in hTERT2-HUVEC/NRP1-BioID2-HA under basal conditions after 1 repeat. 277
Table 6.3 – Comparative levels of carboxylases in hTERT2-HUVEC and HEK293T cells according to the human protein atlas. 286
Table 6.4 – Comparative levels of selected Ras-related proteins in hTERT2-HUVEC and HEK293T cells according to the human protein atlas. 291

Chapter 7: General Discussion

Figure 7.1 – Enriched proteins across all NRP1 C-terminal BioID experiments involved in either vesicular trafficking, cellular adhesion or neuronal processes. 302
Figure 7.2 – Immunofluorescence of transient transfection of NRP1-BioID2-HA in SH-SY5Y cells. 306
Table 7.1 – Known interactors of NRP1 enriched as potential interactors in this project 304

V. Table of Contents

Chapter 1: General Introduction ***17***

1.1 Vascular System **18**
1.1.1 Cardiovascular System 18

1.2 Endothelial Cells **22**
1.2.1 Proliferation of Endothelial Cells and Angiogenesis 22
1.2.2 Transport across Endothelial Cells 25
1.2.3 Endothelial Cell Adhesion 38

1.3 Vascular Endothelial Growth Factors and Receptors **42**
1.3.1 Vascular Endothelial Growth Factors and Receptors 42
1.3.2 Vascular Endothelial Growth Factor Receptor 2 44
1.3.3 Vascular Endothelial Growth Factor Receptor 2 Physiology 45
1.3.4 Vascular Endothelial Growth Factor Receptor 1 47
1.3.5 Vascular Endothelial Growth Factor A 47

1.4 Neuropilin 1 ..... **51**
1.4.1 Neuropilin-1 Structure 52
1.4.2 Neuropilin 1 in Angiogenesis 54
1.4.3 Neuropilin 1 in Endothelial Cell Adhesion 56
1.4.4 Neuropilin 1 in Vascular Permeability 58
1.4.5 Neuropilin-1 in Vesicular Trafficking and Internalisation 59
1.4.6 Current Understanding of the Neuropilin-1 Interactome 65

1.5 BioID Technology **72**
1.5.1 Benefits of BioID Compared to Conventional Protein-Protein Interaction Techniques 72

1.6 NanoBRET **73**

1.7 Thesis Aims **74**

Chapter 2: General Materials and Methods ***76***

2.1 Molecular Biology **77**
2.1.1 Reagents and Buffers 77
2.1.2 Polymerase Chain Reaction (PCR) 78
2.1.3 Restriction Enzyme Digestion 79
2.1.4 Agarose Gel Electrophoresis 79
2.1.5 Gel Extractions and Purification 80
2.1.6 DNA Quantification 81
2.1.7 Ligation Reactions 82
2.1.8 Bacterial Transformation 82
2.1.9 DNA Mini- and Maxipreps 83
2.1.10 DNA Sequencing 84
2.1.11 Cloning of N-terminal BioID2 Fusion Proteins 85
2.1.12 Cloning of C-Terminal BioID2 Fusion Proteins 85
2.1.13 Design of pLV-NRP1-BioID2 Construct 85

2.2 Cell Culture **86**
2.2.1 Cell Maintenance and Passaging 86
2.2.2 Freezing, Storage and Thawing of Cells 87
2.2.3 Cell Seeding 87
2.2.4 HEK293T Wild-type (WT) 89

2.2.5 HEK293-NFAT-HaloTag-VEGFR2/pLV-NRP1-BioID2-HA 90
2.2.6 hTERT-HUVEC 90
2.2.7 hTERT2-HUVEC/pLV-NRP1-BioID2-HA 90
2.3 Recombinant Cell Lines – Transient Transfection Methods 91
2.3.1 Polyethylenimine 91
2.3.2 FuGENE HD 91
2.3.3 Nucleofection 92
2.4 Stable Expression Cell Lines 93
2.4.1 Lentivirus Production 93
2.4.2 Lentivirus Transduction 93
2.4.3 Selection using Blasticidin 93
2.4.4 Fluorescence-Activated Cell Sorting (FACS) 94
2.5 Immunofluorescence 95
2.6 Confocal Microscopy 96
2.7 Colocalisation Analysis 96
2.7.1 Transfection and Immunofluorescence 96
2.7.2 Image Analysis using Segmentation and Quantification of Subcellular Shapes (Squassh) 96
2.7.3 Statistical Analysis of Colocalisation Experiments 97
2.8 BioID Methodology 97
2.8.1 Preparation of HEK293T WT Cell for BioID Analysis 97
2.8.2 Protein Extraction of Biotinylated Proteins 98
2.8.3 Quantification of Protein Concentration 98
2.8.4 Isolation of Biotinylated Proteins 99
2.9 Biochemical Analysis – Western Blotting 100
2.9.1 SDS-PAGE 100
2.9.2 Transfer of Proteins to Nitrocellulose Membrane 101
2.9.3 Immunoblotting of Nitrocellulose Membranes 101
2.9.4 Imaging of Immunoblotted Nitrocellulose Membranes 102
2.10 Bioinformatic Processing 102
2.10.1 Mass Spectrometry 102
2.10.2 Mass Spectrometry Processing by Cambridge Centre for Proteomics 102
2.10.3 Generation of Reference Proteome Database 103
2.10.4 MaxQuant Processing of RAW Mass Spectroscopy Files 103
2.10.5 Statistical Analysis of MaxQuant Processed Data 104
2.10.6 Gene Ontology Analysis 104
2.11 NanoLuciferase Bioluminescence Resonance Energy Transfer (NanoBRET) 104
2.11.1 NanoBRET Validation of BioID Hits 104
2.11.2 Data Analysis 106
Chapter 3: Molecular Cloning and BioID Evaluation 107
3.1 Introduction 108
3.2 Results 110
3.2.1 Comparison of BioID1 and BioID2 Biotinylation Capabilities 110
3.2.2 Cloning of BioID Plasmids 118
3.2.2.1 Cloning of mycBioID2-VEGFR3 119
3.2.2.2 Cloning of VEGFR3-BioID2-HA 121
3.2.2.3 Cloning of mycBioID2-VEGFR2 123

3.2.2.4 Cloning of VEGFR2-BioID2-HA 125
3.2.2.5 Cloning of mycBioID2-NRP1 127
3.2.2.6 Cloning of NRP1-BioID2-HA 129
3.2.2.7 Cloning of NRP2 BioID Constructs 131
3.2.3 Validation of BioID Plasmids 131

3.3 Discussion 136
3.3.1 BioID1 vs BioID2 Comparison 136
3.3.2 BioID2 Plasmid Cloning Discussion 137
3.3.3 Expression of NRP and VEGFR plasmids in HEK293T Cells 138
3.3.4 Conclusion 139

Chapter 4: NRP1 Interactome Analyses in HEK293T Cells 141

4.1 Introduction 142

4.2 Results 145
4.2.1 Neuropilin 1 N-terminal Interactome Analysis using mycBioID2-NRP1 145
4.2.1.1 Expression of mycBioID2-NRP1 in HEK293T Cells 145
4.2.1.2 Optimisation of Streptavidin Pulldown of Biotinylated Proteins from mycBioID2-NRP1 Expressing Cells 147
4.2.1.3 Bioinformatic Processing Optimisation 151
4.2.1.4 Enriched mycBioID2-NRP1 Proteins using Protein Score 154
4.2.1.5 Enriched mycBioID2-NRP1 Proteins using Intensity Based Absolute Quantification (iBAQ) Analysis 155
4.2.1.6 Enriched mycBioID2-NRP1 Proteins using Relative Intensity Based Absolute Quantification (riBAQ) Analysis 155
4.2.2 Neuropilin 1 C-terminal Interactome Analyses using NRP1-BioID2-HA 158
4.2.2.1 Expression of NRP1-BioID-HA in HEK293T Cells 158
4.2.2.2 Reduction of Trace Biotin in Dulbecco's Modified Eagle Medium (DMEM) 159
4.2.2.3 Optimised Streptavidin Pulldown of Biotinylated Proteins from NRP1-BioID2-HA Expressing Cells 162
4.2.2.4 Bioinformatic Analyses of C-terminal NRP1-BioID2-HA 165
4.2.2.4 Enriched Proteins in the NRP1-BioID2-HA Stimulated with $VEGF_{165}$a Analyses 165
4.2.2.5 Gene Ontology Analyses of Enriched Protein List for NRP1-BioID2-HA, $VEGF_{165}$a Stimulated Conditions. 168
4.2.2.6 Enriched Proteins in the NRP1-BioID2-HA in Basal Conditions Analyses 173
4.2.2.7 Gene Ontology Analyses of Enriched Protein List for NRP1-BioID2-HA in Basal Conditions 179
4.2.3 Neuropilin 1 C-terminal Interactome Analysis in the Presence of Vascular Endothelial Growth Factor Receptor 2 using mycBioID2-NRP1 187
4.2.3.1 Transient Expression of Neuropilin 1 Fusion Proteins in HEK293/HaloTag-VEGFR2 Cells 187
4.2.3.2 pLV-NRP1-BioID2-HA Lentiviral Plasmid Design and Synthesis 189
4.2.3.3 Optimisation of Lentiviral Transductions 189
4.2.3.4 Expression of NRP1-BioID2-HA in HEK293/HaloTag-VEGFR2 Cells Following Transduction and Blasticidin Selection 192
4.2.3.5 Fluorescence-activated cell sorting of HEK293T/HaloTag-VEGFR2/NRP1-BioID2-HA Cells 192
4.2.3.6 Expression Analysis of HEK293T/HaloTag-VEGFR2/NRP1-BioID2-HA Cells After Fluorescence-Activated Cell Sorting 195
4.2.3.7 Streptavidin Pulldown of HEK293/HaloTag-VEGFR2/NRP1-BioID2-HA Cells to Improve Protein Coverage 196
4.2.3.8 Enriched Proteins in the HEK293/HaloTag-VEGFR2/NRP1-BioID2-HA Stimulated with $VEGF_{165}$a Analyses 198

4.3 Discussion 200
4.3.1 Proteins Enriched in the mycBioID2-NRP1 Analysis 200

4.3.1.1 Optimised of Transfections....200
4.3.1.2 Optimisation of Streptavidin Pulldowns of mycBioID2-NRP1 200
4.3.2 Optimisation of Mass Spectrometry Processing 201
4.3.3 Proteins Enriched in the extracellular N-terminal mycBioID2-NRP1 Analysis 204
4.3.4 Proteins Enriched in the intracellular NRP1-BioID2-HA Analyses 205
4.3.4.1 Expression of NRP1-BioID2-HA in HEK293T Cells 205
4.3.4.2 Biotin Depletion from DMEM....205
4.3.4.3 Optimisation of Streptavidin Pulldowns of NRP1-BioID2-HA 205
4.3.4.4 Enriched Proteins using NRP1-BioID2-HA stimulated with $VEGF_{165}$a 206
4.3.4.5 Enriched Proteins of C-terminal Intracellular NRP1-BioID2-HA in Basal Conditions 209
4.3.4.6 Comparison Between mycBioID2-NRP1 and NRP1-BioID2-HA Results 212
4.3.4.7 Known Interactors Identified using NRP1-BioID2-HA....213
4.3.5 Proteins Enriched in the HEK293/HaloTag-VEGFR2/NRP1-BioID2-HA Analyses 213
4.3.5.1 Transient Expression of Neuropilin Fusion Proteins in HEK293/HaloTag-VEGFR2 Cells 213
4.3.5.2 pLV-NRP1-BioID2-HA Transductions....214
4.3.5.3 Analysis of NRP1 and VEGFR2 Co-expression in Blasticidin Selected Cells....214
4.3.5.4 Fluorescence-Activated Cell Sorting of HEK293/HaloTag-VEGFR2/NRP1-BioID2-HA Cells....214
4.3.5.5 Streptavidin Pulldown of HEK293/HaloTag-VEGFR2/NRP1-BioID2-HA Cells....215
4.3.5.6 Enriched Proteins using HEK293/HaloTag-VEGFR2/NRP1-BioID2-HA Cells Stimulated with $VEGF_{165}$a 215
4.3.6 Conclusion....217

Chapter 5: Validation of BioID Hits 218

5.1 Introduction 219

5.2 Results 221
5.2.1 Co-localisation Analyses....221
5.2.1.1 GFP-VAPA 223
5.2.1.2 mEmerald-OCLN....225
5.2.1.3 GFP-ZO1 227
5.2.1.4 ITGB1-mEmerald 229
5.2.1.5 mCherry-SEPT9....231
5.2.2 NanoBRET Analyses....233
5.2.2.1 GFP-VAPA 234
5.2.2.2 mEmerald-OCLN....235
5.2.2.3 mCherry-SEPT9....236
5.2.2.4 HRS-RFP NanoBRET 238
5.2.2.5 ITGB1-mEmerald 239
5.2.2.6 GFP-ZO1 240

5.3 Discussion 241
5.3.1 GFP-VAPA 241
5.3.2 mEmerald-OCLN....243
5.3.3 GFP-ZO1 246
5.3.4 mCherry-SEPT9....248
5.3.5 ITGB1-mEmerald 250
5.3.6 HRS-RFP....251
5.3.7 Conclusion....252

Chapter 6: NRP1 Interactome Analyses in hTERT2-HUVEC Cells 254

6.1 Introduction 255

6.2 Results 257

6.2.1 Generation of hTERT2-HUVEC Model Expressing NRP1-BioID2-HA 257
6.2.1.1 Transient Nucleofection Optimisation of hTERT2-HUVEC Cells....257
6.2.1.2 Transient Nucleofection Optimisation of NRP1-BioID2-HA in hTERT2-HUVEC Cells 259
6.2.1.3 Lentiviral Transduction Optimisation of hTERT2-HUVEC Cells with NRP1-BioID2-HA 261
6.2.1.4 Expression Analysis of hTERT2-HUVEC/NRP1-BioID2-HA Stable Cells Following Blasticidin Selection 263
6.2.1.5 Fluorescence-Activated Cell Sorting of hTERT2-HUVEC/NRP1-BioID2-HA Stable Cells....264
6.2.1.6 Post-FACS Expression Analysis of hTERT2-HUVEC/NRP1-BioID2-HA Stable Cells....267
6.2.2 Optimisation of Streptavidin Pulldown of hTERT2-HUVEC/NRP1-BioID2-HA Cells 269
6.2.2.1 Initial Streptavidin Pulldown Attempts....269
6.2.2.2 Optimised Streptavidin Pulldown....270
6.2.3 BioID Bioinformatic Analyses using hTERT2-HUVEC/NRP1-BioID2-HA Stable Cells 272
6.2.3.1 Enriched Proteins in hTERT2-HUVEC/NRP1-BioID2-HA Cells Stimulated with VEGF165a Analyses 273
6.2.3.2 Gene Ontology Analyses of Enriched Protein List for hTERT2-HUVEC/NRP1-BioID2-HA, $VEGF_{165}a$ Stimulated Conditions.....275
6.2.3.3 Enriched Proteins in hTERT2-HUVEC/NRP1-BioID2-HA Cells in Basal Conditions Analyses 276
6.2.3.4 Gene Ontology Analyses of Enriched Protein List for hTERT2-HUVEC/NRP1-BioID2-HA in Basal Conditions 278

6.3 Discussion 283
6.3.1 Initial Nucleofection Experiments 283
6.3.2 pLV-NRP1-BioID2-HA Transductions in hTERT2-HUVEC Cells 284
6.3.2.1 Analysis of NRP1-BioID2-HA Expression in Blasticidin Selected hTERT2-HUVEC Cells 284
6.3.3.2 Fluorescence-Activated Cell Sorting of hTER2-HUVEC/NRP1-BioID2-HA Cells....285
6.3.3.3 Post-FACS Analysis of hTERT2-HUVEC/NRP1-BioID2-HA Cells....285
6.3.4 Streptavidin Pulldowns of hTERT2-HUVEC/NRP1-BioID2-HA Cells....285
6.3.5 Enriched Proteins in hTERT2-HUVEC/NRP1-BioID2-HA Cells, Stimulated with $VEGF_{165}a$ 286
6.3.6 Enriched Proteins in hTERT2-HUVEC/NRP1-BioID2-HA Cells Under Basal Conditions 291
6.3.7 Comparison of Enriched Proteins and Known NRP1 Interactors....296
6.3.8 Conclusion....297

Chapter 7: General Discussion 298

7.1 C-terminal Interactome Analyses of NRP1-BioID2-HA 300
7.1.1 Vesicular Trafficking....301
7.1.2 Cellular Adhesion 302
7.1.3. Neuronal Processes....303
7.1.4 Comparison with NRP1 Interactome in the Literature 303

7.2 Validation of BioID Hits with Colocalisation and NanoBRET Analyses 304

7.3 Future Directions....305

7.4 Key Conclusion 308

Chapter 8: References 309

Chapter 1: General Introduction

1.1 Vascular System

The vascular system is an integral component of the human body which utilises a network of vessels to circulate blood and interstitial fluid. This complex network of arteries, veins, and capillaries facilitates cellular function by supporting cell growth and development, enabling the absorption of essential nutrients and oxygen, and ensuring the removal of cellular and metabolic waste, thereby maintaining homeostasis[1]. The vascular system is essentially two circulatory systems operating in the vertebrate body; the cardiovascular system which circulates blood throughout the body via the heart and vessels[2]; and the lymphatic system which circulates interstitial fluid via lymphatic microvessels and larger lymphatic vessels[3]. The operation, composition and precise functions of these systems are similar in some respects, but generally differ greatly, however, both are essential for maintenance and continued development of human cells and tissues.

1.1.1 Cardiovascular System

1.1.1.1 Vascular Morphology

In general, the morphology of vessels in the cardiovascular network consists of concentric layers of tissues, (Figure 1.1), with their thickness and composition varying depending on the vessel type.

The outermost layer, known as the *tunica adventitia*, consists of densely packed connective tissue comprising of collagen fibres in varying thickness and orientations, along with elastic fibre nets and fibroblasts[4]. In larger arteries and veins, the layer is also characterised by the presence of *vasa vasorum* and *nervi vasorum.* The *vasa vasorum* are microvessels which maintain the health of the larger vessel by supplying oxygen and nutrients, while removing waste and extracellular fluids from the parent vessel[5,6]. The *nervi vasorum* consists of nerves which innervate the artery, influencing smooth muscle tone to regulate pressure and controlling temperature homeostasis[7,8].

Adjacent to the *tunica adventitia*, towards the lumen of the vessels is the *tunica media*. This middle section is generally thicker in vessels more arterial in nature compared to venous and contains concentrically arranged smooth muscle cells which have the propensity to change the calibre of the lumen, influencing blood pressure[9]. The thickness of this layer varies greatly between vessel type, forming the thickest layer in most arteries to being virtually non-existent in some veins[10].

The innermost layer, adjacent to the *tunica media*, is the *tunica intima*, which is exposed to, and interacts with, the contents of the lumen[10]. The *tunica intima* is characterised by layers of continuous, fenestrated or sinusoidally arranged squamous endothelial cells which permits extensive transport of molecules[11]. A highly specialised extracellular matrix consisting of laminins, collagens, and proteoglycans is adjacent to the endothelial cells within the vessel lumen, known as the basement

membrane[12]. The basement membrane is integral in maintaining the structural integrity and stability of blood vessels, as well as modulating cellular processes via interactions with cell surface receptors and acting as a reservoir for growth factors and morphogens[13].

The three layers are separated by membranes consisting of elastic fibres, the external elastic lamina separating the tunica adventitia and the tunica media, with the internal elastic lamina separating the tunica media and the tunica intima[9].

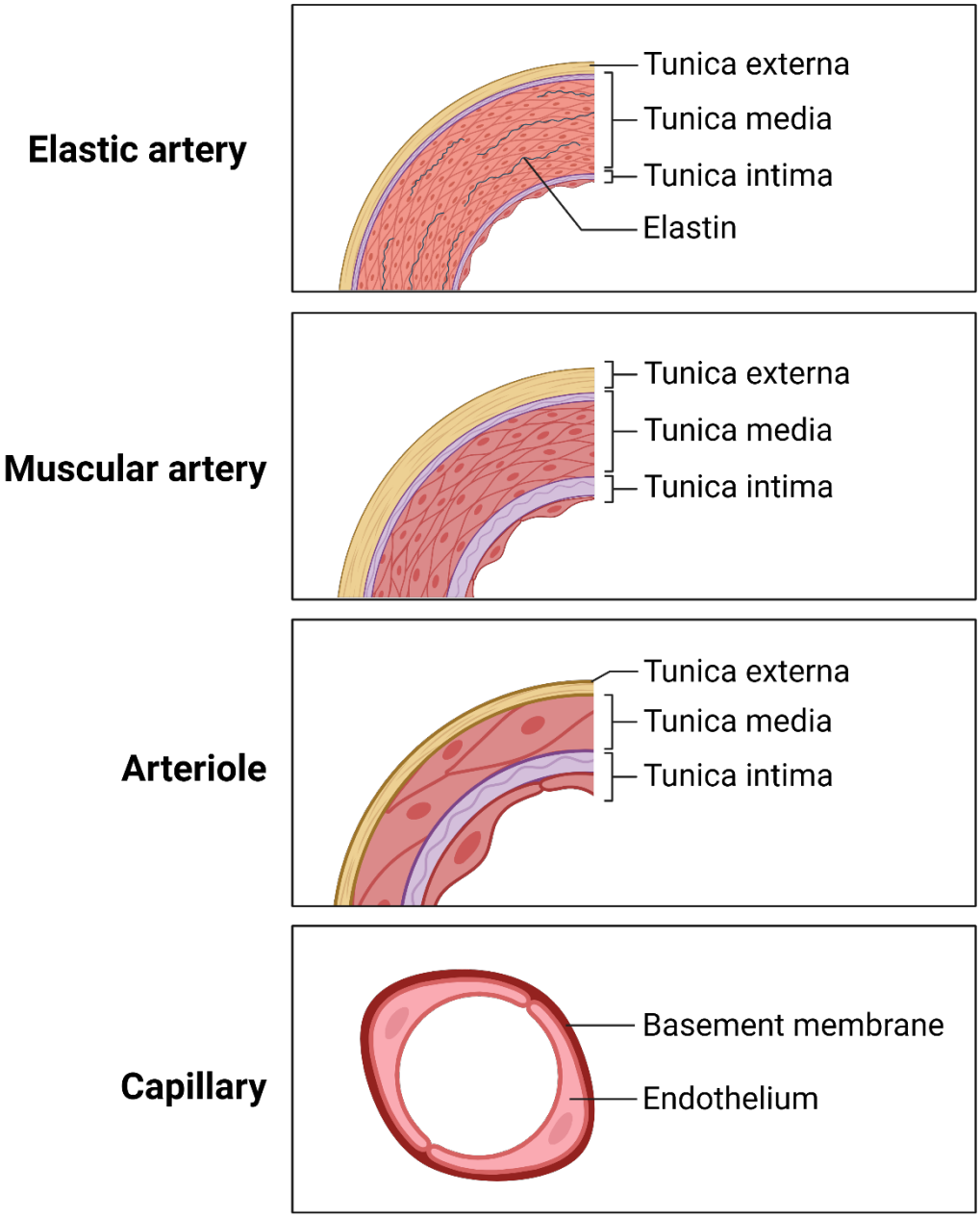

Figure 1.1 – General morphology of vessel types in the cardiovascular system*. All arteries consist of the same layers, the tunica adventitia, tunica media, and tunica intima and primarily function to transport oxygenated blood around the body under high pressure. The relative proportions of these layers vary depending on their function and location within the body. Capillaries differ from larger vessel types, in that they consist of a single layer of endothelial cells designed to exchange solutes with their associated tissues. The figure was created using Biorender.com.*

1.1.1.2 Arteries and Arterioles

Arteries play a critical role in the delivery of blood rich in oxygen and nutrients under high pressures. The stress inflicted by these high pressures are accommodated by an abundance of elastic tissue and smooth muscle. When arteries reach a particular organ or tissue, the vessel undergoes divisions into smaller vessels which consists of more smooth muscle and less elastic fibres[14]. The division of the arterial network is characterised by differing morphology of the vessels. There are two main forms of arteries; the elastic arteries, and the muscular arteries. Elastic arteries are larger and contain substantial amounts of elastin, enabling these vessels to withstand significant pressures[15]. Muscular arteries consist of a thicker smooth muscle layer and distribute blood form the elastic arteries to their proximal peripheral tissue[15,16].

The divisions of the vessel network continue further, with arteries branching into smaller vessels know as arterioles. The diameter of these blood vessels vary significantly depending in species, vascular bed and state of contraction, and are therefore identified by their composition consisting primarily of smooth muscle and a lack of elastic fibres[17]. The arterioles supply capillary beds with blood containing oxygen and nutrients, which are subsequently delivered to tissues.

1.1.1.3 Capillaries

Capillaries are the most numerous of blood vessels and is the primary location of exchange between the blood and tissues. Perfusion into the capillaries is regulated by precapillary sphincters, concentric layers of smooth muscle cells surrounding the proximal end of the vessel. Restricting the flow by these sphincters enables efficient solute exchange and protects the capillary bed from the high pressures observed in arterioles[18]. The morphology of the capillary wall consists of a single layer of endothelial cells, (Figure 1.1)[19]. The organisation of endothelial cells in terms of presence and level of fenestrations enable categorisation of the three capillary types; fenestrated capillaries; continuous capillaries with no fenestrations, and sinusoid capillaries with extensive intercellular gaps and an incomplete basement membrane[20].

Macromolecules, hormones and an abundance of solutes are transferred or transported across the endothelium by vesicular transport, exchange through the endothelial fenestrations and endothelial clefts at cell-cell junctions[21].

1.1.1.4 Veins and Venules

Following an exchange of oxygen, nutrients and metabolic waste in the capillary bed, the blood flows into the smallest veins known as the venules[14]. The immediate post-capillary and collection venules are also major sites for exchange of molecules and water in the microcirculation, similar to the capillary bed[22]. Unlike their arteriole and capillary counterparts, venules typically have a thin layer of smooth

muscle surrounding a larger lumen[23]. As the blood is at much lower pressures, a thicker smooth muscle layer is not necessary. The deoxygenated and nutrient depleted blood flows from the venules into larger venous vessels with an increasing diameter. Similar to venules, these veins have much lower proportion of smooth muscle, lower elasticity and larger lumens compared to arteries[24]. Often veins in the lower extremities contain one-way paired valves, ensuring the unidirectional flow of blood despite the low blood pressure and gravitational forces[25]. The large lumens of the venous vessels enable a high capacity of blood to be stored at relatively low pressures, with two-thirds of the total blood volume present during resting conditions, enabling the venous system to function as a blood reservoir[26].

1.2 Endothelial Cells

The *tunica intima* of the entire vasculature in the human body is lined with an endothelium, which consists of a specialised cell, known as an endothelial cell (EC), in perpetual contact with the vessel contents. ECs are derived from precursor cells called angioblasts, which differentiate into a venous or arterial phenotype in early development, and subsequently, established venous ECs develop into lymphatic ECs (LECs)[27]. The *de novo* formation of vascular networks which form as a result of angioblast differentiation into ECs is termed vasculogenesis, whereas angiogenesis is the development of vessel from a pre-existing vascular network[28]. In either case, the newly formed ECs organise to establish the endothelium, which provides a large surface area for the exchange of molecules between the blood or interstitial fluid and tissues[29].

1.2.1 Proliferation of Endothelial Cells and Angiogenesis

De novo vasculature formation in the adult originates from existing capillaries, sprouting from these vessels during angiogenesis, (Figure 1.2)[30]. Angiogenesis can be further characterised depending on the particular mechanisms driving the formation of vessels, sprouting or intussusceptive angiogenesis. Interestingly, both of these mechanisms may work synergistically in the formation of the vascular network[31].

1.2.1.1 Sprouting Angiogenesis

Sprouting angiogenesis is initiated in response to hypoxia, where the metabolic requirements of the parenchymal cells are not satisfied and formation of new vessels is therefore essential to facilitate demand for oxygen and nutrients[32]. In most cases, parenchymal cells will respond to hypoxic conditions with the secretion of vascular endothelial growth factor (VEGF-A), a proangiogenic growth factor. The filipodia of EC tip cells express high levels of the VEGF receptor (VEGFR2) at their cell surface, which detects secreted VEGF-A[33]. As a result of the highly concentrated VEGFR2 expression,

the filipodia detects differences in VEGF-A concentrations within the extracellular matrix (ECM), aligning itself to the VEGF-A gradient which then guides vessel growth in the direction of the hypoxic environment[34]. VEGF-A can also stimulate the proliferation of the endothelial stalk cells, resulting in elongation of the capillary towards the epicentre of VEGF-A secretion[34].

1.2.1.2 Intussusceptive angiogenesis

Intussusceptive angiogenesis does not initially involve the proliferation of ECs, with *de novo* vessels formed when the vascular wall extends into the lumen resulting in the intravascular separation of an existing vessel into two vessels[35]. Compared to sprouting angiogenesis, intussusceptive angiogenesis occurs much quicker as only EC reorganisation is required, rather than necessity for proliferation and migration[32]. Invaginations in the capillary walls into the lumen results in the formation of pillars. The morphological observations of these pillar formations have been observed and described in four consecutive stages: Phase I, formation of an inter-endothelial bridge linking oppositely facing capillary walls; Phase II, reorganisation of the inter-endothelial cell-cell junctions and central perforation of the capillary bilayer; Phase III, formation of an interstitial pillar which is subsequently invaded by pericytes and myofibroblasts which assemble collagen fibrils; Phase IV; increasing of the pillar girth to a full sized capillary mesh[36,37].

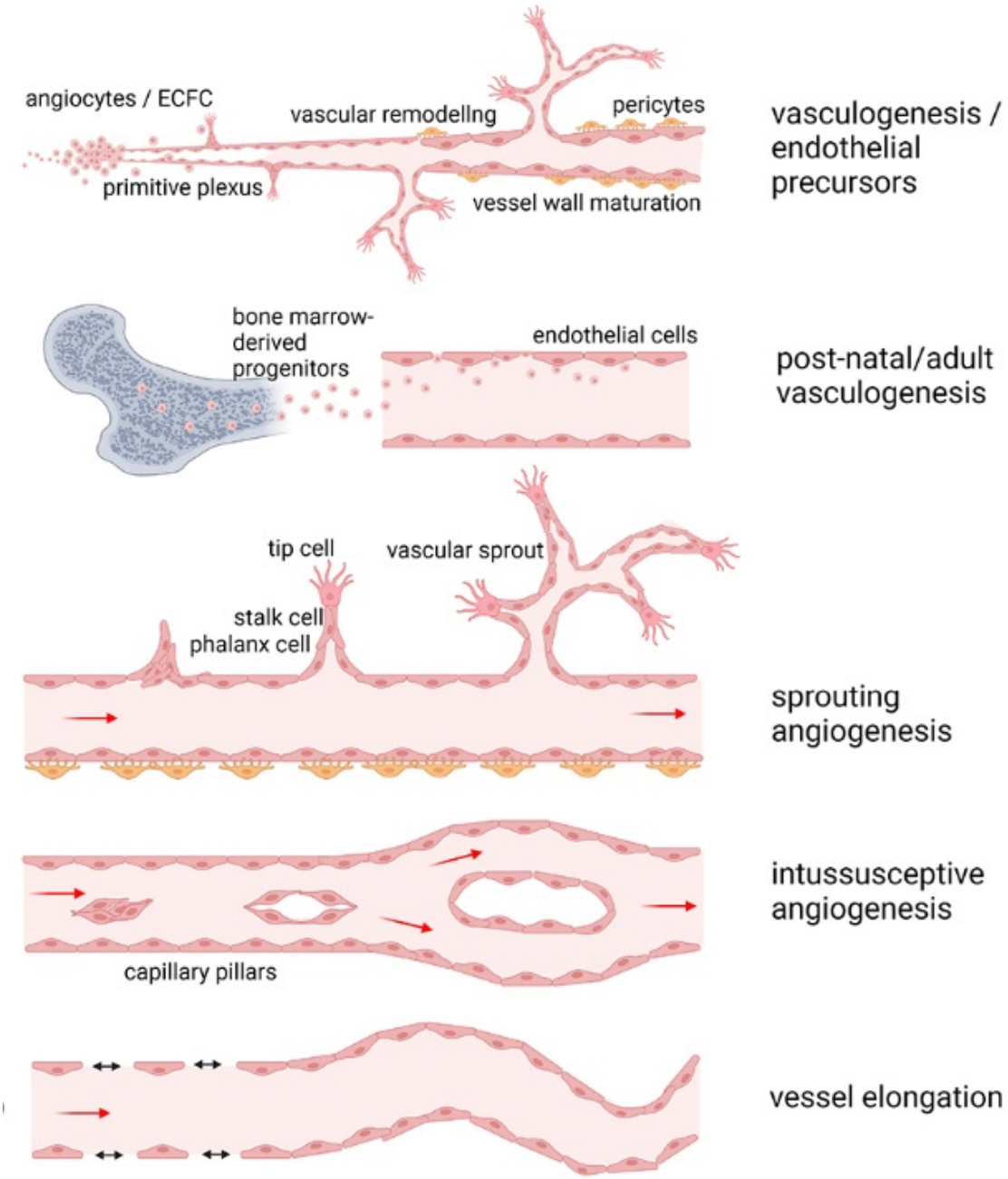

Figure 1.2 – Mechanisms of Vasculogenesis and angiogenesis. *Vasculogenesis occurs during embryonic development, with the differentiation of EC precursors and aggregation into de novo blood vessels, forming the early cardiovascular system. Further extensions of the blood vessels are formed by sprouting angiogenesis. Post-natal Vasculogenesis occurs when progenitors are recruited to ischaemic regions, promoting angiogenesis, notably sprouting angiogenesis. Intussusceptive angiogenesis occurs as a result of bifurcation of vessels due to the formation of pillars between vessel walls*[38].

1.2.2 Transport across Endothelial Cells

A critical feature of the endothelium in maintaining tissue homeostasis is the ability to selectively transport molecules between compartments, ensuring the delivery of nutrients, preventing the accumulation of metabolic waste and enabling communication between distant cells. The established transport routes are either across the ECs (transcellular) or between intercellular junctions of ECs (paracellular), (Figure 1.3)[39]. While the paracellular transport route is defined solely by movement of material through inter-endothelial junctions, there are several mechanisms encompassing transcellular transport. Transcellular transport routes include; passive diffusion where a molecule simply dissolves in the phospholipid bilayer of the plasma membrane and diffuses across it into the cytoplasm[40], membrane transport proteins in the form of ATP powered pumps or passive channels with or without selective permeability for particular molecules[41], and transcytosis where material enveloped by the EC membrane is transported transcellularly via vesicles, (Figure 1.3)[42].

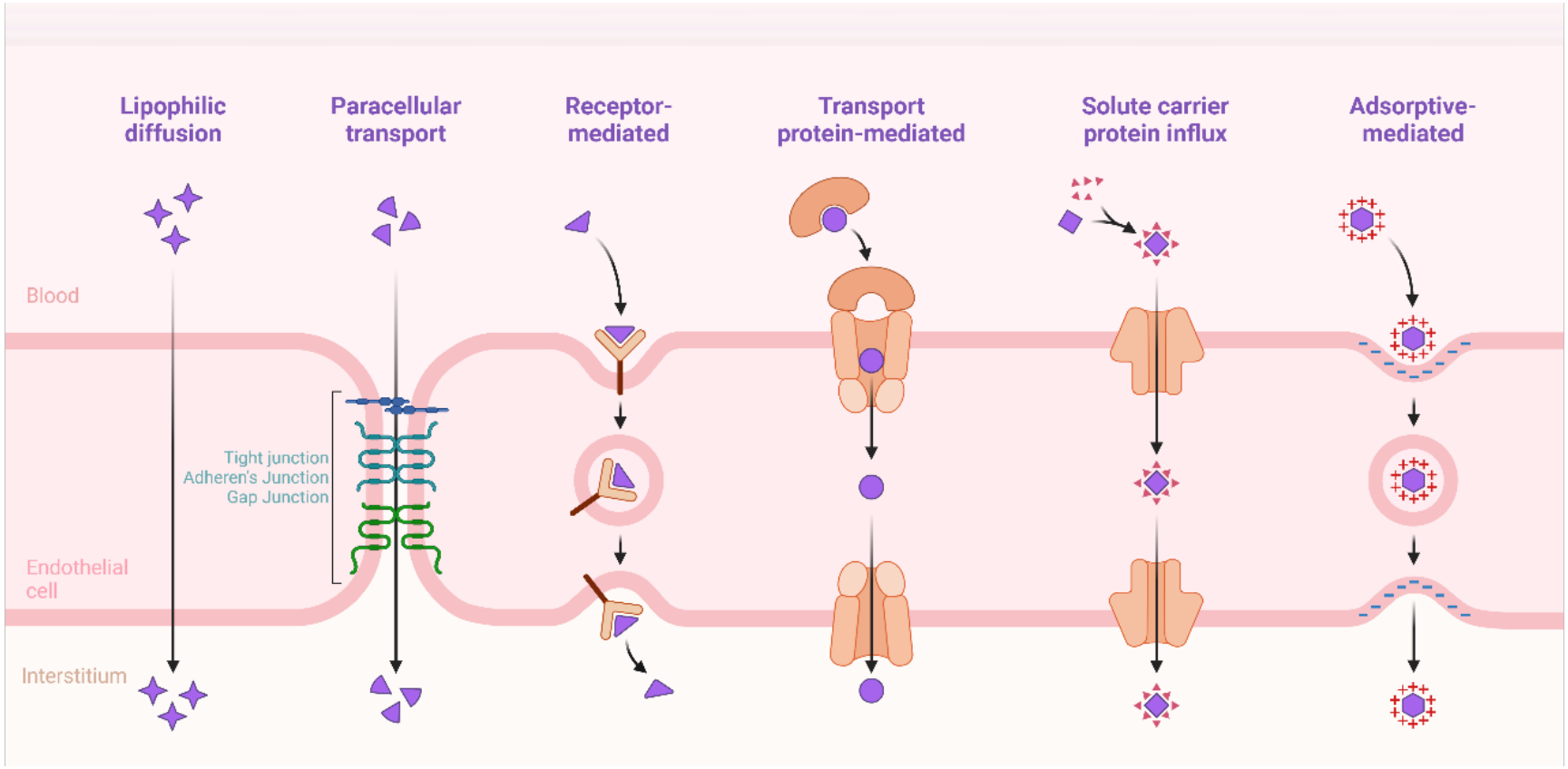

Figure 1.3 – Mechanisms of transport across endothelial cells. *Lipophilic diffusion is driven by concentration gradients and only lipid soluble solutes are transported via this route, such as O_2 and CO_2.* Paracellular transport is the passage of materials through endothelial clefts regulated by various cellular junctions and adhesion proteins and driven by diffusion across trans-endothelial gradients. Other types of transport occur through the ECs which may occur along a concentration gradient. *The figure was created using Biorender.com*

1.2.2.1 Dissolution Across Membrane

The passive diffusion transport pathway occurs without the necessity for membrane proteins, whereby transport is determined by relative concentrations intra- and extracellularly, with the net flow from a higher concentration to a lower concentration[40]. Only molecules which are soluble in the EC lipid bilayer may be transported via this route. It is therefore restricted to small nonpolar molecules, such as O_2 and CO_2, which readily dissolve across the membrane or small uncharged polar molecules such as urea and H_2O, where diffusion occurs significantly slower[43].

1.2.2.2 Transport facilitated by Membrane Transport Proteins

The EC membrane is impermeable to larger hydrophilic polar molecules and ions[40]. For these molecules, alternative transport mechanisms are necessary. Transport is facilitated by carrier proteins and channel proteins, which form a continuous pathways traversing the membrane, enabling solutes to cross without direct contact with the hydrophobic interior of the lipid bilayer, (Figure 1.3). Channel proteins form aqueous pores which extend the length of the EC membrane and allow passage of specific molecules when open[43]. These channels are not coupled to an energy source, meaning the transport they mediate is always passive diffusion of the solute down their concentration or electrochemical gradients[44]. In contrast, carrier proteins bind to specific molecules and undergo reversible conformational changes alternately exposing the molecular binding site first on one site of the membrane and then flipping to the other side[45]. As such, the solutes may be transported against a concentration or electrochemical gradient in a process called active transport. This transport is tightly coupled to an energy source, usually ATP hydrolysis or the utilisation of a coupled ion channel transporting in the energetically favourable direction[40].

1.2.2.3 Transcytosis

Transcellular transport by transcytosis involves the enveloping of material which enters the EC via endocytosis, followed by vesicular trafficking through the cytoplasm and fusion with the oppositely positioned membrane, dispelling the cargo through exocytosis. The initial endocytic process is known to occur by various mechanisms; caveolae-mediated endocytosis (CAV-ME), clathrin-mediated endocytosis (CME), macropinocytosis (MP), and alternative endocytic pathways.

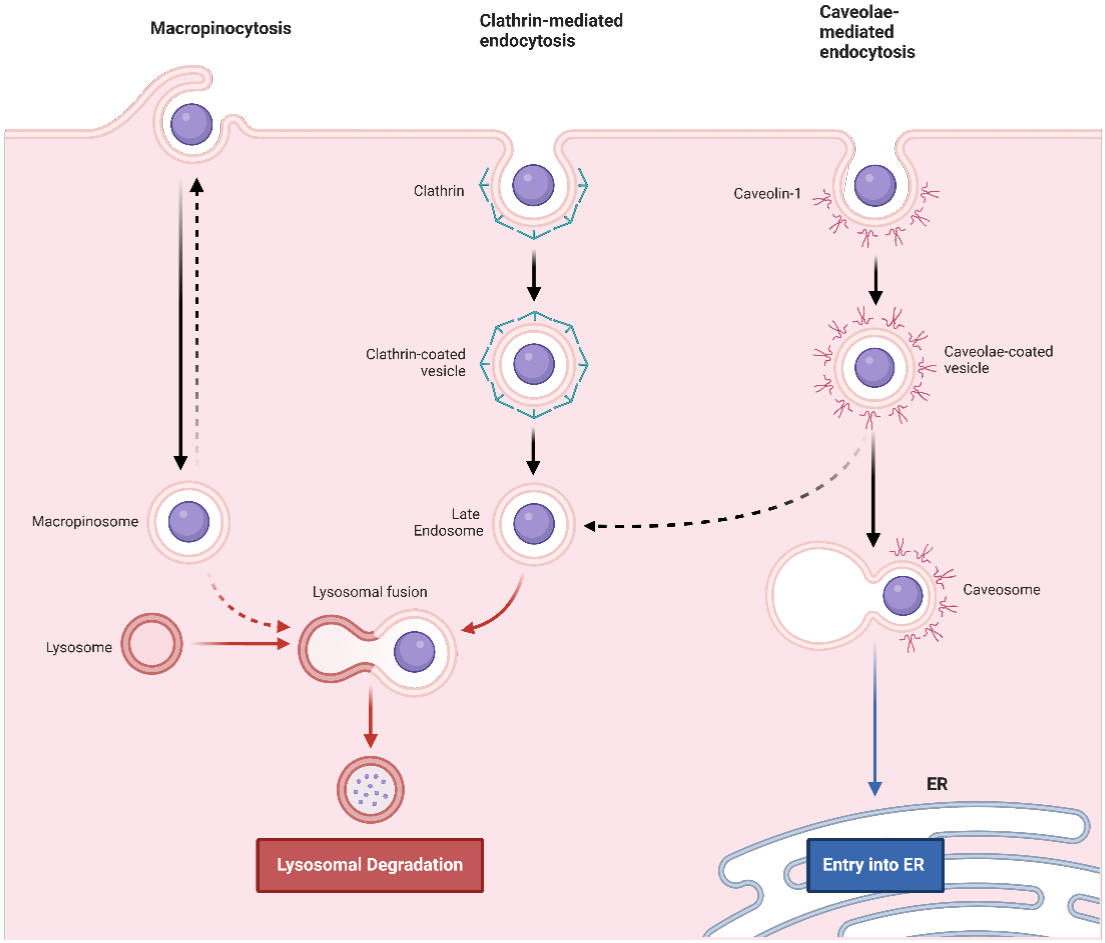

Figure 1.4 – Mechanisms of transcytosis across endothelial cells. *Cellular material is adsorbed to the surface of endothelial cells and engulfed by the membrane for uptake into the cell in a process known as endocytosis. There are several mechanisms of endocytosis. Endocytosis facilitated by caveolin-1 coated pits, forming intracellular caveolin-1 vesicles is known as caveolin-mediated endocytosis (CAV-ME). Alternatively, when the pits and intracellular vesicles are clathrin coated, this is clathrin-mediated endocytosis (CME). Macropinocytosis (MP) is independent of either caveolin-1 or clathrin and driven by actin-rich protrusions. The figure was created using Biorender.com.*

Caveolae-mediated Endocytosis

CAV-ME is characterised by caveolae, which exist as membrane invaginations present in the luminal and abluminal surfaces of the endothelium and as free vesicles in the cytoplasm[46]. Caveolae are enriched with cholesterol and sphingolipids microdomains, distinguished from other lipid-raft based invaginations and endocytic pathways by the presence of caveolin-1 (Cav-1), (Figure 1.4)[47]. Cav-1 self-assembles into homotypic high molecular mass oligomers containing 14-16 individual monomers, which facilitates the formation of the membranous invaginations[48,49]. Following membrane invagination, fission of caveolae from the luminal surface occurs, facilitated by the activation of receptors by ligands, dynamin oligomerisation around the caveolar neck, and dynamin GTP hydrolysis mediated constriction of the caveolar neck resulting in vesicle release from the membrane[50,51]. The

vesical is trafficked to the basolateral membrane, where docking and fusion is dependent on t-SNARES – composed of proteins belonging to the syntaxin, SNAP and SNARE family of proteins[51]. The vesical cargo is then released into the interstitial space by exocytosis.

Clathrin-mediated endocytosis

CME is a form of endocytosis independent of Cav-1. As the name suggests, instead of Cav-1, the main protagonist of the endocytic machinery on CME is the clathrin protein. Unlike Cav-1, clathrin does not directly interact with the plasma membrane, instead mediating endocytosis through adaptor proteins such as the AP-2 complex, CALM family proteins and epsins which are connected to the EC membrane[49,52–54]. The assembly of adaptor proteins promotes bending of the flat membrane, into clathrin coated membrane invaginations or pits, (Figure 1.4)[55]. BAR domain proteins, such as endophillins and amphiphysins, cooperate with dynamin to direct the constriction and fission of the invagination neck[56]. The clathrin cage dissociation, facilitated by the auxilin recruitment of ATPase heat shock cognate 70 (Hsc70) and subsequent ATP hydrolysis, is imperative in enabling transport to subsequent compartments in the endocytic pathway[39]. The vesicle, now free from the clathrin constrictions, is primed to fuse with early endosomes for further processing of the received extracellular material[57].

Macropinocytosis

MP is independent of either Cav-1 or clathrin mediated endocytosis, instead involving actin-driven ruffling of the EC membrane to generate invaginations that envelop extracellular materials. Macropinosomes form through the maturation of actin-rich membrane protrusions, creating a ruffled topography of the membrane, which either folds back on itself or coalesces to form a circular structure which constricts and envelopes the extracellular material[58]. Phosphatidylinositol-trisphosphate (PIP_3) accumulates in the interior of macropinocytic invaginations and is proposed to direct actin polymerisation to the lip resulting in dynamin-independent constriction and vesicular formation[59]. Various mechanisms initiate MP, notably, ligand interactions with cell membrane receptors, oncogenic activation of proteins downstream of a cell membrane protein, or changes in metabolic state. For example, several membranous receptor-tyrosine kinases (RTKs) are known to be regulated by MP following ligand stimulation. Of these RTKs, one of the mechanisms of VEGFR2 internalisation is through VEGF-induced MP[60]. Other membrane RTKs known to be internalised by MP following ligand stimulation include the platelet derived growth factor receptor (PDGFR)[61] and the epidermal growth factor receptor (EGFR)[62], as well as the G protein-coupled receptor the chemokine receptor 4 (CXCR4)[63].

Other Transcytosis Routes

Alternative endocytic pathways may or may not utilise dynamin in the scission of the membrane invagination. Interestingly, all dynamin independent pathways appear to utilise actin polymerisation machinery as the primary driver for scission[64]. Endocytosis of interleukin (IL) receptors are internalised via small non-coated invaginations, mediated by GTPases of the rho family of proteins, rhoA and rac1, and appear to be dependent on dynamin[65,66]. Clathrin-independent carriers (CLICs) are short tubular invaginations that mature into glycosylphosphatidylinositol (GPI)-anchored protein-enriched early endocytic compartments (GEECs)[67]. These tubular constructions are moulded by the BAR domain-containing protein GRAF1[68] and regulated by the small GTPases Arf1 and CDC42[69]. Flotillins are observed in an oligomerised state within cholesterol-rich microdomains of the membrane[70]. Budding of these microdomains from the plasma membrane has been observed as a specific type of endocytic mechanism[71].

1.2.2.4 Paracellular Transport

Paracellular transport describes the transport of material between clefts of adjacent ECs, (Figure 1.3). Paracellular transport appears to exclusively involve passive diffusion driven by transepithelial gradients[72]. These pathways are relatively nonselective compared to transcellular routes, with permeability based on size and charge of the molecule. Permeability of the endothelium through paracellular transport is regulated by specialised intercellular junctions between ECs; adherens junctions and tight junctions. Historically, these specialised microdomains have been viewed as discrete structures, however, evidence suggests formation of tight junctions are dependent on adhesion junction and nectin-based adhesions[73]. A delay in adherens junction formation is observed with mutation of tight junctions[74], suggesting these adhesions are highly interdependent. The number and organisation of these junctions determines vascular permeability, which can be modified by kinases, phosphatases and other enzymatic activity[75]. Gap junctions are another form of intercellular transport that connect adjacent EC via channels.

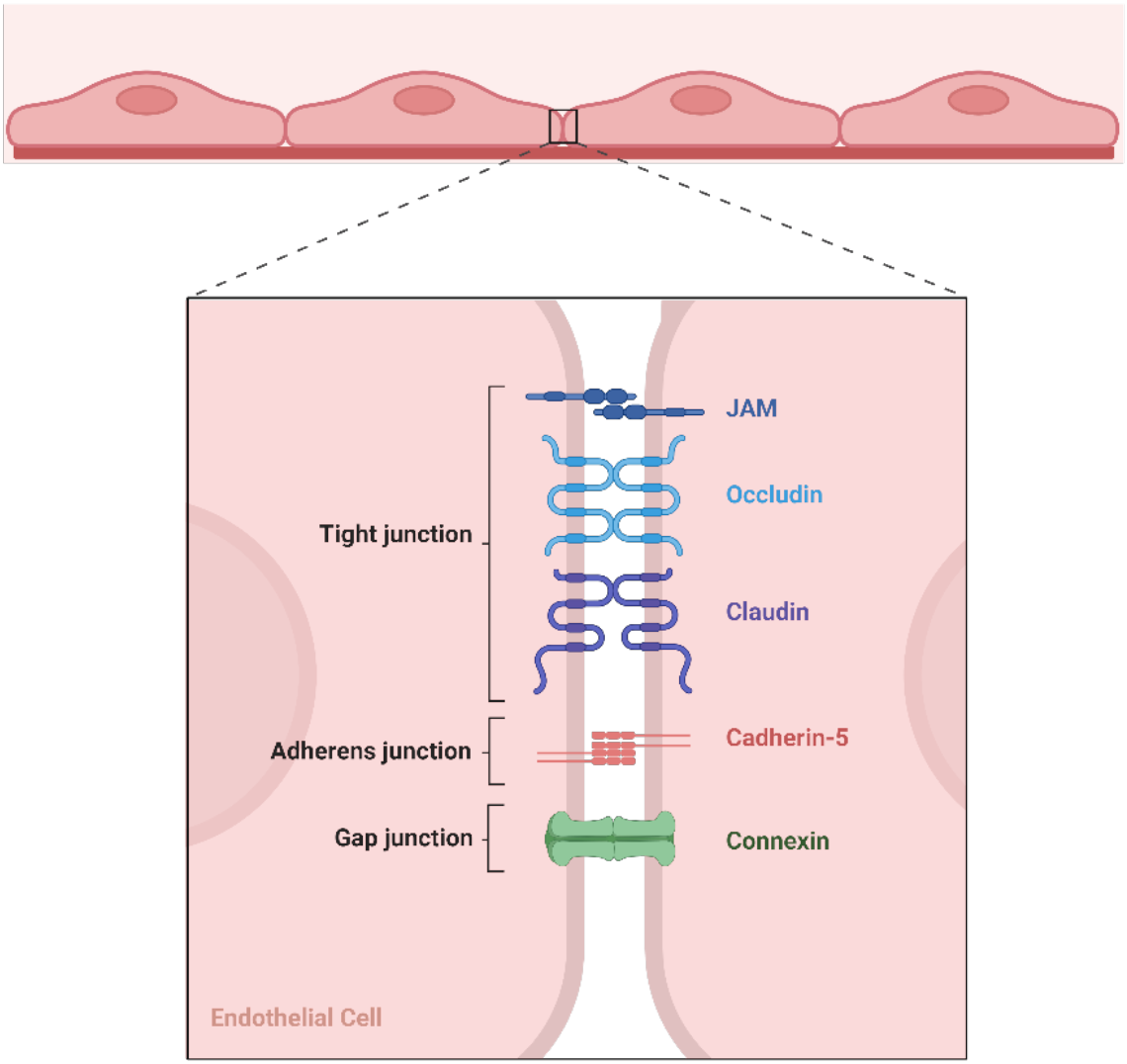

Figure 1.5 – Types of endothelial cell junctions. *Passage of solutes through endothelial cell clefts is highly regulated by cellular junctions and the adhesion proteins incorporated at these junctions. At the apical membrane, closest to the vessel lumen, resides tight junctions. The main constituents of tight junctions include occludin, claudins and junction adhesion molecules (JAMs), along with a multitude of intracellular adaptor proteins. Adherens junctions reside below tight junctions and are comprised of cadherin-5, and a series of intracellular proteins forming a scaffold for the junction. Gap junctions regulate transport through adjacent ECs and are mainly comprised of connexins. The figure was created using Biorender.com.*

Adherens Junctions

Vascular permeability is regulated, in part, by the dynamic opening and closing of adherens junctions. These junctions are recognised in their stabilisation of inter-endothelial contacts and control of permeability for larger molecular weight plasma proteins[76]. Cadherins, notably cadherin-5 (VE-cadherin), are important in the formation of adherens junctions. Cadherin molecules on adjacent cells form complexes which initiate intercellular contact and form the core of the junction, (Figure 1.6)[77].

The cadherin-5 clusters self-assemble through extracellular interactions, independently from processes involving cytosolic proteins[78–81]. Such cadherin-cadherin interactions are dependent on extracellular Ca^{2+}, which facilitates the homophilic adhesion and rigidifies cadherin following chelation[82].

Intracellular proteins are imperative in the structural integrity of the adherens junction. The individual units of an adherens junction are comprised of cadherin motifs, a transmembrane domain, and an intracellular domain which cooperates with β-catenin, catenin delta-1 (p120 catenin) and plakoglobin (γ-catenin), (Figure 1.6)[75]. β-catenin subsequently recruits α-catenin which enhances the stability of cadherin clusters by assisting other catenins in providing a structural foundation and coupling complexes to the actin cytoskeleton[83]. Not only does α-catenin bind to and congregate actin filaments, binary interactions with recognised actin-binding proteins have been observed, including; zonula occludens-1 (ZO1)[84,85], afadin[86,87], spectrins[88], vinculin[89,90], α-actinin[91,92], and ajuba[93]. The aforementioned actin-binding proteins have been observed to interact with each other as well as α-catenin. Such cooperation improves binding of F-actin to the intracellular adherens complexes. As well as proteins which stabilise the clusters, cadherin binds to receptors which mediate vascular permeability, including VEGFR2[94].

The majority of vascular permeability promoting agents can affect the organisation of adherence junctions[95]. Src-dependent phosphorylation of proteins within the cadherin clusters appears important for disassembly and decreased integrity of the junction, resulting in an increase in vascular permeability. Tyrosine phosphorylation of cadherin-5, β-catenin, catenin delta-1 and/or plakoglobin has been observed following stimulation with $VEGF_{165}a$[96] resulting in the dissociation of the junctional complex and an increase in endothelial permeability[97,98]. An increase in vascular permeability has also been observed following stimulation with ligands such as histamine[99,100], tumour necrosis factor-α (TNF-α)[101], EGF[102] and platelet activating factor (PAF)[103].

Another mechanism which may increase permeability involves the internalisation of cadherins, which may occur in a clathrin-dependent[104,105] or clathrin-independent manner[102]. For clathrin-dependent internalisation to occur, it appears dissociation of catenin delta-1 from cadherin-5 is required, with catenin delta-1 suggested to operate as a membrane retention signal[105]. As well as resulting in the phosphorylation of cadherin-5 and its binding partners, $VEGF_{165}a$ stimulation results in the activation of the GTPase Rac by VEGFR2, which in turn initiates the recruitment of β-arrestin-2 and subsequent clathrin-dependent internalisation[95]. The endocytic vesicles are either recycled back to the membrane or degraded by lysosome. Recycling of cadherin-5 back to the EC membrane requires activated Rab GTPases[106].

Cleavage of cadherin-5 is another mechanism which may influence endothelial permeability. Exposure of cells to metalloproteases[107,108], trypsin[109], elastase and cathepsin G[110] facilitate extracellular cleavage of cadherin-5, reducing junctional stability and increasing barrier permeability.

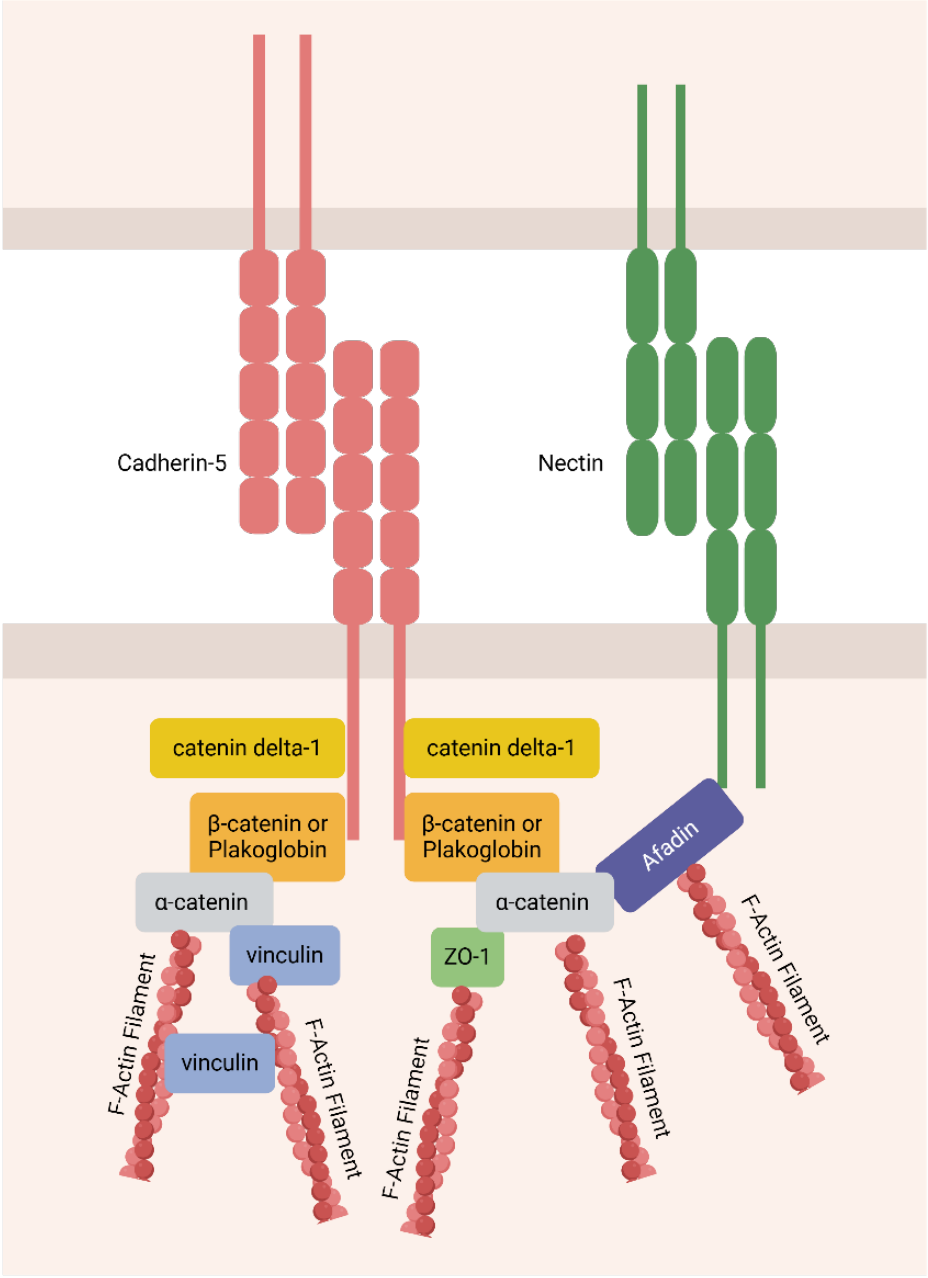

Figure 1.6 – Composition of adherens junction. *The core of the adherens junction is comprised of cadherin-5 units forming a complex on adjacent cells. The junction is anchored to the actin cytoskeleton via a series of adaptor proteins recruited by catenin delta-1 and subsequently either β-catenin or plakoglobin. The recruitment of these proteins enables α-catenin binding, which binds to actin filaments directly, or associates with other actin binding proteins such as ZO1, vinculin and afadin. The association with afadin is important as it is thought to link nectin adhesion complexes to the adherens junction, thereby stabilising the junction. The figure was created using Biorender.com.*

Tight Junctions

Tight junctions are the most apical inter-endothelial junction, and like adherens junctions, they function as a gate controlling the paracellular transport of solutes between ECs. While the adherens junctions are involved in vascular permeability of larger plasma proteins, the tight junctions form a near impenetrable inter-endothelial seal by fusion of adjacent EC membranes which regulates permeability for ions and small molecules[76,111]. Within the vasculature, tight junctions are more complex and abundant in arterioles in comparison with capillaries and venules[112].

Tight junctions are complex microdomains spanning the membrane, involving greater than 40 proteins, either transmembrane proteins establishing cellular contact, or cytoplasmic acting-binding proteins connecting the junction to the actin cytoskeleton[73]. Canonically, the transmembrane proteins involved in cell-cell adhesions are claudins and occludin[113,114], while junction adhesion molecules (JAMs) colocalise and interact with proteins in the tight junction microdomain, they are not involved in the tight junction strands[115,116] (Figure 1.7). The transmembrane proteins are affiliated with proteins with acting-binding capabilities, notably members of the zona occludens family[117].

The critical constituents forming the tight junction strands are the claudins, specifically claudin-5 in endothelial tight junctions[118,119] The claudins have four transmembrane domains, with both the N- and C-terminus located in the cytoplasm, meaning the protein is arranged in a manner that exhibits two protruding extracellular loops[120,121]. Each of these loops have different functions which are imperative for tight junction operation. One of the extracellular loops harbours domains which regulate paracellular ionic transport by creating charge-selective channels[122]. The second loop contains residues responsible for homo- and heterotypic interactions with opposing claudin molecules attached to adjacent cells, forming the integral core of the tight junction[123]. The formation of these inter-endothelial claudin interactions seals the tight junctions and regulates paracellular transport. The C-terminal domain of claudin family members harbours a PDZ (PSD-95/Dlg/ZO1 homology) motif, a protein-protein interaction module capable of binding to short amino acid sequences on interacting proteins[124]. The PDZ domain of claudins are capable of binding scaffolding proteins[125,126], such as the zona occludens (ZO) proteins[127,128].

Occludin, a member of the MARVEL subfamily of proteins, is a second component of the extracellular core of the tight junction and is recruited by claudins[127]. This colocalisation with claudins appears to be phosphorylation dependent, with phosphorylated occludin localising at tight junctions, whereas non-phosphorylated localise to the basolateral membrane and in cytoplasmic vesicles[129]. Interestingly, although a recognised component of the tight junction complex, occludin does not appear to be essential for tight junction formation. Occludin-null mice exhibited tight junctions with normal

morphologies, despite histological abnormalities relating to chronic inflammation, male infertility, hearing loss and failure of families to suckle their litter[130,131]. The aforementioned abnormalities are associated with cellular permeability dysfunction, leading to the supposition that occludin acts as a regulator of tight junction operation, rather than an integral structural component[132]. Similar to claudin, occludin has four transmembrane domains with both its N- and C-termini located intracellularly and two extracellular loops[133]. These loops are thought to have distinct functions, with evidence implicating the second extracellular loop being responsible for interactions with claudins and JAMs and localisation to the tight junction[134,135]. Again, like claudins, occludin binds to ZO proteins via its C-terminus. Contrastingly, this is achieved by a positively charged domain and not through PDZ association[136].

ZO family proteins, are essential for formation of tight junctions, demonstrated in the failure of tight junction assembly in epithelial cells deficient of ZO1 and ZO2[137]. Tight junctions were still able to form in canine epithelial cells if either ZO1, or ZO2 deficiency was induced[138], suggesting ability of ZO1 or ZO2 to induce claudin polymerisation independently of one another. More recent evidence suggests ZO1 harbours EC specific functions, with ZO1 loss inducing disorganisation of the tight junction complex, despite the presence of ZO2[139]. The ZO proteins are proposed to be a membrane scaffold, coordinating the assembly of transmembrane proteins with intracellular proteins, forming multiprotein complexes at tight junction domains[111]. In addition, ZO proteins directly[140] and indirectly facilitate binding of the tight junction complexes to the actin cytoskeleton[141], through the recruitment of actin-binding proteins including; α-catenin[84], protein 4.1[142], cingulin[143], and afadin[144].

JAMs belong to the immunoglobulin (Ig) superfamily and unlike claudins and occludin, are single-pass transmembrane proteins consisting of two extracellular Ig-like loops, a single transmembrane domain and a C-terminal intracellular domain[145,146]. Two subgroups form the JAM family, with classification dependent on the nature of binding domains. JAM-A, JAM-B and JAM-C form the first subgroup defined by C-terminal PDZ motifs, capable of direct interactions with ZO1[147,148]. As well as ZO1, JAM-A is known to directly bind to afadin[149]. The second subgroup, JAM-4 and endothelial cell-selective adhesion molecule (ESAM), harbour C-terminal PDZ motifs. In their extracellular portions, the JAMs are capable of homotypic and heterotypic interactions between JAMs expressed within the same cell or with JAMs localised to membranes of adjacent cells[150]. Notably, JAM-A has been demonstrated to important in barrier function in ECs, as loss or inhibition of JAM-A resulted in increased permeability[151,152]. On the other hand, a decrease in JAM-C expression results in decreased vascular permeability, through modulation of caderin-5 inter-endothelial adhesions[153]. Interestingly, JAMs are capable of forming heterotypic physical interactions with integrins[154].

The absent or modulated expression of some of the components of the tight junction complex results in aberrant permeability, as discussed. However, external factors may cause the reorganisation or disruption of tight junctions, resulting in increased vascular permeability. In response to cytokines TNFα and IFN-γ, claudins, occludin, and JAMs may be internalised away from junction domains, resulting in enhanced paracellular permeability[155]. Phosphorylation state may also be important for tight junction stability and operation. Early research demonstrated enhanced localisation of occludin to the tight junction following phosphorylation[129]. In contrast to more recent research, where $VEGF_{165}$a-induced phosphorylation of occludin resulted in trafficking away from the tight junction, liked to increased EC paracellular permeability[156,157]. Inhibition of PI3 kinase ablated the $VEGF_{165}$a-induced reorganisation of occludin in bovine ECs[158]. While JAM-A in a dephosphorylated state may localise to the tight junction or lateral membrane, phosphorylated JAM-A localises exclusively to the tight junction[159], although the effect on vascular permeability has not been evaluated. In epithelial cells, ion channel reorganisation of tight junction proteins via internalisation has been observed[159], but whether this feature is relevant to ECs is unknown. Growing evidence implies oxidative stress induced by reactive oxygen species (ROS), disrupts endothelial and epithelial tight junctions. For example, hydrogen peroxide induces barrier dysfunction in EC monolayers, leading to elevated paracellular permeability possibly through the redistribution of occludin and ZO1 into intracellular compartments[160,161].

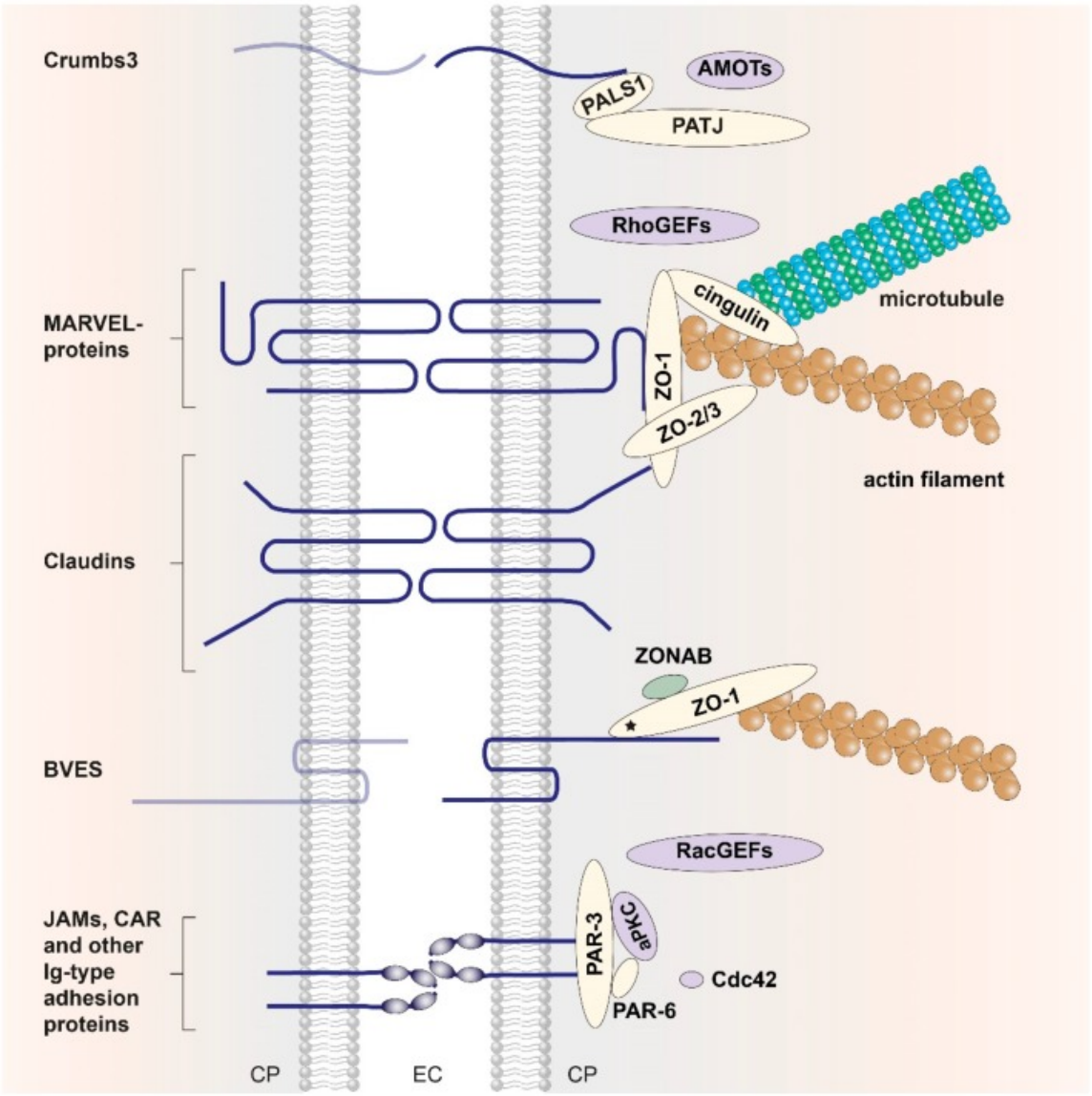

Figure 1.7 – Composition of tight junction. *The core of the tight unction in the centre of the diagram is comprised of claudin and MARVEL-proteins (occludin). The intracellular domains of these proteins form a cytoplasmic plaque consisting of actin-binding proteins, such as ZO-1, anchoring the proteins to the actin cytoskeleton. Association to microtubules is facilitated by cingulin recruitment to ZO1. JAMs are another component of the tight junction, associating through their common binding partner ZO1*[162].

Gap Junctions

Gap junctions are different to adherens junctions and tight junctions, in that they do not regulate transport intracellularly or between EC clefts. Adherens junctions and tight junctions promote adhesion of adjacent cells in the EC monolayer and maintain the integrity of the endothelial barrier, which is not the case for gap junctions. Gap junctions function as non-specific intercellular corridors directly connecting adjacent cells to communicate changes in ion currents and signals[75] and to exchange ions and small molecules by passive diffusion within the contiguous EC monolayer[163]. The gap junctions are formed from homo- or heterohexameric assemblies, termed connexons, consisting

of tetraspan membrane proteins, the connexins[164]. The intercellular channel is formed when two connexions on opposite and adjacent cells dock, with multiple clustering in the plane of the membrane to form a gap junction plaque[163]. Despite its primary function appearing to be in the facilitation of small molecules and signals between adjacent ECs, evidence suggests that modulation of endogenous levels of connexins in ECs influences permeability of the endothelium[165]. In some *in vitro* cell lines, such as MDCK cells, ZO proteins are said to directly bind to connexins[166–168] and determine the localisation of gap junctions[169], although further research is required to determine if this is relevant in ECs.

1.2.3 Endothelial Cell Adhesion

Cellular adhesion is fundamentally important in the development and maintenance of tissues through its connections to the ECM and the ability to form complex structures with other cellular entities. Several of these cellular domains responsible for adhesion have been discussed already. As well as functioning as regulators of vascular permeability, adherens junctions and tight junctions are integral in maintaining cellular adhesions. However, these are not the only important assemblies that are relevant to this process.

1.2.3.1 Nectins

Nectins are important adhesion mediators belonging to the Ig-like superfamily of proteins, consisting of four single pass, transmembrane adhesion proteins extensively expressed in the vascular endothelium[170]. The extracellular domains of nectins contain three Ig-like loops responsible for the interactions with other nectins. These interactions may be homophilic, between the same specific nectin protein, or heterophilic, between differing subtypes of the nectin family. Initially, nectins form dimers within the same cell, cis-dimers, following lateral clustering on the cell surface[171]. These lateral clusters of nectin cis-dimers interact in trans with clusters on adjacent cells in a homo- or heterophilic manner[172–174]. The V-type loop in the extracellular domain has been proposed to be responsible for the formation of cis-dimers as well as trans-interactions between clusters on opposing cells[171,175]. The formation of these heterophilic interactions has exhibited higher affinity than their homophilic counterparts[172,175]. All members of the nectin family possess a PDZ binding motif within their intracellular C-terminal domain, enabling interactions with actin-binding proteins which facilitates anchoring to the cytoskeleton[176]. The presence of the PDZ domain facilitates the recruitment of afadin[177,178], actin binding protein capable of anchoring the nectin clusters to the actin-cytoskeleton. Nectins have been implicated in the formation and maintenance of adherens junctions. The nectin-afadin complex is involved in the development of the corneal endothelium[179] with research demonstrating the colocalisation of nectins with cadherin-5 at adherens junctions and their ability to complex through a shared interactor, afadin[180]. A growing pool of evidence indicates that nectins

recruit cadherins to nectin-based adhesion domains via the nectin-afadin complex, which initiates adherens junction assembly and stabilises the structure[181–183]. In contrast, another proposed model suggests the formation of cadherin microdomains occurs independently prior to or concomitantly with nectin clustering and subsequent recruits the nectin adhesions[184,185]. The apparent contrast in results may be explained by the different endogenous expression levels of nectins and cadherins in the *in vitro* models, however, it is not disputed that nectins appear to be important for organisation and operation of adherens junctions. In *in vitro* vascular ECs, knockdown of endogenous nectins resulted in significant barrier disruption[186]. The inhibition of nectins similarly resulted in the reduced localisation of claudins and occludin at the tight junction, resulting in impaired barrier function, insinuating an involvement of nectins at the tight junctions as well as the adherens junctions[187].

1.2.3.2 Desmosomes

Desmosomes are specialised microdomains mediating cellular contact and adhesions, involving coupling of desmosomal proteins to the intermediate filament of the actin cytoskeleton[188]. The protein core of desmosomes consists of desmogleins, and desmocollins, part of the cadherin subfamily mediating calcium-dependent adhesion[189,190]. These desmosome cores are anchored to the cytoskeleton via desmoplakin[191]. ECs exhibit a lack of desmosome microdomains, despite this, evidence of desmoplakin at both mRNA and protein level has been observed in *in vitro* human umbilical vein endothelial cells (HUVECs)[192]. Interestingly, murine ablation of desmoplakin is lethal, with its subsequent rescue in embryos resulting in a complex phenotype of vascular defects[193]. Although not thought to harbour desmosomes, in some blood ECs, cadherin-5 recruits desmoplakin and vimetin to the membrane, likely bound to the cytoskeleton[194]. This structure is unique to ECs, with these proteins mostly localised with desmogleins and desmocollins, typically absent in the endothelium. Murine knockdown of desmoglein-2 (DSG-2) resulted in reduced angiogenesis assays and modified localisation of actin and claudin-5[195], although its particular role in ECs is yet to be elucidated.

1.2.3.3 Focal Adhesions

Focal adhesions are specialised structures tethering the endothelial cytoskeleton to the ECM through cytoplasmic linker proteins, thereby anchoring the EC to the substratum and transmitting mechanical and biochemical signals between cells and the ECM[196]. The main component of focal adhesions are integrins, a family of transmembrane glycoproteins with the propensity to form heterodimers from multiple homologues of α and β subunits[197] (Figure 1.8). The subunits share structural similarities, with a large extracellular domain, a single pass transmembrane helix, and relatively short cytoplasmic domain[198]. The ectodomains of α integrins are categorised depending on the presence or absence of an inserted domain (α-I domain)[199]. The α-I domain harbours a metal-ion-dependent adhesion site

(MIDAS) facilitating recognition of ligands such as collagens and fibronectin, and integrins with this domain form the collagen and leukocyte receptors[200]. The α-integrins lacking in the α-I domain are classified further based on evolutionary lineage. A notable group within this subclassifications are the RGD sequence receptors, which predominantly heterodimerise with integrin β1 and β3 and recruit RGD containing proteins such as fibronectin in the ECM[201–203]. Although sharing structural similarities with α-integrins, β-integrins possess a more complex composition. β-integrins contain a sequence homologous with the α-I domain, termed the β-I domain, which likewise contains MIDAS domain for ligand recognition. The β-I domain appears to function either directly in binding ligands when heterodimerised with α-integrins lacking an α-I domain or regulating ligand binding in integrins harbouring the α-I domain[204,205].

The cytoplasmic domains of the β-integrins share considerable homology, while the α-integrins have a highly divergent cytoplasmic domain, with the exception of a conserved GFFKR motif responsible for recognition of the β-integrin[206]. The domains are relatively short and lack catalytic activity and instead recruit adaptor proteins that possess either catalytic activity or scaffold and structural functions[200]. These intracellular domains can interact with the cytoskeleton through intermediates, notably vinculin[207], α-actinin[208] and talin[209]. Once such proteins are recruited, the integrin-adaptor protein complexes form specialised microdomains referred to as focal adhesions.

The deletion of integrins and of key regulators of integrin function, results in distinctive vascular phenotypes[210,211]. An influence on vascular permeability and barrier function has been observed in the activation or silencing with particular integrin heterodimer complexes, with contrasting results observed between heterodimers of different compositions[211].

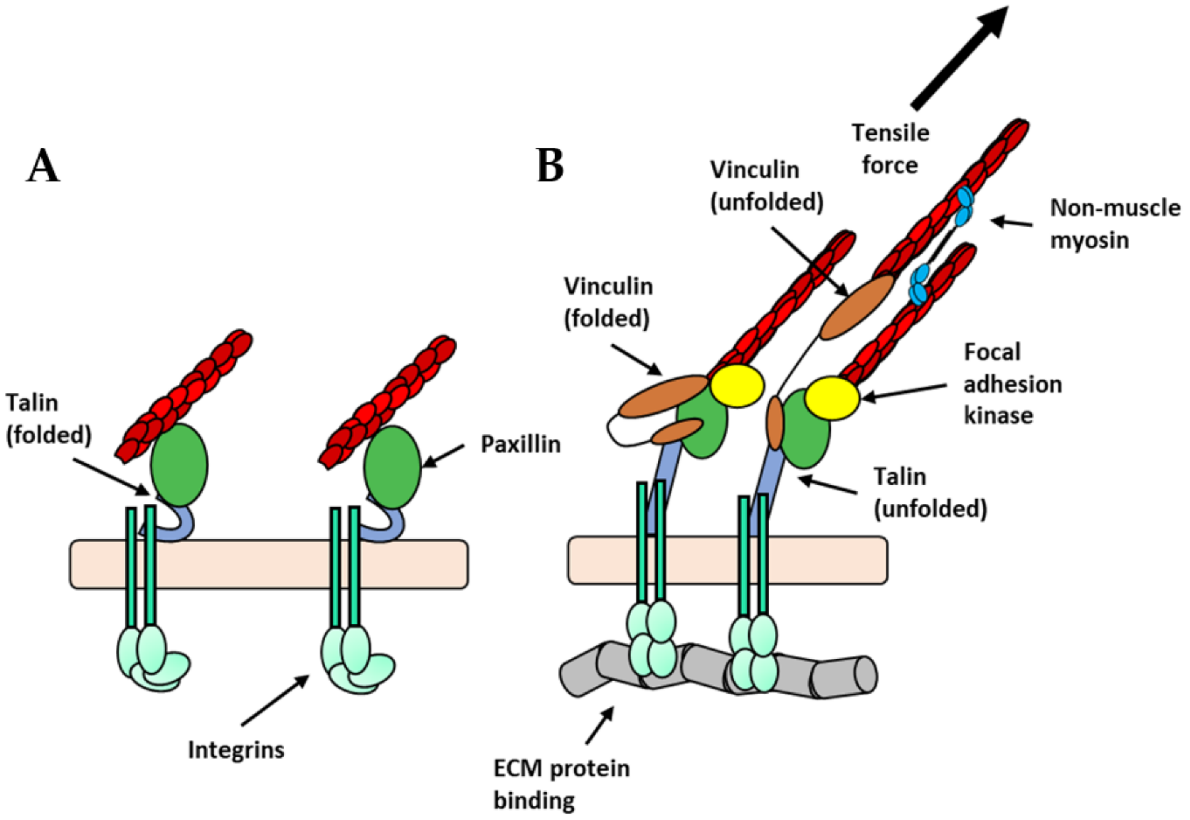

Figure 1.8 – Structure of the folded and unfolded focal adhesion complex. *Integrins are the core constituents of focal adhesions, receiving signals extracellularly and transducing them through intracellular adaptors. The folded and unfolded forms of the focal adhesions are mediated by talin. (**A**) When the focal adhesion complex is not bound to the ECM, talin is folded and the focal adhesion is weakly bound to the cytoskeleton. (**B**) Following ECM binding to integrins within the focal adhesion complex, talin unfolding occurs, resulting in recruitment of adaptor proteins such as vinculin which bind to actin filaments, further engaging the focal adhesion complex to the cytoskeleton*[212].

1.2.3.4 Other Adhesion Proteins

Several other proteins are important for cellular adhesion which may or may not be expressed in adherens or tight junction domains. Like integrins, selectins, VCAM-1, ICAM-1, are transmembrane glycoproteins involved in cellular adhesion. Expression of these adhesion molecules correlates with the presence of inflammatory cytokines, whereby they facilitate infiltration of leukocytes via adhesion to the endothelium[213–215]. In endothelial cells, the main selectins expressed are E- and P-selectin. Unlike other EC adhesion molecules, the function of selectins is restricted to facilitating interactions between leukocytes and vascular endothelium, enabling them to adhere and 'roll' along the endothelium towards blood flow in a process termed extravasation[216]. VCAM-1 and ICAM-1 are localised to the endothelial cell junctions and the luminal surface where they form complexes with integrins and influence leukocyte adhesion and subsequent invasion[217,218].

Platelet endothelial cell adhesion molecule (PECAM1) is another cellular adhesion protein concentrated along the inter-endothelial cleft but expressed in domains outside of adherens or tight junctions[194,219]. Although an influence on vascular permeability has been elucidated through *in* vivo murine silencing experiments, its major function in endothelial cells is facilitating the migration of leukocytes through inter-endothelial clefts[216,220].

1.3 Vascular Endothelial Growth Factors and Receptors

1.3.1 Vascular Endothelial Growth Factors and Receptors

The vascular endothelial growth factor (VEGF) family consists of five endogenously secreted paralogous glycoproteins, which include VEGF-A, VEGF-B, VEGF-C, VEGF-D and PLGF[221]. The VEGF ligands bind preferentially to three closely related RTKs, which are single pass transmembrane proteins capable of binding growth factors to facilitate signal transduction pathways involved in cellular growth, differentiation, metabolism and motility[222]. These are VEGFR1, VEGFR2 and VEGFR3, which bind to particular VEGFs with varying affinities and selectivity, (Figure 1.9)[223–225].

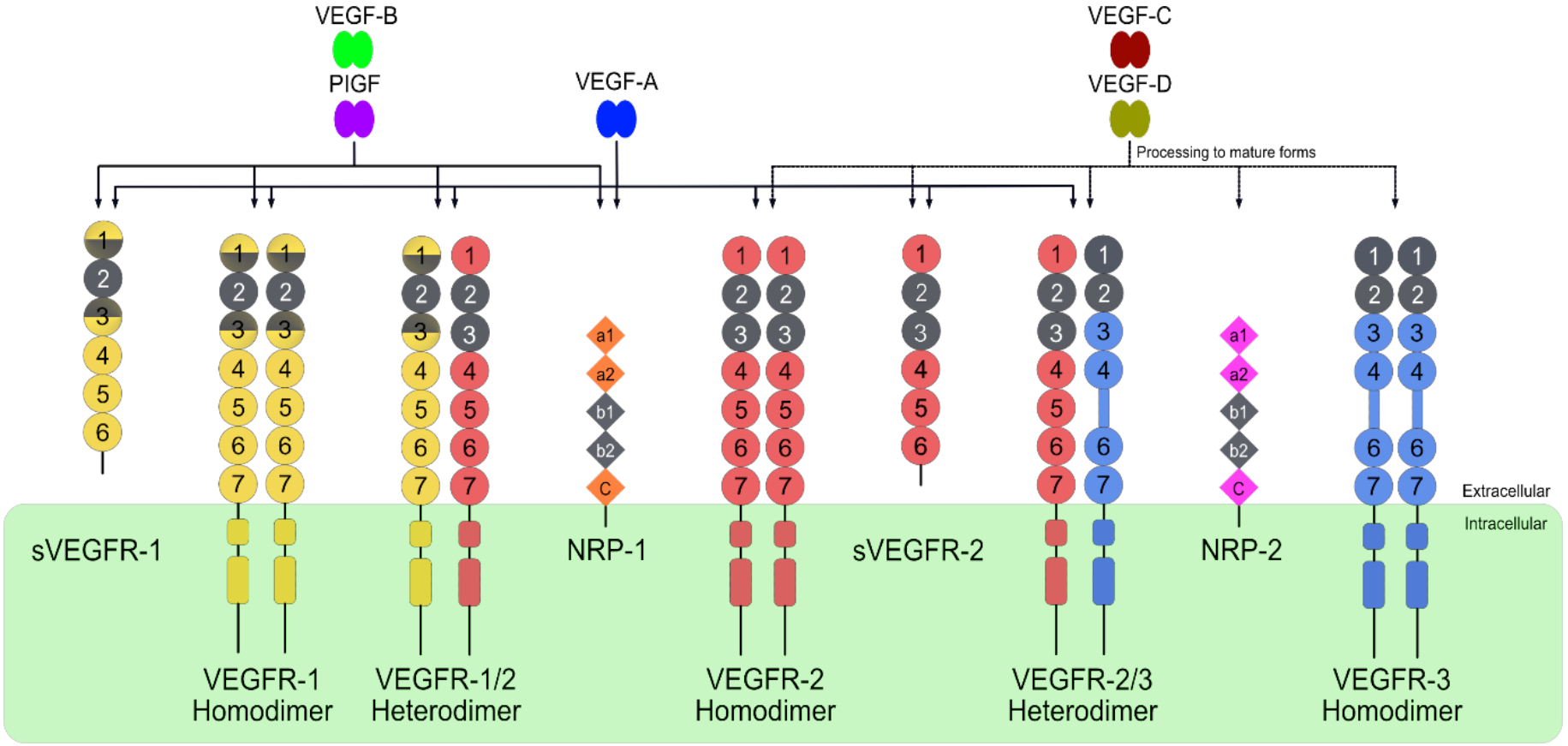

Figure 1.9 – Schematic illustrating ligand-binding selectivity to VEGFR subtypes, NRP-1 and NRP-2. *PIGF, VEGF-A, VEGF-B, VEGF-C and VEGF-D bind to select VEGFRs and NRPs complexes with varied affinities. Unlike other VEGFs and VEGF related ligands, VEGF-C and VEGF-D require processing via proteolysis to the mature form prior to binding to VEGFRs and NRPs. Ligand binding structures in the extracellular portions of the VEGFRs and NRPs are denoted as grey circles. The numbers denote extracellular domain regions of the particular membrane protein.*

1.3.2 Vascular Endothelial Growth Factor Receptor 2

VEGFR2 is an important RTK involved in angiogenesis, vascular permeability and EC survival. Expression is primarily on ECs where it binds to its cognate ligand, $VEGF_{165}$a followed by subsequent activation of downstream signalling pathways such as MAPK, eNOS, PI3K-Akt, FAK, and PLCγ[226,227] regulating EC proliferation, migration and vascular remodelling. Although primarily expressed on ECs, VEGFR2 is found in non-ECs, such as tumour cells[226], macrophages[228], and neuronal cells[229]. For the purposes of this project EC-derived VEGFR2 will be discussed.

1.3.2.1 VEGFR2 Structure

Canonical human VEGFR2 consists of 1356 amino acids and is composed of the classic molecular architecture observed amongst all VEGFRs, with an N-terminal extracellular domain (ECD) consisting of 7 extracellular immunoglobulin-like domains (D1-7), an α-helix transmembrane domain (TM) and a cytoplasmic region, (Figure 1.9)[230]. The cytoplasmic region is further stratified into a juxtamembrane domain (JMD), a kinase domain 1 (KD1) and KD2 split by a kinase insert domain (KID), and a C-terminus. The immature form of the VEGFR2 monomer when expressed, has a mass of around 150 kDa, which then undergoes extensive N- and O-linked glycosylation to result in a mature 230 kDa form which is trafficked to the cell membrane[231].

VEGFs bind to domains D2 and D3, with one VEGF homodimer binding across the two receptor monomers in the VEGFR2 homodimer[232–234]. While domains D4 and D7 are important for stabilisation of VEGFR2 homodimers in the absence of ligand[235,236], conformational changes in the ECD occur following ligand binding. The binding of ligand results in a conformational rotation and intertwining of ECDs of adjacent VEGFR2 monomers[237–239], with proposed new lateral interactions formed between D5 domains of VEGFR2 monomers[236,240]. The ligand-induced conformational changes in the ECD induce reorientation of the transmembrane α-helices with a rotation of 180˚along the helical axis, resulting in increased TKD phosphorylation[236,240]. Further conformational changes occur within the cytoplasmic region following ligand binding, with the kinase insert (KID) in between kinase domains, regulating access of the C-terminus to the enzymatically active kinase domain 1 (KD1) and KD2[241]. Mutations in the C-terminus and KID elicit a reduced propensity to form dimers, implicating these regions in dimerization of VEGFR2[241].

Alternatively spliced variants of VEGFR2 exist endogenously, with a soluble form of VEGFR2, termed soluble VEGFR2 (sVEGFR2), have been identified in humans which lack the transmembrane and cytoplasmic domain of the full-length receptor, (Figure 1.9)[242]. This sVEGFR2 variant is thought to act as a negative regulator of VEGF-C/VEGFR3 induced lymphangiogenesis in murine models, with tissue-specific loss of this isoform resulting in spontaneous lymphatic invasion of the normally aliphatic

cornea and hyperplasia of skin lymphatics[242]. Surprisingly, no accompanying aberrations in vasculature or inhibition of angiogenesis was observed.

1.3.3 Vascular Endothelial Growth Factor Receptor 2 Physiology

Research pertaining to VEGFR2 downstream signalling is well characterised, particularly in comparison with the other VEGFRs subtypes. As discussed, VEGFR2 signalling is critical for EC biology and development of the vasculature. The signalling axis of $VEGF_{165}$a/VEGFR2 is well established in the pathogenesis of diseases such as cancer[243,244], macular degeneration[245] and rheumatoid arthritis[246].

1.3.3.1 Angiogenesis

VEGFR2 is indispensable for early development of the cardiovascular system for embryonic vasculogenesis and angiogenesis. $VEGF_{165}$a binding to VEGFR2 and the subsequent receptor autophosphorylation, is crucial in EC proliferation and mechanisms driving angiogenesis[247], discussed in 1.3.1.1. Generation of *Vegfr2*-null mice using homologous recombination to produce an inactive VEGFR2 variant in mouse embryonic stem cells resulted in embryonic death between E8.5-9.5 characterised by the absence of organised blood vessels[248249]. Whereas inactive or absence of VEGFR1 resulted in elevated angiogenesis and severely disorganised vasculature. In contrast, mice heterozygous for wild-type and inactive VEGFR2 developed normally supporting the role of VEGFR2 as a crucial positive regulator of vascular development[248]. In murine adult tissue, monoclonal antibodies which inhibit $VEGF_{165}$a binding to the ECD of VEGFR2 reduce angiogenesis[248250]. Similarly, utilisation of ribozymes to enhance degradation of *Vegfr2* mRNA exhibited anti-angiogenic properties, further supporting VEGFR2's role as a positive regulator of angiogenesis[251]. To circumvent embryonic lethality, inducible *Vegfr2* loss of function mice were generated, which significantly reduced endothelial sprouting and vessel density in the retinal vasculature[252–254], survival and subsequent differentiation of ECs[255] have also been attributed to $VEGF_{165}$a mediated VEGFR2 signalling. Inhibition of VEGFR2-induced proliferation, migration, invasion and tube formation in HUVECs was observed when treated with kinase inhibitors derived from sorafenib[250], further confirming the role of VEGFR2 activation in the aforementioned biological processes.

VEGFR2 can form complexes with other cell surface proteins which influence angiogenesis. VEGFR2 appears to function in a synergistic manner with integrin β_3. VEGFR2 activation results in phosphorylation of integrin β_3, a critical step in the phosphorylation of VEGFR2 following $VEGF_{165}$a stimulation[256]. The interaction of VEGFR2 and the integrin complex $\alpha_v\beta_3$ is essential for the full phosphorylation of VEGFR2, indicating a complex formation between these two entities is necessary for transducing $VEGF_{165}$a signals related to FAK and SAPK2/p38 motogenic pathways[257].

Vascularisation of tumours and initiation of tumour angiogenesis is an important mechanism for the progression of the disease. Like any tissue in the human body, malignant cells require a supply of oxygen and nutrients for their continued survival, proliferation and metastatic spread. Therefore, proximity to blood vessels is essential. Tumours may become vascularised either by utilising existing blood vessels in a non-angiogenic process, co-opting of vessels[258], or by inducing angiogenesis via a variety of mechanisms[259].

1.3.3.2 Vascular Permeability

Enhanced vascular permeability following VEGFR2 stimulation is well characterised. This physical response is widely observed when VEGFR2 is stimulated with its cognate ligand, $VEGF_{165}$a. However, VEGFR2 itself binds to other entities influencing vascular permeability in a $VEGF_{165}$a dependent or independent manner.

The tyrosine residue Y949 specifically, appears imperative in facilitating the vascular permeability enhancing effects of the $VEGF_{165}$a/VEGFR2 signalling axis. In mice with VEGFR2 deficient of the Y949 residue, they failed to activate c-Src and $VEGF_{165}$a induced vascular permeability was attenuated[260]. The $VEGF_{165}$a dependent phosphorylation of residue Y949 in VEGFR2 *in vivo* promotes interactions with T cell–specific adaptor (TSAd), which initiates binding between c-Src and cadherin-5[261]. As a result of the c-Src/TSAd complex formation, a transient disassembly and opening of inter-endothelial junctions occurs, an effect which was abolished upon the silencing of TSAd. In the same *in vivo* model, a $VEGF_{165}$a-dependent trafficking of cadherin-5 away from EC junctions was observed, as well as a complex formed of VEGFR2, TSAd and cadherin-5 at such junctions[261]. Interestingly, this junctional c-Src activation induced by $VEGF_{165}$a was required for attenuation of EC adhesion during angiogenesis, enabling elongation of the growing sprout[262]. In another murine model, mutation of the Y949 residue resulted in animals with resistance to $VEGF_{165}$a induced reorganisation of adherens junctions, with a phenotype displaying reduced vascular leakage and oedema[263]. These mice exhibited reduced trafficking of cadherin-5 from the adherens junctions when this residue was mutated, further solidifying the role of junctional reassembly in VEGFR2 mediated vascular permeability.

The direct interaction between VEGFR2 and cadherin-5 has been observed several times. In HUVEC lysates expressing modified cadherin-5, it was shown that the transmembrane domain was important for binding with VEGFR2[264]. These cadherin-5/VEGFR2 complexes localised to EC junctions and functioned as a flow sensor. Furthermore, expression of cadherin-5 appeared to retain VEGFR2 at the cell membrane, reducing $VEGF_{165}$a-induced internalisation into signalling compartments[94].

VEGFR2 is thought to form complexes with various integrins, discussed in section 1.3.3.1. Interestingly, the heat shock protein 90 (Hsp90) molecular chaperone was found to bind to VEGFR2, with this binding

being instrumental in the recruitment of vinculin and in the generation of integrin-based focal adhesion[257]. It is unclear whether VEGFR2 influences barrier function at focal adhesions, although a potential role in mediating permeability at these microdomains would be unsurprising, as focal adhesions are known to influence barrier function, discussed in section 1.2.3.3.

1.3.4 Vascular Endothelial Growth Factor Receptor 1

VEGFR1 is structurally similar to VEGFR2, with both harbouring the same domains discussed in section 1.3.2.1. While both bind $VEGF_{165}a$, VEGFR1 has a 10-times higher affinity compared to VEGFR2[265]. Despite the significantly higher affinity for $VEGF_{165}a$, VEGFR1 subunits are up to tenfold less abundant than VEGFR2 on the surface of ECs[266]. Unlike the high kinase activity exhibited by VEGFR2, VEGFR1 is a kinase-impaired receptor, meaning its ability to phosphorylate target proteins and elicit downstream signalling is defective[267]. VEGFR1 is thought to be a negative regulator of VEGFR2 responses. For expression of VEGFR1 as a chimeric form, with a the intracellular VEGFR1 domain fused to the ECD of colony-stimulating factor-1 receptor, a reduction in proliferation and MAPK activation was observed compared to the corresponding chimeric VEGFR2[268]. The same research also demonstrated a similar attenuation with coexpression of the chimeric VEGFR1 and VEGFR2, demonstrating the ability of VEGFR1 in antagonising VEGFR2 responses. Further research with full length receptors shown VEGFR1 can heterodimerise with VEGFR2, and this heterodimerisation primarily responsible for the attenuation of $VEGF_{165}a$/VEGFR2 activity[269].

1.3.5 Vascular Endothelial Growth Factor A

VEGF-A is the most widely researched member of the VEGF family, considered the most significant in the initiation and regulation of angiogenesis[270]. Due to alternative splicing of the *Vegfa* gene, at least 16 known VEGF-A isoforms exist which bind to their target receptors with varying affinities, resulting in distinct signalling outcomes[271]. VEGF-A isoforms bind preferentially to VEGFR1, VEGFR2, NRP1, the soluble variants of these receptors and various heterodimer combinations between the VEGFRs and NRPs[272,273], modulating angiogenesis, vascular permeability, chemotaxis and gene expression.

1.3.5.1 VEGF-A Splicing

The Vegfa coding region, located on chromosome 6p21.1[274], is approximately 14 kilobases (kb) and consists of eight exons and seven introns. Alternative splicing of the primary Vegfa mRNA transcript is well documented, with the dominant splice variant depending on the cellular microenvironment, such as hypoxic conditions[275], in response to stimulation with hormones, cytokines, growth factors or mutagens[276,277], and activity of oncogenes and tumour suppressor genes[278,279]. The alternative splicing of the Vegfa mRNA results in removal of introns and fusion of distinct combinations of exons to generate unique VEGF-A isoforms, resulting in different length isoforms[271]. The isoforms are denoted

$VEGF_{xxx}$ whereby the 'xxx' denotes the number of amino acids present in the specific isoform[271,280]. In total, at least 17 unique VEGF-A isoforms have been identified[271]. All isoforms harbour exons 1-5 and the terminal exon 8, with the exons 5 and 6 either included or excluded in the final isoform sequence[281]. These VEGF-A isoforms include $VEGF_{111}$, $VEGF_{121}$, $VEGF_{145}$, $VEGF_{165}$, $VEGF_{189}$, and $VEGF_{206}$[271].

Further variants are derived from splicing within exon 8, generating two families of isoforms with identical lengths but alternative C-termini amino acid sequences, (Figure 1.10)[281]. $VEGF_{xxx}$a isoforms are considered proangiogenic and are generated by inclusion of exon 8a[283], whereas $VEGF_{xxx}$b isoforms are generally considered anti-angiogenic[282] and splicing out of exon 8a is observed[283]. The first of these isoforms identified and most well characterised is $VEGF_{165}$b.

These isoforms differ in the specific receptor they can interact with, and the level of activation of that receptor. For example, although capable of binding VEGFR2, $VEGF_{165}$b is generally considered anti-angiogenic and cannot bind to NRP1, unlike its $VEGF_{165}$a counterpart[282]. As $VEGF_{165}$a is considered the prototypical angiogenic isoform due to is potency in stimulating angiogenesis[271], this will be the VEGF-A isoform discussed in this chapter unless otherwise stated.

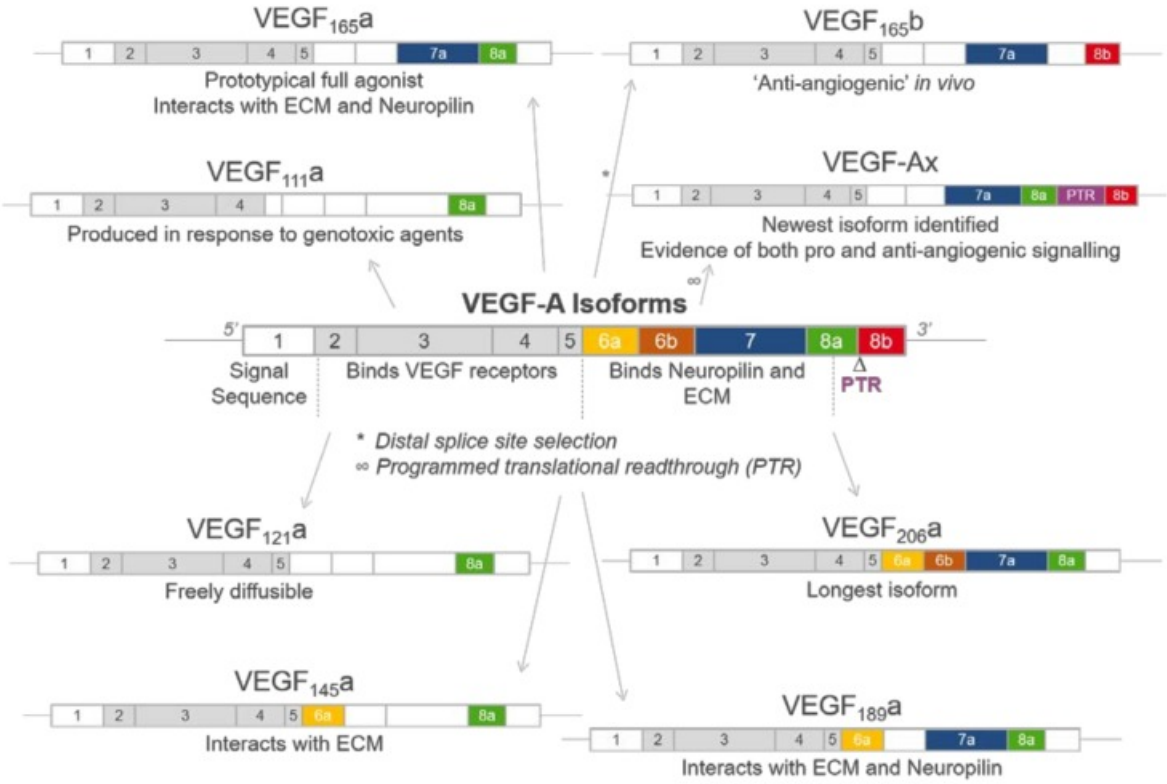

Figure 1.10 – A schematic detailing the VEGF$_{165}$a structure and isoforms generated through alternative splicing. *The VEGF-A gene consist of eight exons which are alternatively spliced to produce isoforms differing in length, designated VEGF$_{xxx}$ where xxx represents the number of amino acids. The differing domains within each isoforms confer distinct properties with respect to VEGFR2 and NRP1 binding. Alternative splicing at the terminal exon 8 results in the generation of two distinct groups of VEGF isoforms, VEGF$_{xxx}$a considered proangiogenic, and anti-angiogenic VEGF$_{xxx}$b variants. Post-translational read-through also results in the formation of isoforms harbouring a 22 amino acid extension at its C-terminus*[271].

1.3.5.2 Angiogenesis

Angiogenesis is primarily regulated through the VEGF$_{165}$a/VEGFR2 signalling axis, the most characterised signalling pathway of the VEGFs to date[245]. Interestingly in developmental angiogenesis, *Vegfa* is unique in its haploid insufficiency, whereby even a single knockout of the *Vegfa* allele in mice, results in heterozygous *Vegfa +/-* mice, which undergo early embryonic death due to dysfunctions in their vascular systems [284]. This observation suggests that sufficient levels of VEGF$_{165}$a are critical in developmental angiogenesis.

VEGF$_{165}$a is an important pro-survival and proliferation mediator in ECs[285,286]. For the *de novo* formation of vasculature in adults, VEGF$_{165}$a is expressed in hypoxic conditions resulting in sprouting angiogenesis. EC tip cells migrate along these VEGF$_{165}$a gradients, propelled by the proliferation of stalk cells, enabling the extensions of capillary sprouts[287]. VEGF$_{165}$a also facilitates the recruitment of endothelial progenitor cells from the bone marrow[288] and promotes the differentiation of the progenitor cells into ECs[289].

The mechanisms driving intussusceptive angiogenesis are less clear, with evidence suggesting mechanical factors such as flow alterations and haemodynamic forces[37,290,291]. Evidence implies the presence of $VEGF_{165}a$ correlates positively with intussusceptive angiogenesis in chicken models [292], although the underlying mechanisms driving this is currently unclear.

1.3.5.3 $VEGF_{165}a$ in Vascular Permeability

$VEGF_{165}a$ is a well characterised modulator of endothelium barrier function, first identified as an antiparallel-homodimeric protein responsible for increased vascular permeability[293]. The effects of $VEGF_{165}a$ on vascular permeability have been investigated utilising *in vitro* and *in vivo* models, with the models evaluated in detail to determine their reliability[294]. The overwhelming consensus across the field indicates increased $VEGF_{165}a$ concentrations results in an increase in vascular permeability. The mechanisms driving the increase in $VEGF_{165}a$-mediated increase in permeability are complex.

Predictably, it appears the principle signalling pathways in which $VEGF_{165}a$ increases vascular permeability is through its cognate receptor, VEGFR2. Addition of $VEGF_{165}a$ results in trans-autophosphorylation of tyrosine residues in the cytoplasmic domains of VEGFR2[295]. This in turn, instigates a signalling cascade whereby phosphorylated VEGFR2 associates with adaptor protein such as PLCγ resulting in an influx of calcium[272,273], c-Src activation[261], eNOS activation[296], RhoGTPases activation[297], and stimulation of the MAP kinase and PI3K pathways[294,298,299] associated with EC proliferation, survival and migration. VEGFR2 activation, phosphorylation and subsequent signalling pathway activation are essential for the $VEGF_{165}a$-mediated increase in vascular permeability[300]. Stimulation of EC lines using $VEGF_{165}a$ can activate eNOS which catalyses nitrous oxide (NO) formation, through VEGFR2 signalling, leading to enhanced vascular permeability[230,301,302].

Following $VEGF_{165}a$ stimulation, c-Src becomes activated in human umbilical vein endothelial cells (HUVECs) through associations with VEGFR2[303], facilitating the increase in permeability, demonstrated in murine models[261]. The inhibition of c-Src activation appears to diminish the permeability modulating effects of $VEGF_{165}a$. The precise mechanisms driving the increases in permeability of the $VEGF_{165}a$/c-Src axis are unknown. However, one explanation may be the c-Src mediated phosphorylation of cadherin-5[304]. Although, c-Src phosphorylation of cadherin-5 alone does not appear to be sufficient to increase permeability of EC monolayers[305] and in murine models[306], suggesting other pathways are required for permeability modulation.

The influence of $VEGF_{165}a$ on the organisation of proteins located at cellular junctions is well characterised. Following treatment with $VEGF_{165}a$, trafficking away from the junction has been observed with integral junctional proteins ZO1[307], occludin[156] cadherin-5[308] in EC monolayers. Similar results have been observed in mice for the internalisation of cadherin-5[309]. As discussed in 2.2.4,

phosphorylation of junctional proteins and in particular, cadherin-5 and proteins localised with the cadherin clusters, appears important in the disassembly and dysfunction of cellular junctions. Phosphorylation of occludin attenuates its interactions with ZO1, reducing its localisation to the tight junctions[310]. The phosphorylation of ZO1 itself similarly resulted in trafficking away from cellular junctions[157]. Phosphorylation of other components of these junctions are known to cause disassembly and increase in permeability, it is less clear if these occurs in a c-Src dependent manner.

The Ras superfamily of GTPases have bene identified in pathways pertaining to modulation of vascular permeability. Specifically, RhoA, RhoC and Rac1, members of the Rho family of GTPases, have demonstrated involvement in regulating a variety of EC functions, including cellular adhesion and permeability. RhoA and its downstream effectors ROCK 1 and ROCK2 regulate $VEGF_{165}$a mediated permeability in EC monolayers[311]. Similarly, RhoC is activated following $VEGF_{165}$a treatment, although *in vivo* zebrafish models indicate it is a negative regulator of $VEGF_{165}$a induced permeability[312]. In agreement, the silencing of RhoC in human breast cancer cells exhibited increased barrier function and cell-cell adhesion compared to wildtype cells[313], supporting prior evidence of its negative regulation of vascular permeability. $VEGF_{165}$a is also able to activate Rac1[314], which is known to facilitate adherens junction reorganisation[315] potentially through interactions with the actin cytoskeleton[316]. In EC monolayers, Rac1 has demonstrated its importance in modulating barrier function, with its knockdown abrogating the enhanced permeability effects observed with $VEGF_{165}$a stimulation[98]. Interestingly, a reduction in cadherin-5 was also observed when silencing Rac1.

1.4 Neuropilin 1

Neuropilins (NRPs) are non-tyrosine kinase type I transmembrane glycoproteins involved in mediating a multitude of essential signalling processes. There are two members of the NRP family, NRP1 and NRP2, which share only a 44% sequence homology[317] but have identical domain structures [318] and a similar size ~ 120 kDa[319,320]. NRP1 is mainly expressed on arterial endothelial cells and is thought to act as a co-receptor for VEGFR2[321] capable of binding several VEGF-A isoforms and PLGF[273]. VEGF-A isoforms, discussed in section 1.3.5.1, lacking exon 7 and a C-terminal arginine ($VEGF_{xxx}$b family members) are incapable of binding to NRP1[322]. Interestingly, there is evidence of interactions with other RTKs, notably tropomyosin-related kinase A (TrkA)[323], epidermal growth factor receptor (EGFR)[324], and transforming growth factor β (TGF-β) receptor[325]. NRP1 is also expressed in immune cells such as machrophages and dendric cells[326], neuronal cells [317], and tumour cells[327].

1.4.1 Neuropilin-1 Structure

NRP1 is a single pass transmembrane glycoprotein with clearly defined domains. The majority of the receptor is comprised of a large N-terminal extracellular domain (~850 amino acids), followed by a short transmembrane (~24 amino acids) and C-terminal intracellular domain (~40 amino acids)[328,329]. The extracellular portion of NRP1 includes five structural motifs: the complement C1r/C1s, Uegf, bone morphogenetic protein 1 (CUB) domains a1, a2; the coagulation factor (FV/VIII) domains b1 and b2 and the MAM domain, (Figure 1.11). In the endogenous cellular membrane, NRP1 is likely to exist as oligomers, as oligomerisation of NRP1 has been demonstrated even in the absence of ligand[330–332].

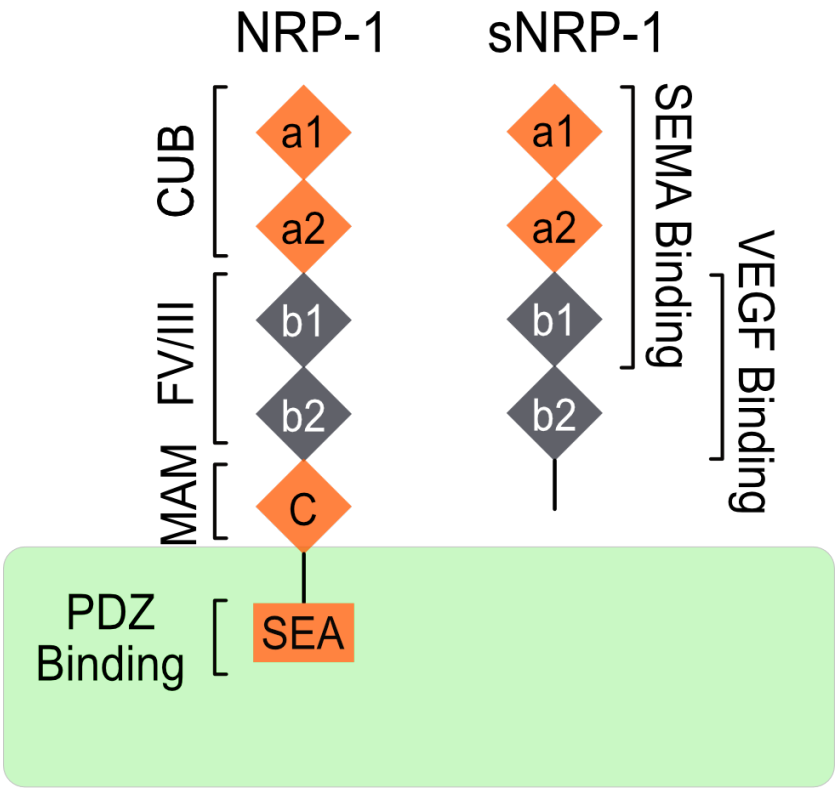

Figure 1.11 – Structure and domains of Neuropilin-1. *The ectopic domain of NRP1 is comprised of 5 notable regions. The complement C1r/C1s, Uegf, bone morphogenetic protein 1 (CUB) domain is further divided into a1 and a2. The coagulation factor (FV/VIII) domains b1 and b2 are adjacent to the CUB domain. A MAM domain links the prior domains to the membrane. Domains a1, a2 and b1 are responsible for binding of semaphorins. Whereas b1 and b2 facilitate the binding of VEGFs. The intracellular domain is short, and harbours a SEA motif capable of binding proteins harbouring a PDZ-motif. The MAM domain is thought to facilitate dimerization of NRP1. sNRP1 consisting of only a1, a2, b1 and b2 domains are not membrane bound, due to the lack of a MAM domain.*

The a1, a2, b1 and b2 are essential for ligand binding[333]. The a1 and a2 domains are chiefly required for the binding of Semaphorin-related ligands, a family of signalling proteins which are key regulators of neuronal growth, (Figure 1.11)[334]. The b1 and b2 domains, facilitate VEGF-A binding, (Figure 1.11)[322,335] and are also required for docking of semaphorin ligands and other VEGFs[336]. Early research into the MAM domain of NRP1 appeared to suggest a contribution to oligomerisation of NRP1[331].

However, the more recent crystal structure of the MAM domain, has suggested this domain alone is insufficient to drive receptor dimerization, perhaps suggesting it functions alternatively in NRP1 membrane assembly and signal transduction[337].

The transmembrane domain, along with the intracellular portions, are required for anchoring NRP1 to the plasma membrane. Further research has identified a putative GxxxG motif in the transmembrane domain, important for NRP1 receptor dimerization and the transduction of semaphorin signalling during axonal guidance[338].

The NRP1 C-terminal intracellular domain is not thought to possess catalytic activity alone, and for a long time, NRP1 was considered a non-signalling receptor due to the small size of this domain. This idea has since been rejected as further investigations have shown that NRP1 can interact with proteins containing a PDZ binding domain through its three amino acids (S-E-A-COOH), the SEA motif, at the end of its C-terminus cytoplasmic domain[328]. PDZ-binding motifs are short sequences at the C-terminus that typically conform to the sequence(-[S/T]-X-Φ-COOH (Class I), where X pertains to any amino acid and Φ denotes a hydrophobic residue. The C-terminal sequence of NRP1 (-S-E-A-COOH) matches this consensus and enables interaction with proteins containing PDZ domains. Further evidence of direct binding to the C-terminal domain is limited, however, its biological significance is well characterised. The SEA motif appears important for promoting $VEGF_{165}$a induced EC migration[339] and ligand-independent EC adhesion to fibronectin[340] , crucial for development of vasculature. The silencing of the NRP1-SEA motif in *in vivo* Zebrafish models and *in vitro* HUVECs elucidated this motif as indispensable for angiogenesis[341].

1.4.1.1 Neuropilin-1 Isoforms

Several endogenous truncated variants of NRP1 exist, generated by alternative splicing mechanisms[342]. Those lacking the transmembrane and cytoplasmic domains are soluble and primarily exert an anti-angiogenic effect, operating in a ligand-sequestering capacity by binding to secreted $VEGF_{165}$a and preventing it from activating membrane-bound VEGFR2, (Figure 1.11)[343,344]. A membrane bound variant of NRP1, lacking exon 16, did not demonstrate functional differences compared to canonical NRP1, with both appearing to mediate $VEGF_{165}$a induced signalling and NRP1/VEGFR2 complex formation in a similar fashion[345]. The emerging pool of evidence of NRP1's significance in other biological processes may mean these soluble forms have alternative functions outside of vascular-related pathology.

1.4.1.2 Neuropilin-1 Post-translational Modifications

NRP1 undergoes post-translational modification, primarily in the form of glycosylation on serine and asparagine residues. N-linked glycosylation on asparagine residues have been demonstrated using

glycoproteomics[346] and through crystallisation of NRP1[347]. The biological relevance of the N-linked glycosylation is yet to be elucidated. In contrast, O-linked glycosylation at Ser_{612} has been identified in HUVECs via western blotting, where Serine was mutated in favour of Alaine resulting in a shift in protein size due to the lack of glycosylation[348]. The mutation at Ser_{612} modulated $VEGF_{165}$a signal transduction, with reduced EC viability observed[348], glioblastoma invasiveness[349] and fibronectin fibril assembly[350].

1.4.2 Neuropilin 1 in Angiogenesis

NRP1s role in vascular development is well established and the signalling axis of the NRP1/VEGFR2 investigated extensively. Indeed, it is generally believed the primary mechanism by which NRP1 modulates angiogenesis, is through its ability to bind VEGF-A isoforms and form complexes with VEGFRs, notably VEGFR2.

There is compelling evidence that expression of NRP1 at the cellular membrane enhances the binding of $VEGF_{165}$a to VEGFR2 and enhances autophosphorylation of the VEGFR2 intracellular domains[351,352]. It was initially though the molecular mechanisms driving the NRP1 and VEGFR2 complex formation was the binding of $VEGF_{165}$a formed a bridge between NRP1 and VEGFR2 subunits[352]. However, a new model of binding is required bridging doesn't explain how NRP1 enhances the phosphorylation of VEGFR2 and proliferation of ECs in the presence of $VEGF_{121}$a[353], which does not bind to NRP1[354]. Therefore, the VEGF-A bridging model does not sufficiently explain the signal enhancing capabilities in the absence of NRP1 ligand binding. There is also disagreement whether $VEGF_{165}$a is required for NRP1/VEGFR2 complex formation. Some reports suggest that the presence of $VEGF_{165}$a is essential for the complex formation[352], while others demonstrate $VEGF_{165}$a is dispensable for the formation of complexes[351,353].

The expression of NRP1 in the presence of VEGFR2 and stimulation with $VEGF_{165}$a enhanced activation of ERK 1 and 2 signalling[355], p38 MAPK[356], PI3K/Akt[357], compared to VEGFR2 expression alone, suggesting NRP1s role in enhancing VEGFR2s ability to activate signalling pathways. Evidence suggests NRP1 increases the phosphorylation of VEGFR2, where absent NRP1 expression resulted in significantly less phosphorylation at tyrosine residue Y1175[321], perhaps postulating a mechanism in which NRP1 increases the signalling output of VEGFR2 by increasing the trans-autophosphorylation of VEGFR2 monomers. As discussed earlier, a normal angiogenic phenotype has been observed following ablation of the VEGF-A binding domains in NRP1, leading to the belief NRP1 functions as a co-receptor, enhancing VEGFR2 activation[358,359] rather than promoting angiogenic signalling in its own right.

For the functions as a coreceptor for VEGFR2 and in the formation of NRP1/VEGFR2 complexes, the SEA motif of NRP1 is required for oligomerisation, suggesting the intracellular region of NRP1 is important for signal transduction pertaining to angiogenesis and other physiological processes mediated by the NRP1/VEGFR2 signalling axis[360].

In vivo models have indicated NRP1 is instrumental in developmental angiogenesis and vasculogenesis. NRP1 deficient mice experience embryonic lethality at E12.5, with impaired angiogenesis and vascularisation, resulting in both neuronal and vascular defects[361]. In contrast overexpression in mice resulted in embryonic lethality due to deregulated angiogenesis causing growth of excess vasculature with a propensity to leak and haemorrhage[362]. The extent of NRP1 overexpression correlated with earlier stage embryonic lethality. NRP1 appears to be essential in the early angiogenic endothelium, specifically at the EC tip where it promotes guidance of the angiogenic sprout[363,364]. The abundance of NRP1 expression on new vasculature in wound healing models of mice, demonstrated its importance in wound angiogenesis in adults[365].

In mice expressing a mutated form of NRP1 capable of binding $VEGF_{165}$a but not semaphorin-3A (SEMA-3A), SEMA-3A binding was dispensable for developmental angiogenesis, although signal transduction through both the $VEGF_{165}$a/NRP1 and SEMA-3A/NRP1 axes are critical for heart development[366]. In contrast, alternative murine models have demonstrated the $VEGF_{165}$a/NRP1 signalling axis to be dispensable for developmental angiogenesis. Mice expressing mutant forms of NRP1 incapable of binding $VEGF_{165}$a, survived to adulthood with normal vasculature[321,367], indicating $VEGF_{165}$a binding to NRP1, is not required for developmental angiogenesis. Considering this in the context of the vascular defects observed in knock out NRP1 mice, implies that NRP1 influences developmental angiogenesis in a $VEGF_{165}$a-independent manner.

Interestingly, ablation of the NRP1 cytoplasmic domain in mice, resulted in normal angiogenesis but impaired developmental and adult arteriogenesis, due to a reduction in NRP1-mediated VEGFR2 trafficking via PDZ domain-interactions[368]. In a similar study, with a murine NRP1 C-terminal knockout, normal vasculogenesis and angiogenesis was observed, demonstrating that the extracellular domain of NRP1 is enough to facilitate these biological processes[369], in contrast to full deletion of NRP1. However, a distinct arteriovenous patterning phenotype of abnormally frequent crossings of arteries and veins was observed in these animals.

NRP1 is able to form complexes with other VEGFR subtypes. An interaction between VEGFR1 has been observed, which is a largely kinase dead VEGFR and thought to act as a decoy receptor for the VEGFs[370], as discussed in section 1.3.4. However, the biological relevance of this interaction is unknown, with current research lacking in the biological outcomes of this interaction.

1.4.2.1 Neuropilin-1 Involvement in Tumour Angiogenesis

NRP1 expression in tumours correlates to poor prognosis and tumour progression in a variety of tumour types, such as: head and neck squamous cell carcinoma (HNSCC)[371], pancreatic cancer[372], lung cancers[373,374], prostate cancer and colon cancer[375,376]. As well as correlating with poor prognosis in solid tumours, a similar correlation has been observed with haematological malignancies, including acute myeloid leukaemia[377–379].

As discussed in section 1.3.3.1, tumour vascularisation is an important mechanism for disease progression, supplying the tumour with oxygen and nutrients for continued proliferation and for metastatic spread. The expression of NRP1 in a variety of tumour cells and tumour-associated vasculature, led to the supposition that NRP1 may contribute to tumour angiogenesis[352]. Early research demonstrated *in vitro* that NRP1 overexpression did not induce proliferation of rat prostate carcinoma cells directly, rather, when these malignant cells were injected in rats *iv vivo* the overexpression of NRP1 significantly increased microvessel density, increased EC proliferation, dilation of blood vessels and less apoptotic tumour cells compared to without NRP1 expression[380]. It was concluded from this *in vivo* model, that NRP1 is important for tumour angiogenesis. In another *in vivo* model, using mice injected with murine melanoma cells, heterozygous mutations resulting in ablation of the NRP1 VEGF-A binding site resulted in mice with no detectable tumours compared to mice expressing WT NRP1, suggesting the NRP1-mediated tumour angiogenesis was dependent on VEGF-A signal transduction[367]. Similarly, when inhibiting VEGF-A using mAbs to ablate its binding capabilities and blocking VEGF-A binding to NRP1 using anti-NRP1 mAbs, murine xenograft tumour size was significantly reduced compared to the anti-VEGF-A mAb alone[381]. These results indicated the proangiogenic activities of NRP1 in malignant cells are mediated by VEGF-A binding and signal transduction.

Interestingly, as well as progression of cancer via angiogenic mechanisms, NRP1 orchestrates fibronectin fibril assembly in the ECM surrounding tumour cells, promoting growth of the tumour[382]

1.4.3 Neuropilin 1 in Endothelial Cell Adhesion

Prior to the discovery of NRP1s influence during angiogenesis, it was originally identified as a cell adhesion molecule of the developing nervous system in chicken models[383]. The primary context of NRP1 research has focused on its angiogenesis modulating properties, however, its role in cellular adhesion is becoming more recognised. The NRP1 extracellular segment, b1 and b2 domains appear to be critical for the cellular adhesion properties exhibited[384].

The specific localisation of membrane bound NRP1 in somatic EC adhesion domains has recently been elucidated with high expression observed at cellular junctions of EC monolayers[385], although this research did not specify the nature of the junctions. This localisation appeared to be independent of

VEGFR2 localisation. Similarly, NRP1 regulated EC adhesion to the to the ECM independently of VEGFR2[386]. Colocalisation of NRP1 and the tight junction protein ZO1, indicated NRP1 may be localising to tight junctions[387]. In addition to tight junctions, colocalisation with the integral adherens junction protein cadherin-5, has also been demonstrated in EC monolayers *in vitro*[385] and *in vivo* vasculature endothelium[388,389].

Building on these observations, functional mechanisms of cellular adhesion properties mediated by NRP1 have been investigated. Following from the NRP1/cadhein-5 localisation *in vivo* observations, a proximity ligation assay (PLA) performed in HUVECs indicated close-proximity between NRP1 and cadherin-5[388]. The research further implicated NRP1 in modulating adherens junctions, in a mechanosensory capacity, whereby NRP1 may detect, respond to and transmit mechanical forces or changes in the physical environment. In the study, the knockdown of NRP1 in ECs exposed to laminar flow induced adherens junction destabilisation and cytoskeletal remodelling. Conversely, mechanosensitive complexes involving NRP1, VEGFR2 and Plexin D1 (PlxnD1) are thought to act upstream of junctional domains and integrins in response to shear stress[390]. An interesting interactome analysis of NRP1 in unstimulated ECs using an extracellular N-terminal modified HaloTag, revealed proximity with cadherin-5 and integrins, known to modulate cellular adhesion[391].

1.4.3.1 Cytoskeletal Assembly

NRP1 appears to be a critical regulator of EC adhesion to ECM proteins and cytoskeletal assembly, independent of its interaction with VEGFR2[386]. Silencing of NRP1 in HUVECs exhibited dysfunction in EC attachment to the ECM, characterised by failed attachment of monolayers and defective intracellular organisation of the actin cytoskeleton. The remodelling of the ECM of ECs and assembly of fibronectin fibrils appears to be mediated by the NRP1 cytoplasmic domain in cooperation with integrins, again independent of the presence of VEGFR2[340,392]. Integrin cooperation has also been observed in tumour cells where the interaction of NRP1 and integrin β_1 promoted cellular adherence[393]. Formation of *cis-* and *trans-,* NRP1 and integrin β_8 complexes, occurring on the same cell or adjacent cells, promotes adhesion between neuroepithelial and ECs during brain development and knockout of NRP1 in cerebral vessels exhibited defective adhesion capabilities[394]. Recent evidence has supported a role for a soluble isomer of VEGFR1 (sVEGFR1) binding with NRP1 in the ECM modulating EC adhesion[395]. The NRP1/sVEGFR1 interaction appeared critical for EC adhesion to an ECM abundant with sVEGFR1 and EC migration towards sVEGFR1. Interestingly, NRP1 also facilitated the interaction between sVEGFR1 and integrins, an interaction known to promote EC adhesion[396].

1.4.3.2 Involvement at Focal Adhesions

Although no difference in focal adhesion has been observed following EC NRP1 knockout[394], removal of the cytoplasmic domain resulted in a significantly slower rate of focal adhesion turnover in response

to $VEGF_{165}a$, possibly due to an inability to bind filamin a (FLNA)[397]. NRP1 trafficking away from focal adhesions was observed following integrin β_3 inhibition and $VEGF_{165}a$ stimulation, resulting in EC migration[398]. The authors suggest NRP1 is usually sequestered at mature focal adhesions, and an escape pathway enables NRP1 to participate in nascent focal adhesion dynamics, influencing EC migration following long term suppression of integrin β_3. Certainly, the interplay between NRP1 and integrins appears important for cellular adhesion and associated processes.

1.4.4 Neuropilin 1 in Vascular Permeability

Given the growing recognition of NRP1 at endothelial junctions, it is unsurprising it may influence vascular permeability. Traditionally, the vascular permeability effects through NRP1 are thought to be mediated by $VEGF_{165}a$ stimulation and VEGFR2 complex formation, hence, many studies have focused on this signalling axis [399]. While evidence exists for NRP1 exerting an effect on barrier function, others claim it is dispensable for $VEGF_{165}a$/VEGFR2-mediated hyperpermeability.

1.4.4.1 Neuropilin-1 Ligand Stimulated Vascular Permeability

Conditional knockdown of NRP1 has been shown to have no influence on $VEGF_{165}a$-induced retinal permeability in mice, however, these knockdown animals were protected against the permeability enhancing effects of NRP1 ligand, SEMA3A[400]. Additionally, when using antibodies intended to block $VEGF_{165}a$ binding to NRP1, but not $VEGF_{165}a$ activity, there was no effect observed on $VEGF_{165}a$ induced permeability in mice models[381].

In contrast, EC monolayers treated with anti-NRP1 mAbs preventing the binding of $VEGF_{165}a$ vascular barrier function was preserved[401]. A similar study using a novel ligand only binding to NRP1, RPARPAR, capable of inducing vascular leakage, demonstrated a reduction in dermal leakage when mice were co-injected with anti-NRP1 mAb[402]. Another study demonstrated a similar reduction of retinal leakage in diabetic models of mice injected with NRP1 inhibitor peptide ATWLPPR[403]. In mice *in vivo* models expressing NRP1 Y297A or D320K mutations incapable of binding $VEGF_{164}a$ (the murine equivalent of human $VEGF_{165}a$), significantly impaired vascular leakage was observed[389]. The same study also determined the cytoplasmic domain was essential for this response, as animals harbouring a NRP1 variant lacking the cytoplasmic domain were resistant to $VEGF_{164}a$-induced hyperpermeability compared to controls. Similarly, mice with selective deletion of NRP1 in ECs exhibited resistance to SEMA3A- and $VEGF_{165}a$-induced hyperpermeability compared to WT animals[404,405]

Interestingly, a $VEGF_{165}a$ mutant with substitutions at amino acids 83–89, lacking the ability to bind to VEGFR2 but retained binding to NRP1, was still able to induce vascular permeability, possibly indicating that NRP1 may modulate barrier function independently of VEGFR2[382,406]. In support of this, $VEGF_{165}a$-

induced vascular hyperpermeability has been observed in *in vivo* mouse models following inhibition of VEGFR2 phosphorylation by kinase inhibitor, vatalanib[385].

Investigation of the molecular mechanisms downstream of NRP1 ligand binding in vascular permeability modulation is an emerging area of research. Importantly, the cytoplasmic domain of NRP1 appears critical for Src kinase activation and subsequent hyperpermeability following $VEGF_{165}a$ treatment[389]. Further mechanisms beyond Src were not evaluated in this model. Indeed, in a mouse model whereby soluble NRP1 (sNRP1) expression was targeted to the epidermis using the keratin 14 (K14) promoter cassette, mice displayed reduced vascular permeability in response to $VEGF_{165}a$[407]. Presumably through the binding and sequestering of $VEGF_{165}a$, potentially indicating sNRP1 is a negative regulator of vascular hyperpermeability. This suggests the important role of the C-terminus of NRP1 in potentiating vascular hyperpermeability.

The presence of NRP1 at cellular junctions, may provide a mechanism for this response. In murine study mentioned earlier, which utilised the NRP1 inhibitor peptide ATWLPPR to reduce retinal vascular leakage, this was accompanied by a reduction in occludin degradation[403]. A possible mechanism of enhanced vascular permeability may therefore be through NRP1 orchestrated reorganisation of junctional proteins, such as occludin. Further, following $VEGF_{165}a$ treatment, a ligand-induced accumulation of NRP1 at cellular junctions has been observed which correlated with vascular leakage[385], suggesting NRP1-modulation of junction microdomains influences barrier functions in ECs. The discovery of a novel secreted extracellular inhibitory ligand, tryptophanyl-tRNA synthetase (mini-WARS), stabilised NRP1 at adherens junctions, which was accompanied by reduced endocytic trafficking of cadherin-5 and a subsequent reduction in EC leakage[391]. Independent of ligand, NRP1 autonomously interacts with cadherin-5 and stabilised adherens junctions, reducing vascular permeability in a mechanosensory capacity in response to sheer stress[388].

1.4.5 Neuropilin-1 in Vesicular Trafficking and Internalisation

NRP1 is known to participate in the internalisation of key signalling receptors, such as VEGFR2 and integrins, influencing cellular migration, adhesion and angiogenesis, (Figure 1.12). Internalisation of these membrane proteins is often proceeding ligand stimulation. As well as endogenous internalisation of proteins, recent evidence suggests an important role or modulating uptake of viral proteins into endosomes.

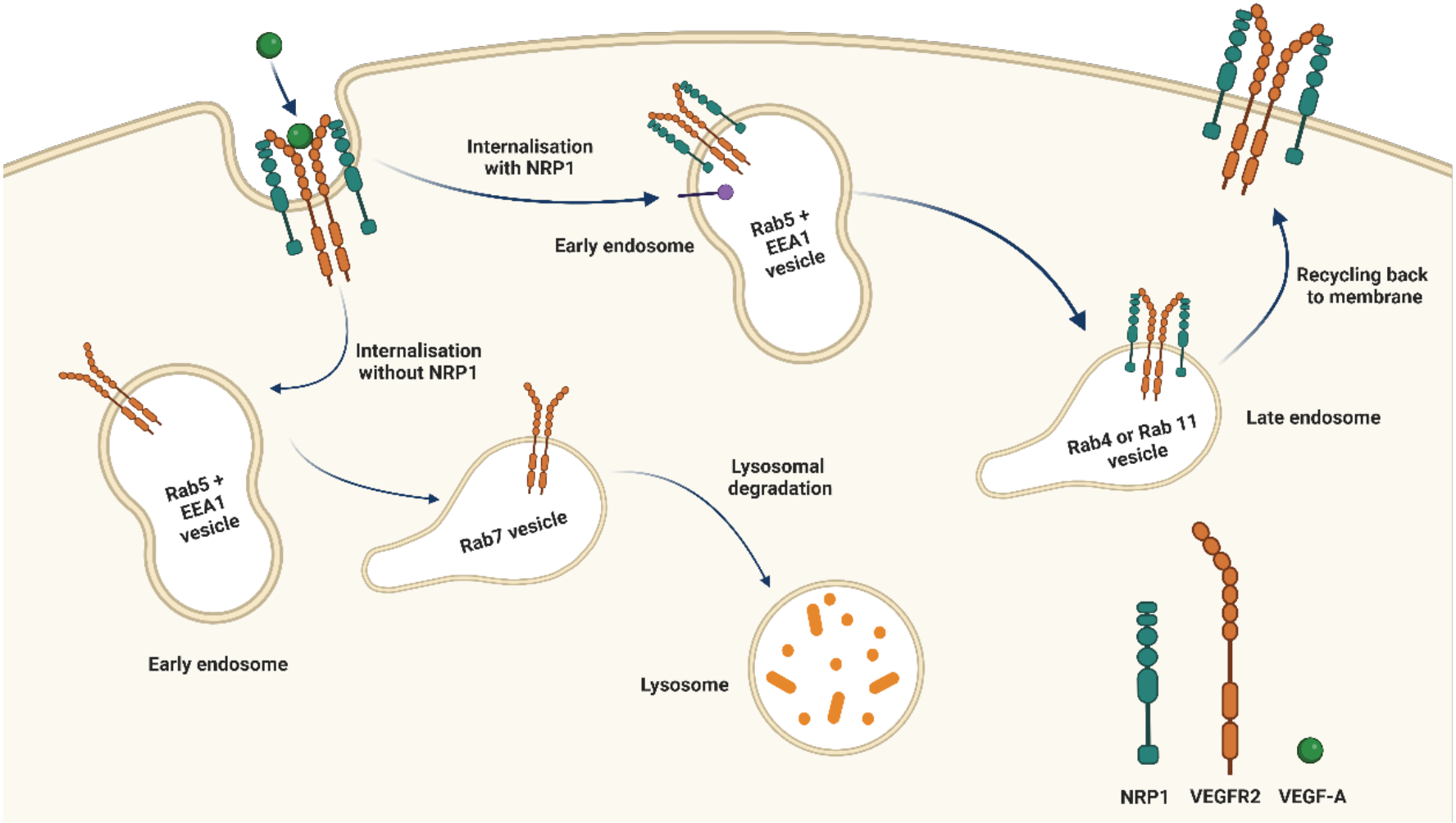

Figure 1.12 – Internalisation and membrane recycling of VEGFR2 facilitated by NRP1. *Following ligand binding of NRP1/VEGFR2 complexes by VEGF-A, both membrane proteins are internalised into early endosomes containing Rab5 and early endosome antigen 1 (EEA1). The presence of NRP1 directs VEGFR2 to late endosomes containing Rab4 or Rab11, associated with recycling back to the membrane. Absence of NRP1 results in VEGFR2 internalisation to Rab5 early endosomes followed by trafficking to Rab7 containing endosomes associated with lysosomal degradation. The figure was created using Biorender.com*

1.4.5.1 Ligand-induced Endocytosis

Observations NRP1 itself is internalised following stimulation with $VEGF_{165}$a and SEMA3A in HUVECs[408] contradict recent experiments in HEK293T cells[354]. Perhaps indicating VEGFR2, present in the HUVECs and not the HEK293T cells, is required for NRP1 internalisation following $VEGF_{165}$a stimulation. The internalisation and trafficking of *cis* NRP1/VEGFR2 complexes following $VEGF_{165}$a stimulation, is well documented, (Figure 1.12).

Specific endocytic pathways induced by NRP1 stimulation, appear to be ligand specific. In ECs, $VEGF_{165}$a stimulation induced clathrin-dependent endocytosis, possibly with NRP1 being internalised within NRP1/VEGFR2 complexes, while SEMA3C stimulation led to lipid-raft dependent endocytosis[409]. VEGFR2, also endocytosed via clathrin-dependent mechanisms when stimulated with $VEGF_{165}$a, undergoes either recycling back to the plasma membrane or is targeted for proteasomal and lysosomal degradation[410]. NRP1 and VEGFR2 remain colocalised to the same endocytic compartments following ligand-induced endocytosis and trafficking[409]. RabGTPase family members, notably Rab4, Rab5, Rab7 and Rab11 are experimentally used to define specific vesicular compartments and can influence whether an intracellular vesicle is directed towards recycling or degradation pathways[411]. Initially, VEGFR2 rapidly enters early endosomes (EEs) localising with the RabGTPase, Rab5 and either early endosome antigen 1 (EEA1), (Figure 1.12) or adaptor protein, phosphotyrosine interaction, PH domain, and leucine zipper-containing (APPL)[412]. Co-localisation of NRP1 to EEA1 has also been observed during endocytosis[391]. Presence of NRP1, and $VEGF_{165}$a capable of binding both NRP1 and VEGFR2, direct VEGFR2 towards Rab4 and Rab11 containing vesicles associated with recycling back towards the membrane, (Figure 1.12)[413]. The colocalisation with these RabGTPases requires the C-terminus of NRP1, and likely the binding of synectin to facilitate this process. In contrast, VEGF-A_{165}b capable of VEGFR2 but not NRP1 binding, induced internalisation of VEGFR2 into Rab7 containing vesicles and subsequent lysosomal degradation[413], further indicating the importance of NRP1 in VEGFR2 recycling. In unstimulated conditions, VEGFR2 has been shown to localise to Rab4 and Rab5 containing vesicles, while NRP1 localised to Rab4, Rab5 and Rab11 vesicles[413]. More recently, following $VEGF_{165}$a stimulation of ECs, the NRP1-mediated recruitment of the protein raftlin, stabilised VEGFR2 at the cell membrane by inhibiting its internalisation and also promoted recycling of internalised VEGFR2 back to the membrane[414]. Interestingly, while *cis* NRP1/VEGFR2 complexes facilitate internalisation, *trans* complexes are associated with inhibition of VEGFR2 internalisation[415].

Similar to VEGFR2, NRP1 may also play a role in the internalisation and trafficking of another receptor tyrosine kinase, the epidermal growth factor receptor (EGFR), in response to stimulation with its cognate ligand, epidermal growth factor (EGF)[324]. Ligand-induced EGFR translocation into EEs containing EEA1 was significantly impaired following NRP1 silencing. The same study also elucidated

the MAM domain in the ECD, required for receptor oligomerisation was responsible for EGFR internalisation.

1.4.5.2 Internalisation of Integrins

Internalisation of integrins by NRP1 has been observed in multiple biological contexts. In EC monolayers, NRP1 facilitates integrin $\alpha_5\beta_1$ internalisation into Rab5-positive EEs, dependent on the SEA-motif in the C-terminus of NRP1 and subsequent synectin binding to this domain[340]. As well as synectin, a GTPase-activating protein, Ras GTPase-activating protein 1 (RasGAP), enabled the NRP1-mediated endocytic trafficking of integrin α_5 towards Rab11 positive vesicles and subsequent recycling back to the membrane[416]. The promotion of NRP1 and integrin α_5 endocytosis, was also observed with SH3 domain-binding protein 4 (SH3BP4). This may be explained by the enhanced binding of synectin to NRP1 in the presence of SH3BP4, which additionally increased internalisation of NRP1 and integrin α_5[417]. NRP1 is also observed to colocalise in endosomal compartments with integrin β_1 in colorectal cancer cells (CRC) under basal conditions[342]. In these CRC cells the identification of two splice variants of NRP1, lacking N-glycosylation regions at the Asn150 or Asn261 sites, correlated with increased endocytosis and co-accumulation of integrin β_1 into endosomal compartments in response to human growth factor (HGF) but not $VEGF_{165}a$ or EGF[342]. The splice variants displayed defective degradation, resulting in recycling and persistent activation of the FAK/p130Cas pathway, promoting CRC migration, invasion and metastasis.

1.4.5.3 Internalisation of microRNAs (miRNAs)

Not only can NRP1 facilitate endocytic processing of membrane proteins, it may additionally regulate the extracellular internalisation of miRNAs. The ectopic domains of full length and sNRP1 can bind to miRNAs and silencing NRP1 reduced the proliferation and migration observed following miRNA treatment[418]. Additionally, NRP1 has been shown to bind the miRNA binding Protein argonaute-2 (AGO2) and facilitate the internalisation of miRNA/AGO2 complexes. Presence of intracellular miRNA may be important for disease pathology, including with coronavirus severe acute respiratory syndrome coronavirus 2 (SARS-CoV-2) infection[419], in which NRP1 appears to mediate.

1.4.5.4 Neuropilin-1 Involvement in SARS-CoV-2 Viral Entry

A multitude of human and animal pathogenic viruses, seemingly biologically distant, harbour surface proteins containing polybasic sites that are cleaved by furin convertase and furin-like proteases, priming the viral surface proteins for fusion to the host cell membrane following their adhesion. This adhesion is mediated by carboxy-terminal RXXR sequences on the viral particle membrane[420]. Peptides with this sequence, described as a C-end Rule (CendR) motif, have been shown to interact with the b1 ectopic domain of NRP1[402] and this CendR/NRP1 interaction facilitates endocytic internalisation of viral particles, (Figure 1.13)[420]. Rather topically, the recent SARS-CoV-2 virus contains these furin-cleavable

sites, generating CendR motifs[421,422], and ablation of these sites attenuates *in vivo* infectivity in ferrets[423] and in hamster and mice models[424]. The blocking of NRP1 ectopic domains b1 and b2, potential binding regions for CendR motifs, using monoclonal antibodies markedly decreased infectivity of viral particles pseudotyped with SARS-CoV-2 in *in vitro* cells either endogenously or transiently expressing angiotensin-converting enzyme 2 (ACE2), identified as a critical factor for SARS-CoV-2 cellular entry[425,426]. In cells expressing NRP1 alone, infectivity was not promoted, demonstrating NRP1 may potentiate infection in the presence of other host factors. When preincubating surrogate SARS-CoV-2 virus with soluble ectopic domain b1/b2, infection of the *in vitro* cells was significantly reduced[425]

In the context of SARS-CoV-2 neurotropism, NRP1 appears to be the primary receptor mediating viral entry into astrocytes, where endogenous ACE2 expression is low[427]. Inhibition of NRP1 in astrocytes via knockdown using siRNAs or blocking with an anti-NRP1 antibody, strongly inhibited the infection of astrocytes.

In contrast to the evidence discussed, blockade of NRP1 using anti-NRP1 antibodies did not significantly affect SARS-CoV-2 viral entry into pancreatic derived spheroids[428]. The authors ultimately concluded this receptor is non-essential for viral entry in this *in vitro* model.

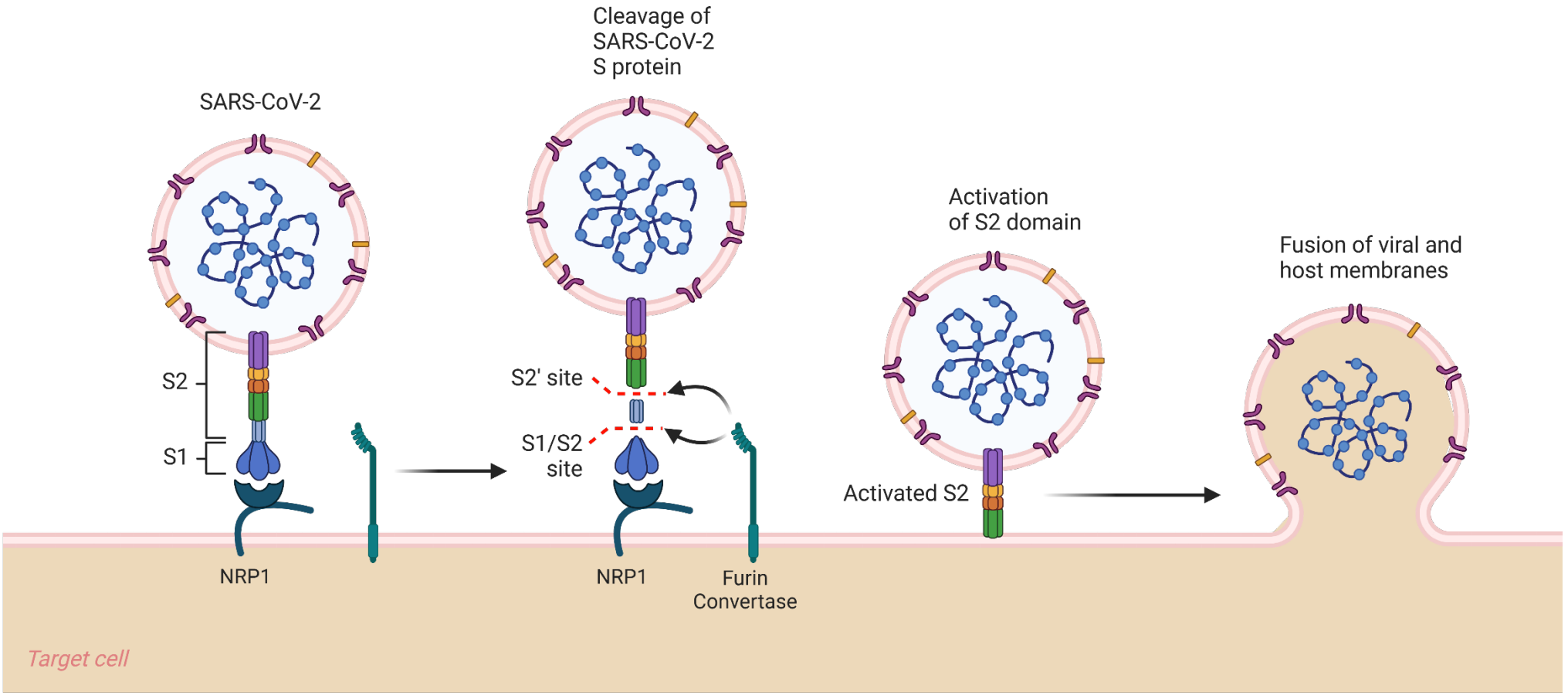

Figure 1.13 – Mechanism of viral entry of SARS-CoV-2 by binding of S1 protein to Neuropilin-1. *The SARS-CoV-2 spike protein S1 harbours a RXXR sequence capable of binding to the b1 and b2 ectopic domains of NRP1. Furin convertases on the cellular surface cleave the S1/S2 spike proteins resulting in activation of the S2 protein, priming the viral particle for fusion with the target cell membrane. The figure was created using Biorender.com*

1.4.5.5 Neuropilin-1 Involvement in Viral Entry of Other Viruses

Earlier research elucidated NRP1s ability to influence infectivity of alternative viruses, besides SARS-CoV-2. NRP1 was found to form complexes with the human T-cell lymphotropic virus (HTLV) type 1 (HTLV-1) envelope glycoproteins and the overexpression of NRP1 in HEK293T cells coincided with increased infectivity of HTVL-1 and HTVL type 2 (HTVL-2)[429]. In this study, silencing of NRP1 had the opposite effect, reducing infection by HTLV-1 and 2. A similar study, investigating the Epstein–Barr virus (EBV), demonstrated a reduced infectivity of the virus in nasopharyngeal epithelial cells with either NRP1 knockdown or pre-treatment with sNRP1[430]. Predictably, overexpression of NRP1 enhanced infection of EBV. Like SARS-CoV-2, EBV harbours a furin-cleavable sites to generate CendR motifs and undergoes internalisation in a similar manner, (Figure 1.13). The evidence presented amongst these experiments provides a compelling argument for the positive role of NRP1 in SARS-CoV-2, and other mammalian viruses, as an important viral entry factor.

1.4.6 Current Understanding of the Neuropilin-1 Interactome

Several binding partners of NRP1, and the biological functions they elicit, have already been discussed extensively. Here, the current knowledge of binding partners of NRP1 at the N-terminal ectopic domain and at the intracellular C-terminal domain will be evaluated, as well as research which details NRP1 binding partners while not specifying the binding region. A full list of proteins interacting with NRP1 identified from current published research, and the method utilised to identify these, are detailed in Table 1.1. A selected few of these will be further discussed.

1.4.6.1 Interactors Identified at Either C-terminal or N-terminal Binding

Complex formation of NRP1 and VEGFR2 monomers has been well established. Co-Immunoprecipitation (Co-IP) has routinely shown these receptors precipitate together[348,351,381]. It is unclear the exact mechanism or by which domains NRP1 and VEGFR2 associate, with suggestions that the ectopic domains associate where binding to their common ligands, including VEGF-A, forms a bridge. Although, as discussed in section 1.4.2, this does not explain the observed NRP1/VEGFR2 complex formation when stimulated with $VEGF_{121}a$, which can only bind to VEGFR2 and not NRP1. Further, there is evidence of constitutive NRP1/VEGFR2 complex formation in HEK293T cells, where a BRET response indicated close-proximity of NRP1 and VEGFR2 in basal conditions[431]. Co-IP of VEGFR1 and NRP1 has also been demonstrated [432], possibly through their ectodomains as demonstrated using enzyme-linked immunosorbent assays (ELISAs)[370]. However, this interaction is much less defined compared to the VEGFR2 homologue.

In research evaluating proangiogenic signalling of VEGFR2, raftlin co-precipitated with NRP1 and was recruited to activated VEGFR2 by NRP1[414]. Raftlin also appeared to stabilise NRP1 at the cellular

membrane, detected by immunofluorescence analyses. Similarly, NRP1 co-precipitated with soluble N-ethylmaleimide sensitive fusion protein attachment protein receptor (SNARE) Synaptobrevin 2 (SYB2, also known as VAMP2) in developing murine brain extracts[433]. Although these methods are indicative of interactions, they provide an inference of binding, rather than evidence and lack temporal sensitivity.

Recently, large proteomic datasets have been published, with the raw data made available to the public domain. These datasets encompass proteomic data of tens of thousands of proteins and hundreds of thousands of identified interactors. The nature of these studies means there are some caveats to the methodology. In the dataset from Huttlin et al., 2021[434], 28 interactors of NRP1 were identified, Table 1.1. However, by the authors own admission, affinity purification mass spectrometry (AP-MS) is poor at identifying transient interactions, and interactions involving membrane proteins may be challenging to detect. Due to the high-throughput nature of this study, for the vast majority of proteins, only technical repeats were performed on the same sample, rather than biological repeats. 10% of the AP-MS experiments were biologically repeated, and a median 60% replication rate was observed[434]. The latter suggesting that a large portion of the identified interactors in the single replicates may be false positives. An earlier version of this research similarly identified several interactors of NRP1, with the same discussed limitations[435]. In a similar smaller dataset focusing on α-arrestins, a single hit for NRP1 was observed. AP-MS identified an interaction between arrestin domain-containing protein 1 (ARRD1) and NRP1[436]. The large proteomic datasets contribute to a significant portion of the 'known' interactors of NRP1. Of note, thioredoxin-related transmembrane protein 1 (TMX1), extended synaptotagmin-1 (ESYT1) and ubiquitin-like modifier-activating enzyme 1 (UBA1) were identified as NRP1 interactors in these datasets. Interestingly, a study investigating a novel protein-protein interaction in intact human nuclei, using crosslinking mass spectrometry (XL-MS), elucidated a potential interaction of nucleolin (NCL) and NRP1[437]. NRP1 has no known nuclear function.

1.4.6.2 N-terminal Binding Interactors

The obvious candidates for interacting with the N-terminal extracellular region of NRP1, are endogenous ligands which stimulate the receptor such as VEGF-A and class III Semaphorins ligands which have been extensively researched in the context of NRP1. In terms of VEGF-A, several splice variants exist discussed in section 1.3.3.1, with different capabilities and affinities concerning NRP1 binding. For example, several conflicting studies either demonstrate or refute binding of VEGF-A_{121}a to NRP1[438]. VEGF-A_{165}b, an anti-angiogenic VEGF isoform, has demonstrated its inability to interact with NRP1[439], due to a lack of a C-terminal arginine in this variant[322]. Previously discussed ligands, SEMA3a and SEMA3c, are class III semphorins binding to NRP1 and eliciting a biological response. However, other class III sempahorins, SEMA3b, SEMA3d, SEMA3 also bind to NRP1[440].

Complex formation between NRP1 and VEGFR2, an imperative unit in facilitating pro-angiogenic signalling, is well defined and discussed in section 1.4.2. However, another peptide has been identified which may bridge or stabilise this complex formation. Endoglin, a vascular endothelial glycoprotein, was found to form complexes with NRP1 and enhance complex formation of NRP1/VEGFR2[355]. The nature of the research in using extracellular tags suggest this interaction is extracellular. Although, it is possible the association is C-terminal and the interaction is detected with N-terminal tags due global conformational changes upon interaction which enable the tags to interact, true for all interaction studies utilising protein tags. The researchers postulate the interaction may be via the MAM domain in ectopic NRP1, however, this was not evaluated further. Another RTK, EGFR, was found to associated with NRP1 in Co-IP experiments under basal conditions via their ECDs[441]. Expression of truncated NRP1 without domains b1/b2, demonstrated this region of the ECD was responsible for complex formation with EGFR.

Consistent with the observations that NRP1 mediates viral entry of SARS-CoV-2 discussed in section 1.4.5.4, direct binding of the S1 spike protein to the b1 ectopic domains has been detected by X-ray crystallography and isothermal titration calorimetry (ITC) via the S1 CendR motif[426]. In the same study, the S1 protein co-immunoprecipitated with NRP1 increasing the confidence of this interaction.

Research utilising a HaloTag epitope fused to the N-terminus of NRP1, and a HaloTag PEG-Biotin ligand provided the most sophisticated analysis of the N-terminal interactome to date[391]. Notable interactions identified in this research include cadherin-5, platelet endothelial cell adhesion molecule (PECAM1, also known as CD31), integrins α_2, α_5 and α_v, ESYT1, reticulon-4 (RTN4), and cytoskeleton-associated protein 4 (CKAP4)[391]. Additionally, the authors elucidate a novel extracellular ligand, a splice variant of tryptophanyl-tRNA synthetase (mini-WARS), which elicits inhibitory effects on NRP1s ability to internalise cadherin-5[391]. In a separate study, NRP1 co-immunoprecipitated with integrin complex $\alpha_5\beta_1$ and the intracellular region appeared dispensable for this interaction, suggesting association via the ectopic domains[340]. The evidence supports NRP1s role in regulating plasticity at adherens junctions, and the interacting partners identified support a proposed role in cellular adhesion.

Further research supported interactions of NRP1 and proteins localised to the adherens junctions. A HRP-based proximity-labelling assay, utilising a horseradish peroxidase (HRP) enzyme incorporated into the N-terminal ectodomain of NRP1, biotinylated proteins in close proximity, allowing elucidation of a potential interaction or complex of NRP1 and either cadherin-5 or catenin delta-1[388]. The authors also performed a proximity-ligation assay (PLA) to demonstrate NRP1 and transforming growth factor beta receptor 2 (TGFβR2) forming a complex, which is modulated by levels of catenin delta-1.

1.4.6.3 C-terminal Binding Interactors

The short intracellular portion of the receptor is historically thought to elicit no recruitment and initiate no direct downstream signalling. The PDZ domain binding motif (SEA) present at the NRP1 C-terminus, provides a potential docking site for interacting proteins. However, few binding partners have been elucidated. One of these, was using chimeric NRP1 receptors, with the extracellular portion substituted with the extracellular region of the EGFR and the transmembrane and cytoplasmic region intact. Interestingly, this chimeric receptor promoted endothelial cell migration in response to EGF[339], which could represent a functional interaction between NRP1 and EGFR.

The most well characterised peptide known to interact with the C-terminus of NRP1 is synectin, a PDZ domain scaffold protein that couples cell-surface receptors to intracellular signaling by binding transmembrane proteins directly or via coreceptors such as neuropilin-1[350]. A two-yeast hybrid model was utilised to discover this interaction, supported by the co-immunoprecipitation of these proteins when transiently expressed in the same cell[328]. Co-immunoprecipitation of these proteins in native murine tissue further reinforced this potential interaction[328]. Similar research demonstrated co-immunoprecipitation of the NRP1 intracellular domain with synectin, and the tyrosine-protein kinase ABL1[350]. The same study observed precipitation of NRP1 and fibronectin (FN1), potentially contributing to NRP1s role in cytoskeletal assembly, consistent with the interaction observed with integrin $\alpha_1\beta_5$ discussed in section 1.4.6.2. In another study, co-precipitation of NRP1 and synectin was again observed likely interacting with the SEA domain of NRP1, in addition to synectin-binding RhoA exchange factor (PKHG5) and p38 mitogen-activated protein kinases (MAPKs), although which specific MAPK was not determined[442]. Interestingly, ablation of the NRP1 SEA domain in which synectin binds to, reduced complex formation between NRP1 and VEGFR2[360]. The authors further characterised synectin-deficient ECs which demonstrated a similar reduction in NRP1/VEGFR2 complex formation, suggesting synectin is important for facilitating this interaction.

A study investigating binding partners of the NRP1 cytoplasmic domain in mouse models elucidated several potential novel interactors. NRP1 is expressed in all vertebrates[318], and human NRP1 shares a 93.17% sequence homology to murine NRP1[443]. The binding partners were identified using Co-IP followed by liquid chromatography mass spectrometry (LC-MS), including variants of myosin heavy chains and filamin-A (FLNA)[397,398], a regulator of focal adhesion turnover[444].

All the techniques mentioned above are indicative of an interaction and provide an inference of binding, rather than direct evidence and also lack temporal sensitivity. The research presented in this project utilises BioID technology which again provides and inference of binding, but has increased temporal capacity compared to the previous methodologies.

Table 1.1 – Observed binding partners with Neuropilin-1 in the literature. *The table details the current research climate regarding potential and known interactors of NRP1. Details regarding interactions identified in Homo sapiens and Mus musculus derived cells/tissues. The method of interaction identification and reference to the research has been detailed. Affinity purification mass spectrometry (AP-MS); Co-immunoprecipitation (Co-IP); enzyme-linked immunosorbent assay (ELISA); fluorescence recovery after photobleaching (FRAP); horse-radish peroxidase proximity-ligation assay (HRP-PLA); isothermal titration calorimetry (ITC); proximity ligation assay (PLA); radioimmunoprecipitation (Radio-IP), surface plasmon resonance (SPR), cross-linking mass spectrometry (XL-MS), X-ray crystallography (XRC).*

Gene Name	Uniprot Identifier	Species	Interaction Assay	DOI
ABCB8	Q9NUT2	*Homo sapiens*	Co-IP	10.1016/j.isci.2018.12.005
Actbl2	Q8BFZ3	*Mus musculus*	AP-MS	10.1242/dmm.019927
Actc1	P68033	*Mus musculus*	AP-MS	10.1242/dmm.019927
Actg1	P63260	*Mus musculus*	AP-MS	10.1242/dmm.019927
Actg1	P63260	*Mus musculus*	AP-MS	10.1242/dmm.019927
AGO2	Q9UKV8	*Homo sapiens*	SPR	0.18632/oncotarget.10929
ALK	Q9UM73	*Homo sapiens*	AP-MS	10.15252/embr.202154041
APP	P05067	*Homo sapiens*	SPR Array	10.3233/JAD-160751
ARRDC1	Q8N5I2	*Homo sapiens*	AP-MS	10.7554/eLife.88328.4
BCAR1	P56945	*Homo sapiens*	Co-IP	10.1016/j.febslet.2013.08.040
BCS1L	Q9Y276	*Homo sapiens*	AP-MS	10.1016/j.cell.2021.04.011
Cald1	E9QA15	*Mus musculus*	AP-MS	10.1242/dmm.019927
CAMKV	Q8NCB2	*Homo sapiens*	AP-MS	10.1016/j.molcel.2020.07.001
Capza1	Q5RKN9	*Mus musculus*	AP-MS	10.1242/dmm.019927
Capza2	P47754	*Mus musculus*	AP-MS	10.1242/dmm.019927
Capzb	P47757	*Mus musculus*	AP-MS	10.1242/dmm.019927
CD63	P08962	*Homo sapiens*	AP-MS	10.1038/s41467-022-31904-1
CD81	P60033	*Homo sapiens*	AP-MS	10.1074/jbc.RA120.014761
CDH5	P33151	*Homo sapiens*	AP-MS HRP-PLA	10.1038/s41467-022-31904-1 10.1126/scisignal.abo4863
CKAP4	Q07065	*Homo sapiens*	AP-MS	10.1038/s41467-022-31904-1
CSNK2A1	P68400	*Homo sapiens*	AP-MS	10.1016/j.cell.2021.04.011
CSNK2A2	P19784	*Homo sapiens*	AP-MS AP-MS AP-MS	10.1038/nmeth.2400 10.1016/j.molcel.2020.07.001 10.1016/j.cell.2021.04.011
CTLA4	P16410	*Homo sapiens*	AP-MS	10.1016/j.cell.2021.04.011
CTNND1	O60716	*Homo sapiens*	HRP-PLA	10.1126/scisignal.abo4863
CXCR4	P61073	*Homo sapiens*	AP-MS	10.1016/j.cell.2021.04.011
DYNC2H1	Q8NCM8	*Homo sapiens*	AP-MS	10.1016/j.febslet.2013.08.040
ECE1	P42892	*Homo sapiens*	AP-MS	10.1038/s41467-022-31904-1
EDNRB	P24530	*Homo sapiens*	AP-MS	10.1038/nature22366
EEF1A1	P68104	*Homo sapiens*	AP-MS	10.1016/j.febslet.2013.08.040
ENG	P17813	*Homo sapiens*	FRAP	10.1038/s42003-024-05798-2
ENO1	P06733	*Homo sapiens*	AP-MS	10.1016/j.febslet.2013.08.040
EPHA2	P29317	*Homo sapiens*	AP-MS	10.1038/s41467-022-31904-1
ESYT1	Q9BSJ8	*Homo sapiens*	AP-MS	10.1038/s41467-022-31904-1
EVA1B	Q9NVM1	*Homo sapiens*	AP-MS	10.1016/j.cell.2021.04.011
EVA1C	P58658	*Homo sapiens*	AP-MS	10.1016/j.cell.2021.04.011

FAM241A	Q8N8J7	*Homo sapiens*	AP-MS	10.1016/j.cell.2021.04.011
Flii	Q9JJ28	*Mus musculus*	AP-MS	10.1242/dmm.019927
FLNA	P21333	*Mus musculus*	SPR, AP-MS AP-MS	10.1016/j.febslet.2013.08.040 10.1242/dmm.019927
FINC	P02751	*Homo sapiens*	Co-IP	10.1158/0008-5472.CAN-11-3907
FZD10	Q9ULW2	*Homo sapiens*	AP-MS	10.1038/nature22366
GINM1	Q9NU53	*Homo sapiens*	AP-MS	10.1038/nature22366
GIPC	O14908	*Homo sapiens*	Yeast-two hybrid, Co-IP Co-IP	10.1523/JNEUROSCI.19-15-06519.1999 10.1002/mc.22943
Gpr158	Q8C419	*Mus musculus*	AP-MS	10.1016/j.celrep.2018.08.068
GPR183	P32249	*Homo sapiens*	AP-MS	10.1016/j.cell.2021.04.011
HADHA	P40939	*Homo sapiens*	AP-MS	10.1016/j.cell.2021.04.011
HLA-C	P10321	*Homo sapiens*	AP-MS	10.1038/s41467-022-31904-1
ICAM2	P13598	*Homo sapiens*	AP-MS	10.1038/nature22366
IL27RA	Q6UWB1	*Homo sapiens*	AP-MS	10.1038/nature22366
ITGA2	P17301	*Homo sapiens*	AP-MS	10.1038/s41467-022-31904-1
ITGA5	P08648	*Homo sapiens*	Co-IP AP-MS	10.1371/journal.pbio.1000025 10.1038/s41467-022-31904-1
ITGAV	P06756	*Homo sapiens*	AP-MS	10.1038/s41467-022-31904-1
ITGB1	P05556	*Homo sapiens*	Co-IP	10.4161/cbt.6.8.4363
KCTD10	Q9H3F6	*Homo sapiens*	AP-MS	10.1016/j.cell.2021.04.011
KCTD9	Q7L273	*Homo sapiens*	AP-MS	10.1016/j.cell.2021.04.011
LAMP1	P11279	*Homo sapiens*	AP-MS	10.1038/s41467-022-31904-1
LAMP2	P13473	*Homo sapiens*	AP-MS	10.1038/s41467-022-31904-1
LIPG	Q9Y5X9	*Homo sapiens*	AP-MS	10.1016/j.cell.2021.04.011
LRRTM4	Q86VH4	*Homo sapiens*	AP-MS	10.1016/j.cell.2021.04.011
MCAM	P43121	*Homo sapiens*	AP-MS	10.1038/s41467-022-31904-1
Mecom	P14404	*Mus musculus*	AP-MS	10.1093/nar/gky1192
MYH10	P35580	*Mus musculus*	AP-MS AP-MS	10.1016/j.febslet.2013.08.040 10.1242/dmm.019927
Myh14	Q6URW6	*Mus musculus*	AP-MS	10.1242/dmm.019927
MYH9	P35579	*Mus musculus*	AP-MS AP-MS	10.1016/j.febslet.2013.08.040 10.1242/dmm.019927
Myo18a	Q9JMH9	*Mus musculus*	AP-MS	10.1242/dmm.019927
Myo1b	P46735	*Mus musculus*	AP-MS	10.1242/dmm.019927
Myo1c	Q9WTI7	*Mus musculus*	AP-MS	10.1242/dmm.019927
Myo1e	E9Q634	*Mus musculus*	AP-MS	10.1242/dmm.019927
NCL	P19338	*Homo sapiens*	XL-MS	10.1074/mcp.RA118.000924
NSUN2	Q08J23	*Homo sapiens*	AP-MS	10.1016/j.cell.2021.04.011
ODF2	Q5BJF6	*Homo sapiens*	AP-MS	10.1016/j.cell.2021.04.011
OR10H1	Q9Y4A9	*Homo sapiens*	AP-MS	10.1016/j.cell.2021.04.011
P38 MAPKs	n/a	*Homo sapiens*	Co-IP	10.1002/mc.22943
PDPK1	O15530	*Homo sapiens*	AP-MS	10.1016/j.cell.2021.04.011
PDS5A	Q29RF7	*Homo sapiens*	AP-MS	10.1016/j.cell.2021.04.011
PECAM1	P16284	*Homo sapiens*	AP-MS	10.1038/s41467-022-31904-1
PIP5K1A	Q99755	*Homo sapiens*	AP-MS	10.1038/nature22366

Plec	Q9QXS1	*Mus musculus*	AP-MS	10.1242/dmm.019927
PLEKHG5	O94827	*Homo sapiens*	Co-IP	10.1002/mc.22943
PLXNA2	O75051	*Homo sapiens*	Co-IP	10.1371/journal.pbio.1000041
RAB7A	P51149	*Homo sapiens*	Co-IP	10.1172/JCI75371
RFTN1	Q14699	*Homo sapiens*	Co-IP	10.1007/s10456-020-09715-z
RPL27	P61353	*Homo sapiens*	Yeast-two hybrid	10.1038/msb.2011.67
RTN4	Q9NQC3	*Homo sapiens*	AP-MS	10.1038/s41467-022-31904-1
RYK	P34925	*Homo sapiens*	AP-MS	10.1016/j.cell.2021.04.011
S	P0DTC2	*SARS-CoV-2*	Co-IP, ITC, XRC	10.1126/science.abd3072
Sptan1	P16546	*Mus musculus*	AP-MS	10.1242/dmm.019927
ST8SIA4	Q92187	*Homo sapiens*	AP-MS	10.1038/nature22366
TAFA4	Q96LR4	*Homo sapiens*	AP-MS	10.1016/j.cell.2021.04.011
TGFBR2	P37173	*Homo sapiens*	PLA	10.1126/scisignal.abo4863
TLK2	P01375	*Homo sapiens*	AP-MS	10.1016/j.xgen.2022.100250
TMEM116	Q8NCL8	*Homo sapiens*	AP-MS	10.1016/j.cell.2021.04.011
Tmod3	Q9JHJ0	*Mus musculus*	AP-MS	10.1242/dmm.019927
TMPRSS11B	Q86T26	*Homo sapiens*	AP-MS	10.1016/j.cell.2021.04.011
TMX1	Q9H3N1	*Homo sapiens*	AP-MS	10.1016/j.cell.2021.04.011
TNF	Q86UE8	*Homo sapiens*	AP-MS	10.1038/nature22366
TNFAIP1	Q13829	*Homo sapiens*	AP-MS	10.1016/j.cell.2021.04.011
Tpm1	P58771	*Mus musculus*	AP-MS	10.1242/dmm.019927
Tpm3	P21107	*Mus musculus*	AP-MS	10.1242/dmm.019927
Tpm4	Q6IRU2	*Mus musculus*	AP-MS	10.1242/dmm.019927
Tuba1b	P05213	*Mus musculus*	AP-MS	10.1242/dmm.019927
UBR1	Q8IWV7	*Homo sapiens*	AP-MS	10.1016/j.cell.2021.04.011
UBR2	Q8IWV8	*Homo sapiens*	AP-MS	10.1016/j.cell.2021.04.011
UBR4	Q5T4S7	*Homo sapiens*	AP-MS	10.1016/j.cell.2021.04.011
VAMP2	P63027	*Homo sapiens*	Co-IP	10.1083/jcb.201106113
VEGF-A	P15692	*Homo sapiens*	Co-IP ELISA	10.1038/sj.emboj.7601188 10.1016/j.ccr.2006.10.018
VEGFR1	P17948	*Homo sapiens*	Co-IP ELISA	10.1016/j.cell.2013.01.036 10.1016/S0021-9258(19)61431-6
VEGFR2	P35968	*Homo sapiens*	Radio-IP Co-IP Co-IP	10.1074/jbc.M102315200 10.1038/sj.emboj.7601188 10.1016/j.ccr.2006.10.018
WARS2 isoform	n/a	*Homo sapiens*	AP-MS	10.1038/s41467-022-31904-1

1.5 BioID Technology

The project aims to further investigate the interactomes of receptors involved in angiogenesis using BioID technology, which incorporates a mutated biotin ligase enzyme (BirA) fused to a protein of interest. When fused to a protein of interest, the mutated form acts as a promiscuous biotin ligase, capable of covalently attaching biotin molecules to proteins in close proximity (around 10-20nm) of the protein of interest, (Figure 1.14)[445,446]. The original BioID tag was herein termed BioID1. As biotinylation of proteins is a rare modification in mammalian cells, these interacting partners may be isolated and identified using mass spectrometry[445,446]. Since the development of the original BirA, several advances have been made in proximity-based biotinylation technology. A newer variant of the biotin ligase, known as BioID2 (25 kDa), has been developed which is roughly a third smaller in size and has an equal or greater efficiency in biotinylating proximate proteins than the original BirA (35 kDa), resulting in more interactors identified[447,448]. More recently, even smaller versions of BioID with quicker biotinylation capabilities are emerging with ultraID an exciting BioID variant [449]. The research in this PhD project will exploit BioID to map the extra- and intracellular interactomes of the VEGFRs and NRPs homo- and heterodimeric complexes.

1.5.1 Benefits of BioID Compared to Conventional Protein-Protein Interaction Techniques

BioID technology has several advantages compared to conventional protein-protein interaction techniques. Firstly, BioID is effective for interactome studies concerning insoluble and membrane-bound proteins, which due to their insoluble nature may be refractory or more difficult to screen using conventional approaches such as co-immunoprecipitation (Co-IP)[450]. Similarly, BioID does not require the use of antibodies essential for techniques such as Co-IP, therefore there are no false-positives due to non-specific antibody binding[451]. With BioID technology the interactome is investigated over a period of time, enabling the detection of dynamic weak or transient interactions[445] which would be missed with a method like Co-IP, which provides a static snapshot of the protein landscape at the point of immobilisation. These transient or weak interactions may be disrupted during the harsh conditions during Co-IP. Additionally, BioID enables interactome screening in a natural cellular setting, unlike in other PPI techniques such as yeast-two hybrid experiments[452] and surface plasmon resonance (SPR), which consists of protein fragments adsorbed to a surface[453].

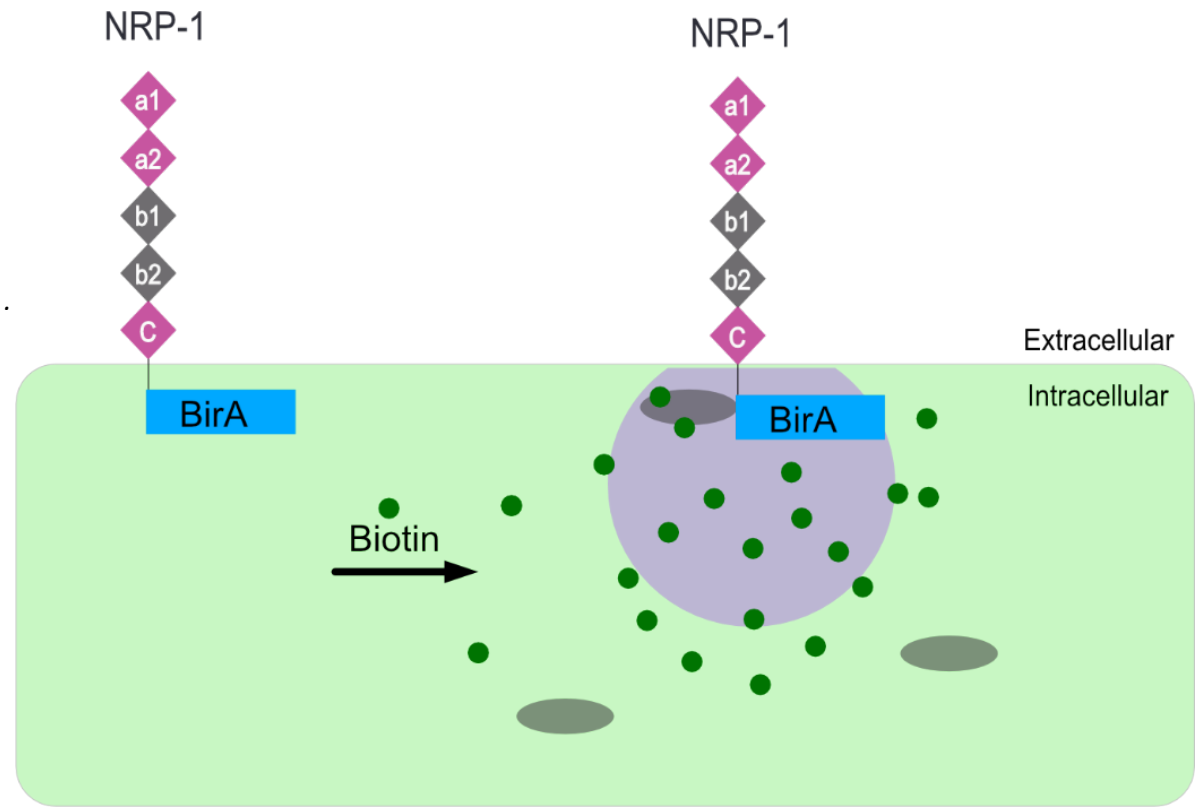

Figure 1.14 – Principles of using BioID technology to identify novel interactors with NRP1. *The biotin ligase (BirA) has the propensity to attach biotin molecules covalently to proteins within close proximity (10-12nm) when exogenous biotin is introduced. As this is a rare modification in mammalian cells, these biotinylated proteins may be isolated and identified.*

1.6 NanoBRET

The hits identified using BioID will then be validated using nanoBRET technology. Bioluminescence resonance energy transfer (BRET) is a proximity-based technique used to investigate protein-protein interactions in live cells. A nano luciferase (NanoLuc) enzyme, which catalyses a substrate resulting in bioluminescent acts as a donor, which transfers energy when in close proximity (<10nm) and correct orientation to an acceptor fluorophore upon addition of substrate furimazine, (Figure 1.15)[454,455]. The light emission wavelengths of the NanoLuc bioluminescence and the fluorophore overlap, which enables BRET to occur. The transferred energy excites the fluorophore resulting in light emission at a different wavelength from the bioluminescence of the NanoLuc. The NanoLuc emission is blue-shifted, whereas the HaloTag fluorophore is green- or red-shifted[456]. Fusing the NanoLuc to a receptor of interest, for example NRP1, and a known or suspected interactor fused to a fluorophore supports the idea a specific protein-protein interaction is occurring. Fusing the C terminus of NRP1 to NanoLuc allowed the validation of interacting proteins identified using BioID, in living cells using a technique with comparable proximity sensitivity. BRET compliments BioID, by providing another technique to

support evidence of interactions identified in the BioID hits and enables interactions to be monitored in real time in live cells.

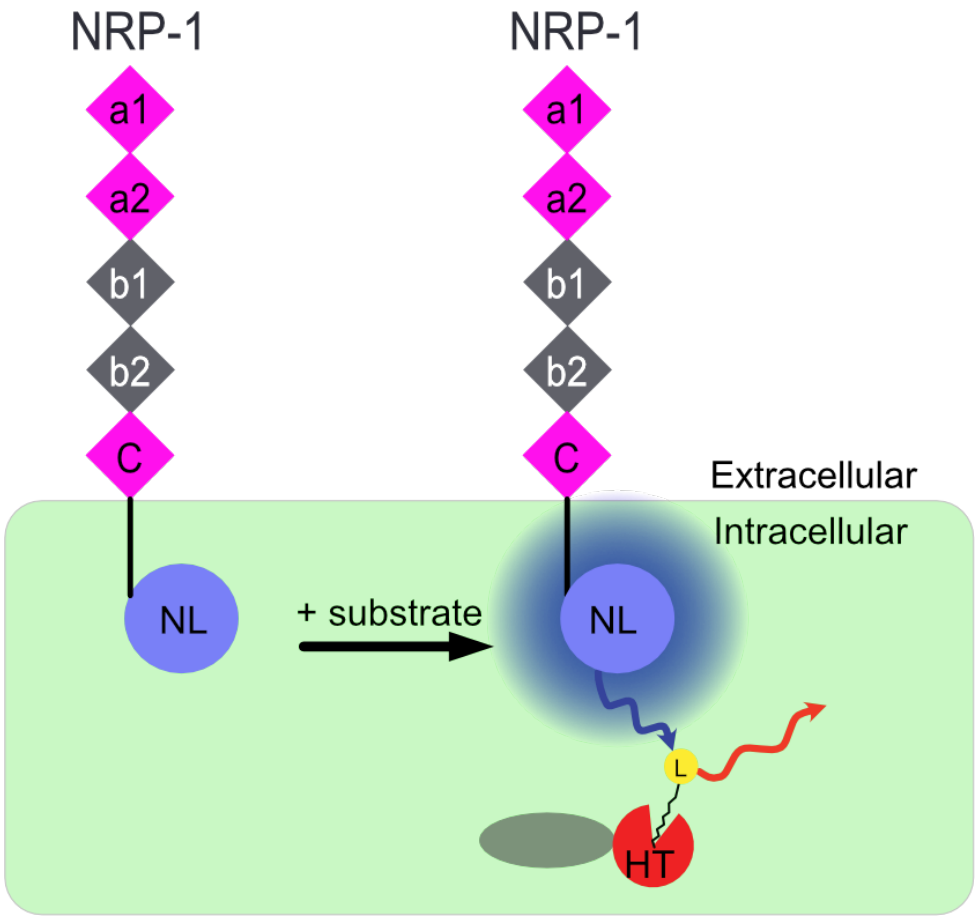

Figure 1.15 – Principles of NanoBRET. *A nano luciferase (NanoLuc) acts as the energy donor and is fused to a protein of interest, in this case NRP1. A suspected interactor of NRP1, identified in the BioID analyses, is conjugated to a HaloTag, capable of binding a HaloTag ligand fluorophore acting as the energy acceptor. Upon the addition of the NanoLuc substrate furimazine, blue-shifted bioluminescence occurs, resulting in energy transfer to the fluorophore in close proximity (<10nm). The energy transfer excites the fluorophore resulting in the emission of a higher wavelength light (typically green- or red-shifted). A ratio between these wavelengths is then calculated.*

1.7 Thesis Aims

As described in this chapter, NRP1 appears to have a complex role in a multitude of biological processes. While recent research has investigated potential NRP1 interactors, the majority have used an affinity-purification mass spectrometry approach (AP-MS) following co-immunoprecipitation (Co-IP) of NRP1. While this is valuable, it may lack the capability to elucidate specific interactors of NRP1. Co-IP experiments are a snapshot of what is currently bound to the protein of interest, and transiently bound proteins may be lost during processing. Utilisation of BioID technology enables the

identification of transient interactors, and interactions occurring over a period of time, rather than what is immediately bound. This may elucidate interactions during specific conditions, such as during cellular division or following stimulation with ligands.

Chapter 3 aimed to evaluate and generate the tool used for this research, including the generation of VEGFRs and NRPs fused to the BirA ligase for use in BioID experiments. Following generation of these plasmid constructs, those most suitable for these experiments were determined, as the addition of a protein tag may adversely affect localisation and dynamics of the receptor. From these experiments it was determined that NRP-1 was the most suitable candidate for further investigation.

Chapter 4 describes the use of NRP constructs, evaluating N- and C-terminally fused constructs in the BioID methodology performed in HEK293T cells. This chapter includes optimisation of the BioID protocol and optimisation of the bioinformatic processing of the raw mass spectroscopy files. Here, potential novel interactors of NRP1 were observed for the first time, providing molecular mechanisms for the various biological processes NRP1 appears to be involved in and inferring potentially novel involvement of NRP1 in other biological processes.

Chapter 5 describes how the BioID protein hits were validated via another protein-protein interaction technique. NanoBRET technology was used to characterise a select panel of identified interactors of NRP1 in real time in living cells.

Chapter 6 further investigates NRP1 interactors, in TERT2-HUVECs, an environment more comparable to the endogenous environment where NRP1 is expressed, when compared to HEK293T cells.

Chapter 2: General Materials and Methods

2.1 Molecular Biology

2.1.1 Reagents and Buffers

Luria Bertani (LB) Lennox Broth

Luria Bertani (LB) Lennox Broth is a nutritionally rich medium containing amino acids, vitamins, trace elements and minerals in a low salt formulation and is primarily used for the culturing and propagation of bacterial cells. To prepare Lennox-LB Broth, Lennox-LB Broth powder (ThermoFisher) was dissolved in ddH_2O at 2%w/v. Following dissolution, the LB broth was autoclaved until sterile. At 2%w/v, Lennox-LB Broth powder (ThermoFisher) contains SELECT Peptone 140 (10g/L), SELECT Yeast Extract (5g/L) and NaCl (5g/L). For antibiotic addition to Lennox-LB Broth, the antibiotic was added following autoclaving and cooling of the broth to RT and used at 0.1% v/v for ampicillin (Gibco; 10790224) and 0.03% v/v for kanamycin (Gibco; 11588676).

For initial culturing of transformed bacterial cells, Sterilin™ 90mm petri dishes (Thermo Fisher; 101R20) containing 20mL of Lennox-LB with agar (Invitrogen; 22700025) was used. To prepare, the Lennox-LB-agar was dissolved in ultrapure water to a final concentration of 3.5% w/v, followed by autoclaving until sterile. The molten Lennox-LB agarose was cooled and either ampicillin (Gibco; 10790224) was added at 0.1% v/v or kanamycin (Gibco; 11588676) at 0.03% v/v to the still molten, cooled culture medium. Adding the antibiotic while the solution is too hot, may denature the antibiotic, rendering it ineffectual. This formulation contained 5g/L agarose, meaning the molten Lennox-LB agarose solution solidified at RT. After pouring the molten Lennox-LB agarose and antibiotic solution into 90mm petri dishes, they were cooled at RT and used the same day for bacterial transformations or stored at 4°C prior to use.

Tris-acetate-EDTA (TAE)

Tris-acetate-EDTA (TAE) buffer was used for DNA gel electrophoresis as a running buffer and to prepare agarose gels. The buffer was made up to a 50x concentration consisting of; 242g Trizma base powder (Sigma-Aldrich; T1503); 57.1mL glacial acetic acid (Sigma-Aldrich; A6283); 100mL 500mM EDTA (Sigma-Aldrich; E4884); up to 1L with ultrapure H_2O. The 50x solution was diluted prior to use to the correct working concentration of; 40mM Trizma pH 8.3; 20mM acetic acid; 1mM EDTA.

Polymerase Chain Reaction (PCR); Restriction Enzyme Digestion; Ligation Buffers

For buffers related to molecular biology techniques including; polymerase chain reaction (PCR), restriction enzyme digestion, ligation of DNA, buffers supplied by the manufacturer of the enzymes were used. For PCR, the Pfu DNA Polymerase 10x Reaction Buffer (Promega Corporation; M776A) was

used. The buffer for all restriction enzyme digestions performed was the rCutSmart Buffer (New England Biolabs (NEB); B6004S). Ligations were performed in the proprietary T4 DNA Ligase Reaction Buffer (NEB; B0202S).

2.1.2 Polymerase Chain Reaction (PCR)

The polymerase chain reaction (PCR) is a technique used to amplify specific regions of DNA facilitated by a DNA polymerase enzyme in an environment containing free nucleic acids[457]. In order to amplify a specific region, complimentary primers are required, which bind to the sequence of DNA requiring amplification. Two primers are usually required, one for the 3'- end and one for the 5'- end of the DNA amplification region. Rigorous design of these primers is essential for a successful PCR. For appropriate primer stability, a GC content of 40-60% is recommended, as these bases form strong hydrogen bonds which bind to the specific DNA sequence. Additionally, having 2 G or C bases in the last 5 bases of the primer sequence promotes specific binding of the primer, this is known as the GC clamp[458]. Primers were designed using SnapGene software (www.snapgene.com), in which the annealing temperature (Tm) of the primers were calculated. All PCRs were performed using bespoke primers manufactured by Sigma-Aldrich, Table 2.1. Pfu polymerase (Promega Corporation; M7741) was used to amplify appropriate regions of DNA using the Mastercycler (Eppendorf) or Mastercycler Gradient (Eppendorf) PCR thermal cycler. Amplifications were performed in a 50 µL reaction volume consisting of; 5 µL Pfu buffer (Promega Corporation; M776A), 10mM dNTPs (Promega Corporation; U1330), 0.25mM-1mM forward primer (Sigma-Aldrich), 0.25mM-1mM reverse primer (Sigma-Aldrich), 20-50ng template DNA, in certain cases 2.5% DMSO (Thermo Scientific; 10761731) was added, and the final volume was made up to 50 µL using nuclease-free water (Promega Corporation; MC1191). DMSO aids in melting template DNA and promotes proper primer annealing, thereby improving specificity and efficiency of DNA amplification[459]. The initial denaturation temperature was set at 95°C for 1.5 minutes, followed by; 28-32 cycles of denaturation at 95°C for 1 minute; annealing temperature between 52-65°C for 30 seconds depending on the PCR reaction; extension at 72°C for 2-4 minutes; and a final extension of 72°C for 10 minutes. Following PCR, the amplified DNA was purified using the Wizard SV Gel and PCR Clean-Up System (Promega Corporation; A9281), following the protocol supplied. The PCR was evaluated using DNA gel electrophoresis to confirm amplification of the expected PCR product size. For molecular cloning downstream of PCR, DNA gel bands were excised and purified using the Wizard SV Gel and PCR Clean-Up System (Promega Corporation; A9281).

Table 2.1 – Sequence of oligos used in the PCR of mycBioID2, BioID2-HA and VEGFR3. *Oligos employed in cloning of BioID and NanoBRET plasmids. Each PCR primer contains a sequence encoding for a restriction enzyme, which enabled editing of double stranded DNA to facilitate molecular cloning.*

PCR Product	Purpose of PCR Product	Sequence	Restriction Enzyme
mycBioID2	BioID2-NRP1 Cloning BioID2-VEGFR2 Cloning	Fwd 5' - gaaccgcgggcagaacaaaaactcatctcagaagaggatctcgac Rev 5' - gcactcgaggcttcttctcaggctgaa	SacII XhoI
mycBioID2	BioID2-VEGFR3 Cloning	Fwd 5' - gaaccgcggatggaacaaaaactcatctcagaagaggatctc Rev 5' - gaacgatcgaacgctcgaggcttcttctcagg	SacII XhoI
VEGFR3	NanoLuc-VEGFR3 Cloning HaloTag-VEGFR3 Cloning	Fwd 5'- atagctcgatcgcatactccatgacccccccgaccttg Rev 5'- aatggttctagagctgcttagtagctgttgtctgtgaagaaagtca	PuvI XbaI
BioID2-HA	NRP1-BioID2 Cloning VEGFR2-BioID2 Cloning VEGFR3-BioID2 Cloning	Fwd 5' - gcattactcgagattcaagaacctgatctggctgaag Rev 5' - gcattctctagactatgcgtaatccggtacatcg	XhoI XbaI

2.1.3 Restriction Enzyme Digestion

In order to resect and insert the desired amplicons, endonuclease enzymes were used which enables editing of specific sequences of DNA. Endonuclease enzymes are used in DNA digestion to cleave double stranded DNA between specific base pairs, which the enzyme can recognise[460]. The cleaved, double stranded DNA harbours overhanging base pairs, in which a DNA fragment with complimentary overhanging base pairs can be fused to, allowing DNA to be inserted into this region. Thus, the restriction enzyme digestion reaction formed the basis of editing the plasmid DNA when generating the constructs. Restriction enzyme digestions were performed in a 50 µL reaction consisting of 1-3 µg of DNA with an excess of restriction enzyme between 20-60 units per enzyme, in the presence of rCutSmart Buffer (NEB; B6004S). Plasmid digestion was confirmed by DNA gel electrophoresis. Heat inactivation of the enzymes was not required, as the enzymes were removed following DNA gel electrophoresis and excision of the DNA bands.

2.1.4 Agarose Gel Electrophoresis

DNA gel electrophoresis was performed to determine the success of these reactions and to further purify the desired DNA fragments. Agarose gel electrophoresis is the most effective method of separating DNA fragments between 100bp-25,000bp[461]. Agarose is a product derived from seaweed consisting of repeating heteropolysaccharide subunits. Heat is required for dissolution into aqueous buffer and upon cooling, gelation occurs in which agarose polymers associate non-covalently to form a network of fibres which operate as a molecular sieve, allowing separation of DNA strands based on size[461]. As the phosphate backbone of the DNA molecule is negatively charged, when an electric field

is applied across the gel, the DNA molecules migrate towards the positively charged anode. To prepare the agarose gels, dissolving agarose gel powder (Sigma-Aldrich; A9539) was added to Tris-acetate-EDTA (TAE) buffer (40mM Tris-acetate pH 8.3; 20mM acetic acid; 1mM EDTA). The agarose gel powder and TAE suspension was heated in a microwave until dissolution of the powder, resulting in a clear liquid. Depending on the number of samples to analyse, the volume of gel prepared was either 50mL using the smaller gel tank or 100mL when using a larger gel tank, capable of analysing a greater number of samples. Agarose gel concentrations varied based on the purpose of the experiment. For PCR reactions, agarose gel was made at 1%. If the DNA fragments were to be extracted via gel purification, a 0.75% gel was used as higher concentrations of agarose resulted in a diminished yield of purified DNA. The molten agarose gel was cooled, before the addition of ethidium bromide (EtBr) (SLS; E8751-5G) to 4% v/v. EtBr is a fluorescent dye used in molecular biology for the visualisation of nucleic acids and binds by intercalation between base pairs[462]. When EtBr is exposed to ultra-violet (UV) light fluorescence occurs meaning the DNA-EtBr complex can be visualised and a DNA banding patter is observed. The cooled, molten agarose gel was then poured into an appropriately sized UV-resistant gel casting tray, sealed at both ends and with a gel comb inserted at one end which forms the sample loading wells. The gel was allowed to cool further for 20-30 minutes at RT to solidify before use. The gel with the UV-resistant gel casting tray was then inserted into the Mini-Sub GT Cell Electrophoresis System (Bio-Rad; 1704406) for 50mL agarose gels or the Wide Mini-Sub Cell GT Electrophoresis System (Bio-Rad; 1704405) for 100mL agarose gels, with both gel tanks attached to a PowerPac (Bio-Rad; 1645050) for regulating voltage across the gels. TAE buffer was added to the gel tanks in order to completely submerge the gel. Samples were prepared by adding Gel Loading Dye, Purple (New England Biolabs; B7024S) at 10% v/v, which contains EDTA to arrest enzymatic reactions and glycerol to facilitate settling of sample in the agarose gel wells. A 1kbp DNA ladder (Promega Corporation; G5711) was used in all agarose gels as a size reference tool for comparison with DNA present in the samples. Depending on the type of experiment performed, the running conditions of the electrophoresis varied. For analysis of DNA following a PCR reaction, the running conditions were 90-110V for 35-45 minutes. For molecular cloning, gels were run at 70-80V for 60-80 minutes. The lower voltages used in the latter resulted in more compact DNA bands, allowing for a greater yield following DNA gel purification. For visualization of the DNA bands the agarose gel was exposed to UV light, using a GelVue UV Transilluminator (Syngene; GVM30) for excision of DNA gel bands. To capture images of UV-illuminated DNA gels, a Geneflash Gel Imaging System (Syngene) was used.

2.1.5 Gel Extractions and Purification

For downstream molecular cloning reactions, the DNA fragments in the agarose gel required isolation. Following visualization of the DNA using UV light, excision of the DNA bands was performed using a

scalpel, cutting as close to the band as possible to minimise excess agarose. The band was cut out rapidly to avoid excess exposure of DNA to UV light, which may damage the DNA causing issues in downstream cloning reactions. The gel slice containing the desired DNA product was stored in a pre-weighed 1.5mL microcentrifuge tube prior to purification. The purification removed any unwanted reagents from the reaction which may interfere with downstream processing such as; nucleotides, primers, enzymes, buffers, and undesirable fragments of DNA. The Wizard SV Gel and PCR Clean-Up System (Promega Corporation; A9281) was used to isolate the DNA fragments from the agarose gel matrix according to the protocol of the kit, using microcentrifugation to pass the DNA through the DNA binding column and for subsequent washes and elution. This DNA extraction kit utilises silica membranes in the DNA binding column, in which DNA adsorbs to the surface of these membranes in the presence of a chaotropic salt, in this case guanidine isothiocyanate in the membrane binding solution[463]. The negatively charged DNA backbone binds with high affinity to the positively charged silica particles in the membrane[464]. Following initial binding of DNA, the membranes are washed with a salt/ethanol solution, which removes contaminating proteins, carbohydrates and small RNA molecules while keeping the DNA tightly bound. The DNA is then eluted from the column under low-salt conditions, using nuclease-free water (Promega Corporation; MC1191), which yields 90-95% of the DNA bound to the silica membrane[464]. A deviation from the protocol is that the dissolved gel slice was passed through a binding column three times prior to washing and elution, allowing retrieval of a higher yield. The nuclease-free water (Promega Corporation; MC1191) was also heated to 50°C for increased efficiency of DNA dissociation from the binding column.

2.1.6 DNA Quantification

Concentration of DNA fragments and plasmids were quantified, and their purity assessed, based on their absorbances of various wavelengths of light using a microvolume UV-Vis spectrophotometer (DeNovix DS-11 Series). 1 µL nuclease-free water (Promega Corporation; MC1191) was used as a blank, with the absorbance of 1 µL of the samples measured against the blank. Nucleic acid concentration is commonly measured by the absorbance of light at a wavelength of 260 nm[465]. Contaminants can be estimated by looking at the absorbance at 280 nm or 230 nm and calculating the ratios of these with the 260 nm absorbance. For the 260/280 ratio, a ratio of around 1.8 or higher was considered a pure sample, with large deviations to this number indicating the presence of contaminants such as protein or phenol[466]. For the 260/230 ratio, a value between 2.0 and 2.2 is considered pure, with a value outside of this range indicating the presence of other contaminants such as proteins, EDTA, carbohydrates, lipids, salts, or phenol. For samples with a concentration below 50 ng/uL, the 260/280 and 260/230 ratios are unreliable hence, if these samples exhibited ratios outside of the permitted range they were still used for downstream processes.

2.1.7 Ligation Reactions

Double stranded DNA inserts were ligated into the destination vector using DNA T4 ligase (New England Biolabs; M0202S). This ligase catalyses the formation of phosphodiester bonds between adjacent 5'-PO_4 and 3'-OH group of two DNA fragments, thus fusing complimentary regions between a DNA insert and plasmid backbone[467]. The ligation reactions were prepared on ice, in a reaction volume of 10uL, which consisted of; 400 units T4 DNA ligase (NEB; M0202S); 1 µL of 10x T4 ligase buffer (NEB; B0202S); varying concentrations of DNA fragment inserts and DNA plasmid backbone; made up to 10 µL using nuclease-free water (Promega Corporation; MC1191). Depending on the size of the DNA fragments and plasmid backbones, and the yield of purified DNA fragments, varying molar ratios of plasmid backbone:insert between 1:3 and 1:20 were used. To calculate the amount of DNA required for the appropriate molar ratios, an online ligation tool created by New England Biolabs (NEB) was used (https://nebiocalculator.neb.com/#!/ligation). Parallel ligation reactions were set up, with different conditions, in order to maximise the success of molecular cloning in one experiment. Ligations were performed at both RT for 2 hours and 16°C for 16 hours using a Biometra TRIO heat block. The T4 DNA ligase was inactivated at 65°C for 10 minutes following culmination of the ligation reactions. The reactions were cooled to RT prior to further processing.

2.1.8 Bacterial Transformation

Bacterial transformation is an invaluable tool in producing large quantities of plasmid DNA in a quick and inexpensive manner[468]. The transformations in this project were performed using chemically competent bacterial strains, meaning a chemical compound, $CaCl_2$, was utilised to weaken the bacterial cell membranes which results in easier passage of the plasmid into the bacterial cells[469]. The Ca^{2+} cations bind to negatively charged components of the bacterial cell membrane, such as phosphate groups, which enables binding of negatively charged plasmid DNA. For translocation of plasmid DNA into the bacterial cell, a heat shock step is required, which increases the Brownian motion of molecules in the membrane, likely forcing the plasmid DNA inside the bacterial cell[470]. A significant portion of the bacterial will have not been transformed and do not contain the plasmid DNA, therefore the bacteria require selection and culturing for downstream applications. To do this, the bacterial cells are plated on growth medium containing a relevant antibiotic, determined by the bacterial resistance cassette harboured within the plasmid. Lennox-LB broth, see section 2.1.1, enabled efficient growth of bacterial cells, hence, using a formulation containing agarose allows a solid medium for cells to grow in. Lennox-LB agarose (Invitrogen; 22700025) provides such a medium.

For bacterial transformations following ligation during molecular cloning, 5-10 µL of ligation reaction was incubated with the Subcloning Efficiency DH5α Chemically Competent *E. Coli* (Invitrogen;

11583117) cells. For verified plasmid DNA, 0.5-2 µL of plasmid DNA was used for bacterial transformation, depending on the concentration of the plasmid sample. In each case, the DNA and chemically competent bacterial cells were incubated on ice for 30 minutes, followed by a heat shock at 42°C for 30 seconds, and a further 5-minute incubation on ice. Following heat shock, 250 µL of Luria Bertani broth was added to the DNA and *E. Coli* mixture and incubated at 37°C/225rpm for 1h-1.5h in a Stuart SI600 orbital shaker (TEquipment; 79520-16). All the transformed competent *E. Coli* cell suspension was spread on the prepared Lennox-LB agarose (Invitrogen; 22700025) Sterilin™ 90mm petri dishes (Thermo Fisher; 101R20), which contained either; ampicillin (Gibco; 10790224) at a final concentration of 0.1% v/v for HaloTag and BioID containing plasmids; or kanamycin (Gibco; 11588676) at 0.03% v/v for NanoLuciferase containing constructs. The plates were incubated upside down to prevent condensation forming on the lids of the plates at 37°C overnight. Successful bacterial transformation was indicated by the presence of individual bacterial colonies, with the plates sealed and stored at 4°C for no more than 4 weeks. Plates stored for longer than this period were not used for downstream applications and subsequently disposed of.

2.1.9 DNA Mini- and Maxipreps

A single bacterial colony, arising from one transformed *E. coli* cell, was chosen from the Lennox-LB agarose petri dish for further culturing on a larger scale. The culturing of the transformed *E. Coli* enables production of large quantities of plasmid DNA in the replicating bacteria, which is then harvested and purified. The single *E. Coli* colony was cultured at 37°C/225rpm overnight in a Stuart SI600 orbital shaker (TEquipment; 79520-16) with either 200mL of Luria Bertani (LB) Lennox Broth for maxipreps, or 5mL LB broth for Minipreps both supplemented with either ampicillin or kanamycin, depending on the bacterial resistance cassette within the plasmid. Following incubation, the plasmid DNA was extracted from the bacterial cells via a modified alkaline lysis method using either the PureYield™ Plasmid Maxiprep System (Promega Corporation; A2392) or the ZymoPURE II Plasmid Maxiprep Kit (Cambridge BioScience; D4203). Initially, centrifugation was required for both kits, in order to pellet the bacterial cells and remove any remaining LB Lennox Broth. The 200mL cultures for maxipreps were pelleted at 5'000 *x g* for 20 minutes at 4°C, with the supernatant discarded and the resulting pellet resuspended in a buffer containing EDTA, which inhibits DNase activity and destabilises the bacterial membranes[471] as well as chelating divalent cations such as Mg^{2+} and Ca^{2+} required for endonucleases to cleave the phosphodiester backbone of DNA[472], thus protecting the plasmid DNA. The alkaline lysis buffer utilises SDS to solubilise the bacterial cell membranes and proteins and NaOH, which degrades the membranes by disrupting fatty acid-glycerol ester bonds[473]. The NaOH additionally disrupts the hydrogen bonds between DNA bases, denaturing the double stranded genomic and plasmid DNA into single strands[474]. Gentle mixing of the resuspended *E. Coli* and the alkaline lysis

buffer is required, as vigorous mixing may shear bacterial genomic DNA which may be co-purified with the plasmid, contaminating the final preparation. Addition of the neutralisation buffer causes the bacterial genomic DNA to renature and aggregate to form an insoluble network along with precipitated proteins and high molecular weight RNA[475], while the renatured plasmid DNA remains in solution. The aqueous phase containing the plasmid DNA is then separated from the insoluble mass of contaminants via filtration using a Vac-Man vacuum manifold system (Promega Corporation; A7231). The solution is then introduced to a silica-based matrix or membrane in which the DNA binds to, as detailed in section 2.1.5. A salt/ethanol buffer was used to wash the DNA bound to the membrane, in order to remove contaminants such as proteins, carbohydrates and small RNA molecules[464]. As the plasmid has been propagated in bacteria, an additional step of endotoxin removal is required, as bacterial endotoxins may reduce transfection efficiency of plasmids into eukaryotic cell lines[476]. For the PureYield™ Plasmid Maxiprep System (Promega Corporation; A2392) 5mL of endotoxin removal wash was passed through the column prior to DNA elution. Plasmid DNA was eluted from the PureYield™ column using 0.5mL-1.5mL of nuclease-free water (Promega Corporation; MC1191). The ZymoPURE II Plasmid Maxiprep Kit (Zymo Research; D4203) required DNA elution using the provided elution buffer, followed by passaging through a proprietary EndoZero II Spin Column (Zymo Research; C1060-25), in order to minimise endotoxin contamination.

For Minipreps, a similar protocol was followed, using the PureYield™ Plasmid Miniprep System (Promega Corporation; A1223). 3mL of initial bacterial culture was pelleted for minipreps in microcentrifuge tubes in two 1.5mL centrifugation steps at 16’000 *x g* for 30 seconds and resuspended in 600 µL of nuclease-free water (Promega Corporation; MC1191) prior to the addition of alkaline lysis buffer. After gentle mixing of the resuspended bacterial cells and the alkaline lysis buffer, the sample was centrifuged at 16’000 *x g* for 3 minutes and the supernatant transferred to a PureYield™ Minicolumn in which the plasmid DNA binds to the silica-based membrane. Subsequent wash steps using endotoxin removal buffer and a salt/ethanol wash buffer was performed, with a final elution in 30 µL of nuclease-free water (Promega Corporation; MC1191) by centrifugation at 16’000 *x g*. The concentration of plasmid DNA isolated via Miniprep and Maxiprep was determined using a microvolume UV-Vis spectrophotometer (DeNovix DS-11 Series), as detailed in section 2.1.6.

2.1.10 DNA Sequencing

DNA sequencing was performed using Plasmidsaurus (https://plasmidsaurus.com/faq), for whole plasmid sequencing. Prior to preparing the samples for sequencing, a more rigorous form of DNA quantification was required. Concentration of plasmids were determined using a Qubit (Thermo Fisher; Q32851) performed by University of Nottingham Deep Seq facility. The plasmids were then

diluted to 100ng/µL and sent to Plasmidsaurus (https://plasmidsaurus.com/faq) for whole plasmid sequencing.

2.1.11 Cloning of N-terminal BioID2 Fusion Proteins

N-terminally tagged BioID2 VEGFR2 and NRP1 constructs were generated by cloning the appropriate cDNA encoding the promiscuous R40G mutant of a biotin protein ligase from *Aquifex aeolicus*[477] into existing HaloTag vectors. The BioID2 was amplified by PCR from a myc-BioID2 vector (Addgene; Plasmid #74223), with subsequent removal of the sequence encoding for the HaloTag using SacII (NEB) and Xho1 (NEB) restriction enzymes for HaloTag-NRP1 and HaloTag-VEGFR2 and SacII (NEB) and PvuI (NEB) restriction enzymes for HaloTag-VEGFR3. For BioID2-NRP1 and BioID-VEGFR2, the ORFs generated resulted in a sequence encoding and IL6 signal sequence fused to the N-terminus of BioID2 in frame with either NRP1 or VEGFR2 via a PRVEISGEPTTEDLYFQSDN(AIA) linker. For BioID2-VEGFR3, the same is true, however, the linker is a LERSIA sequence. For mycBioID2-NRP2, the sequence was generated and sent to GenScript for commercial synthesis.

2.1.12 Cloning of C-Terminal BioID2 Fusion Proteins

C-terminally tagged BioID2 NRP1, VEGFR2 and VEGFR3 constructs were generated by cloning the appropriate cDNA encoding the promiscuous R40G mutant of a biotin protein ligase from *Aquifex aeolicus* 172 into existing HaloTag vectors. The BioID2 was amplified by PCR from a BioID2-HA vector (Addgene; Plasmid #74224), with subsequent removal of the sequence encoding for the HaloTag using XhoI (NEB) and XbaI (NEB) restriction enzymes. The ORFs generated resulted in a sequence encoding an IL6 signal sequence fused to the N-terminus of NRP1, VEGFR2 or VEGFR3 followed by BioID2-HA in frame via a short LE linker. For NRP2-BioID2, the sequence was generated and sent to GenScript for commercial synthesis.

2.1.13 Design of pLV-NRP1-BioID2 Construct

In order to generate a TERT2-HUVEC variant which stably expressed NRP1-BioID2, a lentiviral expression vector was generated. The existing C-terminal NRP1-BioID2 plasmid was sent to GenScript for them to perform the subcloning from this plasmid, in order to generate the lentiviral expression vector. GenScript removed the ORF sequence relating to NRP1-BioID2 and inserted it into their lentiviral vector backbone, which harboured a blasticidin resistance cassette with an IRES region in between this region and the NRP1-BioID2, enabling for both genes to be expressed under the same promoter. The resulting plasmid was suitable for 3rd and 4th generation lentiviral packaging systems.

2.2 Cell Culture

The cell lines used in this research were all passaged using a similar protocol, with minor variations in the media, concentration of trypsin, lengths of incubations and treatment of flasks and dishes for improved adherence. Human Embryonic Kidney 293T (HEK293T) and HEK293T-derived stable cell lines were cultured in high glucose Dulbecco's modified Eagle's medium (DMEM) (Sigma Aldrich; D6429) supplemented with 10% v/v foetal calf serum (FCS) (Sigma Aldrich; F2242). Human telomerase reverse transcriptase (hTERT2) immortalised human umbilical vein endothelial cells (HUVEC) (hTERT2-HUVEC) cells were cultured in Medium 200 (Thermo; M200500) supplemented with 2.2% large vessel endothelial supplement (LVES) (Thermo; A1460801). All cells were cultured at 37°C in 5% CO_2 / 95% air inside cell culture incubators. All reagents and buffers were stored at 4°C prior to passaging of cells. Upon day of passage, the reagents and buffers were incubated in a water bath set to 37°C until they had reached this temperature to avoid cold shock or stress to the cells. Following trypsinisation throughout passaging all cell lines used, cells were pelleted at 300 *x g*. Passaging and plating of cells, along with other cell culture protocols, were performed in a class II laminar flow hood.

2.2.1 Cell Maintenance and Passaging

Cells were grown in either; a 25cm^2 flask (T25); a 75cm^2 flask (T75); or a T175cm^2 flask depending on the downstream application or experiment intended. Regardless of the culture vessel, cells were passaged upon reaching ≥70% confluency. Cells were then washed with 5-15mL of pre-warmed PBS, to remove any residual serum containing media which can inactivate the trypsin. The cells are then incubated for 3-5 minutes at 37°C with 0.5-3.0mL trypsin, depending on the culture vessel size, in which the adherent cells will then detach from the surface of the flask. Trypsin is a serine protease which cleaves C-terminal arginine and lysine residues in the extracellular matrix which leads to the degradation of vessel-anchoring proteins and the detachment of the cells into a suspension for harvesting[478]. The trypsin solution also contains EDTA, which chelates the Ca^{2+} on which cell-cell adhesion interactions depend[479]. Trypsin-EDTA solution (Merck; 59427C) was supplied as a 10X solution and diluted according to use. For HEK293T cells and cell lines derived from HEK293Ts 1X Trypsin-EDTA solution (0.25% w/v) was used. For hTERT2-HUVECs and hTERT2-HUVEC derived cell lines, 4X Trypsin-EDTA solution was required. After incubation with trypsin, the cells agitated to facilitate detachment from the surface of the flask, followed by addition of 5-10mL DMEM (Sigma-Aldrich; D6429) containing 10% v/v FCS (Gibco; 11570506) to inactivate the trypsin, preventing excessive proteolytic degradation and cell toxicity. Cells were then centrifuged at 300 *x g* for 5 minutes, with the supernatant discarded. The pellet containing the cells was resuspended in 5-10mL fresh, pre-

warmed DMEM containing 10% v/v FCS and a portion of this suspension was added to an appropriate flask containing 5-40mL pre-warmed DMEM containing 10% v/v FCS, depending on the vessel size.

2.2.2 Freezing, Storage and Thawing of Cells

For long-term perseveration cells were resuspended in Cellbanker 2 (amsbio; 11914), or FCS (Gibco; 11570506) supplemented with 10% w/v dimethyl sulfoxide (DMSO) (Sigma-Aldrich; D8418) and deposited in liquid nitrogen storage. The latter solution required filter sterilisation through a 0.22µM filter prior to use. The protocol for freezing cell stocks was the same for each type of freezing media used. Cells were detached from the culture vessel, as detailed in section 2.2.1. Following centrifugation at 300 *x g* and disposal of the supernatant, the cells were resuspended in an appropriate volume of freezing media, so that each cryogenic vial of suspended cells contained 0.0-1.0mL depending on the size of the vial. For cells resuspended in Cellbanker 2, cryogenic vials were stored at -80°C for around 1 week, before moving these cells to -150°C liquid nitrogen for long-term storage. When using the freezing media containing FCS supplemented with 10% w/v DMSO, the cryogenic vials containing the cells were placed in a cryogenic freezing container (Sigma-Aldrich; Nalgene® Mr. Frosty, C15620) containing isopropanol, with the container stored at -80°C for 1 week before moving to long-term -150°C liquid or vapour phase nitrogen storage. The isopropanol in the cryogenic freezing container ensures a gradual reduction in the cooling rate, at 1°C per minute when stored in a -80°C freezer.

The stored cryogenic vials were thawed by placing the vials in a water bath at 37°C, enough to cover half of the vial, taking care not to submerge the vial up to the lid, which would cause potential for contamination of the cells. The outside of the cryogenic vial was sterilised using 70% v/v IMS and moved to a Class II laminar flow hood, where the cell suspension with the freezing media was diluted with 3-5mL pre-warmed DMEM supplemented with 10% v/v FCS. The resulting suspension was centrifuged at 300 *x g* for 5 minutes, with the supernatant containing the freezing media discarded. The pellet containing the cells was resuspended in 5mL pre-warmed DMEM supplemented with 10% v/v FCS and transferred to a T25 flask, which was immediately placed in an incubator set at 37°C and 5% CO_2 / 95% air until cells reached ≥70% confluency where they were passaged further.

2.2.3 Cell Seeding

Various vessels were used for seeding cells onto, depending on the nature of the experiment. The number of cells plated, also depended on the cell line used for the experiment, see table 2.2. Cells were passaged using the protocol described in section 2.2.1, upon resuspending the cells in DMEM supplemented with 10% v/v FCS, the concentration of the cell suspension required quantification, in order to plate the appropriate number of cells. 10 µL of the cell suspension was loaded onto a

haemocytometer and cells were counted using a 10X objective on a standard inverted light microscope. The haemocytometer contains gridded areas, allowing for counting of differently sized cells. For the cell lines used in this research, the logical count method was performed, meaning only the cells in the four corner squares of the haemocytometer were counted, (Figure 2.1). Each corner square is further divided into 16 smaller squares. The number of cells in these 16 squares were counted and repeated for two of the other gridded corner squares, for a total of 3 cell counts. A mean of these 3 counts was calculated and multiplied by 10'000, which represented the number of cells per millilitre of cell suspension. The calculated concentration determined the volume of cell suspension required for seeding.

The assay vessel required treatment prior to seeding, to ensure cells would adhere to the surface appropriately. For HEK293 and HEK283T wild-type and derived cell lines, experimental plasticware was incubated with a sufficient volume of 0.1mg/mL poly-D-lysine (PDL) (Sigma-Aldrich; P6407) in PBS, Table 2.2, to cover the surface for 30 minutes at 37°C. PDL is a cationic polymerised amino acid which following absorption to the cell culture surface, increases the number of positively charged binding sites in which the negatively charged cell membranes can access, increasing adherence of cells to the vessel[480]. For human TERT2-HUVEC (hTERT2-HUVEC) and hTERT2-HUVEC derived cell lines, the culture vessels were treated with 0.1% gelatin (Sigma-Aldrich; G1393) in PBS. Gelatin is a collagen-derived cell-attachment substrate, which contains an arginine-glycine-aspartic acid (RGD) sequence which is crucial for cellular interactions with the surrounding extracellular matrix (ECM)[481]. This RGD sequence additionally interacts with integrins, further enhancing cell adhesion capabilities[482]. Immediately before seeding cells, the suspension was drawn up into the pipette and expelled, several times, to ensure cells which have sedimented during the counting process are fully resuspended. Cells were typically incubated for 12-24 h to facilitate adherence to the culture vessel before further experimentation. For immunofluorescence experiments, section 2.5, cells were cultured on sterile 16mm glass coverslips, treated with the appropriate adherence agent.

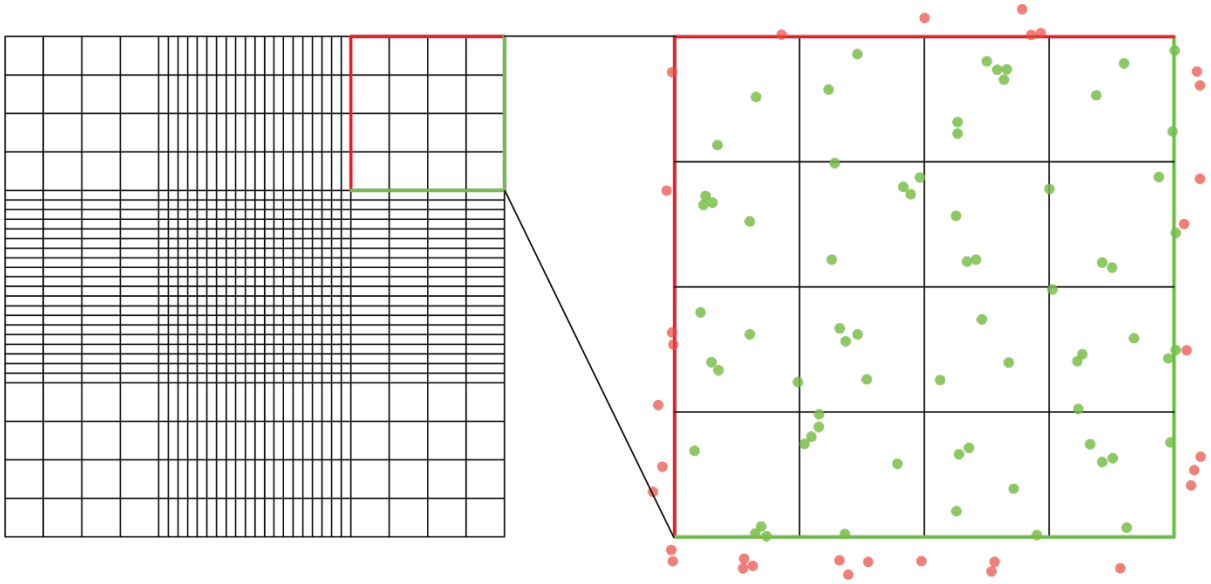

Figure 2.1 – Haemocytometer cell counting visualisation. *One count was performed in each corner of the heamocytomoeter, consisting of a 4 x 4 grid. The green circles represent cells counted, with the red circles representing cells not included in the count. Only cells present within this grid, including cells present on the bottom and right border of the grid were counted. The count was repeated in 2 other 4 x 4 grids, with an average of 3 counts taken as the number of cells per millilitre.*

Table 2.2 – Details describing the volume of media, volume of PDL or gelatine, and number of cells (HEK293T or hTERT2-HUVEC) per well, relating to the culture vessel size.

Culture vessel	Volume of media per well	Volume of PDL or gelatine	Number of HEK293T cells	Number of hTERT2-HUVEC
96-well plate	100uL	50uL	$0.18\text{-}0.22 \times 10^5$	-
48-well plate	300uL	150uL	$0.5\text{-}1 \times 10^5$	-
12-well plate	1mL	500uL	$1.25\text{-}2.00 \times 10^5$	$1\text{-}1.5 \times 10^5$
6-well plate	2mL	800uL	3×10^5	3×10^5
100m dish	5ml	2mL	$2.2\text{-}3.3 \times 10^6$	$2.8\text{-}3.3 \times 10^6$

2.2.4 HEK293T Wild-type (WT)

Human embryonic kidney cells are thought to be originally isolated from the kidney of a donor female embryo, consistent with the absence of the Y chromosome in the genome[483]. The HEK293 cell line was established by transforming these donated cells with sheared adenovirus type 5 DNA to allow the propagation of viral vectors such as non-replicative adenoviruses[484]. The immortalised HEK293 cell line exhibits a complex but stable karyotype, with abnormalities in the chromosome number ranging from 56 to 78, and structural aberrations in the form of deletions and rearrangements, which are common[485]. The HEK293T cell line (ATCC; CRL-3216) is a derivative which stably expresses a temperature sensitive simian virus 40 (SV40) T-antigen mutant, which enables replication of plasmids

containing an SV40 sequence when transfected into the cell[486]. This innate ability of HEK293T cells and their typical high transfection rate, makes them ideal for protein overexpression models, particularly with transient expression. HEK293T cells were used; in the transient transfections of NRP1-BioID1-HA for interactome analyses; in nanoBRET experiments to validate and characterise selected BioID identified interactors; for generating stably expressing cell lines for both BioID and nanoBRET analyses. The HEK293T cells exhibit an epithelial-like morphology and grow as an adherent monolayer.

2.2.5 HEK293-HaloTag-VEGFR2/pLV-NRP1-BioID2-HA

The cell line was derived from a previously produced HEK293 cell line, section 2.2.5, which stably expresses HaloTag-VEGFR2[354]. The cell line was generated in order to obtain a cellular model in which both VEGFR2 and NRP1 are expressed, and incorporating BioID technology to determine how the presence of VEGFR2 influences the interactome of NRP1. The pLV-NRP1-BioID2-HA plasmid was transduced into the existing cell line using a 4th generation lentiviral packaging system and selected for expression as described in section 2.4.2.

2.2.6 hTERT-HUVEC

hTERT2-HUVECs were originally isolated from the umbilical cord of a single donor newborn Caucasian female (ATCC; CRL-4053, LOT# 70023166). The initial primary HUVECs harvested, were virally transduced with hTERT and SV40 large T-antigen (SV40 LT)[487], which offers several advantages compared to the standard primary HUVECs, mainly the elongation of the lifespan of the cells, providing a wider scope for their use. According to ATCC these genetic modifications did not significantly affect the karyotype or nature of the HUVEC cells, with the karyotypically stable hTERT2-HUVECs harbouring 46 chromosomes and >75% expressing the CD31 antigen. CD31 is a transmembrane glycoprotein expressed highly on the surface of endothelial calls at the intercellular junctions. The ubiquitous expression of CD31 on various endothelial cell types mean it has become an established marker to identify human endothelial cells[488].

2.2.7 hTERT2-HUVEC/pLV-NRP1-BioID2-HA

The cell line was derived from a previously produced cell line, section 2.2.6, stably expressing hTERT and SV40 LT, which enables a prolonged passage life of the cell line. The cell line was generated in order to obtain a more translational cellular model for evaluating the interactome of NRP1 using BioID technology. hTERT2-HUVECs endogenously expresses NRP1 and therefore are more representative of the endogenous environment of NRP1 compared to HEK293T cells, where NRP1 RNA presence is minimal[489]. The pLV-NRP1-BioID2-HA plasmid was transduced into the TERT2-HUVECs using a 4th

generation lentiviral packaging system, with positively expressing cells selected as described in section 2.4.2.

2.3 Recombinant Cell Lines – Transient Transfection Methods

2.3.1 Polyethylenimine

Polyethylenimine (PEI) 'MAX' was used as a plasmid DNA delivery vehicle into mammalian cells for transient transfections. PEI is a cationic polymer which forms positively charged complexes with DNA. The positive PEI-DNA complex interacts electrostatically with the external membrane of the cell, followed by endocytosis of the polyplexes and release of the plasmid DNA into the cytoplasm[490]. PEI 'MAX' was generated by dissolving 100mg of PEI (Thermo Fisher; 043896.01) in 90mL ultrapure water, with constant stirring and the pH adjusted to pH 7.0 using 1M HCl, for a final concentration of 1mg/mL. Once the final pH was stable for 5 minutes, the solution was sterilised through a 0.22µm filter, aliquoted and stored at -20°C. For the transient transfections, various ratios of DNA:PEI were used, with the absolute amount varying depending on the size of the culture dish, Table 2.3. Transient transfections were performed using polyethylenimine (PEI) and a 150mM NaCl salt buffer, with HEK293T cells seeded on the day prior to transfection. The DNA was diluted in 150mM NaCl, with the PEI added dropwise to this solution, followed by incubation at RT for 25 minutes. The transfection mix was added to the cell media for 16-24 h at 37°C/5% CO_2 and subsequently replaced with fresh DMEM media and further growth at 37°C/5% CO_2 for another 16-24 h.

Table 2.3 – Details regarding the amount of DNA, volume of polyethylenimine (PEI) and volume of NaCl used in PEI transfections per well. Only 12-well plates and 6 well plates were used.

Culture Vessel	Amount of DNA (ng) per well	Volume of PEI (1mg/ml) per well	Volume of NaCl per well
12-well plate	500-1000ng	1.5-6uL	50uL
6-well plate	1000-2000ng	3-12uL	100uL

2.3.2 FuGENE HD

FuGENE HD (Promega Corporation; E2311) was another reagent used to transiently transfect plasmid DNA into mammalian cells. The formulation and mechanism of action of FuGENE HD is proprietary, although it is thought to interact with nucleic acids and the cell membrane to provide entry of the plasmid DNA into the cell. The plasmid DNA was diluted in Opti-MEM (Gibco; 31985062), with the FuGENE HD added to this solution. The DNA: FuGENE HD ratio was optimised depending on the construct, with the absolute volumes determined by the culture vessel size, Table 2.4. The resulting solution containing DNA and FuGENE HD was incubated for 7 minutes before addition to cell media

for 16-24 h at 37°C/5% CO_2. The media containing the transfection reagents was then replaced with fresh media and the cells were cultured at 37°C/5% CO_2 for a further 16-24 h.

Table 2.4 - Details regarding the amount of DNA, volume of FuGENE HD and volume of Opti-MEM used in FuGENE HD transfections per well. 48-well dishes were not used in these transfections.

Culture Vessel	Amount of DNA (ng) per well	Volume of FuGENE HD per well	Volume of Opti-MEM per well
96-well plate	10-250ng	0.03-0.75uL	10uL
12-well plate	500-1000ng	1.5-3.0uL	50uL
6-well plate	1000-2000ng	3.0-6.0uL	100uL
100m dish	10000ng	30uL	500uL

2.3.3 Nucleofection

Nucleofection was used as a physical method of transfecting plasmid DNA into cells. Nucleofection is a form of electroporation that utilises a transient electric field which induces pore formation in the cell membrane, combines the plasmid DNA with the cell membrane through charge attraction and subsequent endocytosis into the cell[491]. Additionally, with nucleofection, unlike electroporation, the specific parameters of the electric field enable delivery of the plasmid DNA directly to the nucleus. In order to perform nucleofection, the cells required trypsinisation and suspension. For hTERT2-HUVEC cells a T75 culture vessel at 70% confluency was used, for HEK293T cells a T25 culture vessel was sufficient to yield the required number of cells. Cells were trypsinised as described in section 2.2.1. Cells were resuspended in complete media and counted as described in section 2.2.3. The volume of resuspended cells containing 500,000 cells was transferred to another falcon tube and centrifuged again. The supernatant containing media was aspirated and the 500,000 cells were resuspended in 0.1mL Mirus electroporation solution (Mirus; MIR 50114). Following resuspension in Mirus solution, 1 µg plasmid DNA was incorporated into the cell suspension. The solution was gently mixed and carefully transferred to Ingenio Electroporation 0.4mL cuvettes (Mirus; MIR 50121), ensuring no bubbles were present within the cuvette. The cuvette was placed inside the Amaxa Nucleofector II (Lonza Bioscience) and the appropriate programme chosen (either A-024, U-001 or V-001). The nucleofector cells were seeded into pre-warmed vessels containing media and cultured at 37°C/5% CO_2 for the appropriate time, usually 24-48h post-nucleofection.

2.4 Stable Expression Cell Lines

2.4.1 Lentivirus Production

Lentivirus production was performed by Dr. Catherine Probert. The pLV-NRP1-BioID2-HA plasmid was transfected into HEK293T cells along with the accompanying plasmids included in the Lenti-X™ Packaging Single Shots (VSV-G) (Takara Bio; 631275) using FuGENE HD (Promega Corporation; E2311). After 24 h the media was replaced with fresh, complete DMEM and incubated for a further 48 h. The viral packaging proteins produce viral proteins which recognises the recombinant NRP1-BioID2-HA mRNA and packages it into viral cores which are then transported to the cell membrane[492]. The viral cores are then enveloped by the cellular membrane, resulting n the budding of mature, infectious virons from the cell into the DMEM, containing the NRP1-BioID2-HA mRNA[493]. The DMEM containing the virus was harvested 72 h post-transfection and centrifuged at 2100 x g for 20 minutes at 4°C to pellet any cells inadvertently harvested with the virus. The supernatant was filtered through a 0.45 µm filter and stored at -80°C until required.

2.4.2 Lentivirus Transduction

The lentiviral transduction protocol was identical for the generation of NRP1-BioID2 stably expressing HEK293, HEK293T or hTERT2-HUVEC cells. Cells were seeded into 6-well culture vessels 24h prior to lentiviral transduction, ensuring a 70% confluence on the day of transduction. The following morning, a frozen vial of lentivirus containing media was thawed on ice and diluted using fresh culture media appropriate for the cell line. The amount of dilution was optimised whereby the viral containing media was diluted to 75%, for a final volume of 1mL. Immediately prior to addition of lentiviral media to the cells, polybrene (Sigma-Aldrich; TR-1003) was added to a final concentration of 8 µg/mL. Polybrene is widely used to improve efficiency of viral transduction. Also known as hexadimethrine bromide, this cationic polymer promotes virus-host cell fusion by reducing the electrostatic charge repulsion between the approaching viral particles and the negatively charged cell membrane[494,495]. The cells were incubated at 37°C/5% CO_2 for 72h to allow the gene product to accumulate in the cells. Following this incubation period, the lentiviral containing media was replaced with fresh growth media, supplemented with an appropriate amount of blasticidin antibiotic for selection of positively transduced cells.

2.4.3 Selection using Blasticidin

The cells transduced with pLV-NRP1-BioID2-HA should express a blasticidin resistance gene, allowing these cells to survive high concentrations of blasticidin that would be toxic to non-transduced cells.

Blasticidin is a potent inhibitor of the termination step of translation and peptide bond formation by the ribosome, meaning new protein cannot be produced from mRNA translation resulting in the eventual death of the cell[496]. Transduced cells express blasticidin-s-deaminase, which detoxifies blasticidin by catalysing its deamination[497]. For the hTERT2-HUVECs, the media was supplemented with 6µg/mL blasticidin, with selection conditions applied for 8 days. After this selection period, a maintenance concentration of 2µg/mL was used indefinitely to maintain selection pressure. The HEK293 and HEK293T based cell lines exhibited lower sensitivity to blasticidin and required selection concentrations at 8µg/mL for 14 days, with a subsequent maintenance concentration of 5µg/mL. During selection, fresh media and antibiotic was applied every 2 days to the cells. The cells were then trypsinised and transferred to sequentially larger culture vessels to increase stable cell line population, in which cells were used for experiments and surplus cells retained in long-term storage.

2.4.4 Fluorescence-Activated Cell Sorting (FACS)

FACS was used to enrich for cells expressing NRP1-BioID2-HA following lentiviral transduction. A confluent T75 culture vessel was used for growing HEK293T WT and HEK293-NFAT-HaloTag-VEGFR2 transduced with pLV-NRP1-BioID2-HA. For hTERT-HUVEC cells transduced with pLV-NRP1-BioID2-HA, a T175 culture vessel was required. Cells were non-enzymatically detached from the culture flask using an enzyme free dissociation solution, Cellstripper (Corning; 25-056-CI), for 15-20 minutes at 37°C. This non-enzymatic method ensures the presence of NRP1 during probing with the antibodies, detaching using enzymes may cleave target proteins resulting in the reduced efficiency of antibody labelling. The cells were then resuspended in 1mL PBS-based FACS buffer containing 1mM EDTA, 25mM HEPES and 1% BSA. The cells were pelleted initially by centrifugation at 300 *x g* for 5 minutes. The supernatant was discarded, and the cells resuspended again in 1mL FACS buffer. This process was repeated once more, with the cells then resuspended in 50 µL of FACS buffer containing a 1:500 dilution of anti-NRP1 rabbit antibody (Abcam; ab81321) and incubated on ice for 20 minutes with periodic mixing. After antibody incubation, 1mL FACS buffer was added to the cells, which were then pelleted using centrifugation at 300 *x g* for 5 minutes. The supernatant was discarded and Alexa Fluor® 594 AffiniPure™ Goat Anti-Rabbit (Jackson ImmunoResearch; 111-585-003) was prepared in 50 µL FACS buffer at a dilution of 1:100 and used to resuspend the cells. The secondary antibody incubation was performed in the dark, on ice for 20 minutes. For HEK293-NFAT-HaloTag-VEGFR2 transduced with pLV-NRP1-BioID2-HA, HaloTag® Alexa Fluor® 488 Ligand (Promega Corporation; G100B) was added to the 50 µL FACS buffer at a dilution of 1:1000 in order to probe for HaloTag-VEGFR2 expressing cells. Following secondary antibody incubation, 1mL FACS buffer was added to the cells followed by centrifugation at 300 *x g* for 5 minutes. The supernatant was removed, and cells were resuspended in

1mL FACS buffer with subsequent centrifugation. Finally, the cells were resuspended in a final volume of 500 µL FACS buffer and placed on ice prior to sorting.

2.5 Immunofluorescence

Immunofluorescence is a technique that enables detection and localisation of components or specific proteins within a cell or tissue via the use of antibodies either directly conjugated to fluorophores or via secondary conjugated antibodies[498]. The process for immunofluorescence assays for fixed cells was the same across all cell lines used in this research, using cells adhered to 16mm glass coverslips. In the case of cells which were probed for the presence of a HaloTag epitope, the HaloTag ligand was applied to live cells, prior to fixation. HaloTag® Alexa Fluor® 488 Ligand (Promega Corporation; G100B) was diluted in complete DMEM and incubated with the cells for 30 minutes at 37°C/5% CO_2, followed by 3 PBS washes and fixation of the cells. All antibody probing was performed on fixed cells. Initially, pre-warmed 4% paraformaldehyde (PFA) diluted in PBS (16% formalin solution diluted in PBS; Thermo Fisher; 28908) was used as a fixative in preparation for IF processing. The PFA was removed from the cells with 3 x 3-minute PBS washes. Cells were then permeabilised using 0.3% triton in PBS for 5 minutes, which disrupts the cell membrane enabling more efficient penetration of antibodies. The triton based permeabilising solution was removed from the fixed cells and 3 x 5-minute PBS washes followed. The cells were blocked in 2% BSA blocking solution (Thermo Fisher; 37525) for 1h at RT. Blocking improves the sensitivity of immunofluorescence as the BSA in the blocking solution essentially binds all proteins present on the coverslip and as antibodies compete with the BSA for target epitopes, the non-specific binding of primary and secondary antibodies are reduced[498]. Primary antibodies were prepared in 2% BSA blocking solution, with 80 µL of this solution incubated on the coverslips containing the fixed cells at 4°C overnight. Following the primary incubation, 3 x 5-minute washes were performed using 0.1% Triton/PBS. Secondary antibodies were diluted in 2% BSA blocking solution with 80 µL added per coverslip and incubated for 2h at RT. The coverslips were washed a further 3 times in 0.1% Triton/PBS and then incubated with DAPI (Invitrogen; D1306) for 15 minutes at RT diluted in PBS to a final concentration of 2.5µg/mL. The DAPI solution was removed and coverslips washed twice in PBS for 3 minutes. Immediately prior to mounting the 16mm coverslips on to microscope slides, a rinse with ultrapure water was performed. For mounting, 8 µL of Mowiol 4-88 mounting medium (Sigma-Aldrich; 1381) was placed on top of a clean microscope slide, with the coverslip placed face down on top. The mounting medium required an overnight incubation in the dark to harden.

2.6 Confocal Microscopy

Confocal microscopy uses point illumination which enables imaging capabilities deep into cells. In confocal microscopy, the light source is focused through an optical aperture (pinhole) in front of the photon detector so that illumination is confined to a diffraction limited spot so any light which is not within this focal plane (above or below) is not detected and therefore contributes little to the final image[499]. All images in this research were taken using the Leica TCS SPE (Leica-microsystems) with 63x oil immersion objective - ACS APO 63x/1.30 numerical aperture (Leica-microsystems). The exterior of the coverslips was cleaned using isopropanol and a drop of type F immersion liquid oil (Leica; 11944399) was applied. All images were exported from the Leica LAS-X software (Leica-microsystems) as TIFF files and imported to Fiji image software[500] for image analysis.

2.7 Colocalisation Analysis

2.7.1 Transfection and Immunofluorescence

HEK293T cells were transfected with potential interactors conjugated to fluorophores identified in the BioID analyses, Table 2.7, either with or without cotransfection with NRP1-BioID2-HA using FuGENE (Promega Corporation; E2311) as described in section 2.3.2. A negative control using mEmerald-CENPA was also used with or without NRP1-BioID2-HA for comparison with potential interactors. The cells were fixed in 4% PFA and immunofluorescence was performed as described in section 2.5. Anti-HA mouse (Invitrogen; 2-2.2.14) antibody followed by an anti-mouse 594 (Jackson Immuno Research; 115-585-003) or anti-mouse FITC (Jackson Immuno Research; 115-095-003) was used to identify NRP1-BioID2-HA. Streptavidin 488 (Invitrogen; S11223) identified the presence of biotinylated proteins.

2.7.2 Image Analysis using Segmentation and Quantification of Subcellular Shapes (Squassh)

Segmentation and colocalisation analyses between potential interacting proteins conjugated to fluorophores, Table 2.7, and NRP1-BioID2-HA or streptavidin was performed in Image J software[500] using the Squassh plug-in[501]. For the analyses, 20-30 images of a single focal plane from 3 individual experiments were selected for each experiment. Colocalisation signal was measured across the whole image. The TIFF files were selected in the Squassh plug-in and the parameters selected are detailed in Table 2.5. The cell mask reduced image artefacts, restricting the segmentation to the cells.

To extract the results of the Squassh analysis, the SquasshAnalyst programme was launched in R using the script ‘shiny::runGitHub(“SquasshAnalyst”, “a-risk”). The quality of segmentation was evaluated for each image by reviewing images in the ‘segmentation overview’ section, and images displaying

unsuccessful segmentation were excluded. The 'colocalisation (signal)' in the 'Analysis' tab was used to determine colocalisation, whereby the channel containing the potential interactor conjugated to the fluorophore (either GFP or RFP) was selected as 'Percentage of the channel'. The channel representing either NRP1-BioID2-HA or streptavidin was designated the 'colocalising with' option. The colocalisation raw data was exported as a .csv file.

Table 2.5 – Squassh analysis plug-in settings*. The list of parameters selected for colocalisation analyses within this project. The parameters were kept the same and minimal object intensity were changed for different interactors due to different expression level of the potential interactors fused to fluorophores.*

Squassh parameter settings	
Background subtraction	50 pixels
Microscope's PSF	'Compute PSF for confocal microscopy'
Segmentation regulation	Set to 0.100
Minimal object intensity for NRP1 (Channel 1)	0.110
Minimal object intensity for streptavidin (Channel 2)	0.120
Minimal object intensity for interactors	0.120-0.300
Noise model	Set to the optional for confocal microscopy: Poisson model
Output of segmentation	'Object outlines', 'Colored objects', 'Intermediate step'

2.7.3 Statistical Analysis of Colocalisation Experiments

The .csv files containing the raw colocalisation data was imported into Graphpad version 10.3.0 (GraphPad Software, LLC) to perform statistical analyses on the different conditions. To compare between experimental conditions and controls (including mEmerald-CENPA negative controls), one way analysis of variance (ANOVA) was performed.

2.8 BioID Methodology

2.8.1 Preparation of HEK293T WT Cell for BioID Analysis

BioID technology utilises a promiscuous biotin ligase enzyme, which catalyses the formation of covalent bonds between biotin and proximate lysine residues which are able to withstand stringent

lysis and wash conditions[446]. As biotinylation is a rare modification in mammalian cells[502], using a biotin ligase fused to a protein of interest enables an interactome analysis to be performed. The BioID method performed in this research is based on a protocol described by Remnant and Booth et al.[503]. Initial BioID experiments in HEK293T cells concerning NRP1-BioID2-HA were performed transiently in 100mm cell culture dishes. Transfections using FuGENE HD (Promega Corporation; E2311) were performed as per section 2.3.2. following seeding of the cells on the previous day. The media containing the transfection reagents and DNA was changed after 24h. Another incubation followed which consisted of cells treated with vehicle (0.1% BSA) or 10nM $VEGF_{165}$a (R&D Systems; 293-VE-500/CF) and treated and non-treated with 50µM biotin for 20h. For the stable cell lines generated, see section 2.2.7, as the transfection step is not necessary, $VEGF_{165}$a and biotin treatment were performed the following day after cell seeding.

2.8.2 Protein Extraction of Biotinylated Proteins

The protein extraction methodology was identical for transiently transfected cells and stably expressing cells. BioID lysis buffer, containing 50mM Tris pH 7.4, 500mM NaCl, 0.4% SDS, 5mM EDTA, 1mM DTT and 1 x protease inhibitor cocktail (Roche; 11873580001) was prepared fresh, immediately prior to lysis. 100mm cell culture dishes were washed once in ice cold PBS and BioID lysis buffer was applied with the plates kept on ice and incubated for 5 minutes. For the HEK293 and HEK293T cell lines, 400 µL BioID lysis buffer was used per plate. For the hTERT2-HUVEC experiments, 200 µL of BioID lysis buffer was used per plate. A cell scraper was used to remove the cells from the plate, with the lysed material transferred to a prechilled Eppendorf and incubated for a further 30 minutes. The lysis preparations were sonicated at 4°C intermittently for 30 second intervals for 15 minutes with the BioRuptor (Diagenode; B01020001). Triton X-10 was added to the lysis samples to a final concentration of 2%, followed by another intermittent sonication at 4°C for a further 15 minutes. The lysis preparation was diluted with an equal volume of 50mM Tris pH 7.4 and centrifuged at 16,000 *x g* for 30 minutes to remove insoluble cell debris. The supernatant containing the extracted, biotinylated proteins was isolated and stored at -80°C. A blank lysis buffer sample containing no protein was prepared alongside the protein lysates for protein quantification

2.8.3 Quantification of Protein Concentration

All protein quantifications were performed using the using the Pierce™ BCA Protein Assay Kit - Reducing Agent Compatible (Thermo Fisher; 23250). The reducing reagent compatible aspect of the kit is essential as the protein lysates contain DTT. Protein quantification is essential in ensuring the same amount of protein is used in the BioID pulldown assay between test and control samples within a repeat. The blank lysis buffer sample was used to prepare BSA protein standards ranging from 0-

2000µg/mL. 9 µL of protein standard or lysate sample was pipetted in the centre 96-well microplate well, with 4 µL of compatibility reagent subsequently added. The 96-well microplate was covered and placed on a plate shaker at medium speed for one minute. The plate was incubated at 37°C for 15 minutes before addition of 260 µL of prepared Working Reagent, as per the kit requirements. The plated was placed on a pate shaker at medium speed for one minute again and incubated at 37°C for 30 minutes. After this final incubation, the absorbance was measured at 562nm, and a standard curve generated using the POLARStar Omega plate reader (BMG Labtech). From this standard curve, protein concentrations of the lysates could be quantified.

2.8.4 Isolation of Biotinylated Proteins

Streptavidin-coated magnetic beads, Dynabeads MyOne Streptavidin C1 (Invitrogen; 65001) facilitated the isolation of the biotinylated proteins in the bulk cell lysate. Streptavidin is capable of binding biotin, and by extension biotinylated proteins, in a non-covalent manner with high specificity and femtomolar affinity, meaning it is incredibly effective in enriching for these proteins[504]. Before the protein lysates were incubated with Dynabeads MyOne Streptavidin C1, first they needed to be primed for binding. The beads were washed in ice cold 0.1% Tween-20/PBS (PBS-T) three times for four minutes and finally resuspended in 50mM Tris pH7.4. Per lysate sample, 300 µL of beads were used, resuspended in 225 µL 50mM Tris pH7.4. The beads were added to protein lysate samples containing the same amount of protein across test sample lysates and control sample lysates for the repeat, with a portion being reserved for biochemical analysis of the initial protein lysate, see section 2.8. The streptavidin coated magnetic beads were incubated with the lysate for 1.75h at RT. The beads then required a series of washes to remove potential contaminants before elution of the enriched biotinylated proteins. Wash buffers were prepared in ultrapure water on the same day as the isolation, with their constituents detailed in Table 2.6. Initially, the beads were separated from the protein lysates using the DynaMag™-2 Magnet (Thermo Fisher; 12321D) and washed twice for 8 minutes at RT using Wash Buffer 1 (see Table 2.6). The wash was repeated once using Wash Buffer 2, followed by once with Wash Buffer 3. Finally, the beads were washed twice with Wash Buffer 4. The biotinylated peptides were eluted from the beads by resuspending the beads in 4X Bolt™ LDS Sample Buffer (Thermo Fisher; B0007) diluted to 1.5x in a final volume of 70uL and boiled at 96°C for 5 minutes. This boiling process resulted in removal of streptavidin from the beads and breaking of bonds between streptavidin and biotinylated peptides. The beads were separated a final time from the LDS sample buffer and the resulting solution stored at -80°C until biochemical analysis or further proteomic processing was required.

Table 2.6 – Composition of wash buffers used in the isolation of biotinylated proteins protocol.

Wash Buffer 1	2% SDS
Wash Buffer 2	0.1% deoxycholate, 1% Triton X-100, 500 mM NaCl, 1 mM EDTA, and 50 mM HEPES, pH 7.5
Wash Buffer 3	250 mM LiCl, 0.5% NP-40, 0.5% deoxycholate, 1 mM EDTA, and 10 mM Tris, pH 8.1
Wash Buffer 1	50 mM Tris, pH 7.4, and 50 mM NaCl

2.9 Biochemical Analysis – Western Blotting

2.9.1 SDS-PAGE

Sodium dodecyl-sulphate polyacrylamide gel electrophoresis (SDS-PAGE) is used in the high-resolution separation of complex protein mixtures in order to assess purity of samples, identity of proteins present and potentially evaluate or quantify expression of specific proteins[505]. The electrophoresis gels contain SDS, which is ionic and binds to positively charge and hydrophobic residues, imparting a uniform negative charge on the denatured proteins, enabling migration through the polyacrylamide gel when a current is applied[506]. The polyacrylamide forms a molecular matrix which facilitates the separation of proteins, with larger proteins becoming trapped in the gel network, meaning they migrate slower than smaller proteins[507]. SDS-PAGE gels commonly a comprised of a stacking gel and resolving gel region. The stacking gel has a more acidic pH and lower concentration of polyacrylamide, resulting in large pore sizes, allowing proteins to compact into a thin band at the interface of the stacking gel and resolving gel[507]. From here, the proteins enter the resolving gel with a more basic pH and higher concentration of polyacrylamide, the pore sizes in the gel matrix are much smaller, resulting in separation of protein based on their size. In this research, precast Bolt™ Bis-Tris Plus Mini Protein Gels (Thermo Fisher; NW00100BOX), were used for the biochemical analysis of protein samples. The gels were placed in a Mini Gel Tank (Thermo Fisher; A25977) and filled with either 1X Bolt MOPS SDS Running Buffer (Thermo Fisher; B0001) or 1X Bolt MES SDS Running Buffer (Thermo Fisher; B000202). After loading of denatured protein samples and Precision Plus Protein Dual Colour Standards ladder (BioRad; 1610374) to the gel wells, the gel tank was sealed and connected to a PowerEasePower Supply (Thermo Fisher; PS0121), where a constant voltage of 150V was applied for 50 minutes, or until the tracking dye reached the bottom of the gel. For biochemical analyses of BioID experiments, the unpurified cell lysate was loaded on to gels in equal quantities based on BCA results, for the streptavidin immunoprecipitated proteins, 10% of the sample was loaded into the wells. Following SDS-PAGE, the gel cassette was rinsed once with ultrapure water before further processing.

2.9.2 Transfer of Proteins to Nitrocellulose Membrane

Following SDS-PAGE, the proteins migrate in a perpendicular direction to adhere on a nitrocellulose membrane for further analysis. The transfer cassette comprised of sponges, filter paper, a 0.45 µm pore size 8.6 x 13.5 cm nitrocellulose membrane (Thermo Fisher; LC2006) and an SDS-PAGE gel, sealed inside a Mini Blot Module (Thermo Fisher; B1000) as per standard protocols. These components, apart from the SDS-PAGE gel, were soaked in transfer buffer which contains 1X Bolt Transfer Buffer (Thermo Fisher; BT00061), Bolt Antioxidant (Thermo Fisher; BT0005), 10% methanol and 0.015% SDS up to the appropriate volume using ultrapure water. The addition of methanol to the transfer buffer is important, as it promotes dissociation of the SDS-protein complex and improves adsorption of precipitated proteins to the membrane[508]. Addition of SDS to the transfer buffer may seem counterintuitive as it can reduce adherence of proteins on to the membrane, however, its presence results in more efficient release of proteins from polyacrylamide gels. The Mini Blot Module (Thermo Fisher; B1000) cassette is placed inside the Mini Gel Tank (Thermo Fisher; A25977) where an electric field is applied perpendicular to the gel, enabling migration of proteins to the nitrocellulose membrane directly adjacent to the SDS-PAGE gel. The non-hydrophobic nature of nitrocellulose means the proteins adhere to the membrane via electrostatic interactions[509]. The transfer was performed at a constant voltage of 10V for 80 minutes for all immunoblotting experiments.

2.9.3 Immunoblotting of Nitrocellulose Membranes

The immunoblotting protocol detailed is the same used for all membranes in this research. The principles of immunoblotting are similar to that of immunofluorescence discussed in section 2.5, whereby antibodies are used to probe for specific proteins of interest. Initially, the membrane was washed in 20mL of ultrapure water for 2 x 5-minute washes. The membrane was incubated with enough SuperBlock Blocking Buffer (Thermo Fisher; 37515) to completely cover it, for 1 h at RT with constant agitation. The blocking step is essential in preventing the non-specific binding of antibodies to the nitrocellulose membrane, otherwise resulting in artefacts or a higher background signal. As the membranes have a high affinity for protein binding, the BSA in the blocking solution binds to the unoccupied sites on the membrane surface, blocking where the antibody could potentially bind non-specifically[510]. The primary antibody was then diluted in SuperBlock Blocking Buffer (Thermo Fisher; 37515) and incubated with the membrane at 4°C overnight with constant agitation. The following day, the membranes were washed in 0.1% Tween 20 in PBS for 3 x 5 minutes washes. Secondary antibodies or antibodies directly conjugated to a fluorophore were diluted in SuperBlock Blocking Buffer (Thermo Fisher; 37515) and incubated with the membrane for 2h at RT with constant agitation. Membranes were subject to several washes consisting of; 3 x 5-minute washes with 0.1% Tween 20 in PBS; 2 x 3-

minute washes in PBS; and one final rinse with ultrapure water before imaging the gel using the Odyssey XF (LICORbio).

2.9.4 Imaging of Immunoblotted Nitrocellulose Membranes

All images were taken using the Odyssey XF (LICORbio). The Odyssey XF utilises near-infrared (NIR) lasers and LEDs to excite fluorophores conjugated to antibodies. The emission of light at specific regions of the membrane, enabled identification and relative quantification of proteins of interest. The channels utilised were 600, 700, and 800 for fluorescent probes, and the chemiluminescent channel for horse-radish peroxidase (HRP) probes. The exposure time was set for 2 minutes per channel.

2.10 Bioinformatic Processing

2.10.1 Mass Spectrometry

Sample Preparation

The biotinylated protein samples were prepared for mass spectrometry by running 50 µL of isolated biotinylated proteins, prepared in section 2.7.3 on an SDS-PAGE gel. The protein samples were run 1 cm into the SDS-PAGE gel at a slow pace (around 100 Volts for 40 minutes). The gel bands were excised and sent for the Cambridge Centre for Proteomics for mass spectrometry analysis.

2.10.2 Mass Spectrometry Processing by Cambridge Centre for Proteomics

Sample Preparation

From this point forward, the mass spectrometry of biotinylated samples were performed by Cambridge Centre for Proteomics, until bioinformatic processing. Gel bands containing the biotinylated proteins were cut into 1 mm^2 pieces, destained, reduced with DTT and alkylated using iodoacetamide. The samples were then subjected to enzymatic digestion with mass spectrometry grade trypsin (Promega Corporation; VA9000) overnight at 37°C. The supernatant was transferred into a sample vial and loaded onto an autosampler for automated LC-MS/MS.

Mass Spectrometry Analysis

All LC-MS/MS experiments were performed using the Dionex Ultimate 3000 RSLC nanoUPLC (Thermo Fisher) system and a Q Exactive Orbitrap mass spectrometer (Thermo Fisher). Peptide fragment separation was performed by reverse-phase chromatography at a flow rate of 300 nL/min and a Thermo Scientific reverse-phase nano Easy-spray column (Thermo Fisher; PepMap C18, 2 µm particle size, 100A pore size, 75 µm i.d. x 50 cm length). The peptides were applied to a pre-column (Thermo Fisher; PepMap 100 C18, 5 µm particle size, 100A pore size, 300 µm i.d. x 5mm length) from the

Ultimate 3000 autosampler along with 0.1% formic acid for 3-minutes at a flow rate of 15 µL/minute. The column valves were then switched to enable elution of peptide fragments from the pre-column to the analytical column. For elution, solvent A was 0.1% formic acid in H_2O, and solvent B was 80% acetonitrile/0.1% formic acid in H_2O. The linear gradient for increasing solvent B concentration was 2-40% solvent B in 90 minutes. The total run time, including column washing and re-equilibration was 120 minutes.

The eluted peptides from LC were sprayed into the mass spectrometer using an Easy-spray source (Thermo Fisher). The Orbitrap mass analyser was used to measure all m/z values of eluted ions, with resolution set at 70000 and scanned between m/z 380-1500. Data dependent scans (top 20) automatically isolated and generated fragment ions by higher energy collisional dissociation (HCD, Normalised collision energy (NCE):25%) in the HCD collision cell and measurement of the resulting fragment ions was performed in the Orbitrap analyser, set at a resolution of 17500. Ions with unassigned charges and single charged ions were excluded from MS/MS selection and a dynamic exclusion of 40 seconds was used.

2.10.3 Generation of Reference Proteome Database

Prior to bioinformatic analysis, a reference protein database was required which would be used to compare with the BioID samples generated. UniProt is the favoured online repository for proteomics, with the reference database for this research generated using information from this site. The proteome for *Homo Sapiens* was selected and only "Reviewed (Swiss-Prot)" proteins were selected for the database. Reviewed proteins are manually curated by expert biologists, meaning their information is more reliable, especially with regards to sequence[511]. Using these proteins in the mass spectrometry analysis offers higher reliability of protein identification. The FASTA sequences for all these proteins were downloaded and contained within a single file that can be uploaded for analysis software. However, as mass spectroscopy samples are digested using trypsin originating from pig species, a further sequence needs to be added. The FASTA sequence for pig trypsin, UniProt; P00761, was added as the final entry in the database.

2.10.4 MaxQuant Processing of RAW Mass Spectroscopy Files

The MaxQuant platform software version 2.4.2.0 was used in the initial processing of RAW mass spectroscopy files. The software compares experimental mass spectra to *in silico* theoretical spectra deduced from the protein database generated from UniProt. Specific parameters were chosen in the MaxQuant software. Three potential protein modifications were selected for the software to consider when matching spectra, with a maximum of 5 modifications per peptide set. Oxidation of methionine

residues and acetylation of N-terminal protein residues were inputted as variable modifications. Carbidomethylation of cysteine residues was inputted as a fixed modification. For the digestion, pig trypsin was selected as the choice of enzyme and missed protein cleavages were set at a maximum of 2. For the first peptide search the tolerance was set at 20 parts per million (ppm) and set at 4.5ppm for the main peptide search. Posterior error probability, essentially a false positive protein identification, was reduced by setting the peptide spectrum match false discovery rate (PSM-FDR) and protein-FDR to a tolerance of 1%. Additionally, the option to generate values for intensity-based absolute quantification (iBAQ) was selected which was important for further analysis.

2.10.5 Statistical Analysis of MaxQuant Processed Data

For samples with multiple BioID repeats, statistical analyses regarding fold change between control and controls were possible. The relative iBAQ (riBAQ) values were calculated, discussed later in section 4.2.1, and each individual riBAQ was input into GraphPad Prism software version 10.3.0 (GraphPad Software, LLC) and an unpaired t test with Welch's correction was performed on the pooled values. Peptides exhibiting a p value >0.05 was excluded from the final enriched list.

2.10.6 Gene Ontology Analysis

Gene ontology (GO) analyses were performed in order to investigate the biological processes, cellular locations and molecular functions of the proteins identified in the BioID experiments relating to NRP1. Uniprot accession codes were input into Webgestalt[512] and an over-representation gene ontology (GO) analysis was performed for biological processes, cellular components and molecular functions with redundant terms (parent GO terms) excluded. Using only the child GO terms highlighted specific functions, as the parent terms are too broad obscuring specific biological insights. The data is reported as enrichment ratio (ER) which indicates how much more frequently a specific GO term appears in the user-input list, compared to the number of genes enriched by chance in a random list of genes from the whole genome. The significance/false discovery rate (FDR) level was set to <0.05 for all analyses. A minimum number of proteins per category was set at 4, meaning at least 4 proteins per category had to be present for a specific GO term to be enriched.

2.11 NanoLuciferase Bioluminescence Resonance Energy Transfer (NanoBRET)

2.11.1 NanoBRET Validation of BioID Hits

Several of the BioID hits were further analysed with the intention of confirming some of the potentially interacting proteins elucidated from the BioID experiments. BRET is a proximity-based assay which

relies on the energy transfer from a donor luciferase to a proximate fluorophore, discussed in more detail in section 1.6. Numeric BRET ratios can be calculated by dividing the emission from the acceptor fluorescence by the donor luminescence. A saturable increase in BRET ratio as the concentration of acceptor fluorophore increases, is indicative of a specific interactions[513]. However, non-specific BRET interactions can still occur and typically show a linearly increasing BRET ratio with the addition of increasing concentration of acceptor fluorophore.

The nanoBRET experiments detailed in this research consisted of saturation experiments involving luminescent donor, NRP1 tagged at its C terminus with NanoLuciferase (NRP1-NLuc) and fluorescent fusion proteins as the acceptor, as detailed in Table 2.7. HEK293T wildtype cells were seeded into white, clear bottom 96-well F-bottom microplates (Greiner Bio-One; 655074). The following day, cells were transiently co-transfected with a fixed concentration of NRP1-NanoLuc (25-50 ng/well) and an increasing molar ratio of fluorescent fusion protein interactor. The concentration of DNA transfected for the acceptor fluorophore plasmid increased sequentially across the plate resulting in an increasing donor:acceptor ratio from 1:1 to 1:5. The first set of wells excluding any acceptor fluorophore, a donor only control. Each condition was performed in triplicate and differences in total DNA volume in the well were corrected using a pcDNA3.1 empty vector. After 24-48 h expression, the media containing the transfection reagents was aspirated from the microplate and wells were washed once with 0.1% BSA in Hanks' balanced salt solution (HBSS) (2mM sodium pyruvate, 145mM NaCl, 5mM KCl, 1mM $MgSO_4.7H_2O$, 10mM HEPES, 1.3mM $CaCl_2.H_2O$, 1.5mM $NaHCO_3$) supplemented with 5mM glucose. A PHERAstar FSX (BMG Labtech) was used to measure fluorescence, to confirm successful transfection of fluorescently conjugated interactor protein. For GFP proteins the FI 485 520 optic module was used (excitation at 485 nm and emission collection at 520 nm; gain set at 594; focal height 4.3 mm). For RFP proteins the FI 570 610 optic module was used (excitation at 570 nm and emission collection at 610 nm; gain set at 830; focal height 4.3 mm). Furimazine (Promega Corporation; N1110) was then added to each well to a final dilution of 1:400 and microplates were incubated at 37°C/5% CO_2 for 5 minutes before reading dual luminescence and fluorescence emissions on the PHERAstar FSX (BMG Labtech) plate reader. The optic modules used depended on the emission of the acceptor fluorophore, either BRET 1 plus (Emission A measured 535 ± 30 nm and emission B measured 475 ± 30 nm; gain for emission A set at 3200; gain for emission B set at 2300; focal height 10 mm) or LUM 610-LP 450-80 (Emission A measured 535 ± 30 nm and emission B measured 475 ± 30 nm; gain for emission A set at 3300; gain for emission B set at 1800; focal height 10 mm). The selected gain values were fixed between experimental repeats. For each measurement 3 cycles were performed, with 30 second intervals between cycles. The data used in the experiments pertained to cycle 2.

Table 2.7 – Plasmids ordered from addgene containing potential NRP1 interacting partner identified during BioID screening*. Notable features of protein plasmid and any additional information provided by addgene concerning the plasmid is detailed. Green fluorescent protein (GFP); Enhanced green fluorescent protein (EGFP); Red fluorescent protein (RFP).*

Protein ID	Notable Features	Addgene Plasmid Information
ITB1	Integrin beta-1. Cell adhesion, similar function to NRP1, known interactor.	Integrin Beta1-GFP - Expresses GFP tagged Integrin beta-1 in mammalian cells on a CMV promoter. (Plasmid #186302)
SEPT9	Filament-forming cytoskeletal GTPase. Organisation of cytoskeleton. Required for progress through mitosis.	mCherry-C1_SEPT9 i1 - mammalian expression of human SEPT9 with an mCherry fusion. (Plasmid #71622)
ZO1	Tight junction protein ZO-1. TJP1, TJP2, and TJP3 are closely related scaffolding proteins that link tight junction (TJ) transmembrane proteins such as claudins, junctional adhesion molecules, and occluding	pEGFP ZO1 - mammalian expression of human ZO1 fused to an EGFP at the N-terminus. Localises at the tight junctions. (Plasmid #30313).
OCLN	Occludin. formation and regulation of the tight junction (TJ) paracellular permeability barrier.	mEmerald-Occludin-C-14 - mammalian expression of human full length occludin fused to an mEmerald at the N-terminus (Plasmid #54211)
HGS	Hepatocyte growth factor-regulated tyrosine kinase substrate. Down-regulation of receptor tyrosine kinase via multivesicular body (MVBs) when complexed with STAM.	HRS-RFP – Expresses Hepatocyte growth factor-regulated tyrosine kinase substrate. (Plasmid #29685)
VAPA	Vesicle-associated membrane protein-associated protein A. ER-anchored protein	EGFP-hVAP-A - Expression of human VAP-A fused to GFP in mammalian cells (Plasmid #104447).

2.11.2 Data Analysis

All nanoBRET data was plotted in GraphPad Prism software version 10.3.0 (GraphPad Software, LLC), all quantified data is expressed as mean ± standard error from the mean (SEM). Each condition was performed in triplicate and data from 3 individual experiments were pooled. Values were corrected from the baseline luminescence whereby no fluorescent interactor was transfected in the HEK293T cells. To determine if specific protein-protein binding was occurring, a non-linear regression was performed using a 'One site – Total' model.

Chapter 3: Molecular Cloning and BioID Evaluation

3.1 Introduction

Proteomic studies designed to map protein networks are becoming increasingly popular, largely due to technological and computational advancements and the wider availability of tools required to conduct such research. Interactomics denotes a field in which these protein networks are identified, usually focusing on a single protein subject. Determining the interactome of proteins in organisms is important for understanding cellular pathways and identifying potential novel targets for therapy in disease states. Interactomes are elucidated in a variety of ways, often using mass spectrometry (MS) and computational analyses on the raw MS files. However, prior to this processing, a method of isolating protein complexes or interacting proteins is required. Conventionally, this has been achieved using antibody-based, co-immunoprecipitation (Co-IP) of the target protein in a protein complex and using MS to identify the constituents of the protein complex. While a valuable tool, significant information is lost or not attained using this method. Co-IP identifies the interactome of the target protein at a particular juncture, and unable to elucidate transient protein interactions. Alternative technology has therefore been developed to negate these limitations. Proximity biotin labelling assays are one of the methodologies used, which includes techniques involving enzymes such as ascorbate Peroxidases (APEX) or biotin ligases (BirA) fused to a protein of interest. Of these technologies, BioID has been the most utilised, therefore the best characterised[514]. Therefore, one of the reasons BioID was chosen as an investigation tool. In BioID technology, biotinylated proteins are isolated and analysed via MS. The biotin ligase (BirA) incorporated in the method, can biotinylate proteins which interact transiently with the target protein, and depending on the type of BirA used and can elucidate interactors over several hours. This means interactors are identified over different stages of the cell cycle, not at one particular time, as observed with Co-IP. Hence, a technique such as BioID may be superior in evaluating protein interactomes compared with Co-IP. BioID technology has itself evolved during the initial stages of this project which saw the emergence of BioID2, utilising a smaller, but apparently equally functional variant of the BirA[477]. As this has yet to be fully characterised, the initial experiments compared both BirA variants to diligently select the best approach for the forthcoming project.

Since the lab has previously exploited the original BioID BirA variant (termed BioID1 henceforth), with the BirA fused to centromere protein A (CENPA)[503], tools could be generated in order to compare the BioID1 and BioID2 BirA. CENPA is a centromere-specific variant of histone H3 found in the nucleosome which is essential for formation of the kinetochore and hence, mitosis[515]. However, it is not so much the biology of CENPA that was of interest in this experiment, rather the focus was comparing the two variants of the biotin ligase for appropriate localisation and efficiency of biotinylation. The mycBioID1-

CENPA used in the prior published research to investigate the CENPA microenvironment during mitosis[503] was used to generate a mycBioID2-CENPA plasmid, in which direct comparisons between the BirA variants could be made. As well as the BirA's fused to proteins of interest, the freely expressing BirA's were also compared.

The focus of my PhD research was to evaluate the interactome of membrane-bound proteins associated with angiogenesis and lymphangiogenesis. These include neuropilin 1 (NRP1), NRP2, vascular endothelial growth factor 2 (VEGFR2), and VEGFR3. None of these targets have previously been evaluated using BioID technology. Using BioID methodology with any of these proteins of interest, would represent the single most comprehensive interactome analysis of critical mediators of angiogenesis and lymphangiogenesis. Particular attention is required when fusing the BirA to the N- or C-terminus of these proteins, as biological significance may be vastly different. As these are cell surface receptors, when tagging the N-terminus of these proteins, the interactome would be investigated on the extracellular surface of the cell membrane, identifying interactions via the ectopic domains of surface proteins. If the C-terminus is fused to the BirA, intracellular interactions at the cell membrane would be determined. This is only considering the membrane-bound interactions of these receptors, and not any non-membranous interactions such as moonlighting interactions during mitosis or receptor interactions in intracellular compartments due to internalisation. Ideally, the interactomes at both the N- and C-terminus would be investigated.

The fusion of a tag such as BirA to a protein of interest may result in aberrant activity or localisation. The main way of determining if a protein is suitable for BioID analysis following fusion with a BirA tag, is investigating if the fusion protein exhibits proper localisation when expressed in a relevant cell line. Improper localisation suggests the augmentation of the protein interferes with biological function, and is hence, not a suitable modification. In this case, as the proteins in this project are receptors, the fusion proteins are expected to localise to the cellular membrane, with the exception of some possible internalisation located to intracellular vesicles.

The main aims of this chapter are evaluating which BirA variant to use moving forward in my PhD studies and to generate the tools for the project, in terms of NRP and VEGFR plasmid constructs and evaluating whether they are suitable for BioID technology.

3.2 Results

3.2.1 Comparison of BioID1 and BioID2 Biotinylation Capabilities

3.2.1.1 Biotinylation Capabilities Evaluation of unbound mycBioID1 and mycBioID2

Expressing free mycBioID1 and mycBioID2 tags in cells enabled comparison of biotinylation efficiency. Confocal microscopy analyses of transient transfections of the BioID tags were performed to compare biotinylation efficiency, (Figure 3.1).

Total cell fluorescence measurements were then performed on images acquired in the antimyc-AF555 channel and streptavidin-AF488 channel from cells expressing unbound mycBioID1 and mycBioID2, (Figure 3.2). With the mycBioID2 tag, it appeared a greater increase of streptavidin-AF488 intensity was observed per unit increase of antimyc-AF555 when compared with the mycBioID1 vector. Although the R^2 values are low, demonstrating variability in the dataset, there is a correlation. A statistically significant difference between the correlation lines fitted was observed ($P = 0.0017$). As a control, the fluorescence calculations were also performed in cells untreated with biotin. As expected, the majority of data points did not yield significant streptavidin-AF488 signal intensity. From the free BioID BirA experiments, it was thought that mycBioID2 had a greater biotinylation efficiency. More conclusive evidence was then sought.

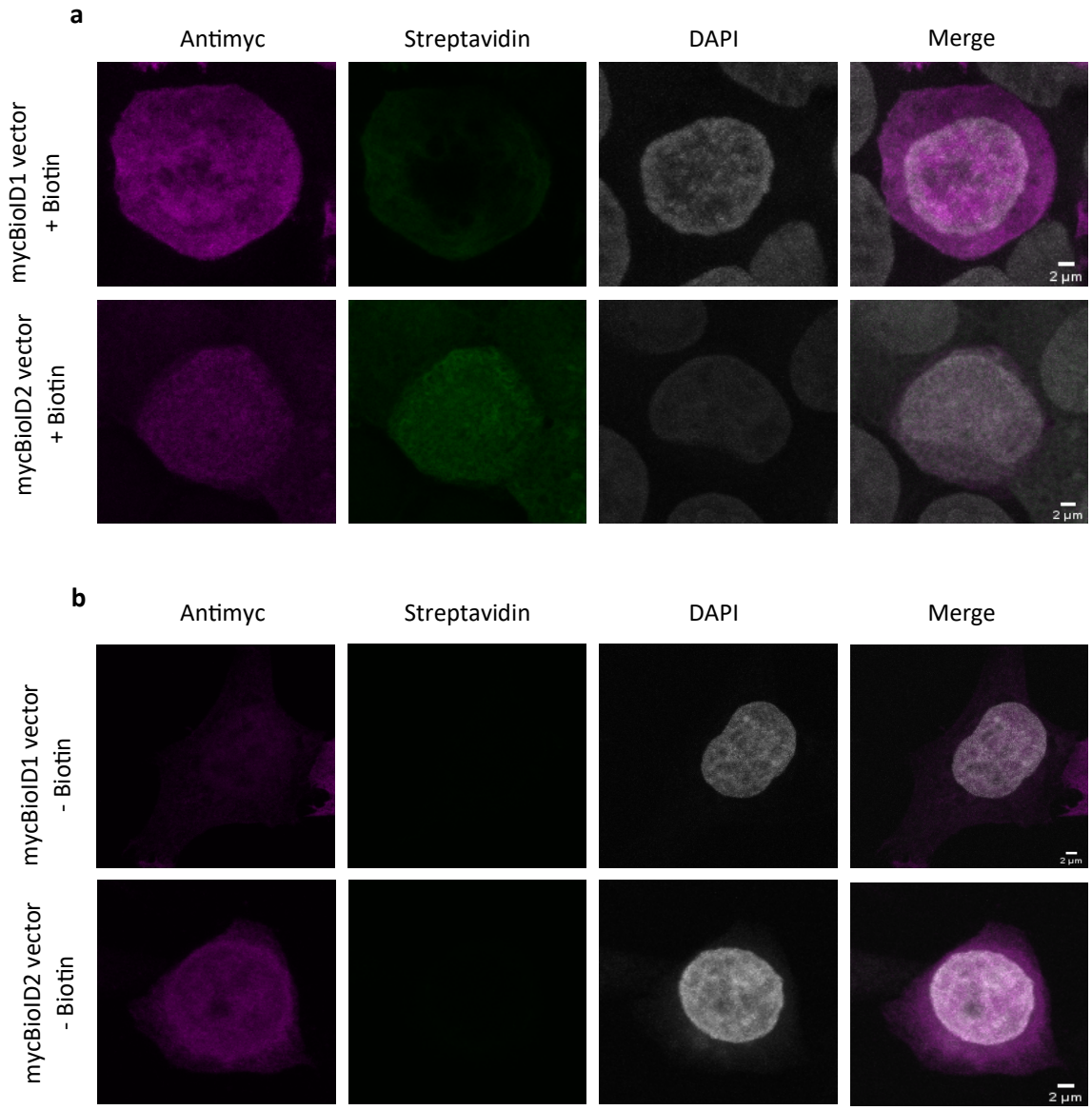

Figure 3.1 – Immunofluorescence images from unbound mycBioID1 BirA and mycBioID2 BirA transient transfections in HeLa Cells. *(a) with the addition of biotin to the cell media. Expression of the BirA is confirmed by antimyc-AF555 (Millipore; 16-255) signal. Correct functioning of the BirA was confirmed by the streptavidin AF488 (Invitrogen; S11223) signal, indicating the presence of biotinylated proteins (b) without the addition of biotin to the cell media.*

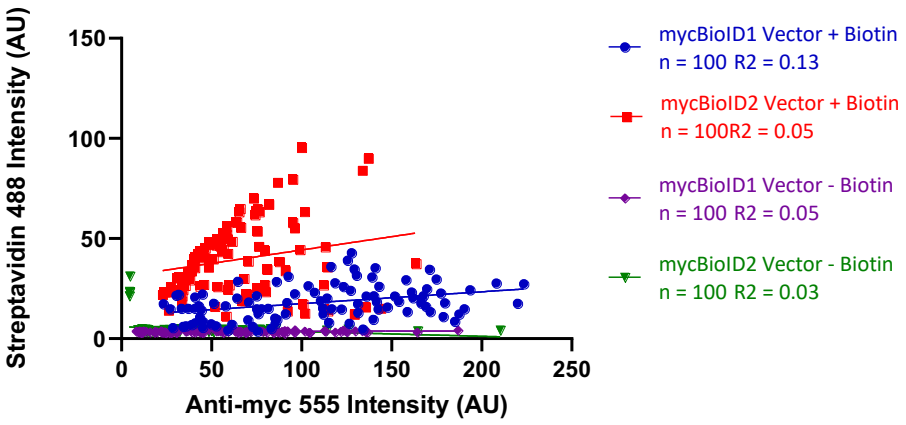

Figure 3.2 – Total cell fluorescence analysis of mycBioID1 compared with mycBioID2. *The total cell fluorescence analysis of BioID tags with and without the addition of biotin to the cell media. mycBioID2 appears to biotinylate proteins with greater efficiency than mycBioID1. No significant streptavidin-AF488 fluorescence is observed in cells devoid of biotin. Each datapoint represents the total cell fluorescence of one cell.*

3.2.1.2 Cloning of mycBioID2-CENPA

Next, a more targeted analysis was performed, comparing BirA variants in real scenarios in a validated model. As discussed in section 3.1, the laboratory has previously employed the original BioID BirA variant (BioID1) fused to centromere protein A (CENPA)[503], thereby enabling comparative analyses with the second-generation BirA (BioID2). CENPA, a centromere-specific histone H3 variant, is integral to nucleosome organization and indispensable for kinetochore assembly and subsequent mitotic progression[515]. mycBioID2-CENPA was subcloned from the existing, previously published BioID1 construct, mycBioID1-CENPA[503]. As the backbones of the BioID vectors are the same, the CENPA could be removed from the existing construct using restriction enzymes and inserted into the new BioID2 vector after digestion with the same enzymes, (Figure 3.3a). The sequence encoding CENPA was initially removed from the original BioID1-CENPA vector by restriction digestion, (Figure 3.3b), with the empty BioID2 vector digested with the same restriction enzymes, (Figure 3.3c). The DNA fragments were then isolated from the gel and ligated together under conditions detailed in Table 3.1. The ligation reactions were then successfully transformed in bacteria, Table 3.2. Individual bacterial colonies were isolated, and plasmids purified to determine if BioID2-CENPA insertion had been successful. Restriction enzymes NheI and XhoI were used to confirm the presence of the BioID2 insert. A positive result would result in a different banding pattern between BioID1-CENPA and BioID2-CENPA, with a smaller second band expected for BioID2-CENPA. Cloning success was confirmed with this restriction enzyme digest, as digestion of the BioID2-CENPA clones resulted in a smaller second band compared to BioID1-CENPA digestion, (Figure 3.3d). Sanger sequencing was performed, which confirmed the expected sequence and cloning of BioID2-CENPA.

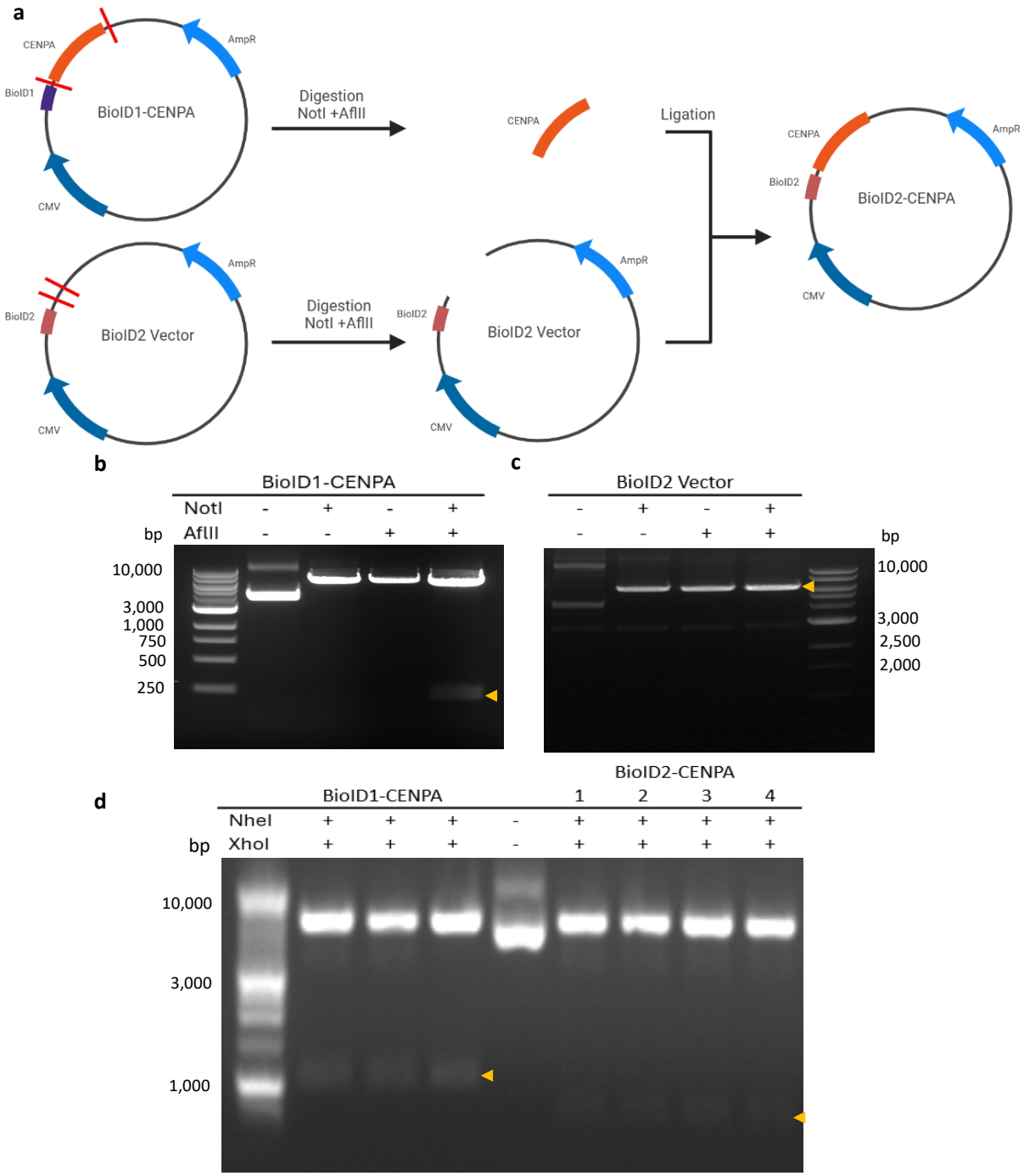

Figure 3.3 – BioID2-CENPA cloning protocol and results. *(a) A schematic representation of the process for generation of BioID2-CENPA, using restriction enzymes NotI and AflII to digest the BioID2 vector and existing BioID1-CENPA to remove the sequence encoding CENPA fragments, followed by fusion of these fragments. (b) Restriction digest of BioID1-CENPA to remove CENPA at 432bp, with the yellow arrow indicating the CENPA band. (c) Restriction enzyme digest of the BioID2 vector showing undigested, single digestions and double digestion reactions. The yellow arrow highlights the extracted band containing the mycBioID2 vector at 6075bp. (d) Test digest of cloned mycBioID2-CENPA using restriction enzymes NheI and XhoI. The original mycBioID1-CENPA was expected to produce bands at 5766bp and 1006bp. The newly cloned mycBioID2-CENPA should elicit bands at 5765bp and 742bp. The difference in lower band size is highlighted with the yellow arrows, indicating successful mycBioID2-CENPA cloning.*

Table 3.1 - Ligation reaction formula for insertion of CENPA into the mycBioID2 vector. *The ratio of BioID2 vector to BioID2 insert was varied with 1:3 and 1:7 ratios used to maximise chances of successful fusion of DNA fragments. A BioID2 vector only control was included to evaluate the propensity of the vector to self-ligate in the absence of insert. Reactions were performed at both room temperature for 2 hours and 16°C for 16 hours.*

Component	**Volume required for a 20µL reaction**		
	1:3	1:7	Control
T4 DNA ligase buffer		2µL	
BioID2 vector		50ng	
CENPA insert	10ng	24ng	0ng
Nuclease free water		To 20µL	
T4 DNA ligase		1µL	

Table 3.2 - Results from the bacterial transformation of BioID2-CENPA ligation reactions in Chemically Competent DH5α E. Coli cells. *Reactions performed at room temperature for 2 hours failed to produce bacterial colonies, whereas several bacterial colonies appeared for both ligation ratios at 16°C for 16 hours. Plasmids were isolated from the colonies for further analysis.*

	Positive Bacterial Colonies	
Ligation Ratio	**RT, 2 h**	**16°C, 16 h**
1:3	0	4
1:7	0	4
Control	0	0

3.2.1.3 Localisation of mycBioID1-CENPA and mycBioID2-CENPA

Initially, validation of correct localisation of the BioID2 fusion protein was required before further assessing biotinylation efficiency. The BioID2-CENPA fusion protein should localise at the centromeres, as has been observed for BioID1-CENPA previously[503], with the appearance of bright puncta within the nuclei of cells. Both BioID1 and BioID2 tags have a myc epitope fused to the N-terminus of the biotin ligase. The myc epitope can be exploited to determine the localisation of the expressed fusion protein within the cell. Figure 3.4a and Figure 3.4b demonstrates the results of HeLa cell transfection, with mycBioID2-CENPA appearing to localise correctly in comparison when compared to mycBioID1-CENPA. As observed, the mycBioID2-CENPA location is highlighted by the bright puncta in antimyc-AF555 channel, which is consistent with the antimyc-AF555 staining in mycBioID1-CENPA.

3.2.1.4 Comparison of Biotinylation Capabilities of mycBioID1-CENPA and mycBioID2-CENPA

The biotinylation efficiency of the tags was then evaluated by measuring the fluorescence intensity of the antimyc-AF555 staining relative to the streptavidin-AF488 staining. Streptavidin is a bacterial protein which has a strong affinity for biotin [504] and hence, biotinylated proteins. Attaching a fluorophore to streptavidin enables visualisation and direct quantification of biotinylation abundance. Hypothetically, the relationship between myc-555 and Strep488 should be linear. However, the

strength of this relationship, accounting for potential differences in biotinylation capabilities of BioID1 and BioID2, remains unknown and was evaluated here. Fluorescence measurements were performed on whole cells and at the puncta for mycBioID1-CENPA and mycBioID2-CENPA constructs, (Figure 3.5).

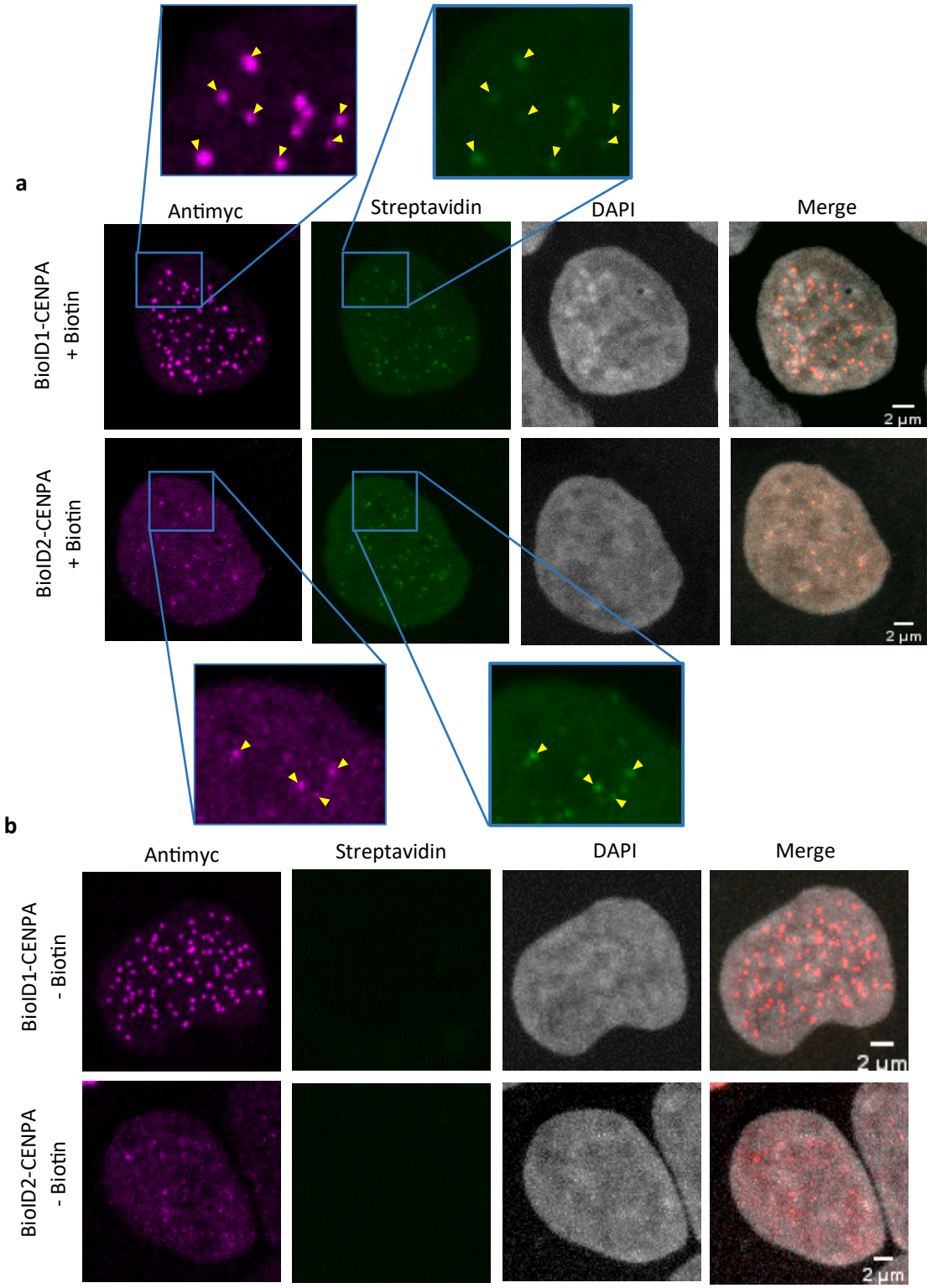

Figure 3.4 – Immunofluorescence images from BioID1-CENPA and BioID2-CENPA transient transfections in HeLa Cells. *Expression of the CENPA fusion proteins is confirmed by antimyc-AF555 (Millipore; 16-255). Correct functioning of the BirA was confirmed by the streptavidin AF488 (Invitrogen; S11223) signal, indicating biotinylated proteins.* ***(a)*** *with the addition of biotin to the cell media. CENPA is highlighted with a magnified portion of the image and identified by the yellow arrows. Fluorescence intensity calculations of these puncta was then performed. (b) without the addition of biotin to the cell media. Centromeres are again identified by the puncta. A lack of streptavidin signal is expectedly observed.*

Fluorescence intensity of antimyc-AF555 and streptavidin-AF488 was measured across whole cells and scored on a 2D plot, (Figure 3.5a). A comparison of linear regression profiles, which demonstrated good R^2 values, revealed BioID2 to have a greater yield of biotinylation to that of BioID 1 (mycBioID1-CENPA vs mycBioID2-CENPA, $P < 0.0001$). As expected, in untreated control cells devoid of biotin, no significant signal is detected in the streptavidin-AF488 channel.

Next, to accommodate for background signal in the nucleoplasm, which potentially dampens the analysis, the same direct quantification was performed specifically at the centromeres, indicated by fluorescent puncta, (Figure 3.5b). Antimyc-AF555 and streptavidin-AF488 fluorescence was measured at the centromeres and scored in a 2D plot. Linear regression profiles furthered evidence of BioID2s greater yield of biotinylation compared to BioID1 (mycBioID1-CENPA vs mycBioID2-CENPA, $P < 0.0001$). Again, no significant fluorescence was observed in the streptavidin-AF488 channel in conditions without biotin added to the cell media.

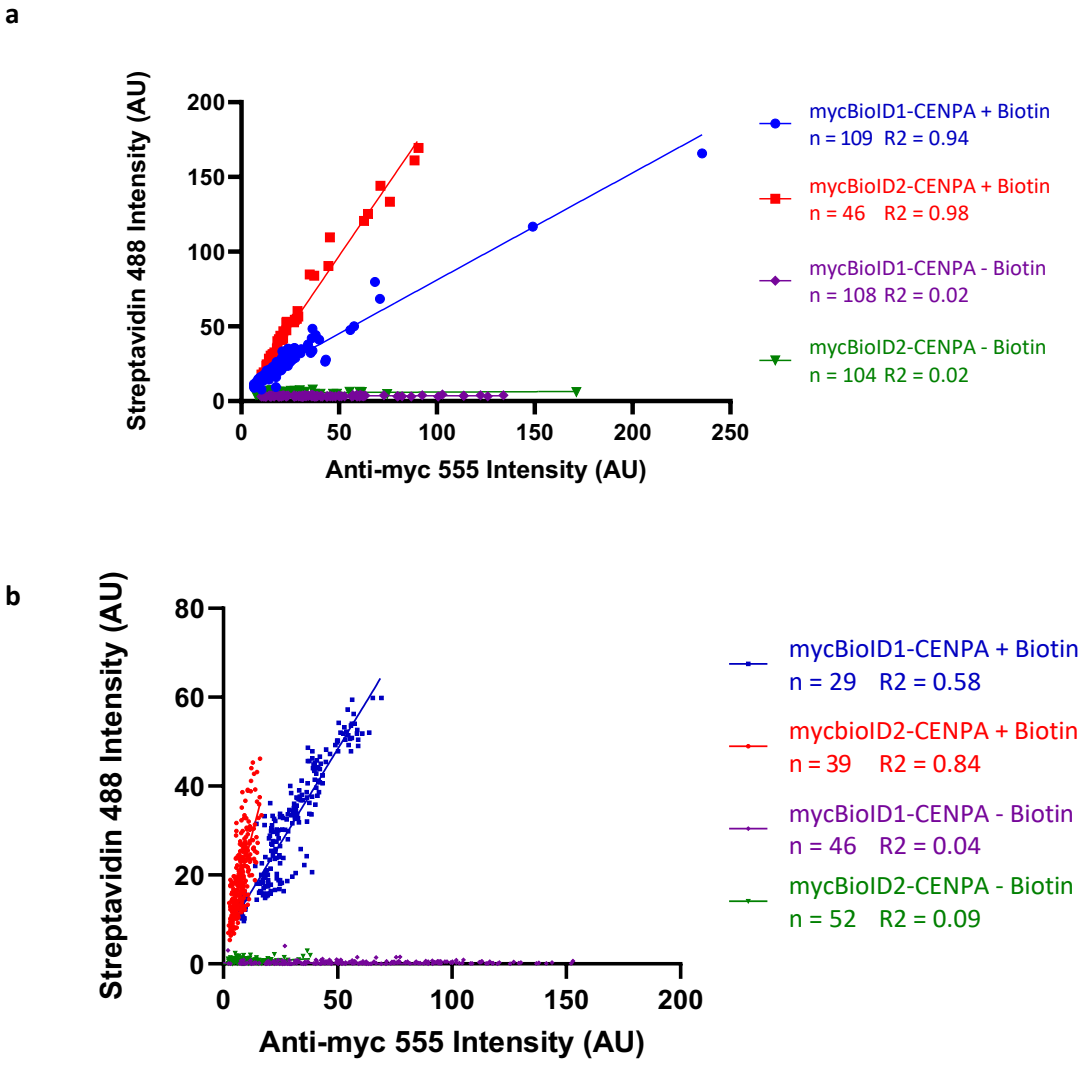

Figure 3.5 – Fluorescence intensity analysis of BioID1-CENPA compared with BioID2-CENPA. *(a) The total cell fluorescence analysis of BioID constructs with and without the addition of biotin to the cell media. Each datapoint represents the total cell fluorescence of one cell (b) The centromeric fluorescence analysis of BioID constructs with and without the addition of biotin to the cell media. Each datapoint represents the fluorescence intensity of one centromere with the results of all cells analysed pooled. The n number denotes number of cells analysed.*

3.2.2 Cloning of BioID2 Plasmids

Following the selection of BioID2 as the appropriate proteomic tool for the rest of the project, a key panel of receptors were identified which have little attention regarding interactome analyses. Thus, the research in this project would be the most comprehensive of its kind. Previous work in the lab group has identified aiming to test and validate around 5-10 candidates provides the best likelihood for success, as the BirA can impede endogenous protein function. The proteins chosen for analysis were vascular endothelial growth factor receptor 2 (VEGFR2), VEGFR3, neuropilin 1 (NRP1) and NRP2,

with both N- and C-terminal BirA fusion proteins generated for a total of 8 plasmids, (Figure 3.6). For all plasmids generated, Sanger sequencing was used to confirm whether cloning had been successful.

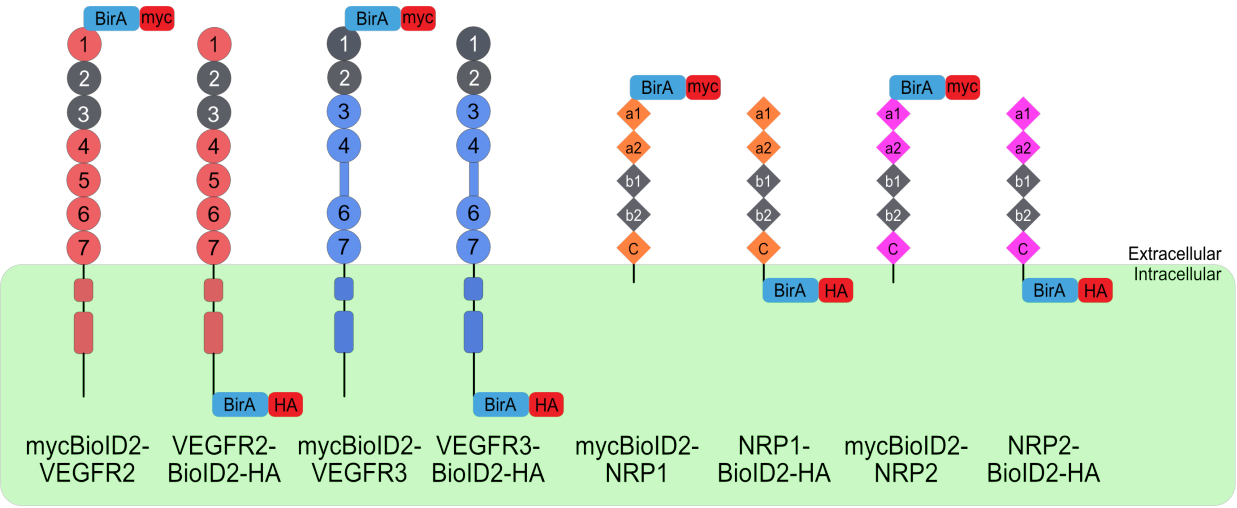

Figure 3.6 – Schematic illustrating the BioID cloned plasmids of VEGFR2, VEGFR3, NRP1 and NRP1 and relative locations of the biotin ligase. *The biotin ligase (BirA) is fused to the N-terminus and C-terminus of proteins of interest which pertain to an extracellular or intracellular BirA, respectively. For fusion protein identification, the BirA is fused to a myc epitope for the extracellular, N-terminal BirA, while the intracellular, C-terminal BirA is fused to a HA epitope. Ligand binding structures in the extracellular portions of the VEGFRs and NRPs are denoted as grey circles. The numbers denote extracellular domain regions of the particular membrane protein.*

3.2.2.1 Cloning of mycBioID2-VEGFR3

To define the N-terminal interactome of VEGFR3, BioD2 BirA was fused to the N-terminus of full length human VEGFR3. The already cloned HaloTag-VEGFR3 (data not shown) was used to subclone in a mycBioID2 tag, (Figure 3.7a). The sequence encoding mycBioID2 was isolated via PCR, (Figure 3.7b), and then ligated into the VEGFR3 backbone after removing the sequence encoding the HaloTag from HaloTag-VEGFR3 using restriction enzymes SacII and PvuI, (Figure 3.7c). Ligation conditions are detailed in Table 3.3. Each ligation condition was then transformed in bacteria, with the number of positive colonies detailed in Table 3.4. Single bacterial colonies were isolated and analysed for correct sequence.

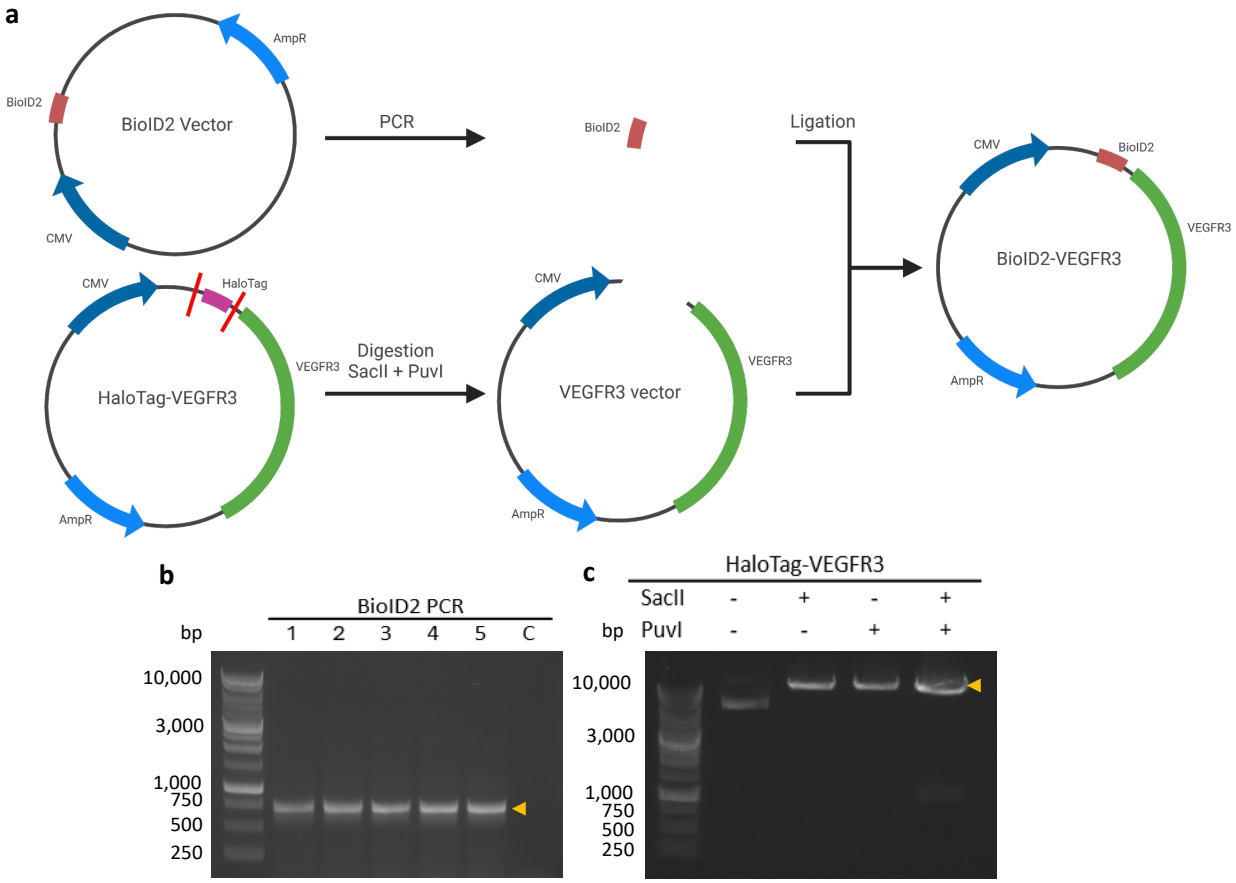

Figure 3.7– mycBioID2-VEGFR3 cloning protocol and results. *(a) A schematic representation of the process used for generation of mycBioID2-VEGFR3, using restriction enzymes SacII and PvuI to digest mycBioID2 PCR fragments and HaloTag-VEGFR previously synthesised, to remove the HaloTag and fuse the mycBioID2 and VEGFR3 fragments. (b) mycBioID2 PCR with 5 repeats. The expected size of amplified product is 735bp, highlighted with the yellow arrow, showing successful amplification of mycBioID2. (c) Restriction enzyme digest of HaloTag-VEGFR3 showing undigested, single digestions and double digestion reactions. The yellow arrow highlights the extracted band containing the VEGFR3 vector, which is 9311bp as demonstrated by the band on the gel. No suitable enzymes were available for a test digest experiment.*

Table 3.3 - Ligation reaction formula for insertion of BioID2 into the VEGFR3 vector. *The ratio of VEGFR3 vector to BioID2 insert was varied from 1:1 to 1:10 to maximise chances of successful fusion of DNA fragments. A VEGFR3 vector only control was included to evaluate the propensity of the vector to self-ligate in the absence of insert. Reactions were performed at both room temperature for 2 hours and 16°C for 16 hours.*

Component	**Volume required for a 10µL reaction**					
	1:1	1:3	1:5	1:7	1:10	Control
T4 DNA ligase buffer				**1µL**		
VEGFR3 vector				50ng		
BioID2 insert	4ng	12ng	20ng	28ng	40ng	0ng
Nuclease free water				To **10µL**		
T4 DNA ligase				**1µL**		

Table 3.4 - Results from the bacterial transformation of BioID2-VEGFR3 ligation reactions in Chemically Competent DH5α *E. Coli* cells. *Several reaction conditions failed to produce viable bacterial colonies. Plasmids were isolated from the conditions which were successfully bacterially transformed.*

	Positive Bacterial Colonies	
Ligation Ratio	**RT, 2 h**	**16°C, 16 h**
1:1	0	0
1:3	0	1
1:5	0	0
1:7	0	3
1:10	1	4
Control	0	0

3.2.2.2 Cloning of VEGFR3-BioID2-HA

Next, we sought to define the C-terminal interactome of VEGFR3. An existing VEGFR3-HaloTag (data not shown) was used as a source of full length human VEGFR3, whereby the BioID2 BirA was ligated into this plasmid replacing the sequence for HaloTag using XhoI and XbaI restriction enzymes, (Figure 3.8a). Initially, appropriate PCR amplification of BioID2-HA was confirmed, (Figure 3.8b). VEGFR3-HaloTag was digested by the same restriction enzymes, and the band relating to the VEGFR3 vector was purified, (Figure 3.8c). A series of ligation reaction conditions were used to maximise ligation success rate, Table 3.5, confirmed by colonies present following bacterial transformation, Table 3.6.

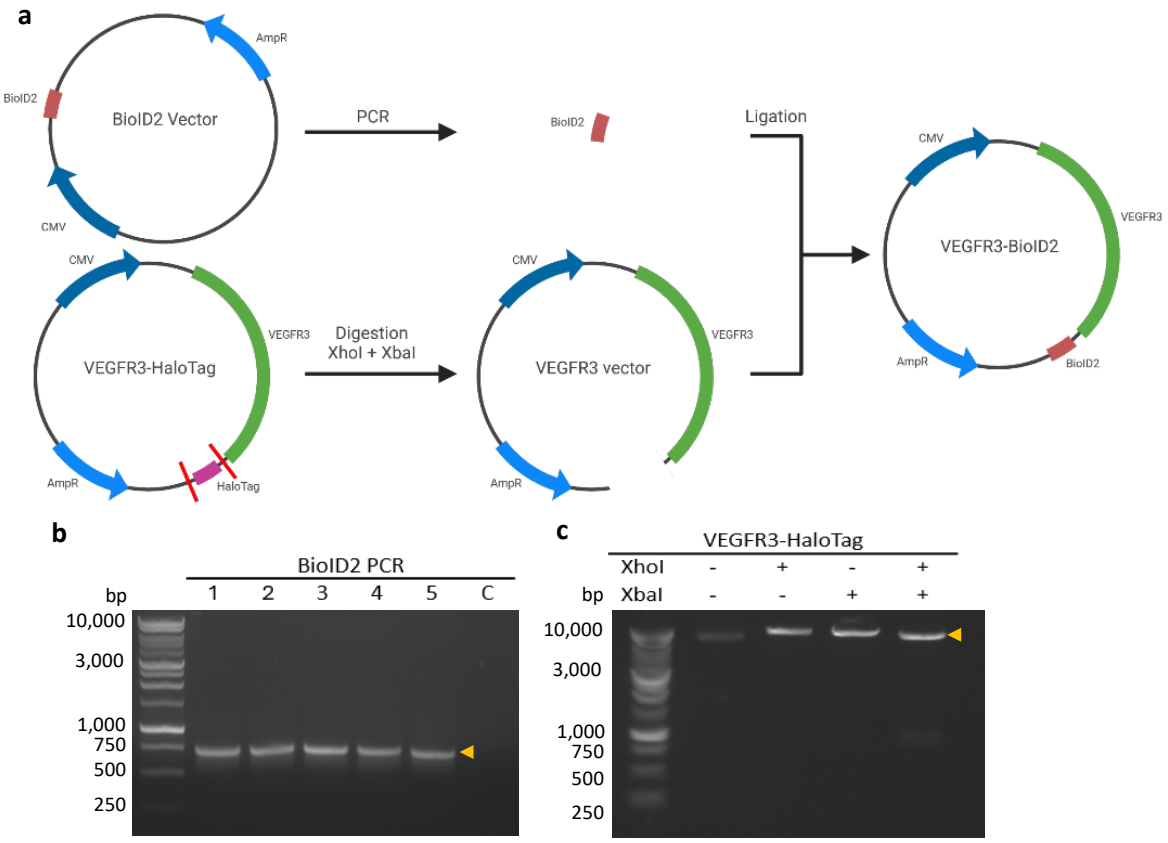

Figure 3.8 – VEGFR3-BioID2-HA cloning protocol and results. *(a) A schematic representation of the process used for generation of VEGFR3-BioID2-HA, using restriction enzymes XhoI and XbaI to digest BioID2-HA PCR fragments and VEGFR3-HaloTag previously synthesised, to remove the HaloTag and fuse the BioID2-HA and VEGFR3 vector fragments. (b) BioID2-HA PCR with 5 repeats. The expected size of amplified product is 732bp, highlighted with the yellow arrow (c) Restriction enzyme digest of VEGFR3-HaloTag showing undigested, single digestions and double digestion reactions. The yellow arrow highlights the extracted band containing the HaloTag vector, which is 9334bp as demonstrated by the band on the gel. No suitable enzymes were available for a test digest experiment.*

Table 3.5 - Ligation reaction formula for insertion of BioID2-HA into the VEGFR3 vector. *The ratio of VEGFR3 vector to BioID2-HA insert was varied from 1:1 to 1:10 to maximise chances of successful fusion of DNA fragments. A VEGFR3 vector only control was included to evaluate the propensity of the vector to self-ligate in the absence of insert. Reactions were performed at both room temperature for 2 hours and 16°C for 16 hours.*

Component	**Volume required for a 10µL reaction**					
	1:1	1:3	1:5	1:7	1:10	Control
T4 DNA ligase buffer				**1 µL**		
VEGFR3 vector				50ng		
BioID2 insert	4ng	12ng	21ng	29ng	42ng	0ng
Nuclease free water				To **10µL**		
T4 DNA ligase				**1µL**		

Table 3.6 - Results from the bacterial transformation of VEGFR3-BioID2-HA ligation reactions in Chemically Competent DH5α E. Coli cells. *Several reaction conditions failed to produce viable bacterial colonies. Plasmids were isolated from the conditions which were successfully bacterially transformed.*

	Positive Bacterial Colonies	
Ligation Ratio	**RT, 2 h**	**16°C, 16 h**
1:1	0	0
1:3	2	3
1:5	0	4
1:7	3	1
1:10	0	2
Control	0	0

3.2.2.3 Cloning of mycBioID2-VEGFR2

The cloning protocol for mycBioID2-VEGFR2 utilised an existing HaloTag-VEGFR2 plasmid[354] whereby the sequence for HaloTag was removed using restriction enzymes SacII and XhoI, followed by insertion of the BioID2 BirA sequence, (Figure 3.9a). The same PCR product used for the cloning of mycBioID2-NRP1 was used in this experiment, (Figure 3.11b). Following successful isolation of BioID2 BirA PCR product, the HaloTag sequence was removed from HaloTag-VEGFR2 using restriction enzymes, (Figure 3.9b). Ligation conditions of the BioID2 BirA into the VEGFR2 backbone was varied to maximise chances of successful cloning, Table 3.7. The ligation reactions were bacterially transformed, Table 3.8, and single colonies were validated for the mycBioID2-VEGFR2 sequence.

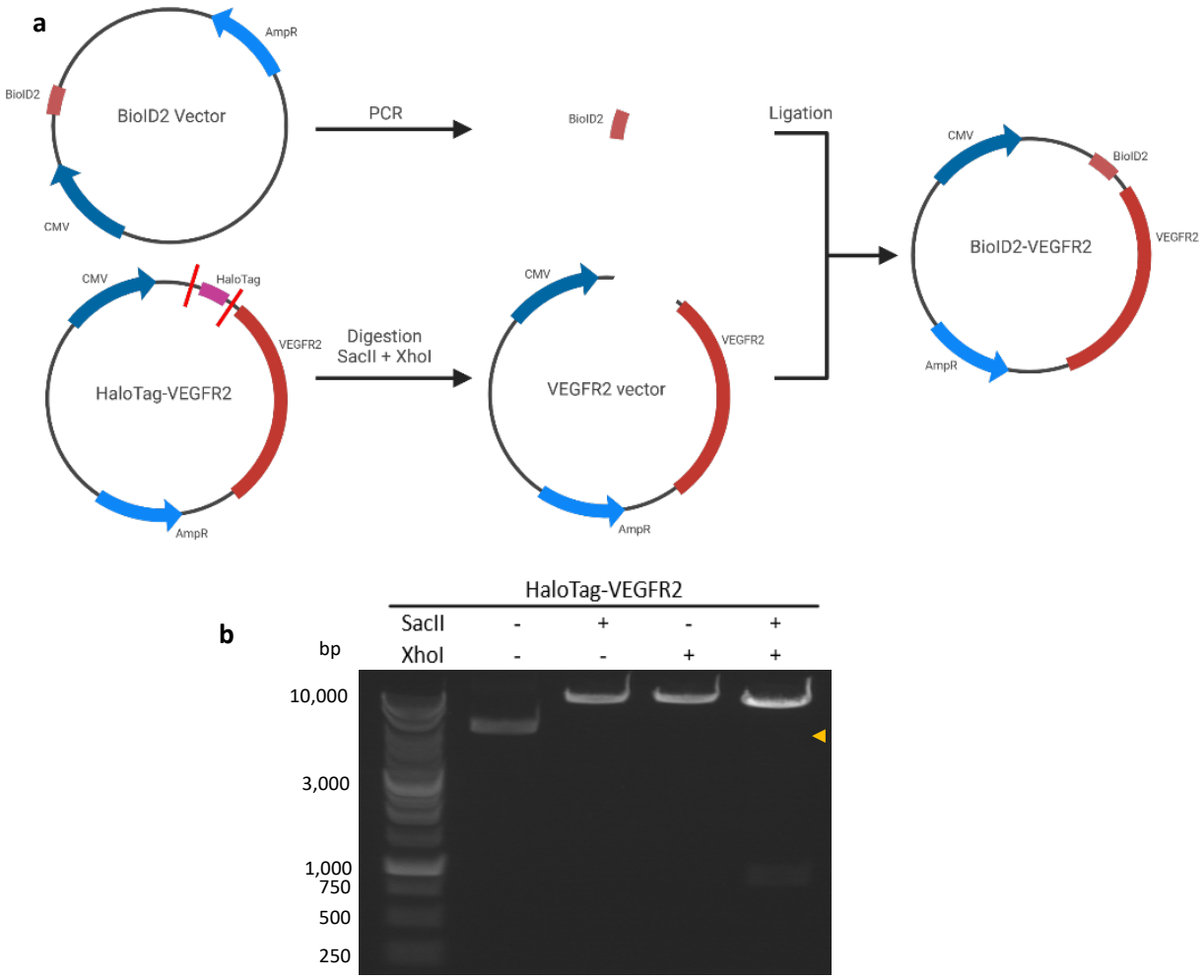

Figure 3.9 – mycBioID2-VEGFR2 cloning protocol and results. *(a) A schematic representation of the process used for generation of BioID2-VEGFR2, using restriction enzymes SacII and XhoI to digest BioID2 PCR fragments and existing HaloTag-NRP1 to remove the NRP1, followed by fusion of these fragments. The BioID2 PCR fragments used was the same as for BioID2-NRP1 cloning. (b) Restriction enzyme digest of HaloTag-VEGFR2 showing undigested, single digestions and double digestion reactions. The yellow arrow highlights the extracted band containing the VEGFR2 vector, which is 9390bp as demonstrated by the band on the gel. No suitable enzymes were available for a test digest experiment.*

Table 3.7 - Ligation reaction formula for insertion of mycBioID2 into the VEGFR2 vector. *The ratio of VEGFR2 vector to mycBioID2 insert was varied from 1:1 to 1:10 to maximise chances of successful fusion of DNA fragments. A VEGFR2 vector only control was included to evaluate the propensity of the vector to self-ligate in the absence of insert. Reactions were performed at both room temperature for 2 hours and 16°C for 16 hours.*

Component	**Volume required for a 10µL reaction**					
	1:1	1:3	1:5	1:7	1:10	Control
T4 DNA ligase buffer				**1µL**		
VEGFR2 vector				50ng		
BioID2 insert	4ng	12ng	20ng	28ng	40ng	0ng
Nuclease free water				To 10**µL**		
T4 DNA ligase				**1µL**		

Table 3.8 - Results from the bacterial transformation of mycBioID2-VEGFR2 ligation reactions in Chemically Competent DH5α E. Coli cells. *Several reaction conditions failed to produce viable bacterial colonies, with only one condition resulting in growth of colonies. Plasmids were isolated from only successful reaction condition for further analysis.*

	Positive Bacterial Colonies	
Ligation Ratio	**RT, 2 h**	**16°C, 16 h**
1:1	0	0
1:3	0	0
1:5	0	0
1:7	0	0
1:10	3	0
Control	0	0

3.2.2.4 Cloning of VEGFR2-BioID2-HA

An existing VEGFR2-HaloTag (unpublished) was used to subclone VEGFR2-BioID2-HA, by removing the sequence coding for HaloTag and replacing it with a sequence for BioID2-HA, (Figure 3.10a). Similar to the previously discussed C-terminal cloning methods, XhoI and XbaI restiriction enzymes were utilised in the removal of the the HaloTag sequence, (Figure 3.10b). The PCR product from VEGFR3-BioID2-HA cloning was also used in VEGFR2-BioID2-HA cloning, (Figure 3.8b). Ligation conditions were again varied to maximise chances of cloning success, Table 3.9, resulting in the presentation of several colonies on agarose plates, Table 3.10. Several colonies were chosen for amplification of plasmid DNA and sequence of VEGFR2-BioID2-HA was confirmed using Sanger sequencing.

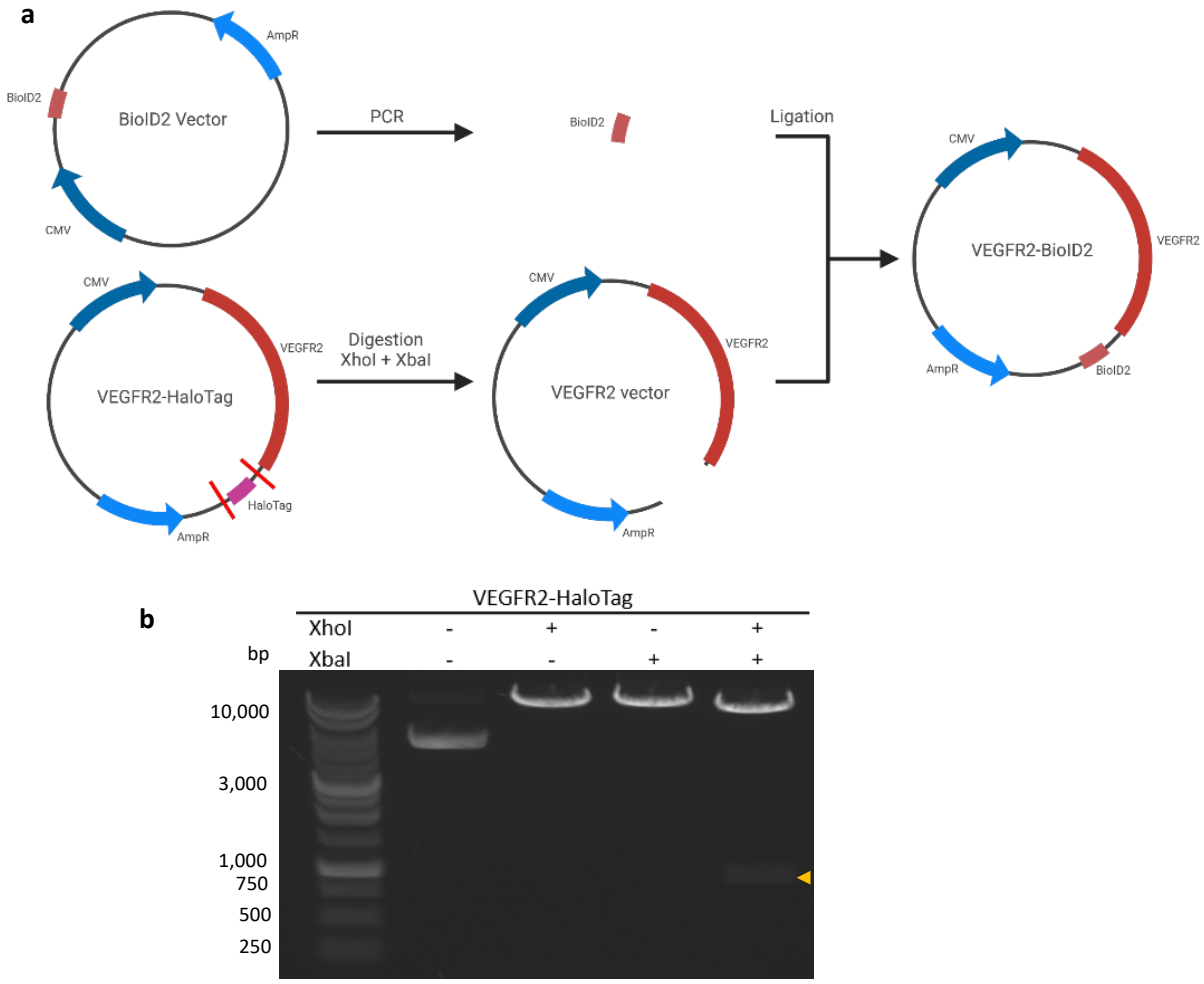

Figure 3.10 – VEGFR2-BioID2-HA cloning protocol and results. *(a) A schematic representation of the process used for generation of VEGFR2-BioID2-HA, using restriction enzymes XhoI and XbaI to digest BioID2-HA PCR fragments and existing VEGFR2-HaloTag to remove the HaloTag, followed by fusion of these fragments. The BioID2-HA PCR fragments used was the same as for NRP1-BioID2-HA cloning. (b) Restriction enzyme digest of VEGFR2-HaloTag showing undigested, single digestions and double digestion reactions. The yellow arrow highlights the extracted band containing the VEGFR2 vector, which is 9407bp as demonstrated by the band on the gel. No suitable enzymes were available for a test digest experiment.*

Table 3.9 - Ligation reaction formula for insertion of BioID2-HA into the VEGFR2 vector. *The ratio of VEGFR2 vector to BioID2-HA insert was varied from 1:1 to 1:10 to maximise chances of successful fusion of DNA fragments. A VEGFR2 vector only control was included to evaluate the propensity of the vector to self-ligate in the absence of insert. Reactions were performed at both room temperature for 2 hours and 16°C for 16 hours.*

Component	**Volume required for a 10µL reaction**					
	1:1	1:3	1:5	1:7	1:10	Control
T4 DNA ligase buffer				**1µL**		
VEGFR2 vector				50ng		
BioID2 insert	5ng	15ng	25ng	35ng	50ng	0ng
Nuclease free water				To 10**µL**		
T4 DNA ligase				**1µL**		

Table 3.10 - Results from the bacterial transformation of VEGFR2-BioID2-HA ligation reactions in Chemically Competent DH5α E. Coli cells. *Several reaction conditions failed to produce viable bacterial colonies. Plasmids were isolated from only successful reaction condition for further analysis.*

	Positive Bacterial Colonies	
Ligation Ratio	**RT, 2 h**	**16°C, 16 h**
1:1	0	0
1:3	0	0
1:5	0	3
1:7	1	1
1:10	0	0
Control	0	0

3.2.2.5 Cloning of mycBioID2-NRP1

To map the extracellular interactome of NRP1, BioID2 was fused to the N-terminus of human NRP1. This already synthesised HaloTag-NRP1 plasmid[354] was used to subclone replacing the region coding for HaloTag with a BioID2 BirA sequence using restriction enzymes SacI and XhoI, (Figure 3.11a). Firstly, the BioID2 BirA PCR was confirmed, (Figure 3.11b), and the NRP1 backbone was generated by restriction enzyme digests to remove the HaloTag sequence, (Figure 3.11c). Varying ligation conditions of BioID2 into the NRP1 backbone as used in order to maximise chances of success, Table 3.11. The ligation reactions were bacterially transformed, Table 3.12, and single colonies were chosen to validate success of cloning.

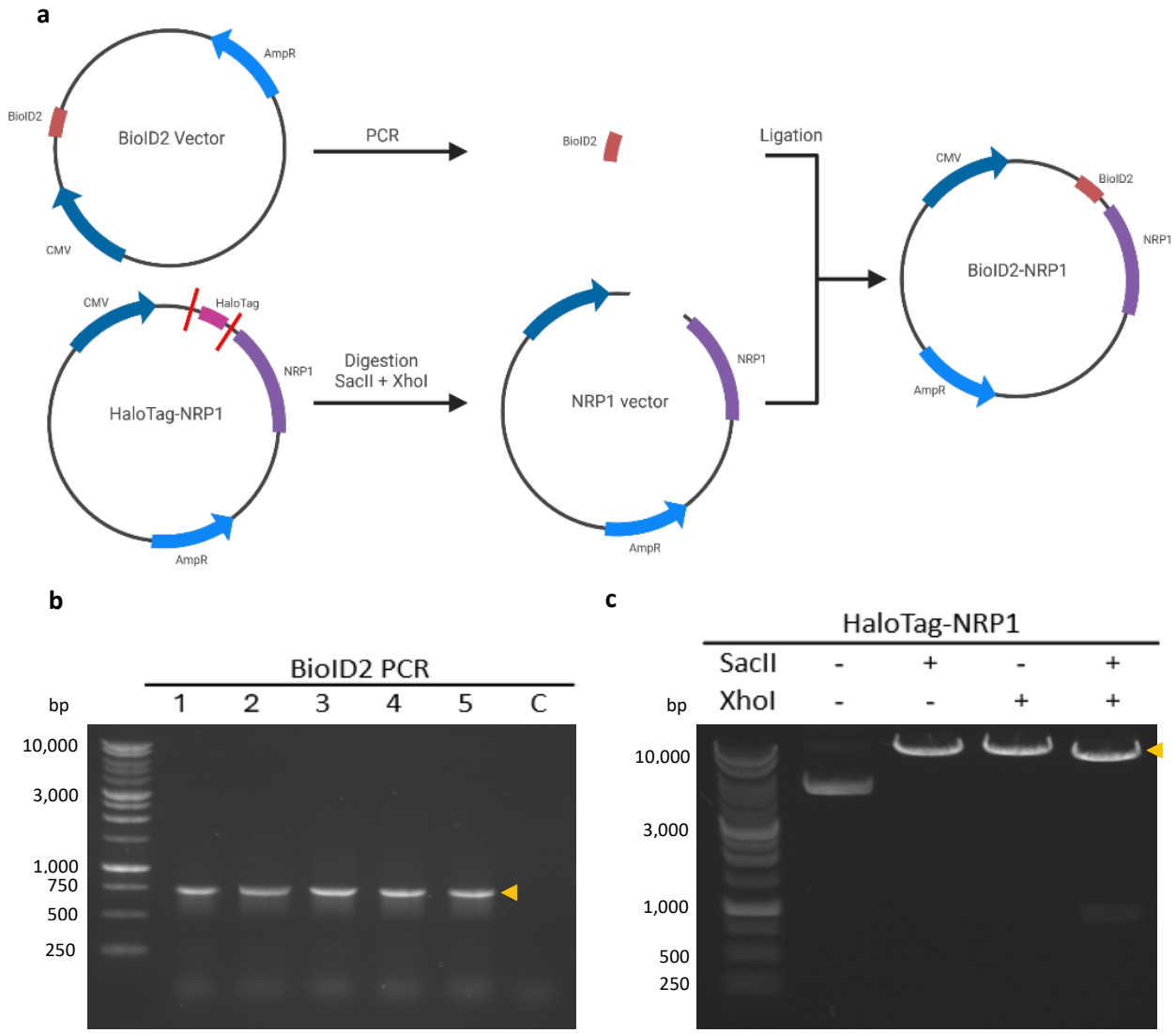

Figure 3.11 – mycBioID2-NRP1 cloning protocol and results. *(a) A schematic representation of the process used for generation of mycBioID2-NRP1, using restriction enzymes SacII and XhoI to digest mycBioID2 PCR fragments and existing HaloTag-NRP1 to remove the HaloTag, followed by fusion of these fragments. (b) mycBioID2 PCR with 5 repeats. The expected size of amplified product is 735bp, highlighted with the yellow arrows (c) Restriction enzyme digest of HaloTag-NRP1 showing undigested, single digestions and double digestion reactions. The yellow arrow highlights the extracted band containing the NRP1 vector, which is 8097bp as demonstrated by the band on the gel. No suitable enzymes were available for a test digest experiment.*

Table 3.11 - Ligation reaction formula for insertion of mycBioID2 into the NRP1 vector. *The ratio of NRP1 vector to mycBioID2 insert was varied from 1:1 to 1:10 to maximise chances of successful fusion of DNA fragments. A NRP1 vector only control was included to evaluate the propensity of the vector to self-ligate in the absence of insert. Reactions were performed at both room temperature for 2 hours and 16°C for 16 hours.*

Component	**Volume required for a 10µL reaction**					
	1:1	1:3	1:5	1:7	1:10	Control
T4 DNA ligase buffer				**1µL**		
NRP1 vector				50ng		
BioID2 insert	4ng	13ng	22ng	30ng	43ng	0ng
Nuclease free water				To **10µL**		
T4 DNA ligase				**1µL**		

Table 3.12 - Results from the bacterial transformation of mycBioID-NRP1 ligation reactions in Chemically Competent DH5α E. Coli cells. *Several reaction conditions failed to produce viable bacterial colonies. Plasmids were isolated from the conditions which were successfully bacterially transformed.*

	Positive Bacterial Colonies	
Ligation Ratio	**RT, 2 h**	**16°C, 16 h**
1:1	0	1
1:3	0	6
1:5	3	4
1:7	4	1
1:10	1	0
Control	0	0

3.2.2.6 Cloning of NRP1-BioID2-HA

For investigation of the recruitment of proteins at the intracellular domain of NRP1, the reciprocal C-terminal BioID plasmid required synthesising, using an existing NRP1-HaloTag plasmid (unpublished) and restriction enzymes XhoI and XbaI, (Figure 3.12a). After successful confirmation of BioID2 amplification via PCR, (Figure 3.12b), the HaloTag sequence was removed from NRP1-HaloTag using restriction enzymes, (Figure 3.12c). Following successful ligation with varied conditions, Table 3.13, and bacterial transformation, Table 3.14, singles colonies were chosen for sequence validation.

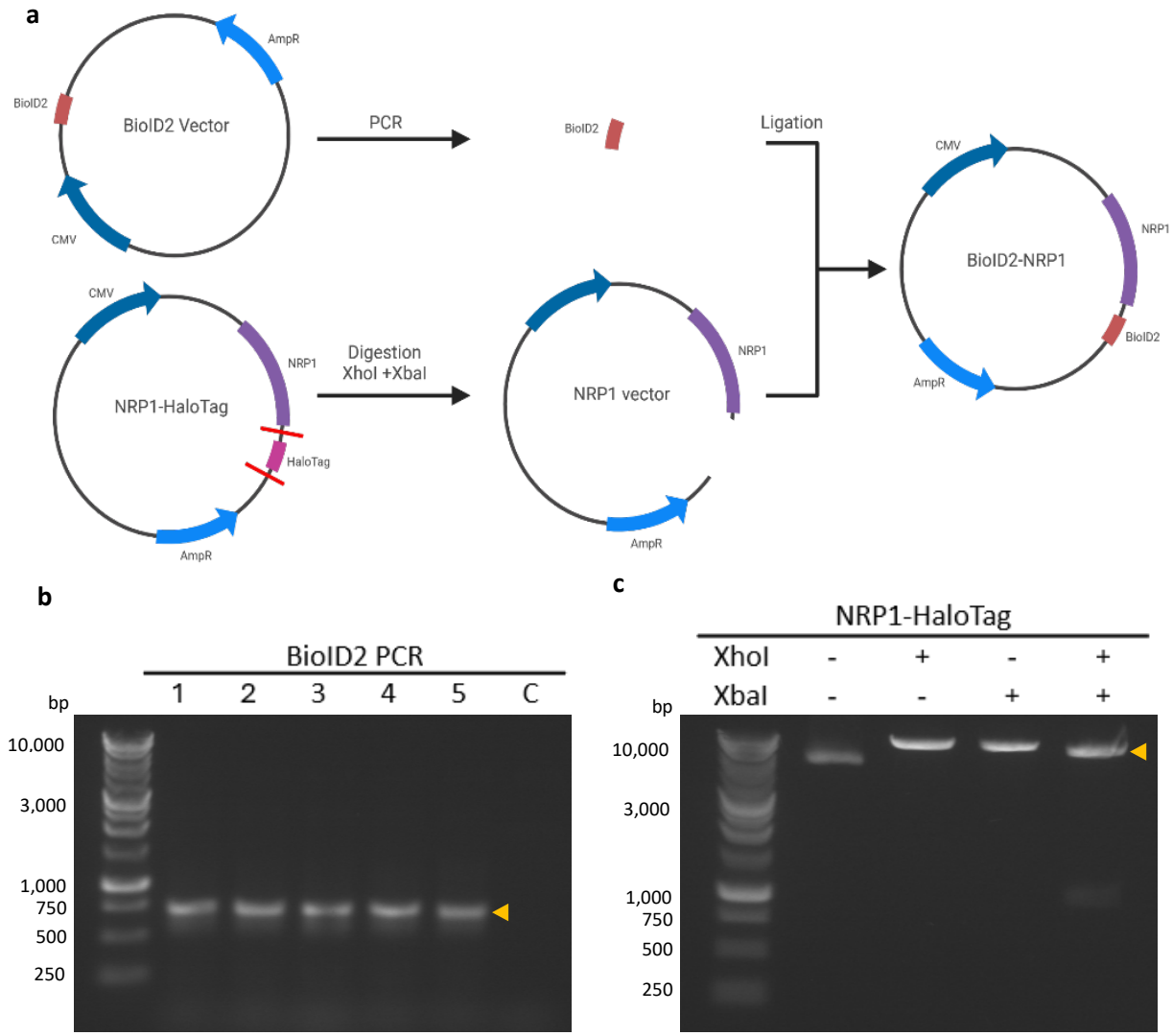

Figure 3.12 – NRP1-BioID2-HA cloning protocol and results. *(a) A schematic representation of the process used for generation of NRP1-BioID2-HA, using restriction enzymes XhoI and XbaI to digest BioID2-HA PCR fragments and existing NRP1-HaloTag to remove the HaloTag, followed by fusion of these fragments. (b) BioID2-HA PCR with 5 repeats. The expected size of amplified product is 732bp, highlighted by the yellow arrows. (c) Restriction enzyme digest of NRP1-HaloTag showing undigested, single digestions and double digestion reactions. The yellow arrow highlights the extracted band containing the NRP1 vector, which is around 8000 bp as demonstrated by the band on the gel. No suitable enzymes were available for a test digest experiment.*

Table 3.13 - Ligation reaction formula for insertion of BioID2-HA into the NRP1 vector. *The ratio of NRP1 vector to BioID2-HA insert was varied from 1:1 to 1:10 to maximise chances of successful fusion of DNA fragments. A NRP1 vector only control was included to evaluate the propensity of the vector to self-ligate in the absence of insert. Reactions were performed at both room temperature for 2 hours and 16°C for 16 hours.*

Component	**Volume required for a 10µL reaction**					
	1:1	1:3	1:5	1:7	1:10	Control
T4 DNA ligase buffer				**1µL**		
NRP1 vector				50ng		
BioID2 insert	4ng	12ng	23ng	31ng	44ng	0ng
Nuclease free water				To **10µL**		
T4 DNA ligase				**1µL**		

Table 3.14 - Results from the bacterial transformation of NRP1-BioID2-HA ligation reactions in Chemically Competent DH5α E. Coli cells. *Several reaction conditions failed to produce viable bacterial colonies. Plasmids were isolated from the conditions which were successfully bacterially transformed.*

	Positive Bacterial Colonies	
Ligation Ratio	**RT, 2 h**	**16°C, 16 h**
1:1	0	0
1:3	0	1
1:5	3	3
1:7	2	4
1:10	0	0
Control	0	0

3.2.2.7 Cloning of NRP2 BioID Constructs

Cloning of both N- and C-terminal BioID2 NRP2 constructs was performed by GenScript and analysed for correct sequence by Plasmidsaurus using Oxford Nanopore Technology with custom analysis and annotation.

3.2.3 Validation of BioID Plasmids

Proximity proteomics is powerful, but laborious and expensive, therefore a systematic approach is required to assess candidate validity. This begins with a localisation assay, but later biochemical, but all prior to scaling up for proteomics. As BioID is a proximity proteomics approach, the key to its success is the correct localisation of fusion candidates. Therefore, validation of the cloned BioID plasmids was performed using IF, which evaluated expression and distribution of the newly generated panel of candidates. All constructs were transiently transfected using FuGENE HD (Promega Corporation; E2311) into HEK293T cells with an expression period of 48 h in the presence or absence of 50µM biotin for 24 h, prior to fixation and preparation for IF. Anti-myc targeting antibodies was used to detect for N-terminal BioID fusion proteins, (Figure 3.13 and Figure 3.14), while anti-HA antibodies detected C-

terminal BioID fusion proteins, (Figure 3.15). Labelling with fluorescent streptavidin, which has strong affinity for biotin and biotinylated proteins[504], confirmed the functionality of the BirA enzyme.

3.2.3.1 Expression of N-terminal BioID Plasmids in HEK293T Cells

Expression of the N-terminally tagged BioID2 constructs demonstrated mixed results between the NRPs and the VEFGRs. For NRP1 and NRP2, (Figure 3.13a and Figure 3.13b), localisation of the fusion protein was observed at the cell membrane. Strong signals in the streptavidin channels indicated sufficient biotinylation, making them promising candidates for future BioID proteomics studies. Diffuse staining of streptavidin-AF488 in the cytoplasm was observed, indicating interactors localised to the cytoplasm. Additionally, transfection efficiency of these constructs was high. The expression of the BioID VEGFR2 and VEGFR3 proteins, (Figure 3.13c and Figure 3.13d), however raised some concerns. Although strong biotinylation signals indicated correct functioning of the BirA, the localisation of tagged VEGFR2 or VEGFR3 was not as expected. The antimyc-AF555 signals appeared intracellular and localised to a structure surrounding the nucleus. Despite this, there were some cells which demonstrated correct localisation, however, they were not representative of the cell population, (Figure 3.14a and Figure 3.14b). The generally poor localisation and a low transfection efficiency of these fusion proteins raised questions whether tagged VEGFR2 or VEGFR3 would be suitable receptors for BioID applications.

3.2.3.2 Expression of C-terminal BioID Plasmids

Expression of the C-terminal BioID2 fusion proteins was generally positive. Again, for the NRPs, (Figure 3.15a and Figure 3.15d), expression of the BioID2 tagged receptor was at the cell membrane, indicated by antimyc-AF555 signals. The correct functioning of the BirA was confirmed in positive streptavidin-AF488 signals. Like their N-terminal counterparts, transfection efficiency was high. The expression of C terminal tagged VEGFR2 or VEGFR3, (Figure 3.15c and Figure 3.15d), also demonstrated expression at the cell membrane and correct functioning of the BirA. A low transfection efficiency was observed with these plasmids in comparison to NRP1.

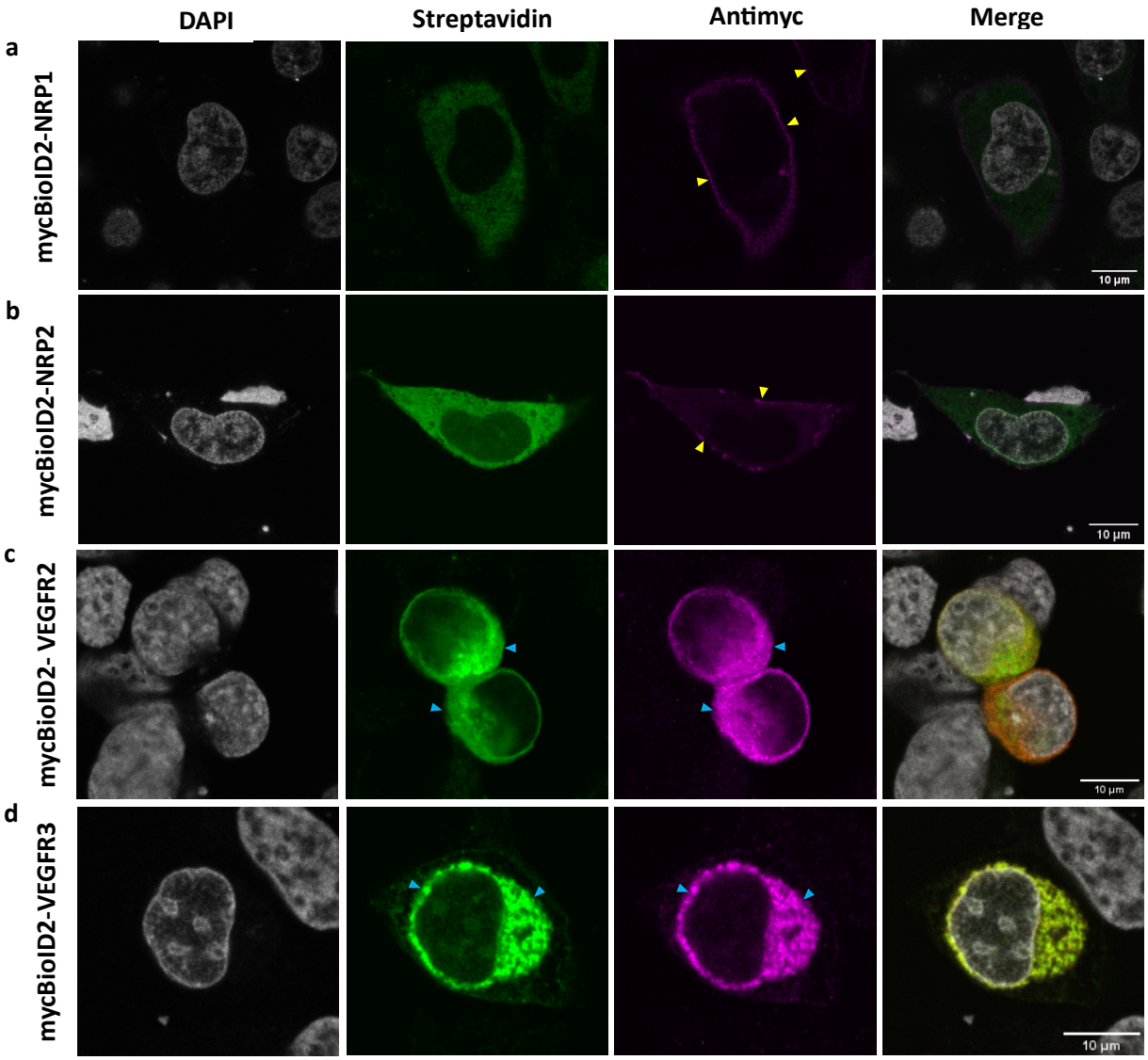

Figure 3.13 - Immunofluorescence of HEK293T cell transfected with N-terminal BioID2 constructs*; (a) mycBioID2-NRP1; (b) mycBioID2-NRP2; (c) mycBioID2-VEGFR2; (d) mycBioID2-VEGFR3. HEK293T cells were incubated with DNA/PEI transfection mix for 24 h, followed by a 50µM biotin supplementation for a further 20 h. Cells were then fixed and incubated with antimyc-AF555 antibody (Millipore; 16-255) which shows localisation of the BioID fusion protein and streptavidin-AF488 (Invitrogen; S11223) which provides information on biotinylated proteins. All images had brightness increased by 40% and contrast reduced 20%. Yellow arrows indicate cellular membrane localisation. Blue arrows indicate localisation to intracellular components.*

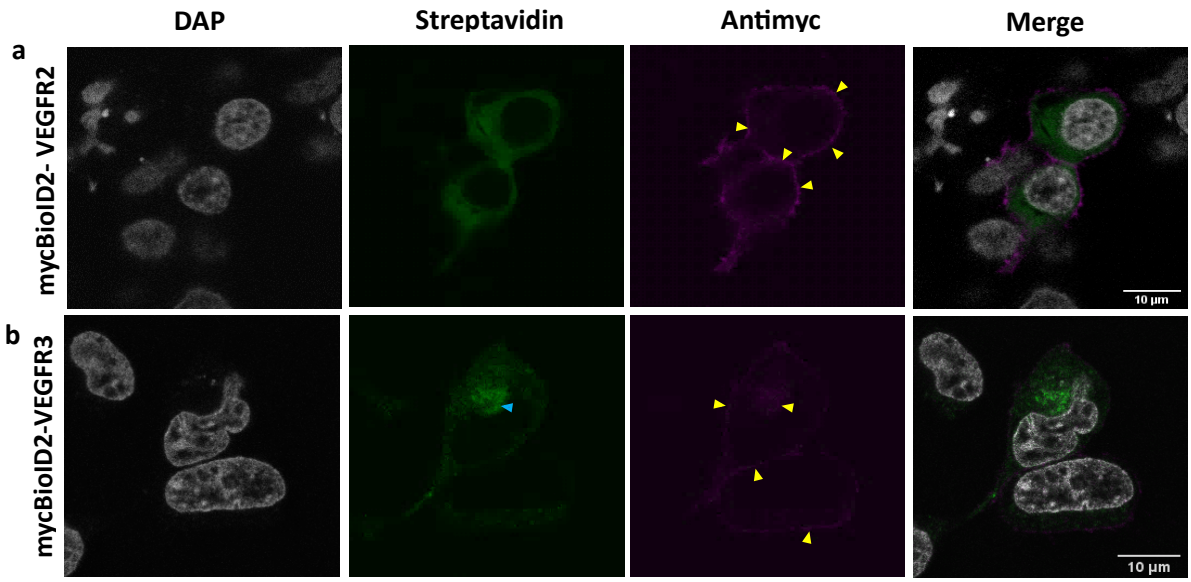

Figure 3.14 – Alternative images for mycBioID2-VEGFR2 and mycBioID2-VEGFR3 not representative of the cell population. *(a) mycBioID2-VEGFR2; (b) mycBioID2-VEGFR3. HEK293T cells were incubated with DNA/PEI transfection mix for 24 h, followed by a 50µM biotin supplementation for a further 20 h. Cells were then fixed and incubated with antimyc-AF555 antibody (Millipore; 16-255) which shows localisation of the BioID fusion protein and Streptavidin-AF488 (Invitrogen; S11223) which provides information on biotinylated proteins. All images had brightness increased by 40% and contrast reduced 20%. Yellow arrows indicate cellular membrane localisation. Blue arrows indicate localisation to intracellular components.*

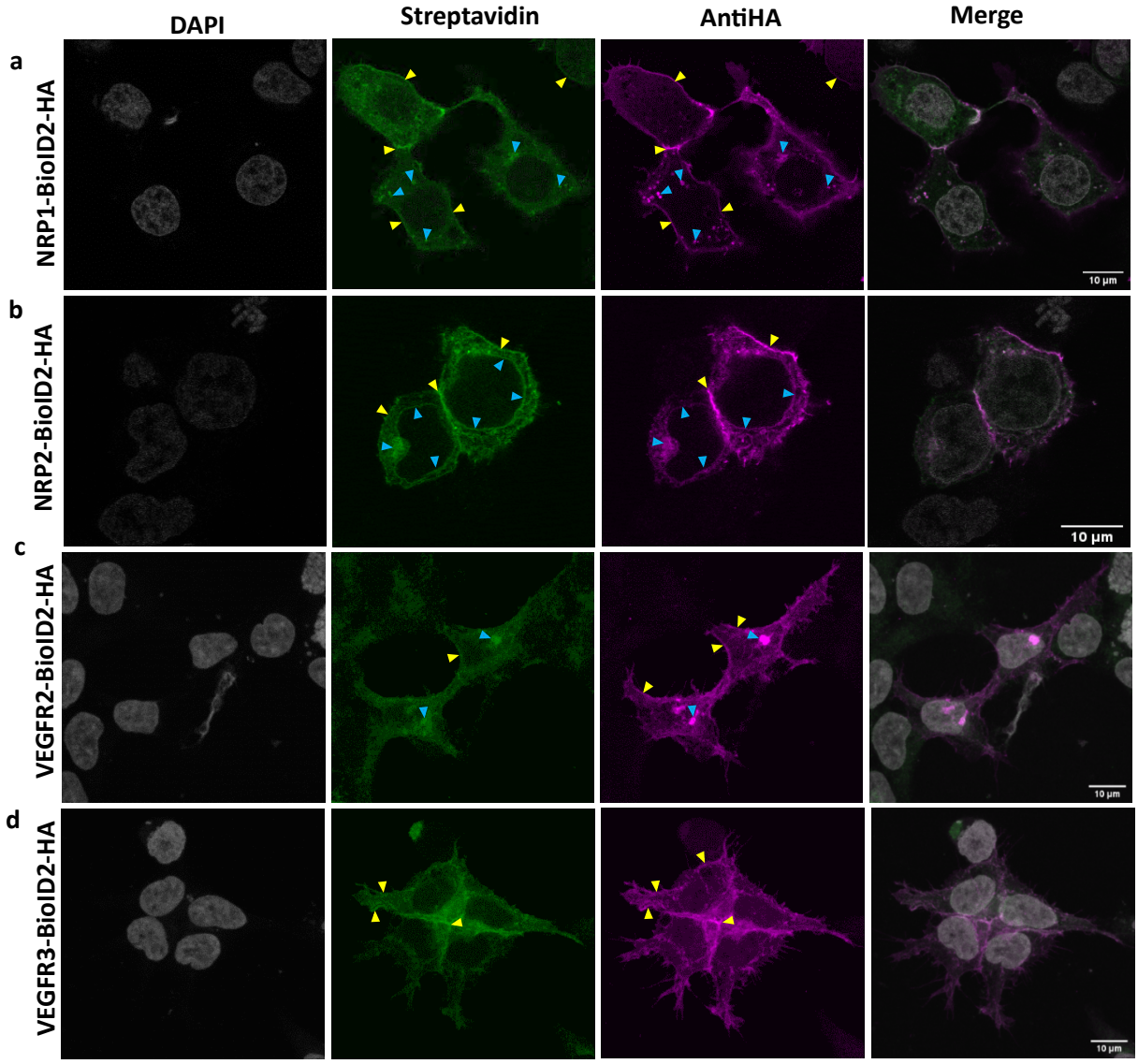

Figure 3.15 - Immunofluorescence of HEK293T cell transfected with C-terminal BioID2 constructs; (a) NRP1-BioID2-HA; (b) NRP2-BioID2-HA; (c) VEGFR2-BioID2-HA; (d) VEGFR3-BioID2-HA. *HEK293T cells were incubated with DNA/PEI transfection mix for 24 h, followed by a 50µM biotin supplementation for a further 20 h. Cells were then fixed and incubated with anti-HA antibody (Abcam; ab137838) which shows localisation of the BioID fusion protein and Streptavidin-AF488 (Invitrogen; S11223) which provides information on biotinylated proteins. All images had brightness increased by 40% and contrast reduced 20%. Yellow arrows indicate cellular membrane localisation. Blue arrows indicate localisation to intracellular components.*

3.3 Discussion

3.3.1 BioID1 vs BioID2 Comparison

As discussed previously, a newer variant of the biotin ligase (BirA) has been developed, which is smaller and has the ability to biotinylate proteins in close proximity with equal or greater efficiency compared to the original biotin ligase in BioID1[477]. The newer, smaller variant is termed BioID2. To compare the original against the newer variant, mycBioID2-CENPA was cloned and compared against a verified, published construct – mycBioID1-CENPA[503]. As the mycBioID1-CENPA is validated, this will be used as the standard for comparison of the different BirA variants. The purpose of the comparison was to determine correct localisation of the CENPA fusion proteins and comparison of biotinylation efficiency of the BioID1 and BioID2 BirA variants via confocal microscopy.

Expression of mycBioID2-CENPA in HeLa cells resulted in fusion protein localisation to the centromeres as expected, (Figure 3.4). This correct localisation implied the fusion of CENPA with the BioID2 BirA variant did not interfere with its biological function, similar to that observed for the BirA in BioID1[503]. The biotinylation efficiency experiments, (Figure 3.5), suggested a greater efficiency of the BioID2 BirA, compared to BioID1 BirA. For the BioID2 BirA, in both centromeric and whole cell analyses, an increase in fusion protein signal, resulted in a larger increase in relative streptavidin signal. Meaning at lower expression levels, biotinylation capacities appeared greater for BioID2 than the BioID1 BirA. However, when considering the centromeric analyses only, (Figure 3.5b), the absolute biotinylation appeared greater with BioID1 BirA. Expression of the empty BioID vectors expressing free BioID1 BirA and BioID2 BirA correlated with the CENPA analyses, (Figure 3.2). Initially, in the inception of the BioID2 BirA, the efficiency of the BirA was compared to that of BioID1 BirA[477]. The authors determined BioID2 BirA to be more efficient in biotinylation but observed less total biotinylation of compared to BioID1 BirA. Although total biotinylation is not the full picture, as this includes specific biotinylation of proximal proteins and contaminants. The authors observed the enhanced specific labelling of proximal proteins with BioID2 BirA, suggesting BioID2 BirA is a less promiscuous ligase and its use results in less contaminants. The previous published comparison of BioID1 vs BioID2 are comparable to the observations in these experiments, leading to the selection of BioID2 BirA as the appropriate biotin ligase tag for subsequent BioID experiments.

Alternative proximity biotinylation technologies exist, differing from the BirA variants incorporated in BioID1 and BioID2. A notable example in the literature utilises an ascorbic acid peroxidase fused to the protein of interest, known as APEX. Upon the addition of hydrogen peroxide (H_2O_2), the rapid kinetics of APEX enable sufficient proximity biotinylation within minutes[516], rather than several hours as

observed with BioID2. A newer version, APEX2, confers higher thermal stability and improved biotinylation activity of the peroxidase[517]. Despite the enhanced biotinylation time, there are some issues with this technology. Namely, the use of H_2O_2 at higher levels than would be endogenously observed and the resultant generation of reactive oxygen species[518], potentially inducing oxidative stress within the cells. The APEX2 peroxidase itself may cause oxidative damage to tyrosine residues of proteins in the local microenvironment[519]. This may have proven problematic for investigating the VEGFRs, which are receptor tyrosine kinases (RTKs), and NRPs which interact and are in close proximity to RTKs, where the APEX2 may ablate protein interactions due to oxidative damage tyrosine residues. The BirA utilised in BioID-based technology does not require the use of oxidising agents, providing rationale for the desired use of BioID compared to APEX.

Since the inception of the project, several other BirA variants have been developed, and their use is becoming more popular. These newer variants vary in size, biotinylation efficiency and biotinylation range. Of these, TurboID is becoming widely used, due to its significantly shorter labelling time compared to BioID1 or BioID2. In certain biological contexts, the proximity labelling achieved with TurboID (in 10 minutes), is almost comparable with BioID1 and BioID2 over 18h in terms of total biotinylation including contaminants, measure by intensity via western blotting[520]. The biotinylation radius of TurboID is thought to be beyond 35 nm, measured using a molecular ruler whereby the biotinylation of TurboID appeared to exceed the lengths of this ruler[521]. Importantly, the biotinylation radius of TurboID appeared significantly larger than that observed for BioID[521] which has an experimentally measured biotinylation radius of approximately 10 nm[522]. Despite enhanced temporal capability of TurboID, it is assumed the larger biotinylation radius increases contaminants, potentially a cause for error in the proteomic analyses. An even newer BirA variant, UltraID, is claimed to be the smallest and most efficient biotin ligase enzyme developed to date[523]. The UltraID research again utilises free BirA expression not fused to a protein of interest, and does not consider specific biotinylation, only measuring total biotinylation. Although the technology is exciting for the field, no examples of its use outside of the publication detailing its development exist at the time of writing.

3.3.2 BioID2 Plasmid Cloning Discussion

The decision to incorporate BioID2 technology in the project meant generation of the appropriate tools. BioID2 plasmids consisting of both N- and C-terminally fused VEGFR2, VEGFR3, NRP1 and NRP2 were synthesised. The final sequence of each plasmid was verified by Plasmidsaurus using Oxford Nanopore Technology with custom analysis and annotation. Following, generation of these tools, the next requirement was to determine if the expressed fusion protein localised correctly in a relevant cell line.

3.3.3 Expression of NRP and VEGFR plasmids in HEK293T Cells

NRP1 and NRP2 Plasmid Expression

An important requirement for determining suitability of the BioID plasmids generated, is the appropriate localisation of the protein of interest. Mis-localisation may suggest aberrant functioning of the protein and would likely result in unreliable interactome analyses. Expression of both BirA N- and C-terminally tagged NRP1 or NRP2 in HEK293Ts showed definitive membrane localisation, detected by anti-myc and anti-HA antibody staining, (Figure 3.13a-b and Figure 3.15a-b), as would be expected based on the nature of these proteins and similar published research[354,431,524]. Fluorescent labelling also indicated intracellular presence of NRPs. Intracellular localisation of NRP1 has been observed in endosomes[416] and in the mitochondria[525], perhaps accounting for the cytoplasmic detection. Likewise, NRP2 expression has been observed in endosomes[526] and recently at the nuclear membrane[527]. Correct functioning of the BirA was demonstrated in the streptavidin-AF488 channel, making these BioID2 tagged NRP1 or NRP2 constructs good candidates for future proteomics experiments.

In the BioID methodology, sufficient expression of the BirA fusion protein is essential for success. For the BioID protocol, generally two confluent 10 cm cell culture dishes per condition is required[446]. This ensures sufficient biotinylated proteins are extracted from the cells, in order to analyse via MS. The high transfection efficiency exhibited by the neuropilin plasmids indicated suitability for future BioID experiments.

VEGFR2 and VEGFR3 Plasmid Expression

When considering N- and C-terminal VEGFR2 and VEGFR3 constructs, there were some concerns with appropriate receptor localisation and suitable expression levels. Expression of the N-terminal mycBioID2-VEGFR2 and mycBioID2-VEGFR3 did not localise to the cellular membrane, (Figure 3.13c-d), as would be expected based on the nature of the proteins and similar published research[354,528]. The expression pattern was intracellular, seemingly localising to an unknown structure. This structure may be the Golgi apparatus and endoplasmic reticulum (ER), which would imply an issue with protein processing, possibly as a result of the addition of an N-terminal BirA sequence. Proteins which undergo misfolding or are modified incorrectly in the Golgi apparatus are known to be diverted back into the ER or selectively degraded[529].

Alternative images were capture of mycBioID2-VEGFR2 and mycBioID2-VEGFR3 constructs expressed in HEK293T cells. The purpose of these images was intended to show that the construct may be valuable, (Figure 3.14a-b). Importantly, these images are not representative of the transiently expressing HEK293T population. Representative images detailing transient expression displayed

mislocalisation of the fusion protein, (Figure 3.13c-d). The alternative images, (Figure 3.14a-b), demonstrated appropriate localisation of the fusion proteins to the cellular membranes, with some internal signals observed. Membrane trafficking of VEGFR2 is well characterised, accounting for intracellular signals for mycBioID2-VEGFR2 expression[354,530]. Although, internalisation is less characterised for VEGFR3, it has been observed, particularly in response to VEGF-C[531,532]. Again, meaning intracellular signal is not unexpected.

The C-terminal VEGFR2-BioID2-HA and VEGFR3-BioID2-HA constructs also exhibited concerning expression patterns when transiently expressed in HEK293T cells, although more promising than their N-terminal counterparts, (Figure 3.15c-d). Some membrane localisation was observed, however there was also a significant diffuse signal of the fusion protein throughout the cell. These concerns with localisation of these constructs provided rationale for excluding these candidates for future BioID analyses.

As discussed, a suitable expression level is required for the BioID methodology. For all VEGFR2 and VEGFR3 fusion proteins evaluated, an extremely low transfection efficiency was observed. As the same CMV promoter is present in the NRP and VEGFR plasmids, differential expression is not due to translation of plasmids. Rather, the issue may lie with the size of the plasmid, with the VEGFR plasmids (~10'500 base pairs (bp)) > 2000 bp larger than the NRP plasmids (~8000 bp). Larger plasmids are more difficult to transfect compared to smaller ones for lipid-based transfection methods (similar to FuGENE HD), often seen when in CRISPR technology, when Cas9/sgRNA plasmids (>9'000 bp) demonstrate poor lipid-based transfection efficiency[533].

3.3.4 Conclusion

The research in this chapter evaluated the BirA variants of BioID1 and BioID2 technology, concluding the BioID2 BirA was more appropriate for the project. The next stages aimed to identify suitable candidates for BioID technology, with receptors which drive angiogenesis and lymphangiogenesis chosen for evaluation. A summary of the sutibility of the BioID plasmids generated are detailed in Table 3.15. Of these plasmids, both NRP1 and NRP2 appeared suitable candidates for selection, based on the expected localisation and biotinylation capabilities of the fusion proteins.

Table 3.15 – Summary of the BioID plasmids synthesised in this project and their characteristics. *In the summary, the nature of the biotin ligase (BirA) tag is detailed and the epitope fusion tag for each plasmid. Additionally, all plasmids demonstrated sufficient activity of the BirA, however, only plasmids pertaining to NRP1 or NRP2 demonstrated sufficient localisation of the fusion protein.*

BioID Plasmid	C- or N-Terminal BirA	Intra- or Extracellular BirA	Epitope Tag of Fusion Protein	Retained Biointylation Capabilities of BirA*	Correct Localisation of Fusion Protein
mycBioID2-VEGFR2	N-	Extracellular	myc	✓	✗
VEGFR2-BioID2-HA	C-	Intracellular	HA	✓	✗
mycBioID2-VEGFR3	N-	Extracellular	myc	✓	✗
VEGFR2-BioID2-HA	C-	Intracellular	HA	✓	✗
mycBioID2-NRP1	N-	Extracellular	myc	✓	✓
NRP1-BioID2-HA	C-	Intracellular	HA	✓	✓
mycBioID2-NRP2	N-	Extracellular	myc	✓	✓
NRP2-BioID2-HA	C-	Intracellular	HA	✓	✓

Chapter 4: NRP1 Interactome Analyses in HEK293T Cells

4.1 Introduction

The current research climate concerning NRP1-interacting proteins generally utilises similar techniques to identify novel interactors. As discussed in 1.4.6. the majority of the potential NRP1 interactors have been identified using co-immunoprecipitation (CO-IP) followed by mass spectrometry. This conventional approach has numerous limitations. One example is missing or indeed losing potential interactors, often during wash-steps – a technical weakness typically amplified for proteins with weak or transient binding, such as those associated with post-translational modifications (PTMs). More than 400 PTMs have been described to date[534], with many of these reversible and highly dynamic[535] conventional CO-IP methods would miss many of these interactions. Even though these interactions are transient, it does not mean they are of less biological significance than stronger interactions. Additionally, a CO-IP is essentially a single snapshot in time of the NRP1 interactors, therefore provides limited temporal power. Interactions that occur, specifically, during different stages of the cell cycle, or under different cellular reorganising events, such as during mitosis, would likely be missed. Therefore, an alternative, superior approach of identifying novel NRP1 interactors was used – for the first time for NRP1. BioID technology is able to identify proteins which interact transiently with NRP1, as close-proximity proteins are biotinylated regardless of their binding affinity. Additionally, the use of the BioID2 enzyme biotinylates interacting proteins over 20 h, transiting multiple cell cycle stages cellular events, such as cell movement. The innovative use of BioID technology to investigate the NRP1 interactome is expected to determine the most comprehensive NRP1 interactome to date.

In Chapter 3, NRP1 BioID fusion proteins underwent initial validation, showing excellent early promise to take forward for affinity purification and mass spectrometry experiments. In Chapter 4, the overarching aim was to establish a robust scaled-up protocol to purify, analyse and interpret, NRP1 interactors. This required bespoke refinement of the purification, but also a bioinformatic approach to analysis of data. Figure 4.1 details the BioID analysis pipeline that will be performed in this research.

Additionally, the question was raised whether NRP1 has any additional interactors in the presence of a receptor it is known to complex with under ligand stimulation, VEGFR2, discussed in section 1.4.2. This required the generation of a stable cell line expressing both VEGFR2 and HaloTag-VEGFR2, followed by the optimised proteomic protocol. These cells were treated with $VEGF_{165}$a to induce complex formation between NRP1 and VEGFR2 to elucidate possible NRP1 interactors when bound to VEGFR2. A control of $VEGF_{165}$b was used, which binds to VEGFR2 but lacks exon 8a and therefore the CendR motif required for NRP1 binding, discussed in section 1.3.5.1. Hence, NRP1/VEGFR2 complex formation would not be induced.

The initial aims of this chapter are focused on the optimisation of the isolation of biotinylated proteins and optimisation of the bioinformatic processing of the samples. The focus then shifts to define novel NRP1 interactors at the N-terminal and C-terminal of the receptor, in the presence and absence of known NRP1 ligand, VEGF-$_{165}$a. Finally, novel potential interactors of NRP1 were investigated in a cellular model of NRP1-BioID2-HA in the presence of VEGFR2.

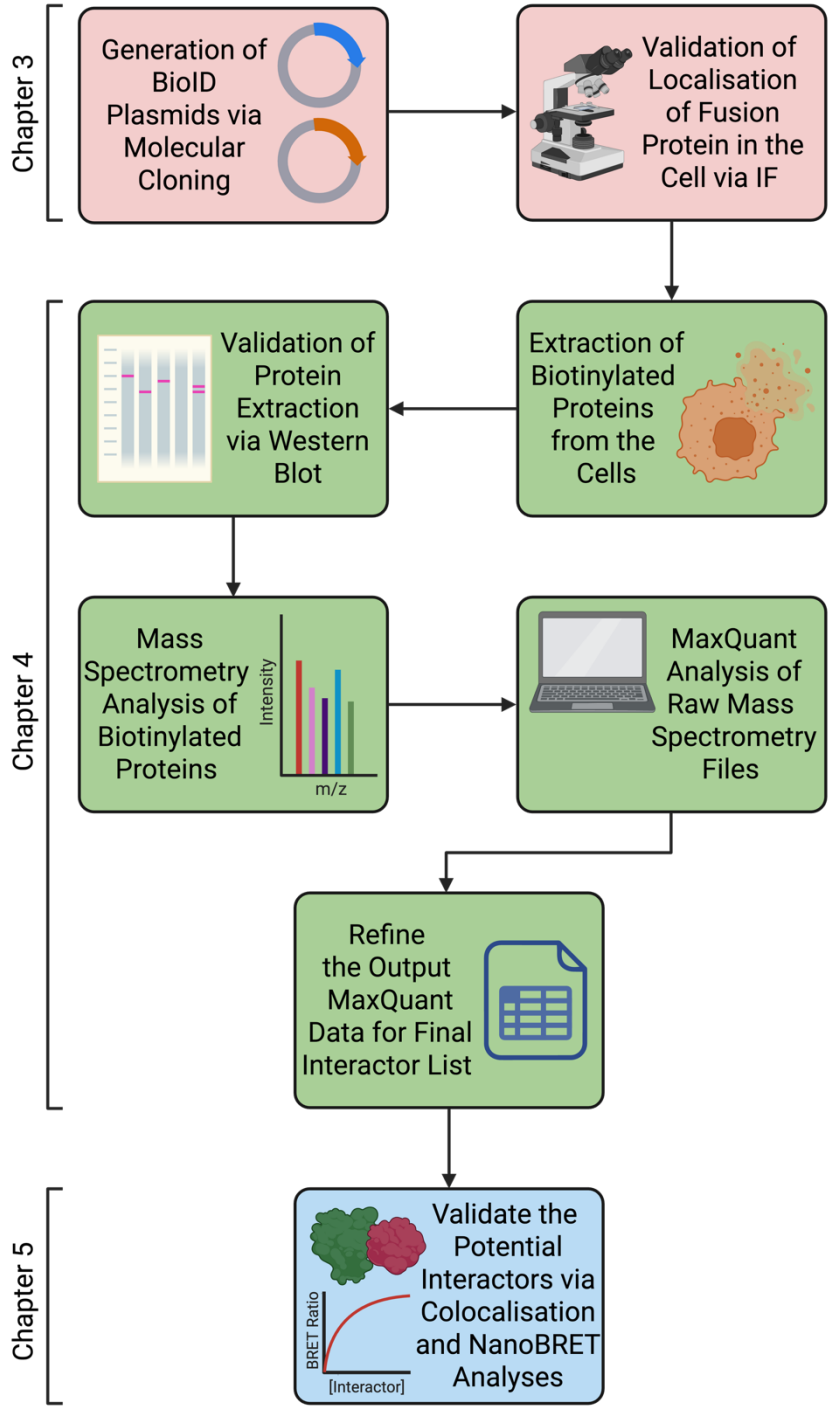

Figure 4.1 – A schematic depicting the BioID analysis protocol pipeline. *First, BioID plasmids are synthesised and correct localisation of the BioID fusion protein is confirmed. Subsequently, optimisation of extraction of biotinylated proteins from cells is determined by western blot. Following successful isolation of biotinylated proteins, the samples are sent for analysis by mass spectrometry to determine composition. The raw mass spectrometry files are processed in MaxQuant software, where a final protein hit list is generated. Selected potential interactors are chosen for further investigation to increase confidence in their interaction, analysed by colocalisation and nanoBRET analyses.*

4.2 Results

4.2.1 Neuropilin 1 N-terminal Interactome Analysis using mycBioID2-NRP1

4.2.1.1 Expression of mycBioID2-NRP1 in HEK293T Cells

Sufficient expression of mycBioID2-NRP1 was observed in wild-type (WT) HEK293T cells following optimisation of the transfection conditions, (Figure 4.2). As observed in the initial mycBioID2-NRP1 validation experiments, the fusion protein localises to the cellular membrane as expected, visualised using an antimyc-AF555 direct conjugate antibody (Sigma; 16-225). Importantly, significant biotinylation was observed in the streptavidin-AF488 (Invitrogen; S11223) channel in the samples supplemented with biotin. In the absence of biotin, a distinct reduction of biotinylation signal was observed. Sufficient biotinylation is imperative for success with the BioID protocol. The observed streptavidin-AF488 signal with optimal expression of mycBioID2-NRP1 was deemed sufficient to continue with the BioID protocol.

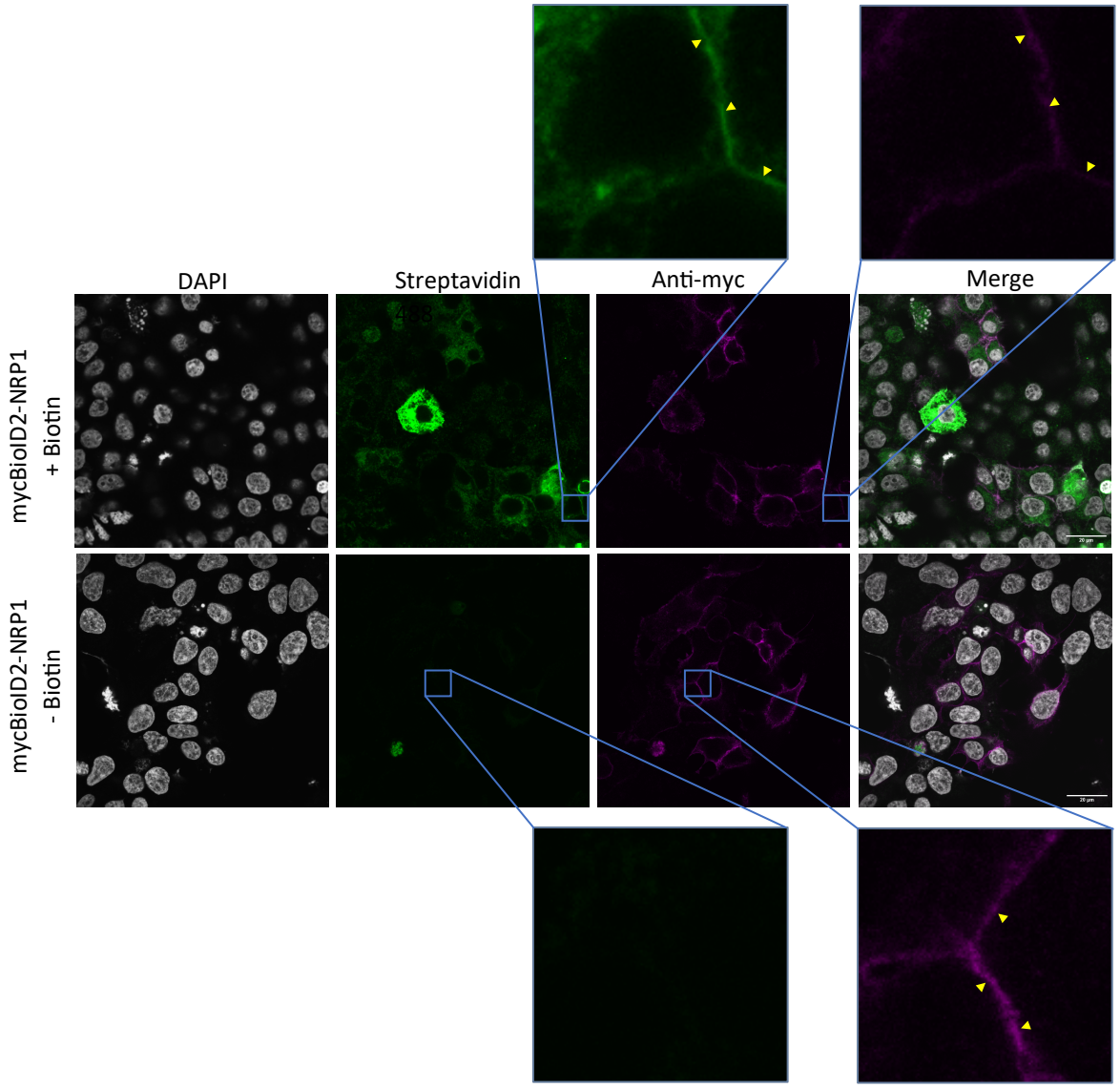

Figure 4.2 – Immunofluorescence of optimised transfection of mycBioID2-NRP1 in HEK293T cells. *Cells were incubated with a mycBioID2-NRP1 plasmid and Fugene HD mixture for 24 hours, followed by supplementation with fresh media and 50 µM biotin for a further 20 h. Cells were fixed and stained with an anti-myc 555 antibody (*Sigma; 16-225*) to visualise the mycBioID2-NRP1 fusion protein. Streptavidin-AF488 (invitrogen; S11223) highlighted the presence of biotinylated proteins. DAPI was used to highlight nuclear material and identify individual cells. Conditions with and without biotin supplementation was performed. The samples supplemented with biotin elicited a stronger streptavidin-AF488 signal. Yellow arrows indicated membrane localisation of signal.*

4.2.1.2 Optimisation of Streptavidin Pulldown of Biotinylated Proteins from mycBioID2-NRP1 Expressing Cells

Initial Streptavidin Pulldown

Following confirmation of appropriate mycBioID2-NRP1-HA localisation and expression, the experiments were scaled up for biochemical analysis of biotinylated proteins. A confluent 10 cm dish of HEK293T cells transiently expressing mycBioID2-NRP1 were harvested by typsination. The cells were pelleted and resuspended in BioID lysis buffer, on ice, for 10mins. The lysate was incubated with Dynabeads C1 (Invitrogen; 65001) to affinity purify biotinylated proteins as described in detail in section 2.8.4. To determine if affinity purification of biotinylated proteins was successful, biochemical analyses via western blotting was performed, (Figure 4.3). As expected, the fusion protein was present in the lysate of transfected cells and absent in the untransfected cells, (Figure 4.3a), assessed in the antimyc 680 channel. Although this banding was relatively weak, and a much stronger band would be expected. Despite biotinylation observable in all lysate samples, it was most abundant in samples treated with biotin, (Figure 4.3a), however again a stronger banding pattern would be expected. The double band present in all lanes from the streptavidin staining are likely pyruvate carboxylase or other mitochondrial carboxylases previously observed in BioID research[536] and known long-standing contaminants for the BioID approach[537]. Unfortunately, little to no banding using antimyc or streptavidin was observed in the eluted fractions, (Figure 4.3b), which is expected for untransfected cells but not for cells expressing NRP1-BioID2-HA. This suggests the isolation of biotinylated proteins had failed, perhaps due to unfavourable pulldown conditions or poor quality of the lysates incubated with the Dynabeads C1. In an effort to overcome these issues, conditions of the cell lysis and streptavidin pulldown were changed.

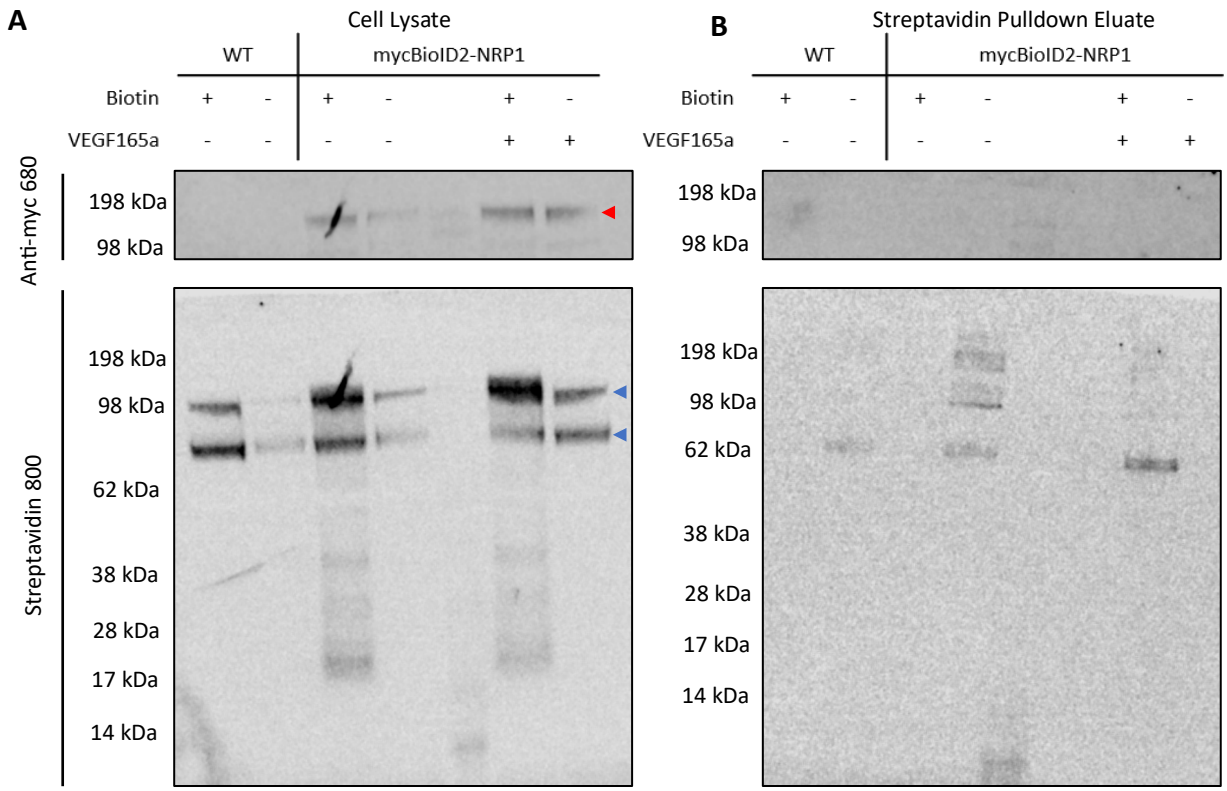

Figure 4.3 – Initial streptavidin pulldown attempts with HEK293T cells transfected with mycBioID2-NRP1 analysed by western blot. *Detection of the mycBioID2-NRP1 fusion protein was attempted using an anti-myc rabbit antibody (Invitrogen; Myc.A7) followed by an anti-rabbit 680 secondary antibody (LiCOR;* 926-68021*). Biotinylated proteins were detected using a streptavidin 800 direct conjugate (Invitrogen; 21851). Cells were treated with $VEGF_{165}a$ and biotin, and conditions without supplementation with these ligands were added as controls. Cell lysates of HEK293Ts were also included as a control.* ***(A)*** *The results of the cell lysates before streptavidin pull down, showed little detection of fusion protein in the anti-myc 680 channel. Weak bands indicated by red arrows at ~150 kDa, the expected size of mycBioID2-NRP1. Contaminants of BioID likely pyruvate carboxylases are indicated by blue arrows.* ***(B)*** *The results of the affinity purification demonstrate little signal in any of the channels, indicating failure of the pulldown. Lysate (L); Eluate (E).*

Repeat of Streptavidin Pulldown

It was considered the lack of purified biotinylated proteins was a result of inefficient cell lysis, indicated by the weak detection of mycBioID2-NRP1 in the previous western blot, (Figure 4.3a). The reason may lie in the trypsinisation of the cells prior to cell lysis. The trypsin detaches cells based on the cleavage of extracellular domains of adhesion proteins on the cellular membrane[538], therefore NRP1 may be lost as a result. To this end two steps were introduced. Cell scrapers were used to physically detach the cells, negating the possibility of cleavage and loss of mycBioID2-NRP1. Additionally, a physical lysis step was introduced, whereby the cells were repeatedly passed through a 33G needle to physically disrupt the cellular membrane. The incubation of the cells with BioID lysis buffer was also increased from 10

minutes to 30 minutes. Despite a stark improvement in the detection of mycBioID2-NRP1 in the cell lysates, there was none detectable in the affinity purified eluates, (Figure 4.4). The abundance of biotinylated proteins captured following affinity purification in eluate samples was still poor, apart from bands likely relating to pyruvate carboxylates, common BioID contaminants discussed earlier[537]. In some eluate samples, no biotinylated proteins were detected indicating inefficient capture by the Dynabeads C1. This meant the methodology required further refinement.

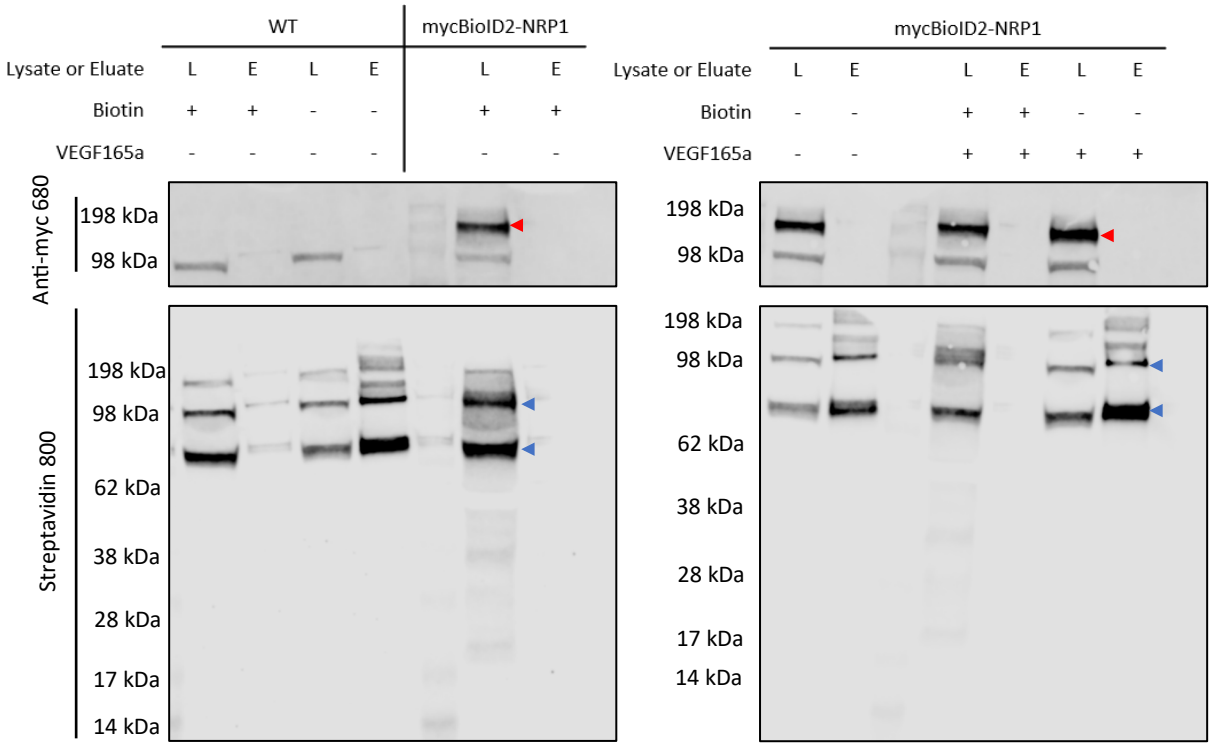

Figure 4.4 – Intermediate streptavidin pulldown attempts with HEK293T cells transfected with mycBioID2-NRP1 analysed by western blot. *Detection of the mycBioID2-NRP1 fusion protein was achieved using an anti-myc rabbit antibody (Invitrogen; Myc.A7) followed by an anti-rabbit 680 secondary antibody (LiCOR; 926-68021). Biotinylated proteins were detected using a streptavidin 800 direct conjugate (Invitrogen; 21851). For this experiment, cell lysates and corresponding pulldown material were paired next to one another. Cells were treated with $VEGF_{165}a$ and biotin, and conditions without supplementation with these were added as controls. Cell lysates of HEK293Ts were also included as a control. The results indicated successful detection of the mycBioID2-NRP1 fusion protein in all transfection conditions indicated red arrows marking a ~150 kDa band in the anti-myc 680 channel, which was absent in the HEK293T WT samples. Little biotinylation was observed in either lysates or pulldown material (eluate). The observed strong bands present in all samples are likely pyruvate carboxylase contaminants indicated by blue arrows. Lysate (L); Eluate (E).*

Optimised Streptavidin Pulldown

Further amendments were made to protocol to improve the abundance of biotinylated proteins captured during affinity purification. It was considered that, as a transmembrane protein, both NRP1 and its interactome network might have a dominant insoluble fraction. To test this a 30-minute sonication step was introduced to aiming to release proteins within the insoluble fraction. For the

affinity capture of biotinylated proteins, the protocol was adjusted to incubate the lysates and Dynabeads C1 at room temperature (RT) incubation for 1.5 h instead of at 4°C overnight. To confirm ideal pulldown conditions, a methodological positive control was introduced. Previously, the lab group have validated Adam23 to be BioID compatible and pulldowns previously optimised for this plasmid. Being a transmembrane protein, Adam23 is an ideal control for this stage. Later in the project, it was decided not to use Adam23 as a control, due to potential common proteins associated with Adam23 and NRP1.

The protocol amendments had a positive effect, with western blotting revealing significant detection of the mycBioID2-NRP1 fusion protein in all transfected cell lysates, (Figure 4.5). However, none was detected in the affinity purified eluates. The absence of this band in Adam23-BioID2-HA is due to the absence of the myc epitope on this fusion protein. The biotinylation patterns of Adam23-BioID-HA control demonstrated conditions of the pulldown were appropriate for isolation of biotinylated proteins, (Figure 4.5). The isolation of biotinylated proteins from HEK293T cells transfected with mycBioID2-NRP1 shows a similar, albeit weaker pattern. Importantly, the smeared banding pattern is absent in biotin-null sample. The most intense bands in the streptavidin 800 channel, are again likely pyruvate carboxylase contaminants, supported by the presence in lysates of WT samples. The substantial improvement in protein recovery, following a variety of technical amendments, was sufficient to progress to mass spectrometry (MS) analysis.

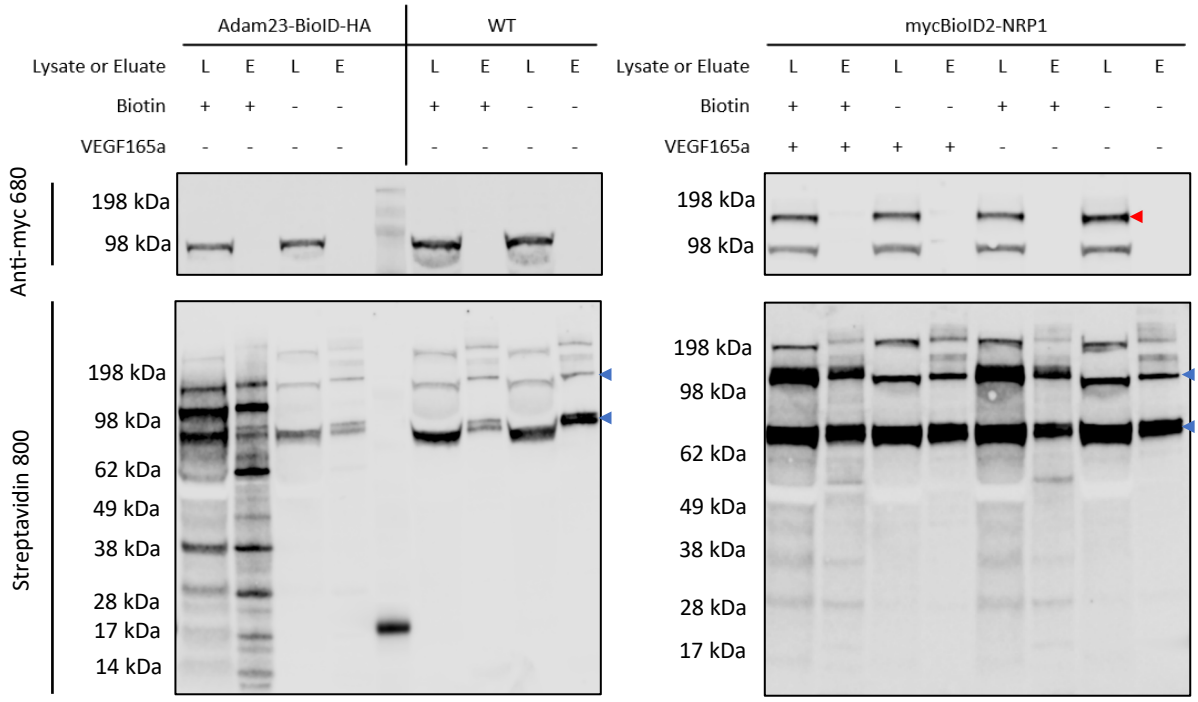

Figure 4.5 – Optimised streptavidin pulldown with HEK293T cells transfected with mycBioID2-NRP1 analysed by western blot. *Detection of the mycBioID2-NRP1 fusion protein was achieved using an anti-myc rabbit antibody (Invitrogen; Myc.A7) followed by an anti-rabbit 680 secondary antibody (LiCOR;* 926-68021*) Biotinylated proteins were detected using a streptavidin 800 direct conjugate (Invitrogen; 21851). Cell lysates and corresponding pulldown material were paired next to one another. Cells were treated with vehicle only, $VEGF_{165}a$ or biotin. Cell lysates of wildtype HEK293Ts were also included as a control. An additional control of Adam23-BioID-HA transfected HEK293Ts was included as a positive control to determine optimal conditions of the streptavidin pulldown, and as a control to determine common contaminants of the biotin ligase (BirA). Optimal streptavidin pulldown conditions were confirmed in the streptavidin 800 channel which indicated strong biotinylation in the Adam23-BioID-HA eluate, the characteristic smear pattern observed with proximity biotinylation is present. The detection of the mycBioID2-HA indicated by red arrows at 150 kDa band in the anti-myc 680 channel of cell lysates. Successful isolation of biotinylated proteins was observed in the mycBioID2-NRP1 eluates treated with biotin. Common contaminants, likely pyruvate carboxylases are indicated by blue arrows. Lysate (L); Eluate (E).*

4.2.1.3 Bioinformatic Processing Optimisation

The initial protein samples were sent to Dr. Christos Spanos at the University of Edinburgh for mass spectrometry analyses. The raw output files obtained from Dr. Spanos were then processed using MaxQuant software. The later samples, after this mycBioID2-NRP1 repeat, were instead sent to the Cambridge Centre for Proteomics (CCP) with the raw data obtained, processed in the same manner using MaxQuant software.

Reference Database Generation

For identification of proteins present in the sample, MaxQuant software requires a reference database. *In silico* trypsin digests of proteins in this reference database was performed in MaxQuant to generate theoretical mass spectrometry spectra for these proteins. The theoretical spectra were then compared to the observed spectra in the protein samples. Initially, a reference database required generation. The chosen database for these proteins was those contained within UniProtKB for *Homo Sapiens*. Following filtering for only proteins with the highest evidence, known as 'reviewed' proteins, the sequences of 20,421 was formatted into a custom database, Table 4.1. Due to the nature of the protocol, the addition of the sequence for porcine trypsin required adding to the database.

Table 4.1 – Example of generated UniProt reference database used in the bioinformatic analysis of the BioID samples sent for mass spectrometry. *The database was generated using the UniProt database, with only 'reviewed' proteins included. A total of 20,421 proteins were formatted into this custom database. For each protein, the UniProt accession number, protein name, gene name and FASTA sequence was included.*

Optimised MaxQuant Input Values

Generated UniProtKB Reference Database for *Homo Sapiens*
>sp|A0A087X1C5|CP2D7_HUMAN Putative cytochrome P450 2D7 OS=Homo sapiens OX=9606 GN=CYP2D7 PE=5 SV=1MGLEALVPLAMIVAIFLLLVDLMHRHQRWAARYPPGPLPLPGLGNLLHVDFQNTPYCFDQLRRRFGDVFSL QLAWTPVVVLNGLAAVREAMVTRGEDTADRPPAPIYQVLGFGPRSQGVILSRYGPAWREQRRFSVSTLRNLGLGK KSLEQWVTEEAACLCAAFADQAGRPFRPNGLLDKAVSNVIASLTCGRRFEYDDPRFLRLLDLAQEGLKEESGFLREV LNAVPVLPHIPALAGKVLRFQKAFLTQLDELLTEHRMTWDPAQPPRDLTEAFLAKKEKAKGSPESSFNDENLRIVVG NLFLAGMVTTSTTLAWGLLLMILHLDVQRGRRVSPGCPIVGTHVCPVRVQQEIDDVIGQVRRPEMGDQAHMPC TTAVIHEVQHFGDIVPLGVTHMTSRDIEVQGFRIPKGTTLITNLSSVLKDEAVWKKPFRFHPEHFLDAQGHFVKPEA FLPFSAGRRACLGEPLARMELFLFFTSLLQHFSFSVAAGQPRPSHSRVVSFLVTPSPYELCAVPR >sp|A0A0B4J2F0|PIOS1_HUMAN Protein PIGBOS1 OS=Homo sapiens OX=9606 GN=PIGBOS1 PE=1 SV=1MFRRLTFAQLLFATVLGIAGGVYIFQPVFEQYAKDQKELKEKMQLVQESEEKKS >sp|A0A0B4J2F2|SIK1B_HUMAN Putative serine/threonine-protein kinase SIK1B OS=Homo sapiens OX=9606 GN=SIK1B PE=5 SV=1MVIMSEFSADPAGQGQGQQKPLRVGFYDIERTLGKGNFAVVKLARHRVTKTQVAIKIIDKTRLDSSNLEKIYR EVQLMKLLNHPHIIKLYQVMETKDMLYIVTEFAKNGEMFDYLTSNGHLSENEARKKFWQILSAVEYCHDHHIVHRD LKTENLLLDGNMDIKLADFGFGNFYKSGEPLSTWCGSPPYAAPEVFEGKEYEGPQLDIWSLGVVLYVLVCGSLPFDG PNLPTLRQRVLEGRFRIPFFMSQDCESLIRRMLVVDPARRITIAQIRQHRWMRAEPCLPGPACPAFSAHSYTSNLGD YDEQALGIMQTLGVDRQRTVESLQNSSYNHFAAIYYLLLERLKEYRNAQCARPGPARQPRPRSSDLSGLEVPQEGLS TDPFRPALLCPQPQTLVQSVLQAEMDCELQSSLQWPLFFPVDASCSGVFRPRPVSPSSLLDTAISEEARQGPGLEEE QDTQESLPSSTGRRHTLAEVSTRLSPLTAPCIVVSPSTTASPAEGTSSDSCLTFSASKSPAGLSGTPATQGLLGACSPVR LASPFLGSQSATPVLQAQGGLGGAVLLPVSFQEGRRASDTSLTQGLKAFRQQLRKTTRTKGFLGLNKIKGLARQVCQ VPASRASRGGLSPFHAPAQSPGLHGGAAGSREGWSLLEEVLEQQRLLQLQHHPAAAPGCSQAPQPAPAPFVIAPC DGPGAAPLPSTLLTSGLPLLPPPLLQTGASPVASAAQLLDTHLHIGTGPTALPAVPPPRLARLAPGCEPLGLLQGDCE MEDLMPCSLGTFVLVQ … + 20'418 reference proteins

The raw data was then processed using MaxQuant software, with the reference database uploaded. Several parameters were changed during optimisation of the data processing. Notable optimised input parameters are found in Table 4.2.

Table 4.2 – Important parameters input into the MaxQuant software during bioinformatic processing of BioID samples. *False discovery rate (FDR). Intensity based absolute quantification (iBAQ).*

Parameter	Input
FDR	0.01
Missed Cleavages	2
Fixed Modifications	Carbidomethyl (C)
Variable Modifications	Oxidation (M) Acetyl (Protein N-term)
Mulitplicity	1
Digestion	Trypsin/P
iBAQ Calculations	Yes

Upon optimisation of the MaxQuant parameter input, the protein lists generated required further processing. The raw file output from MaxQuant consisted of enriched proteins mixed with contaminants and falsely identified sequences. Examples of the type of contaminants and falsely identified peptides are found in Table 4.3. While NRP1 represents a truly enriched protein, contaminants such as keratin required removal prior to further processing of the data. Additionally, MaxQuant generates reverse sequences as an internal control for peptide spectra matching. Any proteins identified with the reverse sequence are also considered contaminants. After filtering of truly enriched proteins, an enriched protein list was generated for each sample.

Table 4.3 – Example of the types of output data in 'proteinGroups' generated by MaxQuant bioinformatic processing. *True enriched interactors were indicated by the standard UniProt ID accession code, as observed with NRP1. For identified contaminants, the UniProt ID followed a 'CON_' prefix. Variants of keratin are often observed as contaminants in mass spectrometry. Peptides matching to bogus sequences were denoted the prefix 'REV_' followed by the UniProt ID. Peptides matched to contaminant and reverse sequences required removal from the final enriched protein list. Origin species (OS); Taxonomic identifier (OX); Gene name (GN); Protein evidence (PE); Sequence version (SV).*

Protein ID	Protein	Gene	FASTA Header
O14786;O14786-3;O14786-2	Neuropilin-1	NRP1	sp|O14786|NRP1_HUMAN Neuropilin-1 OS=Homo sapiens OX=9606 GN=NRP1 PE=1 SV=3;sp|O14786-3|NRP1_HUMAN Isoform 3 of Neuropilin-1 OS=Homo sapiens OX=9606 GN=NRP1;sp|O14786-2|NRP1_HUMAN Isoform 2 of Neuropilin-1 OS=Homo sapiens OX=9606 GN=NRP1
CON__P35527;P35527	Keratin, type I cytoskeletal 9	KRT9	;sp|P35527|K1C9_HUMAN Keratin, type I cytoskeletal 9 OS=Homo sapiens OX=9606 GN=KRT9 PE=1 SV=3
REV__O15067			sp|O15067|PUR4_HUMAN Phosphoribosylformylglycinamidine synthase OS=Homo sapiens OX=9606 GN=PFAS PE=1 SV=4

Optimised Analysis of MaxQuant Output Files

Initial filtering of the MaxQuant output files detailed enriched proteins for bait samples, including mycBioID2-NRP1 expression supplemented with biotin, and control samples, which included biotin-null conditions, WT HEK293T samples and HEK239T cells transfected with Adam23-BioID-HA. In the case of analysis of the NRP1 interactome when treated with $VEGF_{165}a$, samples expressing mycBioID2-NRP1 and treated with biotin in basal conditions were considered controls. Only proteins with >1 unique peptides identified are considered in the analysis. Unique proteins identified in the bait sample are automatically included in the final enriched protein list. Common proteins between bait lists and control lists were matched and compared by either protein score, iBAQ or relative iBAQ (riBAQ) for 1.5 x fold increase, initially during the optimisation of the analyses.

4.2.1.4 Enriched mycBioID2-NRP1 Proteins using Protein Score

The protein score value is an automated output pertaining to the likelihood of the presence of the protein identified. A higher score indicates a higher degree of confidence of the presence of the protein. Initially, protein score was used in the post-MaxQuant processing to determine enriched proteins, Table 4.4. The final protein list consisted of 9 proteins unique to mycBioID2-NRP1 when supplemented with biotin and $VEGF_{165}a$. As the false discovery rate (FDR) is set at 0.01 (0.1%), the confidence that the 9 proteins identified as enriched are true positives was high. However, after these initial analyses, it became apparent that using protein score in the data processing may not be appropriate. While the protein score is a measure of confidence, it does not necessarily correlate with abundance. Therefore, alternative metrics to compare abundance were considered.

Table 4.4 – mycBioID2-NRP1 $VEGF_{165}a$ stimulated enriched protein list using protein score analysis method. *The enriched protein list following a single repeat consisted of 9 proteins. Proteins unique to the* $VEGF_{165}a$ *treated and supplemented with biotin conditions were included in the final list. Proteins with a 1.5-fold increase of protein score in this condition, compared to the controls, were also included in this list.*

UniProt ID	Gene Name	Protein Name	Protein Score
Q13765	NACA	Nascent polypeptide-associated complex subunit alpha	111.88
O14786	NRP1	Neuropilin-1	63.72
Q13428	TCOF	Treacle protein	30.98
P35659	DEK	Protein DEK	13.32
P0DPD6	ECE2	Endothelin-converting enzyme 2	12.20
A4UGR9	XIRP2	Xin actin-binding repeat-containing protein 2	12.10
Q12959	DLG1	Disks large homolog 1	11.63
A4D2P6	GRD2I	Delphilin	11.53
Q12873	CHD3	Chromodomain-helicase-DNA-binding protein 3	9.87

4.2.1.5 Enriched mycBioID2-NRP1 Proteins using Intensity Based Absolute Quantification (iBAQ) Analysis

The intensity-based absolute quantification (iBAQ) value is a metric correlating to protein abundance. As this value is more representative of abundance, fold change between proteins enriched in bait samples compared to controls is calculated more accurately. Processing the MaxQuant output data in this manner led to a slightly different list of enriched proteins, Table 4.5. While the lists are broadly similar, protein DEK within the first list does not appear enriched when using iBAQ to determine fold change and enrichment. Meaning a possible false-positive has been eliminated from the list. Protein score is still useful to compare proteins within the final list of proteins in terms of confidence. The use of iBAQ to calculate fold changes is more stringent than using protein score. However, a further refinement of the analysis methodology was necessary to quantify relative molar abundance of proteins more rigorously.

Table 4.5 – mycBioID2-NRP1 $VEGF_{165}a$ stimulated enriched protein list using iBAQ value analysis method. *The enriched protein list following a single repeat consisted of 8 proteins. Proteins unique to the* $VEGF_{165}a$ *treated and supplemented with biotin conditions were included in the final list. Proteins with a 1.5-fold increase of iBAQ in this condition, compared to the controls, were also included in this list.*

UniProt ID	Gene Name	Protein Name	Protein Score
Q13765	NACA	Nascent polypeptide-associated complex subunit alpha	111.88
O14786	NRP1	Neuropilin-1	63.72
Q13428	TCOF	Treacle protein	30.98
P0DPD6	ECE2	Endothelin-converting enzyme 2	12.20
A4UGR9	XIRP2	Xin actin-binding repeat-containing protein 2	12.10
Q12959	DLG1	Disks large homolog 1	11.63
A4D2P6	GRD2I	Delphilin	11.53
Q12873	CHD3	Chromodomain-helicase-DNA-binding protein 3	9.87

4.2.1.6 Enriched mycBioID2-NRP1 Proteins using Relative Intensity Based Absolute Quantification (riBAQ) Analysis

Further calculations may be derived from MaxQuant iBAQ scores with the purpose of normalising the values for a more accurate representation of protein abundance. Normalising each protein's iBAQ value to the sum of all iBAQ values (minus contaminants and reverse sequences), generates a relative iBAQ (riBAQ) score for each protein. Fold change was calculated in the same manner as for the protein score and iBAQ values and a final list generated, Table 4.6. The output list of this analysis method is similar again to the previous lists using protein score and iBAQ values. Two new proteins were enriched

in this new analysis, leucine-rich repeat-containing protein 59 (LRC59) and putative elongation factor 1-alpha-like 3 (EF1A3), while eliminating potential false positives such as Protein DEK from the final list. The results demonstrated potential novel NRP1-interacting proteins when NRP1 is stimulated with $VEGF_{165}a$. The same method was applied to non- $VEGF_{165}a$ stimulated mycBioID2-NRP1 to determine NRP1-interactors under basal conditions, Table 4.7. Several other proteins were identified which may interact with NRP1 under basal conditions, including serine/arginine repetitive matrix protein 1 (SSRM1), AP-3 complex subunit delta-1 (AP3D1), and ral GTPase-activating protein subunit beta (RLGPB). A summary of this data comparing $VEGF_{165}a$ stimulated and basal conditions is detailed in Figure 4.6.

Table 4.6 – mycBioID2-NRP1 $VEGF_{165}a$ stimulated enriched protein list using riBAQ value analysis method. *The enriched protein list following a single repeat consisted of 9 proteins. Proteins unique to the* $VEGF_{165}a$ *treated and supplemented with biotin conditions were included in the final list. Proteins with a 1.5-fold increase of calculated riBAQ in this condition, compared to the controls, were also included in this list.*

UniProt ID	Gene Name	Protein Name	Protein Score
Q13765	NACA	Nascent polypeptide-associated complex subunit alpha	111.88
Q13428	TCOF	Treacle protein	30.98
Q96AG4	LRC59	Leucine-rich repeat-containing protein 59	28.49
Q5VTE0	EF1A3	Putative elongation factor 1-alpha-like 3	21.82
P0DPD6	ECE2	Endothelin-converting enzyme 2	12.2
A4UGR9	XIRP2	Xin actin-binding repeat-containing protein 2	12.1
Q12959	DLG1	Disks large homolog 1	11.63
A4D2P6	GRD2I	Delphilin	11.53
Q12873	CHD3	Chromodomain-helicase-DNA-binding protein 3	9.87

Table 4.7 – mycBioID2-NRP1 under basal conditions enriched protein list using riBAQ value analysis method. *The enriched protein list following a single repeat consisted of 6 proteins. Proteins unique to basal conditions and supplemented with biotin conditions were included in the final list. Proteins with a 1.5-fold increase of calculated riBAQ in this condition, compared to the controls, were also included in this list.*

UniProt ID	Gene Name	Protein Name	Protein Score
Q8IYB3	SRRM1	Serine/arginine repetitive matrix protein 1	14.79
O14617	AP3D1	AP-3 complex subunit delta-1	5.91
Q13428	TCOF	Treacle protein	2.51
Q86X10	RLGPB	Ral GTPase-activating protein subunit beta	1.48
O14786	NRP1	Neuropilin-1	1.21
P35659	DEK	Protein DEK	0.49

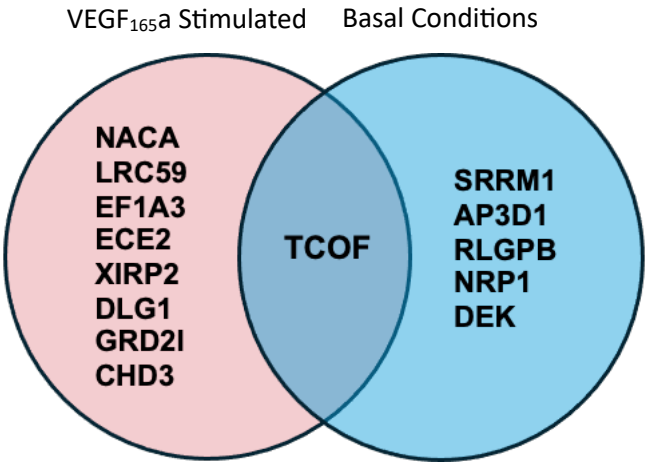

Figure 4.6 – A summary of the enriched proteins in the mycBioID2-NRP1 bioinformatic analysis in both VEGF$_{165}$a stimulated and basal conditions. *For the VEGF$_{165}$a stimulated conditions, 9 proteins were identified as potential NRP1 interactors, with 8 of these unique to VEGF$_{165}$a stimulation. The basal conditions elicited 6 enriched proteins, with 5 of these unique to the basal conditions. There was 1 enriched protein common between both conditions.*

An additional measure was included to filter common contaminants associated with the BirA expression. Inputting the final enriched protein list into the Contaminant Repository for Affinity Purification (CRAPome) database enabled identification of common proteins which have an affinity for the BirA perhaps missed by the controls[539]. The CRAPome is a repository of negative controls of mass spectrometry (MS) data, including experiments incorporating BioID technology. Following input of the protein list into the CRAPome, proteins identified in experiments relating to proximity biotinylation using HEK293T cells with a frequency score of ≥ 20% were excluded from the final list. After defining the proteomic processing pipeline, this was used for future processing of MaxQuant output data, with an overview of the pipeline detailed in Figure 4.7.

The enriched protein lists observed for mycBioID2-NRP1 in VEGF$_{165}$a stimulated and basal conditions were smaller than expected for BioID enrichment analyses. The results must also be interpreted with caution, as only one repeat was performed. Due to the complexity of sample preparation, and the associated costs with mass spectroscopy, before more repeats relating to mycBioID2-NRP1 were completed, the BioID protocol was performed with the C-terminally tagged NRP1-BioID2-HA, where the BirA is intracellular.

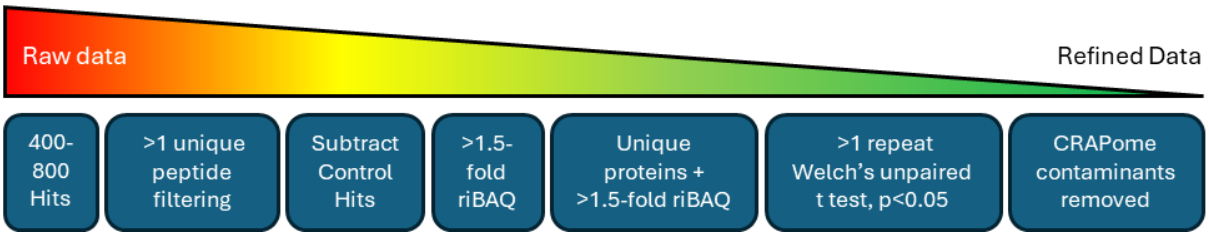

Figure 4.7 – Bioinformatic processing of MaxQuant output files analysis pipeline. *Lists were filterer for proteins with >1 unique peptides identified in mass spectrometry. The filtered individual samples lists were designated as either bait list (experimental sample) or control list. The bait and control lists were compared and proteins unique to the bait samples were included in the final enriched list. For common proteins between lists, fold change calculations were performed on the matched proteins using relative intensity-based absolute quantification (riBAQ) values. Proteins were filtered to include those with a >1.5-fold increase in the bait samples. The unique bait proteins were combined with proteins with a >1.5-fold increase for the final enriched protein list. Where >1 repeat was possible, statistical analysis was performed using Welch's unpaired t test, with only proteins with p<0.05 were included. Proteins were filtered further with using the CRAPome database, which details common contaminants of proximity biotinylation. Proteins with a frequency score of ≥ 20% in HEK293T cells were excluded from the final list.*

4.2.2 Neuropilin 1 C-terminal Interactome Analyses using NRP1-BioID2-HA

4.2.2.1 Expression of NRP1-BioID-HA in HEK293T Cells

The transient transfection of NRP1 tagged at its C terminus with BioID2 BirA (NRP1-BioID2-HA) in HEK293T cells using FuGene HD (Promega Corporation) supplemented with Optimem (Gibco) was first optimised. Following immunolabelling of the incorporated HA tag, sufficient expression and correct localisation of NRP1-BioID2-HA was observed in the anti-HA AF594 channel, along with confirmation of biotinylation capabilities of the expressed fusion protein demonstrated by a streptavidin-AF488 signal, (Figure 4.8). The streptavidin-AF488 signal demonstrated co-localisation of biotinylation signal and anti-HA 594 labelling. The BirA self-biotinylates NRP1 in the fusion protein, resulting in overlapping channels. As expected, biotinylation appeared minimal in the biotin-null conditions, although, a biotinylation signal was still observed. The potential for significant biotinylation occurring in the biotin-null conditions may present a problem when processing the mass spectrometry data. As the biotin-null samples were part of the controls in filtering the bait-enriched lists, this may lead to false negatives in the analysis. This means true interactors are missed due to biotinylation occurring in the biotin-null control conditions. The source of this biotinylation in these samples, was the trace amount of biotin present in the Dulbecco's Modified Eagle Medium (DMEM) media used to culture the HEK293T cells.

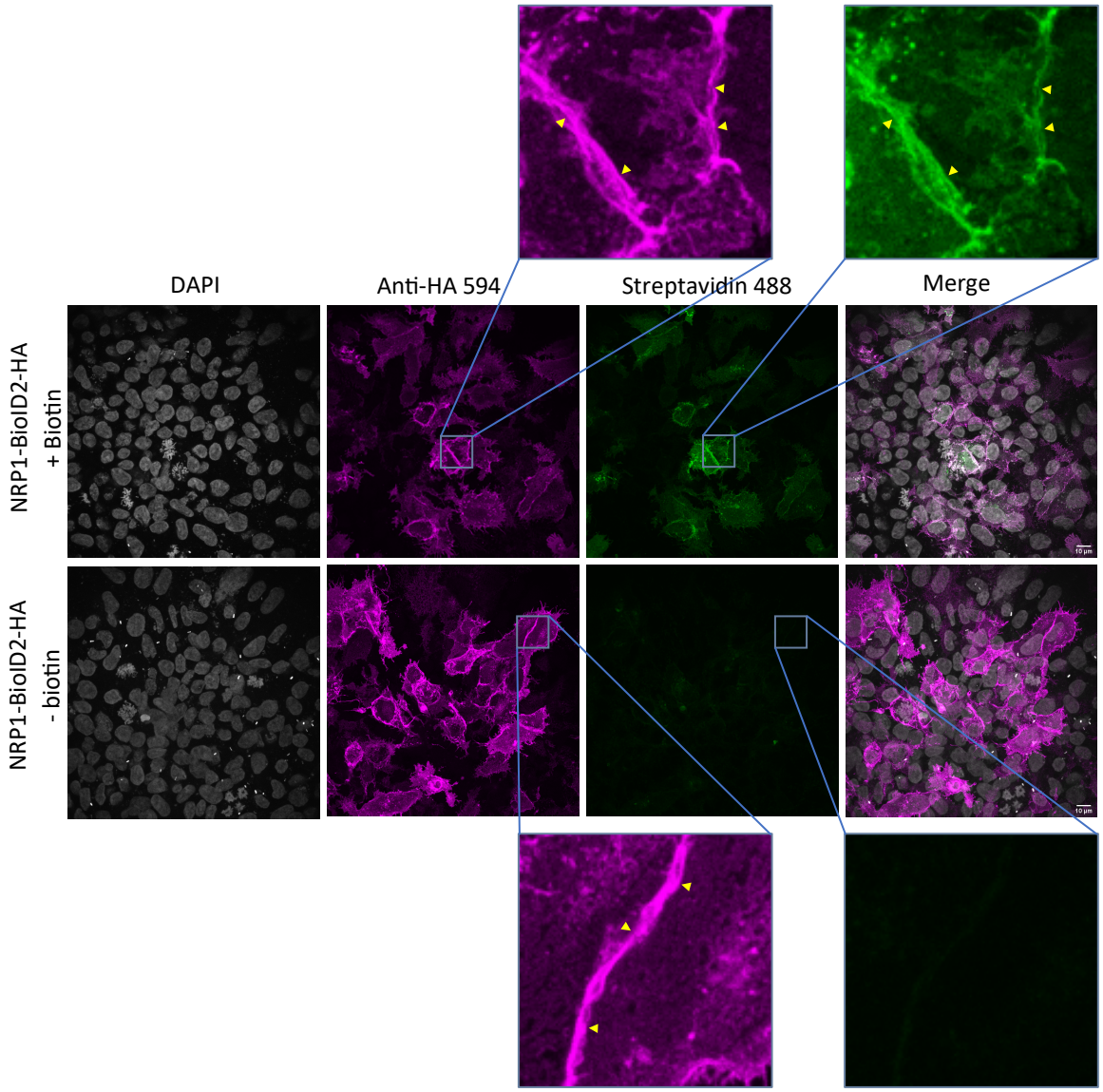

Figure 4.8 – Immunofluorescence of optimised transfection of NRP1-BioID2-HA in HEK293T cells. *Cells were incubated with a NRP1-BioID2-HA plasmid and Fugene HD mixture for 24 hours, followed by supplementation with fresh media and 50 µM biotin for a further 20 h. Cells were fixed and stained with anti-HA mouse (Invitrogen; 2-2.2.14) antibody followed by an anti-mouse AF594 (Jackson Immuno Research; 115-585-003) to visualise the NRP1-BioID2-HA fusion protein. Streptavidin-AF488 (Invitrogen; S11223) highlighted the presence of biotinylated proteins. DAPI was used to highlight nuclear material and identify individual cells. Conditions with and without biotin supplementation was performed. The samples supplemented with biotin elicited a stronger streptavidin-AF488 signal. Yellow arrows indicated membrane localisation of signal.*

4.2.2.2 Reduction of Trace Biotin in Dulbecco's Modified Eagle Medium (DMEM)

To reduce trace amounts of biotin in the Dulbecco's Modified Eagle Medium (DMEM), various concentrations of Dynabeads C1 were incubated with DMEM overnight at 4°C. The streptavidin beads were filtered from the media using a 0.22 µm filter. Transient transfections of HEK293T with NRP1-BioID2-HA was performed using the biotin depleted media, and controls of non-depleted media, media

supplemented with biotin and HEK293T WT cells, (Figure 4.9). All concentrations of Dynabeads incubated with DMEM demonstrated a reduction in residual biotinylation. At the lowest concentration of beads tested, 100 µL bead/50mL DMEM, the reduction in background biotinylation was comparable with the higher concentration of beads tested. For future BioID experiments, the choice was made to use 100 uL beads/50mL media, as this was effective in reducing background biotinylation, while using a small amount of Dynabeads C1 resulting in a cost-effective reduction of trace amounts of biotin.

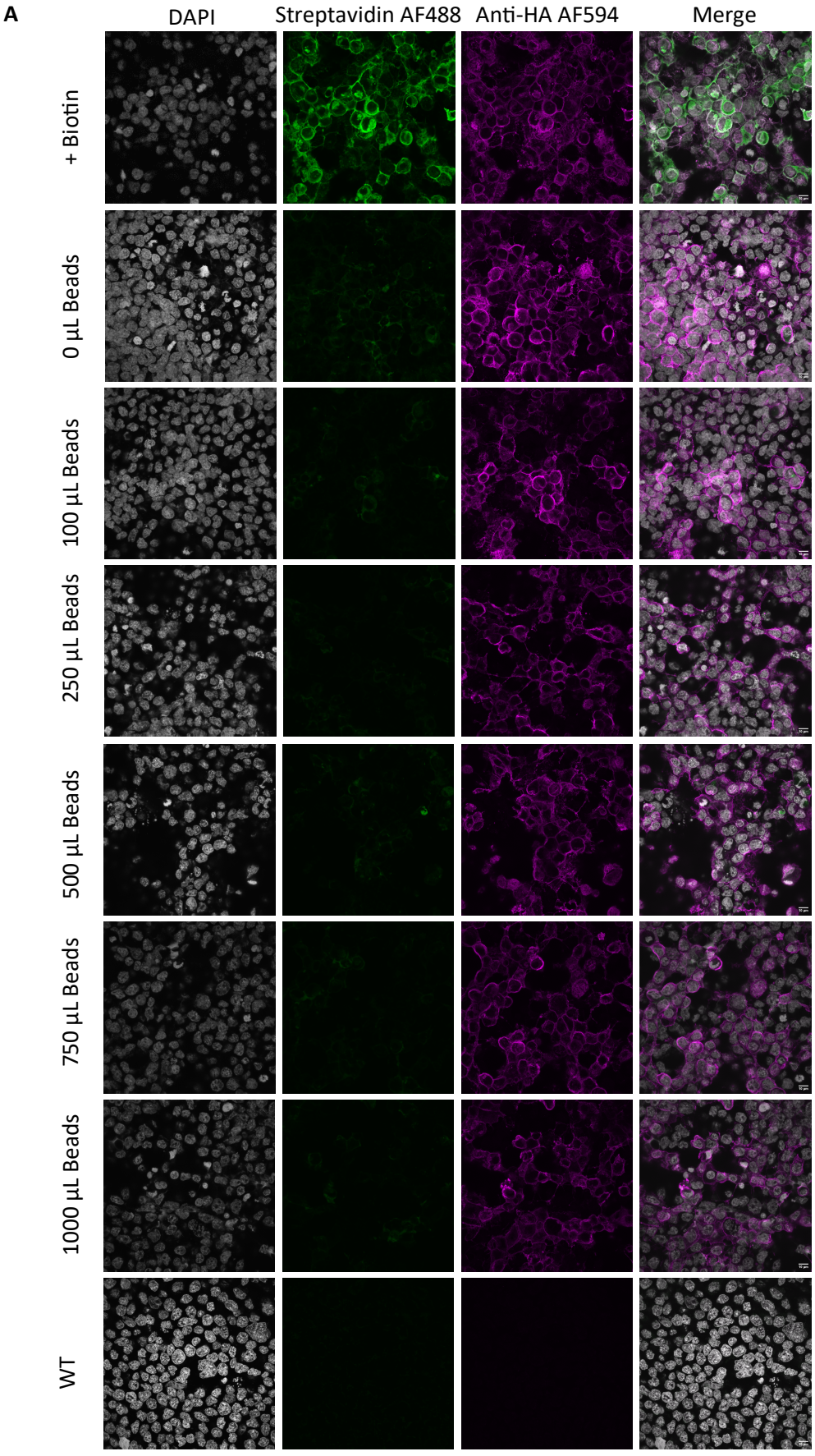

Figure continued following page…

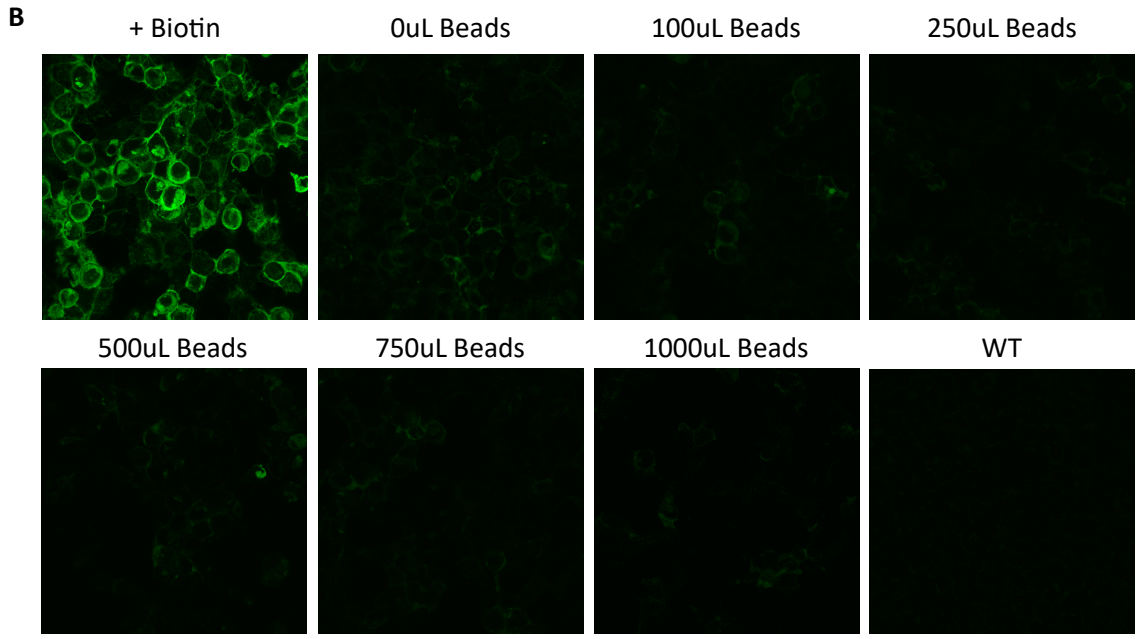

Figure 4.9 – Depletion of biotin from standard Dulbecco's Modified Eagle Medium (DMEM) cultured with HEK293T cells transfected with NRP1-BioID2-HA. *Cells were incubated with a NRP1-BioID2-HA plasmid and Fugene HD mixture for 24 hours. Cells were fixed and stained with anti-HA mouse (Invitrogen; 2-2.2.14) antibody followed by an anti-mouse AF594 (Jackson Immuno Research; 115-585-003) to visualise the NRP1-BioID2-HA fusion protein. Streptavidin-AF488 (Invitrogen; S11223) highlighted the presence of biotinylated proteins. Varying concentrations of Dynabeads C1 (Invitrogen; 65001) were incubated with 50 mL DMEM overnight at 4°C. HEK293T cells were cultured in this biotin depleted media and transfected with NRP1-BioID2-HA. Controls consisting of DMEM without biotin depletion (0uL beads), HEK293T WT cells with no NRP1-BioID2-HA expression, and HEK293T cells expressing NRP1-BioID2-HA supplemented with additional 50 µM biotin. The biotin depleted media demonstrated a reduction in biotinylation signal at all concentrations tested.*

4.2.2.3 Optimised Streptavidin Pulldown of Biotinylated Proteins from NRP1-BioID2-HA Expressing Cells

HEK293T cells were transfected with NRP1-BioID2-HA in 10 cm dishes, and the cells harvested and lysed according to the optimised conditions determined earlier in the project, discussed in section 4.2.1.2. The same optimised streptavidin pulldown conditions determined earlier was used to isolate biotinylated proteins in HEK239T cells expressing NRP1-BioID2-HA. The cell lysates and material eluted from the streptavidin beads were analysed by western blotting to determine if the BioID protocol was successful, (Figure 4.10). The anti-HA 680 channel detected the presence of the NRP1-BioID2-HA at around 150 kDa, the expected size of the fusion protein. As the NRP1 is in close proximity to the BirA, the NRP1 was expected to be self-biotinylated and therefore should be one of the most abundant proteins present in the eluate. This was confirmed by the presence of the NRP1-BioID2-HA in the eluted fractions supplemented with biotin. The streptavidin 800 straining demonstrated equally

positive results. The eluted fraction supplemented with biotin displayed the characteristic smear pattern observed with proximity biotinylation, a pattern which is absent in the biotin-null samples.

At this stage the positive control was changed, this was largely due to the possibility that Adam23 and NRP1 share common interactor proteins. Whilst still useful as a pulldown control, this would render Adam23 BioID as useless to help ID contaminants during bioinformatic enrichment. Thus, mycBioID2-CENPA was returned to, and although not a transmembrane protein, CENPA has no predicted spatial or temporal interactome with NRP1, so it is an ideal control to reveal contaminants. The HEK293T WT samples demonstrated isolation of contaminants which are naturally biotinylated. The successful isolation of biotinylated proteins was confirmed by western blots and warranted mass spectrometry analyses of these samples.

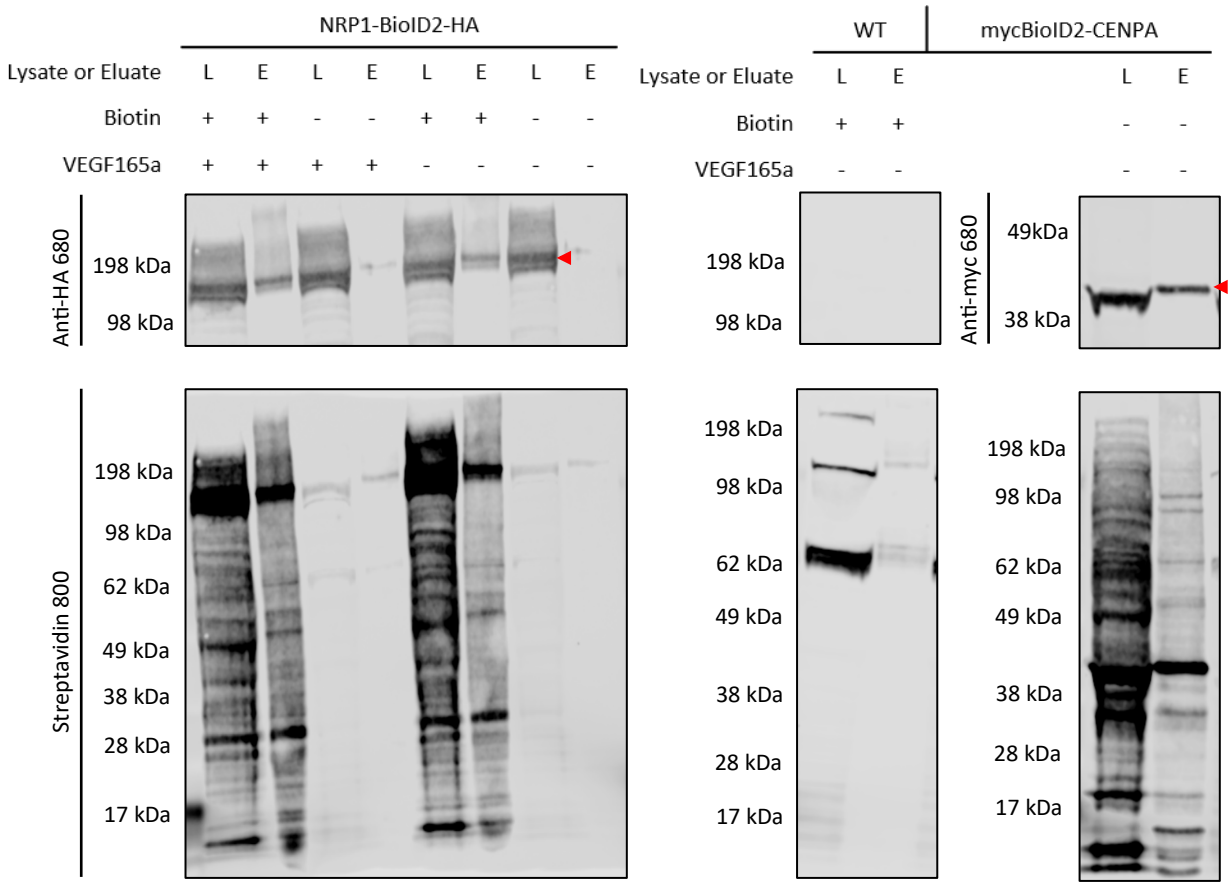

Figure 4.10 – Optimised streptavidin pulldown with HEK293T cells transfected with NRP1-BioID2-HA analysed by western blot. *NRP1-BioID2-HA fusion protein was detected using an anti-HA mouse antibody (Invitrogen; 2-2.2.14) followed by an anti-mouse 680 secondary antibody (LiCOR; 926-68070). Biotinylated proteins were detected using a streptavidin 800 direct conjugate (Invitrogen; 21851). Cell lysates and corresponding pulldown material were paired next to one another. Cells were treated with* $VEGF_{165}a$ *and biotin, and conditions without supplementation with these were added as controls. Cell lysates of HEK293Ts were also included as a control. An additional control of mycBioID2-CENPA transfected HEK293Ts was included determine common contaminants of the biotin ligase (BirA). Anti-myc rabbit antibody (Invitrogen; Myc.A7) followed by anti-rabbit 680 secondary antibody (LiCOR;* 926-68021*), to visualise the mycBioID2-CENPA fusion protein indicated by a red arrow at ~40 kDa. Streptavidin 800 staining confirmed successful isolation of biotinylated proteins, indicated by strong signals in the eluate samples of the biotin supplemented conditions. The presence of the NRP1-BioID2-HA fusion protein is also detected in the lysate and eluate samples, indicated by a red arrow at ~150 kDa band in the anti-HA 680 channel. Successful isolation of mycBioID2-CENPA biotinylated proteins is also observed in the streptavidin channel.*

4.2.2.4 Bioinformatic Analyses of C-terminal NRP1-BioID2-HA

The bioinformatic processing elicited a plethora of potential NRP1 interactors. It was important to evaluate the enriched proteins considering if they were unique to $VEGF_{165}a$ stimulation or under basal conditions. The results are summarised in Figure 4.11, where the majority of interactors were unique to either $VEGF_{165}a$ stimulated or basal conditions. A more detailed description of the enriched proteins in each condition is then discussed, with further analysis regarding gene ontology of these proteins.

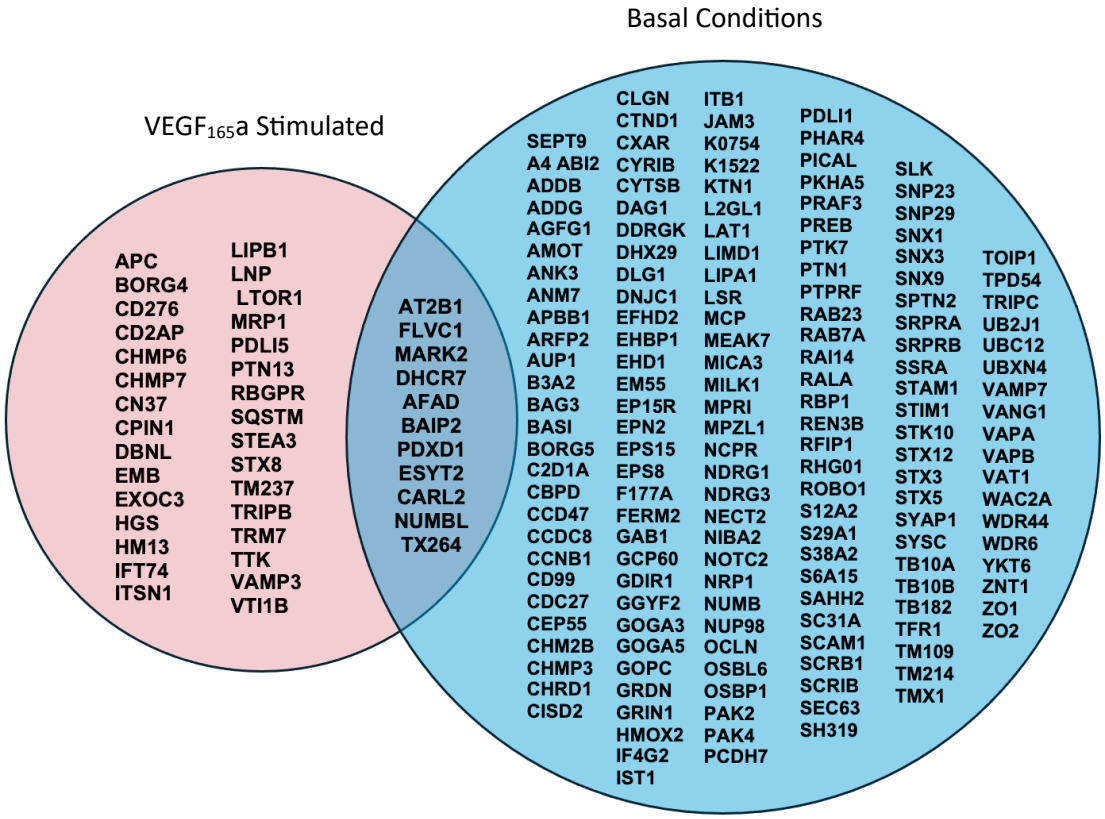

Figure 4.11 – A summary of the enriched proteins in the NRP1-BioID2-HA bioinformatic analyses in both $VEGF_{165}a$ stimulated and basal conditions. *For the $VEGF_{165}a$ stimulated conditions, 42 proteins were identified as potential NRP1 interactors, with 31 of these unique to $VEGF_{165}a$ stimulation. The basal conditions elicited 177 enriched proteins, with 167 of these unique to the basal conditions. There were 11 enriched proteins common between both conditions.*

4.2.2.4 Enriched Proteins in the NRP1-BioID2-HA Stimulated with $VEGF_{165}a$ Analyses

Enriched Proteins of NRP1-BioID2-HA when stimulated with $VEGF_{165}a$ after 4 Repeats

The isolated biotinylated proteins were sent to Cambridge Centre for Proteomics for mass spectroscopy analyses and the raw data files were processed according to the optimised data processing pipeline determined earlier in the project, discussed in section 4.2.1. For NRP1-BioID2-HA when treated with $VEGF_{165}a$ several repeats were performed with a variable number of unique

proteins identified, (Figure 4.12). As several biological repeats were present, statistical analysis was also used in filtering of enriched proteins. An unpaired t test with Welch's correction was performed using the calculated riBAQ calculated for each condition, determining if the fold change between test and control samples were significant. Proteins exhibiting a p value >0.05 was excluded from the final enriched list. These enriched protein lists were compared and proteins which were enriched in all 4 repeats were identified and filtered for contaminants using the CRAPome, Table 4.8. A total of 10 proteins were identified and an average protein score was assigned to each. Proteins which were present in 3 out of 4 repeats were also identified, Table 4.9. A further 32 proteins were identified as potential interactors when NRP1 is stimulated with $VEGF_{165}a$.

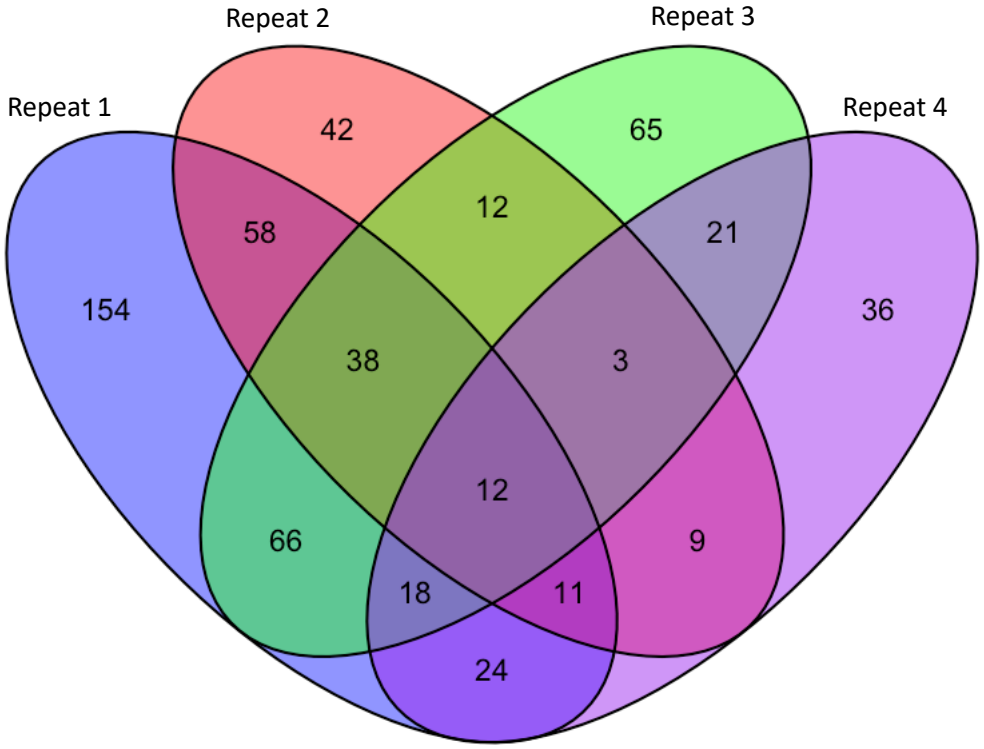

Figure 4.12 – Common proteins between 4 repeats of C-terminal NRP1-BioID2-HA stimulated with $VEGF_{165}a$. *Repeat 1 elicited 381 proteins after initial filtering. For repeat 2 there were 185 enriched proteins, repeat 3 a total of 235 proteins were enriched and repeat 4 enriched 134 proteins. Before further filtering, 12 proteins were common between all repeats. There were also 70 proteins common in 3 out of 4 repeats before further filtering.*

Table 4.8 – Enriched protein list in NRP1-BioID2-HA samples treated with $VEGF_{165}$a of proteins common between all 4 repeats. *Combining the repeats of NRP1-BioID2-HA treated with* $VEGF_{165}$a *and supplemented with biotin, the proteins enriched in all repeats were identified. A total of 10 proteins were enriched in this analysis. Proteins with a >20% frequency in HEK293 cells associated with proximity-biotinylation identified in the CRAPome were excluded from the final list. Statistical analysis by an unpaired t test with Welch's correction was performed on the riBAQ values between test and control samples to determine if fold change was statistically significant. Proteins with a p value of >0.05 were excluded from the final list.*

UniProt ID	Gene Name	Protein Name	Protein Score
P20020	AT2B1	Plasma membrane calcium-transporting ATPase 1	124.03
Q9Y5Y0	FLVC1	Heme transporter FLVCR1	38.92
Q7KZI7	MARK2	Serine/threonine-protein kinase MARK2	31.36
Q658P3	STEA3	Metalloreductase STEAP3	27.43
O14964	HGS	Hepatocyte growth factor-regulated tyrosine kinase substrate	23.89
Q86W92	LIPB1	Liprin-beta-1	23.69
P09543	CN37	2',3'-cyclic-nucleotide 3'-phosphodiesterase	20.84
Q9UBM7	DHCR7	7-dehydrocholesterol reductase	18.61
Q9UJU6	DBNL	Drebrin-like protein	17.44
Q96HC4	PDLI5	PDZ and LIM domain protein 5	13.44

Table 4.9 – Enriched protein list in NRP1-BioID2-HA samples treated with $VEGF_{165}$a of proteins common in 3 of the 4 repeats. *Combining the repeats of NRP1-BioID2-HA treated with* $VEGF_{165}$a *and supplemented with biotin, the proteins enriched in all repeats were identified. A total of 32 proteins were enriched in this analysis. Proteins with a >20% frequency in HEK293 cells associated with proximity-biotinylation identified in the CRAPome were excluded from the final list. Statistical analysis by an unpaired t test with Welch's correction was performed on the riBAQ values between test and control samples to determine if fold change was statistically significant. Proteins with a p value of >0.05 were excluded from the final list.*

Uniprot ID	Gene Name	Protein Name	Protein Score
P55196	AFAD	Afadin	279.05
Q9UQB8	BAIP2	Brain-specific angiogenesis inhibitor 1-associated protein 2	74.73
Q6P996	PDXD1	Pyridoxal-dependent decarboxylase domain-containing protein 1	57.05
A0FGR8	ESYT2	Extended synaptotagmin-2	41.22
Q6F5E8	CARL2	Capping protein, Arp2/3 and myosin-I linker protein 2	33.20
Q9Y5K6	CD2AP	CD2-associated protein	28.89
Q15643	TRIPB	Thyroid receptor-interacting protein 11	28.84
Q9H3Q1	BORG4	Cdc42 effector protein 4	28.42
Q9Y6R0	NUMBL	Numb-like protein	25.63
Q6FI81	CPIN1	Anamorsin	24.52
Q8TCT9	HM13	Minor histocompatibility antigen H13	24.08
Q9UEU0	VTI1B	Vesicle transport through interaction with t-SNAREs homolog 1B	22.98
Q15836	VAMP3	Vesicle-associated membrane protein 3	21.56

Q8WUX9	CHMP7	Charged multivesicular body protein 7	20.93
Q96Q45	TM237	Transmembrane protein 237	20.69
Q96LB3	IFT74	Intraflagellar transport protein 74 homolog	19.81
Q9UET6	TRM7	Putative tRNA (cytidine(32)/guanosine(34)-2-O)-methyltransferase	19.66
Q9Y6I9	TX264	Testis-expressed protein 264	18.86
P25054	APC	Adenomatous polyposis coli protein	18.00
Q9H2M9	RBGPR	Rab3 GTPase-activating protein non-catalytic subunit	17.97
P33981	TTK	Dual specificity protein kinase TTK	17.62
P33527	MRP1	Multidrug resistance-associated protein 1	17.52
Q13501	SQSTM	Sequestosome-1	17.05
O60645	EXOC3	Exocyst complex component 3	16.98
Q96FZ7	CHMP6	Charged multivesicular body protein 6	16.79
Q6IAA8	LTOR1	Ragulator complex protein LAMTOR1	16.12
Q12923	PTN13	Tyrosine-protein phosphatase non-receptor type 13	15.77
Q9UNK0	STX8	Syntaxin-8	15.73
Q9C0E8	LNP	Endoplasmic reticulum junction formation protein lunapark	15.72
Q5ZPR3	CD276	CD276 antigen	14.97
Q15811	ITSN1	Intersectin-1	13.64
Q6PCB8	EMB	Embigin	13.14

4.2.2.5 Gene Ontology Analyses of Enriched Protein List for NRP1-BioID2-HA, $VEGF_{165}a$ Stimulated Conditions.

The total number of proteins identified as potential interactors of NRP1 when stimulated with $VEGF_{165}a$ was 42. A gene ontology (GO) analysis was performed on these 42 proteins using Webgestalt[512], whereby the Uniprot ID codes were input into the software and data pertaining to GO of molecular function, biological processes and cellular component was extracted. Broader parent GO terms were included in a summary analysis to provide a general overview of the types of processes and functions the proteins related to. In the more specific GO analyses, redundant terms were excluded from the analysis, meaning broader parent terms were excluded and only specific child terms were included in the annotations. The identified enriched terms for each analysis was plotted against the 'enrichment ratio' (ER) value calculated by Webgestalt. The ER indicates how much more frequently a specific GO term appears in the user-input list, compared to what would be expected by chance in a random set of genes from the whole genome. Essentially, a measure of how significantly enriched a GO term is within the analysed input gene list. The significance/false discovery rate (FDR) level was set to <0.05 for all analyses.

Molecular Function GO Analysis

The molecular function analysis summary data, (Figure 4.13a), includes broader parent terms identified in the analyses. The majority of these proteins, 42 in total, fall under the protein binding parent term, which itself encompasses a multitude of child terms. The molecular function GO analysis, (Figure 4.13b), reveals more specific information. The most significant GO term associated with molecular function is SNARE binding (ER = 15.30). The other significantly enriched molecular function GO term was cadherin binding (ER = 13.68).

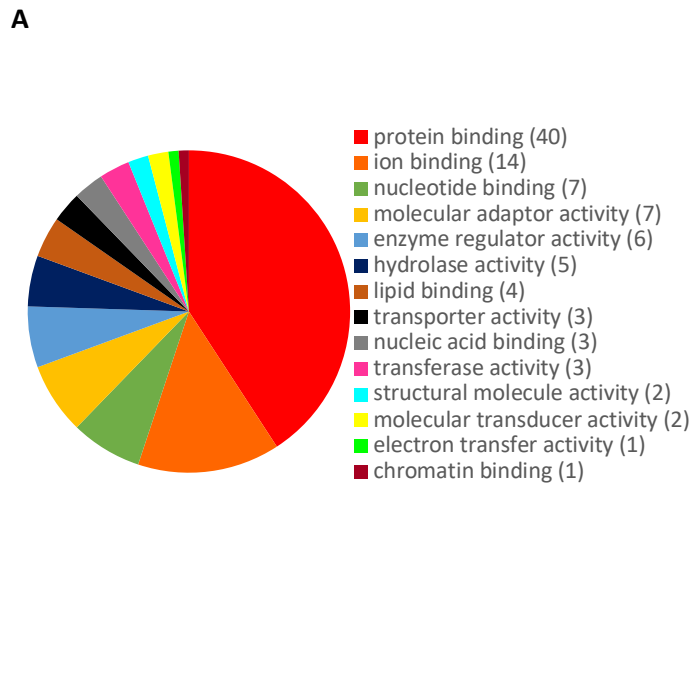

Figure 4.13 – Molecular function gene ontology (GO) analysis of enriched proteins for NRP1-BioID2-HA treated with VEGF$_{165}$a. *Protein lists were analysed by an overrepresentation analysis using Webgestalt, filtering for redundant GO terms. The enriched list was cross-referenced against molecular function GO terms, which describe the fundamental molecular activity of proteins. Enriched terms with a significance level > 0.05 were excluded. The GO terms were ranked based on enrichment ratio (ER), a ratio between the expected number of proteins present for a specific GO term based on a random set of proteins vs the input proteins, in this case those enriched in the BioID analyses of NRP1-BioID2-HA treated with* VEGF$_{165}$a. ***(A)*** *The summary data represents parent GO terms which were enriched.* ***(B)*** *The molecular function GO analysis relating to the enrichment of specific GO child terms.*

Biological Processes GO Analysis

The summary of the biological function analysis highlights the types of biological processes the NRP1-BioID2-HA dataset is involved in, (Figure 4.14a). Several biological processes are enriched in the summary analyses, notably biological regulation (n = 33), cellular compartment organisation (n = 33), response to stimulus (n = 28), localisation (n = 28), and cell communication (n = 20). The more specific biological GO analysis, (Figure 4.14b), details the involvement of the NRP1-BioID2-HA enriched proteins in several processes involving vesicular transport including cellular component organisation child terms, membrane fission (ER = 38.86), membrane docking (ER = 22.34), organelle fusion (ER =

12.59), membrane fusion (ER = 11.20), vesicle organisation (ER = 8.91). GO terms not related to the cellular component organisation parent term which also related to vesicular transport include, endosomal transport (ER = 12.67), vacuolar transport (ER = 11.26), exocytosis (ER = 6.97), and establishment of organelle localization (ER = 5.91). Other unrelated biological processes GO terms are enriched in the input list, ubiquitin-dependent protein catabolic process via the multivesicular body sorting pathway (ER = 33.79), multivesicular body sorting pathway (ER= 25.34), and macroautophagy (ER = 8.30).

A

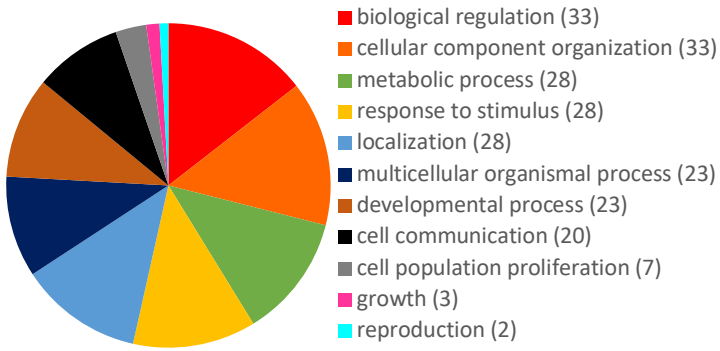

B

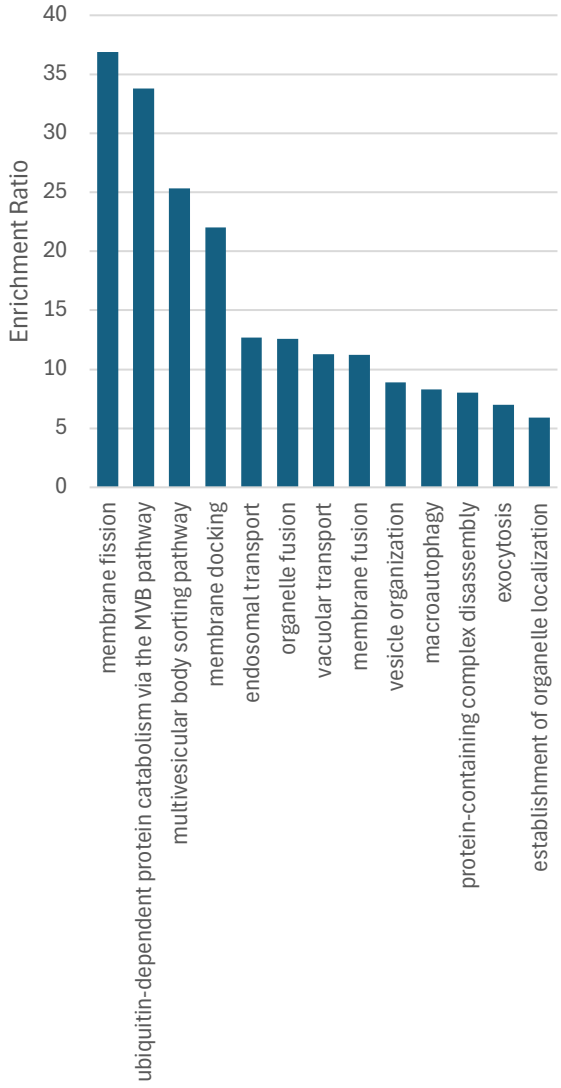

Figure 4.14 – Biological processes gene ontology (GO) analysis of enriched proteins for NRP1-BioID2-HA treated with VEGF$_{165}$a. *Protein lists were analysed by an overrepresentation analysis using Webgestalt, filtering for redundant GO terms. The enriched list was cross-referenced against biological processes GO terms, which describe the pathways and biological objectives a protein contributes to. Enriched terms with a significance level > 0.05 were excluded. The GO terms were ranked based on enrichment ratio (ER), a ratio between the expected number of proteins present for a specific GO term based on a random set of proteins vs the input proteins, in this case those enriched in the BioID analyses of NRP1-BioID2-HA treated with* VEGF$_{165}$a. ***(A)*** *The summary data represents enriched parent GO terms* ***(B)*** *The biological processes GO analysis relating to the enrichment of specific GO child terms.*

Cellular Component GO Analysis

The summary of the cellular component analysis, (Figure 4.15a), shows that 36 of the proteins enriched in NRP1-BioID2-HA $VEGF_{165}$a stimulated analysis are associated with the GO parent term relating to the cellular membrane. The GO component parent term with the second most categorised proteins is the endomembrane system, with 27 proteins. Other notable enriched GO terms include vesicle (n = 23), cell projection (n = 17), and endosome (n = 13). The specific GO terms enriched in the analysis after filtering the parent GO terms are mainly associated with vesicles and the cell membrane, (Figure 4.15b). The most significant GO term relates to proteins within the endosomal sorting complex required for transport (ESCRT) complex (ER = 43.45). Similarly, the GO component terms SNARE complex (ER = 24.33) late endosome (ER = 11.81) are enriched. Other significantly enriched GO component terms related more to cellular membrane and anchoring junctions. A significant portion of these proteins are expected to localise to the adherens junction (ER = 10.84) and cell leading edge (ER = 6.66).

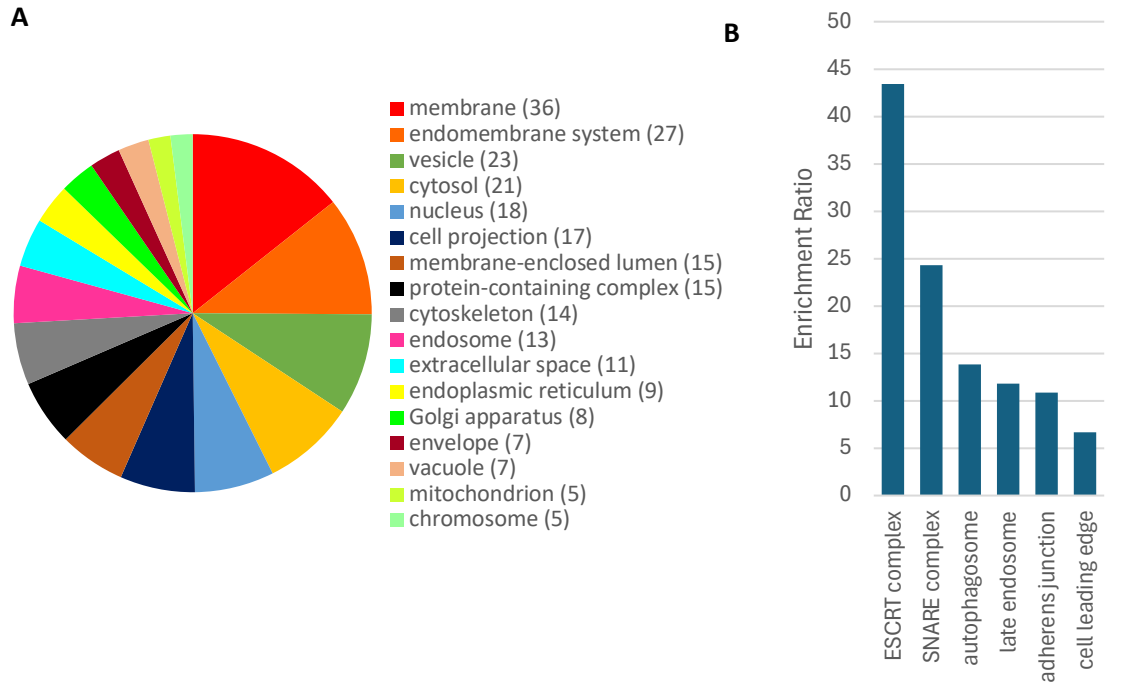

Figure 4.15 – Cellular component gene ontology (GO) analysis of enriched proteins for NRP1-BioID2-HA treated with $VEGF_{165}$a. *Protein lists were analysed by an overrepresentation analysis using Webgestalt, filtering for redundant GO terms. The enriched list was cross-referenced against cellular component GO terms, which describe localisation of the protein within the cellular environment. Enriched terms with a significance level > 0.05 were excluded. The GO terms were ranked based on enrichment ratio (ER), a ratio between the expected number of proteins present for a specific GO term based on a random set of proteins vs the input proteins, in this case those enriched in the BioID analyses of NRP1-BioID2-HA treated with* $VEGF_{165}$a. ***(A)*** *The summary data represents parent GO terms which were enriched.* ***(B)*** *The cellular component GO analysis relating to the enrichment of specific GO child terms.*

4.2.2.6 Enriched Proteins in the NRP1-BioID2-HA in Basal Conditions Analyses

Enriched Proteins of NRP1-BioID2-HA in Basal Conditions after 4 Repeats

To elucidate NRP1 interactions which occur independently of $VEGF_{165}a$, the unstimulated, basal conditions were compared against controls with the NRP1-BioID2-HA $VEGF_{165}a$ stimulated conditions removed from the analysis. The analysis pipeline was the same as described previously, using riBAQ values to perform fold change calculations. Again, the repeats elicited varied numbers of unique proteins identified, and lists were compared for common proteins in four repeats and for proteins in three out of four repeats, (Figure 4.16). Following this, common contaminants of the BirA were identified and excluded using the CRAPome database. In total, 77 proteins were enriched across all repeats and an average protein score was calculated for each protein, Table 4.10. Proteins common in at least 3 out of 4 repeats were also identified to reveal a further 100 potential NRP1 interactors, Table 4.11. Average protein scores were again assigned to each of these proteins.

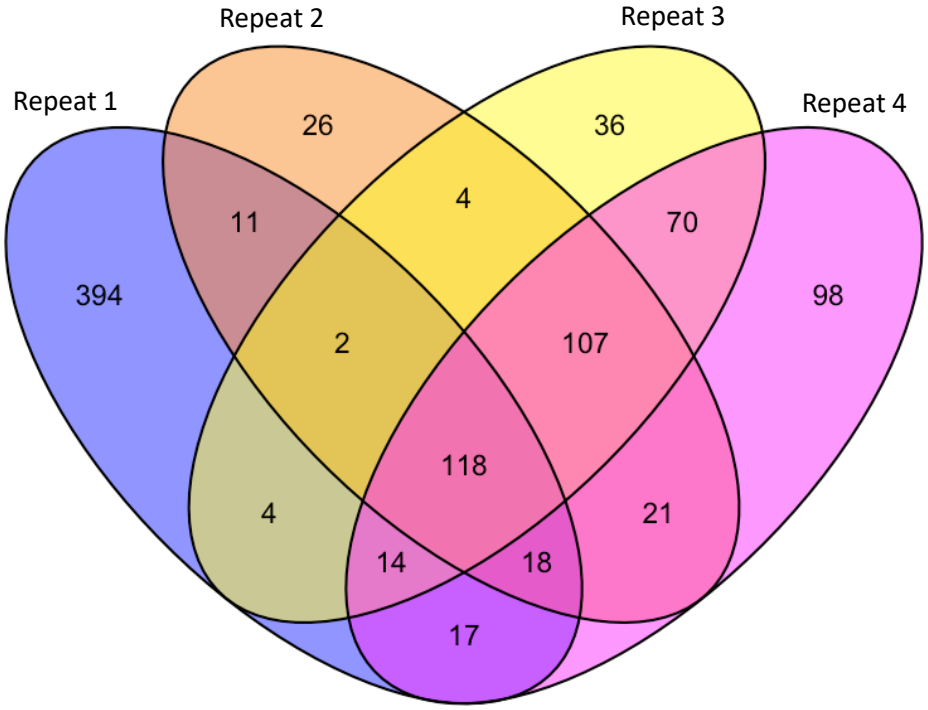

Figure 4.16 – Common proteins between 4 repeats of C-terminal NRP1-BioID2-HA in basal conditions. Repeat 1 elicited 578 proteins after initial filtering. For repeat 2 there were 307 proteins enriched. Repeat 3 yielded 355 enriched proteins and repeat 4, 463 enriched proteins. Before further filtering, there were 118 proteins common in all 4 repeats. There was also a further 141 proteins common in 3 out of 4 repeats before further filtering.

Table 4.10 – Enriched protein list in NRP1-BioID2-HA samples under basal conditions common between all 4 repeats. *Combining the repeats of NRP1-BioID2-HA under basal conditions and supplemented with biotin, the proteins enriched in all repeats were identified. A total of 77 proteins were enriched in this analysis. Proteins with a >20% frequency in HEK293 cells associated with proximity-biotinylation identified in the CRAPome were excluded from the final list. Statistical analysis by an unpaired t test with Welch's correction was performed on the riBAQ values between test and control samples to determine if fold change was statistically significant. Proteins with a p value of >0.05 were excluded from the final list.*

UniProt ID	Gene Name	Protein Name	Protein Score
O14786	NRP1	Neuropilin-1	323.31
Q9C0C2	TB182	182 kDa tankyrase-1-binding protein	209.13
O60716	CTND1	Catenin delta-1	204.16
P55196	AFAD	Afadin	167.55
O15020	SPTN2	Spectrin beta chain, non-erythrocytic 2	157.92
Q86UP2	KTN1	Kinectin	155.82
Q07157	ZO1	Tight junction protein ZO-1	145.51
Q14160	SCRIB	Protein scribble homolog	117.55
Q9UBC2	EP15R	Epidermal growth factor receptor substrate 15-like 1	106.99
P02786	TFR1	Transferrin receptor protein 1	103.73
P35613	BASI	Basigin	101.38
Q9H3N1	TMX1	Thioredoxin-related transmembrane protein 1	98.97
Q9H2G2	SLK	STE20-like serine/threonine-protein kinase	98.14
P11717	MPRI	Cation-independent mannose-6-phosphate receptor	87.70
Q8IZ21	PHAR4	Phosphatase and actin regulator 4	81.86

Q92783	STAM1	Signal transducing adapter molecule 1	77.24
Q13190	STX5	Syntaxin-5	76.62
Q9P0K7	RAI14	Ankycorbin	74.28
Q6WKZ4	RFIP1	Rab11 family-interacting protein 1	72.33
Q07960	RHG01	Rho GTPase-activating protein 1	71.59
Q86X29	LSR	Lipolysis-stimulated lipoprotein receptor	71.33
Q92692	NECT2	Nectin-2	69.80
Q9NNW5	WDR6	WD repeat-containing protein 6	67.92
Q9UEY8	ADDG	Gamma-adducin	67.30
Q9H3P7	GCP60	Golgi resident protein GCP60	64.59
Q4KMP7	TB10B	TBC1 domain family member 10B	59.59
Q16181	SEPT9	Septin-9	56.07
Q13492	PICAL	Phosphatidylinositol-binding clathrin assembly protein	55.86
Q13177	PAK2	Serine/threonine-protein kinase PAK 2	55.33
P05556	ITGB1	Integrin beta-1	54.89
Q9Y5X1	SNX9	Sorting nexin-9	53.59
O95292	VAPB	Vesicle-associated membrane protein-associated protein B/C	50.88
Q6NUQ4	TM214	Transmembrane protein 214	49.85
Q8NDI1	EHBP1	EH domain-binding protein 1	47.72
Q15311	RBP1	RalA-binding protein 1	47.37
Q9UDY2	ZO2	Tight junction protein ZO-2	47.21
O15498	YKT6	Synaptobrevin homolog YKT6	47.11
P78310	CXAR	Coxsackievirus and adenovirus receptor	46.02
O00213	APBB1	Amyloid beta precursor protein binding family B member 1	43.50
Q6P996	PDXD1	Pyridoxal-dependent decarboxylase domain-containing protein 1	43.25
Q9H0W5	CCDC8	Coiled-coil domain-containing protein 8	42.63
Q5JSH3	WDR44	WD repeat-containing protein 44	42.28
Q14118	DAG1	Dystroglycan 1	41.75
Q16625	OCLN	Occludin	40.73
Q92575	UBXN4	UBX domain-containing protein 4	40.46
P55011	S12A2	Solute carrier family 12 member 2	39.85
P30519	HMOX2	Heme oxygenase 2	39.22
Q9H4M9	EHD1	EH domain-containing protein 1	38.64
P08240	SRPRA	Signal recognition particle receptor subunit alpha	37.91
P18031	PTN1	Tyrosine-protein phosphatase non-receptor type 1	37.02
Q3V6T2	GRDN	Girdin	36.96
Q13596	SNX1	Sorting nexin-1	36.86
Q13586	STIM1	Stromal interaction molecule 1	36.18
Q641Q2	WAC2A	WASH complex subunit 2C	36.02
P53990	IST1	ST1 homolog	33.53
P51149	RAB7A	Ras-related protein Rab-7a	32.12
Q96A33	CCD47	PAT complex subunit CCDC47	30.94
O95817	BAG3	BAG family molecular chaperone regulator 3	29.58
Q96HY6	DDRGK	DDRGK domain-containing protein 1	29.11
Q96S66	CLCC1	Chloride channel CLIC-like protein 1	29.06
P22059	OSBP1	Oxysterol-binding protein 1	28.96

O95721	SNP29	Synaptosomal-associated protein 29	27.79
Q9P0L0	VAPA	Vesicle-associated membrane protein-associated protein A	26.88
P14209	CD99	CD99 antigen	26.21
Q9UHD1	CHRD1	Cysteine and histidine-rich domain-containing protein 1	26.01
Q96AC1	FERM2	Fermitin family homolog 2	24.64
Q7Z2K8	GRIN1	G protein-regulated inducer of neurite outgrowth 1	23.74
Q92597	NDRG1	Protein NDRG1	23.66
Q01650	LAT1	Large neutral amino acids transporter small subunit 1	22.35
P49591	SYSC	Serine--tRNA ligase, cytoplasmic	21.74
Q9Y5Y0	FLVC1	Heme transporter FLVCR1	19.81
Q99808	S29A1	Equilibrative nucleoside transporter 1	17.89
Q13277	STX3	Syntaxin-3	17.56
Q9UQN3	CHM2B	Charged multivesicular body protein 2b	16.05
P10586	PTPRF	Receptor-type tyrosine-protein phosphatase F	16.05
O75915	PRAF3	PRA1 family protein 3	15.26
Q99536	VAT1	Synaptic vesicle membrane protein VAT-1 homolog	14.78

Table 4.11 – Enriched protein list in NRP1-BioID2-HA samples under basal conditions common in 3 of the 4 repeats. *Combining the repeats of NRP1-BioID2-HA under basal conditions and supplemented with biotin, the proteins enriched in all repeats were identified. A total of 100 proteins were enriched in this analysis. Proteins with a >20% frequency in HEK293 cells associated with proximity-biotinylation identified in the CRAPome were excluded from the final list. Statistical analysis by an unpaired t test with Welch's correction was performed on the riBAQ values between test and control samples to determine if fold change was statistically significant. Proteins with a p value of >0.05 were excluded from the final list.*

UniProt ID	Gene Name	Protein Name	Protein Score
P20020	AT2B1	Plasma membrane calcium-transporting ATPase 1	96.72
Q9UPN3	K0754	Microtubule-actin cross-linking factor 1, isoforms 6/7	95.42
Q6P1N0	C2D1A	Coiled-coil and C2 domain-containing protein 1A	91.29
P53365	ARFP2	Arfaptin-2	76.91
Q8TBA6	GOGA5	Golgin subfamily A member 5	67.14
Q13136	LIPA1	Liprin-alpha-1	67.00
Q12959	DLG1	Disks large homolog 1	64.60
Q8N3F8	MILK1	MICAL-like protein 1	62.16
Q13480	GAB1	GRB2-associated-binding protein 1	60.74
O00151	PDLI1	PDZ and LIM domain protein 1	59.66
P49757	NUMB	Protein numb homolog	59.35
Q15334	L2GL1	Lethal(2) giant larvae protein homolog 1	57.61
P61081	UBC12	NEDD8-conjugating enzyme Ubc12	54.55
P04920	B3A2	Anion exchange protein 2	52.48
Q08378	GOGA3	Golgin subfamily A member 3	48.84
Q9HAU0	PKHA5	Pleckstrin homology domain-containing family A member 5	48.23

Q9Y6N7	ROBO1	Roundabout homolog 1	47.62
Q9UQB8	BAIP2	Brain-specific angiogenesis inhibitor 1-associated protein 2	47.34
O43399	TPD54	Tumor protein D54	45.74
Q9P206	K1522	Uncharacterized protein KIAA1522	45.38
Q9UGP8	SEC63	Translocation protein SEC63 homolog	44.91
O94804	STK10	Serine/threonine-protein kinase 10	43.81
P35612	ADDB	Beta-adducin	40.90
Q00587	BORG5	Cdc42 effector protein 1	40.59
Q9HD26	GOPC	Golgi-associated PDZ and coiled-coil motif-containing protein	40.37
Q9H2J7	S6A15	Sodium-dependent neutral amino acid transporter B(0)AT2	38.91
Q9Y5M8	SRPRB	Signal recognition particle receptor subunit beta	35.69
Q9NVM4	ANM7	Protein arginine N-methyltransferase 7	35.53
O00161	SNP23	Synaptosomal-associated protein 23	35.45
Q5M775	CYTSB	Cytospin-B	35.31
Q9BX67	JAM3	Junctional adhesion molecule C	35.28
Q13308	PTK7	Inactive tyrosine-protein kinase 7	34.91
Q9UGP4	LIMD1	LIM domain-containing protein 1	34.89
Q6P9B6	MEAK7	MTOR-associated protein MEAK7	34.74
P78344	IF4G2	Eukaryotic translation initiation factor 4 gamma 2	34.40
Q9NUQ9	CYRIB	CYFIP-related Rac1 interactor B	33.79
O60493	SNX3	Sorting nexin-3	32.11
P42566	EPS15	Epidermal growth factor receptor substrate 15	31.07
O75976	CBPD	Carboxypeptidase D	30.86
Q7KZI7	MARK2	Serine/threonine-protein kinase MARK2	30.53
Q9HCU5	PREB	Prolactin regulatory element-binding protein	30.36
Q9ULC3	RAB23	Ras-related protein Rab-23	30.15
P11233	RALA	Ras-related protein Ral-A	29.78
Q4VCS5	AMOT	Angiomotin	29.72
Q96TA1	NIBA2	Protein Niban 2	29.68
O95297	MPZL1	Myelin protein zero-like protein 1	29.61
Q86Y82	STX12	Syntaxin-12	29.12
Q9UGV2	NDRG3	Protein NDRG3	29.00
Q7Z478	DHX29	ATP-dependent RNA helicase DHX29	28.41
Q9Y6M5	ZNT1	Proton-coupled zinc antiporter SLC30A1	28.30
Q8N5K1	CISD2	CDGSH iron-sulfur domain-containing protein 2	27.56
Q5JTV8	TOIP1	Torsin-1A-interacting protein 1	27.28
Q12955	ANK3	Ankyrin-3	27.25
Q9BXI6	TB10A	TBC1 domain family member 10A	26.34
Q15464	SHB	SH2 domain-containing adapter protein B	26.32
O15126	SCAM1	Secretory carrier-associated membrane protein 1	26.25
Q5HYK7	SH319	SH3 domain-containing protein 19	26.25
Q9HC56	PCDH9	Protocadherin-9	24.66
Q9Y6R0	NUMBL	Numb-like protein	24.43

O94979	SC31A	Protein transport protein Sec31A	23.92
P30260	CDC27	Cell division cycle protein 27 homolog	23.80
Q9BZI7	REN3B	Regulator of nonsense transcripts 3B	23.74
O60245	PCDH7	Protocadherin-7	23.72
P05067	A4	Amyloid-beta precursor protein	23.27
Q53EZ4	CEP55	Centrosomal protein of 55 kDa	22.81
Q8WTV0	SCRB1	Scavenger receptor class B member 1	22.75
Q6Y7W6	GGYF2	GRB10-interacting GYF protein 2	22.38
O96013	PAK4	Serine/threonine-protein kinase PAK 4	22.36
O95208	EPN2	Epsin-2	21.25
Q96KC8	DNJC1	DnaJ homolog subfamily C member 1	20.86
A0FGR8	ESYT2	Extended synaptotagmin-2	20.84
P15529	MCP	Membrane cofactor protein	20.58
P52594	AGFG1	Arf-GAP domain and FG repeat-containing protein 1	20.54
Q96C19	EFHD2	EF-hand domain-containing protein D2	20.23
Q9Y6I9	TX264	Testis-expressed protein 264	20.18
Q96A49	SYAP1	Synapse-associated protein 1	20.06
P52948	NUP98	Nuclear pore complex protein Nup98-Nup96	19.49
P16435	NCPR	NADPH--cytochrome P450 reductase	19.31
P43307	SSRA	Translocon-associated protein subunit alpha	19.00
Q04721	NOTC2	Neurogenic locus notch homolog protein 2	18.91
Q7RTP6	MICA3	[F-actin]-monooxygenase MICAL3	18.56
Q14669	TRIPC	E3 ubiquitin-protein ligase TRIP12	18.31
P14635	CCNB1	G2/mitotic-specific cyclin-B1	18.30
Q9NYB9	ABI2	Abl interactor 2	17.94
Q96QD8	S38A2	Sodium-coupled neutral amino acid symporter 2	17.77
P51809	VAMP7	Vesicle-associated membrane protein 7	17.55
Q9Y385	UB2J1	Ubiquitin-conjugating enzyme E2 J1	17.12
Q9UBM7	DHCR7	7-dehydrocholesterol reductase	16.20
P52565	GDIR1	Rho GDP-dissociation inhibitor 1	16.17
Q9BVC6	TM109	Transmembrane protein 109	15.76
Q6F5E8	CARL2	Capping protein, Arp2/3 and myosin-I linker protein 2	15.36
Q8N128	F177A	Protein FAM177A1	15.29
Q12929	EPS8	Epidermal growth factor receptor kinase substrate 8	14.43
Q9Y679	AUP1	Lipid droplet-regulating VLDL assembly factor AUP1	14.27
Q96HN2	SAHH2	S-adenosylhomocysteine hydrolase-like protein 1	14.25
O14967	CLGN	Calmegin	14.06
Q9BZF3	OSBL6	Oxysterol-binding protein-related protein 6	12.55
Q8TAA9	VANG1	Vang-like protein 1	12.19
Q00013	EM55	55 kDa erythrocyte membrane protein	11.68
Q9Y3E7	CHMP3	Charged multivesicular body protein 3	11.51

4.2.2.7 Gene Ontology Analyses of Enriched Protein List for NRP1-BioID2-HA in Basal Conditions

The GO analyses were performed in the same manner for the NRP1-BioID2-HA basal conditions as discussed previously in section 4.2.2.5. Webgestalt was used to identify enriched GO terms relating to molecular function, biological processes and cellular component. A summary analysis was included, providing a general overview of the GO terms which the input protein list related to. More specific analyses were performed, whereby redundant parent terms were excluded and only more specific child GO terms were included in the annotations. Again, enrichment ratio (ER) was plotted against GO terms for each analysis.

Molecular Function GO Analysis

In the summary data from the molecular function analysis, (Figure 4.17a), similar to the NRP1-BioID2-HA $VEGF_{165}$a stimulated data, the majority of the enriched proteins (n = 162) are categorised under the GO parent term of protein binding. Binding to other small molecules and macromolecules is suggested in the summary data, indicated by relevant enriched GO parent terms. GO terms relating to ion binding (n = 56), nucleotide binding (n = 26), nucleic acid binding (n = 23), lipid binding (n = 22), and to a lesser extent carbohydrate binding (n = 2) and chromatin binding (n = 2). When investigating more specific child terms, derived from the parent terms observed in the summary data, a more detailed description on specific enriched GO molecular function terms is observed, (Figure 4.17b). As observed for the NRP1-BioID2-HA $VEGF_{165}$a stimulated molecular function GO analyses, (Figure 4.13b), cadherin binding (ER = 15.70) is a significantly enriched GO term. SNARE binding (ER = 6.50) is another commonly enriched term between these analyses. Cell adhesion mediator activity (ER = 10.44) and actin binding (ER = 2.97) are highly enriched GO terms unique to the NRP1-BioID2-HA fusion protein in basal conditions. Other interesting enriched GO terms were those relating to insulin receptor binding (ER = 13.42), exogenous protein binding (ER = 9.72), and GTPase binding (ER = 5.63).

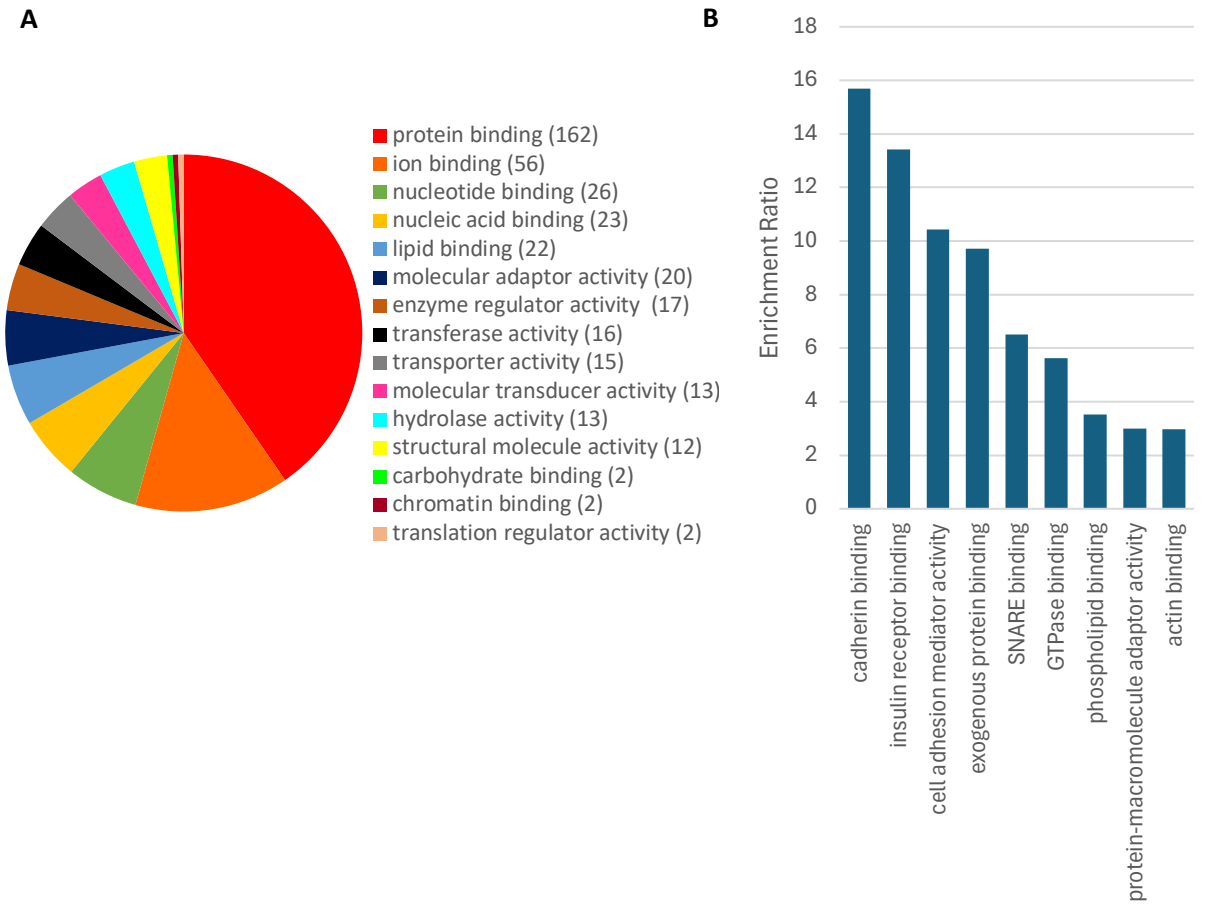

Figure 4.17 – Molecular function gene ontology (GO) analysis of enriched proteins for NRP1-BioID2-HA under basal conditions. *Protein lists were analysed by an overrepresentation analysis using Webgestalt, filtering for redundant GO terms. The enriched list was cross-referenced against molecular function GO terms, which describe the fundamental molecular activity of proteins. Enriched terms with a significance level > 0.05 were excluded. The GO terms were ranked based on enrichment ratio (ER), a ratio between the expected number of proteins present for a specific GO term based on a random set of proteins vs the input proteins, in this case those enriched in the BioID analyses of NRP1-BioID2-HA under basal conditions.* ***(A)*** *The summary data represents parent GO terms which were enriched.* ***(B)*** *The molecular function GO analysis relating to the enrichment of specific GO child terms.*

Biological Processes GO Analysis

The summary of the biological function GO analysis for the NRP1-BioID2-HA under basal conditions, (Figure 4.18a), revealed enriched GO terms common with the NRP1-BioID2-HA $VEGF_{165}a$ stimulated analysis. Notably, the common GO parent terms included biological regulation (n = 137), cellular compartment organisation (n = 116), localisation (n = 108), response to stimulus (n =101) and cell communication (n = 82). The more specific analysis involving GO child terms and filtering for redundant GO parent terms elicited a much greater number of enriched biological processes GO terms, (Figure 4.18b), compared to the NRP1-BioID2-HA $VEGF_{165}a$ stimulated analyses, (Figure 4.14b). Similar to the previous analysis, several GO terms related to vesicular trafficking were enriched including protein localization to endosome (ER = 15.15), membrane docking (ER = 10.70), vesicle-mediated transport to the plasma membrane (ER = 8.59), endosomal transport (ER = 6.49), organelle fusion (ER = 6.11),

membrane fusion (ER = 5.98), vesicle organization (ER = 5.68), receptor-mediated endocytosis (ER = 4.61), vesicle-mediated transport in synapse (ER = 4.47), exocytosis (ER = 3.67), and vesicle localization (ER = 3.56).

Unlike for the NRP1-BioID2-HA $VEGF_{165}$a stimulated GO analysis, several biological processes GO terms relating to cellular adhesion were enriched. For example, protein localization to cell junction (ER = 10.12), cell-cell junction organization (ER = 5.92), and cell junction assembly (n = 3.32). In a similar fashion, GO terms relating to cellular projections were also enriched, including lamellipodium organization (ER = 7.74), positive regulation of cell projection organization (ER = 5.31), regulation of cell projection assembly (ER = 5.11), and regulation of neuron projection development (ER = 3.28).

Several GO terms relating neuronal processes were enriched, unique to the NRP1-BioID2-HA under basal conditions GO analysis. These enriched GO terms related to regulation of postsynaptic membrane neurotransmitter receptor levels (ER = 11.31), vesicle-mediated transport in synapse (ER = 4.47), axonogenesis (ER = 4.36), neurotransmitter transport (ER = 4.32), regulation of neuron projection development (ER = 3.28), dendrite development (ER = 2.36), and synapse organization (ER = 2.88).

Interestingly, the GO term relating to vascular endothelial growth factor receptor signalling pathway (ER = 10.55) was enriched, not observed in the NRP1-BioID2-HA $VEGF_{165}$a stimulated analysis. Similarly related GO terms, specific to this analysis, were vascular process in circulatory system (ER = 4.39), regulation of vasculature development (ER = 3.72), and wound healing (ER = 3.03). The GO term relating to viral processes (ER = 4.00) was also significantly enriched.

A

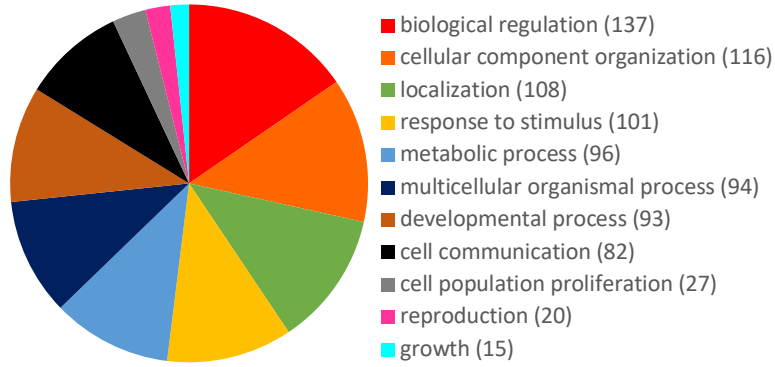

Figure 4.18 – Biological processes gene ontology (GO) analysis of enriched proteins for NRP1-BioID2-HA under basal conditions. *Protein lists were analysed by an overrepresentation analysis using Webgestalt, filtering for redundant GO terms. The enriched list was cross-referenced against biological processes GO terms, which describe the pathways and biological objectives a protein contributes to. Enriched terms with a significance level > 0.05 were excluded. The GO terms were ranked based on enrichment ratio (ER), a ratio between the expected number of proteins present for a specific GO term based on a random set of proteins vs the input proteins, in this case those enriched in the BioID analyses of NRP1-BioID2-HA under basal conditions.* ***(A)*** *The summary data represents parent GO terms which were enriched.* ***(B)*** *The biological processes GO analysis relating to the enrichment of specific GO child terms.* *Figure continued next page…*

B

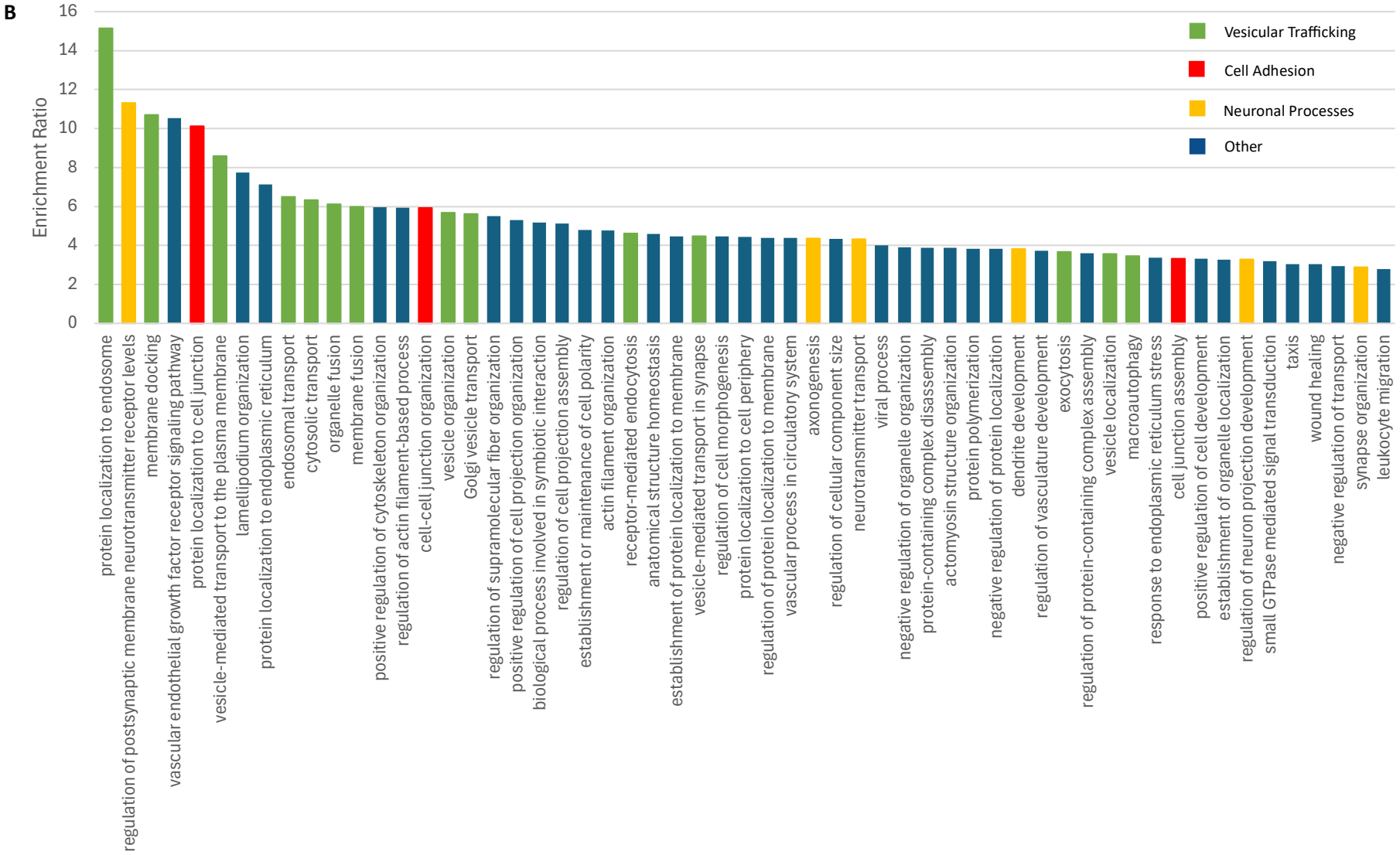
Enrichment Ratio
16
14
12
10
8
6
4
2
0
Vesicular Trafficking
Cell Adhesion
Neuronal Processes
Other
protein localization to endosome
regulation of postsynaptic membrane neurotransmitter receptor levels
membrane docking
vascular endothelial growth factor receptor signaling pathway
protein localization to cell junction
vesicle-mediated transport to the plasma membrane
lamellipodium organization
protein localization to endoplasmic reticulum
endosomal transport
cytosolic transport
organelle fusion
membrane fusion
positive regulation of cytoskeleton organization
regulation of actin filament-based process
cell-cell junction organization
vesicle organization
Golgi vesicle transport
regulation of supramolecular fiber organization
positive regulation of cell projection organization
biological process involved in symbiotic interaction
regulation of cell projection assembly
establishment or maintenance of cell polarity
actin filament organization
receptor-mediated endocytosis
anatomical structure homeostasis
establishment of protein localization to membrane
vesicle-mediated transport in synapse
regulation of cell morphogenesis
protein localization to cell periphery
regulation of protein localization to membrane
vascular process in circulatory system
axonogenesis
regulation of cellular component size
neurotransmitter transport
viral process
negative regulation of organelle organization
protein-containing complex disassembly
actomyosin structure organization
protein polymerization
negative regulation of protein localization
dendrite development
regulation of vasculature development
exocytosis
regulation of protein-containing complex assembly
vesicle localization
macroautophagy
response to endoplasmic reticulum stress
cell junction assembly
positive regulation of cell development
establishment of organelle localization
regulation of neuron projection development
small GTPase mediated signal transduction
taxis
wound healing
negative regulation of transport
synapse organization
leukocyte migration

Cellular Component GO Analysis

The cellular component GO analysis summary, (Figure 4.19a), shows that the majority of the proteins enriched from the NRP1-BioID2-HA under basal conditions analysis, are associated with the GO parent term relating to the cell membrane (n = 151). Similarly, a large portion are associated with the endomembrane system (n = 102). Considering the number of biological processes GO terms associated with vesicular transport, it is unsurprising several cellular component GO child and parent terms related to vesicles. The GO parent terms for vesicle (n = 85), endosome (n = 34), envelope (n = 22), and vacuole (n = 19) were all enriched. Additionally, the GO parent term for cell projection (n = 55) was significantly enriched, (Figure 4.19a). Unsurprisingly, given the biological processes GO results, a number of cellular component GO child terms related to vesicle, (Figure 4.19b). These included GO terms denoted as the retromer complex (ER = 14.06), SNARE complex (ER = 13.78), clathrin-coated pit (ER = 8.95), primary lysosome (ER = 4.45), coated vesicle (ER = 4.39), recycling endosome (ER = 4.36), endocytic vesicle (ER = 4.29), early endosome (ER = 3.92), and transport vesicle (ER = 3.43).

A number of GO terms were also associated with the cellular membrane, in particular at cellular junctions. Enriched GO terms relating to junctions, were the cell-cell contact zone (ER = 13.48), adherens junction (ER = 11.58), tight junction (ER = 8.33), apical junction complex (ER = 7.93), cell-substrate junction (ER = 4.55), and apical part of cell (ER = 2.94). Related Go terms associated with cellular projections were also enriched, the cell leading edge (ER = 4.85) and actin-based cell projection (ER = 4.38).

Several enriched cellular component GO terms were associated with neurology. The terms associated with neuronal processes were the myelin sheath (ER = 9.16), immunological synapse (ER = 8.75), Schaffer collateral - CA1 synapse (ER = 8.47), glutamatergic synapse (ER = 3.87), neuron to neuron synapse (ER = 3.56), postsynaptic specialization (ER = 3.47), synaptic membrane (ER = 3.25), and distal axon (ER = 3.21).

A

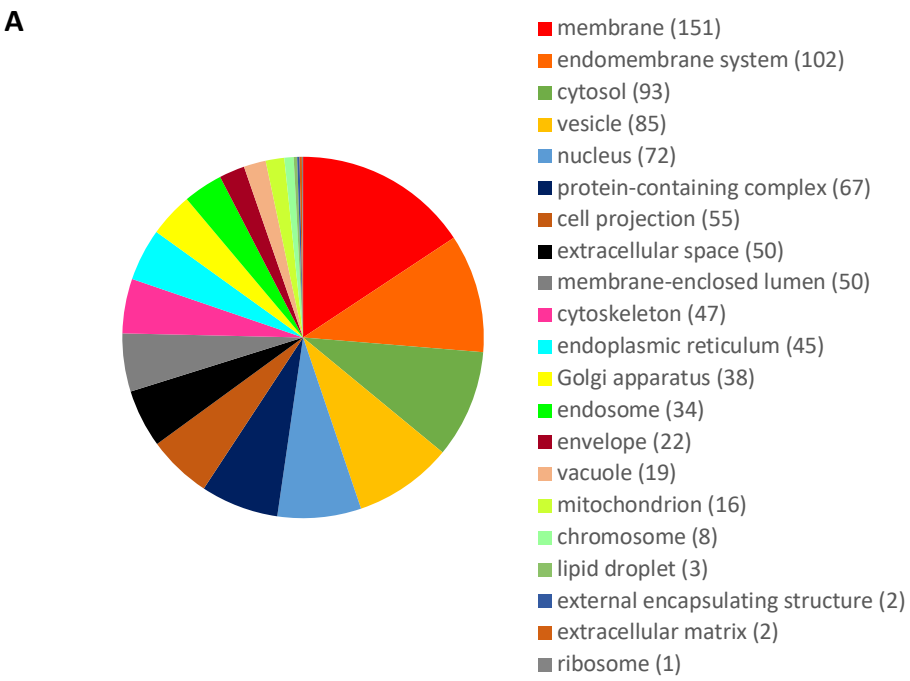

Figure continued next page…

B

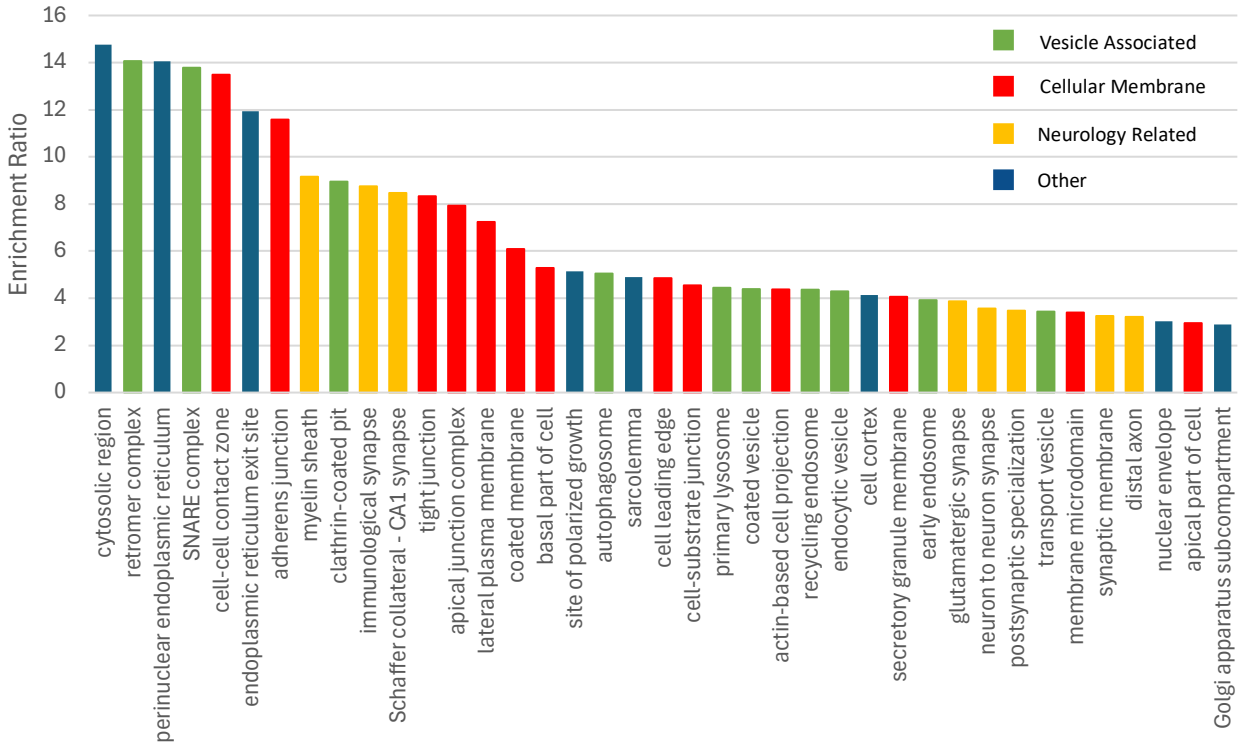

Figure 4.19 – Cellular component gene ontology (GO) analysis of enriched proteins for NRP1-BioID2-HA under basal conditions. *Protein lists were analysed by an overrepresentation analysis using Webgestalt, filtering for redundant GO terms. The enriched list was cross-referenced against cellular component GO terms, which describe localisation of the protein within the cellular environment. Enriched terms with a significance level > 0.05 were excluded. The GO terms were ranked based on enrichment ratio (ER), a ratio between the expected number of proteins present for a specific GO term based on a random set of proteins vs the input proteins, in this case those enriched in the BioID analyses of NRP1-BioID2-HA under basal conditions.* ***(A)*** *The summary data represents parent GO terms which were enriched.* ***(B)*** *The cellular component GO analysis relating to the enrichment of specific GO child terms.*

4.2.3 Neuropilin 1 C-terminal Interactome Analysis in the Presence of Vascular Endothelial Growth Factor Receptor 2 using mycBioID2-NRP1

4.2.3.1 Transient Expression of Neuropilin 1 Fusion Proteins in HEK293/HaloTag-VEGFR2 Cells

NRP1-BioID2-HA

Once the C-terminal interactome analysis had been optimised in WT HEK293T cells and revealed a plethora of potential novel interactors, the analysis was extended to consider the NRP1 interactome in the presence of VEGFR2. This is important as NRP1 and VEGFR2 are known to form complexes, hence, this complex formation may reveal more novel interactors compared to expression of NRP1 alone. Initially a cell model was attempted by transiently expressing NRP1-BioID2-HA in an already generated HEK293 cell line stably expressing HaloTag-VEGFR2[354], (Figure 4.20). Although, sufficient expression of the NRP1-BioID2-HA is observed, indicated by the anti-HA AF594 staining, the pattern of expression did not correlate with HaloTag-VEGFR2 expression, viewed in the HaloTag-AF488 channel. When the two channels are merged, there are few cells with high expression of both NRP1-BioID2-HA and HaloTag-VEGFR2.

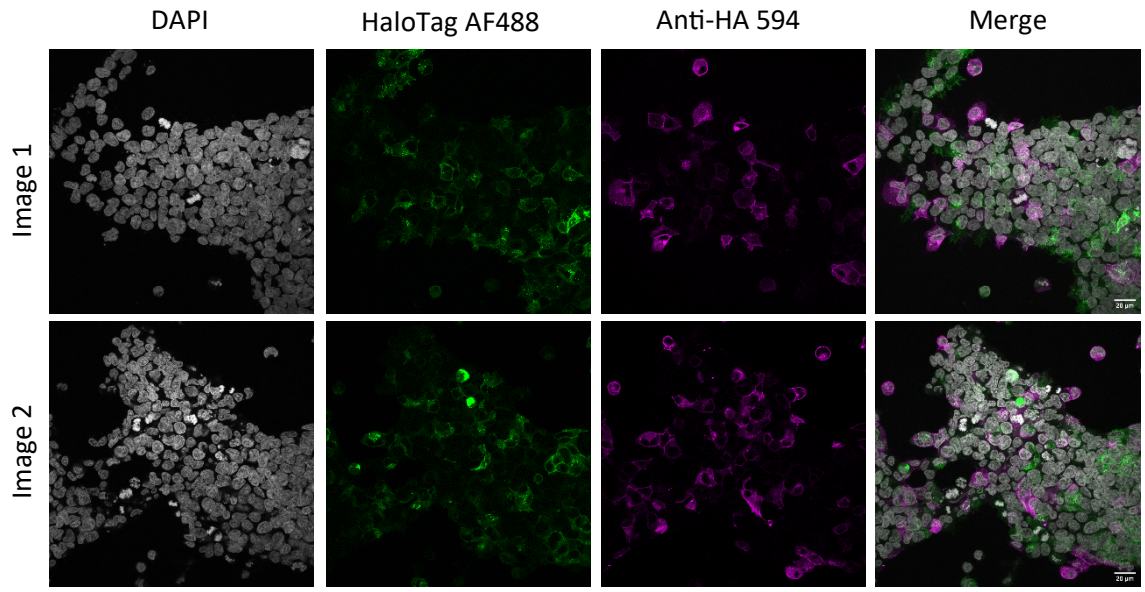

Figure 4.20 – Immunofluorescence of transfection of NRP1-BioID2-HA in HEK293/HaloTag-VEGFR2 stable cell line. *Cells were incubated with a NRP1-BioID2-HA plasmid and Fugene HD mixture for 24 hours, followed by supplementation with fresh media for a further 20 h. Cells were fixed and stained with anti-HA mouse (Invitrogen; 2-2.2.14) antibody followed by an anti-mouse AF594 (Jackson Immuno Research; 115-585-003) to visualise the NRP1-BioID2-HA fusion protein. HaloTag AF488 ligand (Promega; G1001) highlighted the presence of HaloTag-VEGFR2. DAPI was used to highlight nuclear material and identify individual cells. Two representative images from separate repeats were included, labelled image 1 and image 2.*

SNAP-NRP1

SNAP-NRP1 was transiently expressed in the HEK293T HaloTag-VEGFR2 stable cell line to determine if the observed expression issues were specific to NRP1-BioID2-HA or for other reasons, (Figure 4.21). The transient expression analysis was performed in live cells. From the live imaging, a similar pattern is observed as with the transient expression of NRP1-BioID2-HA. The majority of SNAP-NRP1 transiently transfected cells express low amounts, in some cases barely detectable, HaloTag-VEGFR2. While cells expressing HaloTag-VEGFR2 highly, exhibit a low or non-detectable level of SNAP-NRP1. In some cases, sufficient expression of both SNAP-NRP1 and HaloTag-VEGFR2 is observed. However, this would not be sufficient for the BioID protocol. Hence, a means of enriching cells co-expressing both NRP1 and VEGFR2 was sought.

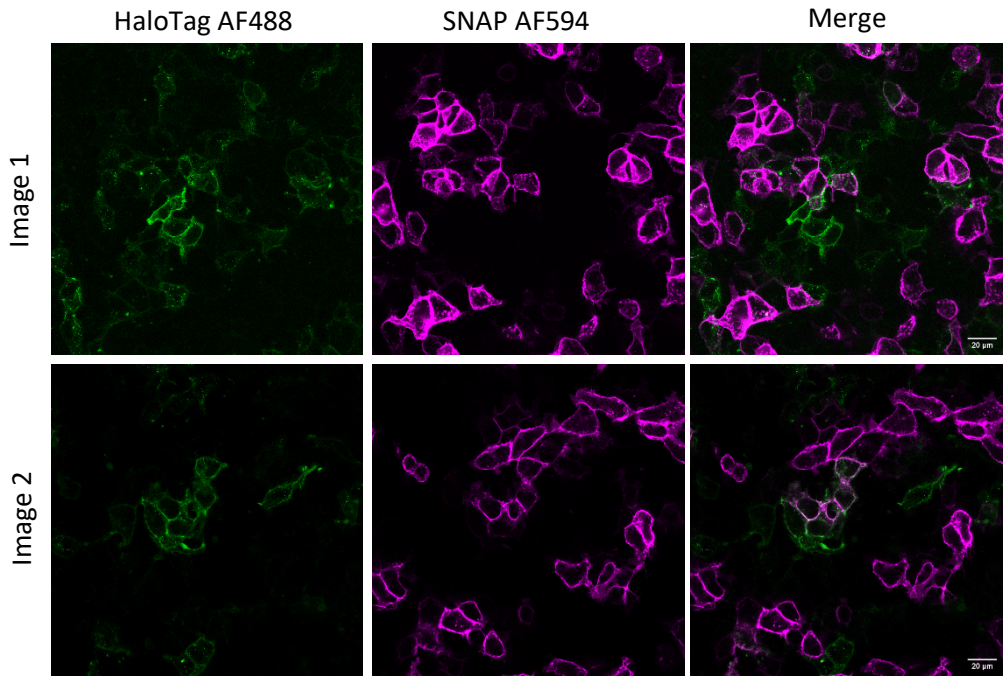

Figure 4.21 – Immunofluorescence of transfection of SNAP-NRP1 in HEK293/HaloTag-VEGFR2 stable cell line. *Cells were incubated with a SNAP-NRP1 plasmid and Fugene HD mixture for 24 hours, followed by supplementation with fresh media for a further 20 h. Cells were stained with SNAP AF594 ligand (New England Biolabs; S9134S) to visualise the SNAP-NRP1 A fusion protein. HaloTag-AF488 ligand (Promega; G1001) highlighted the presence of HaloTag-VEGFR2. The cells were imaged live in with HBSS replacing DMEM for the imaging. Two representative images from separate repeats were included, labelled image 1 and image 2.*

4.2.3.2 pLV-NRP1-BioID2-HA Lentiviral Plasmid Design and Synthesis

The open reading frame (ORF) encoding NRP1-BioID2-HA incorporated in the already cloned plasmid of the same name was sent to GenScript (www.genscript.com/) to synthesise a lentiviral plasmid. The original plasmid was unsuitable for stable cell line generation in this case, as the HEK293T/HaloTag-VEGFR2 cell line was inherently resistant to G418, the resistance cassette in the original NRP1-BioID2-HA plasmid. The new lentiviral plasmid harboured a blasticidin resistance cassette in which the HEK293T/HaloTag-VEGFR2 stable cell line is resistant to.

4.2.3.3 Optimisation of Lentiviral Transductions

Varying concentrations of lentiviral media preparation was mixed with 8 µg/mL polybrene and incubated with the HEK293T/HaloTag-VEGFR2 stable cell line for 72 h before analysis for NRP1-BioID2-HA expression levels, (Figure 4.22). As expected in the polybrene only control, no detectable NRP1-BioID2-HA expression is observed, demonstrated by an absence of signal in the anti-HA AF594 channel. Expression of the fusion protein was observed in all lentiviral concentrations analysed. The lowest transfection efficiency was observed with the 25% lentiviral concentration condition, the lowest

concentration of virus tested. Results were similar with the other lentiviral conditions, perhaps more fusion protein expression observed in the 75% and 100% lentiviral concentrations than the 50% concentration. A lentiviral concentration of 75% was chosen for future lentiviral transduction experiments.

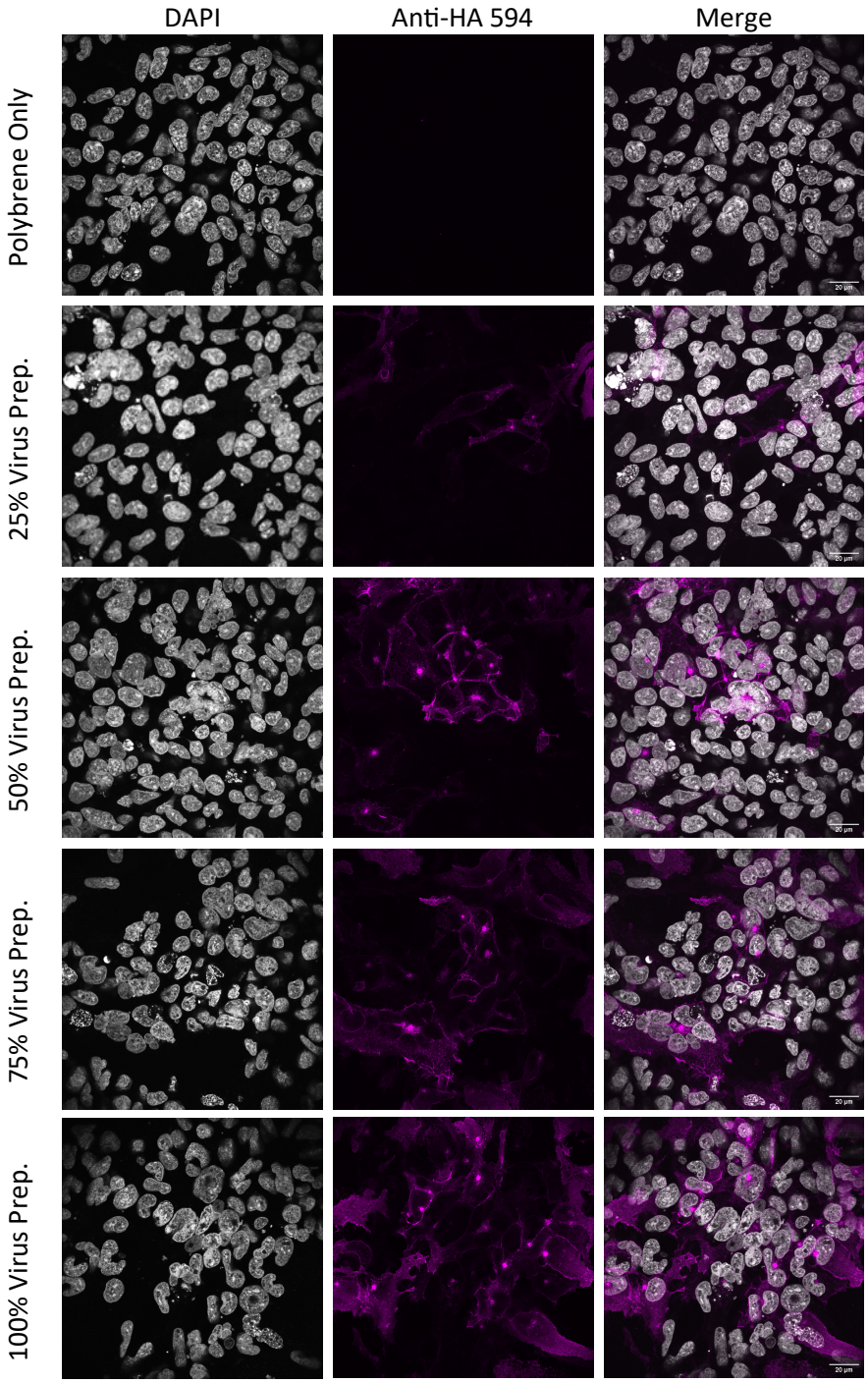

Figure 4.22 – Immunofluorescence of transduction optimisation of pLV-NRP1-BioID2-HA in HEK293/HaloTag-VEGFR2 stable cell line. *Cells were incubated with pLV-NRP1-BioID2-HA lentiviral preparation for 72 h at varying concentrations from 0 – 100 %. A polybrene only control was used at 8 µg/mL. Cells were fixed and stained with anti-HA mouse (Invitrogen; 2-2.2.14) antibody followed by an anti-mouse AF594 (Jackson Immuno Research; 115-585-003) to visualise the NRP1-BioID2-HA fusion protein. DAPI was used to highlight nuclear material and identify individual cells.*

4.2.3.4 Expression of NRP1-BioID2-HA in HEK293/HaloTag-VEGFR2 Cells Following Transduction and Blasticidin Selection

The cells were selected with 8 µg/mL blasticidin for 14 days, followed by analysis of NRP1-BioID2-HA and HaloTag-VEGFR2 co-expression, (Figure 4.23). The anti-HA FITC demonstrated not all cells were highly expressing NRP1-BioID2-HA, despite blasticidin selection. However, there appeared to be more observable cells co-expressing NRP1-BioID2-HA and HaloTag-VEGFR2 demonstrated by the merged anti-HA FITC and anti-VEGFR2 AF channels. Although this was a more positive result than observed previously, further enrichment of the co-expressing cells was warranted.

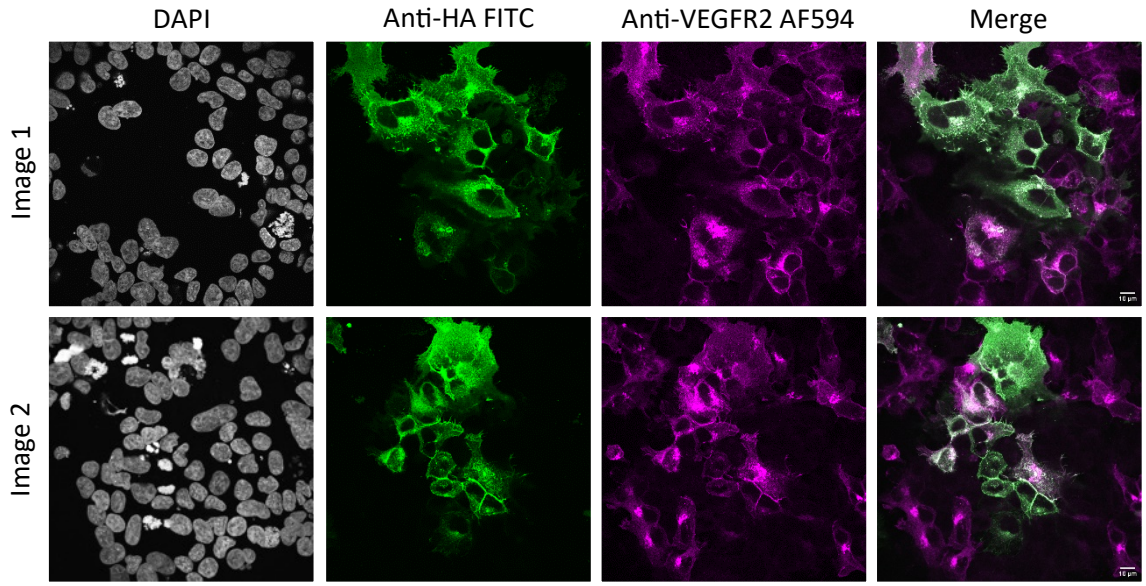

Figure 4.23 – Immunofluorescence of blasticidin selected HEK293/HaloTag-VEGFR2/NRP1-BioID2-HA stable cell line. *Following transduction optimisation, the transduced HEK293/HaloTag-VEGFR2 cells were selected using 8 µg/mL blasticidin for cells expressing NRP1-BioID2-HA. Cells were fixed and stained with anti-HA mouse (Invitrogen; 2-2.2.14) antibody followed by an anti-mouse FITC (Jackson Immuno Research; 115-095-003) to visualise the NRP1-BioID2-HA fusion protein. Anti-VEGFR2 rabbit (Cell Signalling; 2479S) antibody, followed by anti-rabbit AF594 (Jackson Immuno Research; 115-585-003) highlighted the presence of HaloTag-VEGFR2. DAPI was used to highlight nuclear material and identify individual cells. Two representative images from separate repeats were included, labelled image 1 and image 2.*

4.2.3.5 Fluorescence-activated cell sorting of HEK293T/HaloTag-VEGFR2/NRP1-BioID2-HA Cells

Fluorescence-activated cell sorting (FACS) was performed on the stable cell line using HaloTag-AF488 ligand and anti-NRP1, coupled with a AF594 secondary antibody in order to enrich cells expressing high levels of HaloTag-VEGFR2 and NRP1-BioID2-HA. During the FACS, cells were gated based on the forward scatter (FSC), side scatter (SSC) and fluorescence using 594 nm and 488 nm lasers, (Figure

4.24). The regions on the FACS graphs marked R1, R2 and R3 gave an indication of the parameters for sorting cells appropriate cells. Each individual dot on the graph represents either a single cell, a clump of cells or cellular debris. It is therefore important to isolate the single cells from the cell clumps and debris. Cell debris were removed by gating FSC area vs SSC area scatter in the region R1, (Figure 4.24a). Often gating of an FSC vs SSC plot is used for removal of cell debris, which usually appear in the bottom left corner of the graph[540]. Only single cells were isolated in the analysis indicated by region marked R2, (Figure 4.24b). A larger SSC width correlates with cell doublets and clumps of cells[541], hence the bodies with a larger SSC width were excluded. Finally, cells were gated based on fluorescent values by the region marked R3, (Figure 4.24c). As observed by the FACS graph, a large proportion of the cells lacked high expression of both NRP1-BioID2-HA and HaloTag-VEGFR2. Cells along the x-axis indicated HaloTag-VEGFR2 expression. Cells along y-axis indicated NRP1-BioID2-HA expression. Several cell populations appeared to be present in the FACS analysis. Cells in the bottom half indicated a relatively low expression of NRP1-BioID2-HA and higher expression of HaloTag-VEGFR2. Within this area, there was two overlapping populations of cells with higher HaloTag-VEGFR2 expression and cells with lower expression. Another population in the upper left quadrant appeared to be cells with relatively low expression of HaloTag-VEGFR2 and higher expression of NRP1-BioID2-HA. The population valuable for this research appeared in the upper right quadrant, relating to cells expressing both HaloTag-VEGFR2 and NRP1-BioID2-HA. These cells were gated and isolated, marked by the region R3. According to the output data, 65’352 cells were isolated based on these parameters. Extensive cell death occurred during the FACS protocol. Hence, this mixed population of cells was harvested and immediately supplemented with warmed DMEM to prevent further cell death.

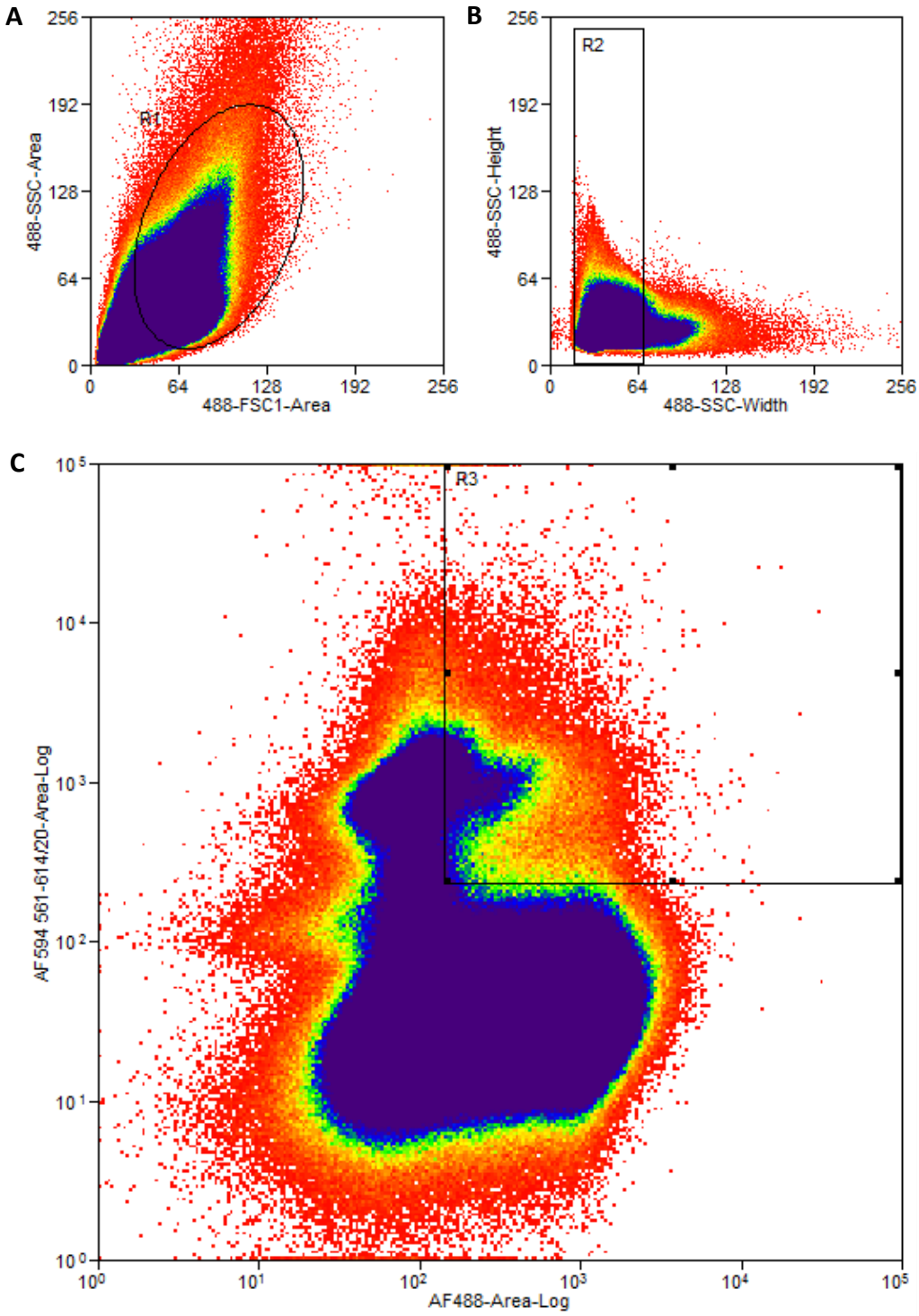

Figure 4.24 – Fluorescence-activated cell sorting (FACS) of blasticidin selected HEK293/HaloTag-VEGFR2/NRP1-BioID2-HA stable cell line. *Cells were detached using cell dissociation buffer (gibco; 13151014) and incubated with anti-NRP1 mouse antibody (Abcam; ab81321) on ice for 20 minutes. Cells were washed and further incubated on ice for 20 mintues with anti-mouse AF594 secondary antibody (Jackson Immuno Research; 115-585-003) and HaloTag-AF488 ligand (Promega; G1001), to indicate presence of NRP1-BioID2-HA and HaloTag-VEGFR2, respectively. Cells were subject to FACS and isolated based on;* ***(A)*** *Forward scatter (FSC) vs side scatter (SSC), marked by the region R1.* ***(B)*** *SSC width vs SSC height, marked by the region R2.* ***(C)*** *488 vs 594 fluorescence, marked by the region R3.*

4.2.3.6 Expression Analysis of HEK293T/HaloTag-VEGFR2/NRP1-BioID2-HA Cells After Fluorescence-Activated Cell Sorting

Following FACS isolation of blasticidin selected HEK293T/HaloTag-VEGFR2/NRP1-BioID2-HA cells, analysis was performed on the co-expression of the fusion proteins, (Figure 4.25). The anti-HA FITC straining correlated with the anti-VEGFR2 AF594 staining in many cells, demonstrated by the merging of the channels. This showed co-expression of the fusion proteins within the same cell. As the population is mixed, the levels of expression of NRP1-BioID2-HA and HaloTag-VEGFR2 vary between cells. Although, some cells still appeared to lack expression of either one or both of the fusion proteins, it was deemed sufficient to proceed with the BioID analysis.

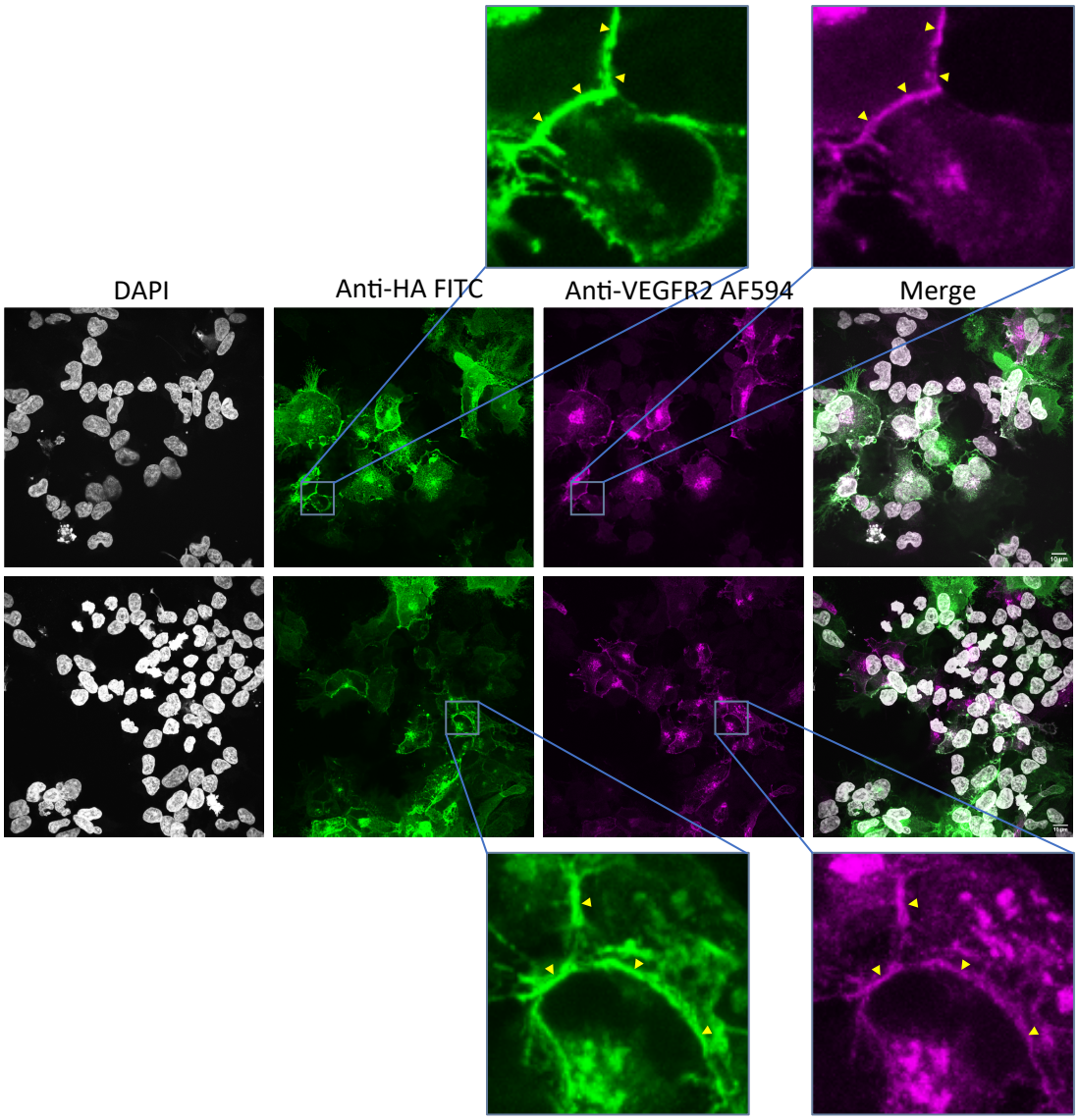

Figure 4.25 – Immunofluorescence of blasticidin selected HEK293/HaloTag-VEGFR2/NRP1-BioID2-HA stable cell line post-FACS. *Following FACS of the cells, the mixed population was cultured and analysed for co-expression of NRP1-BioID2-HA and HaloTag-VEGFR. Cells were fixed and stained with anti-HA mouse (Invitrogen; 2-2.2.14) antibody followed by an anti-mouse FITC (Jackson Immuno Research; 115-095-003) to visualise the NRP1-BioID2-HA fusion protein. Anti-VEGFR2 rabbit (Cell Signalling; 2479S) antibody, followed by anti-rabbit AF594 (Jackson Immuno Research; 111-585-003) highlighted the presence of HaloTag-VEGFR2. DAPI was used to highlight nuclear material and identify individual cells. Two representative images from separate repeats were included, labelled image 1 and image 2. Yellow arrows indicated membrane localisation of signal.*

4.2.3.7 Streptavidin Pulldown of HEK293/HaloTag-VEGFR2/NRP1-BioID2-HA Cells to Improve Protein Coverage

As not all cells appeared to express both NRP1-BioID2-HA and HaloTag-VEGFR2 cells, 2 x 10 cm dishes were used per condition. It may have been appropriate to increase this further, however, costs

associated with the volume of ligand required meant this was not possible. An additional control was added, a VEGF165b treatment supplemented with and without biotin. VEGF165b should bind to VEGFR2 and elicit a biological response. Unlike $VEGF_{165}a$, VEGF165b does not bind to NRP1, hence the inclusion as an extra control. The cell lysates and material eluted from the streptavidin beads were analyses via western blotting, (Figure 4.26). The anti-HA 680 channel detected the presence of bands unique to lysates with NRP1-BioID2-HA expression, indicating the observed bands related to NRP1-BioID2-HA. Due to issues relating to the western blot transfer, a smeared pattern is observed as the proteins have not been transferred perfectly from the SDS-PAGE gel to the nitrocellulose membrane, instead appearing to be pulled to one side. This obscured the true size of some bands in particular lanes. Although these smeared bands likely related to NRP1-BioID2-HA. The streptavidin 800 channel demonstrated the presence of biotinylated proteins in both the lysates and eluted material, indicating successful isolation of biotinylated proteins. The isolated biotinylated proteins were sent for mass spectrometry analyses to determine the nature of the potential interactors.

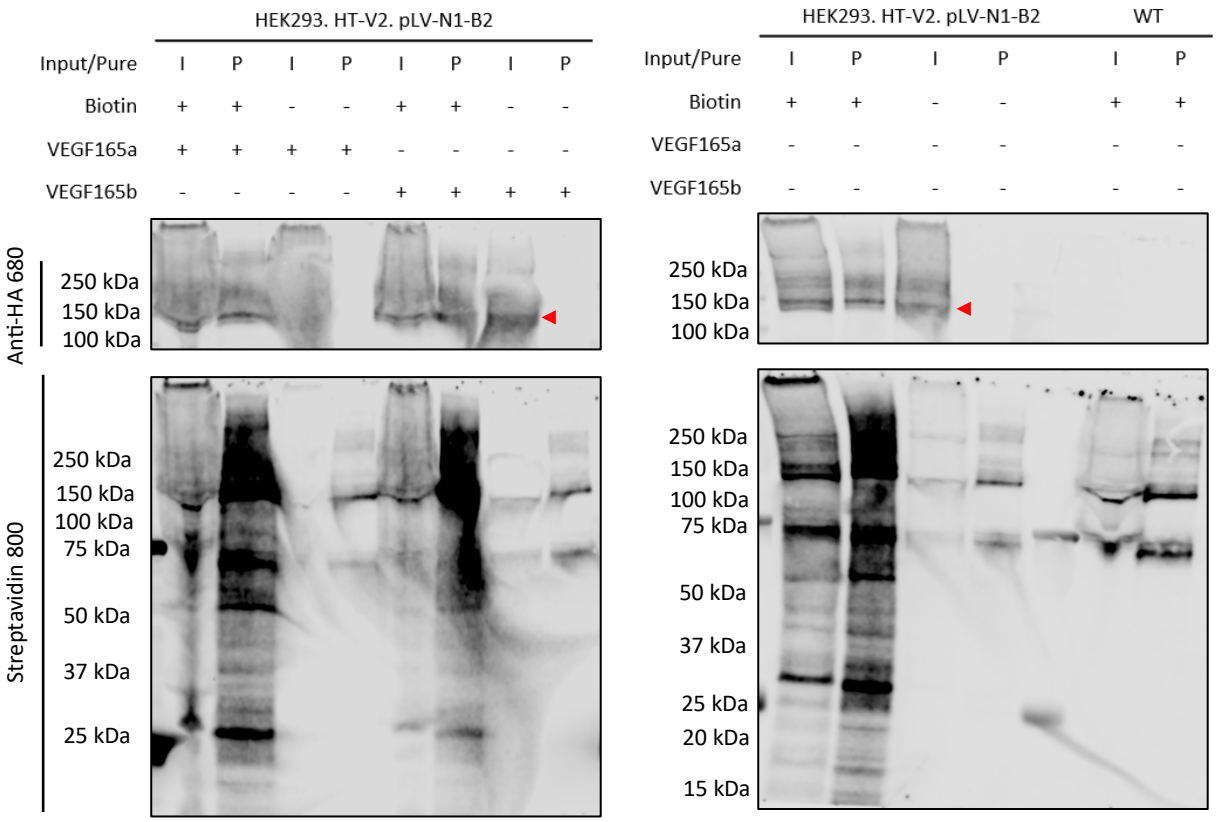

Figure 4.26 – Optimised streptavidin pulldown with HEK293/HaloTag-VEGFR2/NRP1-BioID2-HA stable cell line. *NRP1-BioID2-HA fusion protein was detected using an anti-HA mouse antibody (Invitrogen; 2-2.2.14) followed by an anti-mouse 680 secondary antibody (LiCOR; 926-68070). Biotinylated proteins were detected using a streptavidin 800 direct conjugate (Invitrogen; 21851). Cell lysates and corresponding pulldown material were paired. Cells were treated with* $VEGF_{165}a$ *and biotin, and conditions with VEGF165b treatment and no treatment were used as controls. Cell lysates of the original HEK293/HaloTag-VEGFR2 without NRP1-BioID2-HA expression was also included as a control. Streptavidin 800 staining confirmed successful isolation of biotinylated proteins, indicated by strong signals in the eluate samples of the biotin supplemented conditions. The presence of the NRP1-BioID2-HA fusion protein is also detected in the lysate and eluate samples. Due to faults in the western blot transfer units, the smeared samples are difficult to read the exact band size in some lanes. Bands indicated by the red arrows around ~150 kDa in the Anti-HA 680 channel correspond to the size of the NRP1-BioID2-HA fusion protein.*

4.2.3.8 Enriched Proteins in the HEK293/HaloTag-VEGFR2/NRP1-BioID2-HA Stimulated with $VEGF_{165}a$ Analyses

The raw mass spectrometry files were processed in MaxQuant and the extracted riBAQ values used to calculate fold changes, as discussed in section 4.2.1.3 Protein scores were again assigned to the filtered, enriched proteins, Table 4.12. The analysis elicited 18 enriched proteins when the HEK293T/HaloTag-VEGFR2/NRP1-BioID2-HA cells was treated with $VEGF_{165}a$ and supplemented with biotin. Unfortunately, due to cost constraints of the project, it was only possible to perform one repeat using the HEK293T/HaloTag-VEGFR2/NRP1-BioID2-HA stable cell line.

Table 4.12 – Enriched protein list in HEK293/HaloTag-VEGFR2/NRP1-BioID2-HA treated with $VEGF_{165}$a after 1 repeat. *The enriched protein list following a single repeat consisted of 18 unique proteins. Proteins unique to* $VEGF_{165}$a *treated and supplemented with biotin conditions were included in the final list. Proteins with a 1.5-fold increase of calculated riBAQ in this condition, compared to the controls, were also included in this list. Proteins with a >20% frequency in HEK293 cells associated with proximity-biotinylation identified in the CRAPome were excluded from the final list. Protein score reflects the confidence level of protein identification based on the peptide spectrum matching analysis performed in MaxQuant.*

UniProt ID	Gene Name	Protein Name	Protein Score
Q13136	LIPA1	Liprin-alpha-1	48.86
O60716	CTND1	Catenin delta-1	39.78
Q04656	ATP7A	Copper-transporting ATPase 1	36.51
Q15643	TRIPB	Thyroid receptor-interacting protein 11	29.26
Q9ULF5	S39AA	Zinc transporter ZIP10	28.64
Q14254	FLOT2	Flotillin-2	26.24
Q8TD16	BICD2	Protein bicaudal D homolog 2	24.73
P35968	VGFR2	Vascular endothelial growth factor receptor 2	17.99
O95819	M4K4	Mitogen-activated protein kinase kinase kinase kinase 4	17.82
P02751	FINC	Fibronectin	15.51
Q08554	DSC1	Desmocollin-1	14.48
P98172	EFNB1	Ephrin-B1	12.73
Q9Y6M5	ZNT1	Proton-coupled zinc antiporter SLC30A1	12.65
P52594	AGFG1	Arf-GAP domain and FG repeat-containing protein 1	12.58
Q8WTV0	SCRB1	Scavenger receptor class B member 1	12.51
Q8TBZ3	WDR20	WD repeat-containing protein 20	12.26
Q14160	SCRIB	Protein scribble homolog	11.71
O75054	IGSF3	Immunoglobulin superfamily member 3	11.42

4.3 Discussion

4.3.1 Proteins Enriched in the mycBioID2-NRP1 Analysis

4.3.1.1 Optimised Transfections

Qualitative assessment of immunofluorescence data confirmed robust localisation of mycBioID2-NRP1 to the cell membrane, (Figure 4.2). This is consistent with the body of evidence of NRP1 expression at the cell membrane[431], offering confidence the fusion of NRP1 with the BioID biotin ligase (BiA) had not interfered with the distribution of NRP1. Clear biotin staining confirmed the BirA was active. Interestingly, whilst some biotin signal was found at the cell membrane, there was strong signal localising to, what appear to be more general cytoplasm. Without the use of higher-powered imaging, it was not possible to resolve precisely the source of the signal. However, some intracellular signalling was predictable as NRP1 is known to localise to intracellular compartments, such as endosomes[416] and mitochondria[525]. Additionally, transient NRP1 interactions with dynamic proteins localised in the cytoplasm may also account for some of this signal. These speculations would later be confirmed in the mass spectrometry analyses. The cell line met the criteria as a robust candidate worth of taking forward. To this end, the experiments were scaled up to provide enough material for streptavidin pulldowns.

4.3.1.2 Optimisation of Streptavidin Pulldowns of mycBioID2-NRP1

Following scaling up of the transient transfections, several iterations of the streptavidin pulldown procedure were trialled before optimal conditions were achieved. The initial pulldowns raised questions regarding whether the expression of mycBioID2-NRP1 was poor in the HEK293T cells, or whether the protein extraction from the cells was inefficient, indicated by the lack of signal in the anti-myc 680 channel, (Figure 4.3). However, as the transient expression conditions had already been optimised and sufficient expression and biotinylation was observed with the immunofluorescence images, (Figure 4.2), it was thought the issue related to the protein extraction conditions. The initial use of trypsin to harvest the cells may have also been problematic, given that trypsin cleaves membrane adhesion proteins[542], and NRP1 may be being cleaved and removed during harvesting of the cells. For future experiments, the cell harvesting and protein extraction conditions were modified and the mycBioID2-NRP1 fusion protein was henceforth detected, (Figure 4.4). The bands present in the streptavidin 800 channel of the next major repeat were likely proteins which are naturally biotinylated and therefore common contaminants of the BioID process. This was indicated by the presence of these bands in the HEK293T WT samples. A common contaminant of BioID is pyruvate carboxylases, which are endogenously biotinylated, corresponding to the bands observed on the

western blot. Their presence cannot be avoided, but it is important to be aware of these contaminants to reduce false-positive identification of NRP1 interactors.

Additional measures were then taken in order to maximise yields of protein extractions. The idea of passing the lysed cells through a small gauge needle, was to introduce shear stress to break down cell membranes and releasing the protein[543]. It was thought perhaps some biotinylated proteins may be trapped within the insoluble material during cell lysis, leading to potential false-negatives in the BioID analyses. Hence, an additional sonication step was introduced which would aid the release of the protein bound to insoluble fractions[544]. The conditions for the pulldown were also optimised, modifying the existing conditions from 4°C overnight, to RT for 1 h 45 min. These changes cumulatively assisted in improving the isolation of biotinylated proteins, with successful isolation observed as a result, (Figure 4.5).

Adam23-BioID-HA was added as a control to validate whether streptavidin pulldown was successful. As this is a construct validated within the lab, it served to confirm if streptavidin pulldown conditions were optimal, and as a comparison for mycBioID2-NRP1 biotinylation of proteins. Although the western blots are not directly comparable, the relative biotinylation in the cell lysates and the isolated biotinylated proteins in the eluate appeared greater with Adam23-BioID-HA. This demonstrated the streptavidin pulldown conditions optimised were favourable. Therefore, the weak biotinylation signal observed for mycBioID2-NRP1 may be due to other factors. It was theorised the BirA may not be present in optimal pH conditions and ATP availability may also be unfavourable due to the extracellular localising of the BirA. The Adam23-BioID-HA fusion protein expresses the BirA intracellularly, meaning the BirA is subject to intracellular pH and has access to sufficient ATP, possibly accounting for the improved biotinylation signal observed with this construct. Indeed, few examples of *in vitro* extracellular BirA exist in the literature. For future experiments, the Adam23-BioID-HA was not used as a control. Its inclusion as a control may lead to false-negatives, as Adam23 is involved in cell-cell interactions[545], a potentially similar molecular function of NRP1 and therefore sharing common interactors.

4.3.2 Optimisation of Mass Spectrometry Processing

Uniprot Database Generation

Prior to any processing of the mass spectrometry data, the reference database which would be used to compare all of the observed spectra with, required generation, Table 4.1. It was decided to generate the protein list from the UniProt database, and only proteins which the highest evidence level for existence (i.e. ‘reviewed’ proteins) would be included in the database. This ensured proteins with questionable evidence of their existence were not falsely enriched in the analysis. It was important to

manually input the sequence for porcine trypsin within the database. As porcine trypsin is used in the digestion of protein samples prior to mass spectrometry analysis, this would contribute to a significant number of falsely identified proteins if not included in the database.

MaxQuant Input Parameters

The input values for key MaxQuant parameters, Table 4.2, were chosen to ensure high confidence in the output enriched protein list. The false discovery rate was set at 0.01, meaning 1% of the proteins identified may be false-positives. MaxQuant estimates FDR through target-decoy competition analysis (TDC). TDC is performed by peptide spectrum matching (PSM), whereby spectra of peptides are generated *in* silico from the UniProt database and compared to decoy sequences[546]. Following TDC, the FDR is calculated and the threshold set at <1%. As proteolysis prior to analysing the samples via mass spectrometry is always incomplete, MaxQuant analysis needs to consider the number of missed trypsin cleavages[547]. Potential missed cleavages were set at 2, meaning the software will consider peptides with up to two missed cleavages for identification and quantification. Increasing this number will increase the number of peptides identified, although it may also increase false-positives detected. Protein modifications are also an important factor to consider. Any protein modification will shift the mass for a given amino acid by a known amount. Since the BioID samples are a mixture of generally unknown proteins, common modifications were input into the software[548]. The fixed modification of carbamidomethylation was applied to all peptides identified. Variable modifications expanded the search criteria of the peptides, by considering peptides which may have a mass shift due to this modification. The common variable modifications input into MaxQuant, included methionine oxidation and N-term acetylation. Absence of any modifications in the analysis may lead to a reduced identification rate of peptides[549]. Another important input value was the multiplicity of the samples. Multiplicity was set at 1, meaning only a single set of peptides without any additional tags or labels are being analysed, essentially only one type of peptide ion being considered in each sample. This is essential for performing label-free quantification (LFQ), where the samples are not isotopically labelled. The digestion input was selected as Trypsin/P, indicating to MaxQuant the digestion was performed using porcine trypsin. This is important, as different trypsin variants and proteolysis methods cleave proteins differently. Porcine trypsin specifically cleaves arginine and lysine residues, except when they are immediately followed by proline[538]. The *in silico* digests of the UniProt database and subsequent PSM will be determined based on this specific digestion. Finally, in order to extract values for molar proportions of proteins present, the intensity-based absolute quantification (iBAQ) parameter was selected, where the summed peptide intensities are divided by the number of theoretically observable peptides, giving an estimate of molar abundance.

Processing of MaxQuant Output Files

The output files from MaxQuant processing required further processing before a final enriched protein list was achieved. There were some important considerations with this output list. Initially, the contaminants required filtering from the initial list. Many of the contaminants are automatically detected by the MaxQuant software, indicated by the prefix 'CON' in the UniProt ID, Table 4.3. Contaminants often related to variants of keratin, the most common and abundant contaminant in mass spectrometry analysis[550]. To a lesser degree, the identifications of reverse sequences, denoted by the prefix 'REV', Table 4.3, also require removal. The reverse sequences are decoy sequences used in the TDC analysis.

After filtering of these bogus sequences, further filtering criteria was applied to the list. Only proteins with >1 unique peptides were considered for the final enriched protein list. When considering proteins present in both control and experimental samples, a fold change calculation was performed, filtering the final list further. Only proteins with a 1.5-fold increase in the experimental value (either protein score, iBAQ or relative iBAQ (riBAQ)), were included in the final list.

The initial method of post-MaxQuant processing of the output data utilised protein score, Table 4.4. This was suitable for some of the enriched proteins, unique to the experimental sample. However, for > 1.5 enrichment analysis using protein score was not appropriate. The protein score is an internally calculated value within the MaxQuant software to serve as a means of ranking the proteins present in their confidence, with the highest protein score correlating to a higher confidence of presence within the sample. The exact statistical equation for calculation of protein score is not explicitly published, although it is known the score is derived from the combined peptide intensities and posterior error probability (PEP). The PEP itself is a statistical measure representing the confidence of PSM. Although a measure of confidence in the presence of a sample, the score did not necessarily correlate with abundance. Therefore, using protein score to evaluate fold enrichment between experimental conditions and controls was not appropriate. A metric relating to protein abundance was therefore warranted. MaxQuant is capable of determining abundance of proteins based on the mass spectrometry spectra of the raw files. The quantification calculations are output as an intensity-based absolute quantification (iBAQ) score. The score is calculated by the sum of the intensities of a precursor peptide that correlate to a specific protein, divided by the number of theoretically observable peptides. This calculation converts a metric that is expected to be proportional to mass, the intensity of the spectra, into a metric proportional to molar amounts, the iBAQ score[551]. The difference between analysis via proteins score was minor, Table 4.5. However, it is expected in samples with a larger enriched protein list with more fold change calculations required, this would be more pronounced. Using the iBAQ value in fold change calculation, although improved on issues identified with protein

score, normalisation of the iBAQ scores provides a more accurate representation of protein abundance. Each iBAQ value calculated for a given protein was divided by the sum of all iBAQ values resulting in a relative iBAQ (riBAQ) value. This riBAQ value correlates to mole fraction of the protein more accurately than iBAQ[552]. Again, the change in final enriched list was modest, although two newly enriched proteins were identified, Table 4.6.

4.3.3 Proteins Enriched in the extracellular N-terminal mycBioID2-NRP1 Analysis

The final enriched protein lists for NRP1 interactomes in the presence, Table 4.6, and absence, Table 4.7, of $VEGF_{165}$a revealed few proteins. This is consistent with the relatively weak biotinylation signal observed with the optimised mycBioID2-NRP1 western blot, (Figure 4.5). Perhaps the nature of the extracellular BirA may lead to issues with biotinylation. The BirA expressed outside of the cell may not be in a favourable environment for optimal operation. For example, the extracellular pH may lead to poor biotinylation. Additionally, the availability of ATP may not be sufficient for proper function of the BirA. Intracellular concentrations of ATP range from around 2 – 8 mM[553], while the concentration in the extracellular compartment of healthy tissue is around 10 – 100 nM[554]. Indeed, few examples of extracellular BirA exist in the literature. A recent study highlighted the poor extracellular biotinylation capabilities using the BirA variant TurboID[555]. Sufficient biotinylation was achieved when expressing cells were supplemented with vitamin B_5 and ATP. The high concentrations of ATP required to achieve this (1.5 mM) raises concerns of cellular toxicity, although this was not reported by the authors.

These enriched proteins would all be novel interactors of NRP1, but the caveat is this is a single repeat, with further repeats required to confirm these results. Some of these potential interactors are unsurprising when considering the biology of NRP1. Given the presence of a PDZ binding motif on the C-terminus of NRP1, proteins harbouring a PDZ binding domain, such as Disks large homolog 1 (DLG1), may be expected. Another perhaps interesting interactor may be Endothelin-converting enzyme 2 (ECE2), a membrane bound protein involved in the activation of endothelin, influencing vasoconstriction[556]. The proteins identified as potential interactors of NRP1 under basal conditions, Table 4.7, yielded even fewer proteins. Interestingly, AP-3 complex subunit delta-1 (AP3D1) involved in vesicular trafficking was enriched in this list, a process NRP1 is known to participate in[413]. Due to the associated costs with mass spectrometry analysis, the mixed results relating to the mycBioID2-NRP1, meant NRP1-BioID2-HA could be investigated before further proteomic repeats were performed.

4.3.4 Proteins Enriched in the intracellular NRP1-BioID2-HA Analyses

4.3.4.1 Expression of NRP1-BioID2-HA in HEK293T Cells

The optimised expression of NRP1-BioID2-HA demonstrated sufficient membranous expression of the fusion protein, observed using anti-HA AF594 antibody, (Figure 4.8). Unlike for mycBioID2-NRP1, the biotinylation pattern observed using streptavidin-AF488, co-localised with fluorescence related to the NRP1-BioID2-HA fusion protein. These results were a promising indication this fusion protein would be suitable for BioID analysis. Interestingly, the NRP1-BioID2-HA expression appeared to accumulate at intercellular junctions. Recent evidence exists suggesting NRP1 is expressed at these junctions and controls vascular permeability through juxtracrine regulation of adheren's junctions in endothelial cells[388,557].

4.3.4.2 Biotin Depletion from DMEM

Prior to sending the samples for mass spectrometry analysis, measures were taken to reduce the residual biotinylation in the control samples. The exact concentrations of biotin in the HEK293T cell culture medium (DMEM) are not known, although are stated to be around 2 nM [558]. This is perhaps significant for the BioID2 BirA, considering it utilises lower concentrations of biotin more efficiently compared to the original BirA variant . Biotinylation observed in the biotin null samples, should be minimal. Significant biotinylation in these samples may lead to false-negatives in the final enriched list. Theoretically, a removal of biotin from the media may reduce this background biotinylation signal. From the confocal immunofluorescence images, (Figure 4.9), a reduction in background biotinylation was observed when DMEM was pre-incubated with Dynabeads C1, compared to DMEM incubated with no beads. All bead concentrations appeared to reduce the background biotinylation. For cost-effectiveness, a concentration of 100 µL Dynabeads C1/50mL DMEM was chosen for the remainder of the research.

4.3.4.3 Optimisation of Streptavidin Pulldowns of NRP1-BioID2-HA

The results of the optimised biochemical analysis of the streptavidin pulldown performed on lysates of HEK293T cells transfected with NRP1-BioID2-HA were much more promising than for their N-terminal mycBioID2-NRP1 equivalents. With the C-terminally tagged fusion protein, a much clearer biotinylation pattern was observed, with the characteristic smear seen with proximity-biotinylation, (Figure 4.10). Not only was biotinylation stronger in the cell lysates, the eluted material exhibited a stronger biotinylation pattern. Comparing the biotinylation patterns elicited with mycBioID2-NRP1, (Figure 4.5), and NRP1-BioID2-HA, (Figure 4.10), it was clear the latter was a more promising candidate for BioID analysis. Not only was the fusion protein present in the eluate as would be expected, the

amount of biotinylated proteins appeared greater with NRP1-BioID2-HA. Interestingly, there were no perceived differences in the biotinylation patterns observed between samples expressing NRP1-BioID2-HA under $VEGF_{165}$a stimulation and basal conditions. However, these differences may exceed the capabilities of western blotting and are likely to be observed more efficiently using the mass spectrometry data. As mentioned previously, a possible link between NRP1 and Adam23 meant the Adam23-BioID-HA control was no longer suitable. This control was replaced with mycBioID2-CENPA. The new control has the benefit of the same BirA variant as the NRP1-BioID2-HA, whereas Adam23-BioID-HA utilised the original BirA variant. CENPA is a histone variant previously investigated using BioID technology[503]. Its role pertains to mitotic process, so common proteins enriched between mycBioID2-CENPA and NRP1-BioID2-HA should in theory relate to contaminants of the BirA, and not shared interactors. Additional contaminants not enriched in the controls were identified using the CRAPome database.

4.3.4.4 Enriched Proteins using NRP1-BioID2-HA stimulated with $VEGF_{165}$a

The BioID analysis pipeline differs from other mass spectrometry proteomic approaches. Variation between control samples, such as biotin null conditions, and experimental samples, including biotin supplemented conditions, mean the absolute isolation of proteins varies between samples. The variation is best visualised in the differences between samples in the streptavidin 800 signal indicated by western blotting, (Figure 4.10). With the initial single N-terminal mycBioID2-NRP1 statistical analysis was not possible. For the C-terminal NRP1-BioID2-HA experiments where multiple repeats were completed, after initial filtering of 1.5-fold increase, statistical analysis by an unpaired t test with Welch's correction was performed. This was chosen to account for unequal variances and number of absolute number of proteins identified. Enriched proteins with a p value > 0.05 were excluded. Unpaired t tests with Welch's correction is commonly used for BioID proteomic analyses due to the variable nature of the samples[559,560].

The number of proteins enriched between each repeat varied significantly. Such high variation is commonly observed in proteomic mass spectrometry, often due to the analysis processes including fluctuations in ionisation efficiency, chromatographic separation and instrument performance[561]. Of the 10 proteins identified in 4 out of 4 repeats, Table 4.8, several fall under the cadherin binding molecular function GO term, (Figure 4.13b), and are known regulators of cellular adhesion, including serine/threonine-protein kinase MARK2 (MARK2)[562], liprin-beta-1 (LIPB1)[563], drebrin-like protein (DBNL)[564], and PDZ and LIM domain protein 5 (PDLI5)[565], bolstering evidence of the involvement of NRP1 in cellular adhesion. Cadherin plays a major role in cell junction stability and paracellular transport discussed in section 1.2.2.3 When considering proteins identified across 3 of the 4 repeats,

Table 4.9, a further 6 proteins identified are involved in cadherin binding or cellular adhesion, including afadin (AFAD)[566], BAR/IMD domain-containing adapter protein 2 (BAIP2)[567], and extended synaptotagmin-2 (ESYT2)[568]. Potential binding of ESYT1 to NRP1 has been implied following affinity-purification mass spectrometry (AP-MS)[391], although binding to ESYT2 would be a novel finding.

Interestingly, although many cell adhesion proteins were detected, the highest enrichment ratio for NRP1 interactors in the presence of $VEGF_{165}$a was not related to this cellular process. Although the role of NRP1 in vesicular trafficking is documented in the context of regulation of VEGFR2, the full extent of its role in vesicular trafficking may not yet be fully understood, indicated by the number of vesicular trafficking proteins elucidated in this research. This is reflected in the most significantly enriched molecular function GO term relating to SNARE binding, (Figure 4.13b). The SNARE and SNARE-related proteins form essential components of machinery facilitating fusion of vesicles to the plasma membrane[569], discussed in section 1.2.2.3. The NRP1-enriched proteins known to participate in the SNARE machinery driven vesicular transport and membrane fusion, included vesicle-associated membrane protein 3 (VAMP3)[570], syntaxin 8 (STX8), vesicle transport through interaction with t-SNAREs homolog 1B (VTI1B)[571], and exocyst complex component 3 (EXOC3)[572]. Although all of these would be novel NRP1 interactors, binding to a similar protein, VAMP2 has been suggested following co-immunoprecipitation experiments[433].

The hepatocyte growth factor-regulated tyrosine kinase substrate (HGS) identification in the protein list was of interest. As well as involvement in signal transduction following stimulation with growth factors, HGS is involved with cadherin-5 recycling back towards the cell membrane and vesicular trafficking[573], which NRP1 is known of interacting with[388,391].

The biological processes GO analysis was consistent with the molecular function GO, highlighting NRP1 interactors harbouring common features relating to vesicular transport, (Figure 4.14b). A significant number of the enriched GO terms related to vesicle trafficking. The most significantly enriched term related to membrane fission, which included the aforementioned HGS and EXOC3. Also included in this term were the charged multivesicular body protein 6 (CHMP6), and charged multivesicular body protein 7 (CHMP7), regulator of endosomal cargo sorting[574,575]. The enriched GO term with the most proteins applicable, related to endosomal transport. Proteins belonging to this term similarly included HGS, CHMP6, CHMP6, STX8, VTI1B, and VAMP3. Some additional proteins related to this term were sequestosome 1 (SQSTM), intersectin 1 (ITSN1) and Ragulator complex protein LAMTOR1 (LTOR1).

Interestingly, the GO term relating to the multivesicular body (MVB) sorting pathway, a process involved in the sorting of endocytosed proteins for recycling or lysosomal degradation[576]. This is consistent with evidence demonstrating $VEGF_{165}$a binding to NRP1 promoted the recycling of VEGFR2

through Rab4, Rab5 and Rab 11 vesicles[413]. The rabGTPases mentioned facilitate the recycling through coordination of trafficking, docking and fusion to the plasma membrane[577]. HGS, CHMP6 and CHMP7 fall under this GO term.

The cellular component GO analysis correlated with the GO analyses for molecular function and biological processes. The most significantly enriched GO terms again related to endosomal-related compartments, (Figure 4.15b). The GO term with the highest ER was the endosomal sorting complex required for transport (ESCRT) complex, machinery which is essential for membrane remodelling, facilitating the formation of MVBs[578], internalisation of membrane proteins[579], and cytokinesis during cellular division[580]. The ESCRT is also involved in the budding and release of viruses[581], including HIV[582]. NRP1 is known to facilitate viral entry, as discussed in section 1.4.5.4, but the release of viral particles would be a novel function for NRP1 in viral processes. NRP1 has been shown to act as a co-regulator of RTKs but such a role could potentially extend to other membrane bound receptors. ESCRT modulates signalling of GPCRs such as CXCR4[583]. Interestingly, silencing of NRP1 in hematopoietic stem/progenitor cells (HSPCs), resulted in reduced internalisation of CXCR4 and increased cell surface localisation[584]. Potential binding of CXCR4 to NRP1 was also detected by AP-MS, Table 1.1. Enriched proteins which contribute to this GO term were HGS, CHMP6 and CHMP7. Similarly, the GO term for SNARE complex was also enriched, another cellular machinery complex involved in vesicular membrane deformation, driving the fusion of vesicle membranes rather than the scission. These proteins include VTI1B, VAMP3, and STX8. Another vesicular-related enriched GO term concerned proteins localised to the late endosome. A total of 9 proteins corresponded to this group, including the already mentioned HGS, CHMP6, CHMP7, VTI1B, STX8, SQSTM, and LTOR1. Additionally associated proteins were metalloreductase STEAP3 (STEA3) and CD2-associated protein (CD2AP).

Other significantly enriched GO terms were cellular membrane related, albeit confidence in enrichment was lower than for the vesicular-associated GO terms. The GO term for the adheren's junction was significant, which may be expected given the enrichment for the molecular function GO term for cadherin, discussed in. The known functions of NRP1 in cellular adherence and vascular permeability, discussed in section 1.4.3 and 1.4.4, correlated with the enrichment with this GO term. The proteins involved included previously mentioned PDLI5, BAIP2 and AFAD, as well as adenomatous polyposis coli protein (APC), and Cdc42 effector protein 4 (BORG4). The other membrane associated GO term being the cell leading edge was somewhat unexpected, as the molecular function and biological processes GO analyses did not reveal enrichment of terms related to this, such as cellular projections or cellular taxis. In the context of NRP1 biology, it may be expected this term would be enriched, since NRP1 is expressed at the tip cells of proangiogenic vessels, discussed in section 1.4.2.

4.3.4.5 Enriched Proteins of C-terminal Intracellular NRP1-BioID2-HA in Basal Conditions

The analysis protocol used previously, may be masking potential NRP1 interactors which interact independently of $VEGF_{165}$a. To determine these $VEGF_{165}$a -independent NRP1 interactors, the analysis was repeated, considering the samples relating to NRP1-BioID2-HA expressed under basal conditions as experimental samples and not controls. As expected, the absolute number of proteins enriched in the final lists between the repeats varied. A greater number of proteins were enriched, with 77 proteins common between 4 repeats, Table 4.10, and 100 proteins common between 3 out of 4 repeats, Table 4.11. The majority of which were not identified in the initial analyses with $VEGF_{165}$a stimulation. Similar to the analysis with $VEGF_{165}$a treatment, one of the highest enriched terms was for cadherin binding. In this scenario, the cadherin binding GO term was the most significantly enriched, (Figure 4.17b). In total, 52 proteins were associated with this GO term. Notable associated proteins were ESYT2, AFAD, catenin delta-1 (CTND1), integrin beta-1 (ITGB1), vesicle-associated membrane protein-associated protein A (VAPA) and B (VAPB), septin 9 (SEPT9) and phosphatidylinositol-binding clathrin assembly protein (PICAL). ITGB1 is a known NRP1-interacting protein[393] and recently, CTND1 has also been identified as a potential NRP1 interacting protein[388]. The remaining proteins are considered potentially novel NRP1 interactors. However, alternative research has indicated the binding of NRP1 to related proteins ESYT2 and several integrins, including integrin alpha 2 (ITA2), alpha 5 (ITA5), and alpha V (ITAV), discussed in section 4.6.

Similarly, several proteins were associated with cell adhesion mediator activity. Some of these proteins were also enriched in the $VEGF_{165}$a treatment analysis, including BAIP2 and PDLI5. For this analysis, ITGB1, Serine/threonine-protein kinase PAK 4 (PAK4), Coxsackievirus and adenovirus receptor (CXAR), Cdc42 effector protein 1 (BORG5), and Junctional adhesion molecule C (JAM3).

As with the $VEGF_{165}$a conditions, the potential NRP1 interactors under basal conditions were significantly associated with SNARE binding as a molecular function GO term. VAMP proteins and STX proteins were enriched in both analyses, with the exact proteins enriched in each different. For the basal conditions, VAMP7, STX3, STX5 and STX12 were enriched, compared to VAMP2 and STX8 in the $VEGF_{165}$a stimulated conditions. Unique proteins enriched in the basal conditions were PICAL, synaptosomal-associated protein 23 (SNAP23) and 29 (SNAP29).

Interestingly, the GO terms with the second highest confidence of enrichment was insulin receptor binding, associated with tyrosine-protein phosphatase non-receptor type 1 (PTN1), girdin (GRDN), and sorting nexin-1 (SNX1). Potential functional relations exist between NRP1 and insulin-related signalling, although research is sparse. In pancreatic islet cells expressing a truncated NRP1, not capable of

binding $VEGF_{165}$a, intracellular insulin was low, which is associated with earlier onset of type 1 diabetes[585]. NRP1s involvement in insulin receptor signalling may be area for future research to exploit.

In the biological processes GO analysis, many more GO terms were enriched in the NRP1-BioID2-HA under basal conditions, compared to with $VEGF_{165}$a stimulation, (Figure 4.18b). Again, many of these proteins related to endosomal and vesicular trafficking. Of these GO terms, the 'protein localisation to endosomes' term was the most confidently enriched. As expected NRP1 itself was categorised in this category being defined on endosomes previously[416], while MICAL-like protein 1 (MILK1), WASH complex subunit 2A (WAC2A), and protein scribble homolog (SCRIB) were also associated with this term. The second most confidently enriched process was membrane docking. Several proteins mentioned already were associated with this term, such as ESYT2, STX3, STX5, STX12, VAPA, VAPB, and SNAP29. Additionally, Ras-related protein Rab-7a (RAB7A) was also associated with this term. Rab7-associated vesicles are involved with the trafficking of NRP1 and VEGFR2, associated with late endosomes and trafficking intended for lysosomal degradation[586]. RAB7A has also demonstrated localisation to endosomes in immune fluorescence experiments and complex formation with NRP1 elucidated with co-immunoprecipitation[587].

The biological processes GO terms associated with cellular adhesion were significantly enriched in the NRP1-BioID2-HA analysis under basal conditions when compared to $VEGF_{165}$a stimulation. One such term, relating to protein localisation to cell junctions, correlated with 11 of the enriched proteins, notably, DLG1, SCRIB, STX3, JAM3 and BAIP2. Interestingly other inclusions were the lipolysis-stimulated lipoprotein receptor (LSR) tight junction protein 1 (ZO1) and 2 (ZO2). A number of these proteins are localised to cellular junctions and influence the stability of these junctions. The ZO proteins are known to bind to both AFAD and CTND1, and occludin (OCLN) discussed in 1.2.2.4, also proteins enriched in this analysis. The enrichment of all of these interacting proteins may indicate that NRP1 is part of a larger complex at the cellular junctions. The potential interaction with the LSR may be of interest, as this receptor is involved with the uptake of free fatty acids[588], a potentially novel biological context relating to NRP1.

Research relating to NRP1 is mainly viewed in the context of endothelial cells and angiogenesis. However, another key focus of NRP1 research relates to its expression in neuronal cells. Evidence suggests NRP1 is involved in axonal guidance[589], nervous system development and neurogenesis[590], and neuronal survival and migration[591]. Therefore, it may be expected that several of the enriched biological processes GO terms are associated with neuronal processes. However, as HEK293T cells are of epithelial lineage, this cell model is likely not the best for evaluating NRP1 interactome with neuronal proteins. The GO term with the highest enrichment was for postsynaptic membrane

neurotransmitter receptor levels. Associated proteins included CTND1, DLG1, STX3, and SCRIB. Understanding these interactions in the context of neuronal environments would be an interesting area to explore, to identify novel roles for NRP1 in neuronal development.

The enrichment of the GO term vascular endothelial growth factor receptor signaling pathway is somewhat surprising, given this term was not enriched when NRP1-BioID2-HA was treated with $VEGF_{165}$a. However, as endogenous VEGFR2 expression is negligible in HEK293T cells, it is surprising these proteins are enriched at all. This may be due to shared signalling pathways between NRP1 and VEGFR2, or NRP1 having a role independent of VEGFR2, leading to the enrichment of this GO term. Enrichment of other vascular related GO terms may indicate NRP1 ability to influence angiogenesis and associated processes independently of VEGFR2.

The ability of NRP1 to facilitate cellular entry of SARS-CoV-2, Epstein–Barr virus and other viruses, discussed in 1.4.5.4 and 1.4.5.5, is well established. Hence, the significance of the GO term viral process is consistent with the known biological functions of NRP1. There were 17 proteins identified which are involved in viral processes most already discussed in the context of vesicular trafficking. Notably, SNX3, VAPA, VAPB, ITGB1, and RAB7A were enriched in this GO term. It may indicate further roles for NRP1 beyond viral entry, perhaps in intracellular trafficking of viruses and the release of viral particles from cells.

The cellular component GO analysis further demonstrated the potential involvement of NRP1 in vesicular trafficking, cellular adhesion and neuronal processes, as GO terms relating to one of these categories were the most prevalent, (Figure 4.19b). The most significantly enriched GO term related to the retromer complex, involved in the recycling of membrane proteins. RAB7A was enriched in this term and is an important member of this cellular machinery[592]. For proteins localised to the SNARE complex, these were the expected SNAP, VAMP and STX proteins, observed in SNARE-associated terms previously.

Consistent with the analysis thus far, a number of the cellular component GO terms were affiliated with cellular junctions. The Go term for the cell-cell contact zone was the most significantly enriched, and included proteins such as ZO1, ZO2, AFAD, JAM3, and ITGB1. Also enriched in this term was nectin 2 (NECT2), another cellular adhesion molecule discussed in section 1.2.3.1, capable of interacting with CTND1 through AFAD[593]. The NRP1 interaction with cadherin-5 (CDH5), Table 1.1, has not been observed in this research. Potentially as CDH5 is an endothelial-specific adhesion protein[594], and mRNA levels are undetectable in HEK293T cells – 0.0 normalised transcripts per million (nTPM)[595] accounting for its absence. Although a member of the cadherin family is enriched and also relates to the GO term for the cell-cell contact zone, protocadherin 9 (PCDH9). The most significant GO term specifically

relating to the type of junction, was for the adheren's junction, which included much of the same junctional proteins mentioned previously. The tight junction GO term was also significant and included a key constituent of the tight junctional complex, occuldin (OCLN). VEGF-A stimulation induces trafficking away of OCLN and ZO proteins from junctional complexes, discussed in section 1.3.1.1. Therefore, a possible association with NRP1 is consistent with this observed biological outcome.

GO terms associated with cell-based projections were enriched such as those found at the cell leading edge and that govern actin-based cell projections. NRP1 is essential during early angiogenesis where its expression at endothelia tip cells guides the angiogenic sprout, discussed in section 1.4.2. During sprouting angiogenesis, the actin-based filaments project from the cellular leading edge[596]. Notable proteins categorised in these cellular compartments are OCLN, ITGB1, JAM3 and CTDN1.

Neurology-associated GO terms were similarly enriched in the cellular component GO analysis, the most enriched component being the myelin sheath. The literature supports NRP1s role in myelin sheath development[597]. Silencing of NRP1 on microglial cells has been shown to reduce remyelination capabilities of oligodendrocytes following acute demyelination.

Interestingly, several proteins were enriched which are involved in EC polarisation, important as polarisation is critical in mediating specific endothelial functions and embryonic and adult angiogenesis[681]. Several proteins identified as potential NRP1 interactors are involved with regulation of cell polarity. Notably, Lethal(2) giant larvae protein homolog 1 (L2GL1)[682], Protein scribble homolog (SCRIB)[683] and Disks large homolog 1 (DLG1)[683]. Additionally, inactive tyrosine-protein kinase 7 (PTK7)[684] and Vang-like protein 1 (VANG1)[685] are involved in planar cell polarity, an essential process where polarity is established within a cellular layer, through modulation of the Wnt pathway signalling pathways. The enrichment of such proteins suggests a role for NRP1 in EC polarisation.

4.3.4.6 Comparison Between mycBioID2-NRP1 and NRP1-BioID2-HA Results

Enriched proteins in the repeats with NRP1-BioID2-HA yielded much more promising results, Tables 4.9, 4.10, 4.11 and 4.12, than mycBioID2-NRP1, Tables 4.6 and 4.7. Significantly more proteins were identified, and protein scores were much higher for C-terminally tagged NRP1-BioID2-HA. For example, the top hit for mycBioID2-NRP1 when stimulated with $VEGF_{165}$a was nascent polypeptide-associated complex subunit alpha (NACA) with a protein score of 111.88. Whereas the top hits for NRP1-BioID2-HA elicited a protein score of 323.31 and included proteins such as NRP1, catenin delta-1 (CTND1) and spectrin beta chain, non-erythrocytic 1 (SPTB2). The higher protein scores represent a greater confidence of the presence of these proteins. Additionally, many more proteins were detected for NRP1-BioID2-HA. A total of 14 unique potential interactors were identified for one mycBioID2-NRP1

repeat, while 208 were identified for NRP1-BioID2-HA across four repeats. The latter results are what would be expected of BioID analyses, in terms of number and confidence of proteins identified. The difference may be explained in the capabilities of the extracellular vs the intracellular BirA localisation. As discussed in section 4.3.3, the extracellular BirA may not be operating optimally, in comparison to the intracellularly localised BirA, where ATP concentrations are much higher and pH is more favourable. There were only two common proteins between the analyses for the N-terminal and C-terminal NRP1 BioID experiments. NRP1 was one of these proteins, and DLG1, a PDZ domain containing protein as discussed earlier, was the other.

4.3.4.7 Known Interactors Identified using NRP1-BioID2-HA

As discussed previously, ITGB1[393] and CTND1[388] are already a suspected interactors of NRP1. RAB7A, the vesicular trafficking protein also discussed previously, is known to form complexes with NRP1 following co-immunoprecipitation[587]. There are several other enriched proteins which are also known or suspected interactors. The first is thioredoxin-related transmembrane protein 1 (TMX1), located primarily in the endoplasmic reticulum (ER), a region NRP1 is not known to localise to. One of its primary functions appears to be assisting in the proper folding of membrane-bound proteins[598]. Although this interaction has been previously characterised, its biological significance is still unknown. The final protein already identified as a potential NRP1 interactor is the amyloid-beta precursor protein (A4). Members of this protein family are involved in neuronal development and a notorious proteolytic fragment, amyloid-β (Aβ), in implicated in the pathogenesis of Alzheimer disease (AD). NRP1 itself had demonstrated overexpression in mouse models of AD, with a higher expression correlating with disease progression[599]. The membrane bound amyloid precursor proteins are also involved in cellular adhesion. The potential interaction of NRP1 and A4 correlates with the GO analyses, as it is clear NRP1 is involved in a host of neuronal-associated processes.

4.3.5 Proteins Enriched in the HEK293/HaloTag-VEGFR2/NRP1-BioID2-HA Analyses

4.3.5.1 Transient Expression of Neuropilin Fusion Proteins in HEK293/HaloTag-VEGFR2 Cells

NRP1 is a well-establised co-receptor for VEGFR2[321,358,431]. The interactome analyses thus far was performed in the absence of VEGFR2 coexpression. The complement of proteins that interact with NRP1 may therefore be different when NRP1 is in complex with VEGFR2, particularly following $VEGF_{165}$a stimulation. A cellular model expressing NRP1-BioID2-HA and VEGFR2 was therefore required. The initial attempt to create a model by transiently transfecting NRP1-BioID2-HA into a

HEK293 cell line stably expressing HaloTag-VEGFR2 was unsuccessful, in the sense that cells expressing both NRP1 and VEGFR2 fusion proteins were minimal in number, (Figure 4.20). If these cells had been analysed via mass spectrometry, it is likely results would be similar as for the WT HEK293T model. It remains unclear why the transfections were a failure. The expression of one of these fusion proteins should not negatively regulate the expression of the other. In fact, expression of NRP1 leads to induction of VEGFR2 expression and increased localisation to the HEK293T cell surface[348,357]. To determine if this effect was an issue with the NRP1-BioID2-HA plasmid specifically, SNAPTag-NRP1 was instead transiently transfected and similar results were observed, (Figure 4.21). It became clear that transient transfection of NRP1-BioID2-HA into HEK293T cells stably expressing VEGFR2 was unlikely to yield results. Lentiviral transduction was therefore deemed the most appropriate means of generating a stable cell line for creating a NRP1 and VEGFR2 co-expressing cell model.

4.3.5.2 pLV-NRP1-BioID2-HA Transductions

Varying lentiviral transduction conditions are reported in the literature, meaning transductions first required optimisation. The expected cellular surface expression of NRP1-BioID2-HA was observed in all transduction conditions tested, to varying degrees of efficiency, (Figure 4.22). Increasing concentrations of virus concentration appeared to increase the efficiency of transduction. As the cells would be further selected with blasticidin for NRP1-BioID2-HA fusion protein expression, the choice between the lentiviral concentrations expressing the higher amounts of fusion protein was less important. The decision to choose the 75% viral preparation was based on sufficient expression of NRP1-BioID2-HA and conservation of the viral preparation if further optimisation was required.

4.3.5.3 Analysis of NRP1 and VEGFR2 Co-expression in Blasticidin Selected Cells

Following blasticidin selection of cells expressing NRP1-BioID2-HA, IF was performed to determine if cells were expressing both NRP1-BioID2-HA and HaloTag-VEGFR2, (Figure 4.23). As observed by the merged channel, there appeared to be more cells identified expressing both NRP1-BioID2-HA and HaloTag-VEGFR2, compared with the transient transfections. Unfortunately, a significant number of cells were identified which lacked expression of both. It was thought that this cell model would still be inappropriate for BioID analyses due to the large proportion of cells lacking expression of at least one of the constructs. Further refinement was warranted before use of the cell line.

4.3.5.4 Fluorescence-Activated Cell Sorting of HEK293/HaloTag-VEGFR2/NRP1-BioID2-HA Cells

The cells were then sorted based on expression of both fusion proteins using fluorescence-activated cell sorting (FACS), (Figure 4.24). The FACS analysis indeed indicated there was many cells expressing

either NRP1-BioID2-HA or HaloTag-VEGFR2, and few cells with high expression for both. This demonstrated the necessity for FACS for improving the robustness of the stable cell line if used in mass spectrometry analysis. An expression analysis of the cells post-FACS showed an improved co-expression of NRP1-BioID2-HA and HaloTag-VEGFR2 within the same cells, (Figure 4.25). Meaning the stable cell line was appropriate for further analysis via mass spectrometry.

4.3.5.5 Streptavidin Pulldown of HEK293/HaloTag-VEGFR2/NRP1-BioID2-HA Cells

An additional control of $VEGF_{165}b$ stimulation was incorporated into these analyses. $VEGF_{165}b$ is capable of binding to VEGFR2 with nanomolar affinity, but does not exhibit binding to $NRP1^{354}$. This is to ensure the enrichment of novel NRP1 interactors as a result of complex formation with VEGFR2 induced by $VEGF_{165}a$, which would not be observed with $VEGF_{165}b$. The streptavidin pulldown of the cellular lysates revealed sufficient isolation of biotinylated proteins after optimisation, indicated by the streptavidin 800 staining, (Figure 4.26). Importantly, the comparative streptavidin 800 signal in the biotin-null controls and WT cells was minimal. The question was whether any new potential NRP1 interactors would be enriched, when VEGFR2 is present. At the very least, VEGFR2 should be present in the final enriched list.

4.3.5.6 Enriched Proteins using HEK293/HaloTag-VEGFR2/NRP1-BioID2-HA Cells Stimulated with $VEGF_{165}a$

The results revealed some potentially novel interactors of NRP1 when coexpressed in the presence of VEGFR2, Table 4.12. However, I was only able to perform a single proteomics repeat, therefore results must be interpreted with caution. The presence of VEGFR2 in the final enriched list was important, as this is an expected interactor of NRP1, particularly if they are expressed within the same cell. There were a few common proteins between this analysis and the HEK293T cells transiently transfected with NRP1-BioID2-HA and treated with $VEGF_{165}a$, (Figure 4.27). Common proteins between these lists included Thyroid receptor-interacting protein 11 (TRIPB), Protein bicaudal D homolog 2 (BICD2), and Arf-GAP domain and FG repeat-containing protein 1 (AGFG1). Proteins common between this list and the NRP1-BioID2-HA only under basal conditions were also present. These were AGFG1, liprin-alpha-1 (LIPA1), catenin delta-1 (CTND1), proton-coupled zinc antiporter SLC30A1 (ZNT1), scavenger receptor class B member 1 (SCRB1), and protein scribble homolog (SCRIB). The remaining 10 proteins were unique to the HEK293/HaloTag-VEGFR2/NRP1-BioID2-HA treated with $VEGF_{165}a$ analysis. These common proteins may be shared interactors of NRP1 and VEGFR2 which occur independently of one another. The enrichment of known interactor CTND1 is again positive, given it's a recognised to form

complexes with NRP1[388]. As well as CTND1, NRP1 interacts with fibronectin (FINC) where it facilitates FINC fibril assembly promoting tumour growth[350]. The enrichment of these known interactors increases confidence in the chosen analysis method and confidence in the validity of the results.

Although no direct binding of VEGFR2 to any of these proteins has previously been observed, there are some biological links. CTND1 has been previously shown to augment $VEGF_{165}$a-induced phosphorylation of VEGFR2, possibly through a shared association with CDH5[600]. Similarly, $VEGF_{165}$a/VEGFR2 signalling increases cellular membrane abundance and localisation of SCRB1[601]. Unfortunately, due to funding issues only one repeat was possible for this cell line. The samples are already generated, and only require mass spectrometry analyses, hence, the dataset could be completed in the future.

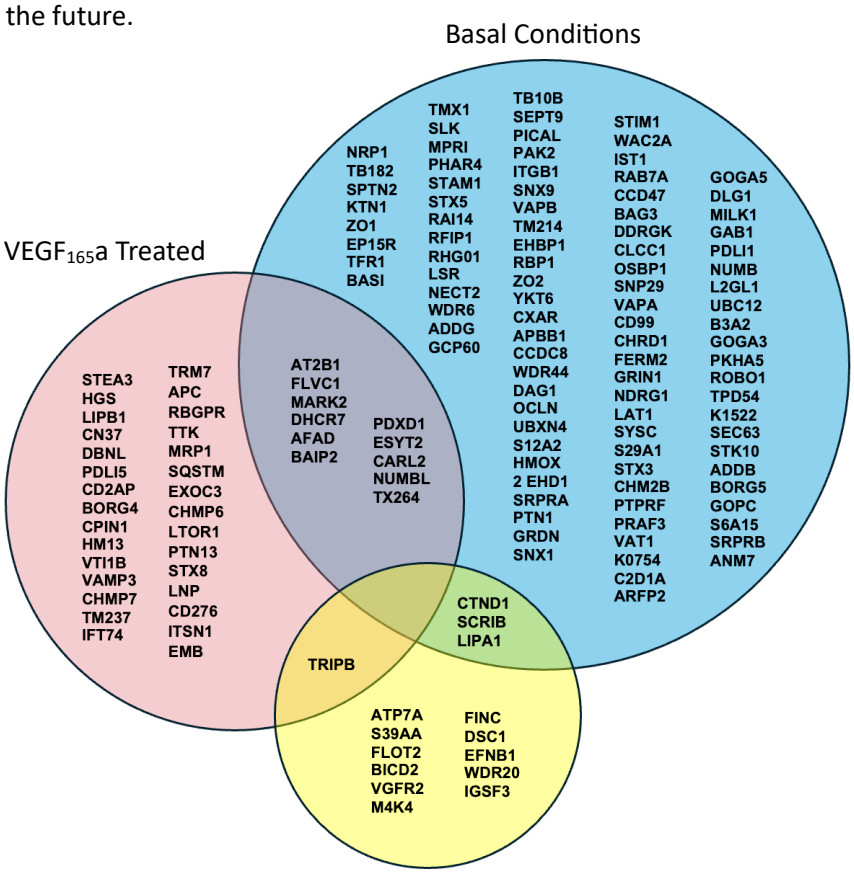

Figure 4.27 - A summary of the enriched proteins in the NRP1-BioID2-HA bioinformatic analyses in conditions of NRP1 expression alone with $VEGF_{165}$a stimulated condtions vs basal conditions vs NRP1 coexpression with VEGFR2 and treated with $VEGF_{165}$a. *For the $VEGF_{165}$a stimulated conditions, 42 proteins were identified as potential NRP1 interactors, with 31 of these unique to $VEGF_{165}$a stimulation. The basal conditions elicited 177 enriched proteins, with 167 of these unique to the basal conditions.Between the NRP1 only $VEGF_{165}$a and basal conditions, 11 interactors were common between conditions. For the NRP1 coexpression with VEGFR2 and treated with $VEGF_{165}$a 15 proteins were identified as potential NRP1 interactors with 11 proteins were identified as unique to this condition, while sharing 1 interactor with the NRP1 alone treated with $VEGF_{165}$a and 3 interactors with the NRP1 alone under basal conditions.*

4.3.6 Conclusion

With the protocol for isolation of streptavidin pulldown and analysis of the mass spectrometry data optimised, it set a platform for future BioID analyses. Despite both constructs yielding interesting data, the C-terminal intracellular proximity analyses provided great protein coverage. Therefore, these tools were prioritised for the next stage of the project, where the aim was to perform interactome analyses in a cell line more similar to NRP1s endogenous environment in chapter 6. The NRP1-BioID2-HA analyses suggested a multitude of novel NRP1 interactors, and potentially revealed novel biological processes NRP1 may be involved with, particularly, with respect to vesicular trafficking. Novel mechanisms of NRP1s involvement in these processes was also highlighted by the specific proteins enriched in the analyses. For example, in cellular junctions where proteins such as ZO proteins, OCLN and CTND1 were significantly enriched, describing a potential mechanism for NRP1s involvement at cellular junctions. The NRP1 interactome was investigated further in the presence of VEGFR2 to moderate success in the single repeat performed. The expected presence of VEGFR2 was confirmed in the enriched protein list, however, few novel interactors were elicited. The strengths of this analysis were that NRP1 interactome was investigated in the presence of an established binding partner VEGFR2. However, an obvious weakness, largely result of time and money constraints, was the low n power. In future, it would be beneficial to perform at least 2 more repeats to improve the robustness of identified interactors. The next stage of the project aimed to validate some of these BioID hits using other techniques to investigate protein-protein interactions.

Chapter 5: Validation of BioID Hits

5.1 Introduction

The HEK293T BioID studies identified potential novel interacting proteins with NRP1 in both $VEGF_{165}$a stimulated and basal contexts. Although these proteins were identified as being enriched a secondary technique was sought to validate some of these interactions in real time and in living cells. Several proteins identified as interactors, involved in a diverse catalogue of biological processes, were selected for further investigation. These selected proteins included Vesicle-associated membrane protein-associated protein A (VAPA), Occludin (OCLN), Zona occludens 1 (ZO1), Septin 9 (SEPT9), Hepatocyte growth factor-regulated tyrosine kinase substrate (HRS) and Integrin β_1 (ITGB1). As ITGB1 is an established NRP1 interactor[393], including this in these validation experiments acted as a positive control. The other proteins were chosen based on the biological mechanisms they are involved with.

A portion of VAPA is anchored to the endoplasmic reticulum (ER) and is involved with vesicular trafficking by mediating interactions between the ER and endosomes[602]. Similarly, HRS accumulates on early endosomes governing vesicular trafficking and forms part of the ESCRT complex[603,604], a complex cellular machinery facilitating a diverse range of biological processes such as membrane remodelling, membrane protein internalisation and cytokinesis as discussed in section 4.3.4.5. The cellular adhesion protein OCLN, critical in the formation of tight junctions[113], was another protein chosen to investigate further. Confirmation of an interaction would provide direct evidence of NRP1 involvement at tight junction microdomains. The versatile scaffolding protein ZO1, localised to various anchoring junctions, was another protein related to cellular adhesion that facilitates the anchoring of junctional proteins to the cytoskeleton for both tight junctions and adheren's junctions[74]. The final protein chosen for investigation was SEPT9, a cytoskeletal GTPase involved in processes such as vesicular trafficking and cytokinesis[605].

These interactions were investigated using two separate techniques. The first related to co-expression experiments, whereby the potential interactor was expressed in HEK293T cells along with NRP1-BioID2-HA. The fluorescent signals were then analysed by microscopy for colocalisation. The cells were also probed for biotinylated proteins and the fluorescent signal compared to the potential interactor. Colocalisation of interactor signal and streptavidin signal indicated close proximity to NRP1. The colocalisation analysis was performed in ImageJ using the Squassh plug-in with the appropriate segmentation protocol followed[501].

The other validation technique used was nanoBRET, described in detail in section 1.6. The energy donor for these experiments, a nano luciferase (NanoLuc) enzyme which was fused to NRP1, NRP1-NanoLuc. Upon the addition of the NanoLuc substrate furimazine, the reaction catalysed by NanoLuc results in bioluminescence, which can excite proximal fluorophores that then emit fluorescence. The

potential interactor, fused to a fluorophore, acted as the energy acceptor. If the potential interactor is in close proximity to NRP1-NanoLuc, fluorescence of the fluorophore would be observed.

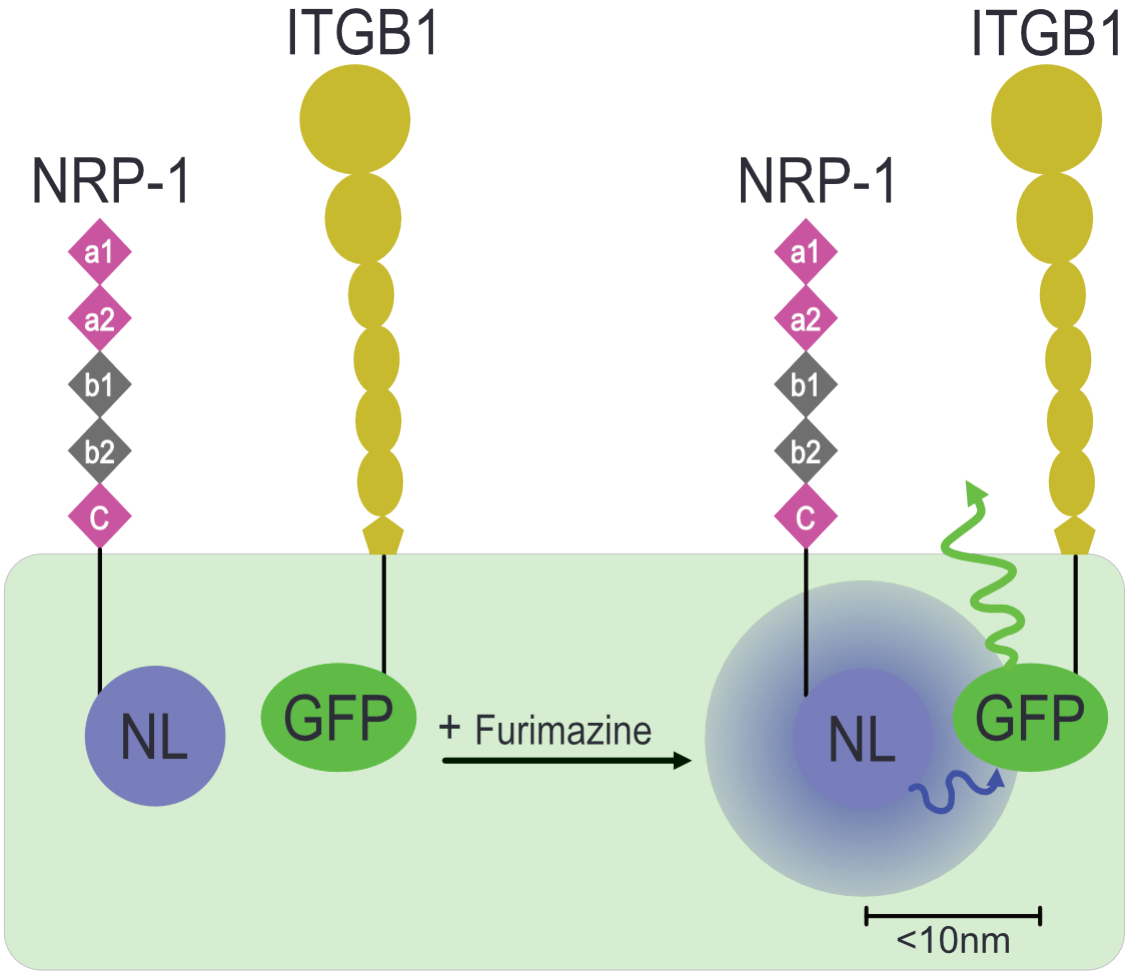

Figure 5.1 – Principles of NanoBRET validation experiments. A nano luciferase (NanoLuc) acts as the energy donor and is fused to Neuropilin 1 (NRP1). A suspected interactor of NRP1, for example Integrin β_1 (ITGB1) identified in the BioID analyses, is conjugated to a fluorescent protein such as GFP acting as the energy acceptor. Upon the addition of the NanoLuc substrate furimazine, blue-shifted bioluminescence occurs, resulting in energy transfer to the fluorophore in close proximity (<10nm). The energy transfer excites the fluorophore resulting in the emission of a higher wavelength light. A ratio between these wavelengths is then calculated.

Validating these interactions using alternative methodology increases the confidence in the potential interactions elucidated from the BioID experiments. The benefit of nanoBRET is, like BioID technology, the interactions are evaluated in a natural cellular setting, enabling observations within the dynamic environment of a cell. This means with nanoBRET the interactions are evaluated in an environment more similar to endogenous conditions, compared to other protein-protein interaction methods such as yeast-two hybrid experiments[452] and surface plasmon resonance (SPR), which consists of protein fragments adsorbed to a surface[453]. Another benefit is nanoBRET does not require the use of antibodies essential for techniques such as Co-IP, therefore there are no false-positives due to non-specific antibody binding[451].

5.2 Results

5.2.1 Co-localisation Analyses

Initially co-localisation experiments were performed with a select number of potential interactors identified in the NRP1-BioID2-HA bioinformatic experiments, fused to a fluorescent protein. These potential interactor fusion proteins were purchased from Addgene, Table 5.1. As HRS-red fluorescent protein (HRS-RFP) also contained a HA epitope, the colocalisation experiments were not performed for this plasmid, as a NRP1 antibody was not available and the NRP1-BioID2-HA fusion protein also harboured a HA epitope. For these experiments, HEK293T cells were co-transfected with NRP1-BioID2-HA and one of the proteins in Table 5.1 and imaged using a Leica TCS SPE (Leica-microsystems) with 63x oil immersion objective - ACS APO 63x/1.30 numerical aperture (Leica-microsystems). Acquired images for NRP1-BioID2-HA and the interacting protein were subject to a colocalisation analysis using the Squassh plugin for ImageJ, across the whole image. As well as fusion protein colocalisation, the streptavidin fluorescence was also compared to the potential interactor fluorescent signal. Colocalisation with the streptavidin signal, indicated the interactor had been biotinylated at some point, and therefore had been in close proximity to NRP1-BioID2-HA. Importantly, the same negative control was used for all colocalisation experiments, with a protein chosen which isn't known to interact with NRP1 and was not enriched in the BioID experiments; mEmerald-CENPA, a histone protein discussed in section 3.1, was chosen and co-expressed with NRP1-BioID2-HA cells in parallel to the experiments, (Figure 5.2). For statistical analyses one-way ANOVA followed by two-side Dunett's comparison test was used in all experiments.

Table 5.1 – Plasmids sourced from Addgene for further investigation as potential NRP Interactors. *Addgene reference numbers detailing the particular features of the fusion proteins. All plasmids contained a CMV promoter sequence.*

Plasmid Identifier	Addgene Reference
GFP-VAPA	#104447
mEmerald-OCLN	#54211
GFP-ZO1	#30313
ITGB1-mEmerald	#54129
mCherry-SEPT9	#71622
HRS-RFP	#29685

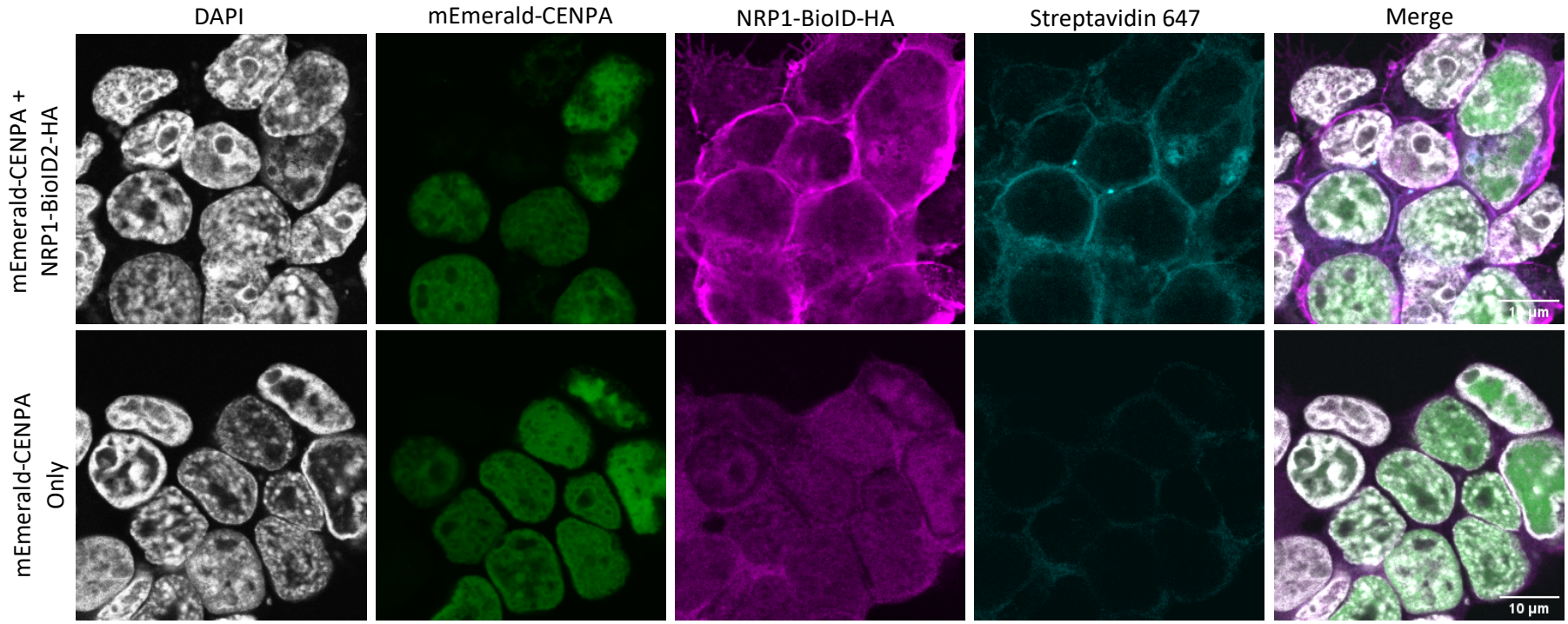

Figure 5.2 – Immunofluorescence of HEK293T cells transfected with mEmerald-CENPA, with and without coexpression of NRP1-BioID2-HA. *Cells were incubated with a mEmerald-CENPA or NRP1-BioID2-HA plasmid and Fugene HD mixture for 24 hours, followed by supplementation with fresh media and 50 µM biotin for a further 20 h. Cells were fixed and stained with anti-HA mouse (Invitrogen; 2-2.2.14) antibody followed by an anti-mouse 594 (Jackson Immuno Research; 115-585-003) to visualise the NRP1-BioID2-HA fusion protein. Streptavidin 647 (Invitrogen; S21374) identified the presence of biotinylated proteins. DAPI was used to highlight nuclear material and identify individual cells. These images were used as controls in the subsequent colocalisation analyses for all proteins investigated, n =3*

5.2.1.1 GFP-VAPA

GFP-VAPA and NRP1-BioID2-HA were co-expressed in HEK293T cells to evaluate colocalisation, (Figure 5.3a). The GFP-VAPA demonstrated localisation to the nuclear membrane and accumulation in what is likely the endoplasmic reticulum (ER), based on the biology of VAPA. Anti-HA antibody indicated the NRP1-BioID2-HA fusion protein localised as observed previously. The colocalisation of NRP1 and VAPA fluorescence was calculated and compared to mEmerald-CENPA controls, as described in section 5.2.1. The quantifications of GFP-VAPA colocalisation with NRP1-BioID2-HA demonstrated significantly greater signal colocalization when compared to controls, (Figure 5.3b). A colocalisation value of 100% would represent the entire fluorescent signal related to the GFP-VAPA perfectly overlapping with the NRP1-BioID2-HA signal. The colocalisation overlap of GFP-VAPA and NRP1-BioID2-HA fluorescent signals was 29.52 ± 4.91%, compared to 10.52 ± 2.00% for mEmerald-CENPA with NRP1-BioID2-HA. The difference between these values were statistically significantly different ($p = 0.0003$). Importantly, in conditions without NRP1-BioID2-HA expression, colocalisation was not significant, indicating the signal was not artefactual due to bleed through between the two channels. Further evidence of an interaction was supported by the colocalisation of GFP-VAPA with streptavidin fluorescence, indicating GFP-VAPA was at some point biotinylated and therefore in close-proximity to NRP1-BioID2-HA, (Figure 5.3c). The colocalisation value for GFP-VAPA and streptavidin signals was 72.03 ± 7.59%, compared to the mEmerald-CENPA with streptavidin control of 7.12 ± 2.26%. Again, a statistically significant difference between these values was observed ($p = < 0.0001$). The no NRP1-BioID2-HA controls similarly indicated the significant differences in the extent of colocalisation were not due to bleed through between channels. These data suggested a fraction of the NRP1 pool colocalised with VAPA, with the biotinylation of VAPA being indicative of this interaction.

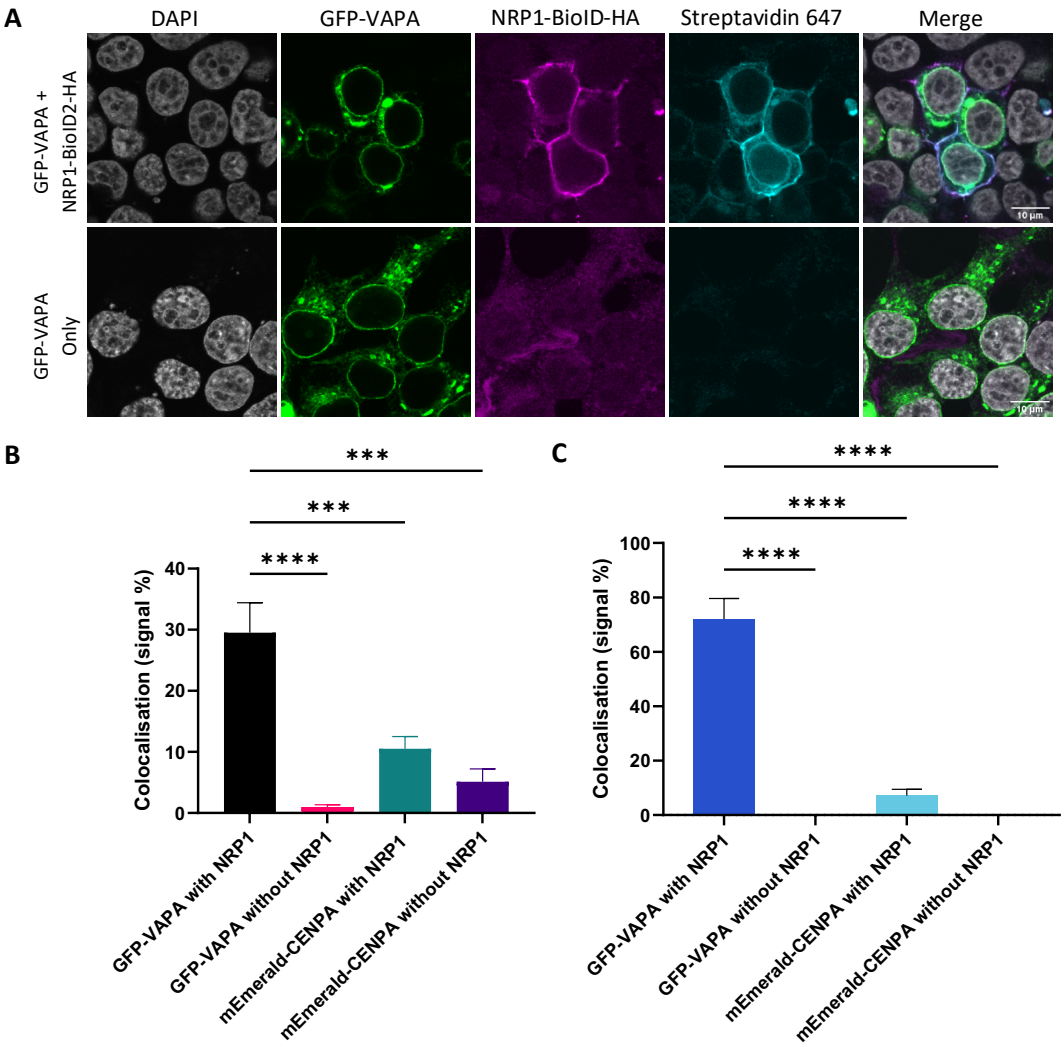

Figure 5.3 – Colocalisation of GFP-VAPA with NRP1-BioID2-HA in HEK293T Cells. (**A**) HEK293T cells *were incubated with a GFP-VAPA or NRP1-BioID2-HA plasmid and Fugene HD mixture for 24 hours, followed 50 µM biotin for a further 20 h. Cells were fixed and stained with anti-HA mouse (Invitrogen; 2-2.2.14) antibody followed by an anti-mouse 594 (Jackson Immuno Research; 115-585-003). Streptavidin 647 (Invitrogen; S21374) identified the presence of biotinylated proteins. DAPI was used to highlight nuclear material and identify individual cells. Scalebar =10µm. (**B**) Colocalisation of GFP-VAPA with NRP1-BioID2-HA fluorescence, compared to controls using mEmerald-CENPA and absent NRP1-BioID2-HA expression (one-way ANOVA followed by two-side Dunett's comparison test if p<0.05 was significant; ***p<0.001, ****p<0.0001; error bars = SEM). (**C**) Colocalisation of GFP-VAPA with streptavidin fluorescence, compared to controls using mEmerald-CENPA and absent NRP1-BioID2-HA expression, (one-way ANOVA followed by two-side Dunett's comparison test if p<0.05 was significant; ****p<0.0001; error bars = SEM). Co-localisation signal was analysed with Squassh Plug in (Image J). n = 24-38 cells from 3 individual experiments. The colocalisation experiments using VAPA, OCLN, ZO1, ITGB1 and SEPT9 were performed in parallel on the same population of HEK293T cells using the same mEmerald-CENPA negative control.*

5.2.1.2 mEmerald-OCLN

To investigate whether NRP1 was localising at the tight junctions and specifically with a major constituent of the tight junction (occuldin), mEmerald-OCLN was co-expressed with NRP1-BioID2-HA in HEK293T cells, (Figure 5.4a). As expected, mEmerald-OCLN accumulated at cellular junctions, a similar pattern to the observed expression of NRP1-BioID2-HA. The colocalisation overlap was quantified and compared to controls, (Figure 5.4b). A colocalisation value for mEmerald-OCLN and NRP1-BioID2-HA fluorescence was 22.70 ± 3.92%, compared to 10.52 ± 2.00% between mEmerald-CENPA and NRP1-BioID2-HA, which was a statistically significant difference in colocalisation value ($p = 0.0094$). With the results being of greater significance than the controls in the absence of NRP1-BioID2-HA expression, this indicated this was a true signal overlap and not due to bleed through between channels. Similarly, the potential interaction concerning OCLN and NRP1 was further supported by the colocalisation of mEmerald-OCLN and streptavidin fluorescence, potentially indicating biotinylation of mEmerald-OCLN indicative of an interaction with NRP1-BioID2-HA, (Figure 5.4c). The colocalisation value for mEmerald-OCLN and streptavidin fluorescence was 46.94 ± 6.19%, compared to controls of mEmerald-CENPA and streptavidin eliciting a value of 7.12 ± 2.26%. The difference between these values, was statistically significant ($p = < 0.0001$). Again, controls with absence of NRP1-BioID2-HA expression suggested colocalization was not artefactual results and due to channel bleed through. The results presented here were supportive of an interaction occurring between NRP1 and OCLN.

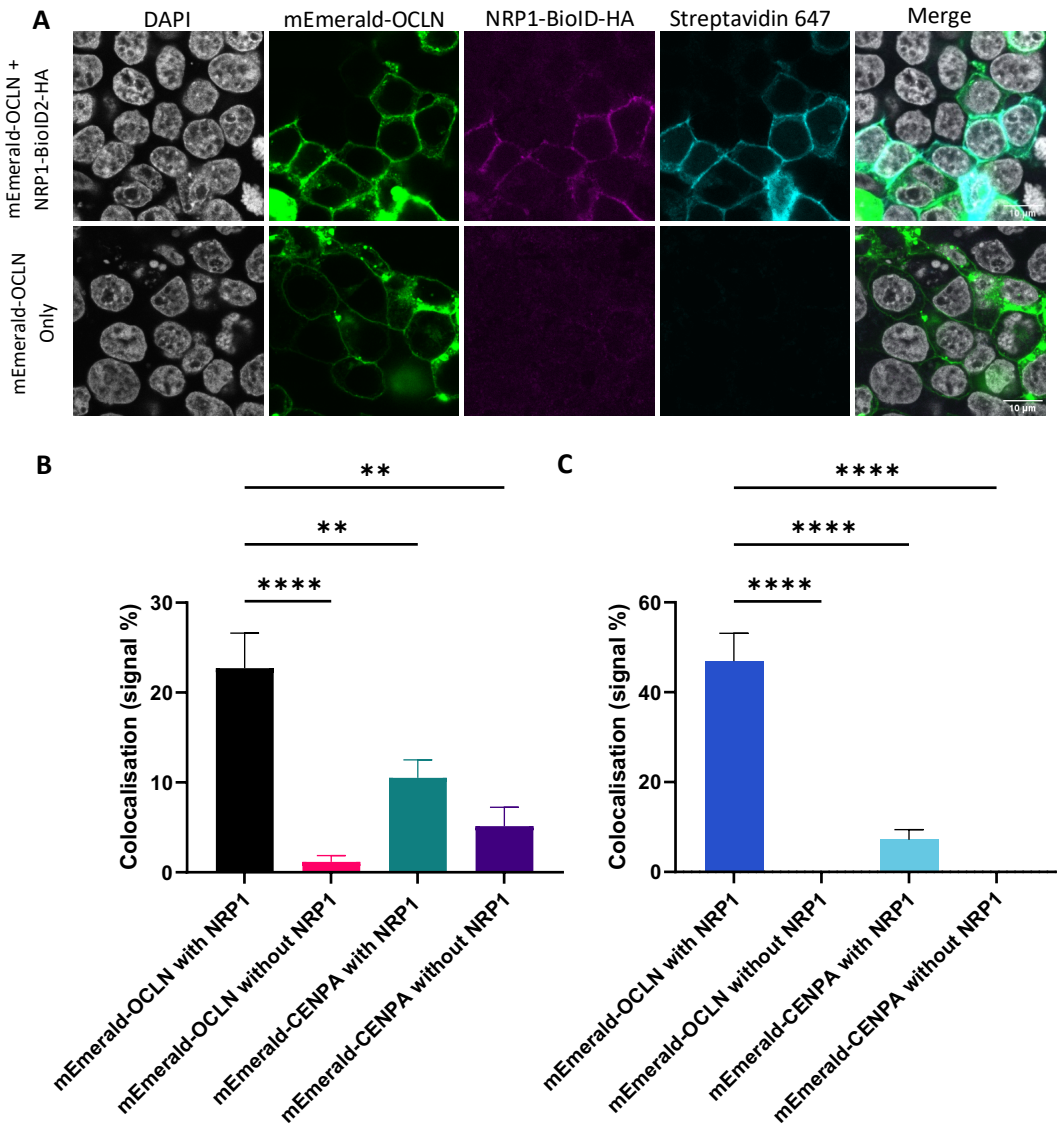

Figure 5.4 – Colocalisation of mEmerald-OCLN with NRP1-BioID2-HA in HEK293T Cells. (**A**) HEK293T cells *were incubated with a mEmerald-OCLN or NRP1-BioID2-HA plasmid and Fugene HD mixture for 24 hours, followed 50 µM biotin for a further 20 h. Cells were fixed and stained with anti-HA mouse (Invitrogen; 2-2.2.14) antibody followed by an anti-mouse 594 (Jackson Immuno Research; 115-585-003). Streptavidin 647 (Invitrogen; S21374) identified the presence of biotinylated proteins. DAPI was used to highlight nuclear material and identify individual cells. Scalebar =10µm. (**B**) Colocalisation of mEmerald-OCLN with NRP1-BioID2-HA fluorescence, compared to controls using mEmerald-CENPA and absent NRP1-BioID2-HA expression, (one-way ANOVA followed by two-side Dunett's comparison test if p<0.05 was significant; **p<0.01, ****p<0.0001; error bars = SEM). (**C**) Colocalisation of mEmerald-OCLN with streptavidin fluorescence, compared to controls using mEmerald-CENPA and absent NRP1-BioID2-HA expression, (one-way ANOVA followed by two-side Dunett's comparison test if p<0.05 was significant; ****p<0.0001; error bars = SEM). Co-localisation signal was analysed with Squassh Plug in (Image J). n = 24-44 cells from 3 individual experiments. The colocalisation experiments using VAPA, OCLN, ZO1, ITGB1 and SEPT9 were performed in parallel on the same population of HEK293T cells using the same mEmerald-CENPA negative control.*

5.2.1.3 GFP-ZO1

Another important protein in the morphology of tight junctions is the scaffolding protein ZO1. Co-expression of GFP-ZO1 and NRP1-BioID2-HA was used to further investigate the presence of NRP1 at tight junctions, (Figure 5.5a). As observed for the co-expression of mEmerald-OCLN and NRP1-BioID2-HA, (Figure 5.4a), GFP-ZO1 and NRP1-BioID2-HA appeared to colocalise at cellular junctions, likely tight junctions given the biology of ZO1. The fluorescence colocalisation was quantified, with GFP-ZO1 and NRP1-BioID2-HA eliciting a value of 52.87 ± 5.39%, much higher than the 10.52 ± 2.00% observed for colocalisation of mEmerald-CENPA and NRP1-BioID2-HA fluorescence, (Figure 5.5b). The difference in colocalisation values were statistically significant ($p = < 0.0001$). Results were also significant compared to controls lacking NRP1-BioID2-HA expression. To investigate this potential interaction further, the colocalisation of GFP-ZO1 and streptavidin was also compared, (Figure 5.5c). As observed for the previous experiments, the fluorescence appeared to colocalise, meaning close proximity of GFP-ZO1 and NRP1-BioID2-HA resulted in biotinylation. The colocalisation analysis for ZO1 and streptavidin fluorescence resulted in a value of 54.65 ± 9.13%, compared to 7.12 ± 2.26% for the Emerald-CENPA with streptavidin control which was statistically significant ($p = < 0.0001$). The colocalisation signal was also significant compared to controls lacking NRP1-BioID2-HA expression, suggesting the result was not due to bleed-through fluorescence. The data represents an indication of an interaction of NRP1 and ZO1 occurring, likely at tight junction microdomains.

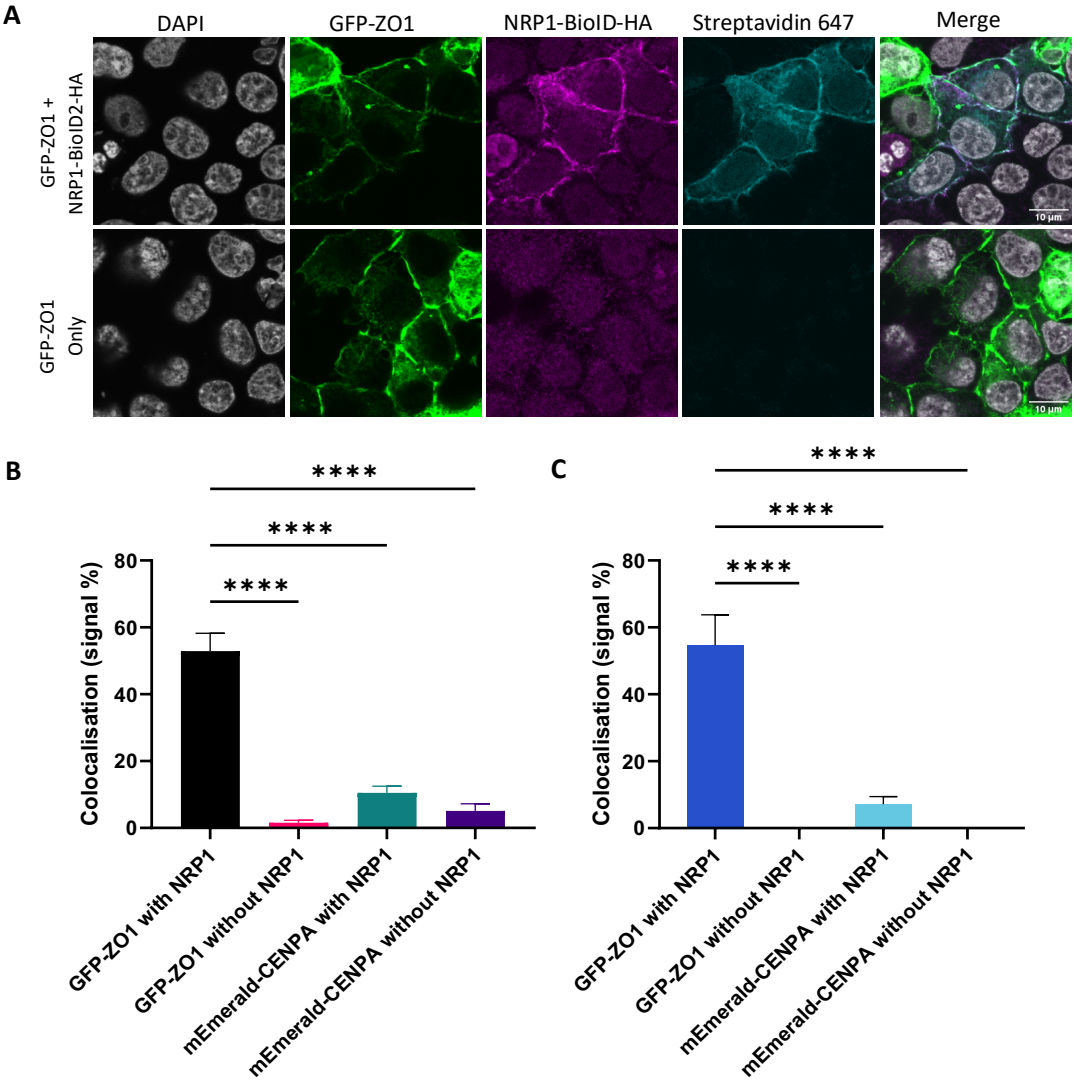

Figure 5.5 – Colocalisation of GFP-ZO1 with NRP1-BioID2-HA in HEK293T Cells*. (**A**) HEK293T cells were incubated with a GFP-ZO1 or NRP1-BioID2-HA plasmid and Fugene HD mixture for 24 hours, followed 50 µM biotin for a further 20 h. Cells were fixed and stained with anti-HA mouse (Invitrogen; 2-2.2.14) antibody followed by an anti-mouse 594 (Jackson Immuno Research; 115-585-003). Streptavidin 647 (Invitrogen; S21374) identified the presence of biotinylated proteins. DAPI was used to highlight nuclear material and identify individual cells. Scalebar =10µm. (**B**) Colocalisation of GFP-ZO1 with NRP1-BioID2-HA fluorescence, compared to controls using mEmerald-CENPA and absent NRP1-BioID2-HA expression, (one-way ANOVA followed by two-side Dunett's comparison test if p<0.05 was significant; ****p<0.0001; error bars = SEM). (**C**) Colocalisation of GFP-ZO1 with streptavidin fluorescence, compared to controls using mEmerald-CENPA and absent NRP1-BioID2-HA expression, (one-way ANOVA followed by two-side Dunett's comparison test if p<0.05 was significant; ****p<0.0001; error bars = SEM). Co-localisation signal was analysed with Squassh Plug in (Image J). n = 24-35 cells from 3 individual experiments. The colocalisation experiments using VAPA, OCLN, ZO1, ITGB1 and SEPT9 were performed in parallel on the same population of HEK293T cells using the same mEmerald-CENPA negative control.*

5.2.1.4 ITGB1-mEmerald

Previous research and the BioID results in this project have suggested a potential interaction between the adhesion protein ITGB1 with NRP1[393]. ITGB1-mEmerald and NRP1-BioID2-HA were co-expressed in HEK293T cells to evaluate potential colocalisation of these proteins, (Figure 5.6a). Importantly, the localisation of ITGB1 in the HEK293T cells was unexpected. As a transmembrane protein, it would be expected ITGB1 would be accumulated at the cell membrane, and particularly, to focal adhesion microdomains within the membrane. As observed in the immunofluorescence images, this was not the case. Instead, the fluorescent signal appeared to be non-specifically distributed in cytoplasmic regions, perhaps to the cellular cytoskeleton. No significant staining at the membrane was observed. The apparent mislocalisation of ITGB1 raised concerns for the experiment and whether it would be appropriate to use this ITGB1-mEmerald plasmid for such an experiment. Nevertheless, the colocalisation of ITGB1-mEmerald and NRP1-BioID2-HA was quantified resulting in a value of 14.34 ± 3.87%, (Figure 5.6b). The corresponding mEmerald-CENPA and NRP1-BioID2-HA negative control elicited a value of 10.52 ± 2.00%. These values did not correlate to a statistically significant difference ($p = 0.4999$). Concerning the colocalisation of ITGB1-mEmerald and streptavidin fluorescence, results must be interpreted with caution. The non-specific distribution of ITGB1 may have falsely inflated the colocalisation value. The analysis for ITGB1 and streptavidin fluorescence resulted in a 40.84 ± 8.87% value, compared to the Emerald-CENPA with streptavidin control of 7.12 ± 2.26%, (Figure 5.6c), which were significantly different ($p = < 0.0001$). Compared to controls without NRP1-BioID2-HA expression, this colocalisation value could not be attributed to bleed-through between channels. These data suggested the ITGB1-mEmerald and NRP1-BioID2-HA do not colocalise, but may have interacted at some point, as a portion of the streptavidin signal appeared to localise with ITGB1. However, as there were concerns with the mislocalisation of the ITGB1-mEmerald fusion protein, there are concerns around the validity of the results, and whether they are sufficiently representative of endogenous untagged ITGB1.

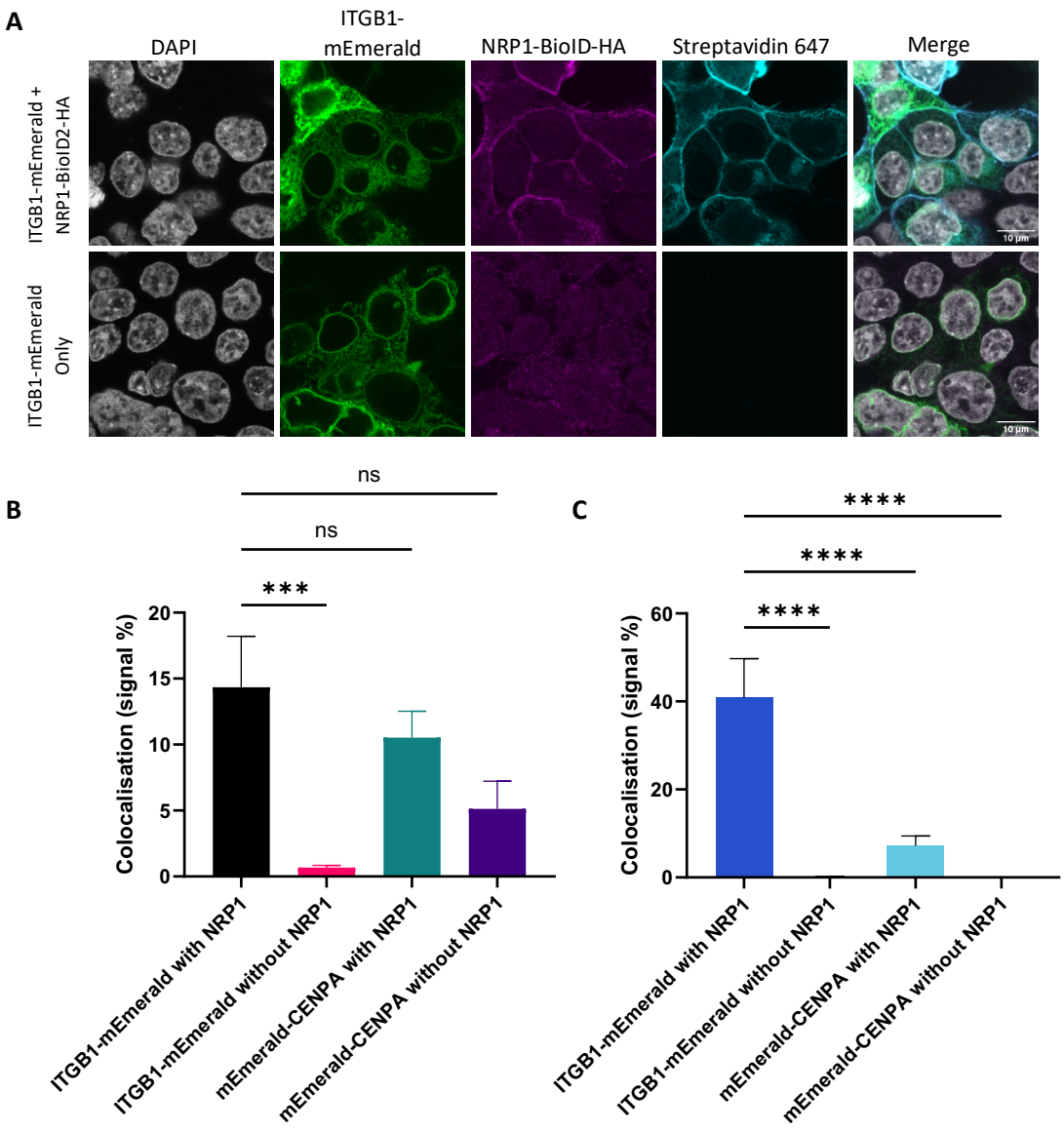

Figure 5.6 – Colocalisation of ITGB1-mEmerald with NRP1-BioID2-HA in HEK293T Cells. (**A**) HEK293T cells *were incubated with a ITGB1-mEmerald or NRP1-BioID2-HA plasmid and Fugene HD mixture for 24 hours, followed 50 µM biotin for a further 20 h. Cells were fixed and stained with anti-HA mouse (Invitrogen; 2-2.2.14) antibody followed by an anti-mouse 594 (Jackson Immuno Research; 115-585-003). Streptavidin 647 (Invitrogen; S21374) identified the presence of biotinylated proteins. DAPI was used to highlight nuclear material and identify individual cells. Scalebar =10µm. (**B**) Colocalisation of ITGB1-mEmerald with NRP1-BioID2-HA fluorescence, compared to controls using mEmerald-CENPA and absent NRP1-BioID2-HA expression, (one-way ANOVA followed by two-side Dunett's comparison test if p<0.05 was significant; ***p<0.001; error bars = SEM). (**C**) Colocalisation of ITGB1-mEmerald with streptavidin fluorescence, compared to controls using mEmerald-CENPA and absent NRP1-BioID2-HA expression, (one-way ANOVA followed by two-side Dunett's comparison test if p<0.05 was significant; ****p<0.0001; error bars = SEM). Co-localisation signal was analysed with Squassh Plug in (Image J). n = 22-32 cells from 3 individual experiments. The colocalisation experiments using VAPA, OCLN, ZO1, ITGB1 and SEPT9 were performed in parallel on the same population of HEK293T cells using the same mEmerald-CENPA negative control.*

5.2.1.5 mCherry-SEPT9

A final colocalisation experiment was performed where mCherry-SEPT9 was co-expressed in HEK293T cells along with NRP1-BioID2-HA, (Figure 5.7a). Similar to the observations with mEmerald-ITGB1, the expression pattern of mCherry-SEPT9 raises some concerns with the analysis method. The expression appeared to be non-specific to any particular cellular compartment, with detection in the nucleus, the cytoplasm and even detection at the cellular membrane. As the mCherry-SEPT9 expression is ubiquitous throughout the cells there may be artificial results with regards to the colocalisation of fluorescent signals. Similar to the previous ITGB1 analyses, the colocalisation values were not significant compared to controls, (Figure 5.7b). For mCherry-SEPT9 and NRP1-BioID2-HA a colocalisation value of 15.88 ± 3.02% was determined, whereas the mEmerald-CENPA and NRP1-BioID2-HA was 10.52 ± 2.00%. The difference of these values was not statistically significant ($p = 0.1765$). Compared to controls without NRP1-BioID2-HA expression, the signal was significant, indicating the colocalisation signal was not related to bleed-through fluorescence. In contrast, the colocalisation of mCherry-SEPT9 and streptavidin fluorescence revealed potentially interesting results, (Figure 5.7c). The colocalisation analysis for mCherry-SEPT9 and streptavidin signals resulted in a value of 19.54 ± 6.35%, compared to mEmerald-CENPA with streptavidin of 7.12 ± 2.26%, with these values being statistically different from one another ($p = 0.0057$). This may indicate mCherry-SEPT9 was biotinylated and therefore in close-proximity to NRP1-BioID2-HA at some point, as evidenced by mCherry-SEPT9 expression observed at the membrane. As observed previously, the controls lacking NRP1-BioID2-HA expression indicated true signal colocalisation. However, the ubiquitous expression throughout the cell may mean the resulting colocalisation value is artificially inflated. Hence, confidence of the interaction being true is low based on these inconclusive results.

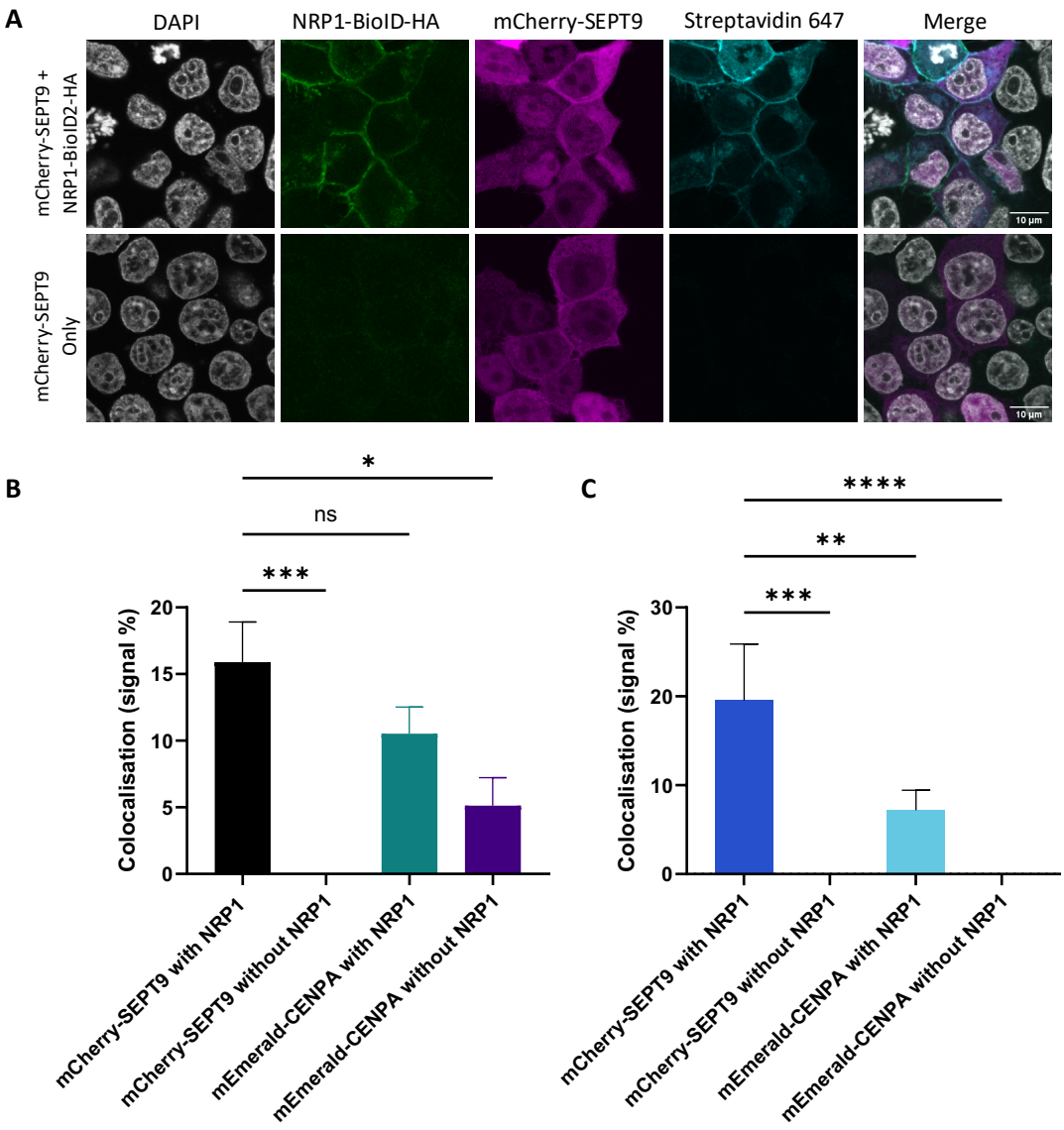

Figure 5.7 – Colocalisation of mCherry-SEPT9 with NRP1-BioID2-HA in HEK293T Cells. (**A**) HEK293T cells *were incubated with a mCherry-SEPT9 or NRP1-BioID2-HA plasmid and Fugene HD mixture for 24 hours, followed 50 µM biotin for a further 20 h. Cells were fixed and stained with anti-HA mouse (Invitrogen; 2-2.2.14) antibody followed by an anti-mouse FITC (Jackson Immuno Research; 115-095-003). Streptavidin 488 (Invitrogen; S11223) identified the presence of biotinylated proteins. DAPI was used to highlight nuclear material and identify individual cells. Scalebar =10µm. (**B**) Colocalisation of mCherry-SEPT9 with NRP1-BioID2-HA fluorescence, compared to controls using mEmerald-CENPA and absent NRP1-BioID2-HA expression, (one-way ANOVA followed by two-side Dunett's comparison test if p<0.05 was significant; ***p<0.001; error bars = SEM). (**C**) Colocalisation of mCherry-SEPT9 with streptavidin fluorescence, compared to controls using mEmerald-CENPA and absent NRP1-BioID2-HA expression, (one-way ANOVA followed by two-side Dunett's comparison test if p<0.05 was significant; **p<0.01, ***p<0.001, ****p<0.0001; error bars = SEM). Co-localisation signal was analysed with Squassh Plug in (Image J). n = 24-26 cells from 3 individual experiments. The colocalisation experiments using VAPA, OCLN, ZO1, ITGB1 and SEPT9 were performed in parallel on the same population of HEK293T cells using the same mEmerald-CENPA negative control.*

5.2.2 NanoBRET Analyses

Further investigation into the potential interactions was warranted, using the same fluorescent plasmids utilised in the colocalisation experiments, Table 5.1. NanoBRET was used to characterise the potential interactions in real time in living cells. As discussed in section 1.6, nanoBRET is a proximity-based assay used to investigate protein-protein interactions. Oxidation of the substrate furimazine, by nano luciferase (NanoLuc) results in bioluminescence. Proteins tagged with NanoLuc therefore can act as an energy donor in BRET experiments. In this case, the donor protein utilised was NRP1 tagged at its C terminus with NanoLuc (NRP1-NLuc). Fluorophores in close proximity to the bioluminescent NanoLuc will be excited by the energy emitted following furimazine oxidation and will then emit fluorescence of a higher wavelength. The proteins fused to the fluorophores therefore act as energy acceptors in this research. Importantly, the donor and acceptor epitopes must be in close proximity, (< 10 nm) and in the correct orientation in order for energy transfer to occur. BRET ratios can then be calculated between the emissions of the differing wavelengths of the donor (luminescence) and acceptor (fluorescence) and these ratios are indicative of whether a specific protein-protein interaction is occurring.

For these experiments, a constant amount of NRP1-NanoLuc cDNA was transiently transfected into HEK293T cells with increasing molar amounts of potential interactor cDNA. For a positive indication of interaction, as the expression of fluorescent interactor increases, the BRET ratios should be saturable. This saturation is an indication that a significant portion of the NRP1-NanoLuc is in close proximity to the fluorescent epitope fused to the potential interactor[607]. A control of only NRP1-NanoLuc without fluorescent interactor was included with other conditions corrected against these BRET ratios to act as a baseline BRET value (bleed through NLuc emission collected in the fluorescent acceptor channel). As well as performing BRET reads, prior to the addition of furimazine, fluorescence intensity of the transfected interactor was also measured. This was to ensure a linear increase in expression of acceptor was observed, and that any possible saturation observed in the nanoBRET luminescence was not artefactual due to a plateau of acceptor expression. A negative control was included in these experiments mEmerald-CENPA, not expected to interact with NRP1-NanoLuc. For a negative result, a saturation in BRET ratio would not be observed. Instead, what may be observed is a linear increase in BRET ratio, indicating a phenomenon known as bystander BRET, whereby the NanoLuc encounters the fluorescent protein by random chance. In this case, the resulting BRET ratios increase linearly as the expression of fluorescent tagged protein increases, due to bystander interactions occurring more frequently as a result of increased abundance of fluorescent protein.

5.2.2.1 GFP-VAPA

The ER protein GFP-VAPA was transfected into the HEK293T cells in increasing molar amounts, relative to the 50ng of NRP1-NanoLuc cDNA transfected across all HEK293T conditions, for a 24 h expression period. The BRET ratios observed demonstrated a small BRET window, with saturation somewhat observed as larger molar amounts of GFP-VAPA were transfected, (Figure 5.8a). The small BRET window indicates limited energy transfer between the donor and acceptor, perhaps as only a small portion of the protein pools in close-proximity, leading to fewer energy transfer events and a limited detection window for changes in interaction levels. Although, the error bars were notably high after 3 replicates, likely due to the small BRET window observed. Importantly, the fluorescence intensity of GFP-VAPA increased as larger amounts were transfected, indicating saturable BRET was not due to a plateaued expression of GFP-VAP, (Figure 5.8b). This saturable phenomenon is indicative of a specific protein-protein interaction between NRP1-NanoLuc and GFP-VAPA. Comparing to the mEmerald-CENPA controls, a different pattern was observed. As increasing molar amounts of mEmerald-CENPA were transfected, BRET ratios did not saturate, instead increasing in an apparently linear manner, (Figure 5.8c). This pattern is more representative as what would be observed during bystander BRET, indicative of a non-specific interaction. For the fluorescence intensity pre furimazine addition, a linear increase was observed with increasing amounts of mEmerald-CENPA transfected, (Figure 5.8d).

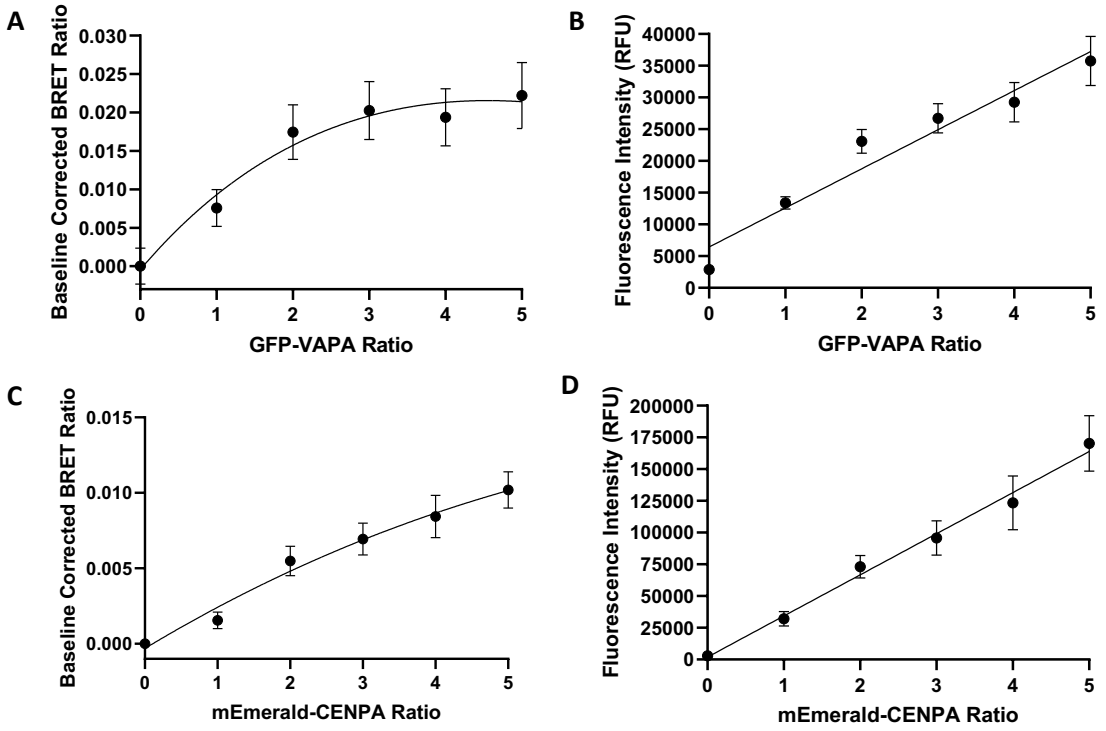

Figure 5.8 – Interaction Analysis using NanoBRET for GFP-VAPA and NRP1-NanoLuc. *HEK293T cells were incubated with a constant amount of donor NRP1-NanoLuc plasmid (50 ng/well) and varying molar ratios of acceptor GFP-VAPA plasmid with Fugene HD mixture for 24 hours. Each ratio was performed in triplicates per experiment. The following day, fluorescence intensity was measured prior to the addition of furimazine for 5 minutes. Luminescence and fluorescence emissions were then simultaneously recorded using a PHERAstar FS plate reader. All BRET values were corrected to the 0ng NLuc only control, which indicated baseline luminescence. BRET ratios were plotted along with ± S.E.M. and pooled from three individual experiments. (**A**) Baseline corrected BRET ratios for GFP-VAPA. (**B**) Fluorescence intensity of GFP-VAPA expressing HEK293T cells. (**C**) Baseline corrected ratios for mEmerald-CENPA. (**D**) Fluorescence intensity of mEmerald-CENPA expressing HEK293T cells.* Relative fluorescence units (RFU).

5.2.2.2 mEmerald-OCLN

The mEmerald-OCLN plasmid was transfected into HEK293T cells in the same manner as for GFP-VAPA, with increasing molar amounts relative to the 50ng of NRP1-NanoLuc in each condition and a 24 h expression period. Again, a small window was observed for the BRET ratio. A trend towards saturation of BRET ratios was observed, (Figure 5.9a). Additional molar ratios higher than the 1:5 ratio used would have been valuable in determining if saturation continued, however, the amount of DNA per well would have been extremely high. These results may have indicated an interaction between NRP1-NanoLuc and mEmerald-OCLN. The saturation observed was not due to a plateau in mEmerald-OCLN expression, as fluorescence intensity increased in a linear manner, as the ratio of transfected mEmerald-OCLN increased, (Figure 5.9b). The BRET ratios observed with the negative control of mEmerald-CENPA did not saturate, and instead appeared to increase in a linear manner, indicative of

a non-specific protein-protein interaction, (Figure 5.9c). The fluorescence intensity of the mEmerald-CENPA transfections increased in a linear manner, similar to the pattern observed for the BRET ratio, (Figure 5.9d).

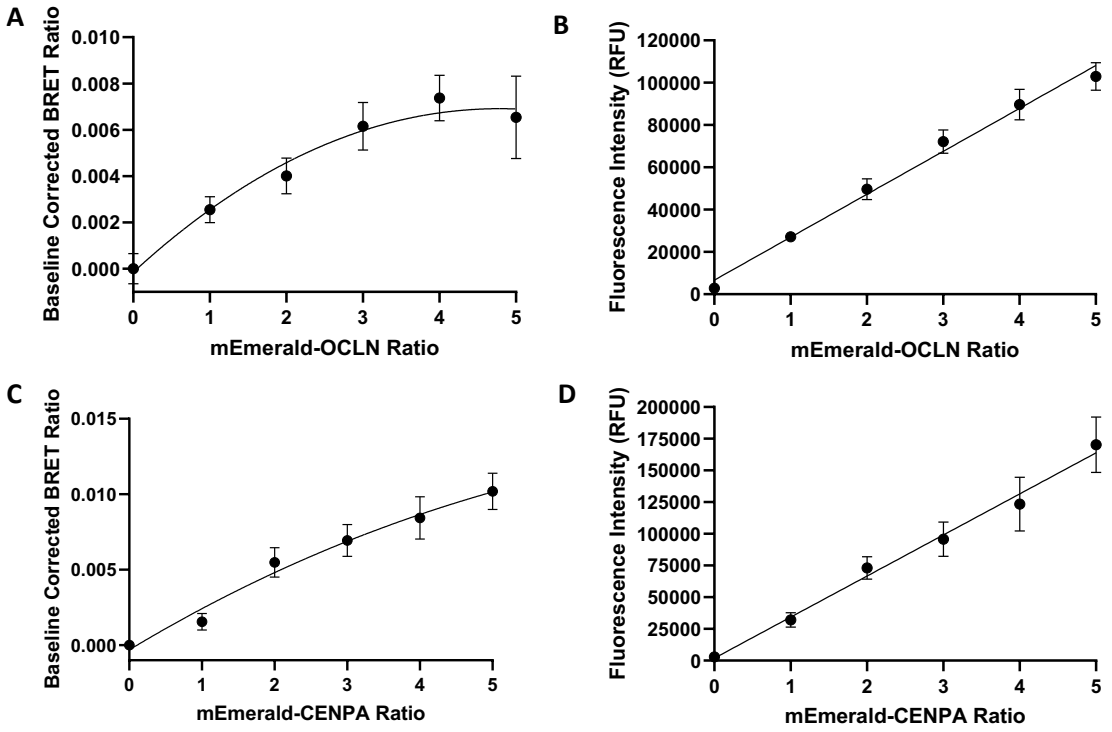

Figure 5.9 – Interaction Analysis using NanoBRET for mEmerald-OCLN and NRP1-NanoLuc. *HEK293T cells were incubated with a constant amount of donor NRP1-NanoLuc plasmid (50 ng/well) and varying molar ratios of acceptor mEmerald-OCLN plasmid with Fugene HD mixture for 24 hours. Each ratio was performed in triplicates per experiment. The following day, fluorescence intensity was measured prior to the addition of furimazine for 5 minutes. Luminescent emissions were then recorded using a PHERAstar FS plate reader. All BRET values were corrected to the 0ng acceptor control, which indicated baseline luminescence. BRET ratios were plotted along with ± S.E.M. and pooled from three individual experiments. (**A**) Baseline corrected BRET ratios for mEmerald-OCLN. (**B**) Fluorescence intensity of mEmerald-OCLN expressing HEK293T cells. (**C**) Baseline corrected ratios for mEmerald-CENPA. (**D**) Fluorescence intensity of mEmerald-CENPA expressing HEK293T cells.* Relative fluorescence units (RFU).

5.2.2.3 mCherry-SEPT9

The next protein investigated was mCherry-SEPT9, transfected in increasing molar amounts in HEK293T cells along with 25ng of NRP1-NanoLuc, with an expression period of 48 h. The lower amount of NRP1-NanoLuc was used in order to reduce possible bystander BRET observed with higher expression of NRP1-NanoLuc. Despite another small BRET window being observed, a saturable response was observed with the mCherry-SEPT9, indicating a potential specific protein interaction, (Figure 5.10a). The fluorescence intensity of mCherry-SEPT9 increased linearly as increasing molar

amounts were transfected, (Figure 5.10b). The corresponding negative control was again mEmerald-CENPA, with the molar ratios transfected relative to the 25ng of NRP1-NanoLuc and a 48 h expression period to correlate with the mCherry-SEPT9 conditions. As observed previously, the mEmerald-CENPA BRET ratios were not saturable, (Figure 5.10c). The linear increase in BRET ratio was not indicative of a specific protein interaction. The fluorescence intensity of the mEmerald-CENPA expression increased linearly up until the final 1:5 ratio, (Figure 5.10d). This may be due to the final dataset for the mEmerald-CENPA control being only an n=2 due to a failed transfection.

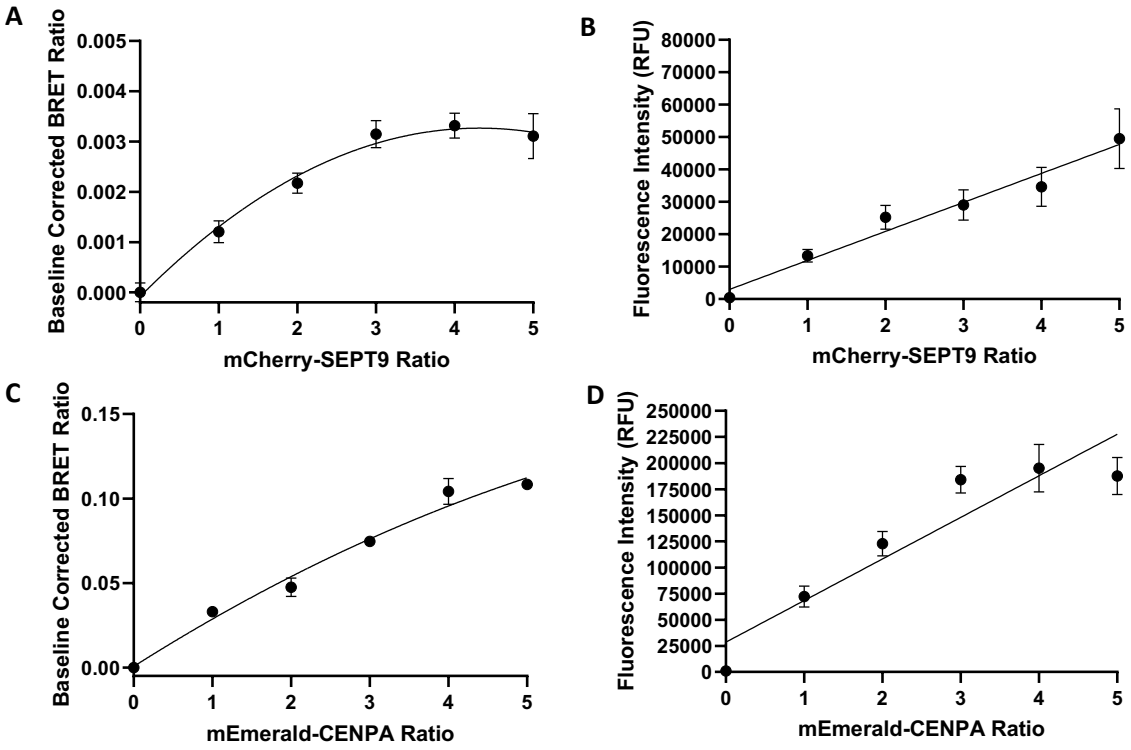

Figure 5.10 – Interaction Analysis using NanoBRET for mCherry-SEPT9 and NRP1-NanoLuc. *HEK293T cells were incubated with a constant amount of donor NRP1-NanoLuc plasmid (50 ng/well) and varying molar ratios of acceptor mCherry-SEPT9 plasmid with Fugene HD mixture for 24 hours. Cells were supplemented with fresh media and incubated for a further 24 h. Each ratio was performed in triplicates per experiment. The following day, fluorescence intensity was measured prior to the addition of furimazine for 5 minutes. Luminescent emissions were then recorded using a PHERAstar FS plate reader. All BRET values were corrected to the 0ng acceptor control, which indicated baseline luminescence. BRET ratios were plotted along with ± S.E.M. and pooled from three individual experiments. The failure of the final mEmerald-CENPA transfection meant only results were pooled from two experiments (**A**) Baseline corrected BRET ratios for mCherry-SEPT9. (**B**) Fluorescence intensity of mCherry-SEPT9 expressing HEK293T cells. (**C**) Baseline corrected ratios for mEmerald-CENPA. (**D**) Fluorescence intensity of mEmerald-CENPA expressing HEK293T cells.* Relative fluorescence units (RFU).

5.2.2.4 HRS-RFP NanoBRET

The final protein to be analysed by nanoBRET was HRS-RFP. As for mCherry-SEPT9, cells were coexpressed with a constant amount of 25ng of NRP1-NanoLuc and varying molar ratios of HRS-RFP for an expression period of 48 h. The BRET ratios elicited did not demonstrate a saturable response, instead appearing to increase linearly, a trend indicative of a non-specific protein interaction, (Figure 5.11a). However, the HRS-RFP ratios 1:4 and 1:5 displayed similar BRET ratios, perhaps indicating that increasing the experimental ratios beyond 1:5 may have demonstrated a saturable response. Although, this effect may be explained by the relative expression of HRS-RFP, as the expression indicated by fluorescence intensity appears to plateau a 1:4 and 1:5, (Figure 5.11b). The mean fluorescence of ratio 1:5 is still larger than that observed for 1:4, although the overlapping error bars reduce confidence in this condition. The same negative control of mEmerald-CENPA was used here, as the mCherry-SEPT9 experiments, with only n=2 performed due to transfection issues. As described previously, the mEmerald-CENPA BRET ratios did not elicit a saturable response and therefore not indicative of a specific protein interaction, (Figure 5.11c). The fluorescence intensity increased linearly until the 1:5 ratio, which may be observed due to the low number of replicates, (Figure 5.11d).

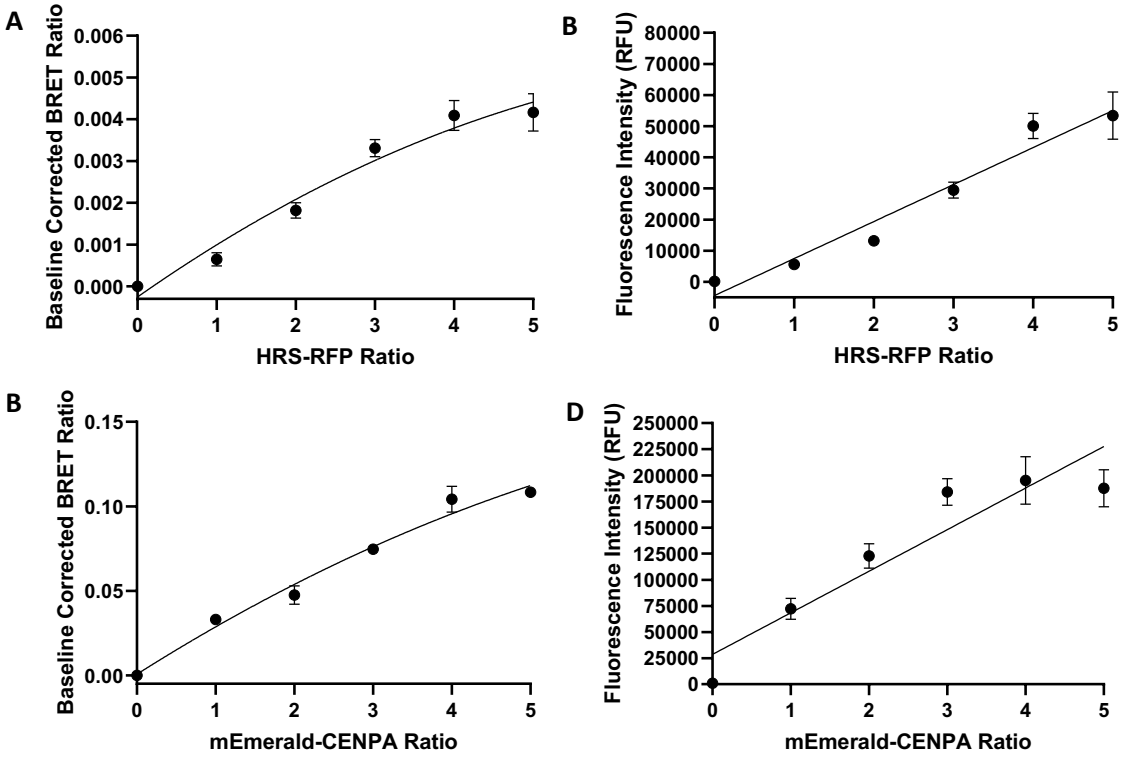

Figure 5.11 – Interaction Analysis using NanoBRET for HRS-RFP and NRP1-NanoLuc. *HEK293T cells were incubated with a constant amount of donor NRP1-NanoLuc plasmid (50 ng/well) and varying molar ratios of acceptor HRS-RFP plasmid with Fugene HD mixture for 24 hours. Cells were supplemented with fresh media and incubated for a further 24 h. Each ratio was performed in triplicates per experiment. The following day, fluorescence intensity was measured prior to the addition of furimazine for 5 minutes. Luminescent emissions were then recorded using a PHERAstar FS plate reader. All BRET values were corrected to the 0ng acceptor control, which indicated baseline luminescence. BRET ratios were plotted along with ± S.E.M. and pooled from three individual experiments. The failure of the final mEmerald-CENPA transfection meant only results were pooled from two experiments. (**A**) Baseline corrected BRET ratios for HRS-RFP. (**B**) Fluorescence intensity of HRS-RFP expressing HEK293T cells. (**C**) Baseline corrected ratios for mEmerald-CENPA. (**D**) Fluorescence intensity of mEmerald-CENPA expressing HEK293T cells.* Relative fluorescence units (RFU).

5.2.2.5 ITGB1-mEmerald

NanoBRET experiments related to ITGB1-mEmerald were aborted due to a lack of significant expression of the fusion protein indicated by the fluorescence intensity, (Figure 5.12). Despite multiple attempts at optimisation, the expression was too low to achieve significant results. As discussed in section 5.2.1.4, this may be due to issues with the plasmid expression.

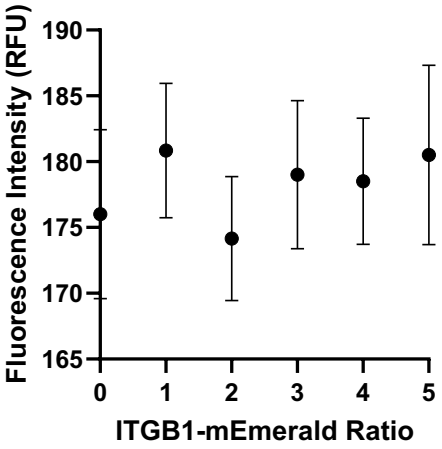

Figure 5.12 – Interaction Analysis using NanoBRET for ITGB1-mEmerald and NRP1-NanoLuc. *HEK293T cells were incubated with a constant amount of donor NRP1-NanoLuc plasmid (50 ng/well) and varying molar ratios of acceptor ITGB1-mEmerald plasmid with Fugene HD mixture for 24 hours. Each ratio was performed in triplicates per experiment. The following day, fluorescence intensity was measured using a PHERAstar FS plate reader. Fluorescent intensity was plotted along with ± S.E.M. and pooled from two individual experiments.* Relative fluorescence units (RFU).

5.2.2.6 GFP-ZO1

The nanoBRET experiments concerning GFP-ZO1 did not yield significant results, (Figure 5.13). The initial screening of the fluorescent plasmids resulted in the exclusion of GFP-ZO1 from further investigation. Following three repeats, the GFP-ZO1 failed to elicit a BRET response compared to wild-type luminescence, indicated by the condition without GFP-ZO1 expression.

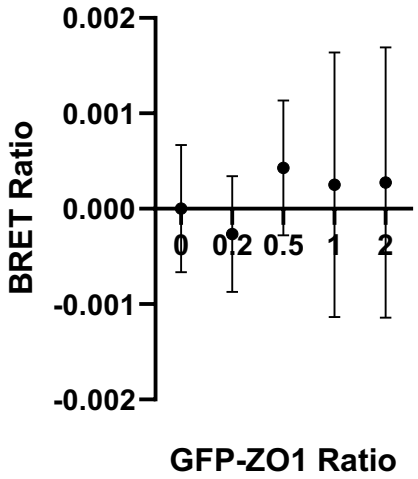

Figure 5.13 – Interaction Analysis using NanoBRET for GFP-ZO1 and NRP1-NanoLuc. *HEK293T cells were incubated with a constant amount of donor NRP1-NanoLuc plasmid (100 ng/well) and varying molar ratios of acceptor GFP-ZO1 plasmid with Fugene HD mixture for 24 hours. Each ratio was performed in triplicates per experiment. The following day, luminescent intensity was measured after the addition of furimazine for 5 minutes using a PHERAstar FS plate reader. All BRET values were corrected to the 0ng acceptor control, which indicated baseline luminescence. BRET ratios were plotted along with ± S.E.M. and pooled from three individual experiments.*

5.3 Discussion

5.3.1 GFP-VAPA

The first potential interactor studied was Vesicle-associated membrane protein-associated protein A (VAPA). The colocalisation analyses revealed significant colocalisation of GFP-VAPA with NRP1-BioID2-HA compared to controls, (Figure 5.3b). Imaging showing instances of NRP1 occupying the same cellular compartment as VAPA increased confidence in this potential interaction. The similar results observed for GFP-VAPA with streptavidin colocalisation, again demonstrated that these fusion proteins are in close proximity at some point in their lifespan, (Figure 5.3c). The expression pattern of VAPA appeared to be predominantly at the nuclear envelope, with highly fluorescent signals in regions surrounding the nucleus, likely the endoplasmic reticulum (ER)[607]. A clear biotinylation pattern was observed at the nuclear membrane, indicating GFP-VAPA biotinylation and therefore close-proximity to NRP1-BioID2-HA during the expression period. Interestingly, NRP1 is not known to have any function at the nuclear envelope or interact with any proteins which localise to this compartment. VAPAs homologue, VAPB, which was also enriched in the HEK293T BioID experiments, is known to localise to the nuclear membrane[608,609], while VAPA at nuclear membrane appears to have not yet been investigated thoroughly, although VAPA is known to interact with constituents of the nuclear envelope elucidated through proximity-based biotinylation assays[607]. Later in the research, the hTERT2-HUVEC data revealed a potential interaction of NRP1 with Torsin-1A-interacting protein 1 (TOIP1), a protein integral in the integrity of the nuclear envelope, discussed in section 6.3.6.

The saturable nanoBRET data observed for GFP-VAPA compared to the controls also increased confidence that VAPA interaction with NRP1 could have biological relevance, (Figure 5.8). The saturable response observed was indicative of specific protein-protein interactions between NRP1-NanoLuc and GFP-VAPA. However, the BRET window was small. This may be due to the specific cellular locations of NRP1 and VAPA. As observed in the immunofluorescence data, (Figure 5.3a), the majority of NRP1 fusion protein localises to the cellular membrane. However, only a small portion of NRP1 may reside in distinct subcellular locations, such as the ER where VAPA localises[607], meaning a less efficient BRET. Additionally, there are other caveats which may result in a smaller BRET window. One reason may be the fluorescent protein is conjugated to the non-optimal terminus for BRET to occur. For example, the NanoLuc conjugated to the NRP1, and the fluorophore conjugated to the VAPA may not be in close proximity, depending on the relative locations of the tags at either the C- or N-terminus. If the tags are not close, energy transfer between the NanoLuc donor and the acceptor fluorophore would be inefficient or non-existent. Repeating the experiment with the tags at differing termini of the proteins of interest or increasing the linker between these to give more flexibility enabling closer contact of the

tags may yield a larger BRET window. Another reason may be the conditions of the interaction are not met during this short analysis window of the endpoint nanoBRET experiments. The luminescent signal was measured over a short period of time and considers all cells without accounting for differing stages in the cell cycle. Therefore, the interaction may be occurring during a particular stage of the cell cycle, during mitosis for example. A possible way to overcome this is performing kinetic reads, whereby BRET measurements are taken continually using a longer acting furimzine[611]. Finally, the fusion of the NanoLuc and the fluorophore with the proteins of interest, may sterically inhibit the interaction or the propensity of this interaction occurring. The attachment of the tags may mean the proteins are no longer in sufficient proximity or in the correct orientation due to additional protein mass preventing close proximity of the interactors.

The VAPA and VAPB interactome has been investigated previously, mainly through affinity-purification mass spectrometry (AP-MS) and proximity biotinylation assays such as BioID and APEX[607]. In these proteomic studies, several common interactors were identified with VAPA and the results of the NRP1 proteomic experiments in this research, Table 5.2. Similarly, there were a some VAPB interacting proteins also enriched in the NRP1 experiments in this research, Table 5.3. As well as direct matches, there were several similar enriched proteins between VAPA and NRP1 BioID, Table 5.4. The enrichment of several common proteins across multiple experiments by different researchers increases confidence that NRP1 and VAPA are involved with some similar biological processes. Notably, NRP1 was not enriched in the VAPA or VAPB proximity-biotinylation research. This may be explained by the nature of the cells used in the VAPA and VAPB experiments. HEK293T cells were used in the AP-MS and proximity biotinylation assays; according to The Human Protein Atlas the normalised transcript per million (nTPM) for NRP1 in HEK293 cells is low (10.5 nTPM)[595]. The low expression of NRP1 may result in these interactions being missed in the previous experiments.

Table 5.2 – Common interactors between VAPA BioID experiments[607] and the NRP1 BioID experiments in this project.

UniProt ID	Gene Name	Protein Name
Q5JSH3	WDR44	WD repeat-containing protein 44
Q96S66	CLCC1	Chloride channel CLIC-like protein 1
P22059	OSBP1	Oxysterol-binding protein 1
Q9P0K7	RAI14	Ankycorbin
Q7RTP6	MICA3	[F-actin]-monooxygenase MICAL3

Table 5.3 – Common interactors between VAPB BioID experiments[607] and the NRP1 BioID experiments in this project.

UniProt ID	Gene Name	Protein Name
O95819	M4K4	Mitogen-activated protein kinase kinase kinase kinase 4
Q9H2M9	RBGPR	Rab3 GTPase-activating protein non-catalytic subunit

Table 5.4 – Related proteins to those identified interactors between VAPB BioID experiments[607] and the NRP1 BioID experiments in this project.

VAPA Interactors	NRP1 Interactors
Serine/threonine-protein kinase 3 (STK3) and Serine/threonine-protein kinase 4 (STK4)	Serine/threonine-protein kinase 10 (STK10)
Sorting nexin-2 (SNX2) **Sorting nexin-5 (SNX5)** **Sorting nexin-25 (SNX25)**	Sorting nexin-1 (SNX1) Sorting nexin-3 (SNX3) Sorting nexin-9 (SNX9)
Extended synaptotagmin-1 (ESYT1)	Extended synaptotagmin-2 (ESYT2)
Protein FAM170A (F170A)	Protein FAM177A1 (F177A)

5.3.2 mEmerald-OCLN

The next protein investigated was the established cellular adhesion protein occludin (OCLN), potential novel NRP1 interactor. The IF analyses revealed significant colocalisation of mEmerald-OCLN with NRP1-BioID2-HA, evidence of NRP1 localising to the tight junction microdomains, (Figure 5.4b). The localisation of NRP1 and OCLN at tight junctions increased confidence of the interaction. The similar biotinylation pattern observed may also indicate the biotinylation of mEmerald-OCLN, and therefore proximal location to NRP1-BioID2-HA, (Figure 5.4c). However, one explanation for this could be that NRP1-BioID2-HA is self-biotinylating and accumulating at the same cellular regions as mEmerald-OCLN. However the high confidence enrichment of OCLN in the BioID HEK293T data indicated biotinylation of OCLN was likely occurring. The localisation of NRP1 to tight junction domains is unsurprising, given the suspected roles of NRP1 in cellular adhesion[386,388], discussed in detail in section 1.4.3. The saturable nanoBRET observed between these proteins was also indicative of a specific protein-protein interaction of NRP1-NanoLuc and mEmerald-OCLN, (Figure 5.9a). As for the GFP-VAPA experiments, the BRET window observed was low, perhaps due to similar reasons as discussed in section 5.3.1, regarding potential issues with tag orientation and snapshot nature of endpoint BRET measurements.

Until now, there has been no direct evidence of NRP1 binding to any constituent proteins found at tight junctions. In mice models with homozygous NRP1 deletion, they exhibited a disruption of endothelial tight junctions with mis-localisation of OCLN[612]. These observations suggest a role for NRP1

at maintaining the integrity of tight junctions, and the evidence presented in this research may indicate the direct binding of NRP1 to OCLN being important in this process. In contrast, as observed in the IF images, (Figure 5.4a), OCLN appeared to localise correctly in the absence of NRP1 expression in HEK293T cells. This would suggest NRP1 may not be an essential component of tight junctions, at least in HEK293T cells. The low expression of NRP1 in HEK293 cells (10.5 of normalized transcript per million (nTPM)[595]) may mean the cell line has adapted compensatory mechanisms to circumvent the requirement for NRP1 at the tight junctions, meaning the NRP1 and OCLN interaction could be cell-line dependent.

BioID experiments have been performed using both N- and C-terminally tagged OCLN[613]. However, there are some caveats to the research. Firstly, the BioID experiments were performed in MDCK II cells, an epithelial-like cell line isolated from the distal renal tubule of a dog. Hence, the interactors identified may not be directly applicable to human cells. Secondly, the level of expression of NRP1 in these cells was unknown. If they are similar to that in HEK293 cells, then expression of NRP1 may be low, resulting in a false-negative result for the NRP1 and OCLN interaction. The use of canine cells themselves should not be an issue, as NRP1 is expressed in all vertebrates[318], with the human and canine sequences exhibiting a 95.45% sequence homology[443]. The proteomic analysis undertaken in the OCLN research meant proteins in 2 out of 3 repeats were included in the final enriched protein list, which is not as robust as the 4 repeats used in this project. In the OCLN BioID experiments performed by Fredriksson *et al.*[613], 48 proteins were commonly enriched with proteins detected in the NRP1 experiments performed in this project, Table 5.5. Many of these proteins are involved with vesicular trafficking and cellular adhesion, consolidating NRP1s roles in these biological processes. Such high number of common interactors increases confidence in the potential interaction between NRP1 and OCLN and perhaps indicates the existence of large protein complexes consisting of NRP1, OCLN and some of their shared interactors. As well as these directly common proteins, there were numerous other similar enriched proteins in the experiments. For example, several VAMPs were enriched with OCLN, notably the bona fide NRP1 Interactor VAMP2[433]. The research in this project did not identify an enrichment of VAMP2, but VAMP3 and VAMP5 were enriched instead. Additionally, semaphorin 4D (SEMA4D) and SEMA4G were thought to interact with OCLN. As discussed in section 1.4.6.2, SEMA3C is a well-defined ligand binding to NRP1.

Table 5.5 – Common interactors between OCLN BioID experiments[613] and the NRP1 BioID experiments in this project.

UniProt ID	Gene Name	Protein Name
Q9UEY8	ADDG	Gamma-adducin
P55196	AFAD	Afadin
Q12955	ANK3	Ankyrin-3
P20020	AT2B1	Plasma membrane calcium-transporting ATPase 1
Q9UQB8	BAIP2	Brain-specific angiogenesis inhibitor 1-associated protein 2
P35613	BASI	Basigin
Q9H3Q1	BORG4	Cdc42 effector protein 4
O60716	CTND1	Catenin delta-1
P78310	CXAR	Coxsackievirus and adenovirus receptor
Q12959	DLG1	Disks large homolog 1
Q14126	DSG2	Desmoglein-2
P98172	EFNB1	Ephrin-B1
O95208	EPN2	Epsin-2
Q8N128	F177A	Protein FAM177A1
P02751	FINC	Fibronectin
Q13480	GAB1	GRB2-associated-binding protein 1
Q9HD26	GOPC	Golgi-associated PDZ and coiled-coil motif-containing protein
P05556	ITB1	Integrin beta-1
Q9P206	K1522	Uncharacterized protein KIAA1522
Q15334	L2GL1	Lethal(2) giant larvae protein homolog 1
Q9UGP4	LIMD1	LIM domain-containing protein 1
Q86X29	LSR	Lipolysis-stimulated lipoprotein receptor
O95819	M4K4	Mitogen-activated protein kinase kinase kinase kinase 4
Q7KZI7	MARK2	Serine/threonine-protein kinase MARK2
P49757	NUMB	Protein numb homolog
Q8IZ21	PHAR4	Phosphatase and actin regulator 4
Q13492	PICAL	Phosphatidylinositol-binding clathrin assembly protein
Q9HAU0	PKHA5	Pleckstrin homology domain-containing family A member 5
Q9HCU5	PREB	Prolactin regulatory element-binding protein
Q13308	PTK7	Inactive tyrosine-protein kinase 7
Q12923	PTN13	Tyrosine-protein phosphatase non-receptor type 13
Q9ULC3	RAB23	Ras-related protein Rab-23
P51149	RAB7A	Ras-related protein Rab-7a
Q6WKZ4	RFIP1	Rab11 family-interacting protein 1
Q8WTV0	SCRB1	Scavenger receptor class B member 1
Q14160	SCRIB	Protein scribble homolog
Q15464	SHB	SH2 domain-containing adapter protein B
O00161	SNP23	Synaptosomal-associated protein 23
O95721	SNP29	Synaptosomal-associated protein 29

O60493	SNX3	Sorting nexin-3
Q658P3	STEA3	Metalloreductase STEAP3
O94804	STK10	Serine/threonine-protein kinase 10
Q86Y82	STX12	Syntaxin-12
P02786	TFR1	Transferrin receptor protein 1
Q8TAA9	VANG1	Vang-like protein 1
O15498	YKT6	Synaptobrevin homolog YKT6
Q07157	ZO1	Tight junction protein ZO-1
Q9UDY2	ZO2	Tight junction protein ZO-2

5.3.3 GFP-ZO1

Similar to OCLN, ZO1 is an established cellular adhesion molecule localising to tight junctions[139], discussed in section 1.2.2.4. The localisation of GFP-ZO1 to these domains were observed in the HEK293T IF analyses, (Figure 5.5a). As observed for mEmerald-OCLN, the GFP-ZO1 fusion protein colocalised with NRP1-BioID2-HA, (Figure 5.5b). The evidence presented thus far for NRP1 activity at tight junction microdomains is compelling. The localisation of NRP1 with two proteins at cell tight junctions increased confidence for its potential biological influence at these domains and potential interactions with OCLN and ZO1. The biotinylation pattern again may be interpreted as self-biotinylation of NRP1-BioID2-HA, resulting in the colocalisation of streptavidin and GFP-ZO1 signal, (Figure 5.5c). Although, as ZO1 was enriched across multiple BioID experiments in this research, it is likely GFP-ZO1 was being biotinylated and the colocalization with streptavidin signal is true. The nanoBRET results were less positive. A specific BRET signal was not observed in these experiments, (Figure 5.13), potentially due to the reasons discussed in section 5.3.1, regarding possible issues with NanoLuc and fluorophore orientation and endpoint BRET measurements.

The orientation of the NanoLuc and the GFP fluorophore conjugated to ZO1 may be the most significant factor adversely affecting potential efficient energy transfer. The ZO1 protein is large (~195 kDa) and has three PDZ domains all located to its C-terminus, the opposite terminus to where the GFP was conjugated. As the SEA domain in the C-terminus of NRP1 is capable of binding to PDZ domains, discussed in section 1.4.1, if NRP1 is interacting with the C-terminus of ZO1, the GFP tag may not be sufficiently proximal for BRET to occur. The failure to achieve BRET here does not necessarily mean an interaction isn't happening but may be due to technical issues with the assay that need to be further optimised (e.g. switching tag location).

The BioID enrichment of ZO1 and colocalisation analyses are again a novel indication of NRP1 interaction with tight junction constituents. Previous microscopy research has also demonstrated colocalisation of NRP1 and ZO1 at endothelial tight junction domains, induced by treatment with PDGF-D[614]. This implies a role for NRP1 at these junctions, perhaps in a dynamic manner in response

to ligand. Correct localisation of GFP-ZO1 in the absence of NRP1 co-expression reinforces that NRP1 tight junctions may be contextual, or may be cell line dependent, (Figure 5.5a), discussed previously. NRP1 may not be a permanent feature of tight junctions but instead may translocate to these domains in certain circumstances to modulate cellular adhesion, as observed with the PDGF-D research mentioned earlier[387]. Conversely, the low expression of NRP1 in WT HEK293T cells may mean compensatory mechanisms have been developed to circumvent the requirement of NRP1 at these junctions, as mentioned previously. Importantly, direct interactions between OCLN and ZO1 at tight[614]. The potential of NRP1 to bind to these proteins highlighted in this project is another positive indication for putative roles of NRP1 at tight junctions and cellular adhesion.

BioID technology has also been used to investigate potential binding partners of ZO1[616]. In this research, both the C- and N-terminus of ZO1 was fused to the original biotin ligase (BirA) variant. As these experiments were also performed in epithelial MDCK II cells, the same caveats as discussed in section 5.3.2 also apply here, with regards to regarding possible issues with orientation of the tags and the single point BRET measurements used. Comparison of the ZO1 BioID research with the NRP1 BioID analyses performed in this project, revealed 43 common interactors, Table 5.6. A link between ZO1, NRP1 and VAPB is implied, as VAPB is enriched in proximity-biotinylation experiments of ZO1 and the NRP1 work in this research. The biological outcome of this complex formation is unknown, with ZO1 not known to participate in vesicular trafficking. However, it has been suggested the tight junctions provide a platform for vesicular docking[617], hence, ZO1 may be involved with the docking of these vesicles. Many of these proteins were also common between NRP1 and OCLN. As discussed in the previous section, the numerous common interactors identified increased confidence that NRP1 and ZO1 are involved in similar biological processes, and therefore increasing the confidence of the significance of this potential interaction.

Table 5.6 – Common interactors between ZO1 BioID experiments[616] and the NRP1 BioID experiments in this project.

UniProt ID	Gene Name	Protein Name
P55196	AFAD	Afadin
Q12955	ANK3	Ankyrin-3
Q9UQB8	BAIP2	Brain-specific angiogenesis inhibitor 1-associated protein 2
Q9Y5K6	CD2AP	CD2-associated protein
Q9UQN3	CHM2B	Charged multivesicular body protein 2b
O60716	CTND1	Catenin delta-1
P78310	CXAR	Coxsackievirus and adenovirus receptor
Q9UJU6	DBNL	Drebrin-like protein
Q96C19	EFHD2	EF-hand domain-containing protein D2

Q9UBC2	EP15R	Epidermal growth factor receptor substrate 15-like 1
Q12929	EPS8	Epidermal growth factor receptor kinase substrate 8
Q96AC1	FERM2	Fermitin family homolog 2
P52565	GDIR1	Rho GDP-dissociation inhibitor 1
P53990	IST1	ST1 homolog
Q9UPN3	K0754	Microtubule-actin cross-linking factor 1, isoforms 6/7
Q9UGP4	LIMD1	LIM domain-containing protein 1
Q86X29	LSR	Lipolysis-stimulated lipoprotein receptor
O95819	M4K4	Mitogen-activated protein kinase kinase kinase kinase 4
Q7KZI7	MARK2	Serine/threonine-protein kinase MARK2
Q92597	NDRG1	Protein NDRG1
Q92692	NECT2	Nectin-2
Q96TA1	NIBA2	Protein Niban 2
Q16625	OCLN	Occludin
Q13177	PAK2	Serine/threonine-protein kinase PAK 2
O00151	PDLI1	PDZ and LIM domain protein 1
Q96HC4	PDLI5	PDZ and LIM domain protein 5
Q13492	PICAL	Phosphatidylinositol-binding clathrin assembly protein
Q9HAU0	PKHA5	Pleckstrin homology domain-containing family A member 5
Q9ULC3	RAB23	Ras-related protein Rab-23
P51149	RAB7A	Ras-related protein Rab-7a
Q07960	RHG01	Rho GTPase-activating protein 1
Q14160	SCRIB	Protein scribble homolog
O00161	SNP23	Synaptosomal-associated protein 23
O95721	SNP29	Synaptosomal-associated protein 29
O60493	SNX3	Sorting nexin-3
Q9Y5X1	SNX9	Sorting nexin-9
P61081	UBC12	NEDD8-conjugating enzyme Ubc12
Q15836	VAMP3	Vesicle-associated membrane protein 3
Q8TAA9	VANG1	Vang-like protein 1
O95292	VAPB	Vesicle-associated membrane protein-associated protein B/C
O15498	YKT6	Synaptobrevin homolog YKT6
Q07157	ZO1	Tight junction protein ZO-1
Q9UDY2	ZO2	Tight junction protein ZO-2

5.3.4 mCherry-SEPT9

The cytoskeletal GTPase SEPT9 was then investigated for potential interactions with NRP1. The results of the colocalisation analysis did not reveal any significant colocalisation of mCherry-SEPT9 with NRP1-BioID2-HA, compared to controls, (Figure 5.7b). However, as SEPT9 is a cytoskeletal GTPase it could be assumed expression would be observed ubiquitously throughout the cell[605] as observed in the IF

images, (Figure 5.7a). Although difficult to detect on the IF images, it does appear a portion of the mCherry-SEPT9 localised to the cellular membrane, (Figure 5.7a). The ubiquitous expression may be masking the relatively small portion which interacts with NRP1, perhaps specifically at the membrane. In contrast, a significant portion of the mCherry-SEPT9 colocalised with the streptavidin fluorescence, (Figure 5.7c). Despite this seemingly significant result, this may be artefactual due to ubiquitous expression of SEPT9 throughout the cell, resulting in more signal overlap. Therefore, these results should be interpreted with caution. With regards to the BRET experiments, there was more positive indications of a specific protein-protein interaction with a saturable BRET ratio observed, (Figure 6.10a), albeit with a relatively small experimental window.

A potential interaction between NRP1 and SEPT9 would be a novel finding, however, the validation results here are not as clear when compared to the previous interactors investigated. It may be only a small portion of SEPT9 is interacting with NRP1, perhaps at the membrane where localisation was observed in the IF. SEPT9 is known to associated with the cellular membrane[618], where it mediates interactions between focal adhesions and the actin cytoskeleton to exert influence on cellular adhesion[619]. The enrichment of several GTPases in the NRP1 BioID experiments, such as the Rab and Ras associated GTPases, suggests NRP1 is able to interact these protein types, notably the Ras, Rab and Rho GTPases discussed in 4.3.4.6, and later in chapter 6 sections 6.3.5 and 6.3.6. Internalisation of NRP1/VEGFR2 complex into Rab7 and Rab11 vesicles has been observed[586], discussed in detail in section 1.4.5. Additionally, Rab7 localises to endosomes and co-immunoprecipitates with NRP1, indicative of an interaction[587].

Unlike the previous proteins discussed, no proximity-dependent biotinylation assays have been published with regards to SEPT9, or for any of the septins. However, an interactome analysis using AP-MS has been performed[620]. Proteomics in this manner is disadvantaged when compared to BioID, as much less interactors are usually identified, due to the nature of the experiment. As discussed preciously, the CO-IP method used in AP-MS is a snapshot of what is interacting with the protein of interest at a fixed timepoint, whereas BioID tracks potential interactions over time. Additionally, transient interactions may be removed during the harsh washing conditions involved in the CO-IP methodology. Only 1 protein was identified as common between this SEPT9 AP-MS study and the NRP1 BioID research in this project, Synaptosomal-associated protein 23 (SNP23). The absence of NRP1 was not surprising given the AP-MS methodology, and because immortalized 1306 skin fibroblast cells were used, with conclusive evidence showing absent NRP1 expression in dermal fibroblasts[621]. Another AP-MS study of SEPT9 of interacting proteins elucidated two more common interactors, Ankyrin-3 (ANK3) and Adenomatous polyposis coli protein (APC)[622]. MCF-7 cells were used in these experiments, which have a higher endogenous NRP1 expression (67.9 nTPM)[595], so enrichment may be expected based on

the BioID data in this project. However, similar limitations of AP-MS as seen with CO-IP still apply, possibly accounting for the lack of NRP1 detected as an interactor. The same study also indicated SEMA6C may interact with SEPT9, indicating possible further connections with the known semaphorin binding protein NRP1.

5.3.5 ITGB1-mEmerald

ITGB1 was another cellular adhesion protein identify from BioID analysis that was then chosen for further investigation using NanoBRET. As a known interactor of NRP1[393], it was hoped this plasmid could be used as a positive control for NanoBRET experiments. However, there were unfortunately concerns regarding the ITGB1-mEmerald plasmid. The IF experiments of ITGB1-mEmerald expression in HEK293T cells, (Figure 5.6a), demonstrated apparent mislocalisation of the fusion protein. The expression appeared ubiquitous throughout the cytoplasm, almost resembling cytoskeletal structures without localising to the cellular membrane as expected. Additionally, expression was low compared to the other fluorescently tagged proteins. Unsurprisingly, the colocalisation of ITGB1-mEmerald with NRP1-BioID2-HA was therefore not significant when compared to the controls, (Figure 5.6b). The colocalisation of ITGB1-mEmerald and streptavidin fluorescence however was significant, (Figure 5.6c), although these results should be interpreted with caution. As discussed for mCherry-SEPT9, this may be due to the non-specific localisation of ITGB1-mEmerald resulting in artefactual overlap with streptavidin fluorescence. The poor expression correlated with the nanoBRET attempts. A sufficient expression of ITGB1-mEmerald could not be achieved, despite optimisation of transfection attempts, (Figure 5.12). Hence, assays were aborted to save reagent costs. The results are therefore inconclusive whether NRP1 interacts with ITGB1. As there appeared to be issues with the ITGB1-mEmerald fusion protein, using a plasmid with improved expression and localisation or alternative fluorescent tag localisation may yield more positive results.

Despite the negative results in this chapter, evidence of NRP1 binding to ITGB1 exists from CO-IP experiments, demonstrating a physical association between these two proteins in human pancreatic cancer cells[393]. NRP1 has also been observed influencing biological processes involving ITGB1. The knockdown of NRP1 resulted in a reduced expression of ITGB1 at both mRNA and protein levels, reducing metastatic potential in two independent models of osteosarcoma[623]. Similarly, NRP1 is thought to interact with integrin $\alpha_5\beta_1$ at adhesion sites, promoting endothelial adhesion to fibronectin (FINC)[340]. The same research also demonstrated the the C-terminus of NRP1 was dispensable for this interaction, but critical for internalisation of activated integrin $\alpha_5\beta_1$.

While no proximity-based biotinylation assays have been performed for ITGB1, several ITGB1 binding partners are consistent with the NRP1 BioID analyses in section 4.2.2.4. Fermitin family homolog 2

(FERM2), also known as Kindlin-2, is colocalised and co-immunoprecipitated with ITGB1[624]. Another common interactor is FINC, discussed earlier where NRP1 modulates endothelial adhesion to this, was identified as a ITGB1 interacting protein determined via cross-linking reactions[625]. Tyrosine-protein phosphatase non-receptor type 1 (PTN1) was another of these common interactors, where ITGB1 was discovered as a substrate for dephosphorylation[626]. Finally, Leukocyte surface antigen CD47 (CD47) was found to physically associate with ITGB1 through CO-IP experiments[627]. The numerous shared interactors between NRP1 and ITGB1 increase the confidence in this potential interaction having biological significance.

5.3.6 HRS-RFP

The endosomal trafficking protein HRS was the final potential NRP1 interactor to be investigated. Unfortunately, as the HRS-RFP plasmid also harboured a HA epitope on the fusion proteins, and due to lack of available primary antibodies against HRS, colocalisation analyses with NRP1-BioID2-HA could not be performed. However, nanoBRET experiments were still possible with this plasmid. The nanoBRET results were not indicative of a specific protein-protein interaction, as the BRET ratio appeared to increase linearly with increasing HRS-RFP cDNA transfection similar to the negative control, (Figure 5.11). As discussed in section 5.3.1, this may not necessarily mean HRS and NRP1 do not interact, rather the conditions of the assay may not be appropriate to detect this interaction.

Compared to the other potential NRP1 interactors, evidence of biological associations with HRS in the literature is scarce. The established NRP1 co-receptor, VEGFR2, has been shown to colocalise with HRS and Signal transducing adapter molecule 1 (STAM1) in endosomes, following stimulation with VEGF-$_{165}$A. The STAMs are a recognised binding partner of HRS[628], and STAM1 was enriched in the NRP1 BioID experiments, perhaps indicating a novel mechanism for VEGFR2 internalisation involving a NRP1/HRS/STAM1 complex. HRS may also be considered a negative regulator of angiogenesis, a process which the VEGF/VEGFR2 signalling axis is a crucial mediator of. The internalisation facilitated by HRS can result in the targeted degradation of VEGFR2 resulting in reduced angiogenic output[629].

Despite little biological association of NRP1 and HRS previously identified, a few common interactors are shared. The interaction of HRS and Abl interactor 2 (ABI2) was predicted in a large-scale proteomic study[630], as well as enrichment in the NRP1 analyses in section 4.2.2.4. ABI2 localises to adherens junctions where it modulates cytoskeletal dynamics[631]. Similar to SEPT9, HRS also associates with APC[632]. It may be unsurprising proteins involved with vesicular trafficking are common interactors with HRS and NRP1. The RabGTPase RAB7A enriched in the NRP1 BioID experiments, was also found to associate with HRS via density centrifugation of the protein complex[633].

As well as common interactors, these proteins are known to interact with other similar proteins. The syntaxin and sortin-nexins are interactors for a number of proteins discussed in this chapter and were suggested as interactors in the NRP1 BioID experiments, section 4.2.2.4. Based on a large proteomic study, HRS is predicted to interact with SNX7[630], similar to the SNX1, SNX3 and SNX9 identified as potential NRP1 interactors in this project. The large-scale proteomics study mentioned earlier also detailed an association between STX11[634], while the BioID experiments indicated an NRP1 interaction with STX3, STX5, STX8 and STX12. The same study also identified Golgin subfamily A member 2 (GOGA2) as an HRS interactor, while GOGA3 and GOGA5 were enriched as NRP1 interactors in this project.

5.3.7 Conclusion

Evidence presented in this chapter are positive indications that many of the proteins enriched in the BioID data are true interactors with NRP1, particularly with regards to VAPA and OLCN as summarised in Table 5.7. However, for some proteins the results were less clear as to whether they are validated NRP1 interactors, notably ITGB1 and HRS. However, this may be due to assay limitations and issues with the expressed fusion proteins. In addition to the results here, the multiple shared interactors identified in the literature and similarly interacting proteins between NRP1 and all of the chosen proteins, increased confidence in these potential interactions as having biological legitimacy. While NanoBRET observations increased this confidence further, it would be prudent to confirm interactions in another manner, classically performed using CO-IP experiments. However, it is important to note the reason BioID was chosen over identification methods such as CO-IP such as the advantages it offers with regards to identifying transient interactions and interactions over a time.

Table 5.7 – Summary of the investigations of the potential NRP1 interactors identified in the BioID experiments. VAPA and OCLN were assigned as high confidence interactors, as positive results were observed across all experiments performed. ITGB1 was also denoted as a high confidence interactor due to the significant evidence in the literature of this interaction. ZO1, HRS and SEPT9 were not denoted as high confidence interactors due to inconclusive results in some of the experiments.

Potential NRP1 Interactor	Enriched in NRP1 BioID Data	Localises with NRP1	Localises with Streptavidin	Positive NanoBRET Results	Known binding partners shared with NRP1	Evidence of NRP1 Interaction in the Literature	High Confidence Interactor
VAPA	✓	✓	✓	✓	✓	×	✓
OCLN	✓	✓	✓	✓	✓	×	✓
ZO1	✓	✓	✓	×	✓	×	×
ITGB1	✓	×	✓	×	✓	✓	✓
HRS	✓	-	-	×	✓	×	×
SEPT9	✓	×	✓	✓	✓	×	×

Chapter 6: NRP1 Interactome Analyses in hTERT2-HUVEC Cells

6.1 Introduction

NRP1 is known to participate in various biological processes across a range of cellular environments. The influence of NRP1 in nervous system development[635], regulation of immune response[334], spermatogenesis in the testis[636], and in the infectivity of viruses in lung epithelial cells has been suggested, discussed in section 1.4.5.4. However, the function of NRP1 has mainly been investigated in the context of cardiovascular development and endothelial cell environments[637,638] and, as discussed in section 1.4.2. With the diverse cellular environments that NRP1 is expressed in, it may be assumed the NRP1-interacting proteins in these differing environments are not equal. The differential expression profiles of the cell types involved in these biological processes, may mean NRP1 interacts with different proteins in different biological contexts. Additionally, potential interacting proteins present in one cell type, may not be expressed significantly in another. Only analysing the NRP1 interactome in one cellular environments may therefore lead to potential interactors being missed.

The interactome analyses thus far have been performed in HEK293T cells, a cellular environment which may not be similar to the endogenous environments occupied by NRP1. This may be reflected in the endogenous mRNA of NRP1 in HEK293 cells being comparatively low, exhibiting a value of 10.5 of normalized transcript per million (nTPM)[595]. Whereas a cell line of endothelial lineage such as hTERT2-HUVECs have a NRP1 mRNA expression value of 280.1 nTPM[595]. The hTERT2-HUVEC cells are an immortalised form of HUVEC cells[487]. Angiogenic vessel forming assays determined comparable tube formation in WT HUVEC and hTERT2-HUVEC cells[611]. The lineage of HEK293T cells is debated, originally though as epithelial, some researchers have demonstrated neuronal lineage by expression of neuron-specific genes[639,640]. A review evaluating research investigating HEK293T lineage concluded there was no evident tissue-specific gene expression signature and expression of markers of several tissues was detected[641]. Cells with an endothelial genetic linage may be more appropriate for investigating the interactome of NRP1, as it represents an environment more comparable to endogenous conditions. The fact expression is so low in HEK293 cells and the cells still function appropriately, may suggest NRP1 biological activity is not as critical in these cells. Although, the data from these cells are still useful, as they represent a more general epithelial cell environment, meaning interactors of NRP1 may be identified which do not occur in endothelial cells. Similarly, the hTERT2-HUVEC expression of select proteins already known to interact with NRP1 appears higher. VEGFR2, an established co-receptor of NRP1, exhibits a 69.1 nTPM in hTERT2-HUVECs compared to 0.0 nTPM (no detectable transcripts) in HEK293 cells[595]. Again, this may imply conditions more favourable for evaluating NRP1 interactome, at least in the context of an endothelial cell environment. Of course, although mRNA expression can be an indicator of protein abundance, it does not always directly correlate with protein translation[642].

The aim of this chapter was to generate a cellular model which may be more representative of an endogenous environment of NRP1 expression. As NRP1 has mainly been investigated in the context of cardiovascular processes, an endothelial cell model was sought. An immortalised hTERT2-HUVEC cell line stably expressing NRP1-BioID2-HA was initially generated to explore the C-terminal interactome of NRP1 in an endothelial cell environment. After the generation and validation of the cell line, the scaled up proteomic experiments were performed and biotinylated proteins were isolated. These biotinylated proteins were analysed by mass spectroscopy to determine their constituents and therefore, potential novel NRP1 interacting proteins. The interactome analysis was performed in cells stimulated with $VEGF_{165}a$ and under basal conditions, the latter to elucidate potential interactors enriched independently of $VEGF_{165}a$ stimulation.

6.2 Results

6.2.1 Generation of hTERT2-HUVEC Model Expressing NRP1-BioID2-HA

6.2.1.1 Transient Nucleofection Optimisation of hTERT2-HUVEC Cells

Nucleofection has successfully been used within the lab group for transfection of hTERT2-HUVEC cells[611]. The optimisation of nucleofection in hTERT2-HUVEC cells for this project was initially performed using an empty C1-mEmerald vector (Addgene; 53975). Nucleofection was achieved using the Nucleofector® II/2b Transfection Device (Lonza; AAB-1001), with different programmes trialled to determine the optimal conditions for transfection of the hTERT2-HUVECs, (Figure 6.1). The programmes used, A-034, V-001, and U-001, utilised varying electrical pulse parameters and voltages for delivery of plasmid DNA. However, the specifics of the parameters are proprietary. In the nucleofection experiments, varying degrees of transfection efficiency was observed. As demonstrated in the C1-mEmerald channel, (Figure 6.1), successful transfection was exhibited in cells expressing C1-mEmerald. When comparing the programmes, the programme exhibiting a higher number of cells expressing C1-mEmerald, and therefore highest transfection efficiency, was A-034, followed by U-001 and V-001, respectively as the next most efficient transfection programmes. This led to the decision to use the A-034 programme, for all future hTERT2-HUVEC transfections with the NRP1-BioID2-HA construct.

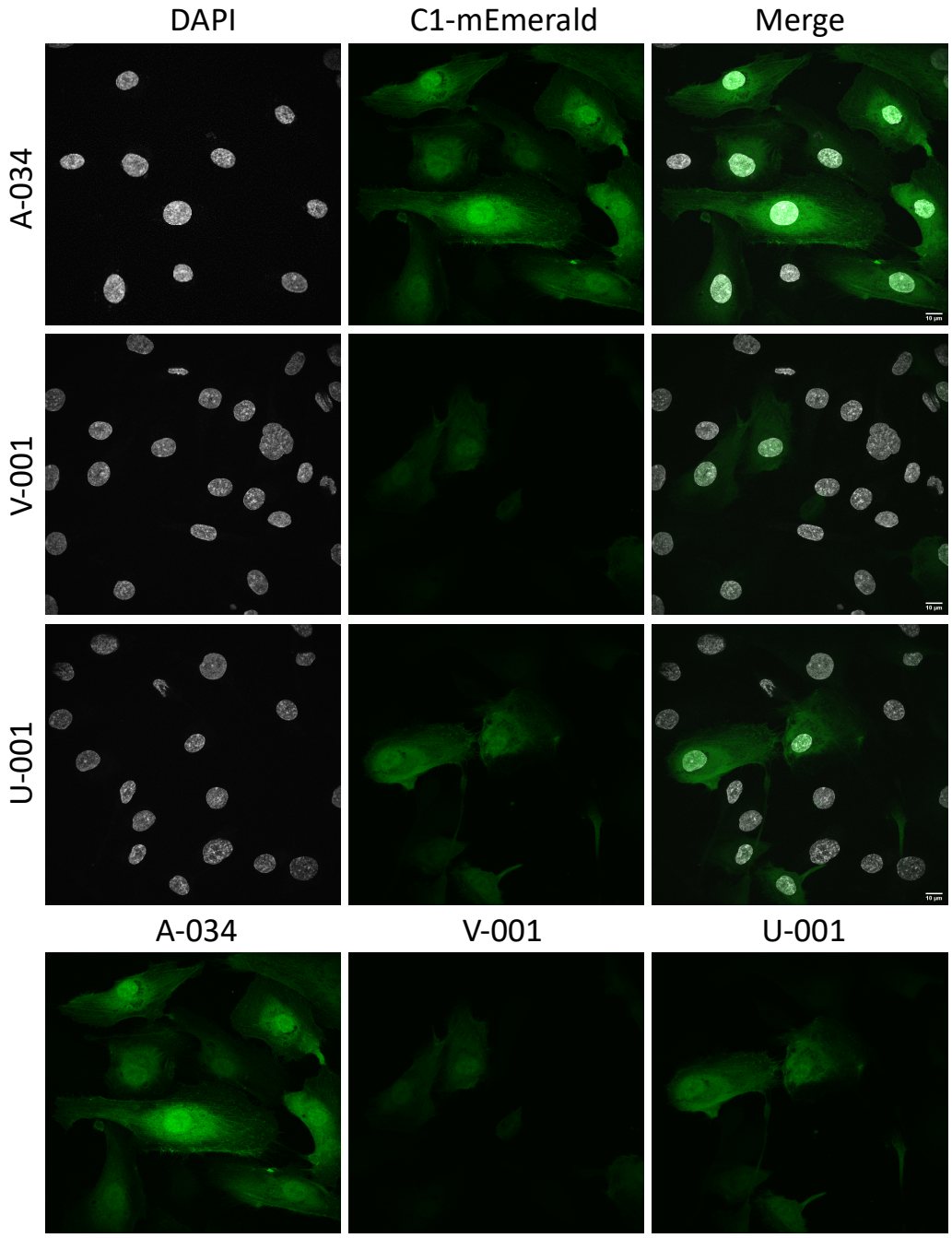

Figure 6.1 – Immunofluorescence of optimised transfection of electroporation of C1-mEmerald in hTERT2-HUVEC cells. *Cells were electroporated with C1-mEmerald plasmid using the Nucleofector® II/2b Transfection Device (Lonza; AAB-1001) with programme A-034, V-001, and U-001. Electroporated cells were seeded on to glass coverslips and cultured for 24 h before fixation and imaging. DAPI was used to highlight nuclear material and identify individual cells. Microscopy gains were kept consistent across image acquisition. The electroporation programme A-034 appeared to be the most efficient in transfecting C1-mEmerald plasmid into the hTERT2-HUVEC cells.*

6.2.1.2 Transient Nucleofection Optimisation of NRP1-BioID2-HA in hTERT2-HUVEC Cells

Following optimisation of transfection conditions using a C1-mEmerald plasmid, the same conditions were used to transiently transfect the NRP1-BioID2-HA plasmid into hTERT2-HUVEC cells, (Figure 6.2a). Using the electroporation programme A-034, successful transfection and expression of NRP1-BioID2-HA was observed. The correct localisation of the NRP1-BioID2-HA fusion protein at the membrane was indicated by immunofluorescence with anti-HA mouse antibody (Invitrogen; 2-2.2.14) and anti-mouse 594 secondary antibody (Jackson Immuno Research; 115-585-003). The biotinylation capabilities of the fusion protein when expressed in hTERT2-HUVECs was also confirmed using the streptavidin 488 direct conjugate (Invitrogen; S11223). Importantly, a stronger biotinylation signal was observed in the samples supplemented with biotin, compared to the biotin-null control. Despite successful transfection, the number of cells expressing the NRP1-BioID2-HA fusion protein was extremely low, too low for the BioID process as an insufficient number of proteins would be biotinylated. Even after copious optimisation strategies of electroporation conditions were attempted. Optimisation with various conditions relating to the U-001 electroporation programme was also attempted, to little success, (Figure 6.2b). As observed in the anti-HA 594 channel and streptavidin 488 channel, no trace of fusion protein expression was detected.

While the localisation of the fusion protein and biotinylation capabilities were promising, the poor transfection meant electroporation could not be used to generate a hTERT2-HUVEC model expressing NRP1-BioID2-HA. As the hTERT2-HUVEC cells are inherently resistant to the antibiotic G418, which is also the resistance cassette in the original NRP1-BioID2-HA plasmid, the expressing cells could not be selected with G418 addition. Hence, an alternative means of generating a hTERT2-HUVEC model with sufficient NRP1-BioID2-HA expression was sought.

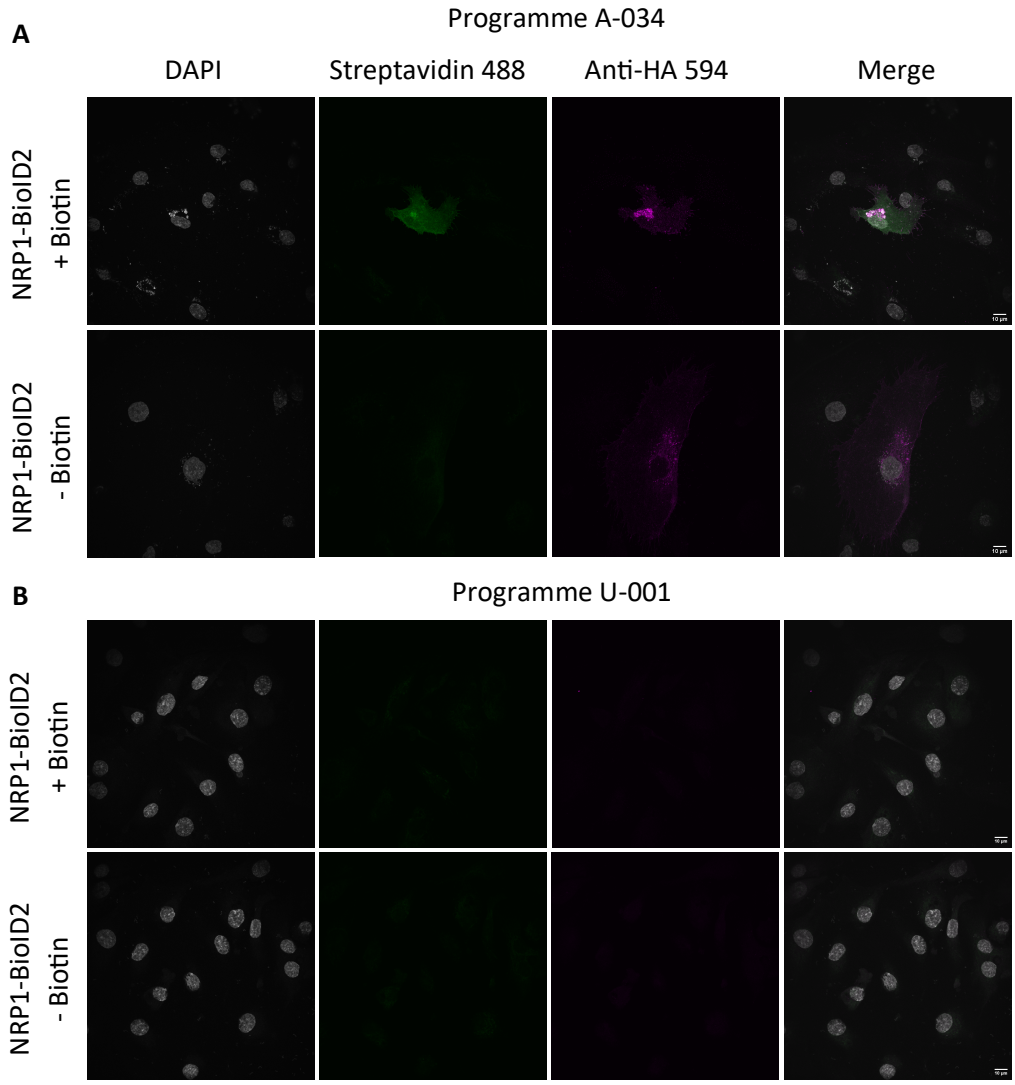

Figure 6.2 – Immunofluorescence of optimised transfection of electroporation of NRP1-BioID2-HA in hTERT2-HUVEC cells. *Cells were electroporated with NRP1-BioID2-HA plasmid using the Nucleofector® II/2b Transfection Device (Lonza; AAB-1001) with programme* ***(A)*** *A-034 or* ***(B)*** *U-001. Electroporated cells were seeded on to glass coverslips and cultured for 24 h. Cells were fixed and stained with anti-HA mouse (Invitrogen; 2-2.2.14) antibody followed by an anti-mouse 594 (Jackson Immuno Research; 115-585-003) to visualise the NRP1-BioID2-HA fusion protein. Streptavidin 488 (Invitrogen; S11223) highlighted the presence of biotinylated proteins. DAPI was used to highlight nuclear material and identify individual cells. Conditions with and without biotin supplementation were performed. Despite demonstrating correct localisation of NRP1 fusion protein and biotinylation capabilities, an extremely poor transfection efficiency was observed.*

6.2.1.3 Lentiviral Transduction Optimisation of hTERT2-HUVEC Cells with NRP1-BioID2-HA

Lentiviral technology was used to generate the appropriate hTERT2-HUVEC model. As the hTERT2-HUVEC cells are known to be sensitive to blasticidin, the same lentiviral plasmid containing NRP1-BioID2-HA discussed in section 4.2.3.2 was used for transduction. The hTERT2-HUVEC cells were incubated with varying concentrations, from 25 – 100%, of lentiviral media preparation diluted with fresh cell media and supplemented with 8 ug/mL polybrene for 72 h, (Figure 6.3). A control of polybrene only was also included. In the polybrene only control, the absence of signal in the anti-HA 594 channel indicated no detectable NRP1-BioID2-HA expression. As the concentration of lentiviral media preparation increased, the number of cells with detectable NRP1-BioID2-HA expression also increased, with the 100% lentiviral media preparation demonstrating the greatest number of cells expressing the fusion protein. Even before blasticidin selection, the number of hTERT2-HUVEC cells expressing NRP1-BioID2-HA was more than that observed for the optimal electroporation transfections, (Figure 6.3). A concentration of 100% was chosen for future lentiviral transductions.

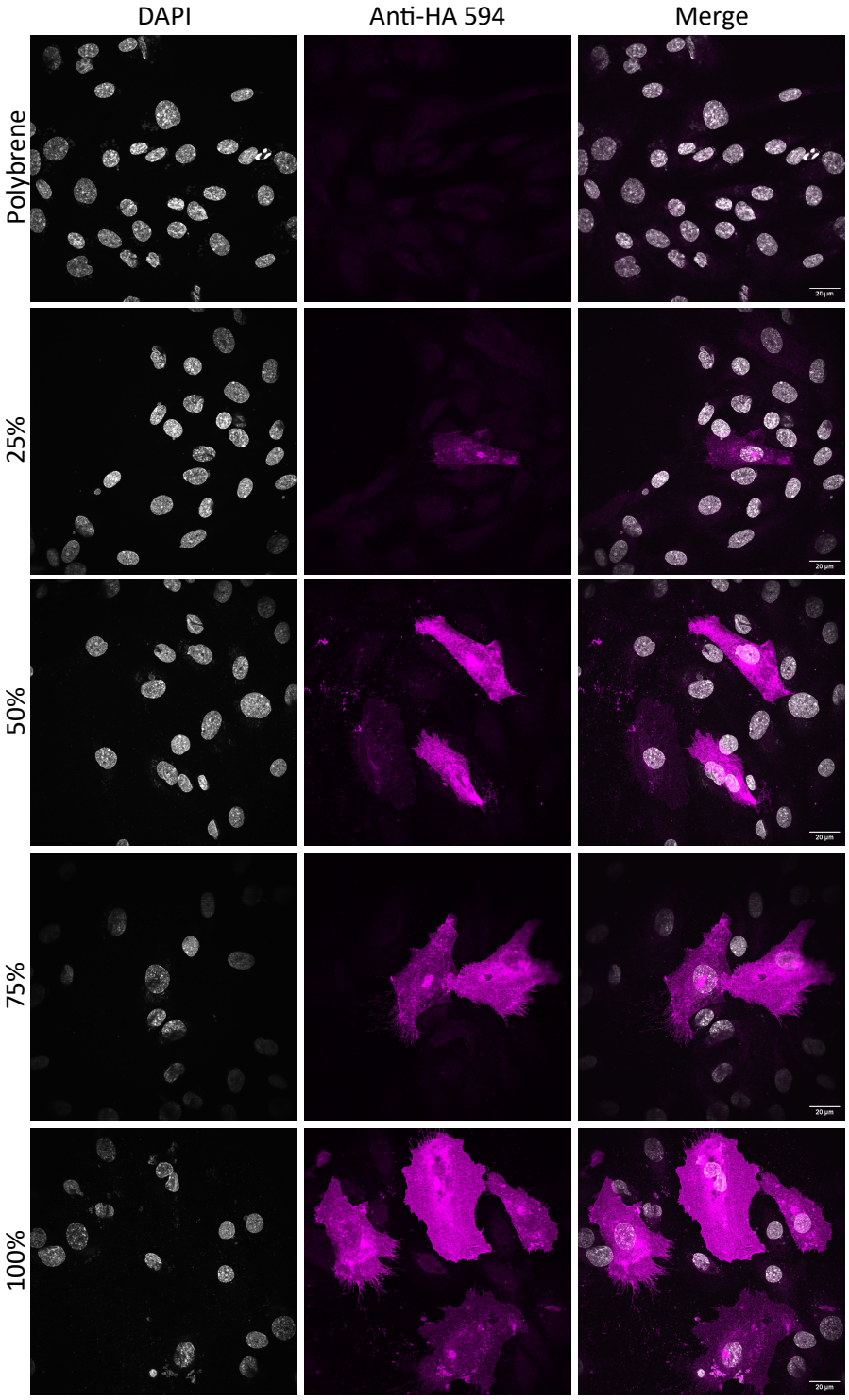

Figure 6.3 – Immunofluorescence of transduction optimisation of pLV-NRP1-BioID2-HA in hTERT2-HUVEC cells. *Cells were incubated with pLV-NRP1-BioID2-HA lentiviral preparation for 72 h at varying concentrations from 0 – 100 %. A polybrene only control was used at 8 µg/mL. Cells were fixed and stained with anti-HA mouse (Invitrogen; 2-2.2.14) antibody followed by an anti-mouse 594 (Jackson Immuno Research; 115-585-003) to visualise the NRP1-BioID2-HA fusion protein. DAPI was used to highlight nuclear material and identify individual cells.*

6.2.1.4 Expression Analysis of hTERT2-HUVEC/NRP1-BioID2-HA Stable Cells Following Blasticidin Selection

The transduced hTERT2-HUVEC cells were selected with 6 µg/mL blasticidin for 14 days and analysed for expression of NRP1-BioID2-HA, (Figure 6.4). As highlighted by the anti-HA mouse antibody and anti-mouse FITC secondary antibody, not all cells had detectable expression of NRP1-BioID2-HA. An anti-NRP1 rabbit antibody with an anti-rabbit 594 secondary antibody was used to detect fusion protein expression and endogenous expression of NRP1 in the hTERT2-HUVECs, (Figure 6.4a). The cells expressing the fusion protein correlated with the highest expression of NRP1 as expected. In cells with absent NRP1-BioID2-HA expression, indicated by signal in the anti-HA FITC channel, hTERT2-HUVEC endogenous NRP1 expression was detected in the anti-NRP1 594 channel. A parallel immunofluorescence experiment was performed to determine the nature of the hTERT2-HUVEC cells. The cells were analysed for expression of endothelial cell marker CD31, using an anti-CD31 rabbit antibody and anti-rabbit 594 secondary antibody, (Figure 6.4b). All cells in the field of view demonstrated sufficient CD31 expression, indicating the cells were still of endothelial lineage despite the genetic modifications. Regardless of blasticidin selection and maintenance of selection pressure, there were still some cells expressing insufficient NRP1-BioID2-HA. While this was the most successful expression of the fusion protein in the hTERT2-HUVECs thus far, further enrichment of the NRP1-BioID2-HA positive cells was required.

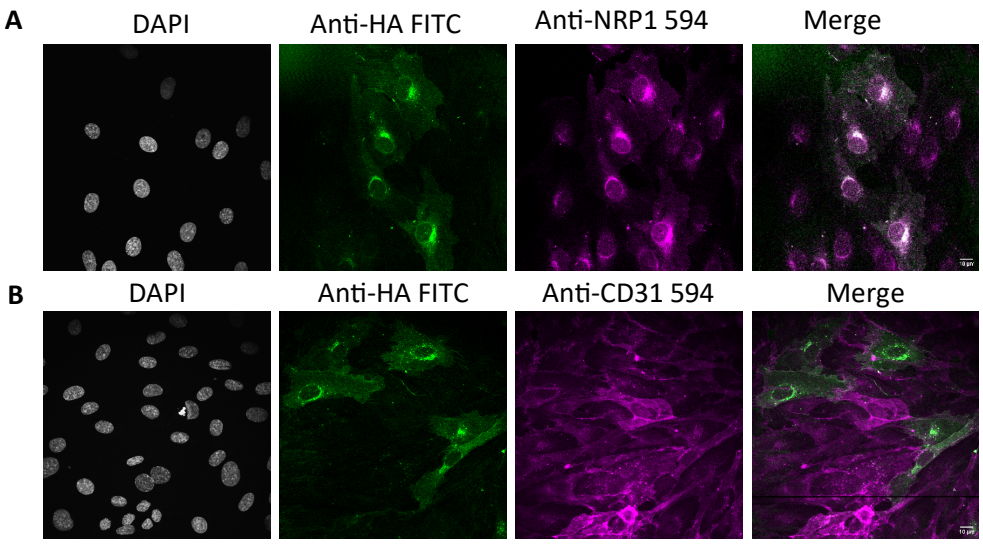

Figure 6.4 – Immunofluorescence of blasticidin selected hTERT2-HUVEC/NRP1-BioID2-HA stable cell line. *Following transduction optimisation, the transduced hTERT2-HUVEC cells were selected using 6 µg/mL blasticidin for cells expressing NRP1-BioID2-HA. Cells were fixed and stained with;* ***(A)*** *anti-HA mouse antibody (Invitrogen; 2-2.2.14) followed by an anti-mouse FITC (Jackson Immuno Research; 115-095-003) to visualise the NRP1-BioID2-HA fusion protein, and anti-NRP1 rabbit antibody (Abcam; ab81321) followed by anti-rabbit 594 antibody (Jackson Immuno Research; 111-585-003) to visualise NRP1;* ***(B)*** *anti-HA mouse antibody (Invitrogen; 2-2.2.14) followed by an anti-mouse FITC (Jackson Immuno Research; 115-095-003) to visualise the NRP1-BioID2-HA fusion protein, and anti-CD31 rabbit antibody (Invitrogen; MA5-32126) and anti-rabbit 594 antibody (Jackson Immuno Research; 111-585-003) to detect endothelial marker CD31. DAPI was used to highlight nuclear material and identify individual cells.*

6.2.1.5 Fluorescence-Activated Cell Sorting of hTERT2-HUVEC/NRP1-BioID2-HA Stable Cells

To enrich hTERT2-HUVEC cells expressing NRP1-BioID2-HA, fluorescence-activated cell sorting (FACS) was performed using an anti-NRP1 rabbit antibody (Abcam; ab81321), coupled with an anti-rabbit 594 secondary antibody (Jackson Immuno Research; 111-585-003). For the FACS, cells were sorted based on the forward scatter (FSC), side scatter (SSC) and 594 nm fluorescence, (Figure 6.5). The FSC vs SSC, (Figure 6.5a), was used to identify hTERT2-HUVEC cells and exclude potential cellular debris generated from the pre-FACS processing. The region marked R1 indicates the cells isolated. Cells were also excluded based on the SSC height vs SSC width, (Figure 6.5b). Fluorescent bodies identified with a larger SSC width are indicative of cell doublets and cellular clumps consisting of multiple cells. Hence, the region marked R2 indicates individual cells isolated and fluorescent reads to the right of this region are more likely to be bodies consisting of multiple cells. To highlight cells expressing the NRP1-BioID2-

HA, cells were also sorted based on 594 nm fluorescence, (Figure 6.5c). The region marked R4 indicates the population of cells isolated, which corresponded to the hTERT2-HUVEC cells exhibiting the highest expression of NRP1. These gated conditions resulted in a reported 135,741 cells isolated with the desired characteristics. However, the FACS conditions were unfavourable for hTERT2-HUVEC survival, demonstrated by the extensive cell death. The cells harvested were immediately supplemented with pre-warmed, fresh media and cultured with blasticidin to maintain selection pressure. The cells were cultured until population size was sufficient for analysis of NRP1-BioID2-HA expression.

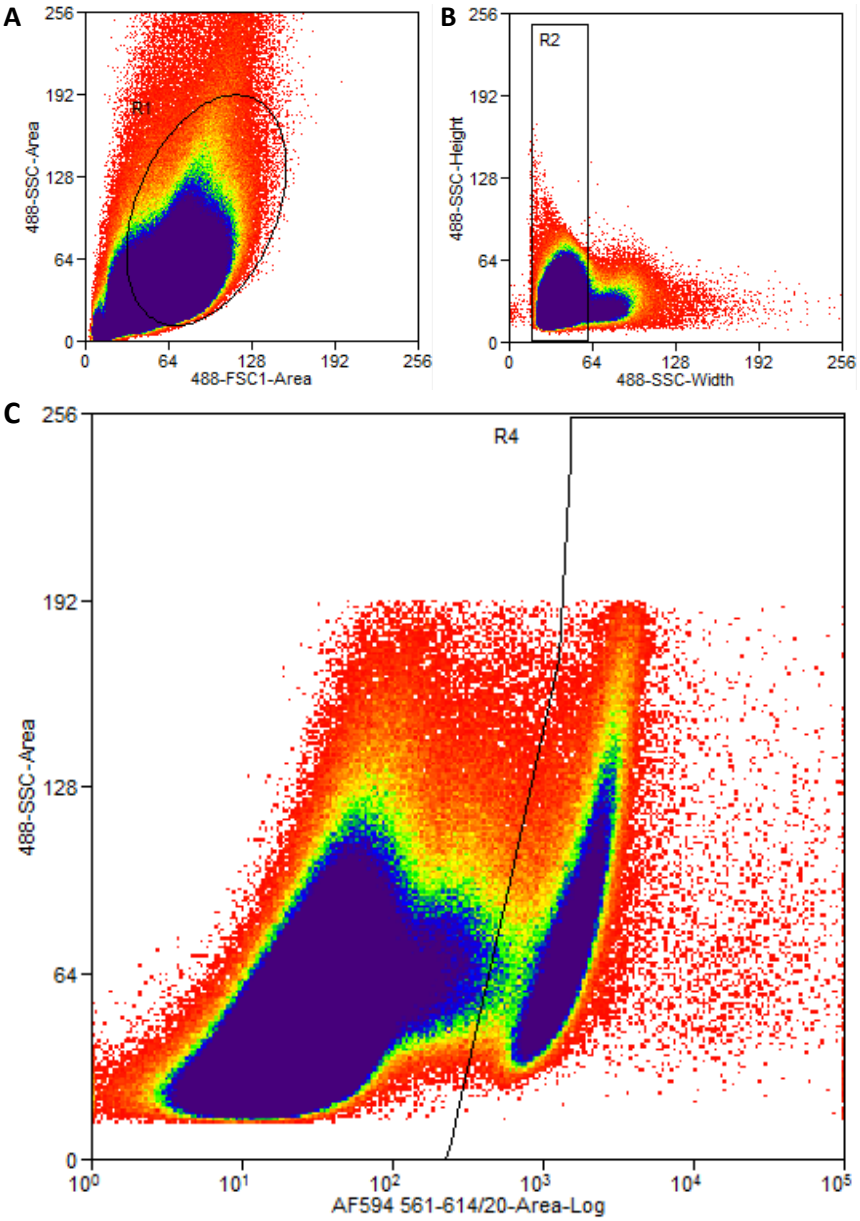

Figure 6.5 – Fluorescence-activated cell sorting (FACS) of blasticidin selected hTERT2-HUVEC/NRP1-BioID2-HA cell line. *Cells were detached using cell dissociation buffer (gibco; 13151014) and incubated with anti-NRP1 rabbit antibody (Abcam; ab81321) on ice for 20 minutes. Cells were washed and further incubated on ice for 20 minutes with anti-rabbit 594 secondary antibody, to indicate presence of NRP1-BioID2-HA. Cells were subject to FACS and isolated based on;* ***(A)*** *Forward scatter (FSC) vs side scatter (SSC), marked by the region R1.* ***(B)*** *SSC width vs SSC height, marked by the region R2.* ***(C)*** *488 vs 594 fluorescence, marked by the region R4.*

6.2.1.6 Post-FACS Expression Analysis of hTERT2-HUVEC/NRP1-BioID2-HA Stable Cells

The blasticidin selected hTERT2-HUVEC/NRP1-BioID2-HA cells were analysed for fusion protein expression following FACS isolation of cells with the highest NRP1 expression, (Figure 6.6a). The signal elicited from the anti-HA mouse antibody and anti-mouse FITC secondary antibody labelling, demonstrated sufficient expression of the NRP1-BioID2-HA fusion protein. The number of hTERT2-HUVEC cells expressing the fusion protein in the field of view, was the most numerous observed thus far. An anti-NRP1 rabbit antibody, coupled with an anti-rabbit 594 secondary antibody, revealed the signal elicited from the FITC was of NRP1 origin, as colocalisation was observed from the signals in both channels. As the hTERT2-HUVEC cells had undergone further genetic modification with the stable expression of NRP1-BioID2-HA, and subject to harsh processing for the FACS analysis, the cells were analysed for the endothelial marker CD31 to ensure cells still resembled an endothelial phenotype, (Figure 6.6b). Cells were labelled with anti-CD31 rabbit antibody and anti-rabbit 594 secondary antibody. All cells demonstrated CD31 expression, indicating the hTERT2-HUVEC/NRP1-BioID2-HA cell were still of endothelial lineage.

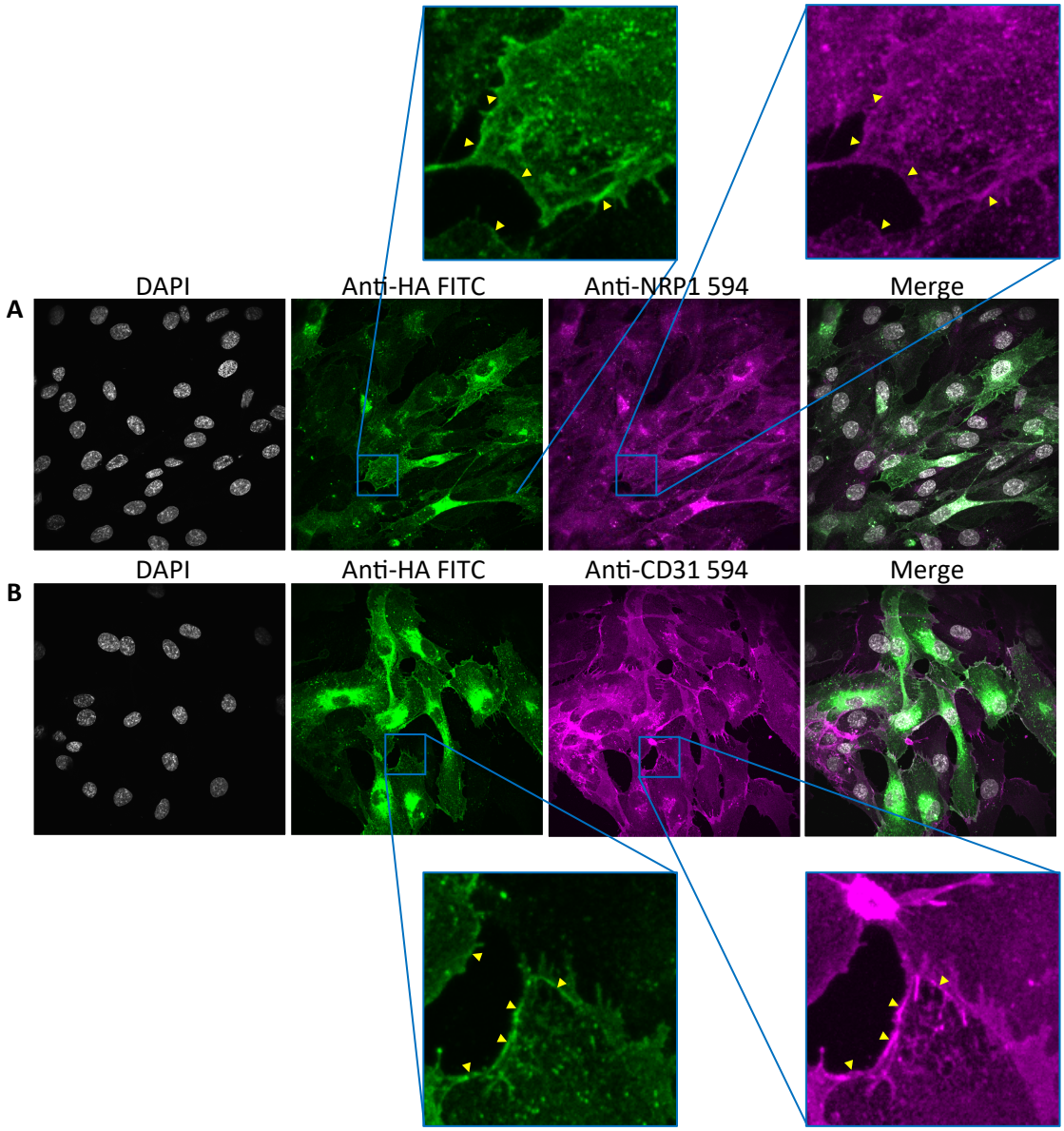

Figure 6.6 – Immunofluorescence of FAC sorted hTERT2-HUVEC/NRP1-BioID2-HA stable cell line. *Following FACS of the cells, the mixed population was cultured and analysed for co-expression of NRP1-BioID2-HA. Cells were fixed and stained with;* ***(A)*** *anti-HA mouse antibody (Invitrogen; 2-2.2.14) followed by an anti-mouse FITC (Jackson Immuno Research; 115-095-003) to visualise the NRP1-BioID2-HA fusion protein, and anti-NRP1 rabbit antibody (Abcam; ab81321) followed by anti-rabbit 594 antibody (Jackson Immuno Research; 111-585-003) to visualise NRP1;* ***(B)*** *anti-HA mouse antibody (Invitrogen; 2-2.2.14) followed by an anti-mouse FITC (Jackson Immuno Research; 115-095-003) to visualise the NRP1-BioID2-HA fusion protein, and anti-CD31 rabbit antibody (Invitrogen; MA5-32126) and anti-rabbit 594 antibody (Jackson Immuno Research; 111-585-003) to detect endothelial marker CD31. DAPI was used to highlight nuclear material and identify individual cells. Yellow arrows indicate cell membrane localisation.*

6.2.2 Optimisation of Streptavidin Pulldown of hTERT2-HUVEC/NRP1-BioID2-HA Cells

6.2.2.1 Initial Streptavidin Pulldown Attempts

As the hTERT2-HUVEC cells occupied more space when compared to HEK293T cells, cells were seeded in 2 x 10 cm dishes per condition. HUVECs exhibit a 'cobblestone' growth pattern[643], and are much flatter than HEK293T cells, with the same number of HUVECs occupying a larger space than HEK293T cells. The lysis and pulldown conditions were initially the same for as for the HEK293T cells, as described in section 4.2.1.2. Cells were treated with $VEGF_{165}$a and supplemented with biotin. Controls consisting of untreated cells and biotin-null were included, along with wild-type (WT) hTERT2-HUVEC cells not expressing the NRP1-BioID2-HA that were also supplemented with biotin. The cell lysates and material eluted from the streptavidin beads were analysed by western blotting for their contents, (Figure 6.7). The anti-HA 680 channel elicited bands at around ~150 kDa, around the expected size of NRP1-BioID2-HA. Importantly, this band was absent in the WT cell lysates which did not express the fusion protein. However, the band at around ~150 kDa was unexpectedly not present in any of the eluted materials. The streptavidin 800 channel highlighted the presence of biotinylated proteins in cell lysates and eluates. Sufficient biotinylated proteins were observed in all cell lysates relating to hTERT2-HUVEC/NRP1-BioID2-HA, demonstrating cell lysate conditions were appropriate. The biotinylation pattern in the eluates were less promising. The presence of biotinylated material in the samples with no biotin supplementation, indicated some conditions were favourable for pulldown. The samples supplemented with biotin, including WT cells, demonstrated a lack of isolation of biotinylated proteins. It was theorised the reason for this was excess free biotin in the conditions where additional biotin was supplemented to the media, despite biotin reduction of the media. An extra step in the protocol was included, to remove the excess free biotin using Zeba™ dye and biotin removal spin columns (Thermo Scientific; A44296S) prior to performing the streptavidin pulldown.

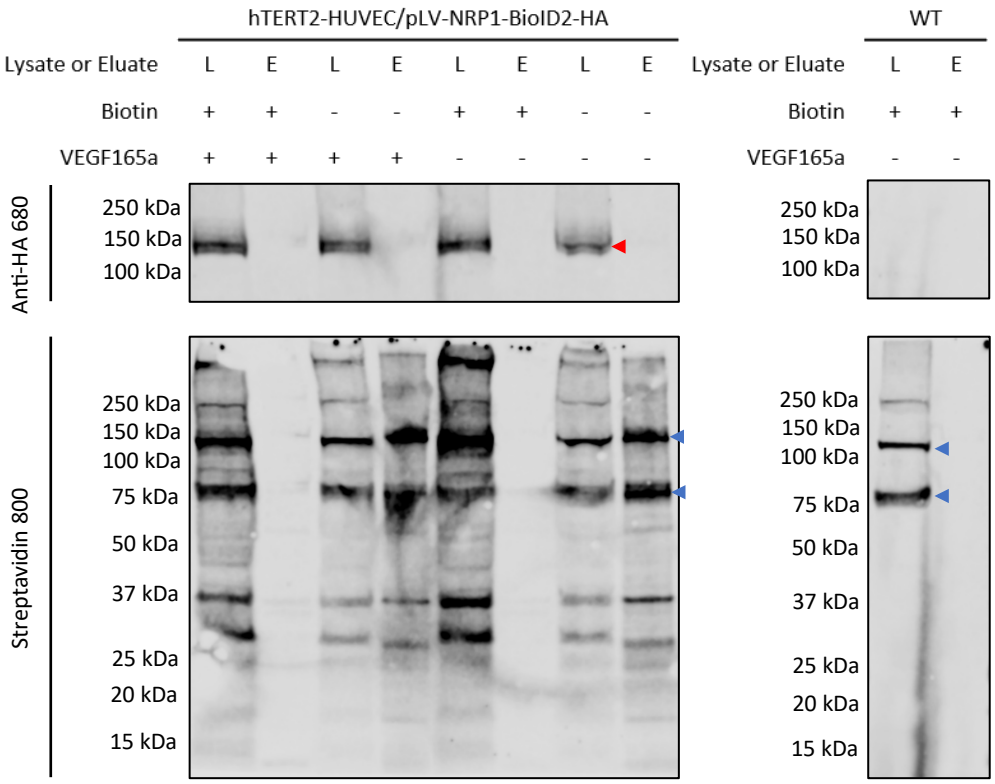

Figure 6.7 – Initial streptavidin pulldowns with hTERT2-HUVEC/NRP1-BioID2-HA stable cell line. *NRP1-BioID2-HA fusion protein was detected using an anti-HA mouse antibody (Invitrogen; 2-2.2.14) followed by an anti-mouse 680 secondary antibody (LiCOR; 926-68070). Biotinylated proteins were detected using a streptavidin 800 direct conjugate (Invitrogen; 21851). Cell lysates and corresponding pulldown material were paired. Cells were treated with $VEGF_{165}$a and biotin. Cell lysates of the original hTERT2-HUVEC WT cells without NRP1-BioID2-HA expression was also included as a control. Streptavidin 800 staining confirmed successful isolation of biotinylated proteins in conditions without biotin supplementation. However, no biotinylated proteins were isolated in samples supplemented with biotin. Bands indicated by the red arrows at ~150 kDa in the Anti-HA 680 channel correspond to the NRP1-BioID2-HA fusion protein. Bands indicated by the blue arrows were likely pyruvate carboxylase contaminants. The bands present in the NRP1-BioID2-HA expressing cells and not the hTERT2-HUVEC WT samples confirms its identity as NRP1-BioID2-HA.*

6.2.2.2 Optimised Streptavidin Pulldown

The removal of biotin from the cell lysates using Zeba™ dye and biotin removal spin columns (Thermo Scientific; A44296S) prior to streptavidin pulldown, yielded improved results, (Figure 6.8). The anti-HA 680 channel elicited bands around ~150 kDa in the conditions with NRP1-BioID2-HA expression. These bands correlated with the expected size of the NRP1-BioID2-HA fusion protein. Unlike the previous streptavidin pulldown attempts, (Figure 6.7), these bands were present in the eluates of biotin supplemented samples, indicating successful isolation of biotinylated material. Additionally, lower bands at ~75 kDa were also present in all cell lysates, including the WT samples, indicating a contaminant which the anti-HA antibody binds to. The biotinylation pattern, observed in the

streptavidin 800 channel, demonstrated the successful isolation of biotinylated proteins in all conditions. The characteristic smear pattern was observed for samples supplemented with biotin and was slightly visible with the biotin-null samples, suggesting residual biotin in the media despite the biotin depletion. The eluates containing the isolated biotinylated proteins were analysed by mass spectrometry to determine their constituents and therefore, potential NRP1-interactors in hTERT2-HUVEC cells.

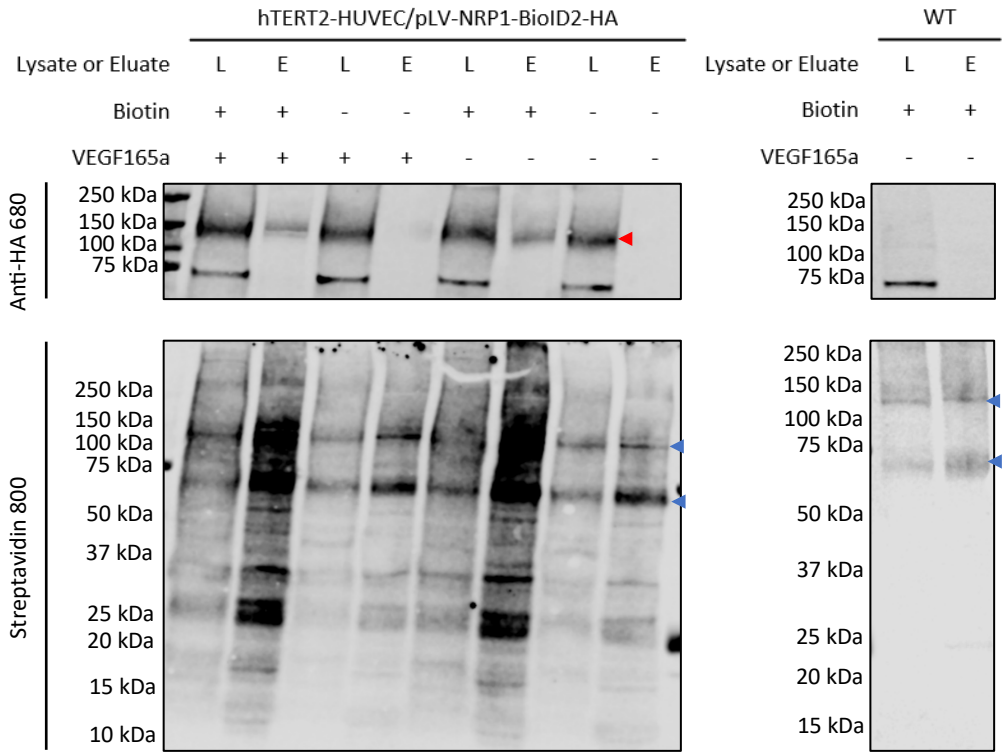

Figure 6.8 – Optimised streptavidin pulldown with hTERT2-HUVEC/NRP1-BioID2-HA stable cell line. *NRP1-BioID2-HA fusion protein was detected using an anti-HA mouse antibody (Invitrogen; 2-2.2.14) followed by an anti-mouse 680 secondary antibody (LiCOR; 926-68070). Biotinylated proteins were detected using a streptavidin 800 direct conjugate (Invitrogen; 21851). Cell lysates and corresponding pulldown material were paired. Cells were treated with $VEGF_{165}a$ and biotin. Cell lysates of the original hTERT2-HUVEC WT cells without NRP1-BioID2-HA expression was also included as a control. Streptavidin 800 staining confirmed successful isolation of biotinylated proteins, indicated by strong signals in the eluate samples of the biotin supplemented conditions. Bands indicated by the red arrow at ~150 kDa in the Anti-HA 680 channel correspond to the NRP1-BioID2-HA fusion protein. Bands indicated by the blue arrows were likely pyruvate carboxylase contaminants. The bands present in the NRP1-BioID2-HA expressing cells and not the hTERT2-HUVEC WT samples confirmed its identity as NRP1-BioID2-HA.*

6.2.3 BioID Bioinformatic Analyses using hTERT2-HUVEC/NRP1-BioID2-HA Stable Cells

The bioinformatic analyses elicited several potential interactors, although the results must be viewed in the context of a single repeat. The majority of the enriched proteins were unique to either the $VEGF_{165}$a stimulated or basal conditions. These results are summarised in (Figure 6.9). A more detailed investigation of the proteins enriched in each condition is then discussed, along with further gene ontology analyses.

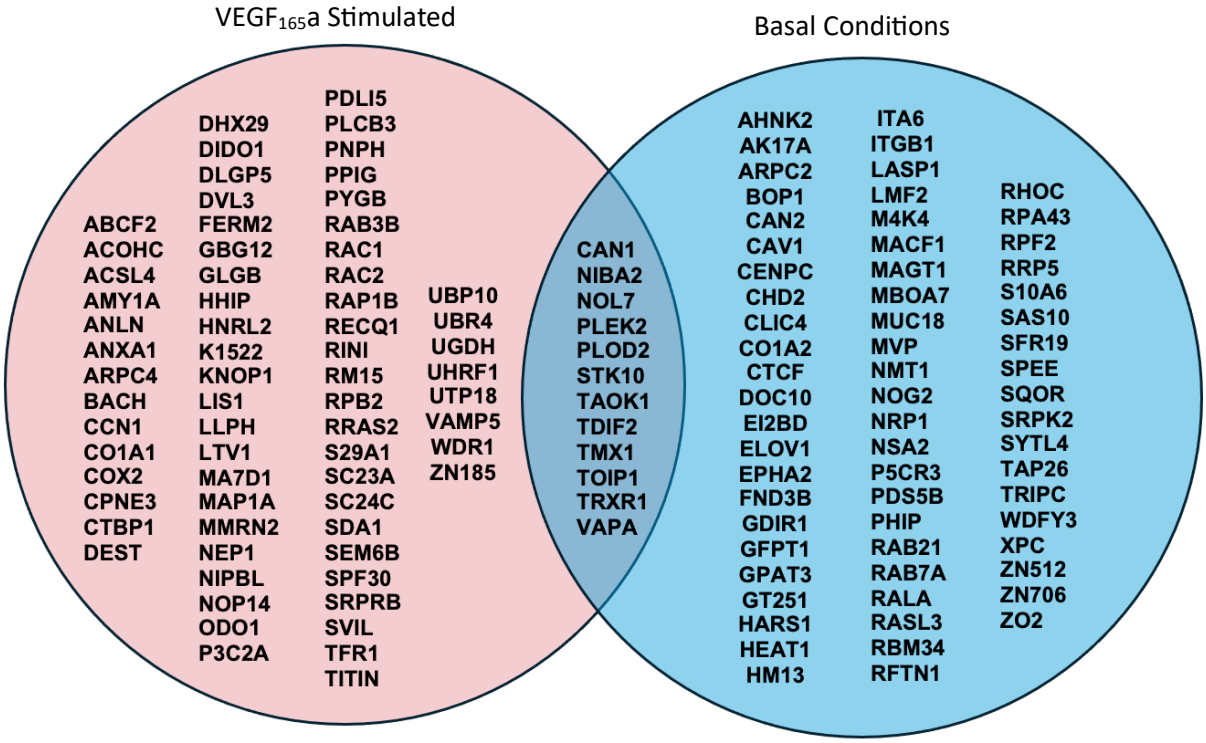

Figure 6.9 – A summary of the enriched proteins in the NRP1-BioID2-HA bioinformatic analyses in both $VEGF_{165}$a stimulated and basal conditions in hTERT2/HUVEC cells. For the $VEGF_{165}$a stimulated conditions**,** 80 proteins were identified as potential NRP1 interactors, with 68 of these unique to $VEGF_{165}$a stimulation. The basal conditions elicited 76 enriched proteins, with 64 of these unique to the basal conditions. There were 12 enriched proteins common between both conditions.

6.2.3.1 Enriched Proteins in hTERT2-HUVEC/NRP1-BioID2-HA Cells Stimulated with VEGF165a Analyses

The isolated biotinylated proteins were sent for mass spectrometry analyses and raw files were processed by the optimised method discussed in section 4.2.1. Due to time and funding constraints, mass spectrometry results were only possible for one repeat in this instance, unlike for the HEK293T samples. The repeat revealed 80 enriched proteins when hTERT2-HUVEC/NRP1-BioID2-HA cells were treated with $VEGF_{165}a$, Table 6.1. The absolute number of proteins in this repeat was fewer than any of the repeats elicited for the HEK293T samples, discussed in section 4.2.2.4. As only 1 repeat was possible, statistical analysis on riBAQ values was not possible.

Table 6.1 – Enriched protein list in hTERT2-HUVEC/NRP1-BioID2-HA treated with $VEGF_{165}a$ after 1 repeat. *The enriched protein list following a single repeat consisted of 80 unique proteins. Proteins unique to $VEGF_{165}a$ treated and supplemented with biotin conditions were included in the final list. Proteins with a 1.5-fold increase of calculated riBAQ in this condition, compared to the controls, were also included in this list. Proteins with a >20% frequency in HEK293T cells associated with proximity-biotinylation identified in the CRAPome were excluded from the final list.*

UniProt ID	Gene Name	Protein Name	Protein Score
P13489	RINI	Ribonuclease inhibitor	96.05
Q9NVU7	SDA1	Protein SDA1 homolog	64.31
O94804	STK10	Serine/threonine-protein kinase 10	61.69
Q1ED39	KNOP1	Lysine-rich nucleolar protein 1	59.55
Q96QV1	HHIP	Hedgehog-interacting protein	54.82
Q3KQU3	MA7D1	MAP7 domain-containing protein 1	53.01
P15153	RAC2	Ras-related C3 botulinum toxin substrate 2	48.79
Q96HC4	PDLI5	PDZ and LIM domain protein 5	48.59
Q9BTC0	DIDO1	Death-inducer obliterator 1	43.70
Q9UG63	ABCF2	ATP-binding cassette sub-family F member 2	41.91
Q96AC1	FERM2	Fermitin family homolog 2	40.80
P00491	PNPH	Purine nucleoside phosphorylase	39.14
P78316	NOP14	Nucleolar protein 14	38.69
Q01970	PLCB3	1-phosphatidylinositol 4,5-bisphosphate phosphodiesterase beta-3	38.29
P46063	RECQ1	ATP-dependent DNA helicase Q1	35.88
Q9UMY1	NOL7	Nucleolar protein 7	34.86
Q96TA1	NIBA2	Protein Niban 2	34.55
Q7Z478	DHX29	ATP-dependent RNA helicase DHX29	33.66
Q02218	ODO1	2-oxoglutarate dehydrogenase complex component E1	31.29
Q7L7X3	TAOK1	Serine/threonine-protein kinase TAO1	30.77
Q9NYT0	PLEK2	Pleckstrin-2	30.64
Q1KMD3	HNRL2	Heterogeneous nuclear ribonucleoprotein U-like protein 2	29.31
Q9Y5M8	SRPRB	Signal recognition particle receptor subunit beta	24.81
P07384	CAN1	Calpain-1 catalytic subunit	24.43

Q9H3N1	TMX1	Thioredoxin-related transmembrane protein 1	24.00
Q5T4S7	UBR4	E3 ubiquitin-protein ligase UBR4	23.08
Q14694	UBP10	Ubiquitin carboxyl-terminal hydrolase 10	22.77
Q96GA3	LTV1	Protein LTV1 homolog	21.94
P61224	RAP1B	Ras-related protein Rap-1b	20.69
O00469	PLOD2	Procollagen-lysine,2-oxoglutarate 5-dioxygenase 2	20.68
P04083	ANXA1	Annexin A1	20.51
O60488	ACSL4	Long-chain-fatty-acid--CoA ligase 4	20.30
Q15398	DLGP5	Disks large-associated protein 5	19.74
P63000	RAC1	Ras-related C3 botulinum toxin substrate 1	19.71
Q16881	TRXR1	Thioredoxin reductase 1, cytoplasmic	19.51
Q15436	SC23A	Protein transport protein Sec23A	19.45
P60981	DEST	Destrin	19.30
Q13427	PPIG	Peptidyl-prolyl cis-trans isomerase G	19.15
Q9Y5J1	UTP18	U3 small nucleolar RNA-associated protein 18 homolog	19.08
Q9P0L0	VAPA	Vesicle-associated membrane protein-associated protein A	18.95
Q5QJE6	TDIF2	Deoxynucleotidyltransferase terminal-interacting protein 2	18.64
O15231	ZN185	Zinc finger protein 185	18.08
O95425	SVIL	Supervillin	18.03
P78559	MAP1A	Microtubule-associated protein 1A	18.02
P21399	ACOHC	Cytoplasmic aconitate hydratase	17.24
Q9P015	RM15	Large ribosomal subunit protein uL15m	16.57
O00154	BACH	Cytosolic acyl coenzyme A thioester hydrolase	15.10
P43034	LIS1	Platelet-activating factor acetylhydrolase IB subunit beta	14.58
O75083	WDR1	WD repeat-containing protein 1	14.10
P00403	COX2	Cytochrome c oxidase subunit 2	14.06
Q92997	DVL3	Segment polarity protein dishevelled homolog DVL-3	13.78
O95183	VAMP5	Vesicle-associated membrane protein 5	13.75
Q9BRT6	LLPH	Protein LLP homolog	13.74
P0DUB6	AMY1A	Alpha-amylase 1A	13.60
Q99808	S29A1	Equilibrative nucleoside transporter 1	13.12
P62070	RRAS2	Ras-related protein R-Ras2	13.06
Q92979	NEP1	Ribosomal RNA small subunit methyltransferase NEP1	12.84
P59998	ARPC4	Actin-related protein 2/3 complex subunit 4	12.61
P20337	RAB3B	Ras-related protein Rab-3B	12.51
P02786	TFR1	Transferrin receptor protein 1	12.43
P02452	CO1A1	Collagen alpha-1(I) chain	12.32
O60701	UGDH	UDP-glucose 6-dehydrogenase	12.22
Q9UBI6	GBG12	Guanine nucleotide-binding protein G(I)/G(S)/G(O) subunit gamma-12	12.13
P11216	PYGB	Glycogen phosphorylase, brain form	12.00
Q9H8L6	MMRN2	Multimerin-2	11.93
Q6KC79	NIPBL	Nipped-B-like protein	11.88
Q13363	CTBP1	C-terminal-binding protein 1	11.81

P30876	RPB2	DNA-directed RNA polymerase II subunit RPB2	11.75
O00443	P3C2A	Phosphatidylinositol 4-phosphate 3-kinase C2 domain-containing subunit alpha	11.53
Q96T88	UHRF1	E3 ubiquitin-protein ligase UHRF1	11.44
Q5JTV8	TOIP1	Torsin-1A-interacting protein 1	11.43
O00622	CCN1	CCN family member 1	11.39
O75940	SPF30	Survival of motor neuron-related-splicing factor 30	11.39
O75131	CPNE3	Copine-3	11.29
Q9NQW6	ANLN	Anillin	11.13
P53992	SC24C	Protein transport protein Sec24C	10.99
Q9H3T3	SEM6B	Semaphorin-6B	10.86
Q04446	GLGB	1,4-alpha-glucan-branching enzyme	10.84
Q8WZ42	TITIN	Titin	10.74
Q9P206	K1522	Uncharacterized protein KIAA1522	10.68

6.2.3.2 Gene Ontology Analyses of Enriched Protein List for hTERT2-HUVEC/NRP1-BioID2-HA, $VEGF_{165}a$ Stimulated Conditions.

The gene ontology (GO) analyses were performed as per section 4.2.2.5, for the protein list elucidated in the hTERT2-HUVEC analyses, Table 6.1. The enrichment ratio (ER) was plotted against the enriched GO terms identified. Despite the identification of 80 proteins in this analysis, enrichment of specific GO terms was sparse. There appeared to be no significantly enriched GO terms relating to molecular function or biological processes. Concerning the cellular component GO analysis, (Figure 6.10a), the summary data indicated the most enriched GO parent terms related to terms such as the membrane, vesicles, and endosomes, in line with the GO analysis for the HEK293T cells, (Figure 4.15a). However, when investigating specific GO terms, only 1 term was enriched, (Figure 6.10b). The term related to the preribosome (ER = 12.21).

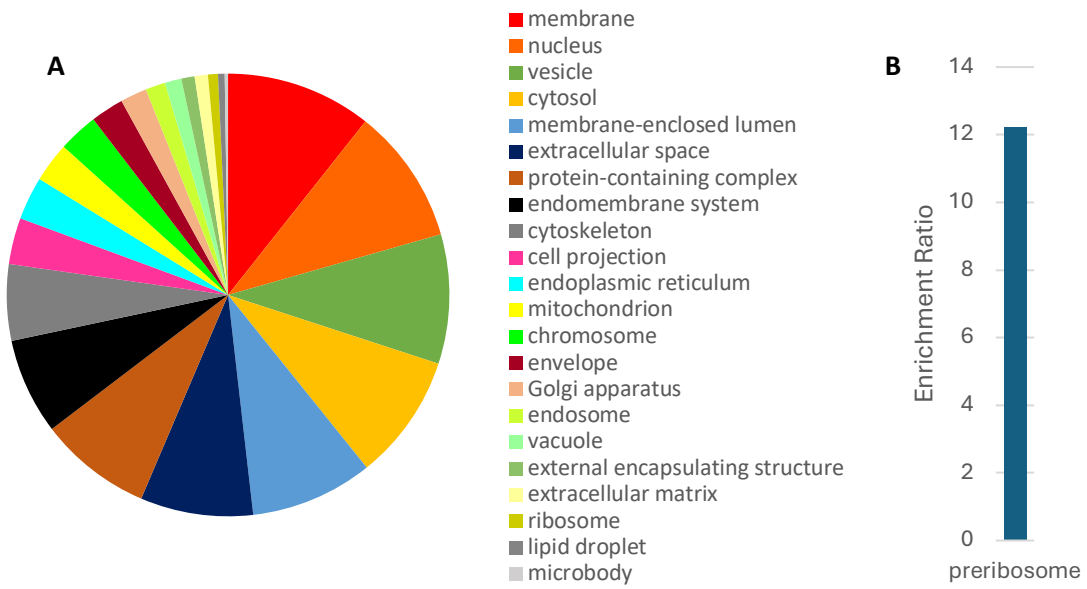

Figure 6.10 – Cellular component gene ontology (GO) analysis of enriched proteins for hTERT2-HUVEC/NRP1-BioID2-HA cells treated with $VEGF_{165}a$. *Protein lists were analysed by an overrepresentation analysis using Webgestalt, filtering for redundant GO terms. The enriched list was cross-referenced against cellular component GO terms, which describe localisation of the protein within the cellular environment. Enriched terms with a significance level > 0.05 were excluded. The GO terms were ranked based on enrichment ratio (ER), a ratio between the expected number of proteins present for a specific GO term based on a random set of proteins vs the input proteins.* ***(A)*** *The summary data represents parent GO terms which were enriched.* ***(B)*** *The cellular component GO analysis relating to the enrichment of specific GO child terms.*

6.2.3.3 Enriched Proteins in hTERT2-HUVEC/NRP1-BioID2-HA Cells in Basal Conditions Analyses

Similar to previous analyses, the raw files were processed to elucidate potential NRP1-interactors which occurred independently of $VEGF_{165}a$. These potential interactors were elucidated using the hTERT2-HUVEC/NRP1-BioID2-HA in basal conditions. Like all previous analyses, riBAQ was used in fold calculations and subsequently to determine enriched proteins. A total of 76 proteins were identified, Table 6.2, again, much fewer proteins than observed in the HEK293T samples in basal conditions, discussed in section 4.2.2.6. Interestingly, fewer proteins were observed for the basal conditions, compared to the $VEGF_{165}a$ stimulated conditions, which have not been observed previously.

Table 6.2 – Enriched protein list in hTERT2-HUVEC/NRP1-BioID2-HA under basal conditions after 1 repeat. *The enriched protein list following a single repeat consisted of 76 unique proteins. Proteins unique to $VEGF_{165}a$ treated and supplemented with biotin conditions were included in the final list. Proteins with a 1.5-fold increase of calculated riBAQ in this condition, compared to the controls, were also included in this list. Proteins with a >20% frequency in HEK293 cells associated with proximity-biotinylation identified in the CRAPome were excluded from the final list.*

UniProt ID	Gene Name	Protein Name	Protein Score
Q86YV0	RASL3	RAS protein activator like-3	163.05
Q9UPN3	MACF1	Microtubule-actin cross-linking factor 1, isoforms 1/2/3/4/5	149.89
O14786	NRP1	Neuropilin-1	117.34
Q9UI10	EI2BD	Translation initiation factor eIF-2B subunit delta	86.01
Q14669	TRIPC	E3 ubiquitin-protein ligase TRIP12	72.02
Q14690	RRP5	Protein RRP5 homolog	59.17
Q13823	NOG2	Nucleolar GTP-binding protein 2	54.87
O94804	STK10	Serine/threonine-protein kinase 10	54.58
P51149	RAB7A	Ras-related protein Rab-7a	52.17
Q8IVF2	AHNK2	Protein AHNAK2	47.98
Q96N66	MBOA7	Lysophospholipid acyltransferase 7	46.69
Q02040	AK17A	A-kinase anchor protein 17A	38.33
Q8IZQ1	WDFY3	WD repeat and FYVE domain-containing protein 3	37.14
O95819	M4K4	Mitogen-activated protein kinase kinase kinase kinase 4	36.92
Q8WWQ0	PHIP	PH-interacting protein	34.67
P17655	CAN2	Calpain-2 catalytic subunit	32.92
Q01831	XPC	DNA repair protein complementing XP-C cells	31.67
P30419	NMT1	Glycylpeptide N-tetradecanoyltransferase 1	30.59
P08123	CO1A2	Collagen alpha-2(I) chain	28.89
Q9UL25	RAB21	Ras-related protein Rab-21	28.84
Q9H7B2	RPF2	Ribosome production factor 2 homolog	27.83
Q96TA1	NIBA2	Protein Niban 2	27.57
Q96ME7	ZN512	Zinc finger protein 512	26.87
P05556	ITGB1	Integrin beta-1	26.56
P11233	RALA	Ras-related protein Ral-A	24.65
Q14699	RFTN1	Raftlin	24.26
Q9UDY2	ZO2	Tight junction protein ZO-2	23.27
P42696	RBM34	RNA-binding protein 34	22.88
Q06210	GFPT1	Glutamine--fructose-6-phosphate aminotransferase [isomerizing] 1	22.05
P08134	RHOC	Rho-related GTP-binding protein RhoC	21.43
Q96C24	SYTL4	Synaptotagmin-like protein 4	21.17
Q53EP0	FND3B	Fibronectin type III domain-containing protein 3B	21.14
P43121	MUC18	Cell surface glycoprotein MUC18	20.67
Q7L7X3	TAOK1	Serine/threonine-protein kinase TAO1	18.75
Q9BU23	LMF2	Lipase maturation factor 2	18.50
O95478	NSA2	Ribosome biogenesis protein NSA2 homolog	18.15
P49711	CTCF	Transcriptional repressor CTCF	18.00
Q9NQZ2	SAS10	Something about silencing protein 10	17.83
P23229	ITA6	Integrin alpha-6	17.68

Q9Y6N5	SQOR	Sulfide:quinone oxidoreductase, mitochondrial	17.55
Q9BW60	ELOV1	Elongation of very long chain fatty acids protein 1	17.41
Q5QJE6	TDIF2	Deoxynucleotidyltransferase terminal-interacting protein 2	17.41
Q9H583	HEAT1	HEAT repeat-containing protein 1	17.35
P78362	SRPK2	SRSF protein kinase 2	17.24
Q03135	CAV1	Caveolin-1	17.01
Q9Y696	CLIC4	Chloride intracellular channel protein 4	16.89
Q53EU6	GPAT3	Glycerol-3-phosphate acyltransferase 3	15.27
O15144	ARPC2	Actin-related protein 2/3 complex subunit 2	15.18
P52565	GDIR1	Rho GDP-dissociation inhibitor 1	13.57
Q9H3N1	TMX1	Thioredoxin-related transmembrane protein 1	13.49
P12081	HARS1	Histidine--tRNA ligase, cytoplasmic	12.98
P06703	S10A6	Protein S100-A6	12.97
Q03188	CENPC	Centromere protein C	12.52
Q14847	LASP1	LIM and SH3 domain protein 1	12.46
P19623	SPEE	Spermidine synthase	12.37
Q53H96	P5CR3	Pyrroline-5-carboxylate reductase 3	12.26
O14647	CHD2	Chromodomain-helicase-DNA-binding protein 2	12.21
Q9H7N4	SFR19	Splicing factor, arginine/serine-rich 19	12.19
Q8NBJ5	GT251	Procollagen galactosyltransferase 1	12.17
Q9NYT0	PLEK2	Pleckstrin-2	12.15
Q9NTI5	PDS5B	Sister chromatid cohesion protein PDS5 homolog B	12.12
O00469	PLOD2	Procollagen-lysine,2-oxoglutarate 5-dioxygenase 2	12.04
Q3B726	RPA43	DNA-directed RNA polymerase I subunit RPA43	11.92
Q9UMY1	NOL7	Nucleolar protein 7	11.88
Q14137	BOP1	Ribosome biogenesis protein BOP1	11.87
P07384	CAN1	Calpain-1 catalytic subunit	11.65
Q9Y5V0	ZN706	Zinc finger protein 706	11.52
Q9P031	TAP26	Thyroid transcription factor 1-associated protein 26	11.47
Q9H0U3	MAGT1	Magnesium transporter protein 1	11.31
Q96BY6	DOC10	Dedicator of cytokinesis protein 10	11.29
Q14764	MVP	Major vault protein	11.24
Q8TCT9	HM13	Minor histocompatibility antigen H13	11.08
Q9P0L0	VAPA	Vesicle-associated membrane protein-associated protein A	11.08
P29317	EPHA2	Ephrin type-A receptor 2	10.97
Q5JTV8	TOIP1	Torsin-1A-interacting protein 1	10.90
Q16881	TRXR1	Thioredoxin reductase 1, cytoplasmic	10.82

6.2.3.4 Gene Ontology Analyses of Enriched Protein List for hTERT2-HUVEC/NRP1-BioID2-HA in Basal Conditions

The GO analyses of the enriched proteins from the hTERT2-HUVEC/NRP1-BioID2-HA analyses were performed as described in section 4.2.2.5. Despite the fewer proteins identified in the samples subject to basal conditions, compared to the $VEGF_{165}$ stimulated conditions, there were more specific GO

terms enriched in the GO analysis relating to molecular function, biological processes, and the cellular component.

Molecular Function Gene Ontology Analysis

The summary data, (Figure 6.11a), revealed enriched GO parent terms similar to the summary data elicited in the HEK293T GO analysis, (Figure 4.17a). The most enriched GO parent term relates to protein binding (n = 61), the same GO term is the highest enriched term in the HEK293T data. Likewise, other parent GO terms are highly enriched in both. These included ion binding (n = 30), nucleic acid binding (n = 25), nucleotide binding (n = 14), and lipid binding (n = 4). Concerning the specific GO terms analysis, only 1 GO term was enriched, (Figure 6.11b). The term related to cadherin binding (ER = 5.66), a term which was enriched in all molecular function GO analyses of HEK293T samples, (Figure 4.13b and Figure 4.17b).

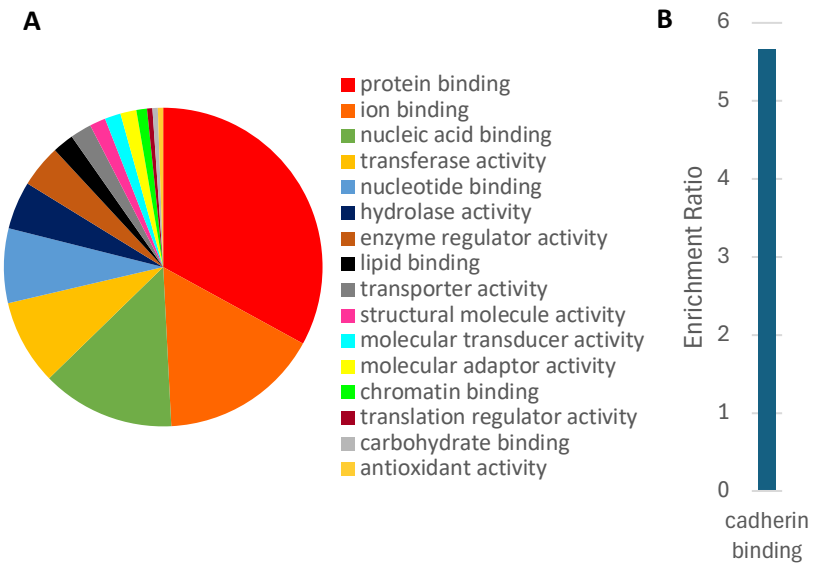

Figure 6.11 – Molecular function gene ontology (GO) analysis of enriched proteins for hTERT2-HUVEC/NRP1-BioID2-HA under basal conditions. *Protein lists were analysed by an overrepresentation analysis using Webgestalt, filtering for redundant GO terms. The enriched list was cross-referenced against molecular function GO terms, which describe the fundamental molecular activity of proteins. Enriched terms with a significance level > 0.05 were excluded. The GO terms were ranked based on enrichment ratio (ER), a ratio between the expected number of proteins present for a specific GO term based on a random set of proteins vs the input proteins.* ***(A)*** *The summary data represents parent GO terms which were enriched.* ***(B)*** *The molecular function GO analysis relating to the enrichment of specific GO child terms.*

Biological Processes Gene Ontology Analysis

The summary data of the biological processes GO analysis using the hTERT2-HUVEC/NRP1-BioID2-HA cells, (Figure 6.12a), again demonstrated similarities with the HEK293T results, (Figure 4.14a). Common enriched GO parent terms between the datasets were metabolic processes (n = 53), biological regulation (n = 53), response to stimulus (n = 45) and cellular component organization (n = 35). The starkest differences between the HEK293T and hTERT2-HUVEC GO analysis were apparent in the more specific child GO terms which were enriched. While the hTERT2-HUVEC GO analysis revealed 3 enriched child terms, (Figure 6.12b), the HEK293T counterpart boasted 57 enriched GO terms, (Figure 4.18b), perhaps reflective of the increased number of proteins enriched in the HEK293T bioinformatic analysis. For 2 of the 3 enriched GO terms, these were unique to the hTERT2-HUVEC analysis. The unique terms were rRNA metabolic process (ER = 7.18) and ribonucleoprotein complex biogenesis (ER = 5.64). The other enriched term, small GTPase mediated signal transduction (ER = 4.68), was common in both the hTERT2-HUVEC and HEK293T biological processes GO analyses.

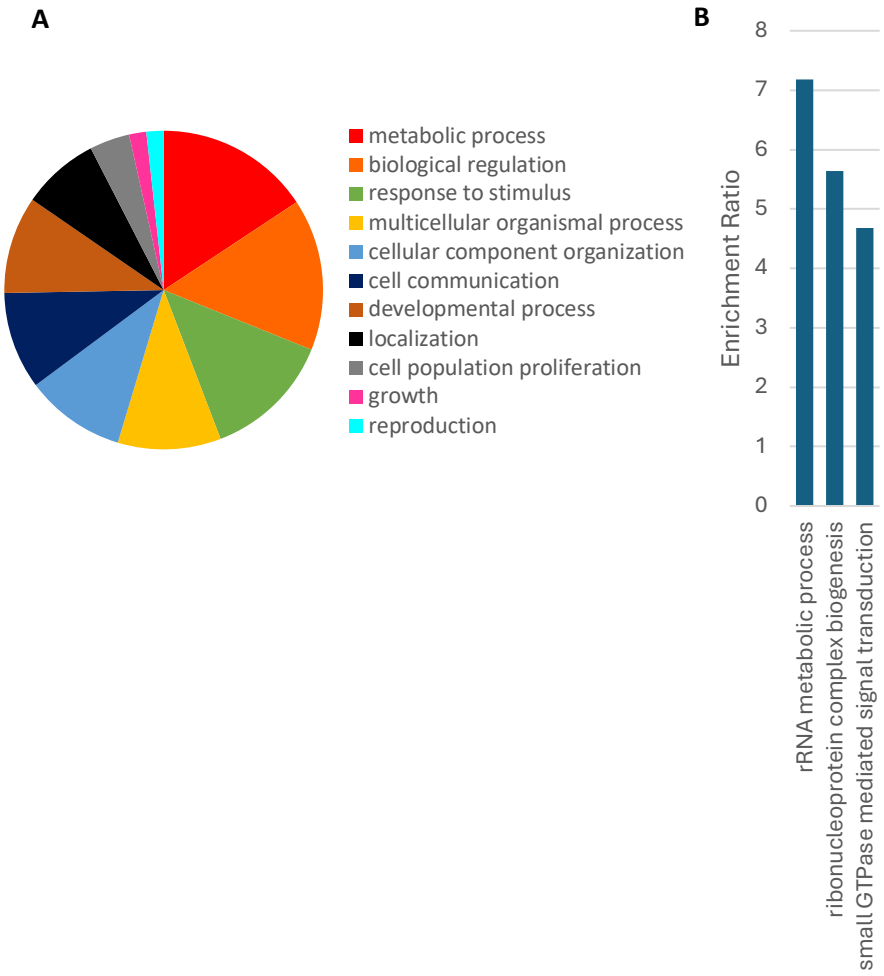

Figure 6.12 – Biological processes gene ontology (GO) analysis of enriched proteins for hTERT2-HUVEC/NRP1-BioID2-HA under basal conditions. *Protein lists were analysed by an overrepresentation analysis using Webgestalt, filtering for redundant GO terms. The enriched list was cross-referenced against biological processes GO terms, which describe the pathways and biological objectives a protein contributes to. Enriched terms with a significance level > 0.05 were excluded. The GO terms were ranked based on enrichment ratio (ER), a ratio between the expected number of proteins present for a specific GO term based on a random set of proteins vs the input proteins.* ***(A)*** *The summary data represents parent GO terms which were enriched.* ***(B)*** *The biological processes GO analysis relating to the enrichment of specific GO child terms*

Cellular Compartment Gene Ontology Analysis

The most enriched parent term in the summary data of the cellular compartment GO analysis was the membrane (n = 45), (Figure 6.13a). As observed for the other GO analyses discussed, this was the highest term enriched for the HEK293T analysis also, (Figure 4.19a). Other notable commonly enriched GO parent terms were the membrane enclosed lumen (n = 30), vesicle (n = 27), cell projection (n = 15) and endosome (n = 8). The specific GO child terms enriched in the hTERT2-HUVEC data, (Figure 6.13b), revealed a far fewer number of enriched GO terms compared to the HEK293T samples, (Figure 4.19b). Only 2 GO child terms were enriched, compared to 39. Only 1 of the 2 enriched terms were unique to the hTERT2-HUVEC analysis, the preribosome (ER = 15.23). This GO term was also enriched in the

hTERT2-HUVEC/NRP1-BioID2-HA conditions treated with $VEGF_{165}a$, (Figure 6.10b). The other child GO term related to the cell-substrate junction (ER = 6.93).

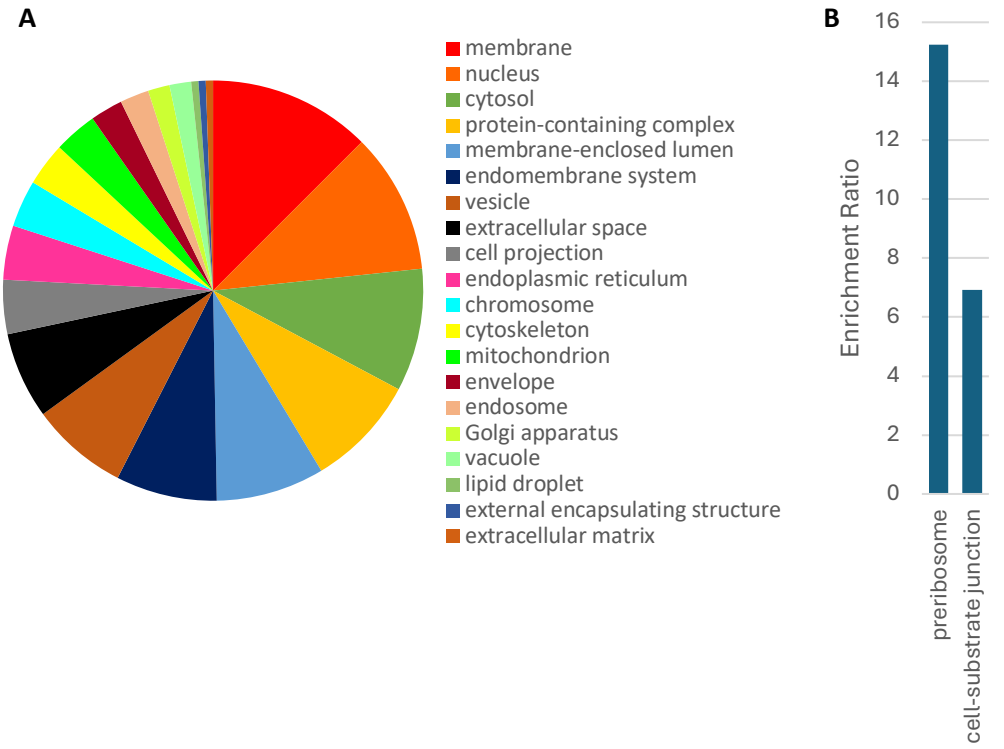

Figure 6.13 – Cellular component gene ontology (GO) analysis of enriched proteins for hTERT2-HUVEC/NRP1-BioID2-HA under basal conditions. *Protein lists were analysed by an overrepresentation analysis using Webgestalt, filtering for redundant GO terms. The enriched list was cross-referenced against cellular component GO terms, which describe localisation of the protein within the cellular environment. Enriched terms with a significance level > 0.05 were excluded. The GO terms were ranked based on enrichment ratio (ER), a ratio between the expected number of proteins present for a specific GO term based on a random set of proteins vs the input proteins.* ***(A)*** *The summary data represents parent GO terms which were enriched.* ***(B)*** *The cellular component GO analysis relating to the enrichment of specific GO child terms.*

6.3 Discussion

6.3.1 Initial Nucleofection Experiments

The initial aims relating to generation of an endothelial cell model expressing the NRP1-BioID2-HA fusion protein was first attempted by transient nucleofection of NRP1-BioID2-HA into hTERT2-HUVEC cells. According to the literature, electroporation or nucleofections is an efficient method of transfecting difficult to manipulate cells, including HUVECs[644]. Firstly, optimal conditions of nucleofection were investigated using a C1-mEmerald empty vector, (Figure 6.1). The different programmes used related to variations in the parameters of the electroporation. Each programme refers to a specific set of electrical pulse durations, intervals of electrical pulsing and voltage parameters, previously validated for efficient DNA delivery in specified cell lines. Efficient transfection and expression was indeed observed using the C1-mEmerald vector, as reported in the literature, particularly using the nucleofection programme A-034. This programme was therefore used in the nucleofection of NRP1-BioID2-HA into the hTERT2-HUVECs, (Figure 6.2). Despite efficient expression observed with the C1-mEmerald vector, this did not correlate with efficient transfections and expression of NRP1-BioID2-HA. Multiple parameters of the nucleofection conditions were attempted to achieve expression of the NRP1 fusion protein similar to the observed expression of C1-mEmerald, to no avail. The transfection efficiency was too low for BioID analysis therefore a poor number of proteins would likely be biotinylated decreasing the accuracy and extent of potential NRP1 interactors detected. The differences observed may be for several reasons. Both C1-mEmerald and NRP1-BioID2-HA plasmids harbour a CMV promoter immediately following a CMV enhancer sequence. Hence, the differences in expression theoretically should not be due to differential transcription of the plasmid. Perhaps the endogenous expression of NRP1 in the hTERT2-HUVECs was causing issues with the exogenous expression of NRP1-BioID2-HA. The endogenous expression of NRP1 may negatively impact the expression of NRP1-BioID2-HA due to potential competition for cellular resources such and transcription factors, RNA polymerase and translation machinery[645]. The starkest differences between the plasmids, lies in their comparative sizes. The C1-mEmerald vector is 4731 bp, while the NRP1-BioID2-HA plasmid is 7751 bp. Plasmids of smaller sizes ~3500 bp routinely demonstrate efficient transfection efficiency and low toxicity to cells, while larger plasmids 6000 – 16000 bp elicit higher cell toxicity and very low transfection efficiency[646].

Even though the nucleofection results were poor, some positive observations regarding the NRP1-BioID2-HA expression in hTERT2-HUVEC cells were made. Correct localisation of the NRP1-BioID2-HA was observed at the cellular membrane, visualised by the anti-HA 594 signal. Likewise, proper function of the biotin ligase (BirA) was demonstrated by the detection of biotinylated proteins using streptavidin

488. This signal was absent in conditions without biotin supplementation. These observations confirmed the suitability of hTERT2-HUVECs as a model to investigate the NRP1 interactome using a BioID fusion protein.

The original NRP1-BioID2-HA plasmid harbours a G418 resistant cassette. In the original generation of the hTERT2-HUVECs, which have been immortalised from HUVEC cells, they have become inherently resistant to G418[487]. This in conjunction with the extremely low transfection efficiency seen in hTERT2-HUVECs made it clear that nucleofection of the original NRP1-BioID2 plasmid would not be appropriate for generating the required endothelial cell model.

6.3.2 pLV-NRP1-BioID2-HA Transductions in hTERT2-HUVEC Cells

As nucleofection resulted in an insufficient number of transfected cells, alternative methods were sought. It was thought lentiviral transductions may be appropriate, as it is a common technique to introduce exogenous DNA into difficult to transfect cells. Lentiviral technology also benefits from more efficient incorporation of the exogenous DNA into the cellular genome[494]. As reported in section 4.3.5.2, the varied transduction conditions reported to be optimal in the literature, meant the transductions with the hTERT2-HUVEC cells required optimisation, (Figure 6.3). The transfection efficiency increased as the concentration of viral preparation increased. As the antibiotic resistance cassette of the pLV-NRP1-BioID2-HA construct was blasticidin, cells expressing NRP1-BioID2-HA could be enriched further by antibiotic selection.

6.3.2.1 Analysis of NRP1-BioID2-HA Expression in Blasticidin Selected hTERT2-HUVEC Cells

After selecting hTERT2-HUVECs expressing NRP1-BioID2-HA using blasticidin, the cells exhibiting expression of the fusion protein were greater than previously observed, (Figure 6.4). Although, there were still cells with no detectable NRP1-BioID2-HA expression. The fact these cells are resistant to blasticidin suggesting the genomic sequence for NRP1-BioID2-HA had been incorporated into the genome but there was issues with its expression. This may be due to the endogenous expression of NRP1 in the hTERT2-HUVECs, as discussed in 6.1. A processes where endothelial cells differentiate into mesenchymal cells, termed the endothelial to mesenchymal transition (EndoMT), is characterised by loss of endothelial cell markers such as CD31[647]. As demonstrated in the anti-CD31 594 channel, extensive expression of CD31 was detected, indicating NRP1-BioID2-HA expressing TERT2-HUVEC were still of endothelial lineage. The low expression of the fusion protein would likely be an issue for the BioID protocol. Hence, further enrichment for cells expression NRP1-BioID2-HA was warranted.

6.3.3.2 Fluorescence-Activated Cell Sorting of hTER2-HUVEC/NRP1-BioID2-HA Cells

The hTERT2-HUVEC cells were sorted based on the expression of NRP1 using fluorescence-activated cell sorting (FACS). Three clear populations were visible relating to the level of NRP1 expression with most cells within the mixed population expressing a comparatively low level of NRP1 and/or likely no or low levels of the NRP1-BioID2-HA fusion protein, (Figure 6.5c). As NRP1 is endogenously expressed in hTERT2-HUVEC cells[595], it was expected all cells would exhibit fluorescent values, even those with low/undetectable expression of NRP1-BioID2-HA. The cells also expressing NRP1-BioID2-HA at higher levels corresponded to a higher fluorescent value. Overlapping with this population, was those hTERT2-HUVECs with higher expression of NRP1 and likely higher levels of NRP1-BioID2-HA fusion protein. However, a third population with even higher 594 fluorescence was detected that corresponded with cells with the highest detected expression NRP1, which were ultimately isolated from the mixed population and cultured further for analysis.

6.3.3.3 Post-FACS Analysis of hTERT2-HUVEC/NRP1-BioID2-HA Cells

Following FACS, NRP1-BioID2-HA and CD31 expression was confirmed in the hTERT2-HUVEC/NRP1-BioID2-HA cells by immunofluorescence analysis (Figure 6.6). A stark contrast to the NRP1 expression levels observed previously using nucleofection, (Figure 6.2), or lentiviral transductions pre-FACS, (Figure 6.4). Importantly, the detectable expression of CD31 in all cells indicates the modified hTERT2-HUVECs were still exhibiting an endothelial phenotype. The endothelial model expressing NRP1-BioID2-HA was of sufficient quality to continue with the BioID protocol.

6.3.4 Streptavidin Pulldowns of hTERT2-HUVEC/NRP1-BioID2-HA Cells

The initial attempts to isolate biotinylated proteins from the hTERT2-HUVEC/NRP1-BioID2-HA cell line were unexpectedly unsuccessful. The cellular lysates in all conditions demonstrated sufficient extraction of biotinylated proteins from cells, (Figure 6.7). Theoretically, these biotinylated proteins should be isolated in the streptavidin pulldown. This was indeed observed for the conditions not supplemented with biotin, for which the biotinylation observed was relatively high despite the absence of biotin supplementation and biotin depletion of the media. The isolation of these proteins demonstrates pulldown conditions are favourable. However, in all conditions with biotin supplementation, no proteins were detected in the eluate. This led to the supposition that in the samples supplemented with biotin, there was an excess of free biotin in the cellular lysates. The free biotin then competed with the biotinylated proteins for binding with the streptavidin-coated magnetic beads. An excess of free biotin in the system is a common cause of failure for streptavidin pulldowns[648].

Measures were then taken to reduce the free biotin in the system, using Zeba™ dye and biotin removal spin columns (Thermo Scientific; A44296S). This also meant proteins < 10 kDa would also be removed from the analyses, however, the benefits were deemed more important than this issue.

Following a free biotin removal from the cell lysates, the successful isolation of biotinylated proteins was observed, (Figure 6.8). It is unknown why the issue of excess free biotin occurred in the hTERT2-HUVEC/NRP1-BioID2-HA experiments, and not for the HEK293T cell model. A possible reason is the increased activity of biotin-dependent carboxylases in hTERT2-HUVEC cells compared to HEK293T cells, although no data is available to suggest this. A comparison of the levels of the common biotin-dependent carboxylases in each cell line, Table 6.3, indicates higher transcription levels of 3 carboxylases in the hTERT2-HUVEC cells which may account for this. Additionally, it is unlikely variation in histone protein levels results in this phenomenon, as HEK293T cells are karyotypically unstable, meaning hypodiploidy is often observed. In these circumstances histone levels may be higher in the HEK293 cells. The answer may alternatively lie in the formulation of the media used to culture cells, whereby the biotin concentration in the media used to culture hTERT2-HUVEC may be higher than the media for HEK293 cells, although as this information is proprietary levels cannot be confirmed. The characteristic biotinylation pattern observed, and the presence of the fusion protein in the cellular lysates meant these samples were appropriate for mass spectrometry analysis. It may have been prudent to use more than 2 x 10 cm dishes per condition, although the associated costs relating to volume of ligand required per 10 cm dish meant it was not possible.

Table 6.3 – Comparative levels of carboxylases in hTERT2-HUVEC and HEK293T cells according to the human protein atlas[595]. *Level of carboxylases is calculated using mRNA for the protein by the number of transcripts per million (nTPM).*

	normalized transcript per million (nTPM)	
Biotin-dependent Carboxylase	hTERT2-HUVEC	HEK293
Acetyl-CoA carboxylase alpha	25.4	21.8
Acetyl-CoA carboxylase beta	0.4	5.0
Pyruvate carboxylase	5.3	10.3
Propionyl-CoA carboxylase subunit alpha	18.0	9.5
Methylcrotonyl-CoA carboxylase subunit 1	26.2	15.8

6.3.5 Enriched Proteins in hTERT2-HUVEC/NRP1-BioID2-HA Cells, Stimulated with $VEGF_{165}a$

As only one repeat was possible using the hTERT2-HUVEC/NRP1-BioID2-HA cells, the results should be considered within this context. Compared with the HEK293T results, for which 4 repeats were

performed, proteins with similar functions and cellular compartments were identified across both cell lines. When comparing the datasets, an obvious discrepancy is between the absolute number of proteins identified. The fewer proteins identified in the enriched list relating to the hTERT2-HUVEC/NRP1-BioID2-HA analysis compared to the HEK293T samples may be due to the presence of less fusion protein and less cells initially lysed, resulting in a lower amount of protein sent for mass spectrometry analysis. This correlates with biological differences between the cell types particularly in terms of their flatness. For example, a confluent 10 cm dish of hTERT2-HUVEC cells contains around 4 million cells, while around 12 million HEK293T cells occupy the same area. Additionally, HEK293T cells are known for their high proliferation rate and ability to synthesise high levels of recombinant proteins, whereas hTERT2-HUVECs have a relatively low proliferation rate and are not optimised for high protein expression. To account for some of inherent differences, 2 x 10 cm cell culture dishes were used for hTERT2-HUVEC/NRP1-BioID2-HA cells per condition. It may have been prudent to increase this to 4 x 10 cm dishes, however, the associated cost of $VEGF_{165}$a ligand meant this was not feasible.

The lack of VEGFR2 enrichment was unexpected, as hTERT2-HUVECs express high amounts of VEGFR2[595], and NRP1 is known to form complexes with $VEGF_{165}$a and VEGFR2[431]. Therefore, VEGFR2 should be present in the final enriched list. A possible reason for its absence is that not enough protein was present in the cell lysates. For some cell types used in BioID experiments more 10 cm dishes are required, and too few may yield detection of fewer candidates[446]. Another reason may be the orientation of the NRP1/VEGFR2 complex, which may be via their extracellular domains[352]. The C-terminal of NRP1 where the BioID2 BirA is located, may not be in close-proximity to the C-terminus of VEGFR2. Additionally, a lack of accessible primary amine (e.g. lysine) residues on VEGFR2s C-terminal domain may mean the BioID2 BirA cannot biotinylate VEGFR2 efficiently[446].

Differences were seen in the types of proteins enriched between HEK293T and hTERT2-HUVEC/NRP1-BioID2-HA samples following treatment with $VEGF_{165}$a, in terms of molecular functions, biological processes and cellular components, demonstrated by the GO analysis. Across the three GO experiments, only one GO term was significantly enriched, part of the cellular component GO term relating to the preribosome, (Figure 6.10b). Enriched proteins in this list included proteins such as Nucleolar protein 14 (NOP14), Nucleolar protein 7 (NOL7), and Protein LTV1 homolog (LTV1). Notably, all of these proteins were unique to the hTERT2-HUVEC/NRP1-BioID2-HA cells and not present in the HEK293T analyses. NRP1 has not been shown to harbour any activity at the preribosome, and binding to ribosomal or associated proteins is undocumented. From previous mass spectrometry analyses in the HEK293T data, ribosomal and similar proteins were also present in significant amount in controls, meaning they may be contaminants. Indeed, the presence of ribosomal proteins appearing as possible contaminants have been noted by other proximity-dependent biotinylation studies using BioID

technology[649]. This may mean that the proteins enriched here and the subsequent enrichment of the preribosome GO term are false-positive results. As observed with the HEK293T data, successive repeats filter these common contaminants from the final enriched protein list across several repeats. It is possible the preribosomal proteins mentioned would not be enriched across several repeats of hTERT2-HUVEC/NRP1-BioID2-HA cells.

Despite no enrichment of other GO terms, there were still some other proteins of interest unique to the hTERT2-HUVEC/NRP1-BioID2 analysis stimulated with $VEGF_{165}a$, Table 6.1. The identification of Semaphorin 6B (SEMA6B) potentially interacting with NRP1 would be a novel finding and may be expected, considering Semaphorin 3C (SEMA3C) is a known ligand binding to the N-terminus of NRP1, discussed in section 1.4.1. Semaphorin classes contain a conserved extracellular domains[650], however, there are notable differences between class 3 and class 6 semaphorins. Perhaps most significantly, class 6 semaphorins may be membrane-bound[651], and while both contain a SEMA domain, required for SEMA3A binding to NRP1[330,336], these domains are not well conserved between SEMA3C and SEMA6B (33.57%)[443]. This may indicate the potential SEMA6B interaction is not occurring at the SEMA domain, unlike for SEMA3A. With the BirA tag at the C-terminus of NRP1, it may indicate a potential novel interaction of NRP1 and sempahorin proteins at the intracellular surface. This intracellular, membrane interaction may be limited to membrane-bound semaphorins such as SEMA6B. As SEMA6B, and semaphorins in general, appear more biologically relevant in the context of neuronal cells, it may be prudent to investigate the NRP1 and semaphorin interactions in such a cellular environment. Perhaps additional interactions with other semaphorin classes would be elucidated in this scenario.

Another interesting potential interactor is one of the top enriched proteins based on protein score, is the Hedgehog-interacting protein (HHIP). The sonic hedgehog pathway is notorious for indispensable signalling in embryogenesis and roles in tumour development and resistance[652]. NRP1 influence on this pathway has been observed previously[653–655] and research has suggested this influence is dependent on the C-terminal intracellular domain of NRP1[656]. The membrane-bound HHIP is the only reported endogenously secreted inhibitor of this signalling pathway[657,658]. The interaction of NRP1 and HHIP at the membrane may present a novel mechanism for NRP1-mediated modulation of the sonic hedgehog pathway.

When comparing $VEGF_{165}a$ treated HEK293T results and the corresponding hTERT2-HUVEC/NRP1-BioID2-HA samples, (Figure 6.14), only one protein was common, PDZ and LIM domain protein 5 (PDLI5). This protein appears to function as a scaffolding protein, capable of linking the actin cytoskeleton to focal adhesion following recruitment by integrins[565]. Integrin β_1 was enriched in the HEK293T data, hence it is not surprising PDLI5 may also interact with NRP1, perhaps forming a complex

with these membrane-bound entities. This interaction may be facilitated by the PDZ-binding domains present on NRP1 and PDLI5. Similar proteins in the $VEGF_{165}$a treated conditions between the differing cell types relates to the vesicle-associated membrane proteins (VAMPs). In the hTERT2-HUVEC/NRP1-BioID2-HA analysis, VAMP3 was significantly enriched, while VAMP5 was enriched in the corresponding HEK293T data. These proteins are involved vesicular transport, particularly the SNARE machinery driven vesicular transport and membrane fusion, discussed in section 4.3.4.5. The enrichment in two difference cellular environments increases confidence as true interactors.

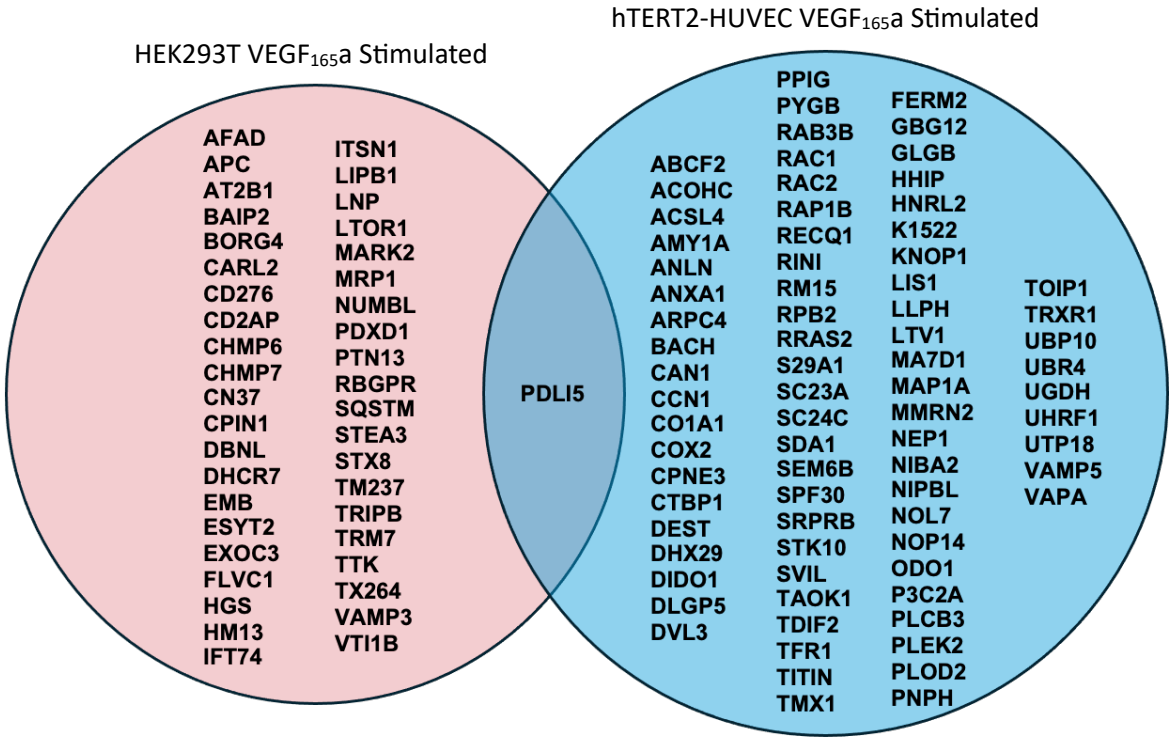

Figure 6.14 – A comparison of NRP1 BioID enriched proteins in HEK293T and hTERT2-HUVEC cells when stimulated with $VEGF_{165}$a. *For the HEK293T data 42 proteins were identified as potential NRP1 interactors, with 41 of these unique. The hTERT2-HUVEC data elicited 80 enriched proteins, with 79 of these unique. There was one protein common between both cell lines, PDZ and LIM domain protein 5 (PDLI5).*

Additional similarities exist between the hTERT2-HUVEC/NRP1-BioID2-HA and the HEK293T data. However, these are between differing conditions. There are proteins commonly enriched in the $VEGF_{165}$a treated hTERT2-HUVEC/NRP1-BioID2-HA conditions, that are instead only seen in the HEK293T cells when under basal conditions, (Figure 6.15). This still increases confidence of enriched proteins being true NRP1 interactors, although it raises the question whether this interaction is dependent on $VEGF_{165}$a and as the TERT-HUVEC data is from a single repeat some caution should be used when interpreting such differences. Nevertheless, the most notable common interactors are Thioredoxin-related transmembrane protein 1 (TMX1), Protein Niban 2 (NIBA2), and Vesicle-associated membrane protein-associated protein A (VAPA). As discussed previously, TMX1 is a bona fide known

interactor of NRP1, hence, its presence here is a positive indication that the enriched proteins identified may be genuine interactors. The biological significance of this protein is not fully understood, although it appears to be involved in protein folding in the endoplasmic reticulum, discussed in section 4.3.4.7. Concerning NIBA2, also known as FAM129B or MINERVA, its molecular functions remain elusive. Translocation of NIBA2 has been observed to adherens junctions in HeLa cells, where it co-localised with catenin-beta 1[659]. In the HEK293T analyses, several proteins associated with adherens junctions were also enriched, in addition to NIBA2. This potential association with NRP1 in two differing cellular environments increases the confidence in this interaction and the proposed involvement of NRP1 at cellular junctions. The involvement of VAPA in several cellular processes such as cadherin binding, vesicular trafficking and membrane docking are discussed in section 4.3.4.6. The identification of a NRP1 interaction with VAPA in hTERT2-HUVEC cells demonstrates more evidence of NRP1s role in vesicular transport. Similarly, VAMP7 in the HEK293T data under basal conditions relates to the VAMP5 enrichment in the hTERT2-HUVEC/NRP1-BioID2-HA $VEGF_{165}$a treated data.

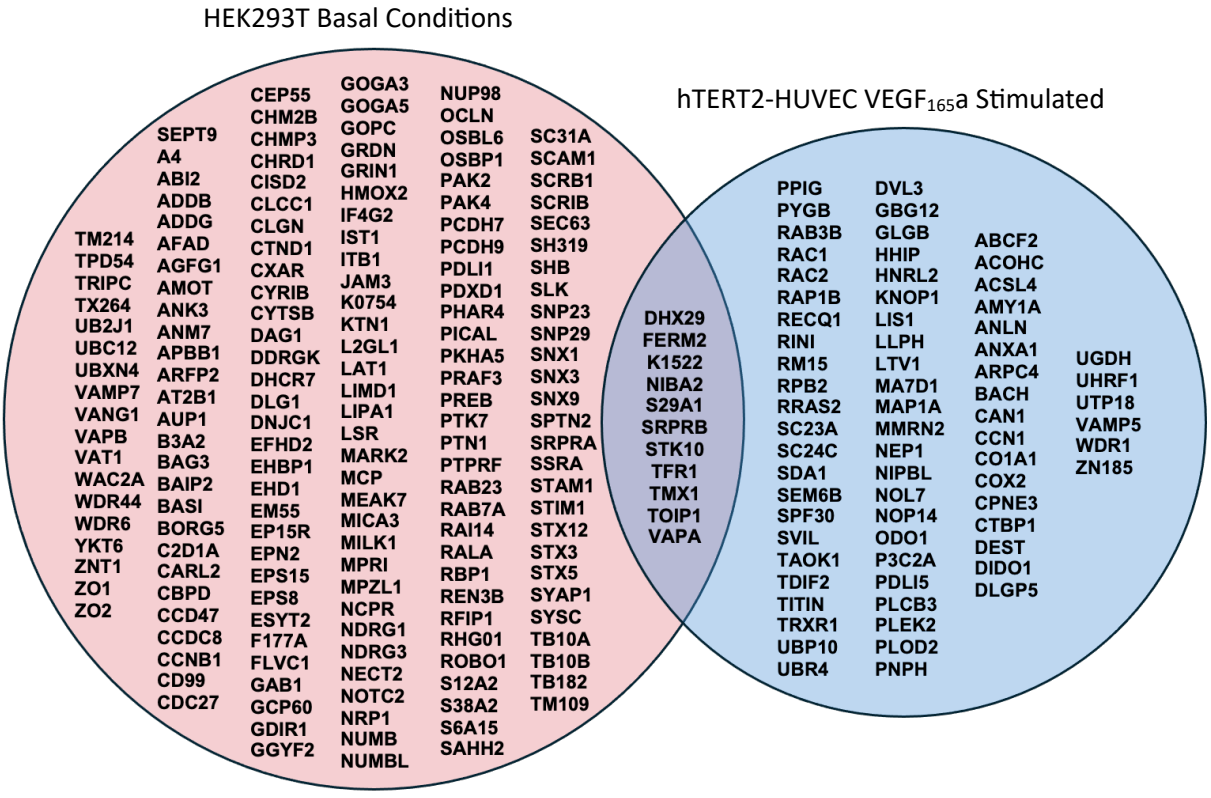

Figure 6.15 – A comparison of NRP1 BioID enriched proteins in HEK293T basal conditions and hTERT2-HUVEC cells when stimulated with $VEGF_{165}$a. *For the HEK293T data 177 proteins were identified as potential NRP1 interactors, with 166 of these unique. The hTERT2-HUVEC data elicited 80 enriched proteins, with 69 of these unique. There were 11 proteins common between these datasets.*

Other similar proteins which are not directly common between the hTERT2-HUVEC and HEK293T data are the presence of Ras-related proteins. In total the 5 Ras-related proteins enriched in the hTERT2-HUVEC experiments were Ras-related C3 botulinum toxin substrate 1 (RAC1), Ras-related C3 botulinum toxin substrate 2 (RAC2), Ras-related protein Rap-1b (RAP1B), Ras-related protein Rab-3B (RAB3B), and Ras-related protein R-Ras2 (RRAS2). In the HEK293T data, similar proteins were enriched, including Ras-related protein Rab-7a (RAB7A), Ras-related protein Rab-23 (RAB23), and Ras-related protein Ral-A (RALA), further supporting the role of NRP1 in vesicular trafficking, perhaps in a Rab/Ras protein dependent manner. The difference observed in the hTERT2-HUVEC and HEK293T cells may be due to differential expression levels of these proteins, Table 6.4. These differences may underline differences in vesicular trafficking machinery in the cell lines, influencing which specific Ras-related protein NRP1 may interact with.

Table 6.4 – Comparative levels of selected Ras-related proteins in hTERT2-HUVEC and HEK293T cells according to the human protein atlas. *Level of carboxylases is calculated using mRNA for the protein by the number of transcripts per million (nTPM).*

	normalized transcript per million (nTPM)	
Potential Ras-related NRP1 Interactor	hTERT2-HUVEC	HEK293
RAC1	307.9	194.4
RAC2	220.9	0.6
RAP1B	275.3	118.7
RAB3B	7.2	1.0
RRAS2	121.5	46.6
RAB7A	82.4	104.7
RAB23	18.8	9.9

6.3.6 Enriched Proteins in hTERT2-HUVEC/NRP1-BioID2-HA Cells Under Basal Conditions

The bioinformatic analyses were also performed with hTERT2-HUVEC/NRP1-BioID2-HA cells under basal conditions, to determine potential interactors of NRP1 which occurred independently of $VEGF_{165}a$, Table 6.2. Despite the enrichment of fewer proteins compared to the conditions stimulated with $VEGF_{165}a$, Table 6.1, the GO analyses revealed more enriched GO terms for molecular function, biological processes and cellular component.

The only enriched GO term for the molecular function analysis was related to cadherin binding, (Figure 6.11b). This GO term was also enriched for the HEK293T experiments when treated with $VEGF_{165}a$, (Figure 4.13b), and under basal conditions, (Figure 4.17b), discussed in sections 4.3.4.5 and 4.3.4.6.

Protein groups attributed to this GO term, were similar to ones discussed previously. These included NIBA2, VAPA, Integrin β_1 (ITGB1), Integrin α_6 (ITGA6), Zona occludens 2 (ZO2), and Ephrin type-A receptor 2 (EPHA2). As discussed in section 6.3.5, evidence of NIBA2 and VAPA interacting with NRP1 was suggested in the HEK293T data.

In the biological processes GO analysis, (Figure 6.12b), the two highest enriched GO terms were related to rRNA metabolic process and ribonucleoprotein complex biogenesis, both not enriched in the HEK293T GO analyses. Proteins attributed to these GO terms were mostly similar and included RNA-binding protein 34 (RBM34), Ribosome biogenesis protein NSA2 homolog (NSA2), Ribosome production factor 2 homolog (RPF2), and Ribosome biogenesis protein BOP1 (BOP1). Again, NRP1 is not known or suspected to be involved with these biological processes and such proteins may therefore be falsely enriched as a result of too few proteomic repeats able to be performed in the remaining time of my studentship. Interestingly, one of the enriched proteins for these terms was SRSF protein kinase 2 (SRPK2), crucial in the splicing of VEGF into different isoforms and thereby influencing angiogenic outcomes [664,665]. This is unexpected as NRP1 is not known to influence VEGF splicing. The final enriched GO term was for small GTPase mediated signal transduction, the only biological processes GO term which was also enriched in the HEK293T experiments. Proteins related to this GO term were Ras-related proteins such as, RALA, Ras-related protein Rab-21 (RAB21), Rho-related GTP-binding protein RhoC (RHOC), and RAS protein activator like-3 (RASL3). Similar, potential interaction have been elucidated in the previous analyses discussed earlier. ITGB1 was also attributed to this term. The evidence presented suggests NRP1 has a significant role in modulating these GTPases. Potential binding to RAB21 also supports evidence of NRP1s involvement in the regulation of vesicular trafficking. The results are somewhat unsurprising, given evidence of NRP1 is known to influence several processes involving GTPases. NRP1s promotion of VEGFR2 recycling back towards the membrane via RAB11 vesicles is well documented [413]. Similarly, a complex formation between NRP1 and RAB7 has been demonstrated by co-immunoprecipitation experiments, likely in endosomes when comparing immunofluorescence results [587]. Additionally, NRP1 facilitates the macropinocytosis-mediated Kaposi's sarcoma–associated herpesvirus (KSHV internalization via the small GTPases Cdc42 and Rac1 [666]. Taken together, it may be expected that GTPases would interact with NRP1.

As observed for the cellular component GO analysis of the hTERT2-HUVEC/NRP1-BioID2-HA cells treated with $VEGF_{165}a$, in the basal conditions analysis the most enriched term related to the preribosome, (Figure 6.13b). Proteins such as NOL7, Ribosome biogenesis protein BOP1 (BOP1) and Ribosome biogenesis protein NSA2 homolog (NSA2). As discussed in 6.3.5, this may be falsely enriched as a result of low repeat numbers. The other enriched cellular component GO term was for the cell-substrate junction, a type of anchoring junction that forms a connection between a cell and the

extracellular matrix. Proteins localised to this cellular component include the aforementioned ITGB1, ITGA6, EPHA2, RAB21 and RALA. Additional enriched proteins were Caveolin-1 (CAV1), Cell surface glycoprotein MUC18 (MUC18), Calpain-1 catalytic subunit (CAN1), and Calpain-2 catalytic subunit (CAN2). The presence of these proteins further supports the influence NRP1 exerts on cellular adhesion. However, these proteins may also insinuate other biological mechanisms NRP1 is involved in. The evidence presented thus far, strongly suggests a role for NRP1 in vesicular trafficking. The enrichment of CAV1 may indicate a role further than only trafficking the vesicle. As discussed in 2.2.3, CAV1 in involved in caveolae-mediated endocytosis (CAV-ME), a form of transcytosis transporting material across the endothelium. Potential binding between NRP1 and CAV1 may indicate a role for NRP1 in CAV-ME and subsequent trafficking of the vesicle across the cell, followed by SNARE-mediated fusion with the basal membrane. For MUC18, similar biological mechanisms and localisation to NRP1 provide confidence in their possible interactions. MUC18, another transmembrane glycoprotein also known as CD146, is a co-receptor for VEGFR2 and influences angiogenic signalling [667,668], similar to the role NRP1 plays as a VEGFR co-receptor. When considering CAN1 and CAN2, it would appear their potential interaction with NRP1 may be more relevant in the context of neuronal environments. These proteins are involved with synaptic plasticity, influencing learning and memory. Activation of CAN1 increases synaptic plasticity corresponding to learning and memory, with CAN2 acting antithetically by inhibiting synaptic plasticity ultimately limiting learning (Wang et al., 2020). Additionally, CAN1 is associated with neuroprotective properties while CAN2 appears to be neurodegenerative. The fact both proteins were enriched is interesting and may point to an important role of NRP1 in regulating the opposing biological outcomes associated with these proteins.

Several proteins already mentioned in the GO analyses of the basal conditions hTERT2-HUVECs were also enriched in the HEK293T analysis under basal conditions, Tables 4.11 and 4.12, including ITGB1, VAPA, ZO2, NIBA2 and RALA, (Figure 6.16). The presence of ITGB1 and ZO2 in both cell types further supportins a role for NRP1 in cellular adhesion, with respect to tight junction complexes and focal adhesions both modulated by the aforementioned proteins. With the enrichment of ITGB1 across several proteomic experiments, it may be unsurprising other integrins, ITGA6 for example, were also enriched. However, other adhesion proteins identified in the HEK293T experiments were not present, for example Occludin (OCLN). A potential reason is HUVECs are not capable of forming a tightly sealed endothelium, meaning certain anchoring junctions may not be representative of an endogenous endothelium and therefore may not be wholly appropriate to investigate NRP1s role in junctional complexes[660]. Interestingly, the presence of EPHA2, another receptor tyrosine kinase (RTK) may indicate a novel co-receptor for NRP1, similar to its well established co-receptor activity with VEGFR2. Indeed, the ligand Ephrin B1 (EFNB1) was also enriched in the HEK293/HaloTag-VEGFR2/NRP1-BioID2-

HA bioinformatic analyses, Table 4.12. The EPHA2 receptor localises and interacts with integrins at focal adhesions[661,662]. The potential involvement of NRP1 at these microdomains is supported by the enrichment of these constituents in this research. Furter, potential interactions between NRP1 and EFNB1 have been suggested, serving to inhibit SEMA3C-mediated signalling[663]. The evidence here may suggest a role for NRP1 in ephrin signalling, in terms of binding to ephrin-related ligands and acting as a co-receptor for the cognate RTKs.

Additional proteins were not associated with any of the enriched GO terms and were significant by virtue of common enrichment in the differing cellular environments. Discussed across several experiments, the presence of Thioredoxin-related transmembrane protein 1 (TMX1) was yet again observed. Another common protein was Ras-related protein Rab-7a (RAB7A), as discussed in section 4.3.4.6, RAB7A is associated with vesicular trafficking. Its presence in this enriched protein list is yet more evidence to support a more important role for NRP1s involvement in vesicular trafficking. Another two proteins enriched in both cell types were Rho GDP-dissociation inhibitor 1 (GDIR1) and Torsin-1A-interacting protein 1 (TOIP1). GDIR1 is a negative regulator of Rho/Ras GTPases, forcing them to remain in an inactive cytosolic state[670], and indicates further involvement of NRP1 in regulation of this family of GTPases. The enrichment of TOIP1, also known as LAP1, is interesting, as it is important in the integrity of the nuclear envelope[671], for which NRP1 has no known function or localisation, perhaps suggesting a novel role for NRP1 here. As TOIP1 is involved in the disassembly and reassembly of nuclear envelope during mitosis[672], it may also suggest a moonlighting/secondary function for NRP1 specifically during cellular division. Other commonly enriched proteins were E3 ubiquitin-protein ligase TRIP12 (TRIPC) and Serine/threonine-protein kinase 10 (STK10). While NRP1 has no known function or localisation here, its homologue NRP2 is known to localise to the nuclear envelope and facilitate recruitment of transcription factors to chromatin[527].

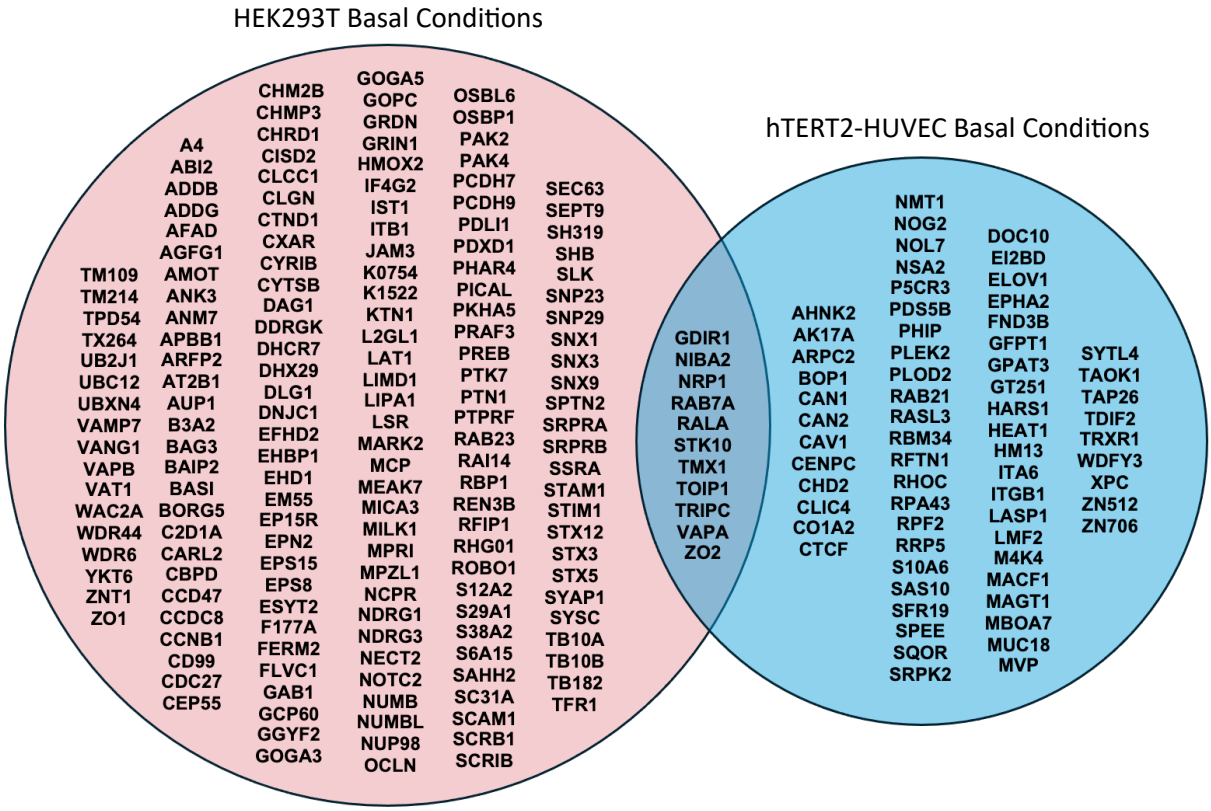

Figure 6.16 – A comparison of NRP1 BioID enriched proteins in HEK293T and hTERT2-HUVEC cells in basal conditions. *For the HEK293T data 177 proteins were identified as potential NRP1 interactors, with 166 of these unique. The hTERT2-HUVEC data elicited 76 enriched proteins, with 65 of these unique. There were 11 proteins common between these datasets.*

Considering the hTERT2-HUVEC basal conditions vs the HEK293T VEGF165a treated conditions, (Figure 6.17), another common protein is identified, Minor histocompatibility antigen H13 (HM13). Similarly to previous discussions, the presence in both lists increases confidence of interaction with NRP1, but raises questions whether it is truly dependent on VEGF165a. HM13 is a peptidase usually bound to the endoplasmic reticulum facilitating the cleavage of proteins, particularly MHC class I signal peptides for immune cell recognition resulting in HLA-E epitopes[673]. Previous research has demonstrated the ability of NRP1 to bind to a similar HLA-C protein[391]. It is currently unknown why NRP1 would interact with such a peptidase, whether itself is cleaved in some manner or in forming a complex to facilitate processing of relevant proteins.

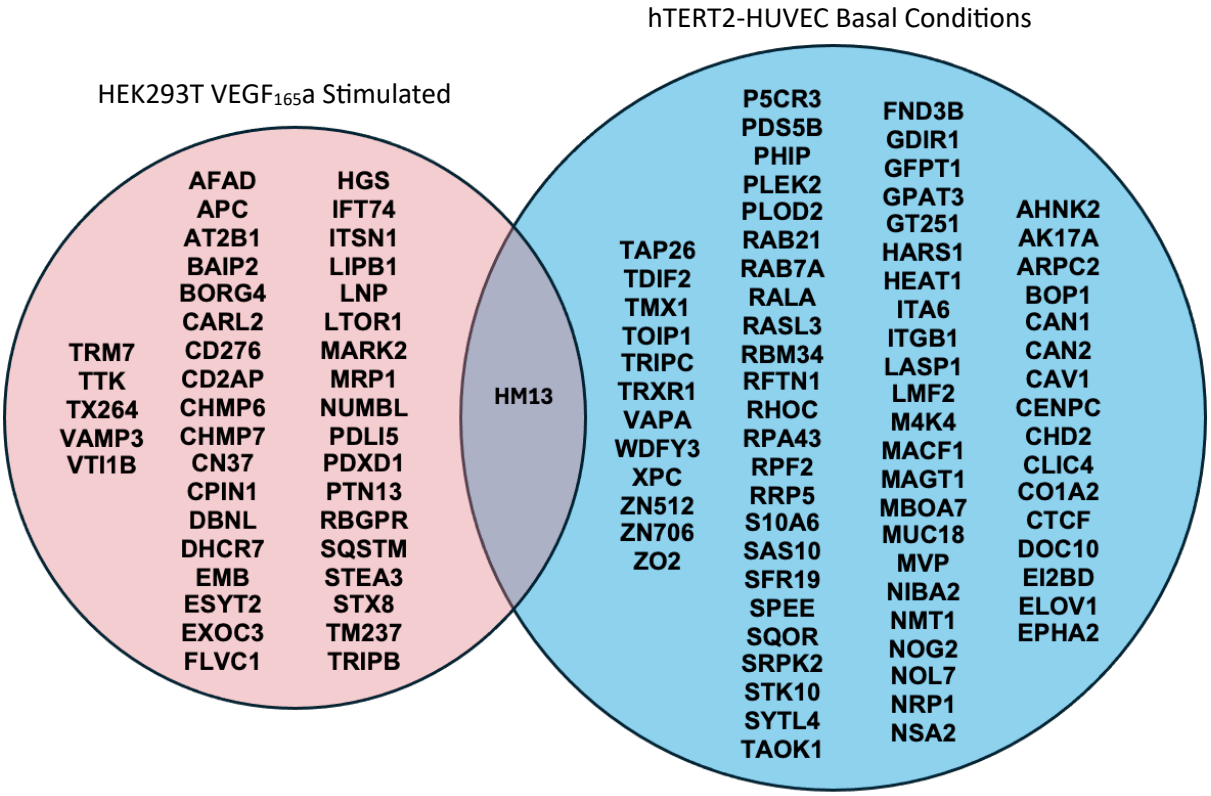

Figure 6.17 – A comparison of NRP1 BioID enriched proteins in HEK293T stimulated with $VEGF_{165}a$ and hTERT2-HUVEC cells in basal conditions. *For the HEK293T data 42 proteins were identified as potential NRP1 interactors, with 41 of these unique. The hTERT2-HUVEC data elicited 76 enriched proteins, with 75 of these unique. There was 1 protein common between these datasets, Minor histocompatibility antigen H13 (HM13).*

6.3.7 Comparison of Enriched Proteins and Known NRP1 Interactors

Some already known or suspected interactors of NRP1 have already been mentioned. For example, the presence of TMX1 across several conditions and cellular environments have been discussed previously. Similarly, potential interactions with ITGB1 and ITGA6 are suggested, correlating with the already suspected integrin homologues claimed to interact with NRP1, ITGA2, ITGA5, and ITGAV, Table 1.1. Several other proteins enriched in the hTERT2-HUVEC/NRP1-BioID2-HA experiments have also been identified as potential NRP1 interactors. As mentioned in section, EPHA2 was enriched by affinity purification mass spectrometry (AP-MS), interestingly the methodology suggested this association occurs on the extracellular surface of the cell membrane[391]. Previously enriched proteins in the HEK293/HaloTag-VEGFR2/NRP1-BioID2-HA data revealed potential binding to EFNB1, perhaps suggesting a mechanism whereby binding of ephrins results in complex formation between NRP1 and ephrin receptors, in a similar manner to the mechanisms observed with VEGF-A, VEGFR2 and NRP1[321,354,431]. The same research that previously identified EPHA2 as a potential NRP1 interactor, MUC18 (MCAM/CD146) was also identified as an N-terminal, extracellular interactor. As a recognised

adhesion protein, the potential interaction with MCAM provides more evidence for the important role of NRP1 in anchoring junctions and increases confidence in the potential NRP1-interactions with other adhesion proteins enriched in the research. Raftlin (RFTN1) and E3 ubiquitin-protein ligase UBR4 (UBR4) were another two enriched proteins correlating to previous NRP1 research. RFTN1 was identified in co-immunoprecipitation (CO-IP) experiments, where it was recruited to the NRP1/VEGFR2 complex by NRP1 to stabilise activated VEGFR2 at the cellular membrane and promoted internalised complexes back towards the membrane[414]. The identification of UBR4, and related proteins UBR1 and UBR2, were performed in a large-scale proteomics experiment whereby single repeats were performed for the majority of proteins, including NRP1[434]. A portion of repeats were performed for around 10% of all proteins investigated, with a replication rate of around 60%, hence, results must be interpreted with caution. It is unknown the biological relevance of a NRP1 and UBR4 interaction, but it may involve potentially ubiquitinating NRP1 for targeted degradation. Finally, VAMP proteins in the hTERT2-HUVEC research are also known interactors of NRP1. VAMP3 was enriched in these experiments, while VAMP2 has been found to complex with NRP1 in CO-IP experiments[433]. Despite the exact VAMP proteins identified here not being consistent with those detected for NRP1 in previous research, the presence of some VAMP subtypes supports the important role for NRP1 in vesicular trafficking.

6.3.8 Conclusion

The generation and validation of the hTERT2-HUVEC/NRP1-BioID2-HA cell line, enabled the interactome of NRP1 to be investigated in the context of endothelial cells. This cellular model may be more representative of the endogenous environment that high levels of NRP1 is expressed within better than the HEK293T cells used previously. The evidence provided using the hTERT2-HUVEC/NRP1-BioID2-HA cells, along with the HEK293T data, supports NRP1s involvement in a diverse catalogue of biological mechanisms and processes. Some of the enriched proteins in the hTERT2-HUVEC experiments complimented the results of the HEK293T work. Further evidence was demonstrated of NRP1s role in cellular adhesion and vesicular trafficking in particular. Additional potential interactors were also identified, correlating to previous NRP1 research. The enrichment of these known interactors increases confidence that potential novel NRP1 interactors are legitimate. As observed with the HEK293T data, evidence of NRP1 interacting with proteins important for neuronal processes, warrants further investigation in an appropriate neuronal cell model. Despite being promising, as only one repeat was possible using the TERT HUVECs, results should be interpreted with some caution.

Chapter 7: General Discussion

There is no debate NRP1 is an integral transmembrane protein involved in a multitude of biological processes, most notably angiogenesis[637], neuronal cell guidance[589,674], immunomodulation[326], and topically viral entry of viruses such as SARS-CoV-2[675]. However, up until recent years, proteomic research into the NRP1 interactome is scarce. Proteins rarely act in isolation, therefore, discerning the interactome of a protein is key in understanding the cellular processes and pathways they mediate and ultimately, how they operate in health and disease, to provide better insights for drug discovery and therapeutic development. Recent studies have investigated the interactome of NRP1 using more complex techniques than previously employed[391], however, these have been restricted to N-terminal extracellular interactome analyses and have identified a moderate number of potential interactors. This project combined two powerful protein-protein interaction techniques, BioID and nanoBRET, to identify and further investigate potential NRP1 interactors, a novel combination of the technologies. The research presented here comprises of the most sophisticated interactome analysis of NRP1 to date. Significantly more potential interactors have been identified in this project compared to published work, particularly at the C-terminal intracellular region of NRP1, where few interactors have been identified. The project aimed to identify potentially novel interactors of NRP1 and how the interactome may change upon stimulation with one of its cognate ligands, $VEGF_{165}$a. Additionally, how the NRP1 interactome changes in the presence of its recognised binding partner, VEGFR2, and an endothelial cell-specific interactome when investigated in hTERT2-HUVEC cells. The identified interactors gave insight into biological processes NRP1 was previously not known to be is involved with, providing a platform for future NRP1 research in these processes.

Chapter 3 began with comparing variants of the biotin ligase (BirA) enzyme that would be used in the project, evaluating the biotinylation capabilities of the original BioID BirA and the newer BioID2 BirA. After evaluating the free BirA, the tags were evaluated in a BioID experimental scenario, using centromere protein A (CENPA), for which the lab has previously used in BioID interactome research[503]. The biotinylation capabilities of the BioID2 BirA appeared greater than that of the original BirA variant, leading to its choice as the tool for NRP1 proteomics experiments in this project. Further tools were generated by fusing the BioID2 BirA to the N or C terminus of NRP1 or NRP2. Validation of expected localisation and biotinylation capabilities of these fusion proteins confirmed they were suitable for further bioinformatic analyses.

In **Chapter 4**, the interactome of NRP1 at both the N-terminus and C-terminus was investigated in HEK293T cells. Initially, the protocol for affinity purification of biotinylated proteins and the subsequent bioinformatic analyses was optimised and used for all future experiments in the project. Despite interesting results with both the N- and C-terminally tagged fusion proteins, the C-terminal intracellular interactome analysis provided much greater protein coverage. The C-terminal analysis

revealed a host of novel potential NRP1 interactors, providing insight into the mechanism by which NRP1 modulates specific biological processes and elucidating novel processes for NRP1 involvement. The NRP1 interactome was investigated further with coexpression of its known interacting partner, VEGFR2. Due to time and financial constraints only one proteomics run was possible, however, interesting novel potential NRP1 interactors were identified.

Chapter 5 then explored some of the potential interactors enriched in the NRP1 experiments using image colocalisation and nanoBRET analyses. Proteins involved in various biological contexts were chosen for further investigation, including those involved in cellular adhesion namely Occludin (OCLN), Zona occludens 1 (ZO1) and Integrin β_1 (ITGB1); in vesicular transport such as Vesicle-associated membrane protein-associated protein A (VAPA) and Hepatocyte growth factor-regulated tyrosine kinase substrate (HRS); and a cytoskeletal GTPase Septin 9 (SEPT9). The evidence presented in this chapter provided positive indications of interactions for some of the proteins investigated, validating the 'hits' detected in the BioID proteomics experiments. Others, including the ITGB1 and HRS experiments, were less clear, possibly due to assay limitations rather than not interacting with NRP1.

The final results **Chapter 6**, built on the BioID experiments performed in HEK293T cells and investigated the NRP1 interactome in an endothelial environment. After generating a suitable model to assess the interactome in hTERT2-HUVEC/NRP1-BioID2-HA stable cells, the bioinformatic analyses supported NRP1s involvement in a diverse catalogue of biological mechanisms and processes. While some of the enriched proteins complemented the HEK293T data, there were many proteins identified as potential NRP1 interactors specific to the hTERT2-HUVEC cells. Despite the single repeat due to financial constraints, valuable interactome data was demonstrated in these experiments, warranting further investigation. The widespread expression of NRP1 in multiple cell types and its roles in multiple cellular processes strongly supports the likelihood of distinct cell type specific NRP1 interactomes.

7.1 C-terminal Interactome Analyses of NRP1-BioID2-HA

For the interactome analyses, a greater coverage was observed with the HEK293T overexpression cell model compared to the hTERT2-HUVEC endothelial cell model, likely due to levels of NRP1 BioID fusion protein expression being much higher in the HEK293T cells and therefore more biotinylation of interactors occurring. These proteomic interactome experiments discussed in this research provided valuable information to the field of NPR1 dynamics in health and disease, elucidating a multitude of novel interactors describing NRP1s involvement in a catalogue of biological processes. In particularly, proteins involved with vesicular trafficking, cellular adhesion and neuronal processes represented a larger portion of the enriched proteins, demonstrated by gene ontology (GO) analyses.

7.1.1 Vesicular Trafficking

Perhaps most evident in this research, is the number of enriched proteins involved in vesicular trafficking. Vesicular trafficking is a fundamental process regulating transport of molecules, proteins, and other cellular components between organelles and the cell membrane critical for maintaining homeostasis in eukaryotic cells[676]. While NRP1 is known to localise to early endosomes[416], modulate internalisation and trafficking of membrane receptors such as VEGFR2[413] and facilitate endocytosis of exogenous agents such as SARS-CoV-2[675], the mechanisms behind NRP1s involvement remain elusive. Therefore, it was expected some vesicular-related proteins would be enriched, however, the sheer number of vesicular trafficking proteins enriched was unprecedented, as NRP1 is not known to bind or even suspected of interacting with the majority of these, (Figure 7.1). The BioID data in this project provides insight into NRP1 involvement in vesicular trafficking, suggesting the extent of NRP1 dynamics in vesicular transport and trafficking machinery is yet to be fully realised. The gene ontology (GO) analyses in the HEK293T experiments in Chapter 4 supports this, with the strong enrichment of vesicular trafficking related terms such as, SNARE binding, membrane docking, the SNARE complex and the ESCRT complex. This demonstrated the significance of the potential NRP1-interacting proteins in vesicular trafficking processes and indicated the importance of NRP1 itself. Such indications warrant future NRP1 research to investigate dynamics of NRP1 in vesicular trafficking, perhaps alongside some of the key vesicular trafficking proteins enriched in the BioID studies.

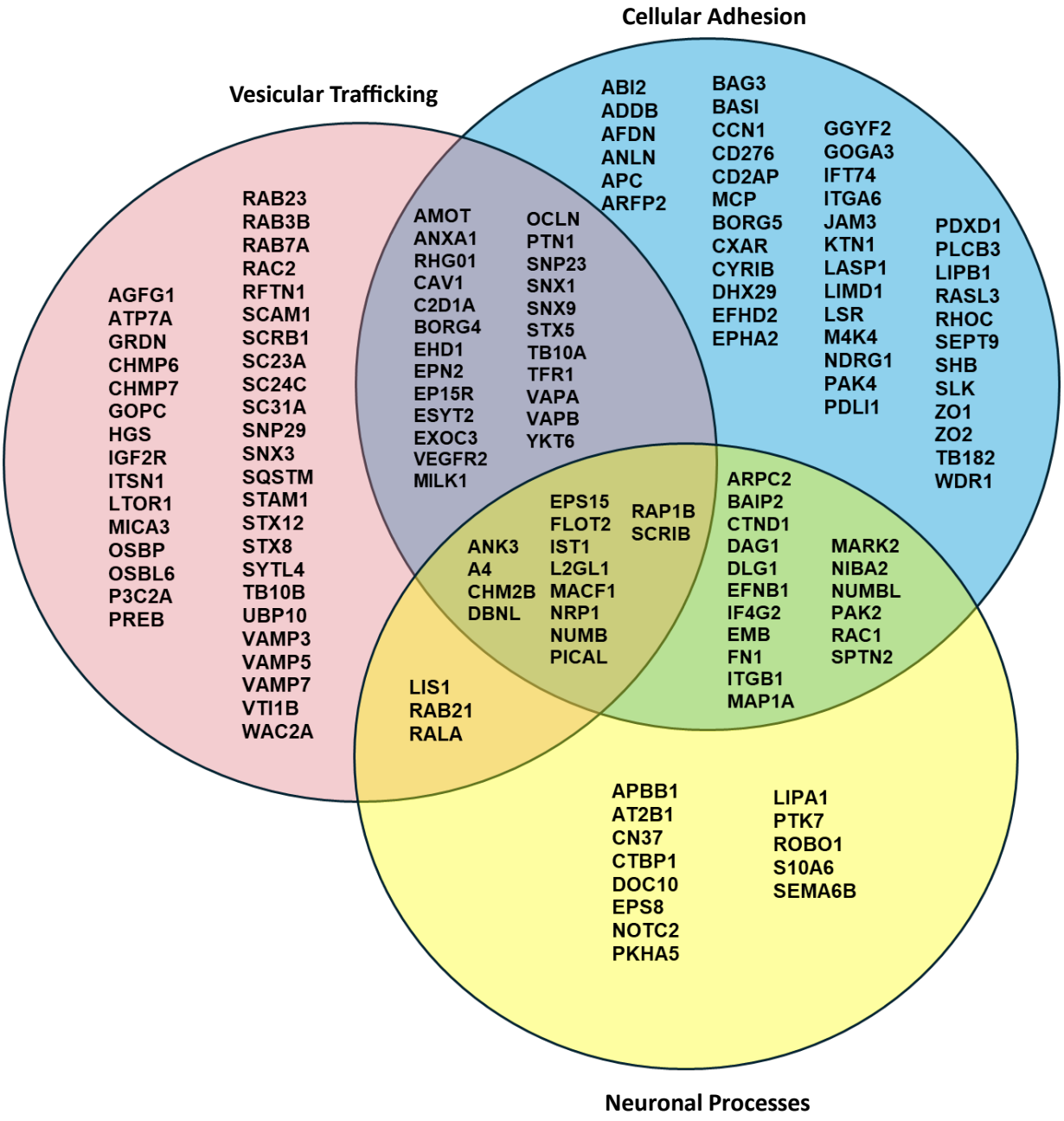

Figure 7.1 – Enriched proteins across all NRP1 C-terminal BioID experiments involved in either vesicular trafficking, cellular adhesion or neuronal processes. *Proteins enriched across HEK293T and hTERT2-HUVEC experiments with NRP1 C-terminal BioID experiments both treated with $VEGF_{165}a$ and in basal conditions. The protein was designated in at least one of the categories based on gene ontology analyses.*

7.1.2 Cellular Adhesion

Proteins regulating cellular adhesion were also enriched in high numbers in the NRP1 interactome experiments, (Figure 7.1). Enrichment of adhesion proteins was expected, given NRP1 was first identified as a cellular adhesion protein[677]. Particularly with respect to proteins at the adherens junctions, where NRP1 is known to localise[388,391]. The majority of adhesion proteins enriched in this

research have not been suspected of interacting with NRP1, with the exception of ITGB1 and catenin delta 1 (CTND1). This suggests a greater involvement of NRP1 in cellular adhesion than is currently reported in the literature. This observation is supported by the GO analyses in HEK293T cells, where highly enriched terms included cadherin binding, cell adhesion mediator activity, the adherens junction and the tight junction. Similarly, the cadherin binding GO term was enriched in the hTERT2-HUVEC analyses. All of which is supportive of an important role for NRP1 in cell adhesion dynamics. Additionally, these potential interactions may provide insight to the vascular permeability enhancing activity of NRP1, through modulation of specialised adhesion microdomains. Taken with the observations in the BioID and GO data, it may suggest a novel role for NRP1 trafficking more of these adhesion proteins, regulating cellular adhesion and vascular permeability.

7.1.3. Neuronal Processes

The enrichment of many proteins relating to neuronal processes was observed, mainly in the HEK293T experiments, likely as these cells exhibit some neuronal features[639,640]. As NRP1 is involved in a host of neuronal processes, including axonal guidance[589], nervous system development and neurogenesis[590], and neuronal survival and migration[591], it would be expected that some neuronal proteins were enriched. Especially as HEK293T cells express several neuron-specific genes[639,640]. Indeed, the majority of these neuronal proteins enriched in this project, (Figure 7.1), would be novel interactors of NRP1, perhaps mechanistically explaining NRP1s role in some of these neuronal processes and implicating further involvement in processes beyond the current literature. While GO analyses supported this, the majority of neuronal-associated GO terms were less significantly enriched than those observed for vesicular trafficking and cellular adhesion. Enriched neuronal process terms in the HEK293T data included postsynaptic membrane neurotransmitter receptor levels, myelin sheath vesicle-mediated transport in synapse, and axonogenesis. It would be expected that interactome studies of NRP1 in an environment more representative of a neuronal cell would elicit more novel NRP1 interactors, specifically expressed or more expressed in cells with neuronal lineage such as SH-SY5Y cells.

7.1.4 Comparison with NRP1 Interactome in the Literature

The enrichment of 11 proteins in the NRP1 interactome analyses presented in this research correlates to already known interactors, Table 7.1. Their presence increases confidence that the potential NRP1-interactors may be legitimately interacting with NRP1. Notably, Thioredoxin related transmembrane protein 1 (TMX1) is a bona fide NRP1 interactor which was present in the majority of proteomic experiments. However, it does raise the question why other known or suspected NRP1 interactors are not present. For example, known interactors VEGFR2 and CDH5 are not enriched in the HEK293T analyses perhaps unsurprisingly as no detectable levels of mRNA are present[595], suggesting no VEGFR2

or CDH5 is present in these cells. As for the hTERT2-HUVEC model, where both VEGFR2 and CDH5 are expressed[595], a reason for their absence may be due to not enough biotinylated material in the cell lysates. This is supported in the interactome experiments where NRP1 and VEGFR2 were co-expressed in HEK293 cells and VEGFR2 was identified as an NRP1 interactor. To combat this, it may be more prudent to increase number of cells lysed, although if stimulation with ligand is desired, an increase in cell number may not be cost-effective. An alternative explanation is It is likely NRP1 has cell-specific and ligand-specific interactomes and the cell types used in this project are not necessarily optimal for detection of all NRP1 interactions. Utilisation of different cell types, including neuronal and immune cells, and alternative ligand stimulation, such as with semaphorin 3A (SEMA3A), could allow a greater protein coverage to be observed.

Table 7.1 – Known interactors of NRP1 enriched as potential interactors in this project. *In total 11 proteins were identified in the BioID proteomic interactome experiments that corresponded with known interactors in the literature.*

UniProt ID	Gene Name	Protein Name
Q9H3N1	TMX1	Thioredoxin-related transmembrane protein 1
Q5T4S7	UBR4	E3 ubiquitin-protein ligase UBR
P05556	ITGB1	Integrin beta-1
Q14699	RFTN1	Raftlin
P43121	MUC18	Cell surface glycoprotein MUC18
P29317	EPHA2	Ephrin type-A receptor 2
P05067	A4	Amyloid-beta precursor protein
O60716	CTND1	Catenin delta-1
P35968	VGFR2	Vascular endothelial growth factor receptor 2
P02751	FINC	Fibronectin
P51149	RAB7A	Ras-related protein Rab-7a

7.2 Validation of BioID Hits with Colocalisation and NanoBRET Analyses

As BioID technology is a proximity-based assay, the results do not explicitly confirm an interaction, rather it confirms close proximity to NRP1 and is indicative of an interaction. Therefore, for greater confidence of an interaction, a secondary technique should be employed. For further investigations various proteins were selected which are involved in processes such as cellular adhesion (OCLN, ZO1, ITGB1) and vesicular transport (VAPA, HRS). This project novelly paired BioID with nanoBRET technology. Ultimately, results were mixed, with a positive indication of interaction for VAPA, OCLN and SEPT9 and less favourable results for HRS, ZO1 and ITGB1. However, the failure to elicit a specific BRET response did not necessarily mean an interaction was not occurring, merely the nanoBRET tags were not sufficiently in close proximity or the optimal orientation for efficient energy transfer to occur. Hence, the assay limitations may have been a factor. Alongside nanoBRET experiments, colocalisation

analyses also gave positive indications of interactions for VAPA, OCLN, and ZO1. These experiments increase the confidence in these BioID hits and the involvement of NRP1 in vesicular trafficking and cellular adhesion.

7.3 Future Directions

The project provided valuable insight into the interactome of the integral membrane protein NRP1 in the presence and absence of $VEGF_{165}$a ligand stimulation. The majority of the potential interactors were not investigated further, hence, there is scope to validate more of these. For the BioID hits with positive nanoBRET data, VAPA, OCLN and SEPT9, further pharmacological characterisation may be performed, such as how the interactions differ upon $VEGF_{165}$a stimulation, or kinetic experiments to determine interactions over a period of time.

The NRP1 interactome was then investigated in the presence of VEGFR2, however, due to time and budget limitations, it was not possible to send the prepared samples for mass spectrometry analysis. Effort was made in generating a HEK293 cell model expressing both NRP1-BioID2-HA and VEGFR2 and preparing the samples and performing the affinity purification of biotinylated material, hence, future work could utilise these samples and complete the dataset for the NRP1/VEGFR2 interactome analysis. The majority of the bioinformatic data utilised HEK293T cells as the primary cell model. This cellular environment may not be representative of a typical NRP1 endogenous environment. Hence, the hTERT2-HUVEC model was then generated. While the single repeat elicited valuable information regarding NRP1 interactome in an endothelial environment, the results must still be viewed in the context of experimental repeats. Again, substantial effort was made in generating the hTERT2-HUVEC/NRP1-BioID2-HA stable cell line and preparing the samples for mass spectrometry analysis, and future work would aim to complete this dataset.

Along with the cell models already evaluated, future work should investigate the NRP1 interactome in a variety of other cellular environments, perhaps most interesting would be in a neuronal cell model. However, there is difficulty in availability of robust *in vitro* neuronal cell models. Some work has already been done in this project regarding neuronal cell models. Preliminary experiments using transient expression of NRP1-BioID2-HA in SH-SY5Y cells, a neuroblastoma cell line which may then be differentiated into a neuron-like phenotype[678], was performed. In these cells, NRP1-BioID2-HA appeared to localise appropriately at the membrane and the biotinylation capabilities of the biotin ligase (BirA) was also demonstrated, (Figure 7.2). For differentiation of the SH-SY5Y cells, a stable expression of NRP1-BioID2-HA would likely be required. This stable cell line may be generated using the lentiviral preparations already used in this project for HEK293 and hTERT2-HUVEC based stable cell lines.

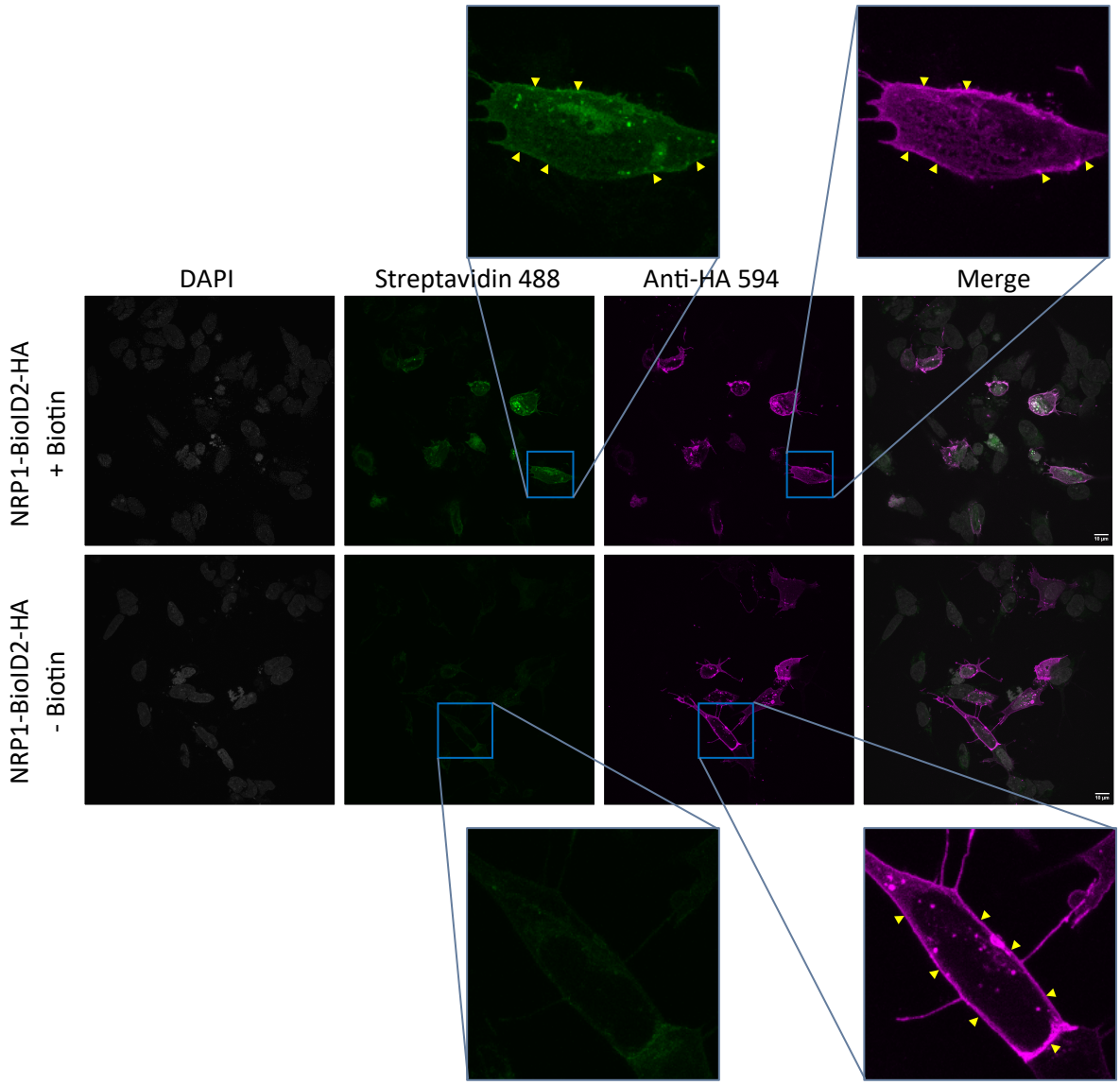

Figure 7.2 – Immunofluorescence of transient transfection of NRP1-BioID2-HA in SH-SY5Y cells. *Cells were incubated with a NRP1-BioID2-HA plasmid and Fugene HD mixture for 24 hours, followed by supplementation with fresh media and 50 µM biotin for a further 20 h. Cells were fixed and stained with anti-HA mouse (Invitrogen; 2-2.2.14) antibody followed by an anti-mouse AF594 (Jackson Immuno Research; 115-585-003) to visualise the NRP1-BioID2-HA fusion protein. Streptavidin AF488 (Invitrogen; S11223) highlighted the presence of biotinylated proteins. DAPI was used to highlight nuclear material and identify individual cells. Conditions with and without biotin supplementation were performed. The samples supplemented with biotin elicited a stronger streptavidin 488 signal. Yellow arrows indicate membrane localisation.*

Determining ligand-specific interactomes would also be of interest. As stimulation of NRP1 with distinct ligands can elicit distinct biological responses[405], it is fair to assume the interactome in these cases would differ. In neuron-like cells, such as differentiated SH-SY5Y cells, it would be interesting to investigate interactome with semaphorin 3A (SEMA3A) stimulation, a known ligand of NRP1 which can

influence processes such as axonal guidance[589]. However, there are significant additional costs associated with these ligand-specific interactome analyses, so this may not be the most appealing area to pursue.

The use of CRISPR technology would be interesting to investigate NRP1 interactome at endogenously expressed NRP1 levels, rather than the overexpression model used in this research. For higher throughput investigations of cell-specific interactome, perhaps CRISPR could be used to generate NRP1 BioID fusion proteins in stem cells, followed by differentiation into specific cell types and subsequent proteomic interactome analyses.

The method of using different *in vitro* cell types may not be the best and most cost-effective method of investigating the NRP1 interactome in different biological contexts. Recently, the utilisation of BioID technology has been optimised in *in vivo* murine models[679–681]. These transgenic BioID mice models enable cell-type-specific proteomes to be determined and may even be exploited to determine interactome at different stages of development (e.g. developmental interactome vs adult interactome). Candidates which show promise during *in vitro* BioID experiments are good candidates to progress further in *in vivo* BioID models.

For future work relating to the potential NRP1 interactors identified in this project, further experiments utilising other methodologies of protein-protein interaction identification should be used to confirm the BioID hits. While the colocalisation analysis and nanoBRET data are indicative of interactions, another validation method, such as co-immunoprecipitation, would increase confidence of the interactions.

As well as the NRP1 research, tools were generated for BioID analysis of NRP2. The NRP2 BioID fusion proteins demonstrated suitable membrane localisation and biotinylation capabilities, meaning they were promising candidates for BioID methodology. Unfortunately, further investigation regarding NRP2 was not possible due to time and financial reasons. As the construct demonstrated promise, and the positive results observed with NRP1 in this project, investigation of the NRP2 interactome using the generated BioID constructs would provide valuable information for the field of Neuropilins. As this research used NRP1 expressed in endothelial cells, the NRP2 experiments could use lymphatic endothelial cells, an environment more similar to the endogenous environment of NRP2.

7.4 Key Conclusion

In summary, this project utilised BioID to investigate the interactome of a membrane receptor under stimulated and basal conditions, a novel use of this technology. While several BioID candidates were proposed, the most promising candidate was Neuropilin 1 (NRP1). Of the BioID analyses the C-terminal BioID fusion protein provided greater protein coverage, with many more potential interactors identified following proteomic bioinformatic analyses. The multitude of proteins enriched, highlighted NRP1s role in a diverse range of biological processes, with particular enrichment of proteins involved in vesicular trafficking and cellular adhesion. Several proteins were identified which were unique to $VEGF_{165}$a stimulated conditions, compared to NRP1 in basal conditions, suggesting these were ligand-stimulated specific interactors of NRP1. A select few of these proteins were investigated further to increase confidence in the BioID hits. Of these proteins, positive results were observed with Occludin (OCLN), Zona occludens 1 (ZO1) and Vesicle-associated membrane protein-associated protein A (VAPA) for colocalisation experiments. In nanoBRET experiments, positive results were observed with OCLN, VAPA and Septin 9 (SEPT9) which were indicative of a specific protein-protein interaction. Finally, the NRP1 interactome was evaluated in the context of an endothelial environment, where distinct potential interactors were elicited in comparison with the HEK293T data. This is suggestive of a cell-type-specific interactome and warrants further investigation.

Chapter 8: References

1. Pugsley MK, Tabrizchi R. The vascular system. *J Pharmacol Toxicol Methods*. 2000;44(2):333-340. doi:10.1016/S1056-8719(00)00125-8

2. Miller LM, Gal A. Cardiovascular System and Lymphatic Vessels. In: *Pathologic Basis of Veterinary Disease*. Elsevier; 2017:561-616.e1. doi:10.1016/B978-0-323-35775-3.00010-2

3. Wiig H, Swartz MA. Interstitial Fluid and Lymph Formation and Transport: Physiological Regulation and Roles in Inflammation and Cancer. *Physiol Rev*. 2012;92(3):1005-1060. doi:10.1152/physrev.00037.2011

4. Witter K, Tonar Z, Schöpper H. How many Layers has the Adventitia? – Structure of the Arterial Tunica Externa Revisited. *Anat Histol Embryol*. 2017;46(2):110-120. doi:10.1111/ahe.12239

5. Mulligan-Kehoe MJ, Simons M. Vasa Vasorum in Normal and Diseased Arteries. *Circulation*. 2014;129(24):2557-2566. doi:10.1161/CIRCULATIONAHA.113.007189

6. Phillippi JA. On vasa vasorum: A history of advances in understanding the vessels of vessels. *Sci Adv*. 2022;8(16):6364. doi:10.1126/sciadv.abl6364

7. Cabrera Fischer EI, Bia D, Camus JM, Zócalo Y, De Forteza E, Armentano RL. Adventitia-dependent mechanical properties of brachiocephalic ovine arteries in in vivo and in vitro studies. *Acta Physiologica*. 2006;188(2):103-111. doi:10.1111/j.1748-1716.2006.01614.x

8. Fischer EC, Santana DB, Zócalo Y, Camus J, Forteza E de, Armentano R. Effects of Removing the Adventitia on the Mechanical Properties of Ovine Femoral Arteries In Vivo and In Vitro. *Circulation Journal*. 2010;74(5):1014-1022. doi:10.1253/circj.CJ-09-0496

9. Belhoul-Fakir H, Wu J, Yeow YL, et al. Injury to the tunica media initiates atherogenesis in the presence of hyperlipidemia. *Front Cardiovasc Med*. 2023;10. doi:10.3389/fcvm.2023.1152124

10. Taylor A, Bordoni B. Histology, Blood Vascular System. [Updated 2023 May 1]. In: StatPearls [Internet]. Treasure Island (FL): StatPearls Publishing; 2024 Jan-. Available from: https://www.ncbi.nlm.nih.gov/books/NBK553217/.

11. Bkaily G, Jacques D. Morphological and Functional Remodeling of Vascular Endothelium in Cardiovascular Diseases. *Int J Mol Sci*. 2023;24(3):1998. doi:10.3390/ijms24031998

12. Mak KM, Mei R. Basement Membrane Type IV Collagen and Laminin: An Overview of Their Biology and Value as Fibrosis Biomarkers of Liver Disease. *Anat Rec*. 2017;300(8):1371-1390. doi:10.1002/ar.23567

13. Mutgan AC, Jandl K, Kwapiszewska G. Endothelial Basement Membrane Components and Their Products, Matrikines: Active Drivers of Pulmonary Hypertension? *Cells*. 2020;9(9):2029. doi:10.3390/cells9092029

14. Tucker W, Arora Y, Mahajan K. Anatomy, Blood Vessels. [Updated 2023 Aug 8]. In: StatPearls [Internet]. Treasure Island (FL): StatPearls Publishing; 2024 Jan-. Available from: https://www.ncbi.nlm.nih.gov/books/NBK470401/.

15. Jadidi M, Razian SA, Habibnezhad M, Anttila E, Kamenskiy A. Mechanical, structural, and physiologic differences in human elastic and muscular arteries of different ages: Comparison of the descending thoracic aorta to the superficial femoral artery. *Acta Biomater*. 2021;119:268-283. doi:10.1016/j.actbio.2020.10.035

16. Zhang W, Jadidi M, Razian SA, Holzapfel GA, Kamenskiy A, Nordsletten DA. A viscoelastic constitutive framework for aging muscular and elastic arteries. *Acta Biomater*. 2024;188:223-241. doi:10.1016/j.actbio.2024.09.021

17. Martinez-Lemus LA. The Dynamic Structure of Arterioles. *Basic Clin Pharmacol Toxicol*. 2012;110(1):5-11. doi:10.1111/j.1742-7843.2011.00813.x

18. Grubb S, Cai C, Hald BO, et al. Precapillary sphincters maintain perfusion in the cerebral cortex. *Nat Commun*. 2020;11(1):395. doi:10.1038/s41467-020-14330-z

19. Roberts WG, Palade GE. Increased microvascular permeability and endothelial fenestration induced by vascular endothelial growth factor. *J Cell Sci*. 1995;108(6):2369-2379. doi:10.1242/jcs.108.6.2369

20. Granger D, Senchenkova E. Inflammation and the Microcirculation. *San Rafael (CA): Morgan & Claypool Life Sciences; 2010 Chapter 3, Anatomical Considerations Available from: https://www.ncbi.nlm.nih.gov/books/NBK53381/*. Published online 2010.

21. van Nieuw Amerongen GP, van Hinsbergh VWM. Targets for pharmacological intervention of endothelial hyperpermeability and barrier function. *Vascul Pharmacol*. 2002;39(4-5):257-272. doi:10.1016/S1537-1891(03)00014-4

22. Jackson WF. Microcirculation. In: *Muscle*. Elsevier; 2012:1197-1206. doi:10.1016/B978-0-12-381510-1.00089-2

23. Pittman R. Regulation of Tissue Oxygenation. *San Rafael (CA): Morgan & Claypool Life Sciences; 2011 Chapter 2, The Circulatory System and Oxygen Transport Available from: https://www.ncbi.nlm.nih.gov/books/NBK54112/*. Published online 2011.

24. Xing C, Guo S, Li W, et al. The brain vasculome. In: *The Vasculome*. Elsevier; 2022:427-438. doi:10.1016/B978-0-12-822546-2.00028-9

25. Mitchell A, Hill B. The vascular system and associated disorders. *British Journal of Nursing*. 2023;32(15):718-724. doi:10.12968/bjon.2023.32.15.718

26. Tansey EA, Montgomery LEA, Quinn JG, Roe SM, Johnson CD. Understanding basic vein physiology and venous blood pressure through simple physical assessments. *Adv Physiol Educ*. 2019;43(3):423-429. doi:10.1152/advan.00182.2018

27. Ramchandran R. Endothelial cells and their role in the vasculature: Past, present and future. *Front Cell Dev Biol*. 2022;10. doi:10.3389/fcell.2022.994133

28. Risau W. Mechanisms of angiogenesis. *Nature*. 1997;386(6626):671-674. doi:10.1038/386671a0

29. Pries AR, Secomb TW, Gaehtgens P. The endothelial surface layer. *Pflugers Arch*. 2000;440(5):653-666. doi:10.1007/s004240000307

30. Alberts B, Johnson A, Lewis J, et al. Blood Vessels and Endothelial Cells. *Molecular Biology of the Cell 4th edition New York: Garland Science; 2002 Blood Vessels and Endothelial Cells Available from: https://www.ncbi.nlm.nih.gov/books/NBK26848/*. Published online 2002.

31. karthik S, Djukic T, Kim JD, et al. Synergistic interaction of sprouting and intussusceptive angiogenesis during zebrafish caudal vein plexus development. *Sci Rep*. 2018;8(1):9840. doi:10.1038/s41598-018-27791-6

32. Adair T, Montani J. Angiogenesis. *San Rafael (CA): Morgan & Claypool Life Sciences; 2010 Chapter 1, Overview of Angiogenesis Available from: https://www.ncbi.nlm.nih.gov/books/NBK53238/*. Published online 2010.

33. Budd S, Byfield G, Martiniuk D, Geisen P, Hartnett ME. Reduction in endothelial tip cell filopodia corresponds to reduced intravitreous but not intraretinal vascularization in a model of ROP. *Exp Eye Res*. 2009;89(5):718-727. doi:10.1016/j.exer.2009.06.011

34. Gerhardt H, Golding M, Fruttiger M, et al. VEGF guides angiogenic sprouting utilizing endothelial tip cell filopodia. *J Cell Biol*. 2003;161(6):1163-1177. doi:10.1083/jcb.200302047

35. Djonov VG, Kurz H, Burri PH. Optimality in the developing vascular system: Branching remodeling by means of intussusception as an efficient adaptation mechanism. *Developmental Dynamics*. 2002;224(4):391-402. doi:10.1002/dvdy.10119

36. Burri PH, Tarek MR. A novel mechanism of capillary growth in the rat pulmonary microcirculation. *Anat Rec*. 1990;228(1):35-45. doi:10.1002/ar.1092280107

37. Djonov V, Baum O, Burri PH. Vascular remodeling by intussusceptive angiogenesis. *Cell Tissue Res*. 2003;314(1):107-117. doi:10.1007/s00441-003-0784-3

38. Dudley AC, Griffioen AW. The modes of angiogenesis: an updated perspective. *Angiogenesis*. 2023;26(4):477-480. doi:10.1007/s10456-023-09895-4

39. Stan R. Channels across Endothelial Cells. *In: Madame Curie Bioscience Database [Internet] Austin (TX): Landes Bioscience; 2000-2013 Available from: https://www.ncbi.nlm.nih.gov/books/NBK6260/*. Published online 2013.

40. Cooper G. Transport of Small Molecules. *The Cell: A Molecular Approach 2nd edition Sunderland (MA): Sinauer Associates; 2000 Transport of Small Molecules Available from: https://www.ncbi.nlm.nih.gov/books/NBK9847/*. Published online 2000.

41. Upadhyay RK. Transendothelial Transport and Its Role in Therapeutics. *Int Sch Res Notices*. 2014;2014:1-39. doi:10.1155/2014/309404

42. Predescu SA, Predescu DN, Malik AB. Molecular determinants of endothelial transcytosis and their role in endothelial permeability. *American Journal of Physiology-Lung Cellular and Molecular Physiology*. 2007;293(4):L823-L842. doi:10.1152/ajplung.00436.2006

43. Alberts B, Johnson A, Lewis J, et al. Principles of Membrane Transport. *Molecular Biology of the Cell 4th edition New York: Garland Science; 2002 Principles of Membrane Transport Available from: https://www.ncbi.nlm.nih.gov/books/NBK26815/*. Published online 2002.

44. Alberts B, Johnson A, Lewis J, et al. Ion Channels and the Electrical Properties of Membranes. *Molecular Biology of the Cell 4th edition New York: Garland Science; 2002 Ion Channels and*

the Electrical Properties of Membranes Available from: https://www.ncbi.nlm.nih.gov/books/NBK26910/. Published online 2002.

45. Alberts B, Johnson A, Lewis J, et al. Carrier Proteins and Active Membrane Transport. *Molecular Biology of the Cell 4th edition New York: Garland Science; 2002 Carrier Proteins and Active Membrane Transport Available from: https://www.ncbi.nlm.nih.gov/books/NBK26896/*. Published online 2002.

46. Komarova Y, Malik AB. Regulation of Endothelial Permeability via Paracellular and Transcellular Transport Pathways. *Annu Rev Physiol*. 2010;72(1):463-493. doi:10.1146/annurev-physiol-021909-135833

47. Stan R V. Structure of caveolae. *Biochimica et Biophysica Acta (BBA) - Molecular Cell Research*. 2005;1746(3):334-348. doi:10.1016/j.bbamcr.2005.08.008

48. Sargiacomo M, Scherer PE, Tang Z, et al. Oligomeric structure of caveolin: implications for caveolae membrane organization. *Proceedings of the National Academy of Sciences*. 1995;92(20):9407-9411. doi:10.1073/pnas.92.20.9407

49. Schlegel A, Lisanti MP. A Molecular Dissection of Caveolin-1 Membrane Attachment and Oligomerization. *Journal of Biological Chemistry*. 2000;275(28):21605-21617. doi:10.1074/jbc.M002558200

50. Predescu SA, Predescu DN, Palade GE. Endothelial Transcytotic Machinery Involves Supramolecular Protein–Lipid Complexes. Scheller RH, ed. *Mol Biol Cell*. 2001;12(4):1019-1033. doi:10.1091/mbc.12.4.1019

51. Minshall RD, Tiruppathi C, Vogel SM, Malik AB. Vesicle formation and trafficking in endothelial cells and regulation of endothelial barrier function. *Histochem Cell Biol*. 2002;117(2):105-112. doi:10.1007/s00418-001-0367-x

52. Ford MGJ, Mills IG, Peter BJ, et al. Curvature of clathrin-coated pits driven by epsin. *Nature*. 2002;419(6905):361-366. doi:10.1038/nature01020

53. Kalthoff C, Alves J, Urbanke C, Knorr R, Ungewickell EJ. Unusual Structural Organization of the Endocytic Proteins AP180 and Epsin 1. *Journal of Biological Chemistry*. 2002;277(10):8209-8216. doi:10.1074/jbc.M111587200

54. Miller SE, Mathiasen S, Bright NA, et al. CALM Regulates Clathrin-Coated Vesicle Size and Maturation by Directly Sensing and Driving Membrane Curvature. *Dev Cell*. 2015;33(2):163-175. doi:10.1016/j.devcel.2015.03.002

55. Schmid SL. CLATHRIN-COATED VESICLE FORMATION AND PROTEIN SORTING: An Integrated Process. *Annu Rev Biochem*. 1997;66(1):511-548. doi:10.1146/annurev.biochem.66.1.511

56. Kaksonen M, Roux A. Mechanisms of clathrin-mediated endocytosis. *Nat Rev Mol Cell Biol*. 2018;19(5):313-326. doi:10.1038/nrm.2017.132

57. Smith SM, Smith CJ. Capturing the mechanics of clathrin-mediated endocytosis. *Curr Opin Struct Biol*. 2022;75:102427. doi:10.1016/j.sbi.2022.102427

58. Salloum G, Bresnick AR, Backer JM. Macropinocytosis: mechanisms and regulation. *Biochemical Journal*. 2023;480(5):335-362. doi:10.1042/BCJ20210584

59. Kay RR. Macropinocytosis: Biology and mechanisms. *Cells & Development*. 2021;168:203713. doi:10.1016/j.cdev.2021.203713

60. Basagiannis D, Zografou S, Murphy C, et al. VEGF induces signalling and angiogenesis by directing VEGFR2 internalisation through macropinocytosis. *J Cell Sci*. 2016;129(21):4091-4104. doi:10.1242/jcs.188219

61. Schmees C, Villaseñor R, Zheng W, et al. Macropinocytosis of the PDGF β-receptor promotes fibroblast transformation by H-RasG12V. Margolis B, ed. *Mol Biol Cell*. 2012;23(13):2571-2582. doi:10.1091/mbc.e11-04-0317

62. Haigler HT, McKanna JA, Cohen S. Rapid stimulation of pinocytosis in human carcinoma cells A-431 by epidermal growth factor. *J Cell Biol*. 1979;83(1):82-90. doi:10.1083/jcb.83.1.82

63. Pacitto R, Gaeta I, Swanson JA, Yoshida S. CXCL12-induced macropinocytosis modulates two distinct pathways to activate mTORC1 in macrophages. *J Leukoc Biol*. 2017;101(3):683-692. doi:10.1189/jlb.2A0316-141RR

64. Mayor S, Parton RG, Donaldson JG. Clathrin-Independent Pathways of Endocytosis. *Cold Spring Harb Perspect Biol*. 2014;6(6):a016758-a016758. doi:10.1101/cshperspect.a016758

65. Lamaze C, Dujeancourt A, Baba T, Lo CG, Benmerah A, Dautry-Varsat A. Interleukin 2 Receptors and Detergent-Resistant Membrane Domains Define a Clathrin-Independent Endocytic Pathway. *Mol Cell*. 2001;7(3):661-671. doi:10.1016/S1097-2765(01)00212-X

66. Grassart A, Dujeancourt A, Lazarow PB, Dautry-Varsat A, Sauvonnet N. Clathrin-independent endocytosis used by the IL-2 receptor is regulated by Rac1, Pak1 and Pak2. *EMBO Rep*. 2008;9(4):356-362. doi:10.1038/embor.2008.28

67. Kirkham M, Fujita A, Chadda R, et al. Ultrastructural identification of uncoated caveolin-independent early endocytic vehicles. *J Cell Biol*. 2005;168(3):465-476. doi:10.1083/jcb.200407078

68. Lundmark R, Doherty GJ, Howes MT, et al. The GTPase-Activating Protein GRAF1 Regulates the CLIC/GEEC Endocytic Pathway. *Current Biology*. 2008;18(22):1802-1808. doi:10.1016/j.cub.2008.10.044

69. Shafaq-Zadah M, Dransart E, Johannes L. Clathrin-independent endocytosis, retrograde trafficking, and cell polarity. *Curr Opin Cell Biol*. 2020;65:112-121. doi:10.1016/j.ceb.2020.05.009

70. Otto GP, Nichols BJ. The roles of flotillin microdomains – endocytosis and beyond. *J Cell Sci*. 2011;124(23):3933-3940. doi:10.1242/jcs.092015

71. Glebov OO, Bright NA, Nichols BJ. Flotillin-1 defines a clathrin-independent endocytic pathway in mammalian cells. *Nat Cell Biol*. 2006;8(1):46-54. doi:10.1038/ncb1342

72. Yu ASL. Paracellular transport as a strategy for energy conservation by multicellular organisms? *Tissue Barriers*. 2017;5(2):e1301852. doi:10.1080/21688370.2017.1301852

73. Campbell HK, Maiers JL, DeMali KA. Interplay between tight junctions & adherens junctions. *Exp Cell Res*. 2017;358(1):39-44. doi:10.1016/j.yexcr.2017.03.061

74. Ikenouchi J, Umeda K, Tsukita S, Furuse M, Tsukita S. Requirement of ZO-1 for the formation of belt-like adherens junctions during epithelial cell polarization. *J Cell Biol*. 2007;176(6):779-786. doi:10.1083/jcb.200612080

75. Claesson-Welsh L, Dejana E, McDonald DM. Permeability of the Endothelial Barrier: Identifying and Reconciling Controversies. *Trends Mol Med*. 2021;27(4):314-331. doi:10.1016/j.molmed.2020.11.006

76. Duong CN, Vestweber D. Mechanisms Ensuring Endothelial Junction Integrity Beyond VE-Cadherin. *Front Physiol*. 2020;11. doi:10.3389/fphys.2020.00519

77. Gumbiner BM. Regulation of cadherin-mediated adhesion in morphogenesis. *Nat Rev Mol Cell Biol*. 2005;6(8):622-634. doi:10.1038/nrm1699

78. Chandran R, Kale G, Philippe JM, Lecuit T, Mayor S. Distinct actin-dependent nanoscale assemblies underlie the dynamic and hierarchical organization of E-cadherin. *Current Biology*. 2021;31(8):1726-1736.e4. doi:10.1016/j.cub.2021.01.059

79. Thompson CJ, Vu VH, Leckband DE, Schwartz DK. Cadherin cis and trans interactions are mutually cooperative. *Proceedings of the National Academy of Sciences*. 2021;118(10). doi:10.1073/pnas.2019845118

80. Wu Y, Jin X, Harrison O, Shapiro L, Honig BH, Ben-Shaul A. Cooperativity between trans and cis interactions in cadherin-mediated junction formation. *Proceedings of the National Academy of Sciences*. 2010;107(41):17592-17597. doi:10.1073/pnas.1011247107

81. Wu Y, Vendome J, Shapiro L, Ben-Shaul A, Honig B. Transforming binding affinities from three dimensions to two with application to cadherin clustering. *Nature*. 2011;475(7357):510-513. doi:10.1038/nature10183

82. Kim SA, Tai CY, Mok LP, Mosser EA, Schuman EM. Calcium-dependent dynamics of cadherin interactions at cell–cell junctions. *Proceedings of the National Academy of Sciences*. 2011;108(24):9857-9862. doi:10.1073/pnas.1019003108

83. Troyanovsky RB, Indra I, Troyanovsky SM. Characterization of early and late events of adherens junction assembly. Published online March 4, 2024. doi:10.1101/2024.03.04.583373

84. Maiers JL, Peng X, Fanning AS, DeMali KA. ZO-1 recruitment to α-catenin: a novel mechanism for coupling the assembly of tight junctions to adherens junctions. *J Cell Sci*. Published online January 1, 2013. doi:10.1242/jcs.126565

85. Itoh M, Nagafuchi A, Moroi S, Tsukita S. Involvement of ZO-1 in Cadherin-based Cell Adhesion through Its Direct Binding to α Catenin and Actin Filaments. *J Cell Biol*. 1997;138(1):181-192. doi:10.1083/jcb.138.1.181

86. Pokutta S, Drees F, Takai Y, Nelson WJ, Weis WI. Biochemical and Structural Definition of the l-Afadin- and Actin-binding Sites of α-Catenin. *Journal of Biological Chemistry*. 2002;277(21):18868-18874. doi:10.1074/jbc.M201463200

87. Sakakibara S, Mizutani K, Sugiura A, et al. Afadin regulates actomyosin organization through αE-catenin at adherens junctions. *Journal of Cell Biology*. 2020;219(5). doi:10.1083/jcb.201907079

88. Pradhan D, Lombardo CR, Roe S, Rimm DL, Morrow JS. α-Catenin Binds Directly to Spectrin and Facilitates Spectrin-Membrane Assembly in Vivo. *Journal of Biological Chemistry*. 2001;276(6):4175-4181. doi:10.1074/jbc.M009259200

89. Seddiki R, Narayana GHNS, Strale PO, et al. Force-dependent binding of vinculin to α-catenin regulates cell–cell contact stability and collective cell behavior. *Mol Biol Cell*. 2018;29(4):380-388. doi:10.1091/mbc.E17-04-0231

90. Weiss EE, Kroemker M, Rüdiger AH, Jockusch BM, Rüdiger M. Vinculin Is Part of the Cadherin–Catenin Junctional Complex: Complex Formation between α-Catenin and Vinculin. *J Cell Biol*. 1998;141(3):755-764. doi:10.1083/jcb.141.3.755

91. Knudsen KA, Soler AP, Johnson KR, Wheelock MJ. Interaction of alpha-actinin with the cadherin/catenin cell-cell adhesion complex via alpha-catenin. *J Cell Biol*. 1995;130(1):67-77. doi:10.1083/jcb.130.1.67

92. Nieset JE, Redfield AR, Jin F, Knudsen KA, Johnson KR, Wheelock MJ. Characterization of the interactions of α-catenin with α-actinin and β-catenin/plakoglobin. *J Cell Sci*. 1997;110(8):1013-1022. doi:10.1242/jcs.110.8.1013

93. Marie H, Pratt SJ, Betson M, et al. The LIM Protein Ajuba Is Recruited to Cadherin-dependent Cell Junctions through an Association with α-Catenin. *Journal of Biological Chemistry*. 2003;278(2):1220-1228. doi:10.1074/jbc.M205391200

94. Lampugnani MG, Orsenigo F, Gagliani MC, Tacchetti C, Dejana E. Vascular endothelial cadherin controls VEGFR-2 internalization and signaling from intracellular compartments. *J Cell Biol*. 2006;174(4):593-604. doi:10.1083/jcb.200602080

95. Dejana E, Orsenigo F, Lampugnani MG. The role of adherens junctions and VE-cadherin in the control of vascular permeability. *J Cell Sci*. 2008;121(13):2115-2122. doi:10.1242/jcs.017897

96. Esser S, Lampugnani MG, Corada M, Dejana E, Risau W. Vascular endothelial growth factor induces VE-cadherin tyrosine phosphorylation in endothelial cells. *J Cell Sci*. 1998;111(13):1853-1865. doi:10.1242/jcs.111.13.1853

97. Sjöberg E, Melssen M, Richards M, et al. Endothelial VEGFR2-PLCγ signaling regulates vascular permeability and antitumor immunity through eNOS/Src. *Journal of Clinical Investigation*. 2023;133(20). doi:10.1172/JCI161366

98. Monaghan-Benson E, Burridge K. The Regulation of Vascular Endothelial Growth Factor-induced Microvascular Permeability Requires Rac and Reactive Oxygen Species. *Journal of Biological Chemistry*. 2009;284(38):25602-25611. doi:10.1074/jbc.M109.009894

99. Shasby DM, Ries DR, Shasby SS, Winter MC. Histamine stimulates phosphorylation of adherens junction proteins and alters their link to vimentin. *American Journal of Physiology-Lung Cellular and Molecular Physiology*. 2002;282(6):L1330-L1338. doi:10.1152/ajplung.00329.2001

100. Andriopoulou P, Navarro P, Zanetti A, Lampugnani MG, Dejana E. Histamine Induces Tyrosine Phosphorylation of Endothelial Cell-to-Cell Adherens Junctions. *Arterioscler Thromb Vasc Biol*. 1999;19(10):2286-2297. doi:10.1161/01.ATV.19.10.2286

101. Angelini DJ, Hyun SW, Grigoryev DN, et al. TNF-α increases tyrosine phosphorylation of vascular endothelial cadherin and opens the paracellular pathway through fyn activation in

human lung endothelia. *American Journal of Physiology-Lung Cellular and Molecular Physiology*. 2006;291(6):L1232-L1245. doi:10.1152/ajplung.00109.2006

102. Lu Z, Ghosh S, Wang Z, Hunter T. Downregulation of caveolin-1 function by EGF leads to the loss of E-cadherin, increased transcriptional activity of β-catenin, and enhanced tumor cell invasion. *Cancer Cell*. 2003;4(6):499-515. doi:10.1016/S1535-6108(03)00304-0

103. Hudry-Clergeon H, Stengel D, Ninio E, Vilgrain I. Platelet-activating factor increases VE-cadherin tyrosine phosphorylation in mouse endothelial cells and its association with the PtdIns3'-kinase. *The FASEB Journal*. 2005;19(6):1-9. doi:10.1096/fj.04-2202com

104. Delva E, Kowalczyk AP. Regulation of Cadherin Trafficking. *Traffic*. 2009;10(3):259-267. doi:10.1111/j.1600-0854.2008.00862.x

105. Xiao K, Garner J, Buckley KM, et al. p120-Catenin Regulates Clathrin-dependent Endocytosis of VE-Cadherin. *Mol Biol Cell*. 2005;16(11):5141-5151. doi:10.1091/mbc.e05-05-0440

106. Yan Z, Wang ZG, Segev N, et al. Rab11a Mediates Vascular Endothelial-Cadherin Recycling and Controls Endothelial Barrier Function. *Arterioscler Thromb Vasc Biol*. 2016;36(2):339-349. doi:10.1161/ATVBAHA.115.306549

107. Herren B, Levkau B, Raines EW, Ross R. Cleavage of β-Catenin and Plakoglobin and Shedding of VE-Cadherin during Endothelial Apoptosis: Evidence for a Role for Caspases and Metalloproteinases. *Mol Biol Cell*. 1998;9(6):1589-1601. doi:10.1091/mbc.9.6.1589

108. Luplerdlop N, Missé D, Bray D, et al. Dengue-virus-infected dendritic cells trigger vascular leakage through metalloproteinase overproduction. *EMBO Rep*. 2006;7(11):1176-1181. doi:10.1038/sj.embor.7400814

109. Xiao K, Allison DF, Kottke MD, et al. Mechanisms of VE-cadherin Processing and Degradation in Microvascular Endothelial Cells. *Journal of Biological Chemistry*. 2003;278(21):19199-19208. doi:10.1074/jbc.M211746200

110. Cohen-Mazor M, Mazor R, Kristal B, Sela S. Elastase and Cathepsin G from Primed Leukocytes Cleave Vascular Endothelial Cadherin in Hemodialysis Patients. *Biomed Res Int*. 2014;2014:1-10. doi:10.1155/2014/459640

111. Adil MS, Narayanan SP, Somanath PR. Cell-cell junctions: structure and regulation in physiology and pathology. *Tissue Barriers*. 2021;9(1):1848212. doi:10.1080/21688370.2020.1848212

112. Wallez Y, Huber P. Endothelial adherens and tight junctions in vascular homeostasis, inflammation and angiogenesis. *Biochimica et Biophysica Acta (BBA) - Biomembranes*. 2008;1778(3):794-809. doi:10.1016/j.bbamem.2007.09.003

113. McCarthy KM, Skare IB, Stankewich MC, et al. Occludin is a functional component of the tight junction. *J Cell Sci*. 1996;109(9):2287-2298. doi:10.1242/jcs.109.9.2287

114. Morita K, Sasaki H, Furuse K, Furuse M, Tsukita S, Miyachi Y. Expression of claudin-5 in dermal vascular endothelia. *Exp Dermatol*. 2003;12(3):289-295. doi:10.1034/j.1600-0625.2003.120309.x

115. Hartmann C, Schwietzer YA, Otani T, Furuse M, Ebnet K. Physiological functions of junctional adhesion molecules (JAMs) in tight junctions. *Biochimica et Biophysica Acta (BBA) - Biomembranes*. 2020;1862(9):183299. doi:10.1016/j.bbamem.2020.183299

116. Muller WA. Leukocyte–endothelial-cell interactions in leukocyte transmigration and the inflammatory response. *Trends Immunol*. 2003;24(6):326-333. doi:10.1016/S1471-4906(03)00117-0

117. Bruewer M, Nusrat A. Regulation of Paracellular Transport across Tight Junctions by the Actin Cytoskeleton. In: Madame Curie Bioscience Database [Internet]. Austin (TX): Landes Bioscience; 2000-2013. Available from: https://www.ncbi.nlm.nih.gov/books/NBK6487/.

118. Morita K, Sasaki H, Furuse K, Furuse M, Tsukita S, Miyachi Y. Expression of claudin-5 in dermal vascular endothelia. *Exp Dermatol*. 2003;12(3):289-295. doi:10.1034/j.1600-0625.2003.120309.x

119. Furuse M, Hata M, Furuse K, et al. Claudin-based tight junctions are crucial for the mammalian epidermal barrier. *J Cell Biol*. 2002;156(6):1099-1111. doi:10.1083/jcb.200110122

120. Furuse M, Fujita K, Hiiragi T, Fujimoto K, Tsukita S. Claudin-1 and -2: Novel Integral Membrane Proteins Localizing at Tight Junctions with No Sequence Similarity to Occludin. *J Cell Biol*. 1998;141(7):1539-1550. doi:10.1083/jcb.141.7.1539

121. Morita K, Furuse M, Fujimoto K, Tsukita S. Claudin multigene family encoding four-transmembrane domain protein components of tight junction strands. *Proceedings of the National Academy of Sciences*. 1999;96(2):511-516. doi:10.1073/pnas.96.2.511

122. Colegio OR, Van Itallie CM, McCrea HJ, Rahner C, Anderson JM. Claudins create charge-selective channels in the paracellular pathway between epithelial cells. *American Journal of Physiology-Cell Physiology*. 2002;283(1):C142-C147. doi:10.1152/ajpcell.00038.2002

123. Piorntek J, Winkler L, Wolburg H, et al. Formation of tight junction: determinants of homophilic interaction between classic claudins. *The FASEB Journal*. 2008;22(1):146-158. doi:10.1096/fj.07-8319com

124. Lee HJ, Zheng JJ. PDZ domains and their binding partners: structure, specificity, and modification. *Cell Communication and Signaling*. 2010;8(1):8. doi:10.1186/1478-811X-8-8

125. Poliak S, Matlis S, Ullmer C, Scherer SS, Peles E. Distinct claudins and associated PDZ proteins form different autotypic tight junctions in myelinating Schwann cells. *J Cell Biol*. 2002;159(2):361-372. doi:10.1083/jcb.200207050

126. Hamazaki Y, Itoh M, Sasaki H, Furuse M, Tsukita S. Multi-PDZ Domain Protein 1 (MUPP1) Is Concentrated at Tight Junctions through Its Possible Interaction with Claudin-1 and Junctional Adhesion Molecule. *Journal of Biological Chemistry*. 2002;277(1):455-461. doi:10.1074/jbc.M109005200

127. Itoh M, Furuse M, Morita K, Kubota K, Saitou M, Tsukita S. Direct Binding of Three Tight Junction-Associated Maguks, Zo-1, Zo-2, and Zo-3, with the Cooh Termini of Claudins. *J Cell Biol*. 1999;147(6):1351-1363. doi:10.1083/jcb.147.6.1351

128. Roh MH, Liu CJ, Laurinec S, Margolis B. The Carboxyl Terminus of Zona Occludens-3 Binds and Recruits a Mammalian Homologue of Discs Lost to Tight Junctions. *Journal of Biological Chemistry*. 2002;277(30):27501-27509. doi:10.1074/jbc.M201177200

129. Sakakibara A, Furuse M, Saitou M, Ando-Akatsuka Y, Tsukita S. Possible Involvement of Phosphorylation of Occludin in Tight Junction Formation. *J Cell Biol*. 1997;137(6):1393-1401. doi:10.1083/jcb.137.6.1393

130. Saitou M, Furuse M, Sasaki H, et al. Complex Phenotype of Mice Lacking Occludin, a Component of Tight Junction Strands. *Mol Biol Cell*. 2000;11(12):4131-4142. doi:10.1091/mbc.11.12.4131

131. Kitajiri S ichiro, Katsuno T, Sasaki H, Ito J, Furuse M, Tsukita S. Deafness in occludin-deficient mice with dislocation of tricellulin and progressive apoptosis of the hair cells. *Biol Open*. 2014;3(8):759-766. doi:10.1242/bio.20147799

132. Kuo W, Odenwald MA, Turner JR, Zuo L. Tight junction proteins occludin and ZO-1 as regulators of epithelial proliferation and survival. *Ann N Y Acad Sci*. 2022;1514(1):21-33. doi:10.1111/nyas.14798

133. Furuse M, Hirase T, Itoh M, et al. Occludin: a novel integral membrane protein localizing at tight junctions. *J Cell Biol*. 1993;123(6):1777-1788. doi:10.1083/jcb.123.6.1777

134. Nusrat A, Brown GT, Tom J, et al. Multiple Protein Interactions Involving Proposed Extracellular Loop Domains of the Tight Junction Protein Occludin. *Mol Biol Cell*. 2005;16(4):1725-1734. doi:10.1091/mbc.e04-06-0465

135. Medina R, Rahner C, Mitic LL, Anderson JM, Van Itallie CM. Occludin Localization at the Tight Junction Requires the Second Extracellular Loop. *Journal of Membrane Biology*. 2000;178(3):235-247. doi:10.1007/s002320010031

136. Li Y, Fanning AS, Anderson JM, Lavie A. Structure of the Conserved Cytoplasmic C-terminal Domain of Occludin: Identification of the ZO-1 Binding Surface. *J Mol Biol*. 2005;352(1):151-164. doi:10.1016/j.jmb.2005.07.017

137. Umeda K, Ikenouchi J, Katahira-Tayama S, et al. ZO-1 and ZO-2 Independently Determine Where Claudins Are Polymerized in Tight-Junction Strand Formation. *Cell*. 2006;126(4):741-754. doi:10.1016/j.cell.2006.06.043

138. McNeil E, Capaldo CT, Macara IG. Zonula Occludens-1 Function in the Assembly of Tight Junctions in Madin-Darby Canine Kidney Epithelial Cells. *Mol Biol Cell*. 2006;17(4):1922-1932. doi:10.1091/mbc.e05-07-0650

139. Tornavaca O, Chia M, Dufton N, et al. ZO-1 controls endothelial adherens junctions, cell–cell tension, angiogenesis, and barrier formation. *Journal of Cell Biology*. 2015;208(6):821-838. doi:10.1083/jcb.201404140

140. Odenwald MA, Choi W, Buckley A, et al. ZO-1 interactions with F-actin and occludin direct epithelial polarization and single lumen specification in 3D culture. *J Cell Sci*. Published online January 1, 2016. doi:10.1242/jcs.188185

141. Bauer H, Zweimueller-Mayer J, Steinbacher P, Lametschwandtner A, Bauer HC. The Dual Role of Zonula Occludens (ZO) Proteins. *J Biomed Biotechnol*. 2010;2010:1-11. doi:10.1155/2010/402593

142. Mattagajasingh SN, Huang SC, Hartenstein JS, Benz EJ. Characterization of the Interaction between Protein 4.1R and ZO-2. *Journal of Biological Chemistry*. 2000;275(39):30573-30585. doi:10.1074/jbc.M004578200

143. D'Atri F, Nadalutti F, Citi S. Evidence for a Functional Interaction between Cingulin and ZO-1 in Cultured Cells. *Journal of Biological Chemistry*. 2002;277(31):27757-27764. doi:10.1074/jbc.M203717200

144. Yamamoto T, Harada N, Kano K, et al. The Ras Target AF-6 Interacts with ZO-1 and Serves as a Peripheral Component of Tight Junctions in Epithelial Cells. *J Cell Biol*. 1997;139(3):785-795. doi:10.1083/jcb.139.3.785

145. Chiba H, Osanai M, Murata M, Kojima T, Sawada N. Transmembrane proteins of tight junctions. *Biochimica et Biophysica Acta (BBA) - Biomembranes*. 2008;1778(3):588-600. doi:10.1016/j.bbamem.2007.08.017

146. Laukoetter MG, Nava P, Lee WY, et al. JAM-A regulates permeability and inflammation in the intestine in vivo. *J Exp Med*. 2007;204(13):3067-3076. doi:10.1084/jem.20071416

147. Itoh M, Sasaki H, Furuse M, Ozaki H, Kita T, Tsukita S. Junctional adhesion molecule (JAM) binds to PAR-3: A possible mechanism for the recruitment of PAR-3 to tight junctions. *J Cell Biol*. 2001;154(3):491-498. doi:10.1083/jcb.200103047

148. Ebnet K, Aurrand-Lions M, Kuhn A, et al. The junctional adhesion molecule (JAM) family members JAM-2 and JAM-3 associate with the cell polarity protein PAR-3: a possible role for JAMs in endothelial cell polarity. *J Cell Sci*. 2003;116(19):3879-3891. doi:10.1242/jcs.00704

149. Ebnet K, Schulz CU, Meyer zu Brickwedde MK, Pendl GG, Vestweber D. Junctional Adhesion Molecule Interacts with the PDZ Domain-containing Proteins AF-6 and ZO-1. *Journal of Biological Chemistry*. 2000;275(36):27979-27988. doi:10.1074/jbc.M002363200

150. Steinbacher T, Kummer D, Ebnet K. Junctional adhesion molecule-A: functional diversity through molecular promiscuity. *Cellular and Molecular Life Sciences*. 2018;75(8):1393-1409. doi:10.1007/s00018-017-2729-0

151. Mandell KJ, Holley GP, Parkos CA, Edelhauser HF. Antibody Blockade of Junctional Adhesion Molecule-A in Rabbit Corneal Endothelial Tight Junctions Produces Corneal Swelling. *Investigative Opthalmology & Visual Science*. 2006;47(6):2408. doi:10.1167/iovs.05-0745

152. Mandell KJ, Berglin L, Severson EA, Edelhauser HF, Parkos CA. Expression of JAM-A in the Human Corneal Endothelium and Retinal Pigment Epithelium: Localization and Evidence for Role in Barrier Function. *Investigative Opthalmology & Visual Science*. 2007;48(9):3928. doi:10.1167/iovs.06-1536

153. Orlova V V., Economopoulou M, Lupu F, Santoso S, Chavakis T. Junctional adhesion molecule-C regulates vascular endothelial permeability by modulating VE-cadherin–mediated cell–cell contacts. *J Exp Med*. 2006;203(12):2703-2714. doi:10.1084/jem.20051730

154. Ebnet K, Suzuki A, Ohno S, Vestweber D. Junctional adhesion molecules (JAMs): more molecules with dual functions? *J Cell Sci*. 2004;117(1):19-29. doi:10.1242/jcs.00930

155. Capaldo CT, Nusrat A. Cytokine regulation of tight junctions. *Biochimica et Biophysica Acta (BBA) - Biomembranes*. 2009;1788(4):864-871. doi:10.1016/j.bbamem.2008.08.027

156. Murakami T, Felinski EA, Antonetti DA. Occludin Phosphorylation and Ubiquitination Regulate Tight Junction Trafficking and Vascular Endothelial Growth Factor-induced Permeability. *Journal of Biological Chemistry*. 2009;284(31):21036-21046. doi:10.1074/jbc.M109.016766

157. Antonetti DA, Barber AJ, Hollinger LA, Wolpert EB, Gardner TW. Vascular Endothelial Growth Factor Induces Rapid Phosphorylation of Tight Junction Proteins Occludin and Zonula Occluden 1. *Journal of Biological Chemistry*. 1999;274(33):23463-23467. doi:10.1074/jbc.274.33.23463

158. Pedram A, Razandi M, Levin ER. Deciphering Vascular Endothelial Cell Growth Factor/Vascular Permeability Factor Signaling to Vascular Permeability. *Journal of Biological Chemistry*. 2002;277(46):44385-44398. doi:10.1074/jbc.M202391200

159. Iden S, Misselwitz S, Peddibhotla SSD, et al. aPKC phosphorylates JAM-A at Ser285 to promote cell contact maturation and tight junction formation. *Journal of Cell Biology*. 2012;196(5):623-639. doi:10.1083/jcb.201104143

160. Rao R. Oxidative stress-induced disruption of epithelial and endothelial tight junctions. *Frontiers in Bioscience*. 2008;Volume(13):7210. doi:10.2741/3223

161. Meyer TN, Schwesinger C, Ye J, Denker BM, Nigam SK. Reassembly of the Tight Junction after Oxidative Stress Depends on Tyrosine Kinase Activity. *Journal of Biological Chemistry*. 2001;276(25):22048-22055. doi:10.1074/jbc.M011477200

162. Heinemann U, Schuetz A. Structural Features of Tight-Junction Proteins. *Int J Mol Sci*. 2019;20(23):6020. doi:10.3390/ijms20236020

163. Kumar NM, Gilula NB. The Gap Junction Communication Channel. *Cell*. 1996;84(3):381-388. doi:10.1016/S0092-8674(00)81282-9

164. Goodenough DA, Goliger JA, Paul DL. CONNEXINS, CONNEXONS, AND INTERCELLULAR COMMUNICATION. *Annu Rev Biochem*. 1996;65(1):475-502. doi:10.1146/annurev.bi.65.070196.002355

165. Hautefort A, Pfenniger A, Kwak BR. Endothelial connexins in vascular function. *Vascular Biology*. 2019;1(1):H117-H124. doi:10.1530/VB-19-0015

166. Singh AJ, Meyer RD, Band H, Rahimi N. The carboxyl terminus of VEGFR-2 is required for PKC-mediated down-regulation. *Mol Biol Cell*. 2005;16(4):2106-2118. doi:10.1091/mbc.e04-08-0749

167. Li X, Olson C, Lu S, Nagy JI. Association of connexin36 with zonula occludens-1 in HeLa cells, BTC-3 cells, pancreas, and adrenal gland. *Histochem Cell Biol*. 2000;122(5):485-498. doi:10.1007/s00418-004-0718-5

168. Kausalya PJ, Reichert M, Hunziker W. Connexin45 directly binds to ZO-1 and localizes to the tight junction region in epithelial MDCK cells. *FEBS Lett*. 2001;505(1):92-96. doi:10.1016/S0014-5793(01)02786-7

169. Palatinus JA, O'Quinn MP, Barker RJ, Harris BS, Jourdan J, Gourdie RG. ZO-1 determines adherens and gap junction localization at intercalated disks. *American Journal of Physiology-Heart and Circulatory Physiology*. 2011;300(2):H583-H594. doi:10.1152/ajpheart.00999.2010

170. Yamada T, Kuramitsu K, Rikitsu E, Kurita S, Ikeda W, Takai Y. Nectin and junctional adhesion molecule are critical cell adhesion molecules for the apico-basal alignment of adherens and tight junctions in epithelial cells. *Genes to Cells*. 2013;18(11):985-998. doi:10.1111/gtc.12091

171. Narita H, Yamamoto Y, Suzuki M, et al. Crystal Structure of the cis-Dimer of Nectin-1. *Journal of Biological Chemistry*. 2011;286(14):12659-12669. doi:10.1074/jbc.M110.197368

172. Satoh-Horikawa K, Nakanishi H, Takahashi K, et al. Nectin-3, a New Member of Immunoglobulin-like Cell Adhesion Molecules That Shows Homophilic and Heterophilic Cell-Cell Adhesion Activities. *Journal of Biological Chemistry*. 2000;275(14):10291-10299. doi:10.1074/jbc.275.14.10291

173. Samanta D, Ramagopal UA, Rubinstein R, Vigdorovich V, Nathenson SG, Almo SC. Structure of Nectin-2 reveals determinants of homophilic and heterophilic interactions that control cell–cell adhesion. *Proceedings of the National Academy of Sciences*. 2012;109(37):14836-14840. doi:10.1073/pnas.1212912109

174. Liu X, An T, Li D, et al. Structure of the heterophilic interaction between the nectin-like 4 and nectin-like 1 molecules. *Proceedings of the National Academy of Sciences*. 2019;116(6):2068-2077. doi:10.1073/pnas.1810969116

175. Reymond N, Fabre S, Lecocq E, Adelaïde J, Dubreuil P, Lopez M. Nectin4/PRR4, a New Afadin-associated Member of the Nectin Family That Trans-interacts with Nectin1/PRR1 through V Domain Interaction. *Journal of Biological Chemistry*. 2001;276(46):43205-43215. doi:10.1074/jbc.M103810200

176. Hermans D, Rodriguez-Mogeda C, Kemps H, Bronckaers A, de Vries HE, Broux B. Nectins and Nectin-like molecules drive vascular development and barrier function. *Angiogenesis*. 2023;26(3):349-362. doi:10.1007/s10456-023-09871-y

177. Takahashi K, Nakanishi H, Miyahara M, et al. Nectin/PRR: An Immunoglobulin-like Cell Adhesion Molecule Recruited to Cadherin-based Adherens Junctions through Interaction with Afadin, a PDZ Domain–containing Protein. *J Cell Biol*. 1999;145(3):539-549. doi:10.1083/jcb.145.3.539

178. Vachharajani VT, DeJong MP, Dunn AR. PDZ Domains from the Junctional Proteins Afadin and ZO-1 Act as Mechanosensors. Published online September 24, 2023. doi:10.1101/2023.09.24.559210

179. Okumura N, Kagami T, Fujii K, Nakahara M, Koizumi N. Involvement of Nectin–Afadin in the Adherens Junctions of the Corneal Endothelium. *Cornea*. 2018;37(5):633-640. doi:10.1097/ICO.0000000000001526

180. Tachibana K, Nakanishi H, Mandai K, et al. Two Cell Adhesion Molecules, Nectin and Cadherin, Interact through Their Cytoplasmic Domain–Associated Proteins. *J Cell Biol*. 2000;150(5):1161-1176. doi:10.1083/jcb.150.5.1161

181. Sakisaka T, Ikeda W, Ogita H, Fujita N, Takai Y. The roles of nectins in cell adhesions: cooperation with other cell adhesion molecules and growth factor receptors. *Curr Opin Cell Biol*. 2007;19(5):593-602. doi:10.1016/j.ceb.2007.09.007

182. Dash S, Biswas J, Goswami S, et al. Molecular Crosstalk Between Adherens Junction Proteins, E-cadherin and Nectin-4. *J Mol Biol*. 2024;436(18):168709. doi:10.1016/j.jmb.2024.168709

183. Sato T, Irie K, Ooshio T, Ikeda W, Takai Y. Involvement of heterophilic trans-interaction of Necl-5/Tage4/PVR/CD155 with nectin-3 in formation of nectin- and cadherin-based adherens junctions. *Genes to Cells*. 2004;9(9):791-799. doi:10.1111/j.1365-2443.2004.00763.x

184. Mizutani K, Takai Y. Nectin spot: a novel type of nectin-mediated cell adhesion apparatus. *Biochemical Journal*. 2016;473(18):2691-2715. doi:10.1042/BCJ20160235

185. Indra I, Hong S, Troyanovsky R, Kormos B, Troyanovsky S. The Adherens Junction: A Mosaic of Cadherin and Nectin Clusters Bundled by Actin Filaments. *Journal of Investigative Dermatology*. 2013;133(11):2546-2554. doi:10.1038/jid.2013.200

186. Rehm K, Panzer L, van Vliet V, Genot E, Linder S. Drebrin preserves endothelial integrity by stabilizing nectin at adherens junctions. *J Cell Sci*. Published online January 1, 2013. doi:10.1242/jcs.129437

187. Fukuhara A, Irie K, Yamada A, et al. Role of nectin in organization of tight junctions in epithelial cells. *Genes to Cells*. 2002;7(10):1059-1072. doi:10.1046/j.1365-2443.2002.00578.x

188. Kowalczyk AP, Green KJ. Structure, Function, and Regulation of Desmosomes. In: ; 2013:95-118. doi:10.1016/B978-0-12-394311-8.00005-4

189. Saito M, Tucker DK, Kohlhorst D, Niessen CM, Kowalczyk AP. Classical and desmosomal cadherins at a glance. *J Cell Sci*. 2012;125(11):2547-2552. doi:10.1242/jcs.066654

190. Thomason HA, Scothern A, McHarg S, Garrod DR. Desmosomes: adhesive strength and signalling in health and disease. *Biochemical Journal*. 2010;429(3):419-433. doi:10.1042/BJ20100567

191. Ishida-Yamamoto A, Igawa S. Genetic skin diseases related to desmosomes and corneodesmosomes. *J Dermatol Sci*. 2014;74(2):99-105. doi:10.1016/j.jdermsci.2014.02.005

192. Valiron O, Chevrier V, Usson Y, Breviario F, Job D, Dejana E. Desmoplakin expression and organization at human umbilical vein endothelial cell-to-cell junctions. *J Cell Sci*. 1996;109(8):2141-2149. doi:10.1242/jcs.109.8.2141

193. Gallicano GI, Bauer C, Fuchs E. Rescuing desmoplakin function in extra-embryonic ectoderm reveals the importance of this protein in embryonic heart, neuroepithelium, skin and vasculature. *Development*. 2001;128(6):929-941. doi:10.1242/dev.128.6.929

194. Bazzoni G, Dejana E. Endothelial Cell-to-Cell Junctions: Molecular Organization and Role in Vascular Homeostasis. *Physiol Rev*. 2004;84(3):869-901. doi:10.1152/physrev.00035.2003

195. Ebert LM, Tan LY, Johan MZ, et al. A non-canonical role for desmoglein-2 in endothelial cells: implications for neoangiogenesis. *Angiogenesis*. 2016;19(4):463-486. doi:10.1007/s10456-016-9520-y

196. Wu MH. Endothelial focal adhesions and barrier function. *J Physiol*. 2005;569(2):359-366. doi:10.1113/jphysiol.2005.096537

197. Barczyk M, Carracedo S, Gullberg D. Integrins. *Cell Tissue Res*. 2010;339(1):269-280. doi:10.1007/s00441-009-0834-6

198. Campbell ID, Humphries MJ. Integrin Structure, Activation, and Interactions. *Cold Spring Harb Perspect Biol*. 2011;3(3):a004994-a004994. doi:10.1101/cshperspect.a004994

199. Larson RS, Corbi AL, Berman L, Springer T. Primary structure of the leukocyte function-associated molecule-1 alpha subunit: an integrin with an embedded domain defining a protein superfamily. *J Cell Biol*. 1989;108(2):703-712. doi:10.1083/jcb.108.2.703

200. Anderson LR, Owens TW, Naylor MJ. Structural and mechanical functions of integrins. *Biophys Rev*. 2014;6(2):203-213. doi:10.1007/s12551-013-0124-0

201. Brown AC, Dysart MM, Clarke KC, Stabenfeldt SE, Barker TH. Integrin α3β1 Binding to Fibronectin Is Dependent on the Ninth Type III Repeat. *Journal of Biological Chemistry*. 2015;290(42):25534-25547. doi:10.1074/jbc.M115.656702

202. Danen EHJ, Sonneveld P, Brakebusch C, Fässler R, Sonnenberg A. The fibronectin-binding integrins α5β1 and αvβ3 differentially modulate RhoA–GTP loading, organization of cell matrix adhesions, and fibronectin fibrillogenesis. *J Cell Biol*. 2002;159(6):1071-1086. doi:10.1083/jcb.200205014

203. Charo IF, Nannizzi L, Smith JW, Cheresh DA. The vitronectin receptor alpha v beta 3 binds fibronectin and acts in concert with alpha 5 beta 1 in promoting cellular attachment and spreading on fibronectin. *J Cell Biol*. 1990;111(6):2795-2800. doi:10.1083/jcb.111.6.2795

204. Xiao T, Takagi J, Coller BS, Wang JH, Springer TA. Structural basis for allostery in integrins and binding to fibrinogen-mimetic therapeutics. *Nature*. 2004;432(7013):59-67. doi:10.1038/nature02976

205. Xiong JP, Stehle T, Diefenbach B, et al. Crystal Structure of the Extracellular Segment of Integrin αVβ3. *Science (1979)*. 2001;294(5541):339-345. doi:10.1126/science.1064535

206. Takada Y, Ye X, Simon S. The integrins. *Genome Biol*. 2007;8(5):215. doi:10.1186/gb-2007-8-5-215

207. Wilson ZS, Witt H, Hazlett L, et al. Context-Dependent Role of Vinculin in Neutrophil Adhesion, Motility and Trafficking. *Sci Rep*. 2020;10(1):2142. doi:10.1038/s41598-020-58882-y

208. Otey CA, Pavalko FM, Burridge K. An interaction between alpha-actinin and the beta 1 integrin subunit in vitro. *J Cell Biol*. 1990;111(2):721-729. doi:10.1083/jcb.111.2.721

209. Lu F, Zhu L, Bromberger T, et al. Mechanism of integrin activation by talin and its cooperation with kindlin. *Nat Commun*. 2022;13(1):2362. doi:10.1038/s41467-022-30117-w

210. Malinin NL, Pluskota E, Byzova T V. Integrin signaling in vascular function. *Curr Opin Hematol*. 2012;19(3):206-211. doi:10.1097/MOH.0b013e3283523df0

211. Sarelius IH, Glading AJ. Control of vascular permeability by adhesion molecules. *Tissue Barriers*. 2015;3(1-2):e985954. doi:10.4161/21688370.2014.985954

212. Cronin NM, DeMali KA. Dynamics of the Actin Cytoskeleton at Adhesion Complexes. *Biology (Basel)*. 2021;11(1):52. doi:10.3390/biology11010052

213. Milošević N, Rütter M, David A. Endothelial Cell Adhesion Molecules- (un)Attainable Targets for Nanomedicines. *Front Med Technol*. 2022;4. doi:10.3389/fmedt.2022.846065

214. Moreira MB, Garcia-Cardeña G, Saffi MAL, Libby P. Endothelium: A Coordinator of Acute and Chronic Inflammation. In: *Endothelium and Cardiovascular Diseases*. Elsevier; 2018:485-491. doi:10.1016/B978-0-12-812348-5.00032-5

215. Kreuger J, Phillipson M. Targeting vascular and leukocyte communication in angiogenesis, inflammation and fibrosis. *Nat Rev Drug Discov*. 2016;15(2):125-142. doi:10.1038/nrd.2015.2

216. Golias C, Batistatou A, Bablekos G, et al. Physiology and Pathophysiology of Selectins, Integrins, and IgSf Cell Adhesion Molecules Focusing on Inflammation. A Paradigm Model on Infectious Endocarditis. *Cell Commun Adhes*. 2011;18(3):19-32. doi:10.3109/15419061.2011.606381

217. Cook-Mills JM, Marchese ME, Abdala-Valencia H. Vascular Cell Adhesion Molecule-1 Expression and Signaling During Disease: Regulation by Reactive Oxygen Species and Antioxidants. *Antioxid Redox Signal*. 2011;15(6):1607-1638. doi:10.1089/ars.2010.3522

218. Walpola PL, Gotlieb AI, Cybulsky MI, Langille BL. Expression of ICAM-1 and VCAM-1 and Monocyte Adherence in Arteries Exposed to Altered Shear Stress. *Arterioscler Thromb Vasc Biol*. 1995;15(1):2-10. doi:10.1161/01.ATV.15.1.2

219. Vestweber D. Adhesion and signaling molecules controlling the transmigration of leukocytes through endothelium. *Immunol Rev*. 2007;218(1):178-196. doi:10.1111/j.1600-065X.2007.00533.x

220. Muller WA, Weigl SA, Deng X, Phillips DM. PECAM-1 is required for transendothelial migration of leukocytes. *J Exp Med*. 1993;178(2):449-460. doi:10.1084/jem.178.2.449

221. Hsu MC, Pan MR, Hung WC. Two Birds, One Stone: Double Hits on Tumor Growth and Lymphangiogenesis by Targeting Vascular Endothelial Growth Factor Receptor 3. *Cells*. 2019;8(3):270. doi:10.3390/cells8030270

222. Hubbard SR, Miller WT. Receptor tyrosine kinases: mechanisms of activation and signaling. *Curr Opin Cell Biol*. 2007;19(2):117-123. doi:10.1016/j.ceb.2007.02.010

223. Shibuya M. VEGFR and type-V RTK activation and signaling. *Cold Spring Harb Perspect Biol*. 2013;5(10):1-13. doi:10.1101/cshperspect.a009092

224. Peng K, Bai Y, Zhu Q, Hu B, Xu Y. Targeting VEGF–neuropilin interactions: a promising antitumor strategy. *Drug Discov Today*. 2019;24(2):656-664. doi:10.1016/j.drudis.2018.10.004

225. Mercurio M, Kooi CW Vander. Sequestration by a Soluble Splice Form. 2016;23(4):677-687. doi:10.1016/j.str.2015.01.018.Structural

226. Wong C, Jin ZG. Protein Kinase C-dependent Protein Kinase D Activation Modulates ERK Signal Pathway and Endothelial Cell Proliferation by Vascular Endothelial Growth Factor. *Journal of Biological Chemistry*. 2005;280(39):33262-33269. doi:10.1074/jbc.M503198200

227. Shibuya M. Vascular Endothelial Growth Factor (VEGF) and Its Receptor (VEGFR) Signaling in Angiogenesis: A Crucial Target for Anti- and Pro-Angiogenic Therapies. *Genes Cancer*. 2011;2(12):1097-1105. doi:10.1177/1947601911423031

228. Okikawa S, Morine Y, Saito Y, et al. Inhibition of the VEGF signaling pathway attenuates tumor-associated macrophage activity in liver cancer. *Oncol Rep*. 2022;47(4):71. doi:10.3892/or.2022.8282

229. Okabe K, Fukada H, Tai-Nagara I, et al. Neuron-derived VEGF contributes to cortical and hippocampal development independently of VEGFR1/2-mediated neurotrophism. *Dev Biol*. 2020;459(2):65-71. doi:10.1016/j.ydbio.2019.11.016

230. Holmes K, Roberts OL, Thomas AM, Cross MJ. Vascular endothelial growth factor receptor-2: Structure, function, intracellular signalling and therapeutic inhibition. *Cell Signal*. 2007;19(10):2003-2012. doi:10.1016/j.cellsig.2007.05.013

231. Takahashi T, Shibuya M. The 230 kDa mature form of KDR/Flk-1 (VEGF receptor-2) activates the PLC-γ pathway and partially induces mitotic signals in NIH3T3 fibroblasts. *Oncogene*. 1997;14(17):2079-2089. doi:10.1038/sj.onc.1201047

232. Brozzo MS, Bjelić S, Kisko K, et al. Thermodynamic and structural description of allosterically regulated VEGFR-2 dimerization. *Blood*. 2012;119(7):1781-1788. doi:10.1182/blood-2011-11-390922

233. Shinkai A, Ito M, Anazawa H, Yamaguchi S, Shitara K, Shibuya M. Mapping of the sites involved in ligand association and dissociation at the extracellular domain of the kinase insert domain-containing receptor for vascular endothelial growth factor. *Journal of Biological Chemistry*. 1998;273(47):31283-31288. doi:10.1074/jbc.273.47.31283

234. Leppänen VM, Prota AE, Jeltsch M, et al. Structural determinants of growth factor binding and specificity by VEGF receptor 2. *Proceedings of the National Academy of Sciences*. 2010;107(6):2425-2430. doi:10.1073/pnas.0914318107

235. King C, Wirth D, Workman S, Hristova K. Cooperative interactions between VEGFR2 extracellular Ig-like subdomains ensure VEGFR2 dimerization. *Biochimica et Biophysica Acta (BBA) - General Subjects*. 2017;1861(11):2559-2567. doi:10.1016/j.bbagen.2017.08.021

236. Sarabipour S, Ballmer-Hofer K, Hristova K. VEGFR-2 conformational switch in response to ligand binding. *Elife*. 2016;5(APRIL2016):1-23. doi:10.7554/eLife.13876

237. Ruch C, Skiniotis G, Steinmetz MO, Walz T, Ballmer-Hofer K. Structure of a VEGF-VEGF receptor complex determined by electron microscopy. *Nat Struct Mol Biol*. 2007;14(3):249-250. doi:10.1038/nsmb1202

238. Markovic-Mueller S, Stuttfeld E, Asthana M, et al. Structure of the Full-length VEGFR-1 Extracellular Domain in Complex with VEGF-A. *Structure*. 2017;25(2):341-352. doi:10.1016/j.str.2016.12.012

239. Kisko K, Brozzo MS, Missimer J, et al. Structural analysis of vascular endothelial growth factor receptor-2/ligand complexes by small-angle X-ray solution scattering. *The FASEB Journal*. 2011;25(9):2980-2986. doi:10.1096/fj.11-185397

240. Manni S, Mineev KS, Usmanova D, et al. Structural and functional characterization of alternative transmembrane domain conformations in VEGF receptor 2 activation. *Structure*. 2014;22(8):1077-1089. doi:10.1016/j.str.2014.05.010

241. Manni S, Kisko K, Schleier T, Missimer J, Ballmer-Hofer K. Functional and structural characterization of the kinase insert and the carboxy terminal domain in VEGF receptor 2 activation. *FASEB Journal*. 2014;28(11):4914-4923. doi:10.1096/fj.14-256206

242. Albuquerque RJC, Hayashi T, Cho WG, et al. Alternatively spliced vascular endothelial growth factor receptor-2 is an essential endogenous inhibitor of lymphatic vessel growth. *Nat Med*. 2009;15(9):1023-1030. doi:10.1038/nm.2018

243. Modi SJ, Kulkarni VM. Vascular Endothelial Growth Factor Receptor (VEGFR-2)/KDR Inhibitors: Medicinal Chemistry Perspective. *Med Drug Discov*. 2019;2:100009. doi:10.1016/j.medidd.2019.100009

244. Lian L, Li XL, Xu MD, et al. VEGFR2 promotes tumorigenesis and metastasis in a pro-angiogenic-independent way in gastric cancer. *BMC Cancer*. 2019;19(1):479-489. doi:10.1186/s12885-019-5322-0

245. Örnek N, Örnek K, Aydin S, Yilmaz M, Ölmez Y. Serum vascular endothelial growth factor receptor-2 and adropin levels in age-related macular degeneration. *Int J Ophthalmol*. 2016;9(4):556-560. doi:10.18240/ijo.2016.04.13

246. Beazley-Long N, Moss CE, Ashby WR, et al. VEGFR2 promotes central endothelial activation and the spread of pain in inflammatory arthritis. *Brain Behav Immun*. 2018;74:49-67. doi:10.1016/j.bbi.2018.03.012

247. Abhinand CS, Raju R, Soumya SJ, Arya PS, Sudhakaran PR. VEGF-A/VEGFR2 signaling network in endothelial cells relevant to angiogenesis. *J Cell Commun Signal*. 2016;10(4):347-354. doi:10.1007/s12079-016-0352-8

248. Shalaby F, Rossant J, Yamaguchi TP, et al. Failure of blood-island formation and vasculogenesis in Flk-1-deficient mice. *Nature*. 1995;376(6535):62-66. doi:10.1038/376062a0

249. Shalaby F, Ho J, Stanford WL, et al. A requirement for Flk1 in primitive and definitive hematopoiesis and vasculogenesis. *Cell*. 1997;89(6):981-990. doi:10.1016/S0092-8674(00)80283-4

250. Zhang J, Liu C, Shi W, et al. The novel VEGF receptor 2 inhibitor YLL545 inhibits angiogenesis and growth in breast cancer. *Oncotarget*. 2016;7(27):41067-41080. doi:10.18632/oncotarget.9392

251. Parry TJ, Cushman C, Gallegos AM, et al. Bioactivity of anti-angiogenic ribozymes targeting Flt-1 and KDR mRNA. *Nucleic Acids Res*. 1999;27(13):2569-2577. doi:10.1093/nar/27.13.2569

252. Kroll J, Waltenberger J. The vascular endothelial growth factor receptor KDR activates multiple signal transduction pathways in porcine aortic endothelial cells. *Journal of Biological Chemistry*. 1997;272(51):32521-32527. doi:10.1074/jbc.272.51.32521

253. Takahashi T, Shibuya M. The 230 kDa mature form of KDR/Flk-1 (VEGF receptor-2) activates the PLC-γ pathway and partially induces mitotic signals in NIH3T3 fibroblasts. *Oncogene*. 1997;14(17):2079-2089. doi:10.1038/sj.onc.1201047

254. Holmes K, Roberts OL, Thomas AM, Cross MJ. Vascular endothelial growth factor receptor-2: Structure, function, intracellular signalling and therapeutic inhibition. *Cell Signal*. 2007;19(10):2003-2012. doi:10.1016/j.cellsig.2007.05.013

255. Benedito R, Rocha SF, Woeste M, et al. Notch-dependent VEGFR3 upregulation allows angiogenesis without VEGF-VEGFR2 signalling. *Nature*. 2012;484(7392):110-114. doi:10.1038/nature10908

256. Mahabeleshwar GH, Feng W, Reddy K, Plow EF, Byzova T V. Mechanisms of Integrin–Vascular Endothelial Growth Factor Receptor Cross-Activation in Angiogenesis. *Circ Res*. 2007;101(6):570-580. doi:10.1161/CIRCRESAHA.107.155655

257. Masson-Gadais B, Houle F, Laferrière J, Huot J. Integrin αvβ3 requirement for VEGFR2-mediated activation of SAPK2/p38 and for Hsp90-dependent phosphorylation of focal adhesion kinase in endothelial cells activated by VEGF. *Cell Stress Chaperones*. 2003;8(1):37. doi:10.1379/1466-1268(2003)8<37:IVRFVA>2.0.CO;2

258. Kuczynski EA, Vermeulen PB, Pezzella F, Kerbel RS, Reynolds AR. Vessel co-option in cancer. *Nat Rev Clin Oncol*. 2019;16(8):469-493. doi:10.1038/s41571-019-0181-9

259. Lugano R, Ramachandran M, Dimberg A. Tumor angiogenesis: causes, consequences, challenges and opportunities. *Cellular and Molecular Life Sciences*. 2020;77(9):1745-1770. doi:10.1007/s00018-019-03351-7

260. Smith RO, Ninchoji T, Gordon E, et al. Vascular permeability in retinopathy is regulated by VEGFR2 Y949 signaling to VE-cadherin. *Elife*. 2020;9. doi:10.7554/eLife.54056

261. Sun Z, Li X, Massena S, et al. VEGFR2 induces c-Src signaling and vascular permeability in vivo via the adaptor protein TSAd. *Journal of Experimental Medicine*. 2012;209(7):1363-1377. doi:10.1084/jem.20111343

262. Gordon EJ, Fukuhara D, Weström S, et al. The endothelial adaptor molecule TSAd is required for VEGF-induced angiogenic sprouting through junctional c-Src activation. *Sci Signal*. 2016;9(437). doi:10.1126/scisignal.aad9256

263. Li X, Padhan N, Sjöström EO, et al. VEGFR2 pY949 signalling regulates adherens junction integrity and metastatic spread. *Nat Commun*. 2016;7(1):11017. doi:10.1038/ncomms11017

264. Coon BG, Baeyens N, Han J, et al. Intramembrane binding of VE-cadherin to VEGFR2 and VEGFR3 assembles the endothelial mechanosensory complex. *Journal of Cell Biology*. 2015;208(7):975-986. doi:10.1083/jcb.201408103

265. Sawano A, Takahashi T, Yamaguchi S, Aonuma M, Shibuya M. Flt-1 but not KDR/Flk-1 tyrosine kinase is a receptor for placenta growth factor, which is related to vascular endothelial growth factor. *Cell Growth Differ*. 1996;7(2):213-221.

266. Imoukhuede PI, Popel AS. Quantification and cell-to-cell variation of vascular endothelial growth factor receptors. *Exp Cell Res*. 2011;317(7):955-965. doi:10.1016/j.yexcr.2010.12.014

267. Shibuya M. Vascular endothelial growth factor receptor-1 (VEGFR-1/Flt-1): a dual regulator for angiogenesis. *Angiogenesis*. 2006;9(4):225-230. doi:10.1007/s10456-006-9055-8

268. Rahimi N, Dayanir V, Lashkari K. Receptor Chimeras Indicate That the Vascular Endothelial Growth Factor Receptor-1 (VEGFR-1) Modulates Mitogenic Activity of VEGFR-2 in Endothelial Cells *. *Journal of Biological Chemistry*. 2000;275(22):16986-16992. doi:10.1074/jbc.M000528200

269. Cudmore MJ, Hewett PW, Ahmad S, et al. The role of heterodimerization between VEGFR-1 and VEGFR-2 in the regulation of endothelial cell homeostasis. *Nat Commun*. 2012;3(1):972. doi:10.1038/ncomms1977

270. Ferrara N, Adamis AP. Ten years of anti-vascular endothelial growth factor therapy. *Nat Rev Drug Discov*. 2016;15(6):385-403. doi:10.1038/nrd.2015.17

271. Peach CJ, Mignone VW, Arruda MA, et al. Molecular pharmacology of VEGF-A isoforms: Binding and signalling at VEGFR2. *Int J Mol Sci*. 2018;19(4). doi:10.3390/ijms19041264

272. Yokota Y, Nakajima H, Wakayama Y, et al. Endothelial Ca2+ oscillations reflect VEGFR signaling-regulated angiogenic capacity in vivo. *Elife*. 2015;4. doi:10.7554/eLife.08817

273. Koch S, Tugues S, Li X, Gualandi L, Claesson-Welsh L. Signal transduction by vascular endothelial growth factor receptors. *Biochemical Journal*. 2011;437(2):169-183. doi:10.1042/BJ20110301

274. Vincenti V, Cassano C, Rocchi M, Persico MG. Assignment of the Vascular Endothelial Growth Factor Gene to Human Chromosome 6p21.3. *Circulation*. 1996;93(8):1493-1495. doi:10.1161/01.CIR.93.8.1493

275. Yadav P, Pandey A, Kakani P, et al. Hypoxia-induced loss of SRSF2-dependent DNA methylation promotes CTCF-mediated alternative splicing of VEGFA in breast cancer. *iScience*. 2023;26(6):106804. doi:10.1016/j.isci.2023.106804

276. Nowak DG, Woolard J, Amin EM, et al. Expression of pro- and anti-angiogenic isoforms of VEGF is differentially regulated by splicing and growth factors. *J Cell Sci*. 2008;121(20):3487-3495. doi:10.1242/jcs.016410

277. Mineur P, Colige AC, Deroanne ChristopheF, et al. Newly identified biologically active and proteolysis-resistant VEGF-A isoform VEGF111 is induced by genotoxic agents. *J Cell Biol*. 2007;179(6):1261-1273. doi:10.1083/jcb.200703052

278. Wagner KD, El Maï M, Ladomery M, et al. Altered VEGF Splicing Isoform Balance in Tumor Endothelium Involves Activation of Splicing Factors Srpk1 and Srsf1 by the Wilms' Tumor Suppressor Wt1. *Cells*. 2019;8(1):41. doi:10.3390/cells8010041

279. Arcondeguy T, Lacazette E, Millevoi S, Prats H, Touriol C. VEGF-A mRNA processing, stability and translation: a paradigm for intricate regulation of gene expression at the post-transcriptional level. *Nucleic Acids Res*. 2013;41(17):7997-8010. doi:10.1093/nar/gkt539

280. Harris S, Craze M, Newton J, et al. Do Anti-Angiogenic VEGF (VEGFxxxb) Isoforms Exist? A Cautionary Tale. *PLoS One*. 2012;7(5):e35231. doi:10.1371/journal.pone.0035231

281. Varey AHR, Rennel ES, Qiu Y, et al. VEGF165b, an antiangiogenic VEGF-A isoform, binds and inhibits bevacizumab treatment in experimental colorectal carcinoma: balance of pro- and antiangiogenic VEGF-A isoforms has implications for therapy. *Br J Cancer*. 2008;98(8):1366-1379. doi:10.1038/sj.bjc.6604308

282. Woolard J, Wang WY, Bevan HS, et al. VEGF165b, an Inhibitory Vascular Endothelial Growth Factor Splice Variant. *Cancer Res*. 2004;64(21):7822-7835. doi:10.1158/0008-5472.CAN-04-0934

283. Bates DO, Cui TG, Doughty JM, et al. VEGF165b, an inhibitory splice variant of vascular endothelial growth factor, is down-regulated in renal cell carcinoma. *Cancer Res*. 2002;62(14):4123-4131.

284. Carmeliet P, Ferreira V, Breier G, et al. Abnormal blood vessel development and lethality in embryos lacking a single VEGF allele. *Nature*. 1996;380(6573):435-439. doi:10.1038/380435a0

285. Aiello LP, Wong JS. Role of vascular endothelial growth factor in diabetic vascular complications. *Kidney Int*. 2000;58:S113-S119. doi:10.1046/j.1523-1755.2000.07718.x

286. Byrne AM, Bouchier-Hayes DJ, Harmey JH. Angiogenic and cell survival functions of Vascular Endothelial Growth Factor (VEGF). *J Cell Mol Med*. 2005;9(4):777-794. doi:10.1111/j.1582-4934.2005.tb00379.x

287. Pauty J, Usuba R, Cheng IG, et al. A Vascular Endothelial Growth Factor-Dependent Sprouting Angiogenesis Assay Based on an In Vitro Human Blood Vessel Model for the Study of Anti-Angiogenic Drugs. *EBioMedicine*. 2018;27:225-236. doi:10.1016/j.ebiom.2017.12.014

288. Hattori K, Dias S, Heissig B, et al. Vascular Endothelial Growth Factor and Angiopoietin-1 Stimulate Postnatal Hematopoiesis by Recruitment of Vasculogenic and Hematopoietic Stem Cells. *J Exp Med*. 2001;193(9):1005-1014. doi:10.1084/jem.193.9.1005

289. Li L, Liu H, Xu C, et al. VEGF promotes endothelial progenitor cell differentiation and vascular repair through connexin 43. *Stem Cell Res Ther*. 2017;8(1):237. doi:10.1186/s13287-017-0684-1

290. Belle J, Ysasi A, Bennett RD, et al. Stretch-induced intussuceptive and sprouting angiogenesis in the chick chorioallantoic membrane. *Microvasc Res*. 2014;95:60-67. doi:10.1016/j.mvr.2014.06.009

291. Lee GS, Filipovic N, Miele LF, et al. Blood flow shapes intravascular pillar geometry in the chick chorioallantoic membrane. *J Angiogenes Res*. 2010;2(1):11. doi:10.1186/2040-2384-2-11

292. Baum O, Suter F, Gerber B, et al. VEGF-A promotes intussusceptive angiogenesis in the developing chicken chorioallantoic membrane. *Microcirculation*. Published online May 2010:no-no. doi:10.1111/j.1549-8719.2010.00043.x

293. Senger DR, Galli SJ, Dvorak AM, Perruzzi CA, Harvey VS, Dvorak HF. Tumor Cells Secrete a Vascular Permeability Factor That Promotes Accumulation of Ascites Fluid. *Science (1979)*. 1983;219(4587):983-985. doi:10.1126/science.6823562

294. Bates DO. Vascular endothelial growth factors and vascular permeability. *Cardiovasc Res*. 2010;87(2):262-271. doi:10.1093/cvr/cvq105

295. Wang X, Bove AM, Simone G, Ma B. Molecular Bases of VEGFR-2-Mediated Physiological Function and Pathological Role. *Front Cell Dev Biol*. 2020;8. doi:10.3389/fcell.2020.599281

296. Bosma EK, Darwesh S, Habani YI, et al. Differential roles of eNOS in late effects of VEGF-A on hyperpermeability in different types of endothelial cells. *Sci Rep*. 2023;13(1):21436. doi:10.1038/s41598-023-46893-4

297. El Baba N, Farran M, Khalil EA, Jaafar L, Fakhoury I, El-Sibai M. The Role of Rho GTPases in VEGF Signaling in Cancer Cells. *Analytical Cellular Pathology*. 2020;2020:1-11. doi:10.1155/2020/2097214

298. Wu MH, Yuan SY, Granger HJ. The protein kinase MEK1/2 mediate vascular endothelial growth factor- and histamine-induced hyperpermeability in porcine coronary venules. *J Physiol*. 2005;563(1):95-104. doi:10.1113/jphysiol.2004.076075

299. Six I, Kureishi Y, Luo Z, Walsh K. Akt signaling mediates VEGF/VPF vascular permeability in vivo. *FEBS Lett*. 2002;532(1-2):67-69. doi:10.1016/S0014-5793(02)03630-X

300. Yang GL, Li LY. Counterbalance: modulation of VEGF/VEGFR activities by TNFSF15. *Signal Transduct Target Ther*. 2018;3(1):21. doi:10.1038/s41392-018-0023-8

301. Gliki G, Abu-Ghazaleh R, Jezequel S, Wheeler-Jones C, Zachary I. Vascular endothelial growth factor-induced prostacyclin production is mediated by a protein kinase C (PKC)-dependent activation of extracellular signal-regulated protein kinases 1 and 2 involving PKC-δ and by mobilization of intracellular CA2+. *Biochemical Journal*. 2001;353(3):503-512. doi:10.1042/0264-6021:3530503

302. Blanes MG, Oubaha M, Rautureau Y, Gratton JP. Phosphorylation of tyrosine 801 of vascular endothelial growth factor receptor-2 is necessary for Akt-dependent endothelial nitric-oxide synthase activation and nitric oxide release from endothelial cells. *Journal of Biological Chemistry*. 2007;282(14):10660-10669. doi:10.1074/jbc.M609048200

303. Chou MT, Wang J, Fujita DJ. Src Kinase becomes preferentially associated with the VEGFR, KDR/Flk-1, following VEGF stimulation of vascular endothelial cells. *BMC Biochem*. 2002;3(1):32. doi:10.1186/1471-2091-3-32

304. Eliceiri BP, Paul R, Schwartzberg PL, Hood JD, Leng J, Cheresh DA. Selective Requirement for Src Kinases during VEGF-Induced Angiogenesis and Vascular Permeability. *Mol Cell*. 1999;4(6):915-924. doi:10.1016/S1097-2765(00)80221-X

305. Adam AP, Sharenko AL, Pumiglia K, Vincent PA. Src-induced Tyrosine Phosphorylation of VE-cadherin Is Not Sufficient to Decrease Barrier Function of Endothelial Monolayers. *Journal of Biological Chemistry*. 2010;285(10):7045-7055. doi:10.1074/jbc.M109.079277

306. Orsenigo F, Giampietro C, Ferrari A, et al. Phosphorylation of VE-cadherin is modulated by haemodynamic forces and contributes to the regulation of vascular permeability in vivo. *Nat Commun*. 2012;3(1):1208. doi:10.1038/ncomms2199

307. Wang W, Dentler WL, Borchardt RT. VEGF increases BMEC monolayer permeability by affecting occludin expression and tight junction assembly. *American Journal of Physiology-Heart and Circulatory Physiology*. 2001;280(1):H434-H440. doi:10.1152/ajpheart.2001.280.1.H434

308. Gavard J, Gutkind JS. VEGF controls endothelial-cell permeability by promoting the β-arrestin-dependent endocytosis of VE-cadherin. *Nat Cell Biol*. 2006;8(11):1223-1234. doi:10.1038/ncb1486

309. De Rossi G, Vähätupa M, Cristante E, et al. Pathological Angiogenesis Requires Syndecan-4 for Efficient VEGFA-Induced VE-Cadherin Internalization. *Arterioscler Thromb Vasc Biol*. 2021;41(4):1374-1389. doi:10.1161/ATVBAHA.121.315941

310. Elias BC, Suzuki T, Seth A, et al. Phosphorylation of Tyr-398 and Tyr-402 in Occludin Prevents Its Interaction with ZO-1 and Destabilizes Its Assembly at the Tight Junctions. *Journal of Biological Chemistry*. 2009;284(3):1559-1569. doi:10.1074/jbc.M804783200

311. Bryan BA, Dennstedt E, Mitchell DC, et al. RhoA/ROCK signaling is essential for multiple aspects of VEGF-mediated angiogenesis. *The FASEB Journal*. 2010;24(9):3186-3195. doi:10.1096/fj.09-145102

312. Hoeppner LH, Sinha S, Wang Y, et al. RhoC maintains vascular homeostasis by regulating VEGF-induced signaling in endothelial cells. *J Cell Sci*. Published online January 1, 2015. doi:10.1242/jcs.167601

313. Abraham HG, Ulintz PJ, Goo L, et al. RhoC Modulates Cell Junctions and Type I Interferon Response in Aggressive Breast Cancers. *Front Oncol*. 2021;11. doi:10.3389/fonc.2021.712041

314. Garrett TA, Van Buul JD, Burridge K. VEGF-induced Rac1 activation in endothelial cells is regulated by the guanine nucleotide exchange factor Vav2. *Exp Cell Res*. 2007;313(15):3285-3297. doi:10.1016/j.yexcr.2007.05.027

315. Akhtar N, Hotchin NA. RAC1 Regulates Adherens Junctions through Endocytosis of E-Cadherin. *Mol Biol Cell*. 2001;12(4):847-862. doi:10.1091/mbc.12.4.847

316. Moztarzadeh S, Sepic S, Hamad I, Waschke J, Radeva MY, García-Ponce A. Cortactin is in a complex with VE-cadherin and is required for endothelial adherens junction stability through Rap1/Rac1 activation. *Sci Rep*. 2024;14(1):1218. doi:10.1038/s41598-024-51269-3

317. Schwarz Q, Ruhrberg C. Neuropilin, you gotta let me know: should I stay or should I go? *Cell Adh Migr*. 2010;4(1):61-66. doi:10.4161/cam.4.1.10207

318. Guo HF, Vander Kooi CW. Neuropilin Functions as an Essential Cell Surface Receptor. *Journal of Biological Chemistry*. 2015;290(49):29120-29126. doi:10.1074/jbc.R115.687327

319. Chen H, Chédotal A, He Z, Goodman CS, Tessier-Lavigne M. Neuropilin-2, a novel member of the neuropilin family, is a high affinity receptor for the semaphorins Sema E and Sema IV but not Sema III. *Neuron*. 1997;19(3):547-559. doi:10.1016/s0896-6273(00)80371-2

320. Lu Y, Xiang H, Liu P, et al. Identification of circulating neuropilin-1 and dose-dependent elevation following anti-neuropilin-1 antibody administration. *MAbs*. 2009;1(4):364-369. doi:10.4161/mabs.1.4.8885

321. Gelfand M V, Hagan N, Tata A, et al. Neuropilin-1 functions as a VEGFR2 co-receptor to guide developmental angiogenesis independent of ligand binding. *Elife*. 2014;3. doi:10.7554/eLife.03720

322. Parker MW, Xu P, Li X, Vander Kooi CW. Structural Basis for Selective Vascular Endothelial Growth Factor-A (VEGF-A) Binding to Neuropilin-1. *Journal of Biological Chemistry*. 2012;287(14):11082-11089. doi:10.1074/jbc.M111.331140

323. Peach CJ, Tonello R, Damo E, et al. Neuropilin-1 is a co-receptor for Nerve Growth Factor-evoked pain. Published online December 6, 2024. doi:10.1101/2023.12.06.570398

324. Rizzolio S, Rabinowicz N, Rainero E, et al. Neuropilin-1–Dependent Regulation of EGF-Receptor Signaling. *Cancer Res*. 2012;72(22):5801-5811. doi:10.1158/0008-5472.CAN-12-0995

325. Glinka Y, Stoilova S, Mohammed N, Prud'homme GJ. Neuropilin-1 exerts co-receptor function for TGF-beta-1 on the membrane of cancer cells and enhances responses to both latent and active TGF-beta. *Carcinogenesis*. 2011;32(4):613-621. doi:10.1093/carcin/bgq281

326. Roy S, Bag AK, Singh RK, Talmadge JE, Batra SK, Datta K. Multifaceted Role of Neuropilins in the Immune System: Potential Targets for Immunotherapy. *Front Immunol*. 2017;8. doi:10.3389/fimmu.2017.01228

327. Soker S, Takashima S, Miao HQ, Neufeld G, Klagsbrun M. Neuropilin-1 Is Expressed by Endothelial and Tumor Cells as an Isoform-Specific Receptor for Vascular Endothelial Growth Factor. *Cell*. 1998;92(6):735-745. doi:10.1016/S0092-8674(00)81402-6

328. Cai H, Reed RR. Cloning and Characterization of Neuropilin-1-Interacting Protein: A PSD-95/Dlg/ZO-1 Domain-Containing Protein That Interacts with the Cytoplasmic Domain of Neuropilin-1. *The Journal of Neuroscience*. 1999;19(15):6519-6527. doi:10.1523/JNEUROSCI.19-15-06519.1999

329. Alshawaf E, Hammad MM, Marafie SK, et al. Discovery of natural products to block SARS-CoV-2 S-protein interaction with Neuropilin-1 receptor: A molecular dynamics simulation approach. *Microb Pathog*. 2022;170:105701. doi:10.1016/j.micpath.2022.105701

330. Chen H, He Z, Bagri A, Tessier-Lavigne M. Semaphorin–Neuropilin Interactions Underlying Sympathetic Axon Responses to Class III Semaphorins. *Neuron*. 1998;21(6):1283-1290. doi:10.1016/S0896-6273(00)80648-0

331. Nakamura F, Tanaka M, Takahashi T, Kalb RG, Strittmatter SM. Neuropilin-1 Extracellular Domains Mediate Semaphorin D/III-Induced Growth Cone Collapse. *Neuron*. 1998;21(5):1093-1100. doi:10.1016/S0896-6273(00)80626-1

332. Takahashi T, Nakamura F, Jin Z, Kalb RG, Strittmatter SM. Semaphorins A and E act as antagonists of neuropilin-1 and agonists of neuropilin-2 receptors. *Nat Neurosci*. 1998;1(6):487-493. doi:10.1038/2203

333. Vieira JM, Ruhrberg C, Schwarz Q. VEGF receptor signaling in vertebrate development. *Organogenesis*. 2010;6(2):97-106. doi:10.4161/org.6.2.11686

334. Chuckran CA, Liu C, Bruno TC, Workman CJ, Vignali DA. Neuropilin-1: a checkpoint target with unique implications for cancer immunology and immunotherapy. *J Immunother Cancer*. 2020;8(2):e000967. doi:10.1136/jitc-2020-000967

335. Lee CC, Kreusch A, McMullan D, Ng K, Spraggon G. Crystal Structure of the Human Neuropilin-1 b1 Domain. *Structure*. 2003;11(1):99-108. doi:10.1016/S0969-2126(02)00941-3

336. Gu C, Limberg BJ, Whitaker GB, et al. Characterization of Neuropilin-1 Structural Features That Confer Binding to Semaphorin 3A and Vascular Endothelial Growth Factor 165. *Journal of Biological Chemistry*. 2002;277(20):18069-18076. doi:10.1074/jbc.M201681200

337. Yelland T, Djordjevic S. Crystal Structure of the Neuropilin-1 MAM Domain: Completing the Neuropilin-1 Ectodomain Picture. *Structure*. 2016;24(11):2008-2015. doi:10.1016/j.str.2016.08.017

338. Roth L, Nasarre C, Dirrig-Grosch S, et al. Transmembrane Domain Interactions Control Biological Functions of Neuropilin-1. *Mol Biol Cell*. 2008;19(2):646-654. doi:10.1091/mbc.e07-06-0625

339. Wang L, Zeng H, Wang P, Soker S, Mukhopadhyay D. Neuropilin-1-mediated Vascular Permeability Factor/Vascular Endothelial Growth Factor-dependent Endothelial Cell Migration. *Journal of Biological Chemistry*. 2003;278(49):48848-48860. doi:10.1074/jbc.M310047200

340. Valdembri D, Caswell PT, Anderson KI, et al. Neuropilin-1/GIPC1 Signaling Regulates α5β1 Integrin Traffic and Function in Endothelial Cells. *PLoS Biol*. 2009;7(1):e1000025. doi:10.1371/journal.pbio.1000025

341. Wang L, Mukhopadhyay D, Xu X, Wang L, Mukhopadhyay D, Xu X. C terminus of RGS-GAIP-interacting protein conveys neuropilin-1-mediated signaling during angiogenesis. *The FASEB Journal*. 2006;20(9):1513-1515. doi:10.1096/fj.05-5504fje

342. Huang X, Ye Q, Chen M, et al. N-glycosylation-defective splice variants of neuropilin-1 promote metastasis by activating endosomal signals. *Nat Commun*. 2019;10(1):3708. doi:10.1038/s41467-019-11580-4

343. Cackowski FC, Xu L, Hu B, Cheng SY. Identification of two novel alternatively spliced Neuropilin-1 isoforms. *Genomics*. 2004;84(1):82-94. doi:10.1016/j.ygeno.2004.02.001

344. Gagnon ML, Bielenberg DR, Gechtman Z, et al. Identification of a natural soluble neuropilin-1 that binds vascular endothelial growth factor: In vivo expression and antitumor activity. *Proceedings of the National Academy of Sciences*. 2000;97(6):2573-2578. doi:10.1073/pnas.040337597

345. Tao Q, Spring SC, Terman BI. Characterization of a new alternatively spliced neuropilin-1 isoform. *Angiogenesis*. 2003;6(1):39-45. doi:10.1023/A:1025884628155

346. Chen R, Jiang X, Sun D, et al. Glycoproteomics Analysis of Human Liver Tissue by Combination of Multiple Enzyme Digestion and Hydrazide Chemistry. *J Proteome Res*. 2009;8(2):651-661. doi:10.1021/pr8008012

347. Appleton BA, Wu P, Maloney J, et al. Structural studies of neuropilin/antibody complexes provide insights into semaphorin and VEGF binding. *EMBO J*. 2007;26(23):4902-4912. doi:10.1038/sj.emboj.7601906

348. Shintani Y, Takashima S, Asano Y, et al. Glycosaminoglycan modification of neuropilin-1 modulates VEGFR2 signaling. *EMBO J*. 2006;25(13):3045-3055. doi:10.1038/sj.emboj.7601188

349. Frankel P, Pellet-Many C, Lehtolainen P, et al. Chondroitin sulphate-modified neuropilin 1 is expressed in human tumour cells and modulates 3D invasion in the U87MG human glioblastoma cell line through a p130Cas-mediated pathway. *EMBO Rep*. 2008;9(10):983-989. doi:10.1038/embor.2008.151

350. Yaqoob U, Cao S, Shergill U, et al. Neuropilin-1 Stimulates Tumor Growth by Increasing Fibronectin Fibril Assembly in the Tumor Microenvironment. *Cancer Res*. 2012;72(16):4047-4059. doi:10.1158/0008-5472.CAN-11-3907

351. Whitaker GB, Limberg BJ, Rosenbaum JS. Vascular Endothelial Growth Factor Receptor-2 and Neuropilin-1 Form a Receptor Complex That Is Responsible for the Differential Signaling Potency of VEGF165 and VEGF121. *Journal of Biological Chemistry*. 2001;276(27):25520-25531. doi:10.1074/jbc.M102315200

352. Soker S, Miao H, Nomi M, Takashima S, Klagsbrun M. VEGF165 mediates formation of complexes containing VEGFR-2 and neuropilin-1 that enhance VEGF165-receptor binding. *J Cell Biochem*. 2002;85(2):357-368. doi:10.1002/jcb.10140

353. Shraga-Heled N, Kessler O, Prahst C, Kroll J, Augustin H, Neufeld G. Neuropilin-1 and neuropilin-2 enhance VEGF $_{121}$ stimulated signal transduction by the VEGFR-2 receptor. *The FASEB Journal*. 2007;21(3):915-926. doi:10.1096/fj.06-6277com

354. Peach CJ, Kilpatrick LE, Friedman-Ohana R, et al. Real-Time Ligand Binding of Fluorescent VEGF-A Isoforms that Discriminate between VEGFR2 and NRP1 in Living Cells. *Cell Chem Biol*. 2018;25(10):1208-1218.e5. doi:10.1016/j.chembiol.2018.06.012

355. Sharma S, Ehrlich M, Zhang M, Blobe GC, Henis YI. NRP1 interacts with endoglin and VEGFR2 to modulate VEGF signaling and endothelial cell sprouting. *Commun Biol*. 2024;7(1):112. doi:10.1038/s42003-024-05798-2

356. Kawamura H, Li X, Goishi K, et al. Neuropilin-1 in regulation of VEGF-induced activation of p38MAPK and endothelial cell organization. *Blood*. 2008;112(9):3638-3649. doi:10.1182/blood-2007-12-125856

357. Wang L, Feng Y, Xie X, et al. Neuropilin-1 aggravates liver cirrhosis by promoting angiogenesis via VEGFR2-dependent PI3K/Akt pathway in hepatic sinusoidal endothelial cells. *EBioMedicine*. 2019;43:525-536. doi:10.1016/j.ebiom.2019.04.050

358. Kofler NM, Simons M. Angiogenesis versus arteriogenesis: neuropilin 1 modulation of VEGF signaling. *F1000Prime Rep*. 2015;7. doi:10.12703/P7-26

359. Uniewicz KA, Cross MJ, Fernig DG. Exogenous Recombinant Dimeric Neuropilin-1 Is Sufficient to Drive Angiogenesis. *Journal of Biological Chemistry*. 2011;286(1):12-23. doi:10.1074/jbc.M110.190801

360. Prahst C, Héroult M, Lanahan AA, et al. Neuropilin-1-VEGFR-2 Complexing Requires the PDZ-binding Domain of Neuropilin-1. *Journal of Biological Chemistry*. 2008;283(37):25110-25114. doi:10.1074/jbc.C800137200

361. Kawasaki T, Kitsukawa T, Bekku Y, et al. A requirement for neuropilin-1 in embryonic vessel formation. *Development*. 1999;126(21):4895-4902. doi:10.1242/dev.126.21.4895

362. Kitsukawa T, Shimono A, Kawakami A, Kondoh H, Fujisawa H. Overexpression of a membrane protein, neuropilin, in chimeric mice causes anomalies in the cardiovascular system, nervous system and limbs. *Development*. 1995;121(12):4309-4318. doi:10.1242/dev.121.12.4309

363. Gerhardt H, Ruhrberg C, Abramsson A, Fujisawa H, Shima D, Betsholtz C. Neuropilin-1 is required for endothelial tip cell guidance in the developing central nervous system. *Developmental Dynamics*. 2004;231(3):503-509. doi:10.1002/dvdy.20148

364. Fantin A, Vieira JM, Plein A, et al. NRP1 acts cell autonomously in endothelium to promote tip cell function during sprouting angiogenesis. *Blood*. 2013;121(12):2352-2362. doi:10.1182/blood-2012-05-424713

365. Matthies AM, Low QEH, Lingen MW, DiPietro LA. Neuropilin-1 Participates in Wound Angiogenesis. *Am J Pathol*. 2002;160(1):289-296. doi:10.1016/S0002-9440(10)64372-6

366. Gu C, Rodriguez ER, Reimert D V, et al. Neuropilin-1 Conveys Semaphorin and VEGF Signaling during Neural and Cardiovascular Development. *Dev Cell*. 2003;5(1):45-57. doi:10.1016/S1534-5807(03)00169-2

367. Fantin A, Herzog B, Mahmoud M, et al. Neuropilin 1 (NRP1) hypomorphism combined with defective VEGF-A binding reveals novel roles for NRP1 in developmental and pathological angiogenesis. *Development*. 2014;141(3):556-562. doi:10.1242/dev.103028

368. Lanahan A, Zhang X, Fantin A, et al. The Neuropilin 1 Cytoplasmic Domain Is Required for VEGF-A-Dependent Arteriogenesis. *Dev Cell*. 2013;25(2):156-168. doi:10.1016/j.devcel.2013.03.019

369. Fantin A, Schwarz Q, Davidson K, Normando EM, Denti L, Ruhrberg C. The cytoplasmic domain of neuropilin 1 is dispensable for angiogenesis, but promotes the spatial separation of retinal arteries and veins. *Development*. 2011;138(19):4185-4191. doi:10.1242/dev.070037

370. Fuh G, Garcia KC, de Vos AM. The Interaction of Neuropilin-1 with Vascular Endothelial Growth Factor and Its Receptor Flt-1. *Journal of Biological Chemistry*. 2000;275(35):26690-26695. doi:10.1016/S0021-9258(19)61431-6

371. Napolitano V, Russo D, Morra F, et al. Neuropilin-1 Expression Associates with Poor Prognosis in HNSCC and Elicits EGFR Activation upon CDDP-Induced Cytotoxic Stress. *Cancers (Basel)*. 2021;13(15):3822. doi:10.3390/cancers13153822

372. Parikh AA, Liu WB, Fan F, et al. Expression and regulation of the novel vascular endothelial growth factor receptor neuropilin-1 by epidermal growth factor in human pancreatic carcinoma. *Cancer*. 2003;98(4):720-729. doi:10.1002/cncr.11560

373. Kawakami T, Tokunaga T, Hatanaka H, et al. Neuropilin 1 and neuropilin 2 co-expression is significantly correlated with increased vascularity and poor prognosis in nonsmall cell lung carcinoma. *Cancer*. 2002;95(10):2196-2201. doi:10.1002/cncr.10936

374. Dong JC, Gao H, Zuo SY, et al. Neuropilin 1 expression correlates with the Radio-resistance of human non-small-cell lung cancer cells. *J Cell Mol Med*. 2015;19(9):2286-2295. doi:10.1111/jcmm.12623

375. Parikh AA, Fan F, Liu WB, et al. Neuropilin-1 in Human Colon Cancer. *Am J Pathol*. 2004;164(6):2139-2151. doi:10.1016/S0002-9440(10)63772-8

376. Fernández-Palanca P, Payo-Serafín T, Fondevila F, et al. Neuropilin-1 as a Potential Biomarker of Prognosis and Invasive-Related Parameters in Liver and Colorectal Cancer: A Systematic Review and Meta-Analysis of Human Studies. *Cancers (Basel)*. 2022;14(14):3455. doi:10.3390/cancers14143455

377. Zhao J, Gu L, Li C, Ma W, Ni Z. Investigation of a novel biomarker, neuropilin-1, and its application for poor prognosis in acute myeloid leukemia patients. *Tumor Biology*. 2014;35(7):6919-6924. doi:10.1007/s13277-014-1942-9

378. H. Sallam T, A.shams Eldin El Telbany M, M. Mahmoud H, A. Iskander M. Significance of Neuropilin-1 Expression in Acute Myeloid Leukemia. *The Turkish Journal of Hematology*. 2013;30(3):300-306. doi:10.4274/Tjh.2011.0005

379. Kreuter M, Woelke K, Bieker R, et al. Correlation of neuropilin-1 overexpression to survival in acute myeloid leukemia. *Leukemia*. 2006;20(11):1950-1954. doi:10.1038/sj.leu.2404384

380. Miao H, Lee P, Lin H, Soker S, Klagsbrun M. Neuropilin-1 expression by tumor cells promotes tumor angiogenesis and progression. *The FASEB Journal*. 2000;14(15):2532-2539. doi:10.1096/fj.00-0250com

381. Pan Q, Chanthery Y, Liang WC, et al. Blocking Neuropilin-1 Function Has an Additive Effect with Anti-VEGF to Inhibit Tumor Growth. *Cancer Cell*. 2007;11(1):53-67. doi:10.1016/j.ccr.2006.10.018

382. Plein A, Fantin A, Ruhrberg C. Neuropilin Regulation of Angiogenesis, Arteriogenesis, and Vascular Permeability. *Microcirculation*. 2014;21(4):315-323. doi:10.1111/micc.12124

383. Takagi S, Kasuya Y, Shimizu M, et al. Expression of a Cell Adhesion Molecule, Neuropilin, in the Developing Chick Nervous System. *Dev Biol*. 1995;170(1):207-222. doi:10.1006/dbio.1995.1208

384. Shimizu M, Murakami Y, Suto F, Fujisawa H. Determination of Cell Adhesion Sites of Neuropilin-1. *J Cell Biol*. 2000;148(6):1283-1294. doi:10.1083/jcb.148.6.1283

385. Roth L, Prahst C, Ruckdeschel T, et al. Neuropilin-1 mediates vascular permeability independently of vascular endothelial growth factor receptor-2 activation. *Sci Signal*. 2016;9(425). doi:10.1126/scisignal.aad3812

386. Murga M, Fernandez-Capetillo O, Tosato G. Neuropilin-1 regulates attachment in human endothelial cells independently of vascular endothelial growth factor receptor-2. *Blood*. 2005;105(5):1992-1999. doi:10.1182/blood-2004-07-2598

387. Muhl L, Folestad EB, Gladh H, et al. Neuropilin 1 binds PDGF-D and is a co-receptor in PDGF-D–PDGFRβ signaling. *J Cell Sci*. 2017;130(8):1365-1378. doi:10.1242/jcs.200493

388. Bosseboeuf E, Chikh A, Chaker AB, et al. Neuropilin-1 interacts with VE-cadherin and TGFBR2 to stabilize adherens junctions and prevent activation of endothelium under flow. *Sci Signal*. 2023;16(786). doi:10.1126/scisignal.abo4863

389. Fantin A, Lampropoulou A, Senatore V, et al. VEGF165-induced vascular permeability requires NRP1 for ABL-mediated SRC family kinase activation. *Journal of Experimental Medicine*. 2017;214(4):1049-1064. doi:10.1084/jem.20160311

390. Mehta V, Pang KL, Rozbesky D, et al. The guidance receptor plexin D1 is a mechanosensor in endothelial cells. *Nature*. 2020;578(7794):290-295. doi:10.1038/s41586-020-1979-4

391. Gioelli N, Neilson LJ, Wei N, et al. Neuropilin 1 and its inhibitory ligand mini-tryptophanyl-tRNA synthetase inversely regulate VE-cadherin turnover and vascular permeability. *Nat Commun*. 2022;13(1):4188. doi:10.1038/s41467-022-31904-1

392. Yaqoob U, Cao S, Shergill U, et al. Neuropilin-1 Stimulates Tumor Growth by Increasing Fibronectin Fibril Assembly in the Tumor Microenvironment. *Cancer Res*. 2012;72(16):4047-4059. doi:10.1158/0008-5472.CAN-11-3907

393. Fukasawa M, Matsushita A, Korc M. Neuropilin-1 interacts with integrin β1 and modulates pancreatic cancer cell growth, survival and invasion. *Cancer Biol Ther*. 2007;6(8):1184-1191. doi:10.4161/cbt.6.8.4363

394. Hirota S, Clements TP, Tang LK, et al. Neuropilin-1 balances β8 integrin-activated TGFβ signaling to control sprouting angiogenesis in the brain. *Development*. Published online January 1, 2015. doi:10.1242/dev.113746

395. Colotti G, Failla CM, Lacal PM, et al. Neuropilin-1 is required for endothelial cell adhesion to soluble vascular endothelial growth factor receptor 1. *FEBS J*. 2022;289(1):183-198. doi:10.1111/febs.16119

396. Orecchia A, Lacal PM, Schietroma C, Morea V, Zambruno G, Failla CM. Vascular endothelial growth factor receptor-1 is deposited in the extracellular matrix by endothelial cells and is a ligand for theα5β1 integrin. *J Cell Sci*. 2003;116(17):3479-3489. doi:10.1242/jcs.00673

397. Seerapu HR, Borthakur S, Kong N, et al. The cytoplasmic domain of neuropilin-1 regulates focal adhesion turnover. *FEBS Lett*. 2013;587(21):3392-3399. doi:10.1016/j.febslet.2013.08.040

398. Ellison TS, Atkinson SJ, Steri V, et al. Suppressing β3-integrin triggers a neuropilin-1 dependent change in focal adhesion remodelling that can be targeted to block pathological angiogenesis. *Dis Model Mech*. Published online January 1, 2015. doi:10.1242/dmm.019927

399. Domingues A, Fantin A. Neuropilin 1 Regulation of Vascular Permeability Signaling. *Biomolecules*. 2021;11(5):666. doi:10.3390/biom11050666

400. Cerani A, Tetreault N, Menard C, et al. Neuron-Derived Semaphorin 3A Is an Early Inducer of Vascular Permeability in Diabetic Retinopathy via Neuropilin-1. *Cell Metab*. 2013;18(4):505-518. doi:10.1016/j.cmet.2013.09.003

401. Becker PM, Waltenberger J, Yachechko R, et al. Neuropilin-1 Regulates Vascular Endothelial Growth Factor–Mediated Endothelial Permeability. *Circ Res*. 2005;96(12):1257-1265. doi:10.1161/01.RES.0000171756.13554.49

402. Teesalu T, Sugahara KN, Kotamraju VR, Ruoslahti E. C-end rule peptides mediate neuropilin-1-dependent cell, vascular, and tissue penetration. *Proceedings of the National Academy of Sciences*. 2009;106(38):16157-16162. doi:10.1073/pnas.0908201106

403. Wang J, Wang S, Li M, et al. The Neuropilin-1 Inhibitor, ATWLPPR Peptide, Prevents Experimental Diabetes-Induced Retinal Injury by Preserving Vascular Integrity and Decreasing Oxidative Stress. *PLoS One*. 2015;10(11):e0142571. doi:10.1371/journal.pone.0142571

404. Pal S, Su Y, Claesson-Welsh L, Richards M. Neuropilin-1 controls vascular permeability through juxtacrine regulation of endothelial adherens junctions. Published online April 11, 2024. doi:10.7554/eLife.95934.1

405. Acevedo LM, Barillas S, Weis SM, Göthert JR, Cheresh DA. Semaphorin 3A suppresses VEGF-mediated angiogenesis yet acts as a vascular permeability factor. *Blood*. 2008;111(5):2674-2680. doi:10.1182/blood-2007-08-110205

406. Stacker SA, Vitali A, Caesar C, et al. A Mutant Form of Vascular Endothelial Growth Factor (VEGF) That Lacks VEGF Receptor-2 Activation Retains the Ability to Induce Vascular Permeability. *Journal of Biological Chemistry*. 1999;274(49):34884-34892. doi:10.1074/jbc.274.49.34884

407. Mamluk R, Klagsbrun M, Detmar M, Bielenberg DR. Soluble neuropilin targeted to the skin inhibits vascular permeability. *Angiogenesis*. 2005;8(3):217-227. doi:10.1007/s10456-005-9009-6

408. Narazaki M, Tosato G. Ligand-induced internalization selects use of common receptor neuropilin-1 by VEGF165 and semaphorin3A. *Blood*. 2006;107(10):3892-3901. doi:10.1182/blood-2005-10-4113

409. Salikhova A, Wang L, Lanahan AA, et al. Vascular Endothelial Growth Factor and Semaphorin Induce Neuropilin-1 Endocytosis via Separate Pathways. *Circ Res*. 2008;103(6). doi:10.1161/CIRCRESAHA.108.183327

410. Eichmann A, Simons M. VEGF signaling inside vascular endothelial cells and beyond. *Curr Opin Cell Biol*. 2012;24(2):188-193. doi:10.1016/j.ceb.2012.02.002

411. Zwang Y, Yarden Y. Systems Biology of Growth Factor-Induced Receptor Endocytosis. *Traffic*. 2009;10(4):349-363. doi:10.1111/j.1600-0854.2008.00870.x

412. Simons M. An Inside View: VEGF Receptor Trafficking and Signaling. *Physiology*. 2012;27(4):213-222. doi:10.1152/physiol.00016.2012

413. Ballmer-Hofer K, Andersson AE, Ratcliffe LE, Berger P. Neuropilin-1 promotes VEGFR-2 trafficking through Rab11 vesicles thereby specifying signal output. *Blood*. 2011;118(3):816-826. doi:10.1182/blood-2011-01-328773

414. Bayliss AL, Sundararaman A, Granet C, Mellor H. Raftlin is recruited by neuropilin-1 to the activated VEGFR2 complex to control proangiogenic signaling. *Angiogenesis*. 2020;23(3):371-383. doi:10.1007/s10456-020-09715-z

415. Koch S, van Meeteren LA, Morin E, et al. NRP1 Presented in trans to the Endothelium Arrests VEGFR2 Endocytosis, Preventing Angiogenic Signaling and Tumor Initiation. *Dev Cell*. 2014;28(6):633-646. doi:10.1016/j.devcel.2014.02.010

416. Benwell CJ, Johnson RT, Taylor JAGE, Lambert J, Robinson SD. A proteomics approach to isolating neuropilin-dependent α5 integrin trafficking pathways: neuropilin 1 and 2 co-traffic α5 integrin through endosomal p120RasGAP to promote polarised fibronectin fibrillogenesis in endothelial cells. *Commun Biol*. 2024;7(1):629. doi:10.1038/s42003-024-06320-4

417. Burckhardt CJ, Minna JD, Danuser G. SH3BP4 promotes neuropilin-1 and α5-integrin endocytosis and is inhibited by Akt. *Dev Cell*. 2021;56(8):1164-1181.e12. doi:10.1016/j.devcel.2021.03.009

418. Prud'homme GJ, Glinka Y, Lichner Z, Yousef GM. Neuropilin-1 is a receptor for extracellular miRNA and AGO2/miRNA complexes and mediates the internalization of miRNAs that modulate cell function. *Oncotarget*. 2016;7(42):68057-68071. doi:10.18632/oncotarget.10929

419. Pawlica P, Yario TA, White S, et al. SARS-CoV-2 expresses a microRNA-like small RNA able to selectively repress host genes. *Proceedings of the National Academy of Sciences*. 2021;118(52). doi:10.1073/pnas.2116668118

420. Balistreri G, Yamauchi Y, Teesalu T. A widespread viral entry mechanism: The C-end Rule motif–neuropilin receptor interaction. *Proceedings of the National Academy of Sciences*. 2021;118(49). doi:10.1073/pnas.2112457118

421. Örd M, Faustova I, Loog M. The sequence at Spike S1/S2 site enables cleavage by furin and phospho-regulation in SARS-CoV2 but not in SARS-CoV1 or MERS-CoV. *Sci Rep*. 2020;10(1):16944. doi:10.1038/s41598-020-74101-0

422. Romeu AR. Probable human origin of the SARS-CoV-2 polybasic furin cleavage motif. *BMC Genom Data*. 2023;24(1):71. doi:10.1186/s12863-023-01169-8

423. Peacock TP, Goldhill DH, Zhou J, et al. The furin cleavage site in the SARS-CoV-2 spike protein is required for transmission in ferrets. *Nat Microbiol*. 2021;6(7):899-909. doi:10.1038/s41564-021-00908-w

424. Johnson BA, Xie X, Bailey AL, et al. Loss of furin cleavage site attenuates SARS-CoV-2 pathogenesis. *Nature*. 2021;591(7849):293-299. doi:10.1038/s41586-021-03237-4

425. Cantuti-Castelvetri L, Ojha R, Pedro LD, et al. Neuropilin-1 facilitates SARS-CoV-2 cell entry and infectivity. *Science (1979)*. 2020;370(6518):856-860. doi:10.1126/science.abd2985

426. Daly JL, Simonetti B, Klein K, et al. Neuropilin-1 is a host factor for SARS-CoV-2 infection. *Science (1979)*. 2020;370(6518):861-865. doi:10.1126/science.abd3072

427. Kong W, Montano M, Corley MJ, et al. Neuropilin-1 Mediates SARS-CoV-2 Infection of Astrocytes in Brain Organoids, Inducing Inflammation Leading to Dysfunction and Death of Neurons. *mBio*. 2022;13(6). doi:10.1128/mbio.02308-22

428. Szlachcic WJ, Dabrowska A, Milewska A, et al. SARS-CoV-2 infects an in vitro model of the human developing pancreas through endocytosis. *iScience*. 2022;25(7):104594. doi:10.1016/j.isci.2022.104594

429. Ghez D, Lepelletier Y, Lambert S, et al. Neuropilin-1 Is Involved in Human T-Cell Lymphotropic Virus Type 1 Entry. *J Virol*. 2006;80(14):6844-6854. doi:10.1128/JVI.02719-05

430. Wang HB, Zhang H, Zhang JP, et al. Neuropilin 1 is an entry factor that promotes EBV infection of nasopharyngeal epithelial cells. *Nat Commun*. 2015;6(1):6240. doi:10.1038/ncomms7240

431. Peach CJ, Kilpatrick LE, Woolard J, Hill SJ. Use of NanoBiT and NanoBRET to monitor fluorescent VEGF-A binding kinetics to VEGFR2/NRP1 heteromeric complexes in living cells. *Br J Pharmacol*. 2021;178(12):2393-2411. doi:10.1111/bph.15426

432. Snuderl M, Batista A, Kirkpatrick ND, et al. Targeting Placental Growth Factor/Neuropilin 1 Pathway Inhibits Growth and Spread of Medulloblastoma. *Cell*. 2013;152(5):1065-1076. doi:10.1016/j.cell.2013.01.036

433. Zylbersztejn K, Petkovic M, Burgo A, et al. The vesicular SNARE Synaptobrevin is required for Semaphorin 3A axonal repulsion. *Journal of Cell Biology*. 2012;196(1):37-46. doi:10.1083/jcb.201106113

434. Huttlin EL, Bruckner RJ, Navarrete-Perea J, et al. Dual proteome-scale networks reveal cell-specific remodeling of the human interactome. *Cell*. 2021;184(11):3022-3040.e28. doi:10.1016/j.cell.2021.04.011

435. Huttlin EL, Bruckner RJ, Paulo JA, et al. Architecture of the human interactome defines protein communities and disease networks. *Nature*. 2017;545(7655):505-509. doi:10.1038/nature22366

436. Lee KT, Pranoto IK, Kim SY, et al. Comparative interactome analysis of α-arrestin families in human and Drosophila. *Elife*. 2024;12. doi:10.7554/eLife.88328.4

437. Fasci D, van Ingen H, Scheltema RA, Heck AJR. Histone Interaction Landscapes Visualized by Crosslinking Mass Spectrometry in Intact Cell Nuclei. *Molecular & Cellular Proteomics*. 2018;17(10):2018-2033. doi:10.1074/mcp.RA118.000924

438. Sarabipour S, Mac Gabhann F. VEGF-A121a binding to Neuropilins – A concept revisited. *Cell Adh Migr*. 2018;12(3):204-214. doi:10.1080/19336918.2017.1372878

439. Cébe Suarez S, Pieren M, Cariolato L, et al. A VEGF-A splice variant defective for heparan sulfate and neuropilin-1 binding shows attenuated signaling through VEGFR-2. *Cellular and Molecular Life Sciences*. 2006;63(17):2067-2077. doi:10.1007/s00018-006-6254-9

440. Nakamura F, Goshima Y. Structural and Functional Relation of Neuropilins. In: Madame Curie Bioscience Database [Internet]. Austin (TX): Landes Bioscience; 2000-2013. Available from: https://www.ncbi.nlm.nih.gov/books/NBK6408/.

441. Zhang P, Chen L, Zhou F, He Z, Wang G, Luo Y. NRP1 promotes prostate cancer progression via modulating EGFR-dependent AKT pathway activation. *Cell Death Dis*. 2023;14(2):159. doi:10.1038/s41419-023-05696-1

442. Grun D, Adhikary G, Eckert RL. NRP-1 interacts with GIPC1 and SYX to activate p38 MAPK signaling and cancer stem cell survival. *Mol Carcinog*. 2019;58(4):488-499. doi:10.1002/mc.22943

443. Altschul S. Gapped BLAST and PSI-BLAST: a new generation of protein database search programs. *Nucleic Acids Res*. 1997;25(17):3389-3402. doi:10.1093/nar/25.17.3389

444. Xu Y, Bismar TA, Su J, et al. Filamin A regulates focal adhesion disassembly and suppresses breast cancer cell migration and invasion. *Journal of Experimental Medicine*. 2010;207(11):2421-2437. doi:10.1084/jem.20100433

445. Roux KJ, Kim DI, Burke B, May DG. BioID: A Screen for Protein-Protein Interactions. *Curr Protoc Protein Sci*. 2018;91(November 2013):19.23.1-19.23.15. doi:10.1002/cpps.51

446. Sears RM, May DG, Roux KJ. BioID as a Tool for Protein-Proximity Labeling in Living Cells. In: ; 2019:299-313. doi:10.1007/978-1-4939-9546-2_15

447. Yang X, Wen Z, Zhang D, et al. Proximity labeling: an emerging tool for probing in planta molecular interactions. *Plant Commun*. 2021;2(2):100137. doi:10.1016/j.xplc.2020.100137

448. Kim DI, Jensen SC, Noble KA, et al. An improved smaller biotin ligase for BioID proximity labeling. *Mol Biol Cell*. 2016;27(8):1188-1196. doi:10.1091/mbc.E15-12-0844

449. Zhao X, Bitsch S, Kubitz L, et al. ultraID: a compact and efficient enzyme for proximity-dependent biotinylation in living cells. *bioRxiv*. Published online 2021:2021.06.16.448656. https://doi.org/10.1101/2021.06.16.448656

450. Rawlings AE. Membrane proteins: always an insoluble problem? *Biochem Soc Trans*. 2016;44(3):790-795. doi:10.1042/BST20160025

451. Buchwalow I, Samoilova V, Boecker W, Tiemann M. Non-specific binding of antibodies in immunohistochemistry: fallacies and facts. *Sci Rep*. 2011;1(1):28. doi:10.1038/srep00028

452. He R, Li X. Mammalian Two-Hybrid Assay for Detecting Protein-Protein Interactions in Vivo. In: ; 2008:327-337. doi:10.1007/978-1-59745-188-8_22

453. Douzi B. Protein–Protein Interactions: Surface Plasmon Resonance. In: ; 2017:257-275. doi:10.1007/978-1-4939-7033-9_21

454. Hall MP, Unch J, Binkowski BF, et al. Engineered luciferase reporter from a deep sea shrimp utilizing a novel imidazopyrazinone substrate. *ACS Chem Biol*. 2012;7(11):1848-1857. doi:10.1021/cb3002478

455. Dale NC, Johnstone EKM, White CW, Pfleger KDG. NanoBRET: The bright future of proximity-based assays. *Front Bioeng Biotechnol*. 2019;7(MAR):1-13. doi:10.3389/fbioe.2019.00056

456. Wade M, Ph D, Méndez J, et al. Inhibition of Protein-Protein Interactions : Cell-Based Assays. In: S M, GS S, S G, et al., eds. *Assay Guidance Manual [Internet]*. Bethesda (MD): Eli Lilly & Company and the National Center for Advancing Translational Sciences; 2017.

457. Markham. The polymerase chain reaction: a tool for molecular medicine. *BMJ*. 1993;306:441-446.

458. Hanapi UK, Desa MNM, Ismail A, Mustafa S. A higher sensitivity and efficiency of common primer multiplex PCR assay in identification of meat origin using NADH dehydrogenase subunit 4 gene. *J Food Sci Technol*. 2015;52(7):4166-4175. doi:10.1007/s13197-014-1459-7

459. Varadaraj K, Skinner DM. Denaturants or cosolvents improve the specificity of PCR amplification of a G + C-rich DNA using genetically engineered DNA polymerases. *Gene*. 1994;140(1):1-5. doi:10.1016/0378-1119(94)90723-4

460. Roberts RJ. How restriction enzymes became the workhorses of molecular biology. *PNAS*. 2005;102(17):5905-5908. www.pnas.orgcgidoi10.1073pnas.0500923102

461. Lee PY, Costumbrado J, Hsu CY, Kim YH. Agarose gel electrophoresis for the separation of DNA fragments. *Journal of Visualized Experiments*. 2012;(62). doi:10.3791/3923

462. Galindo-Murillo R, Cheatham TE. Ethidium bromide interactions with DNA: An exploration of a classic DNA-ligand complex with unbiased molecular dynamics simulations. *Nucleic Acids Res*. 2021;49(7):3735-3747. doi:10.1093/nar/gkab143

463. Günal G, Kip Ç, Eda Öğüt S, İlhan H, Kibar G, Tuncel A. Comparative DNA isolation behaviours of silica and polymer based sorbents in batch fashion: monodisperse silica microspheres with bimodal pore size distribution as a new sorbent for DNA isolation. *Artif Cells Nanomed Biotechnol*. 2018;46(1):178-184. doi:10.1080/21691401.2017.1304404

464. Esser KH, Marx WH, Lisowsky T. maxXbond: First regeneration system for DNA binding silica matrices. *Nat Methods*. 2006;3(1):i-ii. doi:10.1038/nmeth845

465. García-Alegría AM, Anduro-Corona I, Pérez-Martínez CJ, Corella-Madueño MAG, Rascón-Durán ML, Astiazaran-Garcia H. Quantification of DNA through the nanodrop spectrophotometer: Methodological validation using standard reference material and sprague dawley rat and human DNA. *Int J Anal Chem*. 2020;2020. doi:10.1155/2020/8896738

466. Lucena-Aguilar G, Sánchez-López AM, Barberán-Aceituno C, Carrillo-Ávila JA, López-Guerrero JA, Aguilar-Quesada R. DNA Source Selection for Downstream Applications Based on DNA Quality Indicators Analysis. *Biopreserv Biobank*. 2016;14(4):264-270. doi:10.1089/bio.2015.0064

467. Cherepanov A V., De Vries S. Kinetics and thermodynamics of nick sealing by T4 DNA ligase. *Eur J Biochem*. 2003;270(21):4315-4325. doi:10.1046/j.1432-1033.2003.03824.x

468. Liu J, Chang W, Pan L, et al. An Improved Method of Preparing High Efficiency Transformation Escherichia coli with Both Plasmids and Larger DNA Fragments. *Indian J Microbiol*. 2018;58(4):448-456. doi:10.1007/s12088-018-0743-z

469. Ren J, Karna S, Lee HM, Seung &, Yoo M, Na D. Artificial transformation methodologies for improving the efficiency of plasmid DNA transformation and simplifying its use. *Appl Microbiol Biotechnol*. 2019;103:9205-9215. doi:10.1007/s00253-019-10173-x/Published

470. Asif A, Mohsin H, Tanvir R, Rehman Y. Revisiting the mechanisms involved in calcium chloride induced bacterial transformation. *Front Microbiol*. 2017;8(NOV). doi:10.3389/fmicb.2017.02169

471. Salwan and Sharma. Expression of recombinant proteins in prokaryotic host. In: *Laboratory Methods in Microbiology and Molecular Biology*. Academic Press; 2023:145-153.

472. DeSanctis ML, Soranno EA, Messner E, et al. Greater than pH 8: The pH dependence of EDTA as a preservative of high molecular weight DNA in biological samples. *PLoS One*. 2023;18(1). doi:10.1371/journal.pone.0280807

473. Islam MS, Aryasomayajula A, Selvaganapathy PR. A review on macroscale and microscale cell lysis methods. *Micromachines (Basel)*. 2017;8(3):83. doi:10.3390/mi8030083

474. Wang X, Lim HJ, Son A. Characterization of denaturation and renaturation of DNA for DNA hybridization. *Environ Health Toxicol*. 2014;29:e2014007. doi:10.5620/eht.2014.29.e2014007

475. Bimboim HC, Doly J. A rapid alkaline extraction procedure for screening recombinant plasmid DNA. *Nucleic Acids Res*. 1979;7(6):1513-1523. doi:https://doi.org/10.1093/nar/7.6.1513

476. Butash KA, Natarajan P, Young A, Fox DK. Reexamination of the effect of endotoxin on cell proliferation and transfection efficiency. *Biotechniques*. 2000;29(3):610-619. doi:10.2144/00293rr04

477. Kim DI, Jensen SC, Noble KA, et al. An improved smaller biotin ligase for BioID proximity labeling. *Mol Biol Cell*. 2016;27(8):1188-1196. doi:10.1091/mbc.E15-12-0844

478. Olsen J V., Ong SE, Mann M. Trypsin cleaves exclusively C-terminal to arginine and lysine residues. *Molecular and Cellular Proteomics*. 2004;3(6):608-614. doi:10.1074/mcp.T400003-MCP200

479. Sharma M, Kumar R, Sharma S, et al. Sustained exposure to trypsin causes cells to transition into a state of reversible stemness that is amenable to transdifferentiation. Published online June 23, 2019. doi:10.1101/679928

480. Yu C, Zhao W, Duan C, Xie J, Yin W. Poly- l -lysine-caused cell adhesion induces pyroptosis in THP-1 monocytes. *Open Life Sci*. 2022;17(1):279-283. doi:10.1515/biol-2022-0028

481. Hoch E, Schuh C, Hirth T, Tovar GEM, Borchers K. Stiff gelatin hydrogels can be photochemically synthesized from low viscous gelatin solutions using molecularly functionalized gelatin with a high degree of methacrylation. *J Mater Sci Mater Med*. 2012;23(11):2607-2617. doi:10.1007/s10856-012-4731-2

482. Wu SC, Chang WH, Dong GC, Chen KY, Chen YS, Yao CH. Cell adhesion and proliferation enhancement by gelatin nanofiber scaffolds. *J Bioact Compat Polym*. 2011;26(6):565-577. doi:10.1177/0883911511423563

483. Binz RL, Tian E, Sadhukhan R, Zhou D, Hauer-Jensen M, Pathak R. Identification of novel breakpoints for locus- and region-specific translocations in 293 cells by molecular cytogenetics before and after irradiation. *Sci Rep*. 2019;9(1). doi:10.1038/s41598-019-47002-0

484. Singh S, Kumar R, Agrawal B. Adenoviral Vector-Based Vaccines and Gene Therapies: Current Status and Future Prospects. In: *Adenoviruses*. IntechOpen; 2019. doi:10.5772/intechopen.79697

485. Binz RL, Tian E, Sadhukhan R, Zhou D, Hauer-Jensen M, Pathak R. Identification of novel breakpoints for locus- and region-specific translocations in 293 cells by molecular cytogenetics before and after irradiation. *Sci Rep*. 2019;9:10554. doi:10.1038/s41598-019-47002-0

486. Tan E, Chin CSH, Lim ZFS, Ng SK. HEK293 Cell Line as a Platform to Produce Recombinant Proteins and Viral Vectors. *Front Bioeng Biotechnol*. 2021;9:96991. doi:10.3389/fbioe.2021.796991

487. Bian C, Zhao K, Tong GX, Zhu YL, Chen P. Immortalization of human umbilical vein endothelial cells with telomerase reverse transcriptase and simian virus 40 large T antigen. *J Zhejiang Univ Sci*. 2005;6(7):631-636. doi:10.1631/jzus.2005.B0631

488. Pusztaszeri MP, Seelentag W, Bosman FT. Immunohistochemical expression of endothelial markers CD31, CD34, von Willebrand factor, and Fli-1 in normal human tissues. *Journal of Histochemistry and Cytochemistry*. 2006;54(4):385-395. doi:10.1369/jhc.4A6514.2005

489. Karlsson M, Zhang C, Méar L, et al. *A Single-Cell Type Transcriptomics Map of Human Tissues*. Vol 7.; 2021. Accessed November 18, 2024. https://www.proteinatlas.org/ENSG00000099250-NRP1/cell+line

490. Sabin J, Alatorre-Meda M, Miñones J, Domínguez-Arca V, Prieto G. New insights on the mechanism of polyethylenimine transfection and their implications on gene therapy and DNA vaccines. *Colloids Surf B Biointerfaces*. 2022;210. doi:10.1016/j.colsurfb.2021.112219

491. Ren R, Guo J, Liu G, et al. Nucleic acid direct delivery to fibroblasts: a review of nucleofection and applications. *J Biol Eng*. 2022;16(1). doi:10.1186/s13036-022-00309-5

492. Sweeney NP, Vink CA. The impact of lentiviral vector genome size and producer cell genomic to gag-pol mRNA ratios on packaging efficiency and titre. *Mol Ther Methods Clin Dev*. 2021;21:574-584. doi:10.1016/j.omtm.2021.04.007

493. Milone MC, O'Doherty U. Clinical use of lentiviral vectors. *Leukemia*. 2018;32(7):1529-1541. doi:10.1038/s41375-018-0106-0

494. Elegheert J, Behiels E, Bishop B, et al. Lentiviral transduction of mammalian cells for fast, scalable and high-level production of soluble and membrane proteins. *Nat Protoc*. 2018;13(12):2991-3017. doi:10.1038/s41596-018-0075-9

495. Denning W, Das S, Guo S, Xu J, Kappes JC, Hel Z. Optimization of the transductional efficiency of lentiviral vectors: Effect of sera and polycations. *Mol Biotechnol*. 2013;53(3):308-314. doi:10.1007/s12033-012-9528-5

496. Svidritskiy E, Ling C, Ermolenko DN, Korostelev AA. Blasticidin S inhibits translation by trapping deformed tRNA on the ribosome. *Proc Natl Acad Sci U S A*. 2013;110(30):12283-12288. doi:10.1073/pnas.1304922110

497. Carpentier F de, Le Peillet J, Boisset ND, Crozet P, Lemaire SD, Danon A. Blasticidin S Deaminase: A New Efficient Selectable Marker for Chlamydomonas reinhardtii. *Front Plant Sci*. 2020;11. doi:10.3389/fpls.2020.00242

498. Im K, Mareninov S, Diaz MFP, Yong WH. An introduction to performing immunofluorescence staining. *Methods in Molecular Biology*. 2019;1897:299-311. doi:10.1007/978-1-4939-8935-5_26

499. Elliott AD. Confocal Microscopy: Principles and Modern Practices. *Curr Protoc Cytom*. 2020;92(1):e68. doi:10.1002/cpcy.68

500. Schindelin J, Arganda-Carreras I, Frise E, et al. Fiji: An open-source platform for biological-image analysis. *Nat Methods*. 2012;9(7):676-682. doi:10.1038/nmeth.2019

501. Rizk A, Paul G, Incardona P, et al. Segmentation and quantification of subcellular structures in fluorescence microscopy images using Squassh. *Nat Protoc*. 2014;9(3):586-596. doi:10.1038/nprot.2014.037

502. Chapman-Smith A, Cronan Jr JE. Molecular Biology of Biotin Attachment to Proteins. *J Nutr*. 1999;129(2):477S-484S. doi:10.1093/jn/129.2.477S

503. Remnant L, Booth DG, Vargiu G, Spanos C, Kerr ARW, Earnshaw WC. In vitro BioID: mapping the CENP-A microenvironment with high temporal and spatial resolution. *Mol Biol Cell*. 2019;30(11):1314-1325. doi:10.1091/mbc.E18-12-0799

504. Chivers CE, Koner AL, Lowe ED, Howarth M. How the biotin-streptavidin interaction was made even stronger: Investigation via crystallography and a chimaeric tetramer. *Biochemical Journal*. 2011;435(1):55-63. doi:10.1042/BJ20101593

505. Nowakowski AB, Wobig WJ, Petering DH. Native SDS-PAGE: High resolution electrophoretic separation of proteins with retention of native properties including bound metal ions. *Metallomics*. 2014;6(5):1068-1078. doi:10.1039/c4mt00033a

506. Jafari M, Mehrnejad F, Rahimi F, Asghari SM. The Molecular Basis of the Sodium Dodecyl Sulfate Effect on Human Ubiquitin Structure: A Molecular Dynamics Simulation Study. *Sci Rep*. 2018;8(1):2150. doi:10.1038/s41598-018-20669-7

507. Rath A, Cunningham F, Deber CM. Acrylamide concentration determines the direction and magnitude of helical membrane protein gel shifts. *Proc Natl Acad Sci U S A*. 2013;110(39):15668-15673. doi:10.1073/pnas.1311305110

508. Pettegrew CJ, Jayini R, Islam MR. Transfer buffer containing methanol can be reused multiple times in protein electrotransfer. *J Biomol Tech*. 2009;20(2):93-95. http://www.ncbi.nlm.nih.gov/pubmed/19503619

509. Xu J, Sun H, Huang G, et al. A fixation method for the optimisation of western blotting. *Sci Rep*. 2019;9:6649. doi:10.1038/s41598-019-43039-3

510. Mahmood T, Yang PC. Western blot: Technique, theory, and trouble shooting. *N Am J Med Sci*. 2012;4(9):429-434. doi:10.4103/1947-2714.100998

511. Bowler-Barnett EH, Fan J, Luo J, Magrane M, Martin MJ, Orchard S. UniProt and Mass Spectrometry-Based Proteomics—A 2-Way Working Relationship. *Molecular & Cellular Proteomics*. 2023;22(8):100591. doi:10.1016/j.mcpro.2023.100591

512. Elizarraras JM, Liao Y, Shi Z, Zhu Q, Pico AR, Zhang B. WebGestalt 2024: faster gene set analysis and new support for metabolomics and multi-omics. *Nucleic Acids Res*. 2024;52(W1):W415-W421. doi:10.1093/nar/gkae456

513. Borroto-Escuela DO, Flajolet M, Agnati LF, Greengard P, Fuxe K. Bioluminescence Resonance Energy Transfer Methods to Study G Protein-Coupled Receptor-Receptor Tyrosine Kinase Heteroreceptor Complexes. *Methods Cell Biol*. 2013;117:141-164. doi:10.1016/B978-0-12-408143-7.00008-6

514. Guo J, Guo S, Lu S, et al. The development of proximity labeling technology and its applications in mammals, plants, and microorganisms. *Cell Communication and Signaling*. 2023;21(1):269. doi:10.1186/s12964-023-01310-1

515. McKinley KL, Cheeseman IM. The molecular basis for centromere identity and function. *Nat Rev Mol Cell Biol*. 2016;17(1):16-29. doi:10.1038/nrm.2015.5

516. Nguyen TMT, Kim J, Doan TT, Lee MW, Lee M. APEX Proximity Labeling as a Versatile Tool for Biological Research. *Biochemistry*. 2020;59(3):260-269. doi:10.1021/acs.biochem.9b00791

517. Lam SS, Martell JD, Kamer KJ, et al. Directed evolution of APEX2 for electron microscopy and proximity labeling. *Nat Methods*. 2015;12(1):51-54. doi:10.1038/nmeth.3179

518. Mishra PK, Park I, Sharma N, Yoo CM, Lee HY, Rhee HW. Enzymatic Recording of Local Hydrogen Peroxide Generation Using Genetically Encodable Enzyme. *Anal Chem*. 2022;94(43):14869-14877. doi:10.1021/acs.analchem.2c01966

519. Martell JD, Deerinck TJ, Lam SS, Ellisman MH, Ting AY. Electron microscopy using the genetically encoded APEX2 tag in cultured mammalian cells. *Nat Protoc*. 2017;12(9):1792-1816. doi:10.1038/nprot.2017.065

520. Branon TC, Bosch JA, Sanchez AD, et al. Efficient proximity labeling in living cells and organisms with TurboID. *Nat Biotechnol*. 2018;36(9):880-887. doi:10.1038/nbt.4201

521. May DG, Scott KL, Campos AR, Roux KJ. Comparative Application of BioID and TurboID for Protein-Proximity Biotinylation. *Cells*. 2020;9(5):1070. doi:10.3390/cells9051070

522. Kim DI, KC B, Zhu W, Motamedchaboki K, Doye V, Roux KJ. Probing nuclear pore complex architecture with proximity-dependent biotinylation. *Proceedings of the National Academy of Sciences*. 2014;111(24). doi:10.1073/pnas.1406459111

523. Kubitz L, Bitsch S, Zhao X, et al. Engineering of ultraID, a compact and hyperactive enzyme for proximity-dependent biotinylation in living cells. *Commun Biol*. 2022;5(1):657. doi:10.1038/s42003-022-03604-5

524. Alghamdi AAA, Benwell CJ, Atkinson SJ, Lambert J, Johnson RT, Robinson SD. NRP2 as an Emerging Angiogenic Player; Promoting Endothelial Cell Adhesion and Migration by Regulating Recycling of α5 Integrin. *Front Cell Dev Biol*. 2020;8. doi:10.3389/fcell.2020.00395

525. Issitt T, Bosseboeuf E, De Winter N, et al. Neuropilin-1 Controls Endothelial Homeostasis by Regulating Mitochondrial Function and Iron-Dependent Oxidative Stress. *iScience*. 2019;11:205-223. doi:10.1016/j.isci.2018.12.005

526. Diaz-Vera J, Palmer S, Hernandez-Fernaud JR, et al. A proteomic approach to identify endosomal cargoes controlling cancer invasiveness. *J Cell Sci*. 2017;130(4):697-711. doi:10.1242/jcs.190835

527. Dutta S, Polavaram NS, Islam R, et al. Neuropilin-2 regulates androgen-receptor transcriptional activity in advanced prostate cancer. *Oncogene*. 2022;41(30):3747-3760. doi:10.1038/s41388-022-02382-y

528. Korhonen EA, Murtomäki A, Jha SK, et al. Lymphangiogenesis requires Ang2/Tie/PI3K signaling for VEGFR3 cell-surface expression. *Journal of Clinical Investigation*. 2022;132(15). doi:10.1172/JCI155478

529. Schwabl S, Teis D. Protein quality control at the Golgi. *Curr Opin Cell Biol*. 2022;75:102074. doi:10.1016/j.ceb.2022.02.008

530. Wang Y, Nakayama M, Pitulescu ME, et al. Ephrin-B2 controls VEGF-induced angiogenesis and lymphangiogenesis. *Nature*. 2010;465(7297):483-486. doi:10.1038/nature09002

531. Deng Y, Zhang X, Simons M. Molecular controls of lymphatic VEGFR3 signaling. *Arterioscler Thromb Vasc Biol*. 2015;35(2):421-429. doi:10.1161/ATVBAHA.114.304881

532. Zhang X, Simons M. Receptor tyrosine kinases endocytosis in endothelium: biology and signaling. *Arterioscler Thromb Vasc Biol*. 2014;34(9):1831-1837. doi:10.1161/ATVBAHA.114.303217

533. Sousa DA, Gaspar R, Ferreira CJO, Baltazar F, Rodrigues LR, Silva BFB. In Vitro CRISPR/Cas9 Transfection and Gene-Editing Mediated by Multivalent Cationic Liposome–DNA Complexes. *Pharmaceutics*. 2022;14(5):1087. doi:10.3390/pharmaceutics14051087

534. Ramazi S, Zahiri J. Post-translational modifications in proteins: resources, tools and prediction methods. *Database*. 2021;2021. doi:10.1093/database/baab012

535. Zhong Q, Xiao X, Qiu Y, et al. Protein posttranslational modifications in health and diseases: Functions, regulatory mechanisms, and therapeutic implications. *MedComm (Beijing)*. 2023;4(3). doi:10.1002/mco2.261

536. Schopp IM, Béthune J. Split-BioID — Proteomic Analysis of Context-specific Protein Complexes in Their Native Cellular Environment. *Journal of Visualized Experiments*. 2018;(134). doi:10.3791/57479

537. Batsios P, Meyer I, Gräf R. Proximity-Dependent Biotin Identification (BioID) in Dictyostelium Amoebae. In: ; 2016:23-42. doi:10.1016/bs.mie.2015.09.007

538. Siepen JA, Keevil EJ, Knight D, Hubbard SJ. Prediction of Missed Cleavage Sites in Tryptic Peptides Aids Protein Identification in Proteomics. *J Proteome Res*. 2007;6(1):399-408. doi:10.1021/pr060507u

539. Mellacheruvu D, Wright Z, Couzens AL, et al. The CRAPome: a contaminant repository for affinity purification–mass spectrometry data. *Nat Methods*. 2013;10(8):730-736. doi:10.1038/nmeth.2557

540. Barnette A. A guide to gating in flow cytometry. https://www.bio-rad-antibodies.com/blog/a-guide-to-gating-in-flow-cytometry.htm.

541. Kim KH, Sederstrom JM. Assaying Cell Cycle Status Using Flow Cytometry. *Curr Protoc Mol Biol*. 2015;111(1). doi:10.1002/0471142727.mb2806s111

542. Huang HL, Hsing HW, Lai TC, et al. Trypsin-induced proteome alteration during cell subculture in mammalian cells. *J Biomed Sci*. 2010;17(1):36. doi:10.1186/1423-0127-17-36

543. Thermo Fisher Scientific. Traditional Methods of Cell Lysis for Protein Extraction. https://www.thermofisher.com/uk/en/home/life-science/protein-biology/protein-biology-learning-center/protein-biology-resource-library/pierce-protein-methods/traditional-methods-cell-lysis.html.

544. Xie X, Chamoli M, Bhaumik D, et al. Quantification of Insoluble Protein Aggregation in Caenorhabditis elegans during Aging with a Novel Data-Independent Acquisition Workflow. *Journal of Visualized Experiments*. 2020;(162). doi:10.3791/61366

545. Black RA, White JM. ADAMs: focus on the protease domain. *Curr Opin Cell Biol*. 1998;10(5):654-659. doi:10.1016/S0955-0674(98)80042-2

546. Freestone J, Short T, Noble WS, Keich U. Group-walk: a rigorous approach to group-wise false discovery rate analysis by target-decoy competition. *Bioinformatics*. 2022;38(Supplement_2):ii82-ii88. doi:10.1093/bioinformatics/btac471

547. Lawless C, Hubbard SJ. Prediction of Missed Proteolytic Cleavages for the Selection of Surrogate Peptides for Quantitative Proteomics. *OMICS*. 2012;16(9):449-456. doi:10.1089/omi.2011.0156

548. Bugyi F, Szabó D, Szabó G, et al. Influence of Post-Translational Modifications on Protein Identification in Database Searches. *ACS Omega*. 2021;6(11):7469-7477. doi:10.1021/acsomega.0c05997

549. Bagwan N, El Ali HH, Lundby A. Proteome-wide profiling and mapping of post translational modifications in human hearts. *Sci Rep*. 2021;11(1):2184. doi:10.1038/s41598-021-81986-y

550. Ahmed S, Altman J, Jones G, et al. Mass spectrometric detection of keratins in tear fluid. *Exp Eye Res*. 2025;251:110231. doi:10.1016/j.exer.2025.110231

551. Krey JF, Wilmarth PA, Shin JB, et al. Accurate Label-Free Protein Quantitation with High- and Low-Resolution Mass Spectrometers. *J Proteome Res*. 2014;13(2):1034-1044. doi:10.1021/pr401017h

552. Shin JB, Krey JF, Hassan A, et al. Molecular architecture of the chick vestibular hair bundle. *Nat Neurosci*. 2013;16(3):365-374. doi:10.1038/nn.3312

553. Greiner J V., Glonek T. Intracellular ATP Concentration and Implication for Cellular Evolution. *Biology (Basel)*. 2021;10(11):1166. doi:10.3390/biology10111166

554. Allard B, Longhi MS, Robson SC, Stagg J. The ectonucleotidases CD39 and CD73: Novel checkpoint inhibitor targets. *Immunol Rev*. 2017;276(1):121-144. doi:10.1111/imr.12528

555. Al Mismar R, Samavarchi-Tehrani P, Seale B, Kasmaeifar V, Martin CE, Gingras AC. Extracellular proximal interaction profiling by cell surface–targeted TurboID reveals LDLR as a partner of liganded EGFR. *Sci Signal*. 2024;17(861). doi:10.1126/scisignal.adl6164

556. Pacheco-Quinto J, Herdt A, Eckman CB, Eckman EA. Endothelin-Converting Enzymes and Related Metalloproteases in Alzheimer's Disease. *Journal of Alzheimer's Disease*. 2012;33(s1):S101-S110. doi:10.3233/JAD-2012-129043

557. Pal S, Su Y, Nwadozi E, Claesson-Welsh L, Richards M. Neuropilin-1 controls vascular permeability through juxtacrine regulation of endothelial adherens junctions. *Angiogenesis*. 2025;28(1):7. doi:10.1007/s10456-024-09963-3

558. Nesbeth D, Williams SL, Chan L, et al. Metabolic Biotinylation of Lentiviral Pseudotypes for Scalable Paramagnetic Microparticle-Dependent Manipulation. *Molecular Therapy*. 2006;13(4):814-822. doi:10.1016/j.ymthe.2005.09.016

559. Ryu SW, Stewart R, Pectol DC, et al. Proteome-wide identification of HSP70/HSC70 chaperone clients in human cells. *PLoS Biol*. 2020;18(7):e3000606. doi:10.1371/journal.pbio.3000606

560. Niinae T, Imami K, Sugiyama N, Ishihama Y. Identification of Endogenous Kinase Substrates by Proximity Labeling Combined with Kinase Perturbation and Phosphorylation Motifs. *Molecular & Cellular Proteomics*. 2021;20:100119. doi:10.1016/j.mcpro.2021.100119

561. Tabb DL, Vega-Montoto L, Rudnick PA, et al. Repeatability and Reproducibility in Proteomic Identifications by Liquid Chromatography−Tandem Mass Spectrometry. *J Proteome Res*. 2010;9(2):761-776. doi:10.1021/pr9006365

562. Pasapera AM, Heissler SM, Eto M, et al. MARK2 regulates directed cell migration through modulation of myosin II contractility and focal adhesion organization. *Current Biology*. 2022;32(12):2704-2718.e6. doi:10.1016/j.cub.2022.04.088

563. Wei Z, Zheng S, Spangler SA, Yu C, Hoogenraad CC, Zhang M. Liprin-Mediated Large Signaling Complex Organization Revealed by the Liprin-α/CASK and Liprin-α/Liprin-β Complex Structures. *Mol Cell*. 2011;43(4):586-598. doi:10.1016/j.molcel.2011.07.021

564. Herrera A, Menendez A, Torroba B, Ochoa A, Pons S. Dbnl and β-catenin promote pro-N-cadherin processing to maintain apico-basal polarity. *Journal of Cell Biology*. 2021;220(6). doi:10.1083/jcb.202007055

565. Huang X, Qu R, Ouyang J, Zhong S, Dai J. An Overview of the Cytoskeleton-Associated Role of PDLIM5. *Front Physiol*. 2020;11. doi:10.3389/fphys.2020.00975

566. Ikeda W, Nakanishi H, Miyoshi J, et al. Afadin: A key molecule essential for structural organization of cell-cell junctions of polarized epithelia during embryogenesis. *J Cell Biol*. 1999;146(5):1117-1132. doi:10.1083/jcb.146.5.1117

567. Stephenson JR, Paavola KJ, Schaefer SA, Kaur B, Van Meir EG, Hall RA. Brain-specific Angiogenesis Inhibitor-1 Signaling, Regulation, and Enrichment in the Postsynaptic Density. *Journal of Biological Chemistry*. 2013;288(31):22248-22256. doi:10.1074/jbc.M113.489757

568. Herdman C, Tremblay MG, Mishra PK, Moss T. Loss of Extended Synaptotagmins ESyt2 and ESyt3 does not affect mouse development or viability, but in vitro cell migration and survival under stress are affected. *Cell Cycle*. 2014;13(16):2616-2625. doi:10.4161/15384101.2014.943573

569. Han J, Pluhackova K, Böckmann RA. The Multifaceted Role of SNARE Proteins in Membrane Fusion. *Front Physiol*. 2017;8. doi:10.3389/fphys.2017.00005

570. Hu C, Hardee D, Minnear F. Membrane fusion by VAMP3 and plasma membrane t-SNAREs. *Exp Cell Res*. 2007;313(15):3198-3209. doi:10.1016/j.yexcr.2007.06.008

571. Antonin W. A SNARE complex mediating fusion of late endosomes defines conserved properties of SNARE structure and function. *EMBO J*. 2000;19(23):6453-6464. doi:10.1093/emboj/19.23.6453

572. Walsh TG, Li Y, Williams CM, Aitken EW, Andrews RK, Poole AW. Loss of the exocyst complex component EXOC3 promotes hemostasis and accelerates arterial thrombosis. *Blood Adv*. 2021;5(3):674-686. doi:10.1182/bloodadvances.2020002515

573. Yu Z, Zeng J, Wang J, et al. Hepatocyte growth factor-regulated tyrosine kinase substrate is essential for endothelial cell polarity and cerebrovascular stability. *Cardiovasc Res*. 2021;117(2):533-546. doi:10.1093/cvr/cvaa016

574. Yorikawa C, WAGURI S, HATTA K, et al. Human CHMP6, a myristoylated ESCRT-III protein, interacts directly with an ESCRT-II component EAP20 and regulates endosomal cargo sorting. *Biochemical Journal*. 2005;387(1):17-26. doi:10.1042/BJ20041227

575. Horii M, Shibata H, Kobayashi R, et al. CHMP7, a novel ESCRT-III-related protein, associates with CHMP4b and functions in the endosomal sorting pathway. *Biochemical Journal*. 2006;400(1):23-32. doi:10.1042/BJ20060897

576. Piper RC, Katzmann DJ. Biogenesis and Function of Multivesicular Bodies. *Annu Rev Cell Dev Biol*. 2007;23(1):519-547. doi:10.1146/annurev.cellbio.23.090506.123319

577. Xu M, Ji J, Jin D, et al. The biogenesis and secretion of exosomes and multivesicular bodies (MVBs): Intercellular shuttles and implications in human diseases. *Genes Dis*. 2023;10(5):1894-1907. doi:10.1016/j.gendis.2022.03.021

578. Boura E, Ivanov V, Carlson LA, Mizuuchi K, Hurley JH. Endosomal Sorting Complex Required for Transport (ESCRT) Complexes Induce Phase-separated Microdomains in Supported Lipid Bilayers. *Journal of Biological Chemistry*. 2012;287(33):28144-28151. doi:10.1074/jbc.M112.378646

579. Stuffers S, Brech A, Stenmark H. ESCRT proteins in physiology and disease. *Exp Cell Res*. 2009;315(9):1619-1626. doi:10.1016/j.yexcr.2008.10.013

580. Elia N, Sougrat R, Spurlin TA, Hurley JH, Lippincott-Schwartz J. Dynamics of endosomal sorting complex required for transport (ESCRT) machinery during cytokinesis and its role in abscission. *Proceedings of the National Academy of Sciences*. 2011;108(12):4846-4851. doi:10.1073/pnas.1102714108

581. Nabhan JF, Hu R, Oh RS, Cohen SN, Lu Q. Formation and release of arrestin domain-containing protein 1-mediated microvesicles (ARMMs) at plasma membrane by recruitment of TSG101 protein. *Proceedings of the National Academy of Sciences*. 2012;109(11):4146-4151. doi:10.1073/pnas.1200448109

582. Schmidt O, Teis D. The ESCRT machinery. *Current Biology*. 2012;22(4):R116-R120. doi:10.1016/j.cub.2012.01.028

583. Verma R, Marchese A. The Endosomal Sorting Complex Required for Transport Pathway Mediates Chemokine Receptor CXCR4-promoted Lysosomal Degradation of the Mammalian Target of Rapamycin Antagonist DEPTOR. *Journal of Biological Chemistry*. 2015;290(11):6810-6824. doi:10.1074/jbc.M114.606699

584. Ghode SS, Bajaj MS, Kulkarni RS, Limaye LS, Shouche YS, Kale VP. Neuropilin-1 Is an Important Niche Component and Exerts Context-Dependent Effects on Hematopoietic Stem Cells. *Stem Cells Dev*. 2017;26(1):35-48. doi:10.1089/scd.2016.0096

585. MacDonald MJ, Ansari I ul H, Riedemann AS, et al. A Novel Intron-Encoded Neuropilin-1 Isoform in Pancreatic Islets Associated With Very Young Age of Onset of Type 1 Diabetes. *Diabetes*. 2022;71(9):2058-2063. doi:10.2337/db21-1070

586. Xie Y, Mansouri M, Rizk A, Berger P. Regulation of VEGFR2 trafficking and signaling by Rab GTPase-activating proteins. *Sci Rep*. 2019;9(1):13342. doi:10.1038/s41598-019-49646-4

587. Okon IS, Coughlan KA, Zhang C, et al. Protein kinase LKB1 promotes RAB7-mediated neuropilin-1 degradation to inhibit angiogenesis. *Journal of Clinical Investigation*. 2014;124(10):4590-4602. doi:10.1172/JCI75371

588. Yen FT, Roitel O, Bonnard L, et al. Lipolysis Stimulated Lipoprotein Receptor. *Journal of Biological Chemistry*. 2008;283(37):25650-25659. doi:10.1074/jbc.M801027200

589. Telley L, Cadilhac C, Cioni JM, et al. Dual Function of NRP1 in Axon Guidance and Subcellular Target Recognition in Cerebellum. *Neuron*. 2016;91(6):1276-1291. doi:10.1016/j.neuron.2016.08.015

590. Fujisawa H. Discovery of semaphorin receptors, neuropilin and plexin, and their functions in neural development. *J Neurobiol*. 2004;59(1):24-33. doi:10.1002/neu.10337

591. Vanacker C, Trova S, Shruti S, et al. Neuropilin-1 expression in GnRH neurons regulates prepubertal weight gain and sexual attraction. *EMBO J*. 2020;39(19). doi:10.15252/embj.2020104633

592. Carosi JM, Denton D, Kumar S, Sargeant TJ. Receptor Recycling by Retromer. *Mol Cell Biol*. 2023;43(7):317-334. doi:10.1080/10985549.2023.2222053

593. Sato T, Fujita N, Yamada A, et al. Regulation of the Assembly and Adhesion Activity of E-cadherin by Nectin and Afadin for the Formation of Adherens Junctions in Madin-Darby Canine Kidney Cells. *Journal of Biological Chemistry*. 2006;281(8):5288-5299. doi:10.1074/jbc.M510070200

594. Breviario F, Caveda L, Corada M, et al. Functional Properties of Human Vascular Endothelial Cadherin (7B4/Cadherin-5), an Endothelium-Specific Cadherin. *Arterioscler Thromb Vasc Biol*. 1995;15(8):1229-1239. doi:10.1161/01.ATV.15.8.1229

595. Pontén F, Jirström K, Uhlen M. The Human Protein Atlas—a tool for pathology. *J Pathol*. 2008;216(4):387-393. doi:10.1002/path.2440

596. Mentzer SJ, Konerding MA. Intussusceptive angiogenesis: expansion and remodeling of microvascular networks. *Angiogenesis*. 2014;17(3):499-509. doi:10.1007/s10456-014-9428-3

597. Sherafat A, Pfeiffer F, Reiss AM, Wood WM, Nishiyama A. Microglial neuropilin-1 promotes oligodendrocyte expansion during development and remyelination by trans-activating

platelet-derived growth factor receptor. *Nat Commun*. 2021;12(1):2265. doi:10.1038/s41467-021-22532-2

598. Matsuo Y. Introducing Thioredoxin-Related Transmembrane Proteins: Emerging Roles of Human TMX and Clinical Implications. *Antioxid Redox Signal*. 2022;36(13-15):984-1000. doi:10.1089/ars.2021.0187

599. Lim KH, Yang S, Kim SH, Joo JY. Identifying New COVID-19 Receptor Neuropilin-1 in Severe Alzheimer's Disease Patients Group Brain Using Genome-Wide Association Study Approach. *Front Genet*. 2021;12. doi:10.3389/fgene.2021.741175

600. Lampugnani MG, Zanetti A, Corada M, et al. Contact inhibition of VEGF-induced proliferation requires vascular endothelial cadherin, β-catenin, and the phosphatase DEP-1/CD148. *J Cell Biol*. 2003;161(4):793-804. doi:10.1083/jcb.200209019

601. Velagapudi S, Yalcinkaya M, Piemontese A, et al. VEGF-A Regulates Cellular Localization of SR-BI as Well as Transendothelial Transport of HDL but Not LDL. *Arterioscler Thromb Vasc Biol*. 2017;37(5):794-803. doi:10.1161/ATVBAHA.117.309284

602. Di Mattia T, Martinet A, Ikhlef S, et al. FFAT motif phosphorylation controls formation and lipid transfer function of inter-organelle contacts. *EMBO J*. 2020;39(23). doi:10.15252/embj.2019104369

603. Hurley JH, Emr SD. THE ESCRT COMPLEXES: Structure and Mechanism of a Membrane-Trafficking Network. *Annu Rev Biophys Biomol Struct*. 2006;35(1):277-298. doi:10.1146/annurev.biophys.35.040405.102126

604. Bache KG, Brech A, Mehlum A, Stenmark H. Hrs regulates multivesicular body formation via ESCRT recruitment to endosomes. *J Cell Biol*. 2003;162(3):435-442. doi:10.1083/jcb.200302131

605. Sun J, Zheng MY, Li YW, Zhang SW. Structure and function of Septin 9 and its role in human malignant tumors. *World J Gastrointest Oncol*. 2020;12(6):619-631. doi:10.4251/wjgo.v12.i6.619

606. Besson B, Eun H, Kim S, Windisch MP, Bourhy H, Grailhe R. Optimization of BRET saturation assays for robust and sensitive cytosolic protein–protein interaction studies. *Sci Rep*. 2022;12(1):9987. doi:10.1038/s41598-022-12851-9

607. James C, Kehlenbach RH. The Interactome of the VAP Family of Proteins: An Overview. *Cells*. 2021;10(7):1780. doi:10.3390/cells10071780

608. James C, Müller M, Goldberg MW, Lenz C, Urlaub H, Kehlenbach RH. Proteomic mapping by rapamycin-dependent targeting of APEX2 identifies binding partners of VAPB at the inner nuclear membrane. *Journal of Biological Chemistry*. 2019;294(44):16241-16254. doi:10.1074/jbc.RA118.007283

609. James C, Möller U, Spillner C, et al. Phosphorylation of ELYS promotes its interaction with VAPB at decondensing chromosomes during mitosis. *EMBO Rep*. 2024;25(5):2391-2417. doi:10.1038/s44319-024-00125-6

610. Ogrodzinski L, Platt S, Goulding J, et al. Probing expression of E-selectin using CRISPR-Cas9-mediated tagging with HiBiT in human endothelial cells. *iScience*. 2023;26(7):107232. doi:10.1016/j.isci.2023.107232

611. Wang Y, Cao Y, Mangalam AK, et al. Neuropilin-1 modulates interferon-γ-stimulated signaling in brain microvascular endothelial cells. *J Cell Sci*. 2016;129(20):3911-3921. doi:10.1242/jcs.190702

612. Fredriksson K, Van Itallie CM, Aponte A, Gucek M, Tietgens AJ, Anderson JM. Proteomic Analysis of Proteins Surrounding Occludin and Claudin-4 Reveals Their Proximity to Signaling and Trafficking Networks. *PLoS One*. 2015;10(3):e0117074. doi:10.1371/journal.pone.0117074

613. Muhl L, Folestad EB, Gladh H, et al. Neuropilin 1 binds PDGF-D and is a co-receptor in PDGF-D–PDGFRβ signaling. *J Cell Sci*. 2017;130(8):1365-1378. doi:10.1242/jcs.200493

614. Van Itallie CM, Anderson JM. Claudin interactions in and out of the tight junction. *Tissue Barriers*. 2013;1(3):e25247. doi:10.4161/tisb.25247

615. Van Itallie CM, Aponte A, Tietgens AJ, Gucek M, Fredriksson K, Anderson JM. The N and C Termini of ZO-1 Are Surrounded by Distinct Proteins and Functional Protein Networks. *Journal of Biological Chemistry*. 2013;288(19):13775-13788. doi:10.1074/jbc.M113.466193

616. Zahraoui A, Louvard D, Galli T. Tight Junction, a Platform for Trafficking and Signaling Protein Complexes. *J Cell Biol*. 2000;151(5):F31-F36. doi:10.1083/jcb.151.5.F31

617. Omrane M, Camara AS, Taveneau C, et al. Septin 9 has Two Polybasic Domains Critical to Septin Filament Assembly and Golgi Integrity. *iScience*. 2019;13:138-153. doi:10.1016/j.isci.2019.02.015

618. Paradžik T, Podgorski II, Vojvoda Zeljko T, Paradžik M. Ancient Origins of Cytoskeletal Crosstalk: Spectraplakin-like Proteins Precede the Emergence of Cortical Microtubule Stabilization Complexes as Crosslinkers. *Int J Mol Sci*. 2022;23(10):5594. doi:10.3390/ijms23105594

619. Hecht M, Rösler R, Wiese S, Johnsson N, Gronemeyer T. An Interaction Network of the Human SEPT9 Established by Quantitative Mass Spectrometry. *G3 Genes|Genomes|Genetics*. 2019;9(6):1869-1880. doi:10.1534/g3.119.400197

620. Bielenberg DR, Pettaway CA, Takashima S, Klagsbrun M. Neuropilins in neoplasms: Expression, regulation, and function. *Exp Cell Res*. 2006;312(5):584-593. doi:10.1016/j.yexcr.2005.11.024

621. Devlin L, Okletey J, Perkins G, et al. Proteomic profiling of the oncogenic septin 9 reveals isoform-specific interactions in breast cancer cells. *Proteomics*. 2021;21(19). doi:10.1002/pmic.202100155

622. Nerlakanti N, McGuire JJ, Bishop RT, et al. Histone deacetylase upregulation of neuropilin-1 in osteosarcoma is essential for pulmonary metastasis. *Cancer Lett*. 2024;606:217302. doi:10.1016/j.canlet.2024.217302

623. Harburger DS, Bouaouina M, Calderwood DA. Kindlin-1 and -2 Directly Bind the C-terminal Region of β Integrin Cytoplasmic Tails and Exert Integrin-specific Activation Effects. *Journal of Biological Chemistry*. 2009;284(17):11485-11497. doi:10.1074/jbc.M809233200

624. Humphries JD, Byron A, Bass MD, et al. Proteomic Analysis of Integrin-Associated Complexes Identifies RCC2 as a Dual Regulator of Rac1 and Arf6. *Sci Signal*. 2009;2(87). doi:10.1126/scisignal.2000396

625. McParland V, Varsano G, Li X, et al. The Metastasis-Promoting Phosphatase PRL-3 Shows Activity toward Phosphoinositides. *Biochemistry*. 2011;50(35):7579-7590. doi:10.1021/bi201095z

626. Chung J, Wang XQ, Lindberg FP, Frazier WA. Thrombospondin-1 Acts Via IAP/CD47 to Synergize With Collagen in α2β1-Mediated Platelet Activation. *Blood*. 1999;94(2):642-648. doi:10.1182/blood.V94.2.642

627. Asao H, Sasaki Y, Arita T, et al. Hrs Is Associated with STAM, a Signal-transducing Adaptor Molecule. *Journal of Biological Chemistry*. 1997;272(52):32785-32791. doi:10.1074/jbc.272.52.32785

628. Würdinger T, Tannous BA, Saydam O, et al. miR-296 Regulates Growth Factor Receptor Overexpression in Angiogenic Endothelial Cells. *Cancer Cell*. 2008;14(5):382-393. doi:10.1016/j.ccr.2008.10.005

629. Rolland T, Taşan M, Charloteaux B, et al. A Proteome-Scale Map of the Human Interactome Network. *Cell*. 2014;159(5):1212-1226. doi:10.1016/j.cell.2014.10.050

630. Grove M, Demyanenko G, Echarri A, et al. Abi2-Deficient Mice Exhibit Defective Cell Migration, Aberrant Dendritic Spine Morphogenesis, and Deficits in Learning and Memory. *Mol Cell Biol*. 2004;24(24):10905-10922. doi:10.1128/MCB.24.24.10905-10922.2004

631. Bandyopadhyay S, Chiang C yuan, Srivastava J, et al. A human MAP kinase interactome. *Nat Methods*. 2010;7(10):801-805. doi:10.1038/nmeth.1506

632. Proikas-Cezanne T, Gaugel A, Frickey T, Nordheim A. Rab14 is part of the early endosomal clathrin-coated TGN microdomain. *FEBS Lett*. 2006;580(22):5241-5246. doi:10.1016/j.febslet.2006.08.053

633. Yang X, Coulombe-Huntington J, Kang S, et al. Widespread Expansion of Protein Interaction Capabilities by Alternative Splicing. *Cell*. 2016;164(4):805-817. doi:10.1016/j.cell.2016.01.029

634. Rodrigues EM, Giovanini AF, Ribas CAPM, Malafaia O, Roesler R, Isolan GR. The Nervous System Development Regulator Neuropilin-1 as a Potential Prognostic Marker and Therapeutic Target in Brain Cancer. *Cancers (Basel)*. 2023;15(20):4922. doi:10.3390/cancers15204922

635. Sargent KM, Bremer ML, Pohlmeier WE, Brauer VM, Cupp AS. Neuropilin-1 (NRP-1) Loss in Sertoli Cells Increases Testis Weight and Alters Expression of Genes Necessary for Undifferentiated Spermatogonia Self-Renewal, Differentiation, and Cell Survival. *Biol Reprod*. 2012;87(Suppl_1):92-92. doi:10.1093/biolreprod/87.s1.92

636. Lampropoulou A, Ruhrberg C. Neuropilin regulation of angiogenesis. *Biochem Soc Trans*. 2014;42(6):1623-1628. doi:10.1042/BST20140244

637. Raimondi C, Brash JT, Fantin A, Ruhrberg C. Progress in Retinal and Eye Research NRP1 function and targeting in neurovascular development and eye disease. *Prog Retin Eye Res*. 2016;52:64-83. doi:10.1016/j.preteyeres.2016.02.003

638. Shaw G, Morse S, Ararat M, Graham FL. Preferential transformation of human neuronal cells by human adenoviruses and the origin of HEK 293 cells. *The FASEB Journal*. 2002;16(8):869-871. doi:10.1096/fj.01-0995fje

639. Thomas P, Smart TG. HEK293 cell line: A vehicle for the expression of recombinant proteins. *J Pharmacol Toxicol Methods*. 2005;51(3):187-200. doi:10.1016/j.vascn.2004.08.014

640. Stepanenko AA, Dmitrenko VV. HEK293 in cell biology and cancer research: phenotype, karyotype, tumorigenicity, and stress-induced genome-phenotype evolution. *Gene*. 2015;569(2):182-190. doi:10.1016/j.gene.2015.05.065

641. Nie L, Wu G, Zhang W. Correlation of mRNA Expression and Protein Abundance Affected by Multiple Sequence Features Related to Translational Efficiency in Desulfovibrio vulgaris : A Quantitative Analysis. *Genetics*. 2006;174(4):2229-2243. doi:10.1534/genetics.106.065862

642. Rhim J, Tsai W P, Chen Z Q, et al. A human vascular endothelial cell model to study angiogenesis and tumorigenesis. *Carcinogenesis*. 1998;19(4):673-681. doi:10.1093/carcin/19.4.673

643. Jordan ET, Collins M, Terefe J, Ugozzoli L, Rubio T. Optimizing electroporation conditions in primary and other difficult-to-transfect cells. *J Biomol Tech*. 2008;19(5):328-334.

644. Di Blasi R, Marbiah MM, Siciliano V, Polizzi K, Ceroni F. A call for caution in analysing mammalian co-transfection experiments and implications of resource competition in data misinterpretation. *Nat Commun*. 2021;12(1):2545. doi:10.1038/s41467-021-22795-9

645. Lesueur LL, Mir LM, André FM. Overcoming the Specific Toxicity of Large Plasmids Electrotransfer in Primary Cells In Vitro. *Mol Ther Nucleic Acids*. 2016;5:e291. doi:10.1038/mtna.2016.4

646. Hong L, Du X, Li W, Mao Y, Sun L, Li X. EndMT: A promising and controversial field. *Eur J Cell Biol*. 2018;97(7):493-500. doi:10.1016/j.ejcb.2018.07.005

647. Luong JHT, Vashist SK. Chemistry of Biotin–Streptavidin and the Growing Concern of an Emerging Biotin Interference in Clinical Immunoassays. *ACS Omega*. 2020;5(1):10-18. doi:10.1021/acsomega.9b03013

648. Pfannenstein J, Tyryshkin M, Gulden ME, Doud EH, Mosley AL, Reese JC. Characterization of BioID tagging systems in budding yeast and exploring the interactome of the Ccr4-Not complex. *G3: Genes, Genomes, Genetics*. 2024;14(11). doi:10.1093/g3journal/jkae221

649. Yazdani U, Terman JR. The semaphorins. *Genome Biol*. 2006;7(3):211. doi:10.1186/gb-2006-7-3-211

650. Wagner W, Ochman B, Wagner W. Semaphorin 6 Family—An Important Yet Overlooked Group of Signaling Proteins Involved in Cancerogenesis. *Cancers (Basel)*. 2023;15(23):5536. doi:10.3390/cancers15235536

651. Carballo GB, Honorato JR, de Lopes GPF, Spohr TCL de S e. A highlight on Sonic hedgehog pathway. *Cell Communication and Signaling*. 2018;16(1):11. doi:10.1186/s12964-018-0220-7

652. Hillman RT, Feng BY, Ni J, et al. Neuropilins are positive regulators of Hedgehog signal transduction. *Genes Dev*. 2011;25(22):2333-2346. doi:10.1101/gad.173054.111

653. Pontarollo G, Kollar B, Mann A, et al. Author Correction: Commensal bacteria weaken the intestinal barrier by suppressing epithelial neuropilin-1 and Hedgehog signaling. *Nat Metab*. 2023;5(9):1639-1639. doi:10.1038/s42255-023-00901-z

654. Ge X, Milenkovic L, Suyama K, et al. Phosphodiesterase 4D acts downstream of Neuropilin to control Hedgehog signal transduction and the growth of medulloblastoma. *Elife*. 2015;4. doi:10.7554/eLife.07068

655. Pinskey JM, Franks NE, McMellen AN, Giger RJ, Allen BL. Neuropilin-1 promotes Hedgehog signaling through a novel cytoplasmic motif. *Journal of Biological Chemistry*. 2017;292(37):15192-15204. doi:10.1074/jbc.M117.783845

656. Holtz AM, Peterson KA, Nishi Y, et al. Essential role for ligand-dependent feedback antagonism of vertebrate hedgehog signaling by PTCH1, PTCH2 and HHIP1 during neural patterning. *Development*. 2013;140(16):3423-3434. doi:10.1242/dev.095083

657. Holtz AM, Griffiths SC, Davis SJ, Bishop B, Siebold C, Allen BL. Secreted HHIP1 interacts with heparan sulfate and regulates Hedgehog ligand localization and function. *Journal of Cell Biology*. 2015;209(5):739-758. doi:10.1083/jcb.201411024

658. Chen S, Evans HG, Evans DR. FAM129B/MINERVA, a Novel Adherens Junction-associated Protein, Suppresses Apoptosis in HeLa Cells. *Journal of Biological Chemistry*. 2011;286(12):10201-10209. doi:10.1074/jbc.M110.175273

659. Nowak DG, Amin EM, Rennel ES, et al. Regulation of Vascular Endothelial Growth Factor (VEGF) Splicing from Pro-angiogenic to Anti-angiogenic Isoforms. *Journal of Biological Chemistry*. 2010;285(8):5532-5540. doi:10.1074/jbc.M109.074930

660. Li Q, Zeng C, Liu H, et al. Protein-protein interaction inhibitor of SRPKs alters the splicing isoforms of VEGF and inhibits angiogenesis. *iScience*. 2021;24(5):102423. doi:10.1016/j.isci.2021.102423

661. Lu ZZ, Sun C, Zhang X, et al. Neuropilin 1 is an entry receptor for KSHV infection of mesenchymal stem cell through TGFBR1/2-mediated macropinocytosis. *Sci Adv*. 2023;9(21). doi:10.1126/sciadv.adg1778

662. Jiang T, Zhuang J, Duan H, et al. CD146 is a coreceptor for VEGFR-2 in tumor angiogenesis. *Blood*. 2012;120(11):2330-2339. doi:10.1182/blood-2012-01-406108

663. Wang Z, Xu Q, Zhang N, Du X, Xu G, Yan X. CD146, from a melanoma cell adhesion molecule to a signaling receptor. *Signal Transduct Target Ther*. 2020;5(1):148. doi:10.1038/s41392-020-00259-8

664. Wang Y, Liu Y, Bi X, Baudry M. Calpain-1 and Calpain-2 in the Brain: New Evidence for a Critical Role of Calpain-2 in Neuronal Death. *Cells*. 2020;9(12):2698. doi:10.3390/cells9122698

665. Stenman JM, Rajagopal J, Carroll TJ, Ishibashi M, McMahon J, McMahon AP. Canonical Wnt Signaling Regulates Organ-Specific Assembly and Differentiation of CNS Vasculature. *Science (1979)*. 2008;322(5905):1247-1250. doi:10.1126/science.1164594

666. Makarov A, Ylivinkka I, Nyman TA, Hyytiäinen M, Keski-Oja J. Ephrin-As, Eph receptors and integrin α3 interact and colocalise at membrane protrusions of U251MG glioblastoma cells. *Cell Biol Int*. 2013;37(10):1080-1088. doi:10.1002/cbin.10134

667. Finney AC, Scott ML, Reeves KA, et al. EphA2 signaling within integrin adhesions regulates fibrillar adhesion elongation and fibronectin deposition. *Matrix Biology*. 2021;103-104:1-21. doi:10.1016/j.matbio.2021.09.001

668. Mire E, Hocine M, Bazellières E, et al. Developmental Upregulation of Ephrin-B1 Silences Sema3C/Neuropilin-1 Signaling during Post-crossing Navigation of Corpus Callosum Axons. *Current Biology*. 2018;28(11):1768-1782.e4. doi:10.1016/j.cub.2018.04.026

669. DerMardirossian C, Rocklin G, Seo JY, Bokoch GM. Phosphorylation of RhoGDI by Src Regulates Rho GTPase Binding and Cytosol-Membrane Cycling. *Mol Biol Cell*. 2006;17(11):4760-4768. doi:10.1091/mbc.e06-06-0533

670. Kayman-Kurekci G, Talim B, Korkusuz P, et al. Mutation in TOR1AIP1 encoding LAP1B in a form of muscular dystrophy: A novel gene related to nuclear envelopathies. *Neuromuscular Disorders*. 2014;24(7):624-633. doi:10.1016/j.nmd.2014.04.007

671. Santos M, Costa P, Martins F, da Cruz e Silva EF, da Cruz e Silva OAB, Rebelo S. LAP1 is a crucial protein for the maintenance of the nuclear envelope structure and cell cycle progression. *Mol Cell Biochem*. 2015;399(1-2):143-153. doi:10.1007/s11010-014-2241-x

672. Lemberg MK, Bland FA, Weihofen A, Braud VM, Martoglio B. Intramembrane Proteolysis of Signal Peptides: An Essential Step in the Generation of HLA-E Epitopes. *The Journal of Immunology*. 2001;167(11):6441-6446. doi:10.4049/jimmunol.167.11.6441

673. Erskine L, François U, Denti L, et al. VEGF-A and neuropilin 1 (NRP1) shape axon projections in the developing CNS via dual roles in neurons and blood vessels. *Development*. 2017;144(13):2504-2516. doi:10.1242/dev.151621

674. Gudowska-Sawczuk M, Mroczko B. The Role of Neuropilin-1 (NRP-1) in SARS-CoV-2 Infection: Review. *J Clin Med*. 2021;10(13):2772. doi:10.3390/jcm10132772

675. Cui L, Li H, Xi Y, et al. Vesicle trafficking and vesicle fusion: mechanisms, biological functions, and their implications for potential disease therapy. *Molecular Biomedicine*. 2022;3(1):29. doi:10.1186/s43556-022-00090-3

676. Takagi S, Tsuji T, Amagai T, Takamatsu T, Fujisawa H. Specific cell surface labels in the visual centers of Xenopus laevis tadpole identified using monoclonal antibodies. *Dev Biol*. 1987;122(1):90-100. doi:10.1016/0012-1606(87)90335-6

677. Shipley MM, Mangold CA, Szpara ML. Differentiation of the SH-SY5Y Human Neuroblastoma Cell Line. *Journal of Visualized Experiments*. 2016;(108). doi:10.3791/53193

678. Murata K, Mimura A, Suzuki H, et al. Efficient induction of proximity-dependent labelling by biotin feeding in BMAL1-BioID knock-in mice. *The Journal of Biochemistry*. 2021;170(4):453-461. doi:10.1093/jb/mvab059

679. Yang R, Meyer AS, Droujinine IA, et al. A genetic model for in vivo proximity labelling of the mammalian secretome. *Open Biol*. 2022;12(8). doi:10.1098/rsob.220149

680. Liu J, Jang JY, Pirooznia M, Liu S, Finkel T. The secretome mouse provides a genetic platform to delineate tissue-specific in vivo secretion. *Proceedings of the National Academy of Sciences*. 2021;118(3). doi:10.1073/pnas.2005134118

681. Wang C, Qu K, Wang J, et al. Biomechanical regulation of planar cell polarity in endothelial cells. Biochimica et Biophysica Acta (BBA) - Molecular Basis of Disease. 2022;1868(12):166495. doi:10.1016/j.bbadis.2022.166495

682. Cao F, Miao Y, Xu K, Liu P. Lethal (2) Giant Larvae: An Indispensable Regulator of Cell Polarity and Cancer Development. Int J Biol Sci. 2015;11(4):380-389. doi:10.7150/ijbs.11243

683. Khoury MJ, Bilder D. Distinct activities of Scrib module proteins organize epithelial polarity. Proceedings of the National Academy of Sciences. 2020;117(21):11531-11540. doi:10.1073/pnas.1918462117

684. Lhoumeau AC, Puppo F, Prébet T, Kodjabachian L, Borg JP. PTK7: A cell polarity receptor with multiple facets. Cell Cycle. 2011;10(8):1233-1236. doi:10.4161/cc.10.8.15368

685. He CW, Liao CP, Chen CK, Teulière J, Chen CH, Pan CL. The polarity protein VANG-1 antagonizes Wnt signaling by facilitating Frizzled endocytosis. Development. 2018;145(24). doi:10.1242/dev.168666